Unconventional aspects of MR1 restricted T-cells

Hossain Delowar Akther
St. Edmund Hall
University of Oxford
Trinity term 2022

Thesis submission for the degree of
Doctor of Philosophy in Clinical Medicine

Supervisors:
Professor Paul Klenerman, MRCP, FRCP, DPhil
Dr Carolina Arancibia
Dr Marco Lepore
Dr David Cole

In loving memory of dad…

I wish you could have seen the end of this journey and be proud one last time. I would have never dreamed of achieving a DPhil if it weren't for you. Thank you for always encouraging me. Thank you for always seeing the best in me.

Unconventional functions of MR1 restricted T-cells

Hossain Delowar Akther, St. Edmund Hall.

Submitted for DPhil in Clinical Medicine, Trinity term 2022

Abstract

The non-polymorphic MHC class I-related protein 1 (MR1) is an antigen presenting receptor that displays endogenous or microbial-derived metabolic intermediates. The commensal antigens, such as intermediates of the riboflavin synthesis pathway, are the most well understood so far and, these are known to activate mucosal associated invariant T (MAIT) cells. MAIT cells have been widely studied for their innate-like properties and, their strong pro-inflammatory and anti-microbial functions in response to TCR-dependent and TCR-independent signalling. These characteristics confers them with an important, but so far unclear, role in mucosal immunity and autoimmune diseases. Other non-MAIT MR1-restricted T (MR1T) cells have shown specificity to both commensal and endogenous antigens; however, we are still far from understanding the diversity in their functions, phenotype, antigenic specificity and, TCR repertoire.

In this thesis, we used RNAseq analysis to dissect the downstream effects of TCR-dependent and TCR-independent signals on their own and in combination. Our experiments revealed that while the inflammatory responses are tightly regulated and primarily driven by TCR-independent signalling, TCR-mediated activation elicit other unexpected functions related to homeostasis and tissue repair. These data provide a deeper insight on how MAIT cells balance inflammatory and protective functions at barrier sites under constant exposure to the microbiota.

We also explored MR1 as a target molecule for TCR-based immunotherapy against cancer disease. We hypothesised that the endogenous metabolic intermediates could be antigens of interest for the specific targeting of cells undergoing metabolic stress, such

as transformed cancerous cells. In this thesis, we collaborated with Immunocore, a leader in TCR-based immunotherapies, to validate the role of MR1T cells in cancer disease and analysed the specificity of 2 new autoreactive MR1T cells. This work also proposes new methods to accelerate the discovery of antigens and TCR sequences in the unexplored field of MR1T cells.

Acknowledgements

My thanks go, firstly, to my supervisor, Paul, for the guidance, for always being kind and supportive to me and, for giving me the opportunity to work in his lab and embark in this journey that is my DPhil. I could have not asked for a better supervisor.

I would like to express my gratitude to everyone at the Klenerman lab, especially Dr Carl-Philipp Hackstein, for being such great co-workers, for teaching and supporting me throughout my research and for making it such a great place to work. I also want to thank everyone at Immunocore, especially Marco and Dave for welcoming me into their team and co-supervising my research. It has been 4 amazing years and, I feel privileged to have worked beside such talented, generous, and fun people.

I will always be grateful to MRC, Immunocore and Nuffield Department of Medicine for funding my DPhil project and for providing me with all the learning opportunities I need to complete my research.

Thank you to all my friends in Oxford and Abingdon for reminding me that there is life outside the DPhil and, for experiencing Oxford with me. I specially want to thank my fiancé, Laia Puertas, for your patience, for holding me up during hard times, for putting up with my moods, for ensuring that I stayed healthy and, for always being my safe place. I would have not survived this DPhil without you.

Lastly, I want to thank my family for their love, their unwavering support and, for guiding me to where I am today. To my mom, for teaching me patience and resilience. To my dad, for giving me courage, grit, and ambition. And to my sister, for always looking after me.

Contributions

Chapter 3

- Data in sections from 3.3.1 and 3.3.2, MAIT characterisation data were generated in collaboration with **Dr Carl-Philipp Hackstein**.
- In section 3.3.3, data from gut-derived MAIT cells were generated by **Dr Tianqui Leng.**
- RNAseq dataset in section 3.3.4 was generated by Dr Tianqui Leng, while I conducted the presented dataset analysis.
- In section 3.3.6, quantification of growth factors in MAIT supernatants was measured by **Irina Tasin** and Dr Carl-Philipp Hackstein.

Chapters 4

- In sections 4.3.2 and 4.3.3, CRISPR/Cas9 KO guides for β2m and CIITA were designed at Immunocore by **Dr Rahul Khanolkar**. I used these reagents to perform β2m and CIITA KO on THP1 and CRC target cells.
- In sections 4.3.4, DNA constructs for single-chain MR1 (scMR1) and CD1c (scCD1c) were generated at Immunocore by the Discovery research team (**Dr Thomas Gligoris** and **Dr Johanne Pentier**). I transduced these in THP1 and CRC target cells.
- In sections 4.3.5, the E8- and VT001-Jurkat reagents were generated by the Discovery research team at Immunocore. I used these reagents to validate the functionality of scMR1 in target cells. In posterior work, I also used them as controls in experiments with MR1T cells.
- In sections 4.3.9, TCR-sequencing was conducted in house with help from the scPCR team at Immunocore Ltd. (**Dr Nicola Smith**, **Dr Shaliny Ramachandran** and **Dr Lauren Chessum**)
- In section 4.3.10, the refolded MR1 reagents with 5FSA, 5OPRU and 6FP were generated at Immunocore by **Dr Rob Simmons**. I used these reagents to characterise MR1T cells.
- In section 4.3.12, the expression and purification of soluble MR1 reagents from mammalian cells were done by **Dr Rich Suckling** at Immunocore. I used these reagents to characterise MR1T cells.

Chapters 5

- Dr Rich Suckling did the expression and purification of soluble MR1 reagents from mammalian cells at Immunocore. I used these reagents to detect MR1T cells in overnight activation assays.
- Sample collection from CRC donors was coordinated by **James Chivenga** and **Dr Carolina Arancibia** at the Oxford Biobank.

Table of contents

Abbreviations

5ARU	5-amino-6-d-ribityl-aminouracil
5FSA	5- formyl sialic
5OERU	5-(2-oxoethylideneamino)-6-D-ribityl-aminouracil
5OPPRU	5-(2-oxopropylideneamino)-6-D-ribityl-aminouracil
6FP	6-formylpterin
Ac-6FP	Acetyl-6-formylpterin
αGalCer	Alpha-Galceramide
AIM	Activation induced markers
APC	Antigen presensing cells
ATG	Autophagy-related gene/protein
β2m	Beta-2-microglobulin
BCR	B-cell receptor
Bp	Base-pairs
BPC	Bacteria per cell
BTN	Butyrophilin
CCL	C-C motif ligand (followed by number)
CCR	Chemokine Receptor (followed by number)
CD	Cluster of differentiation (followed by number)
CD_R/L	CD (followed by number) receptor/ligand
cDNA	Complementary DNA
CFU	Colony-forming units
CIITA	Class II MHC transactivator
CLIP	Class II-associated invariant chain
CLT	Cytotoxic T lymphocyte
CRC	Colorectal carcinoma
CRISPR	Clustered regularly interspaced short palindromic repeats
CSF	Colony Stimulating Factor (followed by number)
CTV	Cell trave violet
CXCR	CXC chemokine receptors
DB28	3-([2,6-dioxo-1,2,3,6-tetrahydropyrimidin-4-yl] formamido) propanoic acid
DC	Dendritic cells
Ds	Disulphide bond
DETC	Dendritic epidermal T cells
DKO	Double knock-out
DMSO	Dimethyl sulfoxide
DN	Doubl**5**e negative (CD4- CD8-)
DP	Double positive (CD4+ CD8+)

E.coli	*Escherichia coli*
EBSS	Earle's balanced salt
EDTA	Ethylenediaminetetraacetic
ELISA	Enzyme-linked immunosorbent assay
ELISPOT	Enzyme-linked immunospot
EOMES	Eomesodermin 3
EPCR	Endothelial protein c receptor
ER	Endoplasmic reticulum
F.tularensis	*Francisella tularensis*
FACS	Fluorescence-activated cell sorting
FBS/FCS	*Foetal bovine/calf serum*
FDA	Food and drug administration
FO	7,8-dideme-thyl-8-hydroxy-5-deazariboflavin
FOXP3	Forkhead box protein P3
GATA3	GATA-binding factor 3
GF mice	Germ free mice
GFP	Green fluorescent protein
GPI	Glycosyl-phosphatidyl-inositol
Grz	Granzyme
GSEA	Gene set enrichment analysis
H.pylori	*Helicobacter pylori*
HCC	Hepatocellular carcinoma
HLA	Human leukocyte antigen
HRP	Horseradish peroxidase
IBD	Inflammatory bowel disease
ICOS	Inducible T-cell costimulator
ICS	Intracellular staining
IFN	Interferon
IFNGR	IFNγ receptor 1
IgG	Immunoglobulin G
Ii	Invariant chain
IL	Interleukin (followed by number)
IL_R	Interleukin receptor
ILC	Innate lymphoid cells
iNKT	Invariant Natural killers T-cell
K.pneumoniae	*Klebsiella pneumoniae*
KD	Knock-down
KO	Knock-out
L.longbeachae	*Legionella longbeachae*
LC3	Microtubule-associated protein 1A/1B-light chain 3
LEAF	Low endotoxin, azide-free
LLT1	Lectin-like transcript 1

LPMC	Lamina propria mononuclear cells
LPS	Lipopolysaccharides
M.smegmatis	*Mycobacterium smegmatis*
MAIT	Mucosal associated invariant T-cells
MALT	Mucosa associated lymphoid tissue
MG	Methylglyoxal
MHC	Major histocompatibility complex
MICA/B	MHC class I polypeptide-related sequence A
MICB	MHC class I polypeptide-related sequence B
MR1	Major histocompatibility complex class I-related gene protein
MR1T	MR1 restricted T-cells
Mtb	*Mycobacterium tuberculosis*
NEAA	*Non-essential aminoacid*
NFAT	Nuclear Factor of Activated T-cells
NFkb	Nuclear factor kappa-light-chain-enhancer of activated B cells
NK	Natural killers
NKT	Natural killers T-cell
NOD	Non-obese diabetic
NV18.1	3-([2,6-dioxo-1,2,3, 6-tetrahydropyrimidin-4-yl] formamido) propanoate
P. mirabilis	*Proteus mirabilis*
PAMP	Pathogen associated molecular pattern
PBMC	Human peripheral blood mononuclear cells
PBS	Phosphate buffered saline
PCA	Principal component analysis
PCR	Polymerase chain reaction
PD1	Programmed cell death protein 1
PDGF	Platelet derived growth factor
PDL1	Programmed cell death 1 ligand 1
PHA	Phytohemagglutinin
PLC	Peptide loading complex
PLI	6-(2-carboxyethyl)-7-hydroxy-8-ribityl-lumazine
PLIII	6-(1H-indol-3-yl)-7-hydroxy-8- ribityl-luma- zine
PLZF	Zinc finger and BTB domain-containing protein 16
PMA	Phorbol 12-myristate 13-acetate
PRR	Pattern recognition receptor
RACE	Rapid amplification of cdna ends
ribA	GTP cyclohydrolase
ribB	3,4-dihydroxy-2-butanone 4-phosphate synthase
ribD	5-amino-6-(5-phosphoribosylamino)uracil reductase
RL-6-Me-7-OH	7-hydroxy-6-methyl-8-D-ribityllumazine
RL-6,7-diMe	6,7-dimethyl-8-D-ribityllumazine

RNA	*Ribonucleic acid sequencing*
RNP	Ribonucleoprotein complexed
RORγt	Retinoid-related orphan receptor-gamma
RPM	Revolutions per minute
S.O.	Sub-optimal
SAP	SLAM-associated protein
Sc	Single chain (followed by MR1 or CD1c)
SFU	Spot forming units
SLAM	Signalling-lymphocytic-activation-molecule
SLO	Secondary lymphoid organs
STAT	Signal transducer and activator of transcription (followed by number)
T1D	Type 1 diabetes
TAP	Transporter associated with antigen processing
Tbet	T-box transcription factor TBX21
Tc	Cytotoxic T-cell (followed by 1, 2, 3 or 17)
TCR	T-cell receptor
Tet	Tetramer
TGF	Transforming growth factor
Th	Helper T-cell (followed by 1, 2, 3 or 17)
TIL	Tumour infiltrating lyphocyte
TL1A	Histocompatibility 2, M region locus 3
TLR	Toll like receptor
TNF	Tumor necrosis factor
TRAJ	T cell receptor alpha joining genes
TRAV (Va)	T cell receptor alpha variable genes
TRBV (Vb)	T cell receptor beta variable genes
TRDV (Vd)	T cell receptor delta variable genes
TRGV (Vg)	T cell receptor gamma variable genes
TSO	Template switching oligo
Tyr	Tyrosine
VEGF	Vascular endothelial growth factor

1. Introduction

1.1. Innate and adaptive systems

The innate and adaptive systems are 2 arms of the immune response that work together to protect us against pathogens and clear infections. The innate system is the first line of defence and eliminates most invading pathogens while maintaining a homeostatic balance with commensal microorganisms. It provides a broader (less specific) and faster response than the adaptive system. On the other hand, the adaptive system can generate a targeted and bespoke response to each pathogen. However, the adaptive response does not provide immediate protection against newly invading microorganisms as an inductive period is required to build up pathogen-specific responses and posterior memory. Immunological memory allows rapid adaptive response against reoccurring infections from the same pathogen or other agents generating similar antigens (Ahmed and Gray 1996; Bachmann *et al.* 1996).

1.1.1. Innate system

Besides cellular components, the innate system is also composed of physical and chemical elements of protection. This is evident in mucosal tissues that coat the gastrointestinal, respiratory, and urogenital tracts. This epithelial coating repels pathogens from establishing an infection through the secretion of mucin, antimicrobial peptides, enzymes, and IgA antibodies. This topic is explained in more detail in Ref: (Murphy and Weaver 2017).

Microorganisms that overcome the mucosal barrier rapidly activate innate immune cells and the complement system. The complement system can be described as a network

of molecular cascades that opsonise invading pathogens, and either have a direct microbicidal effect or flag them for phagocytosis and killing by immune cells (Dunkelberger and Song 2009). Besides the complement system, immune cells also use pattern-recognition receptors (PRR) to recognise broad pathogen-associated-molecular-patterns (PAMP). One example of PRRs is the Toll-like receptor family (TLR), which recognises intracellular and extracellular infections (Medzhitov and Janeway 1998).

There are several populations within the cellular component of innate immunity. These are phagocytes, dendritic cells (DC), innate-lymphoid cells (ILC) and natural killer cells (NK) (Murphy and Weaver 2017). Phagocytes clear pathogens by phagocytosis and antimicrobial activity. Macrophages and neutrophils are the most abundant phagocytes in host tissues and are the first to control the spread of invading pathogens. Both local phagocytes and the complement cause local inflammation, which increases the local influx of neutrophils and monocytes (that differentiate into macrophages) and circulating cells from the adaptive immune system (Mosser and Edwards 2008; Kolaczkowska and Kubes 2013). On the other hand, DC specialise in processing and presenting pathogen-derived antigens in secondary lymphoid organs (SLO) to activate the adaptive arm of the immune system (Banchereau and Steinman 1998).

ILCs and NK cells are lymphoid cells that do not carry a T-cell or B-cell receptor (TCR or BCR, respectively) but are activated either through PRR- or complement-mediated pathogen recognition or through cytokines produced by myeloid, epithelial, and stromal cells. ILC1, ILC2 and ILC3 are 3 broad subsets that provide early response against intracellular pathogens, parasites, and extracellular pathogens, respectively. The activation of these different sub-types shapes the adaptive response into type-1, type-2 and type-3 responses. These axes imply the differentiation of T-cell subsets that amplify the initial ILC inputs (explained in more detail in section 1.1.4). NK cells are mostly part of the type-1 response and elicit early cytotoxic functions against cells infected by intracellular pathogens (Sun and Lanier 2011; Eberl *et al.* 2015).

1.1.2. Adaptive system

Parallel to the innate response, the adaptive system provides a tailored response to pathogens consisting of antibody-mediated opsonisation of microbes and parasites and, T-cell-mediated signal amplification to enhance phagocytosis and cytotoxic killing of infected cells. The effector cells in the adaptive arm are primarily T-cell and B-cell lymphocytes (Murphy and Weaver 2017).

Antigen-presenting cells (APC) are an important link between the innate and adaptive arms. As innate cells, they combat the spread of invading pathogens and engulf pathogens to extract antigens that are presented to T-cells through antigen-presenting molecules, such as the MHC complex. DC are regarded as professional APC; however, macrophages and B-cells can also present antigens. When APC capture pathogens, they migrate to SLOs, such as lymph nodes or mucosal-associated lymphoid organs (MALTs), following the gradient of CCL19/21 through CCR7 receptors (Banchereau and Steinman 1998; Mosser and Edwards 2008; Yuseff *et al.* 2013). In SLOs, T-cells are presented with different antigens, and those that carry antigen-reactive TCRs are primed to undergo clonal expansion and differentiate into effector and memory phenotypes. During priming, T-cells upregulate CD69, a retention marker that prevents T-cells from scaping the SLOs until they finish the clonal expansion and downregulate CD69 (Mempel, Henrickson and von Andrian 2004). CD69 is regularly used as an early T-cell activation marker.

In SLOs, follicular T-cells also prime B-cells with BCRs that recognise relevant epitopes, which expand and differentiate into memory and IgG antibody-producing plasma cells. After priming, effector T-cells enter circulation and infiltrate into inflamed tissues, where they realise their functions. On the other hand, plasma cells also enter circulation and produce soluble BCRs, also known as antibodies, which opsonise pathogens and speeds their clearance (Lee *et al.* 2011; Shulman *et al.* 2014).

1.1.3. T-cell subsets

T-cell progenitors originate in the bone marrow and fully mature in the thymus. There, they acquire the expression of the CD3 complex and the CD4 and CD8 co-receptors. CD4 and CD8 expression is determined by the transcription factors ThPOK and RUNX3, respectively (He *et al.* 2005; Singer, Adoro and Park 2008). Most T-cells will be categorised either as CD4+ or as CD8+; however, some can have both (double positive, DP) or none (double negatives, DN). Additionally, every T-cell undergoes rearrangements of the variability (V), diversity (D) and joining (J) gene segments, giving rise to a heterogeneous TCR-carrying population (Schatz, Oettinger and Baltimore 1989). Mature T-cells circulate through different SLOs via the bloodstream until they are primed by an APC presenting their cognate antigen. During this differentiation process, T-cells switch surface expression of the CD45A isoform to the CD45RO isoform; therefore, the lack of CD45RA expression is usually associated with an effector-memory phenotype (Murphy and Weaver 2017).

APC activate CD4+ T-cells by presenting cognate antigens in the context of MHC class II (MHCII) receptors (Doyle and Strominger 1987; Grusby *et al.* 1991). After activation, CD4 T-cells can differentiate into lineages such as Th1, Th2, Th17 and Treg, among others. Every lineage is defined by the expression of specific transcription factors and cytokines (as elucidated in Figure 1) and differentiation into each lineage is conditioned by a particular priming microenvironment determined by the innate system (Dong 2006; Cesare, Meglio and Nestle 2009). It is generally accepted that Th1, Th2 and Th17 amplify the type-1, type-2, type-3 immune axis, respectively and, are the adaptive counterparts of ILC1, ILC2 and ILC3, respectively (Fang and Zhu 2017).

On the other hand, CD8+ T-cells are the adaptive counterparts of NK cells, and they respond to antigens presented by MHC class-I (MHCI) receptors, eliciting cytotoxic functions against antigen-bearing cells. Differentiated CD8+ cells are also called

cytotoxic lymphocytes (CTL) (Fowlkes *et al.* 1985; Wax Ma N *et al.* 1988), and there are also Tc1, Tc2, and Tc17 subsets expressing cytokines involved in type-1, type-2 and type-3 responses, respectively (Mittrücker, Visekruna and Huber 2014).

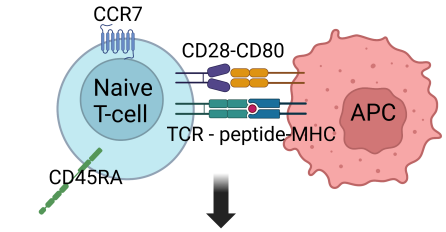

		Key Transcription Factor	Chemokine receptors	Effector cytokines	Functions
IL12/IFNg	Th1/ Tc1	T-bet STAT1	CCR5 CXCR3	IFNγ TNFα	- Intracellular pathogen control - Cell-mediated immunity
IL4	Th2/ Tc2	GATA3	CCR3 CCR4 CCR8 CRTH2	IL4 IL5 IL13	-Humoral immunity -Allergy -Parasite control
TGFβ/IL6	Th17/ Tc17	RORγt STAT3	CCR6	IL17A IL17F IL22	-Cell-mediated immunity -Autoimmunity -Chronic inflammation -Extracellular pathogen control
TGFβ/Retinoic-acid	Treg	FOXP3	CCR9	IL10 TGFβ	-Immunosuppression -Peripheral tolerance

Figure 1- 1. Differentiation of CD4 and CD8 into T-cell subsets. T-helper and T-cytotoxic subsets differentiate from primed CD4+ and CD8+ T-cell subsets. Different lineages are regulated under different key transcription factors, have different homing properties and, release different effector molecules and elicit different biological functions upon triggering. Created with BioRender.com

1.1.4. T-cell functions

The type-1 response corresponds to immunity against intracellular pathogens, and it is initiated by phagocytes (macrophages and DC) and ILC1 cells through the early production of IL12 and IFNγ, respectively (Hsieh *et al.* 1993). Th1 cells produce pro-inflammatory molecules like TNFα, CCL3 and GM-CSF, which activate the endothelia and increase the recruitment of monocytes and macrophages (Muñoz-Fernández, Fernández and Fresno 1992). Expression of CD40L and IFNγ by Th1 cells favour the polarisation of macrophages into M1-phenotype, which elicits enhanced killing and antigen presentation of engulfed bacteria (Stout *et al.* 1996).

The type-2 response is initiated by IL5 and IL13. These cytokines are produced by ILC2 cells in response to IL33 alarmin, IL25, and TSLP made by stromal and epithelial cells damaged by large multicellular parasites (Camelo *et al.* 2017). IL5 and IL13 induce granulocytes to produce IL4, the main cytokine involved in the Th2 polarisation of naïve T-cells (McLeod, Baker and Ryan 2015). Th2 cells are producers of IL5, IL13 and IL4 cytokines; IL5 activates anti-parasite activity in eosinophils, while IL13 and IL4 promote polarisation of M2-macrophages, which carry out essential anti-parasitic and tissue-repair functions (van Dyken and Locksley 2013). In addition, IL13 prevents parasites from adhering to the epithelia by boosting mucus production and increasing cellular turnover (Alevy *et al.* 2012). Th2 cells are also involved in humoral immunity against toxins and noxious substances and, in some cases, can cause allergic inflammations due to the excessive triggering of mast cells and increased IgE production (Fort *et al.* 2001; Ohnmacht *et al.* 2010; Liang *et al.* 2011).

The type-3 (or type 17) response provides anti-microbial immunity. This axis is initiated by IL17A/F cytokines produced by ILC3 cells in response to IL23 and IL1β produced by macrophages and DC (Hoorweg *et al.* 2012; Golebski *et al.* 2019). IL17A/F induces the production of IL6 in stromal, epithelial, and myeloid cells (Chang and Dong

2007; Dubin and Kolls 2009). Th17 differentiation requires the presence of IL6 and TGFβ (Kimura, Naka and Kishimoto 2007; Qin *et al.* 2009); this lineage express CCR6, a homing receptor for skin and mucosal sites, where they combat extracellular pathogens and keep the microbiota at bay through the expression of IL17A/F and IL22 (Cesare, Meglio and Nestle 2009). While IL17 is a pro-inflammatory cytokine that increases the production and recruitment of neutrophils from the bone marrow, IL22 cytokine induces the expression of anti-microbial peptides and cellular turnover in the epithelia (Zheng *et al.* 2008). Interestingly different studies have shown that Th17 cells can polarise macrophages into both M1- or M2-phenotypes (Shi *et al.* 2013; Nishikawa *et al.* 2014; Shen *et al.* 2018). However, it is still unclear how they drive either of the 2 phenotypes (Nakai *et al.* 2017).

On the other hand, Treg differentiation requires retinoic-acid and TGFβ. The balance between IL6 and retinoic-acid at barrier sites controls differentiation to Th17 or induced Tregs (iTregs), respectively (Eisenstein and Williams 2009). Tregs produce TGFβ and IL10 inhibitory cytokines that block T-cell activation and maintain tissue homeostasis and tolerance (Taylor *et al.* 2006).

1.2. Unconventional and innate-like T-cells

While the priming of conventional T-cells requires the recognition of MHC-peptide complexes, unconventional T-cells escape the classical MHC restriction and can be triggered by non-polymorphic MHCIb receptors (Godfrey *et al.* 2015). Some of these specificities include lipid presentation by CD1 molecules (such as αGalCer by CD1d), metabolite presentation by MR1 (such as riboflavin derivates) and HLA-E molecules presenting MHC leader peptides. On the other hand, the γδT-cell compartment is also interesting for its broad recognition patterns; not only have they shown specificities to CD1 and MR1 molecules, but also, they can recognise surface proteins like endothelial-protein-C-receptor (EPCR) and, phospho-antigens presented by Butyrophilin 3A1 (BTN3A1) or Annexin A2 (Godfrey *et al.* 2015). Most of these unconventional specificities are associated with cellular stress due to infections or aberrant metabolism (Godfrey *et al.* 2018).

Within unconventional T-cells, the most well-characterised subsets are Vγ9Vδ2 T-cells, invariant natural-killer T-cells (iNKT) and mucosal-associated invariant T-cells (MAIT) (Kurioka *et al.* 2016; Crosby and Kronenberg 2018; Provine *et al.* 2018). These subsets are unique because of their abundance in either mice or humans, their semi-invariant TCRs, the limited number of antigens they can recognise, and their innate-like characteristics. Innate-like T-cells have an effector-memory phenotype (CD45RA-) imprinted during their development in the thymus or very early in the organism's development (Pellicci, Koay and Berzins 2020). Unlike conventional T-cells, they do not require priming in SLO, and as a result, they are poised for rapid activation both by TCR-dependent or TCR-independent triggers. These characteristics are necessary for innate-like T-cells as they reside in barrier tissues where they are constantly exposed to antigens (Kurioka *et al.* 2016; Crosby and Kronenberg 2018; Provine *et al.* 2018).

1.2.1. γδ T-cells

The CDR3 from the Vδ chains are significantly longer than those found in Vα or Vβ chains (Rock *et al.* 1994), allowing γδT-cells to have a broader recognition of stress-associated ligands outside the MHC context (Bonneville, O'Brien and Born 2010).

Most of them are DN T-cells. There are 2 major subgroups of γδ T-cells depending on their δ chain: Vδ2- and Vδ2+ (TRDV2+). Vδ2 cells are the predominant γδT-cell population in the blood (Constant *et al.* 1994; Hayday 2009). Most Vδ2 have the Vγ9Vδ2 chain pairing and recognise phosphorylated intermediaries of the isoprenoid biosynthesis pathway presented by BTN3 and BTN8 (Vantourout and Hayday 2013). These phospho-antigens can be produced by mammalian cells and bacteria; however, the Vγ9Vδ2 TCRs have ~10000-fold higher affinity to those of bacterial origin (Gu, Nawrocka and Adams 2015).

Vδ1 (TRDV1+) cells are the most abundant in the Vδ2- compartment and are found in peripheral tissues and the thymus (Constant *et al.* 1994; Hayday 2009). Vδ2- populations exhibited clonal diversity with diverse TCR chain pairing. Mice studies suggests that Vδ2-cells, similar to adaptive T-cells, undergo clonal expansion in response to microbial and non-microbial ligands, like adaptive T-cells (Davey *et al.* 2017). The larger diversity of TCRs in the Vδ2- compartment allows them to recognise a broader range of antigens than Vδ2+ cells, which vary from surface proteins such as EPCR (Willcox *et al.* 2012) to soluble ligands and small lipids presented in the context of CD1a,c,d and MR1 molecules (Porcelli *et al.* 1989; van Rhijn and le Nours 2021). The differences between the 2 subgroups suggest that γδ T-cells are not all innate-like.

During thymic development, γδT-cells are pre-programmed to elicit Th1, Th2 and Th17-like phenotypes depending on their TCR pairing and localisation (Ness-Schwickerath, Jin and Morita 2010; Ribot *et al.* 2014). These functions allow them to perform anti-viral and anti-microbial duties in peripheral tissue (Hoq *et al.* 1997; Carding

and Egan 2000; Willcox *et al.* 2012). Their functions depend on the presence of cytokines; for instance, cytokines such as IL2, IL12, IL15, and IL18 in the local microenvironment induce type-1 functions (Domae *et al.* 2017; Schilbach *et al.* 2020), while TGFβ, IL6 and IL10 at barrier sites promote the type-3 and regulatory functions (Peng *et al.* 2007; Do *et al.* 2010; Petermann *et al.* 2010). Additionally, mice have Vγ5+ or Vγ3+ dendritic epidermal T-cells (DETC) with antigen-presenting capabilities located in the skin epidermis, which are not found in their human counterparts (Girardi *et al.* 2002; Jameson *et al.* 2004).

Because γδT-cells have specificities for stress markers, they have been linked with tumour immunity (Willcox and Willcox 2019; Payne *et al.* 2020). On one side, they can elicit antitumour activity by releasing IFNγ and other cytotoxic molecules such as granzymes (Grz) and perforins. Moreover, they can also exert direct killing through TCR-independent receptors such as FASL, TRAIL and NKG2D mediated MICA/B recognition on tumour cells. On the other hand, they can also have pro-tumour functions by promoting angiogenesis and promote M2 polarisation of macrophages through IL17A (Park and Lee 2021). While the Th17 module is seen in Vγ9vδ2 subsets, it is more prevalent in the tissue-resident Vδ2- cells (Maher *et al.* 2015; Bai *et al.* 2016; McKenzie *et al.* 2018); although there is no clear correlation between chain-pairings and T-cells function. In addition, Vδ1 subsets can express CD39, PDL1 and FOXP3 and, in activation assays, they blocked T-cell proliferation in an IL10-dependent manner (Casetti *et al.* 2009; Rutkowski *et al.* 2015; Mao *et al.* 2016; Hu *et al.* 2017).

1.2.2. NKT cells

These share expression of surface markers with NK cells, such as NK1.1 (CD161) (Bendelac *et al.* 1997). They react to small lipids presented by CD1d molecules through αβ TCRs (Godfrey *et al.* 2004). There are 2 subgroups: type-I NK T-cells (also referred to as invariant or iNKT cells) and type-II NK T-cells. In mice, NKT cells are mostly CD4+ or DN, while in humans, they can be CD4+, CD8+ or DN (Godfrey *et al.* 2004).

Like Vδ2- cells, type-II NK T-cells have a diverse TCR repertoire (Rhost *et al.* 2012). They recognise CD1d-associated sulfatides and phospholipids produced by mammalian cells and microbes (Roy *et al.* 2008; Girardi *et al.* 2012; Tatituri *et al.* 2013). They are more abundant than iNKT cells and have exhibited immunosuppressive functions, contributing to cancer progression in mouse studies (Rhost *et al.* 2012).

On the other hand, iNKT cells have limited TCR diversity with an invariant Vα24-Jα18 (TRAV10*01-TRAJ18*01) chain coupled with different Vβ-chains (Godfrey *et al.* 2004). The most well-studied agonistic ligand for iNKT cells is αGalCer, which led to the discovery of the antigenic motif for iNKT cells, the α-anomeric linkages between carbohydrate moieties and a lipid tail (Pei *et al.* 2012). Although lipid antigens are mostly produced in pathogens and commensals, mammalian cells can also produce similar CD1d-associated antigens (Kain *et al.* 2014).

iNKT cells can elicit different effector functions depending on the transcription factors they express. In mouse studies, several subsets have been identified: IFNγ producing NKT1 cells, IL4 producing NKT2, IL17 producing NKT17 or IL10 producing NK10 (Michel *et al.* 2007; Lee *et al.* 2013; Sag *et al.* 2014). Although the distribution of these subsets can vary between strains of mice, resident iNKT cells shape the local microenvironment and profoundly affect how the local immune response is shaped (Lee *et al.* 2015). Some iNKT cells also remain in the thymus after differentiation, where they

condition the polarisation of primed CD8 and CD4 T-cells (Eberl, Brawand and MacDonald 2000). After egressing from the thymus, they establish long-term residencies in peripheral tissues. In parabiosis studies, these subsets could establish residency in peripheral tissues: liver, lungs, spleen, lymph nodes, intestine, skin, adipose tissue, and bone marrow (Thomas *et al.* 2011; Lynch *et al.* 2015). NK10 cells were exclusively found in adipose tissues, where they secrete IL10 and contribute to the immunosuppressive microenvironment (Lee *et al.* 2015). Because this subset is not found in the thymus, one of the other 3 subsets is thought to differentiate into NK10 in response to the local conditions in the adipose tissues (Lynch *et al.* 2015).

This heterogeneity explains why depending on the subset of iNKT cells, they can be beneficial or detrimental to the host in response to disease. For example, against CD1d+ tumours, NKT1 cells exert cytotoxic responses and boost DC activity by upregulating CD40L (CD154) (Vincent *et al.* 2002; Wingender *et al.* 2010). In contrast, the NKT2 subset can adopt a homeostasis role by producing IL13 and hinder the clearance of cancer cells (Lee *et al.* 2013). In autoimmune diseases like obesity and diabetes, NKT2 and NKT10 subsets have a protective role by creating an immunosuppressive environment (Wu and van Kaer); in other cases, NKT2, alongside NKT17 cells, are responsible for hyper-reactivity in respiratory diseases being detrimental to the host (Pichavant *et al.* 2008);

1.2.3. MR1-reactive cells

MR1 specific T-cells are the main topic of study in this thesis. They are characterised by their specificity to metabolic intermediates presented in the context of MR1 molecules. There are 2 types of populations: the innate-like MAIT cells and other MR1-reactive T-cells (Gherardin *et al.* 2018a). The latter compartment has not been extensively characterised, and, in this thesis, they will be referred to as MR1T cells.

MAIT cells are an innate-like population characterised by the expression of a semi-invariant TCR with a constant Vα7.2-J33/12/20 (TRAV1-2, TRAJ33/12/20) associated with limited TRBV chains, which recognises intermediates from the riboflavin synthesis pathways from bacterial and fungal origin presented in the context of MR1. They are present in barrier sites and, exert strong antimicrobial functions (Kurioka *et al.* 2016). These cells will be explained in more detail in section 1.4.

On the other hand, MR1T cells are thought to be heterogeneous in their TCR repertoire. They can recognise both microbial and endogenous ligands. However, the bulk of this population is yet to be fully characterised regarding TCR diversity, unique antigen specificity and functions (Koay *et al.* 2019a; Seneviratna *et al.* 2022). These cells will be explained in more detail in section 1.3.

1.2.4. The interplay between innate-like populations

Innate-like T-cells, such as Vγ9vδ2, iNKT and MAIT cells, acquire an effector phenotype at neonatal stages, and consequently, they can colonise peripheral tissues before conventional T-cells (Salou *et al.* 2019; Pellicci, Koay and Berzins 2020). Several studies, including work in this thesis, point out that innate-like T-cells are crucial to strike a balance between controlling the commensal microbiota at barrier sites and minimising tissue damage due to persistent T-cell activation (Constantinides and Belkaid 2021).

Studies with mice showed that mice housed under different conditions had a considerable variability in the MAIT frequency (Constantinides *et al.* 2019). Using the PLZF transcription factor as a marker for innate-like T-cells, impaired thymic development of PLZF+ T-cells was observed in germ-free (GF) neonate mice (Ennamorati *et al.* 2020). More specifically, the rise of MAIT population required early exposure to riboflavin-producing microbiota (Koay *et al.* 2016; Constantinides *et al.* 2019; Legoux *et al.* 2019a). This indicated that the frequency of innate T-cells is determined by non-genetic factors such as exposure to specific commensal antigens. In additional studies, antibiotic treatment in early-life reduced the abundance of innate-like T-cells in adult mice however, perturbation in the microbiota of adult mice did not affect their innate-like T-cell populations (Zeissig and Blumberg 2014). This suggested that the microbiota-derived signals to expand innate-like T-cell populations need to happen in a limited window of time early in the life of mice.

Because innate-like T-cells share similarities in their behaviour and transcriptional programmes (Gutierrez-Arcelus *et al.* 2019), regulated under PLZF transcription factor (Savage *et al.* 2008), compensatory effects are possible in order to retain specific functions in host tissues despite the absence of specific T-cell populations. For example, in TCRδ knock-out C57BL mice, the absence of Th17 effector γδT-cells in the skin is compensated by Th17 MAIT and iNKT cells (Constantinides *et al.* 2019), thus retaining a

strong anti-microbial module against commensals. In another study with CD1d knock-out mice, the missing iNKT populations in the thymus, spleen and liver were replaced by an increased MAIT frequency (Koay *et al.* 2016). Similarly, the loss of MAIT populations in a patient with a homozygous point MR1 mutation ($MR1^{R9H}$) was associated with a concomitant increase of γδT-cells (Howson *et al.* 2020).

Despite the compensatory effects, the predominance of innate-like subsets can be observed in specific localizations and niches, suggesting that they have different biological functions and compete during the early colonisation of peripheral tissues and barrier sites. Although this is not yet fully understood, the composition of innate-like T-cells is likely to be determined by the presence of relevant antigens (Wei *et al.* 2010; Legoux *et al.* 2019a; Lin *et al.* 2020) in addition to cytokine/chemokine signals that favour specific subsets and functions (Koay *et al.* 2019b; Howson *et al.* 2020; Constantinides and Belkaid 2021).

1.3. MR1 biology

Early studies with MAIT cells showed that this population persisted in mice deficient in MHCI, MHCII, TAP (transporter associated with antigen loading) and CD1 molecules; nevertheless, β-2-microglobulin (β2m) deficient mice did not develop MAIT populations (Tilloy *et al.* 1999). These findings indicated that MAIT cells recognised a non-classical MHC molecule different from CD1. In 2003, Treiner *et al.* found that these cells reacted with ligands associated with the non-polymorphic MHCI-related protein-1 (MR1) receptor (Treiner *et al.* 2003).

1.3.1. MR1 structure

Initial structural studies showed that MR1 molecules resembled MHCI molecules, consisting of a heavy chain non-covalently associated with β2m. The heavy chain has 3 domains named α1, α2, α3 and a transmembrane domain (Yamaguchi and Hashimoto 2002). The Mr1 gene is located outside the MHC locus and is evolutionarily conserved across mammalians, especially in the α1 and α2 domains, which contain the antigen binding cleft composed by the A' and F' pockets (López-Sagaseta *et al.* 2013; Reinink and van Rhijn 2016).

Using conformation-specific anti-MR1 antibodies, it was found that MR1 switched between an open and a folded conformation and, in the latter conformation, MR1 was able to activate MAIT hybridomas. These conformational changes were reminiscent of the peptide-induced changes seen in MHCI, underlining that MR1 was able to present antigens (Huang *et al.* 2005a). Both human and murine MAIT cells could cross-react with other mammalian MR1 orthologs. This and the evolutionarily conserved nature of MR1 suggested that MR1 antigens had to be conserved across mammalians (Huang *et al.* 2009).

Structural studies by Kjer-Nielsen *et al*. showed that MR1 could present microbial-derived chemical moieties (Kjer-Nielsen *et al*. 2012). These antigens were presented in the A' pocket, which contained both aromatic and charged residues, confering it with the versatility to present both hydrophobic and charged antigens (Keller *et al*. 2017). Mass spectrometry analysis of MR1-eluted compounds indicated that MR1 antigen sizes ranged between 280-1200 Daltons (Harriff *et al*. 2018). These 2 studies alone suggest that the A' pocket may accommodate a wide range of chemical structures.

Most structural models so far elucidated ligands between 150-300 Dalton associated to the A' pocket, leaving the F' pocket empty (Eckle *et al*. 2014; Keller *et al*. 2017); nevertheless, given that these studies were biased toward the discovery of ligands that formed canonical interactions (similar to 5OPRU or 6FP) with MR1, they may have overlooked the possibility of unconventional binding modes where the F' pocket could be partially occupied by ligands in the upper end of the size range (Seneviratna *et al*. 2022). Another theory is that the F' pocket has a role in MR1 trafficking by binding to chaperones that allow antigen loading and exchange (Harriff *et al*. 2016; Karamooz *et al*. 2019; McWilliam *et al*. 2020; McShan *et al*. 2022).

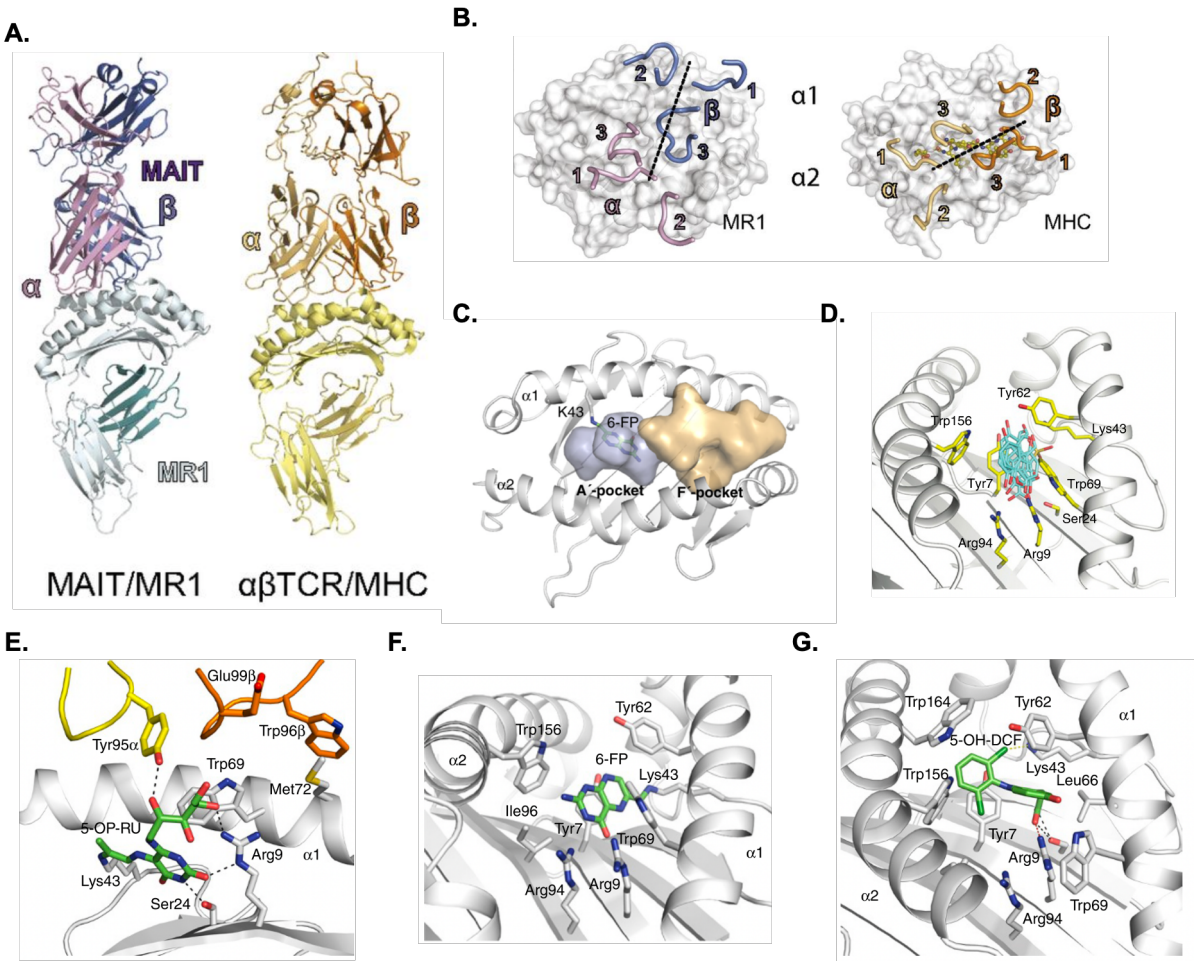

Figure 1- 2. MR1 resemble MHC molecules and can accommodate different chemical structures. (**A**) MR1 (blue) and MHC (yellow) are structurally similar, and both of them associate to β2m. Nevertheless, MR1 associates the MAIT TCR with a different docking orientation than conventional TCRs (**A, B**). (**C**) MR1 binding grooves have 2 pockets, and most described antigens were found in the A' pocket, where they can form a Schiff base. (**D-G**) In addition to 5OPRU (**E**) and 6FP (**F**), which form Schiff bases, MR1 can also accommodate a wide range of chemical structures (**D**). One such structure is the Diplofenac drug (**G**), which canasspciate to MR1 without forming a Schiff base.

Figure and caption from **A** and **B** panels were adapted and reprinted from PNAS, 2013;110:E1771–8, López-Sagaseta J, Dulberger CL, Crooks J, Erin J. Adams, The molecular basis for Mucosal-Associated Invariant T cell recognition of MR1 proteins, Copyright (2013), with permission from PNAS (No Licence needed).

Figure and caption from **C** were adapted and reprinted from Current Opinion in Immunology 2015, 34:28–34, Hamish EG McWilliam, Richard W Birkinshaw, Jose A Villadangos, James McCluskey, Jamie Rossjohn, MR1 presentation of vitamin B-based metabolite ligands, pp. 28-34, Copyright (2015), with permission from Elsevier (Licence number 5373780287434)

Figure and caption from **D-G** were adapted and reprinted from Nature Immunology 2017, 18:402–11, Keller AN, Eckle SBGG, Xu W, James McCluskey, Jamie Rossjohn, Drugs and drug-like molecules can modulate the function of mucosal-associated invariant T cells, Copyright (2017), with permission from Nature Immunology (Licence number 12600a58-1)

1.3.2. Intracellular trafficking and presentation pathways MR1

1.3.2.1. Conventional antigen-presentation pathway

MHCI and MHCII have different intracellular trafficking. Both MHCI and MHCII molecules start at the endoplasmic reticulum (ER), where they are synthesised in a partially open conformation. MHCI molecules associate with β2m and associate with the peptide loading complex (PLC) in the ER. In the PLC, Tapasin and other chaperones mediate the loading of high-affinity peptides onto MHCI molecules. MHCI peptides come from the degradation of proteins in the cytosol by the proteasomes, which are then transported to the ER by the TAP complex. This topic is reviewed in Ref: (Neefjes *et al.* 2011).

On the other hand, MHCII molecules associate with the invariant chain (Ii) in the ER, which allows their transportation to late endosomes. There, Ii is cleaved by cathepsin proteases and dissociates from MHCII molecules leaving a small peptide occupying the antigen-binding groove of the MHCII molecules. This peptide is called MHCII-associated-invariant-chain (CLIP). Like tapasin, HLA-DM molecules in endosomes mediate CLIP exchange for higher affinity peptides. MHCII peptides come from proteins degraded at endosomal compartments. This topic is reviewed in Ref: (Neefjes *et al.* 2011; Roche and Furuta 2015)

For both MHCI and MHCII molecules, the binding of high-affinity peptides stabilises them and allows their expression to the cell surface. At the surface, MHC complexes are stable for a limited period after which they are internalised for degradation in lysosomes or loaded with new peptides in late endosomal compartments in a process called antigen cross-presentation. In the case of MHCI molecules, cross-presentation of antigens allows the priming of CD8 T-cells against extracellular pathogens. Moreover, cross-presentation is also useful to induce CD8 immunity against viruses that do not target APC. In the latter

scenario, APC cells would engulf viral particles from the extracellular matrix and present them through MHCI using the cross-presentation method. In cancer disease, cross-presentation also allows CD8-mediated antigen spreading. This topic is reviewed in Ref: (Joffre *et al.* 2012).

Another important concept in antigen presentation is autophagy. In this process, cytosolic content can be encapsulated in phagosomes, which can be presented by both MHCI molecules through cross-presentation or by MHCII molecules. This mechanism allows CD4 activation against intracellular pathogens or against extracellular pathogens that avoid lysosomal degradation by escaping to the cytosol (Crotzer and Blum 2010). This mechanism is also relevant and interesting for cancer therapy (Levy, Towers and Thorburn 2017).

1.3.2.2. MR1 antigen-presentation pathway

Although MR1 is a class-I related molecule and requires β2m association to present antigens, cellular studies showed that MR1 surface expression and MAIT activation were independent of the TAP complex and proteosomes (Huang *et al.* 2008). On the other hand, overexpression of Ii and HLA-DM showed that, while they do not change the surface levels of MR1, they increased MR1-mediated MAIT activation (Huang *et al.* 2008). Confocal studies have also shown that GFP-tagged MR1 colocalised with Lamp1+, which is a late endosomal and lysosomal marker. Furthermore, in the case of bacterial infection, blocking endosomal acidification completely inhibited MAIT activation (Huang *et al.* 2008). These data suggested that MR1 does not present antigens originating from the cytosol and, like MHCII molecules, its antigen presentation pathway could involve trafficking through the endosomal compartment. On the other hand, primary DC from TAP/Ii KO mice could activate MAIT cells as efficiently as those from wild-type mice (le Bourhis *et al.* 2010), showing that MR1-mediated antigen presentation was not strictly like MHCII molecules.

Studies with confocal microscopy revealed that at steady-state, the majority of MR1 was in the ER compartment however, the addition of VitBAgs-derivates stabilised MR1 molecules in the folded conformation, presumably through the formation of a Schiff base, and translocated them to the surface (McWilliam *et al.* 2016). These results indicated that MR1 surface expression was ligand-dependent; however, that also begged the question of why basal surface MR1 was detected in the absence of ligands and why this surface level increased in cells overexpressing MR1.

One study found that MR1 surface expression, like MHCI molecules, was temperature sensitive (Abós *et al.* 2011). This led to the conformational theory by McWilliam and Villadangos, suggesting that at low temperatures, empty MR1 molecules could be stabilised into the folded conformation without the formation of a Schiff base and spontaneously egress from the ER to the plasmatic membrane (McWilliam and Villadangos 2017). There, they would directly load antigens that cannot reach the ER (Schumacher *et al.* 1990). Like MCHI molecules, MR1 molecules also use cross-presentation mechanisms. Studies by Karamooz *et al.*, elucidated that MR1-GFP colocalised with late-endosomal proteins and recycled back to the surface if APC were spiked with 6FP (Harriff et al. 2016a). In addition, they also found that after loading 6FP, MR1 molecules could also go through ligand exchange and present both exogenous ligands and antigens generated in post-Golgi compartments from intracellular pathogens like *Mycobacterium tuberculosis* (*Mtb*) (Karamooz *et al.* 2019). This not only indicates that MR1 can be recycled after being internalised but also that they can sample through different compartments and have access to different pools of antigens. One caveat with all the studies so far is the reliance on transduced-, overexpressed- or GFP-tagged MR1, which could lead to experimental artefacts; however, studies with endogenously expressed MR1 are challenging because of its low basal expression.

Currently, it is accepted that MR1 can follow 4 different mechanisms for antigen presentation (**Figure 1- 3**) (Kulicke *et al.* 2020). In the ER pathway, ligands that reach the ER bind to MR1, stabilising the folded conformation and allowing it to associate with β2m and translocate to the surface (McWilliam *et al.* 2016). From the study of different chemical structures, it was found that the formation of a Schiff base stabilises MR1 in the folded conformation, thus causing ER egress and surface upregulation (Keller *et al.* 2017). A more recent experiment also showed that MR1 bound to their ligands in the ER in as little as 10min after ligand exposure (McWilliam *et al.* 2020). These results hint that extracellular MR1 antigens reach the ER directly without transiting through the endosomal compartment; however, metabolites like 5OPRU cannot passively cross lipid membranes, therefore suggesting the exitance of transport mechanisms that rapidly transfer metabolites between phagosomes and the ER (Gagnon *et al.* 2002; Levin-Konigsberg and Grinstein 2020).

At steady-state (**Figure 1- 3**), MR1 can constitutively translocate to the extracellular membrane by presenting endogenous antigens. From the surface, MR1 may be recycled into endosomal compartments to access microbial-derived antigens or self-ligands proceeding from autophagy as part of the ligand exchange pathway (Karamooz *et al.* 2019; Ye *et al.* 2021). This pathway is very interesting for cancer therapy as many transformed cells undergo metabolic stress. Consequently, differential expression of MR1 binding metabolites could be found between healthy and cancer cells.

In the ligand exchange pathway (**Figure 1- 3**), surface MR1 molecules are recycled into an intracellular compartment, where they can re-load other exogenous or endogenous antigens (Harriff et al. 2016a). Treatment with Brefeldin-A (a drug that blocks transport from ER to the Golgi apparatus) inhibits ligand exchange as well as 6FP mediated surface upregulation of MR1, meaning that the majority of surface MR1 come from the ER pathway, while only a fraction of MR1 molecules follow the exchange pathway (Harriff et al. 2016a). Engineered MR1 associated with the plasmatic membrane

through Glycosyl-phosphatidyl-inositol (GPI) linkage had a reduction in ligand exchange compared to wild-type MR1 (Salio *et al.* 2020), suggesting that specific motifs in the intracellular domain of MR1 might be involved to selectively internalise MR1 into endosomal compartments. In a more recent experiment, MR1 cross-presentation was further confirmed by MAIT activation against a pro-drug agonist, designed to be accessible only in endo-lysosomal compartments. Simultaneous pulsing with Ac-6FP did not show MAIT inhibition, indicating that MR1 accessed Ac-6FP and the pro-drug agonist from 2 separate compartments (Lange *et al.* 2020).

Finally, in the *Mtb* pathway (**Figure 1- 3**), MR1 molecules are recycled like in the exchange pathway; however, they load antigens that derive from the processing of intracellular pathogens. There is some data suggesting that loading of soluble ligands and loading of antigens derived from processed bacteria require slightly different mechanisms; for example, in the Klenerman group, it was shown that activation by intact *E.coli* and *Salmonella*, led to a much stronger MAIT stimuli than their respective lysates and supernatants. Nevertheless, blocking of lysosomal acidification reduced MAIT activation for intact *E.coli*, but not for its supernatants (Ussher *et al.* 2016). MAIT cells are hyporesponsive to 5OPRU trigger, however co-stimulation with bacteria deficient in the riboflavin synthesis pathway restored optimal MAIT activation. This could be due to TLRs and NFkβ activation (seen only in the presence of bacterial infection), which may be a differential factor between the antigen presentation of exogenous-soluble ligands and intact bacteria (Ussher *et al.* 2016; Chen *et al.* 2017). In the case of *Mtb*, bacterial infections are required for MAIT activation (Harriff *et al.* 2014), meaning that its degradation in phagosomes is required to generate specific groups of antigens at a sufficient concentration to activate MAIT cells. MR1 is also known to interact with MHCII-associated chaperones (Huang *et al.* 2008), however, it is still unclear how these are involved with MR1 in the presentation of antigens from intracellular pathogens.

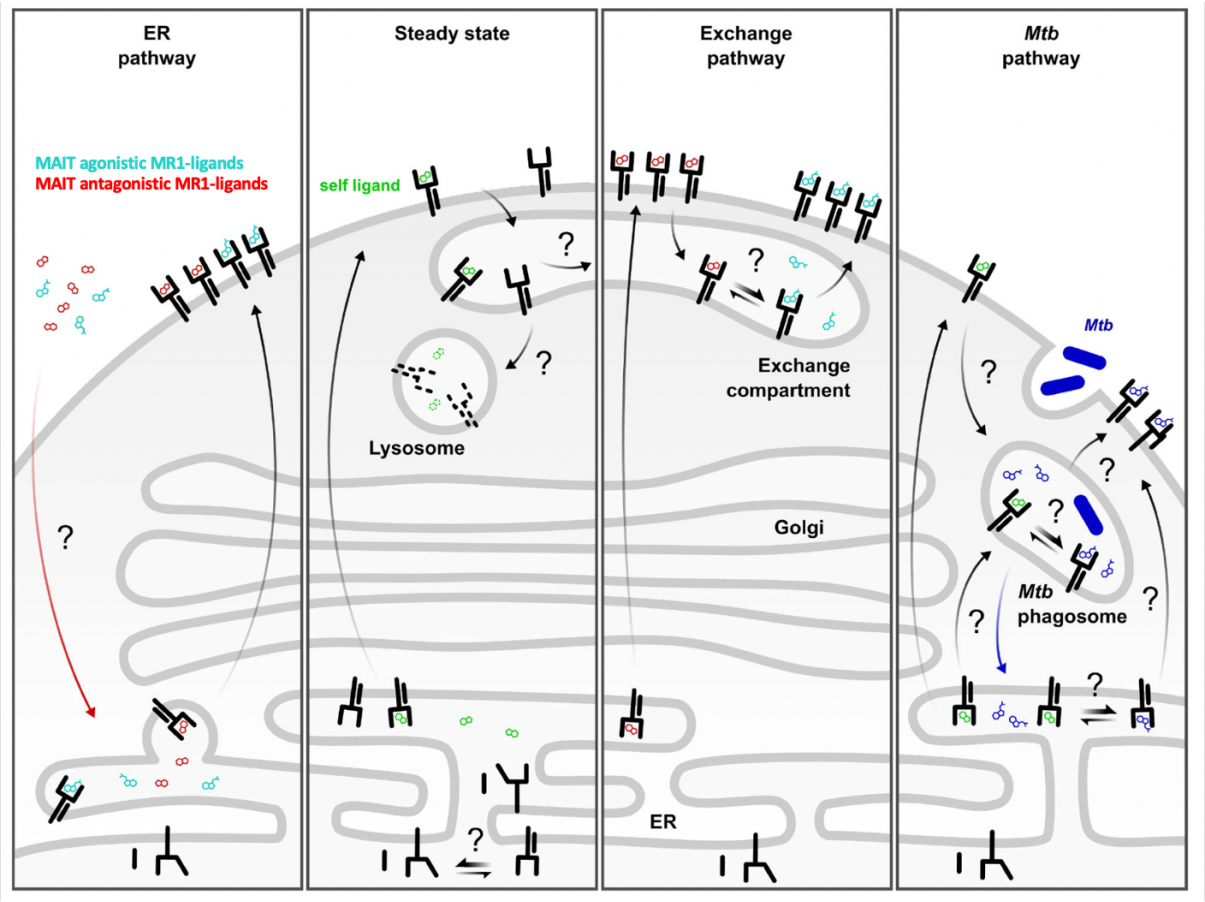

Figure 1- 3. Antigen presentation and trafficking pathways of MR1. In the ER pathway, MR1 antigens travel directly to the ER where they bind to MR1 and are presented to the cell surface. At steady-state, MR1 can also present self-ligands that are compatible with the MR1 binding pockets and reach the extracellular membrane. In the exchange pathways, surface MR1 molecules are internalised for degradation or recycled in endosomal compartments where their ligands are exchanged for alternative ones (either endogenous or exogenous). In the *Mtb* pathway, MR1 is recycled into phagosomes where they encounter antigens from extracellular pathogens (internalised through phagocytosis) or intracellular pathogens (engulfed through autophagy).

Figure and caption adapted and reprinted from Frontiers in Immunology 2020, 11:2034, Kulicke C, Karamooz E, Lewinsohn D, Antigen Presentation Pathways Sample Diverse Antigens and Intracellular Compartments, Copyright (2020), with permission from Frontiers in Immunology.

1.3.3. MR1 antigens: Microbial-derived

Mass-spectrometry and structural studies by Kjer-Nielsen *et al*. from refolded MR1 molecules identified 6-formylpterin (6FP) as the first described MR1-antigen, which is generated from the photo-degradation of folic-acid (vitamin-B9); however, follow-up studies with 6FP showed that it failed to activate Jurkat T cells (Jurkats) transduced with MAIT-TCR and, reduced activation of MAIT cells by competing with agonistic ligands for the MR1 binding cleft (Kjer-Nielsen *et al.* 2012; Eckle *et al.* 2014).

Treiner *et al.* inferred that MR1 ligands had to be microbe-derived since GF mice did not have MAIT cells in gut tissue (Treiner *et al.* 2003). This hypothesis was confirmed in studies showing MAIT cells reactive to some species of bacteria however, the nature of the microbial antigens were unclear (le Bourhis *et al.* 2010). The analysis of MAIT-stimulating chemical fractions from *Salmonella* supernatants identified ribityl-lumazine molecules as MAIT agonists (Kjer-Nielsen *et al.* 2012). These metabolites are: 7-hydroxy-6-methyl-8-D-ribityllumazine (RL-6-Me-7-OH) and 6,7-dimethyl-8-D-ribityllumazine (RL-6,7-diMe), and they result from the riboflavin (vitamin-B2) synthesis pathway. Further studies identified riboflavin precursors, such as 5-(2-oxopropylideneamino)-6-D-ribityl-aminouracil (5OPRU) or 5-(2-oxoethylideneamino)-6-D-ribityl-aminouracil (5OERU), from *Escherichia col*i and *Salmonella enterica* supernatants as potent MAIT agonists (Corbett *et al.* 2014). Both 5OPRU and 5OERU originate from the spontaneous reaction of the microbe-derived 5-amino-6-d-ribityl-aminouracil (5ARU) with methylglyoxal (MG) and glyoxal, respectively (Corbett *et al.* 2014).

Both 6FP and 5OPRU/5OERU share a structural scaffold structure of pyrimidine heterocycles with a carbonyl moiety that can establish a reversible covalent Schiff base with the Lys43 of the MAIT-TCR. The Schiff base anchors the ligands in the A' pocket of MR1 (Corbett *et al.* 2014). Unlike 6FP, the uracil analogues have a ribityl group that forms hydrogen bonds with the Tyr95 of the MAIT-TCR (Patel *et al.* 2013). Studies with 5OPRU

analogues have shown that modifications in the ribityl tail reduced the potency of MAIT activation (Awad *et al.* 2020). 5ARU and 5OPRU/5OERU, due to their low stability as soluble molecules (Mak *et al.* 2017), often condense into RL-6,7-diMe and RL-6-Me-7-OH, respectively. In ribityl-lumazines, the carbonyl moiety is converted into a second aromatic ring and, as a result, cannot form Schiff bases in the A' pocket of MR1. This makes them weaker agonists than their non-condensed counterparts, as their positioning in the A' pocket is less stable (Corbett *et al.* 2014; Eckle *et al.* 2015a).

Recently mass-spectrometry studies of chemicals eluted from soluble-MR1 expressed in mammalian cells under infection with *E.coli* or *M.smegmatis* showed several compounds with similar backbones thats clustered with riboflavin intermediates, underlining the relevance of this pathway as a source of MR1 antigens (Harriff *et al.* 2018). Some of these additional compounds were identified as lumazines: 6-(2-carboxyethyl)-7-hydroxy-8-ribityl-lumazine (photo-lumazine I; PLI) and 6-(1H-indol-3-yl)-7-hydroxy-8- ribityl-luma- zine (photo-lumazine III; PLIII) and the riboflavin analogue 7,8-dideme-thyl-8-hydroxy-5-deazariboflavin (FO) (Harriff et al. 2018a). In these studies, other major clusters indicated the existence of additional antigenic backbones however, concerning MAIT-activating antigens, the riboflavin pathway is likely to be the most relevant one. In studies with neonatal GF mice mono-colonised with different *Enterobacteriaceae*, only those with intact riboflavin synthesis pathways (*P. mirabilis* express ribA, ribD, and pyrp2 genes) can cause the emergence of MAIT populations (Constantinides *et al.* 2019). Similarly, mono-colonisation studies with *E.coli* with ribD knock-out failed to generate MAIT populations in mice as their wild-type counterparts (Legoux *et al.* 2019a).

Besides MAIT cells, MR1T cells can also recognise microbial antigens (Gherardin *et al.* 2016; Meermeier *et al.* 2016; Koay *et al.* 2019a; Seneviratna *et al.* 2022). Meermeier *et al.* described a TRAV12-2+ MR1T clone reactive to microbes, however, with a different specificity to MAIT cells. This result suggests the existence of unexplored microbial

ligands, potentially unrelated to riboflavin derivates (Meermeier *et al.* 2016). The identification of more MR1T sequences can be helpful in the discovery to new antigens.

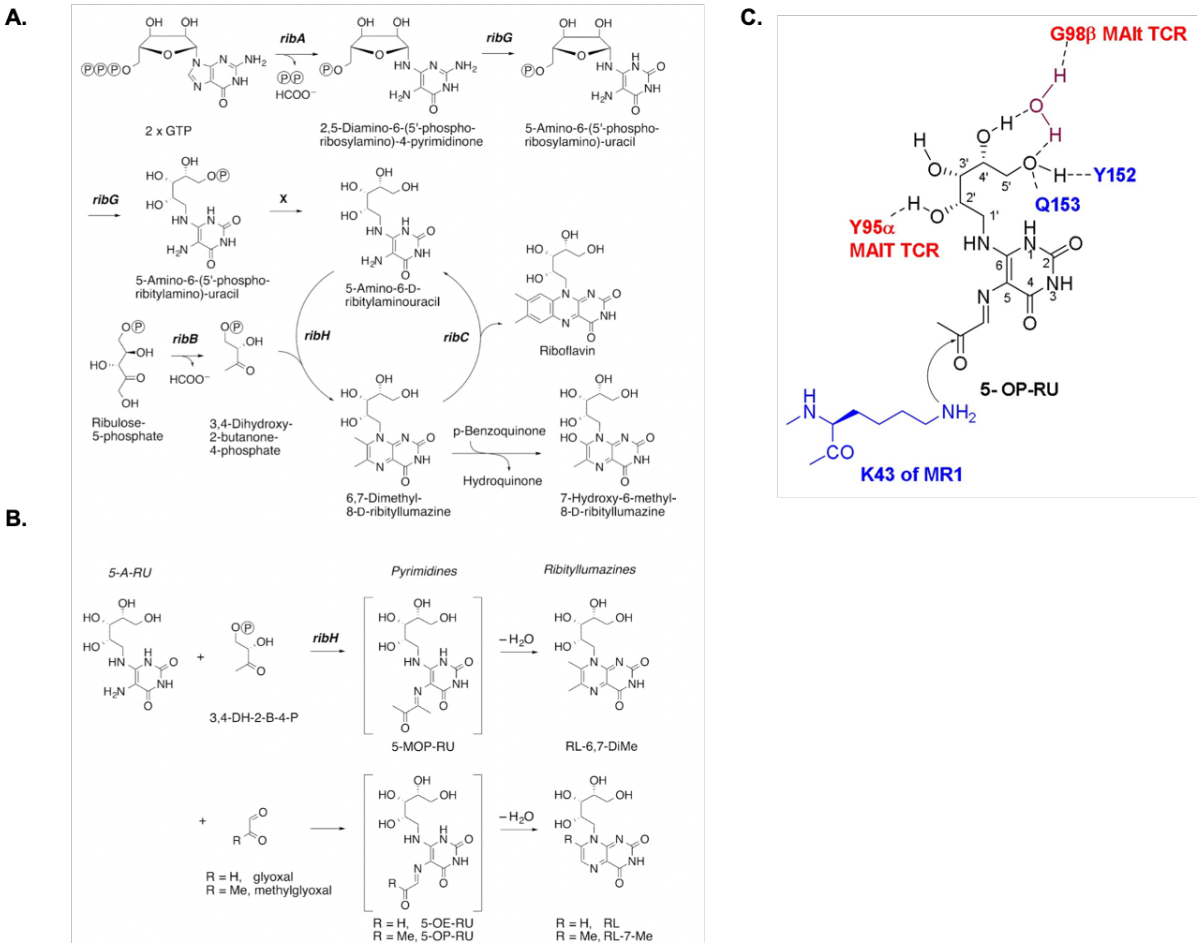

Figure 1- 4. Generation of microbial-derived MAIT agonists. (**A**) 5ARU is a metabolic intermediate of the Riboflavin synthesis pathway. (**B**) 5ARU can react with different groups to generate pyrimidine intermediates; for instance, 5OPRU is generated by the spontaneous reaction of 5ARU with methylglyoxal. Pyrimidine intermediates are inherently unstable and spontaneously condense into Ribityllumazimes. (**C**) Although Ribityllumazimes are chemically more stable molecules than their Pyrimidine counterparts, the latter group can form more stable interaction with MR1 through the covalent Schiff base link with the K34. The presence of the Rybityl group interacts with T95α and G98β residues of the MAIT TCR. The latter described interactions do not exist in other MR1 ligands such as 6FP; therefore, they cannot activate MAIT cells.
Figure and caption from **A** and **B** were adapted and reprinted from JBC, 2015, 290:30204–11, Eckle SBG, Corbett AJ, Keller AN *et al.,* Recognition of Vitamin B Precursors and Byproducts by Mucosal Associated Invariant T Cells, Copyright (2015), with permission from JBC (Licence number 1260064-1)
Figure and caption from **C** were adapted and reprinted from Molecular Immunology, 2021, 129:114–20, Veerapen N, Hobrath J, Besra AK et al., Chemical insights into the search for MAIT cells activators, Copyright (2021), with permission from Molecular Immunology (Licence number 1260066-1)

1.3.4. MR1 antigens: Non-Microbial

In silico screening of small molecules found several hits corresponding to chemical species that can bind to MR1 forming similar interactions as 5OPRU or 6FP (canonical binding) (Keller *et al.* 2017).

In the studies by Keller *et al.*, most of the identified binders had a size between 150-300 Daltons and had hydrophobic aromatic rings. Nonetheless, the diversity in chemical groups attached to the aromatic rings highlighted the versatility of MR1 to accommodate diverse chemical structures (Keller et al. 2017; Table 1-1). Structural and *in-vitro* studies of the 81 identified binders showed that not all of them were able to upregulate MR1 to the surface or elicit MAIT activation. Upregulation of MR1 to the cellular surface was only seen in Schiff base forming ligands, while MAIT activation required a direct contact between the TCR and antigen moiety, such as that of 5OPRU's ribityl-tail with Tyr95 (Keller *et al.* 2017; Awad *et al.* 2020). Therefore, the surface levels of MR1 on APC do not always correlate with its ability to activate MAIT or MR1-specific T-cells. While compounds like lumazines and derivates of diclofenac (FDA-approved drug) were identified as MAIT agonists, they do not upregulate the surface expression of MR1. On the other hand, examples like 5-formylsalicylic-acid (5FSA) and derivates of chemotherapy drugs like methotrexate and aminopterin could both activate the MAIT-TCR and increase MR1 expression (Keller *et al.* 2017). In the case of both 5FSA, and diclofenac derivates, the triggering of the MAIT-TCR required it to have a specific β-chain. In line with this, there is growing evidence that the TCRβ-chain may play a role in discriminating between different groups of antigens (Meermeier *et al.* 2016; Harriff *et al.* 2018; Awad *et al.* 2020).

In more recent findings, DB28 and its derivative NV18.1 were identified as non-microbial ligands that retained MR1 in the ER and competed with agonistic ligands and, as a result, downregulated the surface expression of MR1 (Salio *et al.* 2020).

Structure	Name	Group	MR1 upreg./ downreg	MAIT agonist	Ref
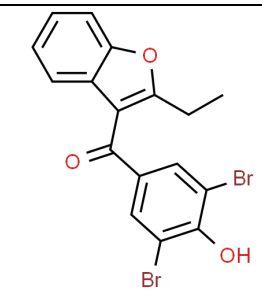	Benzbromarone	Drug or Drug-like	--	↑	(Keller *et al.* 2017)
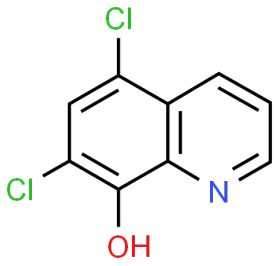	Chloroxine	Drug or Drug-like	--	↑	(Keller *et al.* 2017)
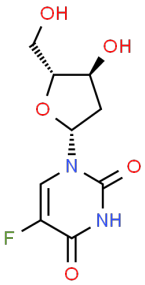	Floxuridine	Pyrimidine Based	--	↑	(Keller *et al.* 2017)
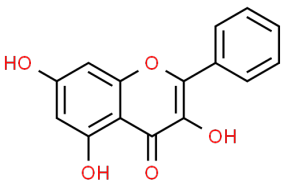	Galangin	Drug or Drug-like	--	↑	(Keller *et al.* 2017)
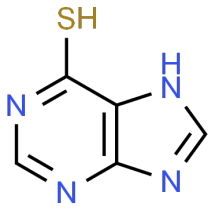	Mercaptopurine	Purine Based	--	↑	(Keller *et al.* 2017)

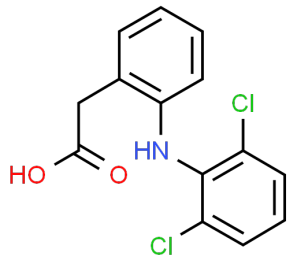	Diclofenac	Drug or Drug-like	--	↑↑	(Keller *et al.* 2017)
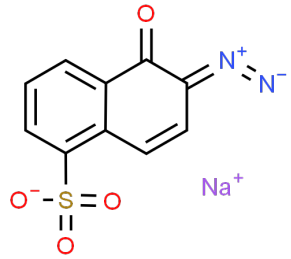	1,2-Naphtoquinone-4-sulfonic acid	Drug or Drug-like	↑	--	(Keller *et al.* 2017)
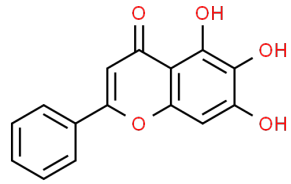	Baicalein	Drug or Drug-like	↑	--	(Keller *et al.* 2017)
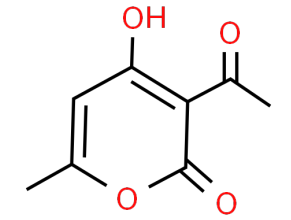	Dehydroacetic acid	Drug or Drug-like	↑	--	(Keller *et al.* 2017)
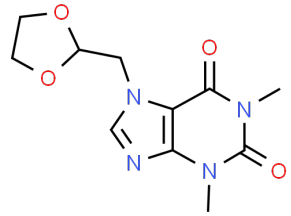	Doxofylline	Purine Based	↑	--	(Keller *et al.* 2017)
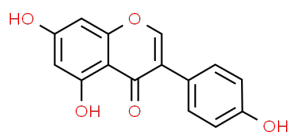	Genistein	Drug or Drug-like	↑	--	(Keller *et al.* 2017)

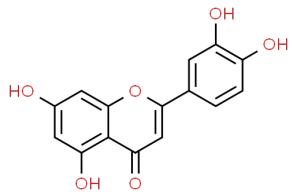	Luteolin	Drug or Drug-like	↑	--	(Keller *et al.* 2017)
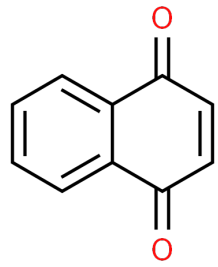	1,4-Naphthoquinone	Drug or Drug-like	↑↑	--	(Keller *et al.* 2017)
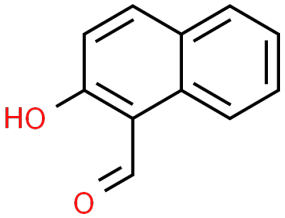	2-Hydroxy-1-naphthaldehyde	Drug or Drug-like	↑↑	--	(Keller *et al.* 2017)
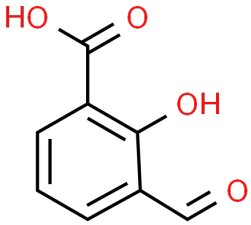	3-Formylsalicylic acid	Drug or Drug-like	↑↑	--	(Keller *et al.* 2017)
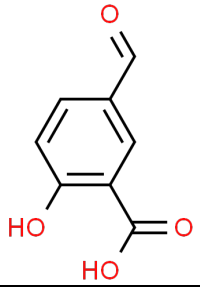	5-Formylsalicylic acid	Drug or Drug-like	↑↑	--	(Keller *et al.* 2017)
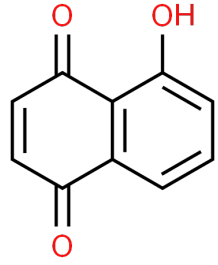	5-Hydroxy-1,4-naphtoquinone	Drug or Drug-like	↑↑	--	(Keller *et al.* 2017)

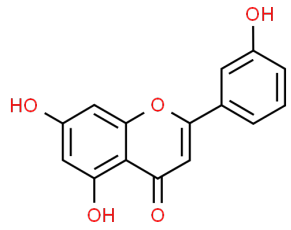	Apigenin	Drug or Drug-like	↑↑	--	(Keller *et al.* 2017)
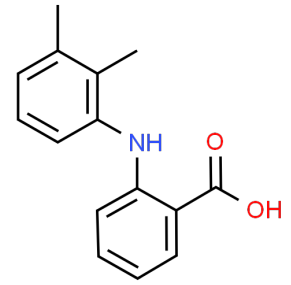	Mefenamic acid	Drug or Drug-like	↑↑	--	(Keller *et al.* 2017)
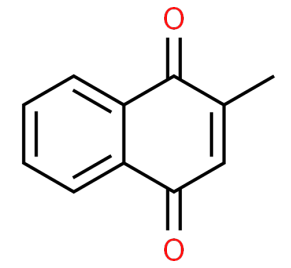	Menadione	Drug or Drug-like	↑↑	--	(Keller *et al.* 2017)
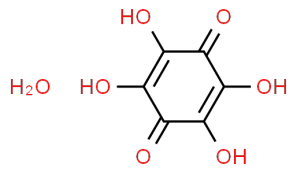	Tetrahydroxy-1,4-quinone hydrate	Drug or Drug-like	↑	↑	(Keller *et al.* 2017)
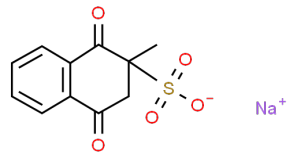	Menadione sodium bisulfite	Drug or Drug-like	↑↑	↑	(Keller *et al.* 2017)
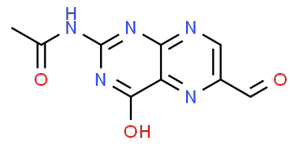	Acetyl-6-formylpterin	Pterin Based	↑↑	--	(Keller *et al.* 2017)

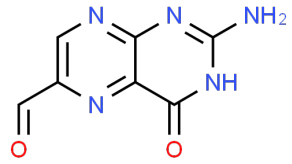	6-formylpterin	Pterin Based	↑	--	(Keller *et al.* 2017)
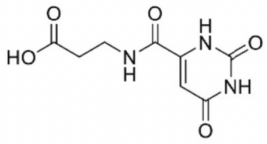	3-([2,6-dioxo-1,2,3,6-tetrahydropyrimidin-4-yl] formamido) propanoic acid (DD28)	Pyrimidine Based	↓	--	(Salio *et al.* 2020)
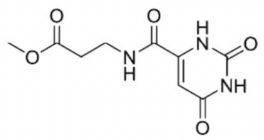	3-([2,6-dioxo-1,2,3, 6-tetrahydropyrimidin-4-yl] formamido) propanoate NV18.1	Pyrimidine Based	↓	--	(Salio *et al.* 2020)

Table 1- 1. Examples of small molecules that alter MR1 expression or activate MAIT cells.

Validation of several of these molecules in MAIT activation experiments validated that besides microbial-derived antigens, there are other small organic (mostly purines and pyrimidines) molecules, drugs, drug-like metabolites, and drug-like molecules that could bind MR1 with biological relevance (Keller *et al.* 2017). It also underlined the cross-reactivity of MAIT-TCRs with other compounds outside the riboflavin synthesis pathway. While a significant portion of MR1 binders do not activate MAIT cells nor change the expression of MR1, it does not exclude them as biologically relevant species as they could still be agonistic for unexplored MR1T cells. For instance, while some purines and pyrimidine-based antigens failed to activate MAIT cells, De Libero's group described several MR1T cells that could recognise nucleotide-like antigens with purine and pyrimidine groups (de Libero *et al.* 2021). In line with this hypothesis, there is an increasing body of data about self-derived metabolites that can be presented by MR1 to activate MR1T-cells (explained in section 1.3.5).

1.3.5. Non-MAIT MR1T cells

Although many MR1T clones show reactivity to 5OPRU, there is evidence suggesting that their recognition of microbial infections happens through specificities different to MAIT cells (Gherardin *et al.* 2016; Meermeier *et al.* 2016; Harriff *et al.* 2018). Similarly, MR1T cells have also shown recognition of non-microbial antigens, some of which are drug-like molecules or endogenous self-antigens expressed inside APC (Lepore *et al.* 2017; Harriff *et al.* 2018; Crowther *et al.* 2020; de Libero *et al.* 2021). The reactivity to self-antigens is particularly interesting for the design of immunotherapy strategies aiming to use MR1 as an antigen-presenting platform. This is partly due to the belief that in cancer disease and infections, cells undergo significant changes in the regulation of metabolic pathways, which can generate a differential expression of MR1-associated antigens. In recent reports, excessive generation of glyoxal and oxidative stress contributed to the formation of nucleotide adducts, some of which are MR1 antigens (de Libero *et al.* 2021). Other studies identified the MR1T G5 clone, which showed preferential reactivity against cancer cells over their healthy counterparts (Crowther *et al.* 2020).

Although we define MR1T cells as any MR1-restricted T-cell that falls outside the MAIT definition (TRAV1-2+, CD161+, PLZF+, Tbet+, RORγt+ and 5OPRU reactivity), many of the identified MR1T clones can recognise 5OPRU-tetramers. Surprisingly, some of the 5OPRU-tetramer+/TRAV1-2- T-cells have MAIT-like characteristics, such as the expression of CD161 NK receptor and PLZF transcription factor for innateness (Koay *et al.* 2019a). Within these MAIT-like MR1T cells, a subset was identified with a public invariant TCR (TRAV36+, TRBV28+) (Koay *et al.* 2019a). The frequency of MAIT-like characteristics inside the 5OPRU-tetramer+/TRAV1-2- compartment was only ~10% (Koay *et al.* 2019a), which explains why prior bulk-phenotyping studies of the 5OPRU-tetramer+/TRAV1-2- compartment did not identify any significant trend of T-cell innateness (ex: PLZF expression) and CD161 expression (Gherardin *et al.* 2016). While the

MAIT-like features in MR1T cells could be explained because the 5OPRU recognition led them to the same development and differentiation pathway as MAIT cells, these results still underline that MR1T cells are not exclusively adaptive-like, and therefore more studies should be conducted to make a better representative classification.

Phenotyping of the 5OPRU-tetramer+/TRAV1-2- compartment showed a higher Tbet expression in MR1T cells than in conventional T-cells (Gherardin *et al.* 2016), corresponding with an increased type-1 functionality. On the other hand, analysis of the cytokine expression in different MR1T clones also showed Th2 functions (expression of IL4, IL5 and IL13), Th17 functions (IL17A), Immunosuppressive functions (IL10) and expression of pleiotropic cytokines (TNFα, CSF1, CSF2, VEGF, PDGF and CCL3) involved in the activation of tissue endothelia, increased recruitment of macrophages and effector cells (Lepore *et al.* 2017). The expression profile for these cytokines was clone-dependent, indicating functional diversity within the MR1T compartment.

Studies so far have also confirmed that MR1T cells are polyclonal, with diverse TCR chain pairings that react to diverse antigens (Gherardin *et al.* 2016; Lepore *et al.* 2017; Harriff *et al.* 2018; Koay *et al.* 2019a; Crowther *et al.* 2020; de Libero *et al.* 2021; Seneviratna *et al.* 2022). In the current state of literature, it is unclear if there is a predominance of specific TCR chain pairings, although the studies by Koay *et al.* show the existence of public MR1T sequences (Koay *et al.* 2019a) in the 5OPRU reactive subset. The diversity in MR1T sequences can be further appreciated if we consider the existence of $\gamma\delta$TCRs that can recognise MR1 in an open conformation. These ligand-agnostic $\gamma\delta$MR1T populations were found in several donors although it is unclear if they have any biological relevance (le Nours *et al.* 2019). The study of the total MR1T compartment is still not possible due to the lack of specific markers to discern them from the rest of conventional T-cells. This is also one of the bottlenecks for understanding the diversity and nature of MR1-associated antigens.

Studies by Lepore *et al*. used *ex-vivo* activation assays to quantify MR1T cells in circulating blood around 1:2500 to 1:5000 (0.02-0.04%) (Lepore *et al*. 2017). One caveat to these results is that they may only represent MR1T cells with innate-like properties, which do not require any priming, thus being detectable in overnight activation assay. On the other hand, Harriff *et al*. used soluble MR1-molecules to elute and analyse MR1-associated antigens through mass-spectrometry (Harriff *et al*. 2018). However, this strategy does not guarantee that the resulting antigens can be used for therapy or the existence corresponding MR1T populations *in vivo*.

1.4. MAIT cells

These were identified in 1993 by Porcelli *et al.* as a αβ T-cell population with an invariant α-chain: Vα7.2-Jα33 (TRAV1-2-TRAJ33) in humans (Porcelli *et al.* 1993) and mVα19-Jα33 in mice (Tilloy *et al.* 1999). Treiner *et al.* found a significant enrichment of the Vα7.2-Jα33 or mVα19-Jα33 rearrangements in mucosal sites, especially in the gut lamina propria (Treiner *et al.* 2003), which is why these cells are named mucosal-associated invariant T-cells (MAIT). As explained throughout the introduction, MAIT cells react mostly to riboflavin precursors in the context of the MR1 receptor (Treiner et al. 2003), and they have been instrumental in studies related to MR1-biology.

The discovery of 5OPRU as an MR1-associated MAIT agonist (Kjer-Nielsen *et al.* 2012) allowed the development of 5OPRU-MR1 tetramer reagents for the identification and characterisation of MAIT cells in both humans and mice (Reantragoon *et al.* 2013). These tetramers revealed some heterogeneity in the invariant αTCR chain where the TRAV1-2 segment could also be arranged with the TRAJ12 and TRAJ20, in addition to the pre-established TRAJ33 (Reantragoon *et al.* 2013). In humans, most MAIT characterisation studies were conducted using the anti-Vα7.2 3C10 antibody and CD161 or CD26 marker. Comparative studies in peripheral T-cells showed an almost complete overlap between 5OPRU-tetramer+ T-cells and TRAV1-2+/CD161^{high} T-cells (Reantragoon *et al.* 2013); confirming that CD161 receptor could be used as a reliable surrogate marker to 5OPRU-tetramers to identify the MAIT subset within the TRAV1-2+ T-cells. This correlation still needs to be validated in tissue resident MAIT cells due to the varying CD161 expression levels in different locations. Nevertheless, the development of 5OPRU-tetramers was still relevant because it allows the identification of MAIT cells in mouse models, which do not have the CD161 gene.

1.4.1. MAIT cell phenotype and functions

Circulating MAIT cells are ~80% CD8+ and ~20% DN (Gherardin *et al.* 2018b). There are also small frequencies of CD4+ (Gherardin *et al.* 2018b), although their functional and biological role is still to be explored. A significant portion of CD8+ T-cells express the CD8αα homodimer instead of the more conventional CD8αβ heterodimer. Although the differences are not major, these 2 populations have slightly different transcriptional signatures, with a more pronounced Th17 functionality in CD8αα group (Walker *et al.* 2012). CD8αα is frequently seen in mucosal-resident T-cells, and some reports consider it to mark T-cells that follow an unconventional thymus-selection process. Notably, CD8αα has a weaker affinity to class-I receptors than CD8αβ; therefore, it may also be a modulation mechanism to reduce the antigen sensitivity of MAIT cells (Cheroutre and Lambolez 2008). This hypothesis would align with the hyporesponsiveness of MAIT cells under TCR-stimuli. Similarly, DN MAIT cells are also transcriptionally different to CD8+ MAIT cells. Reports show that they have less functionality, less TCR diversity, and a pronounced pro-apoptotic signature. Altogether, these findings suggest that DN MAIT cells simply represent a subset of chronically stimulated MAIT cells with an exhausted phenotype. In line with this, prolonged *in vitro* stimulation of CD8+ MAIT cells downregulated de surface expression of CD8 co-receptor (Dias *et al.* 2018).

MAIT cells have a "pre-primed" effector-memory phenotype (CD45RA-CD45RO+CD62L^{Low}CD95^{High}) (Dusseaux et al. 2011). Like iNKT cells, MAIT cells also express the PLZF transcription factor (Martin *et al.* 2009), which provides them with innate-like properties and upregulates the surface expression of IL18R1 and IL12R (Gleimer, von Boehmer and Kreslavsky 2012). The expression of these cytokines receptors allows MAIT activation in response to IL12/IL18 without concomitant TCR stimuli (Ussher *et al.* 2014a). MAIT cells also express very high levels of the C-type lectin CD161 (Dusseaux *et al.* 2011) ; nevertheless, its function is still unclear. A report by Fergusson *et al.* proposes that CD161 expression in MAIT and other T-cell subsets marks a shared

transcriptional signature associated with PLZF (innate-like phenotype), RORγt (Th17-like functions) and TCR-independent response to cytokines (Fergusson *et al.* 2014).

Function-wise, MAIT cells can produce GrzB, IFNγ and IL17 in response to phorbol myristate acetate (PMA) and ionomycin stimulation (Dusseaux *et al.* 2011). From studies so far, MAIT cells express the CTL-associated factors EOMES and Blimp-1, the type-1 transcription factor T-bet and the type-3 transcription factor RORγt (Billerbeck *et al.* 2010; Dusseaux *et al.* 2011; Rahimpour *et al.* 2015; Koay *et al.* 2016). These proteins impart MAIT cells with concomitant cytotoxic Tc1-like and Tc17-like functions in humans (Kurioka *et al.* 2015; Leeansyah *et al.* 2015), although the tissue localisation may influence the functional profile of resident MAIT subsets. In the case of mice, these 2 functions are segregated in 2 different MAIT populations where the expression of T-bet (MAIT1) and RORγt (MAIT17) are mutually exclusive (Rahimpour *et al.* 2015). Recent reports suggest that after activation in mice, these 2 populations collapse into a homogenous population (Hinks *et al.* 2019).

T-bet, EOMES and Blimp-1 provide MAIT cells with the capacity to produce IFNγ and cytotoxic-granules, respectively (Szabo *et al.* 2000; Pearce *et al.* 2003; Kallies *et al.* 2009; Rutishauser *et al.* 2009). From the cytotoxic granules, components such as Perforin, GrzB and Granulysin, among others, are released (Walch *et al.* 2014; Kurioka *et al.* 2015; Leeansyah *et al.* 2015). On the other hand, RORγt is responsible for the upregulation of IL17 and IL22 expression in MAIT cells (Billerbeck *et al.* 2010). The Th17 modules seem to be tightly regulated in circulating MAIT cells as prolonged stimulations are needed to elicit strong IL17 expression; conversely, higher IL17 production was observed in tissue resident MAIT cells (Gibbs *et al.* 2017; Sobkowiak *et al.* 2019).

A.

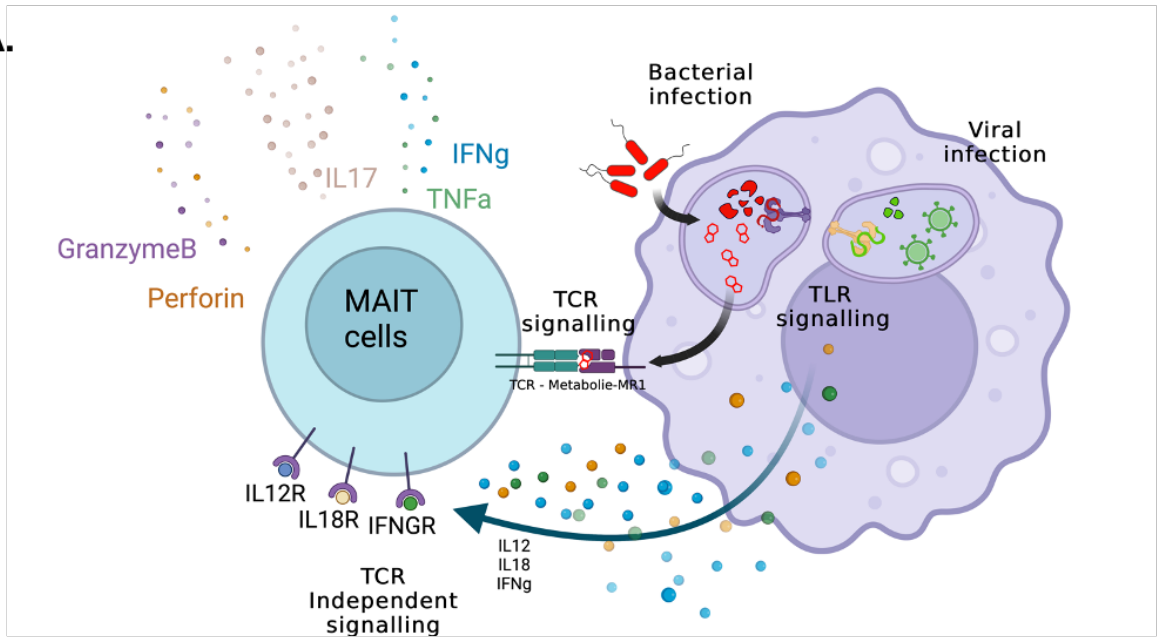

B.

	Human	Mouse
Coreceptors	-CD8αα -CD8αβ (majority) -DN -CD4 (low frequency)	-CD8αα -CD8αβ -DN (majority) -CD4
Memory and other markers	CD54RO+, CD161high, CD26high	CD44+
Homing Markers	CCR2+, CCR5+, CCR6+, CXCR6+, CCR7-	CXCR6+, CCR7-
Chemokine receptors	IL1R, IL7R, IL12R, IL18R, IL15R, IL22R	IL2R, IL7R, IL12R, IL18R
Main transcription factor	Tbet, RORγt, Eomes, PLZF	PLZF, Tbet+ or -, RORγt+ or -
Cytokines and effector molecules	IFNγ, TNFα, IL17A, IL17F, IL22, Granzyme B, Perforin	IFNγ (if Tbet+), TNFα, IL17A (if RORγt+)

Figure 1- 5. MAIT cells respond to TCR-dependent and -independent signals. (**A**) While bacterial infections generate MAIT antigens that are involved in the TCR-dependent signal through the MR1 molecules, they also activate TLR signalling pathways that result in cytokine signalling through IL12/18. Viral responses, despite not generating MAIT agonists, can elicit MAIT activation through the TCR-independent activation pathways. (**B**) The main differences between MAIT phenotype in humans and murine species are the expression of CD161 and the co-expression of T-bet and RORγt in human MAIT cells. Created with BioRender.com

1.4.2. MAIT development

Like conventional T-cells, MAIT cells develop in the thymus from CD4+CD8+ double positive (DP) thymocytes. At the DP stage, thymocytes undergo positive and negative selection, where those that recognise MHC molecules but do not react strongly to self-antigens receive survival signals (Klein *et al.* 2014). Although the nuances of non-MAIT MR1T cell development are still unexplored, in the case of MAIT cells, only DP thymocytes expressing TCRs reactive to MR1-5OPRU will commit to the lineage (Martin *et al.* 2009; Koay *et al.* 2016). Unlike conventional T-cells that are selected by positive selection in thymic epithelial cells, MAIT cells are selected through MR1-5OPRU recognition on cortical DP thymocytes (Seach et al. 2013). This selection process has also been described in iNKT cells through recognition of CD1d receptor (Bendelac 1995) and, is further supported by recent reports demonstrating that microbial ligands such as 5OPRU can cross the mucosal barrier and reach other organs such as the liver and thymus (Legoux *et al.* 2019a). The requirement of MR1-5OPRU recognition limits the diversity of MAIT TCRs in humans, mice, cattle, pigs, and other species that have MR1 (Porcelli *et al.* 1993; Tilloy *et al.* 1999; Goldfinch *et al.* 2010; Xiao *et al.* 2019). Species lacking MR1, such as Lagomorphs and Carnivora, not only lack MAIT cells, but they also do not have the TRAV1 gene segment, suggesting a tight interdependence between the 2 (Boudinot *et al.* 2016).

While mice have a low frequency of MAIT cells, these are significantly more abundant in humans. In both species, MAIT cells undergo 3 differentiations stages that require interaction with MR1 and relevant antigens (Koay *et al.* 2016). MAIT cells at stage 1 are defined as CD24+CD44- in mice and CD27-CD161- in humans. The transition to stage 2 requires the expression of miR18a/b-1 (Koay *et al.* 2016; Winter *et al.* 2019). The expression of this microRNA is dependent on the presence of bacterial antigens, as in GF mice, this transition is less efficient (Rahimpour *et al.* 2015; Koay *et al.* 2016). In mice, signalling-lymphocytic-activation-molecule (SLAM) signalling via SLAM-associated

protein (SAP) also seems critical for the MAIT transition to stage 2, although it is still unclear if these are important for humans (Legoux *et al.* 2019b). At stage 2, MAIT cells are defined as CD24-CD44- in mice and $CD27^{High}$CD161- in humans (Koay *et al.* 2016; Winter *et al.* 2019).

At stage 2, MAIT cells acquire their innate-like phenotype by expressing PLZF and IL18R (Koay *et al.* 2016; Winter *et al.* 2019). The transition to stage 3 happens intrathymically in mice, while in humans it can happen both in the thymus or the periphery, as stage 2 and 3 MAIT cells could be found in cord-blood. This transition is regulated by PLZF, IL18, miR18a/b-1 and requires microbial antigens (Koay *et al.* 2016). At stage 3, MAIT cells are defined as CD24-CD44+ in mice and $CD27^{High}CD161^{High}$ in humans (Koay *et al.* 2016). At stage 3, MAIT cells also acquire their Tc1 and Tc17 functions through the expression of T-bet and RORγt, respectively. In the case of mice, T-bet and RORγt expression are mutually exclusive, leading to functional segregation between MAIT1 and MAIT17, respectively (Rahimpour *et al.* 2015; Koay *et al.* 2016). Conversely, in humans, MAIT population are homogeneous in terms of functional capabilities at steady-state, although they may show an inclination towards either of the 2 phenotypes depending on their tissue localisation and stimulation (Koay *et al.* 2016).

After thymic egression, MAIT cells remain in circulation or colonise peripheral niches where they receive adequate stimuli. Post-natal tissue colonisation coincides with their differentiation into memory cells (CD45RO+) (Dusseaux *et al.* 2011; Gherardin *et al.* 2018b; Youssef *et al.* 2018). While thymic MAIT frequencies are low, these cells expand in the periphery reaching peak frequencies at the age of 25-30 and gradually decreasing afterwards (Novak *et al.* 2014).

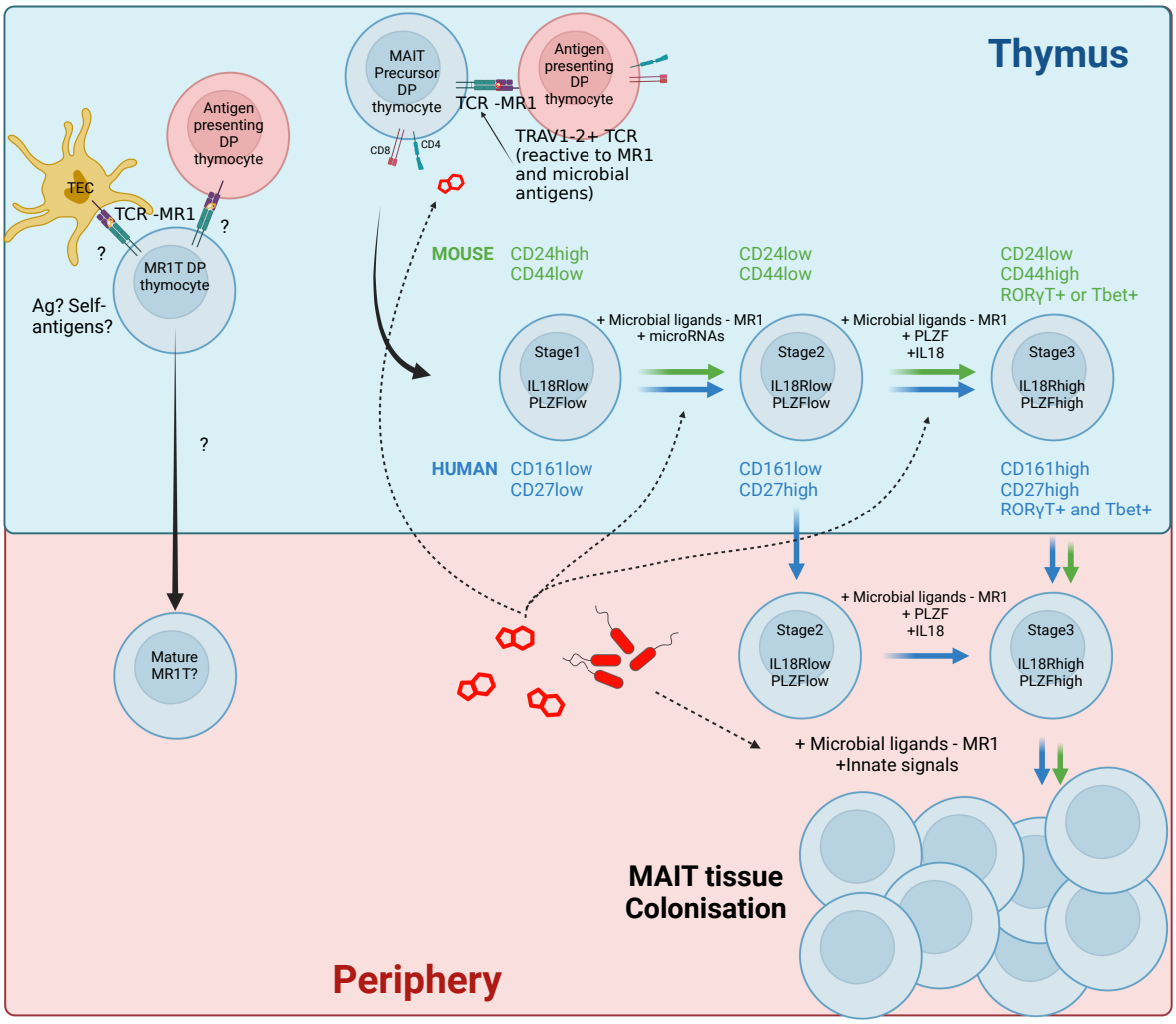

Figure 1- 6. Developmental stages of MAIT cells in mice and humans. MAIT cells undergo 3 stages of differentiations where they gradually acquire innate-like phenotypes. The development stage requires the presence of MR1 and microbial ligands, which travel from peripheral tissues. Mature MAIT cells travel to the periphery and migrate to inflamed tissues; if they receive adequate stimuli from commensals, they expand and colonise specific tissues. Conversely, not much is know about MR1T development, althouhg they are likely to follow the same developmental route as conventional T-cells. Created with BioRender.com

1.4.3. MAIT subsets and tissue distribution

MAIT cells are 10-100 times more frequent in humans than in mice (Tilloy *et al.* 1999; Rahimpour *et al.* 2015). Notably, in humans, they are the largest αβ T-cell subset that shares specificity to a specific antigen. Although the MAIT population was initially defined in mucosal tissues (Treiner *et al.* 2003), further studies found them in blood and non-mucosal sites. Their distribution in lymphoid tissues is low due to their lack of CCR7 and CD62L expression. Instead, their homing receptor profile is CCR2+CCR5+CCR6+ and CXCR6+ (Dusseaux *et al.* 2011; Tang *et al.* 2013; Jo *et al.* 2014; Lee *et al.* 2018). CXCR6 is a chemokine receptor that follows the CXCL16 gradient to the liver and explains the high abundance of 6-15% of total T-cells in the human liver, although, in some donors, it can be as high as 50% (Dusseaux *et al.* 2011; Tang *et al.* 2013; Jo *et al.* 2014). CCR6 is another chemokine receptor that follows the CCL20 gradient to mucosal sites such as the gut and the skin (Wang *et al.* 2009; Campbell *et al.* 2017). CCR6 is important in maintaining Th17 functions at mucosal sites, and it is regulated under RORγt and PLZF (Singh *et al.* 2015). CCR5 has also been associated with homing to mucosal sites, especially the female genital tract (Gibbs *et al.* 2017), while CCR2 is associated with T-cell extravasation to inflamed tissues and it is also associated to Th17 functions at mucosal sites (Kara *et al.* 2015; Bakos *et al.* 2017).

Tetramer-based studies identify MAIT cells at a frequency of 3% in blood (Gherardin *et al.* 2018b). Their frequency across the gut varies depending on the segment, which reflects how some niches are more propitious for MAIT colonisation than others. MAIT frequencies were as high as 60% of CD4- T-cells from the Jejunum (Reantragoon *et al.* 2013), while in the ileum, colon and rectum segments, the frequencies are similar to blood (Serriari *et al.* 2014; Haga *et al.* 2016; Provine *et al.* 2018; Hama *et al.* 2019). MAIT cells have also been identified at a frequency of ~4% in the lungs (Loh *et al.* 2016), ~1-2% in the female genital tract (Gibbs *et al.* 2017) and 2-3% in adipose tissue (Carolan *et*

al. 2015). Other studies have also identified MAIT cells or TRAV1-2 transcripts in oral mucosa, tonsils, lymph, prostate, ovaries and kidney (Lepore *et al.* 2014a).

Whether MAIT cells can recirculate between tissues is still a topic of debate. MAIT cells also express tissue retention receptors such as CD69 and CD103 (Booth *et al.* 2015; Salou *et al.* 2019), which can also be used as early activation markers. In parabiosis studies with mice, MAIT cells show low recirculation levels between tissues (Salou *et al.* 2019), which is consistent with the tissue-residency gene signature found in murine and human MAIT cells (Salou *et al.* 2019). Conversely, recent studies showed a significant degree of overlap in terms of phenotype, transcriptome, and TCR-sequence between MAIT cells derived from the blood and the lymph of patients, suggesting they are coming from the same pool and that MAIT cells use the lymph to recirculate between tissues (Voillet *et al.* 2018).

Although human MAIT cells are considered homogeneous across tissues in terms of functional capabilities, a unique IL10-producing subset was identified in adipose tissues (Carolan *et al.* 2015). In obese patients, this population drastically decreased in adipose tissue and became less likely to produce IL10 and IFNγ; instead, they increased their production of IL17 (Carolan *et al.* 2015). These changes are likely to play a role in sterile inflammation and co-morbidities associated with obesity. Similarly, an iNKT10 subset was also identified in mice adipose tissues (Sag *et al.* 2014). In the case of mice, MAIT1 cells are predominant in spleen and liver, while MAIT17 are widely found across barrier sites such as skin, gut, and lungs, although they still have a presence in spleen and liver (Rahimpour *et al.* 2015; Salou *et al.* 2019). The differential tropism between the 2 subsets is explained by their chemokine receptor and integrin profile. For instance, higher expression of CCR6 in MAIT17 explains their relative abundance over MAIT1 cells in skin and gut (Salou *et al.* 2019). A more detailed review of MAIT subsets and localisation can be found in Ref: (Salou, Legoux and Lantz 2021).

1.4.4. MAIT cell in disease: Bacterial and viral infections

As explained in previous sections, MAIT cells are heavily involved in anti-microbial immunity through a mix of Tc1 and Tc17 functions. In animal studies, the absence of MAIT cells correlates with higher mortality in *K.pneumoniae*, *F.tularensis, L.longbeachae* or *Mtb* infections (Gold *et al.* 2010; Georgel *et al.* 2011; Meierovics, Yankelevich and Cowley 2013; Wang *et al.* 2018). Later studies by Legoux *et al.* showed that MAIT activation was consistent against bacteria with intact riboflavin biosynthesis pathways (Legoux *et al.* 2019a). While it is known that MAIT antigens can be generated in APC from phagocyted pathogens, riboflavin derivates can also exist in circulation and induce MAIT activation in distal tissue or organs (Legoux *et al.* 2019a; Lett *et al.* 2022). In general, MAIT activation through the TCR is tightly regulated through different mechanisms. One is the intrinsic hyporesponsiveness of MAIT cells activated through single TCR trigger (Turtle *et al.* 2011; Slichter *et al.* 2016). In addition, the short half-life of classical MAIT-antigens hampers the TCR-mediated MAIT activation under low bacterial load (Mak *et al.* 2017; Lange *et al.* 2020). The microenvironment also influences MAIT activity as commensals reduce the production of MAIT-antigens under hypoxic conditions (Schmaler *et al.* 2018). These regulation methods are important at steady-state as MAIT cells are constantly exposed to commensals that produce soluble MAIT-agonists.

In the case of bacterial infections that breach the mucosal barrier, APC also generate additional co-signalling through TLR-mediated recognition of PAMPs and release of IL12, IL18 and other pro-inflammatory cytokines (Jo *et al.* 2014). Cytokine and TCR co-signalling are important to overcome the MAIT hyporesponsiveness at steady-state and control the spread of pathogens (Ussher *et al.* 2014a). The Tc1/Tc17 functional balance and the weight of cytokine- and TCR-signalling in MAIT activation may vary depending on the pathogen and the tissue. This interplay does not always result in a protective or beneficial outcome for the host; for instance, in the case of *H.pylori* infections, the presence of MAIT seems to have a deleterious effect, potentially due to excessive

inflammation (D'Souza *et al.* 2018). Whether MAIT cells contribute directly or indirectly to the inflammation severity remains unclear.

On the other hand, intracellular pathogens such as viral infections do not generate cognate TCR signals for MAIT cells. Nevertheless, they can be sensed through TLRs to generate inflammatory signals in the extracellular milieu; these cytokine signals activate MAIT cells in a TCR-independent manner (van Wilgenburg *et al.* 2016). Early viral studies showed that virus-infected cells could not stimulate MAIT cells, which aligned with the MAIT specificity to riboflavin antigens (le Bourhis *et al.* 2010); however, later studies demonstrated an IL18 dependency in MAIT activation during Influenza-challenge (Ussher *et al.* 2014a; Loh *et al.* 2016). Additional data showing changes in MAIT frequency under chronic infections from HIV and HCV also emphasised the non-redundancy of MAIT cells in viral immunity (Cosgrove *et al.* 2013; Leeansyah *et al.* 2013; Spaan *et al.* 2016; Bolte and Rehermann 2018). In the case of H7N9 and H1N1, low MAIT frequency correlated with negative clinical prognostics (Loh *et al.* 2016; Wilgenburg *et al.* 2018).

1.4.5. MAIT cell in disease: Autoimmunity and Cancer

In several autoimmune diseases such as diabetes type-1 (T1D), arthritis, multiple sclerosis (MS), liver fibrosis or IBD, it was found using CD161+TRAV1-2+ markers that circulating MAIT cells decreased with a concomitant increase at the site of inflammation (Serriari *et al.* 2014; Willing *et al.* 2014; Haga *et al.* 2016; Hayashi *et al.* 2016; Rouxel *et al.* 2017; Hegde *et al.* 2018; Toussirot *et al.* 2018). Therefore, there is enough evidence to infer MAIT activity outside the context of microbial and viral infections either through TCR activation by self-antigens or circulating microbial-derived antigens or, through TCR-independent mechanisms resulting from innate cues (proinflammatory cytokines) in an autoimmune microenvironment.

In most autoimmune diseases, the characterisation of circulating MAIT cells showed an enhanced expression of IL17A and IL22 (Serriari *et al.* 2014; Willing *et al.* 2014; Haga *et al.* 2016; Hayashi *et al.* 2016; Rouxel *et al.* 2017; Hegde *et al.* 2018; Toussirot *et al.* 2018). Assuming that the phenotype of circulating MAIT cells reflects their state at the site of the lesion, it is unclear whether the prominent Tc17 function has a protective or pathogenic effect. In autoimmune arthritis mouse models, MR1 deficiency is associated with a better prognosis and lower disease severity, which can be reversed by MAIT transfer (Chiba *et al.* 2012). Moreover, in the TD1-susceptible non-obese diabetic (NOD) mouse model, the MAIT frequency (detected by MR1-tetramers) was reduced in peripheric lymphoid tissues and increased in the pancreatic islets where they produced effector molecules (IFNγ, TNFα, IL17A and GrzB) that exacerbated the inflammation and destruction of the pancreatic islets (Rouxel *et al.* 2017). Other mouse models showed that MR1-deficiency increased susceptibility to TD1, while increased MAIT frequency delayed the disease onset (Shimamura *et al.* 2011; Rouxel *et al.* 2017).

The MAIT role in cancer disease has been primarily studied in colorectal cancers (CRC) and hepatocellular carcinomas (HCC). While in CRC disease, MAIT cells had an increased

intratumoral presence compared to healthy adjacent tissues and blood, the opposite was observed in liver tumours of HCC patients (Sundström *et al.* 2015; Zabijak *et al.* 2015; Ling *et al.* 2016; Shaler *et al.* 2017; Zheng *et al.* 2017; Duan *et al.* 2019). Analysis of diverse cancer types suggested a trend where circulating MAIT frequency diminished only in patients with mucosal cancers (Won *et al.* 2016). In general, high frequency of MAIT cells within the TIL population is associated with poor clinical outcomes and low survivability in both CRC and HCC. Nonetheless, the mechanistic aspects of how MAIT cells contribute to cancer disease are not clear. Some hypotheses suggest a potential pro-tumour role of IL17 (Zhao *et al.* 2020) or potentially immunosuppressive abilities. Given the role of MAIT cells in the control of microbial infections, it is possible that some infections can lead to chronic inflammations, such as in the case of *H.pylori* (D'Souza *et al.* 2018), and potentially lead to dysregulation and cancer development at mucosal sites.

1.5. Research objectives and importance

This thesis is an industrial collaboration between the Klenerman group at Oxford University and the discovery research group at Immunocore Ltd. The project aims to obtain a deeper understanding of MR1 biology by studying the role MAIT cells at steady-state and the potential of MR1T cells in cancer immunotherapy.

While we understand that MAIT cells can respond to TCR-dependent and TRC-independent signals, we still do not understand how these 2 signals interplay with each other or whether there are nuances in the pathways that are activated through these 2 types of activations. In chapter 3, we build on previously generated RNAseq data to further study gene signatures in MAIT cells under TCR and cytokine triggers. This analysis and validation will give us a better understanding of MAIT cells at steady-state and how they would potentially contribute to autoimmune and cancer diseases.

On the other hand, because MR1 can display stress-associated antigens such as abnormally accumulated metabolic intermediates, autoreactive MR1 specific TCRs reactive to these non-microbial metabolites could become useful reagents for cancer immunotherapy. In chapter 4 of this thesis, we aimed to isolate and study autoreactive MR1 restricted TCRs and understand the nature of their no-microbial antigens. Because there are no clear markers to identify MR1T cells, in chapter 5, we explored methods to speed their discovery and isolation in a setting close to *ex-vivo*. This will allow us to study MR1T frequency, functionality, and phenotype. In addition, building a database of MR1T TCR sequences may become a relevant tool in the future discovery of cancer-specific antigens and development of TCR-based immunotherapies.

2. Methods

2.1. Cells, Media, and Buffers

2.1.1. Cell lines

Cells	Provider	Identifier
THP1	ATCC	TIB-202
CACO2	ATCC	HTB-37
JURKATS	ATCC (Kindly provided by Immunocore Ltd)	TIB-152
HEK293T	ATCC	CRL-3216
COLO205	ATCC (Kindly provided by Immunocore Ltd)	CCL-222
NCIH508	ATCC (Kindly provided by Immunocore Ltd)	CCL-253
DLD1	ATCC (Kindly provided by Immunocore Ltd)	CCL-221
PSN1	ATCC (Kindly provided by Immunocore Ltd)	CRM-CRL-3211
MEL526	- (Kindly provided by Immunocore Ltd)	-
MEL642	- (Kindly provided by Immunocore Ltd)	-
7860	ATCC (Kindly provided by Immunocore Ltd)	CRL-1932
U266	ATCC (Kindly provided by Immunocore Ltd)	TIB-196
MOLT4	ATCC (Kindly provided by Immunocore Ltd)	CRL-1582

Table 2- 1. List of cell lines used in chapter 3-5

2.1.2. Reagents

Culture Reagents	Provider	Catalogue number
RPMI 1640 media	Sigma Aldrich	R7388-500ML
DMEM media	Sigma Aldrich	D0819-500ML
Foetal bovine serum (FBS)	Sigma Aldrich	12103C-500ML
Ethylenediaminetetraacetic acid (EDTA)	Sigma Aldrich	T9285-100ML
Penicillin/Streptomycin	Sigma Aldrich	P4333-100ML
L-Glutamine	Sigma Aldrich	G7513-100ML
0.25%Trypsin-EDTA	Glibco	25200056
Human Serum	Sigma Aldrich	H5667-100ML
Non-essential amino acids (NEAA)	Sigma Aldrich	M7145-100ML
Sodium Pyruvate	Sigma Aldrich	S8636-100ML

Table 2- 2. List of reagents for cell culture media

Culture Reagents	Provider	Catalogue number
hIL2	R&D Systems	202-IL-010
PHA	Sigma Aldrich	L8902
Dimethyl sulfoxide (DMSO)	Sigma Aldrich	D2438-50ML
5OPRU	Courtesy of David P. Farley group	
DH5α *E.coli*	Invitrogen	18265017
hIL12	Miltenyi Biotech	130-096-705
hIL18	MBL	B001-5
hIL15	Miltenyi Biotech	130-095-764
hTL1A	R&D Systems	1319-TL-010
LEAF anti-CD3 (UCHT1)	Biolegend	300438
LEAF anti-CD3 (OKT3)	Biolegend	317326
LEAF anti-CD28 (CD28.2)	Biolegend	302934
Purified anti-CD8 (SK1)	Biolegend	344702
LEAF anti-MR1 (26.5)	Biolegend	361110
LEAF anti-CD1c (L161)	Biolegend	331502

Table 2- 3. List of reagents used in T-cell activation assays

2.1.3. Buffers and medias

Components' percentages indicate the volume of component/total media volume.

R0 media

RPMI-1640, 1%Penicillin/Streptomycin, 1%L-Glutamine.

R10 media

RPMI-1640, 10% FBS, 1%Penicillin/Streptomycin, 1%L-Glutamine.

C10 media

DMEM media, 10%FBS, 1%Penicillin/Streptomycin, 1% L-Glutamine, 1%NEAA.

Freezing media

90% FBS + 10% DMSO.

MACS buffer

250mL PBS, 1% FBS, 1mM EDTA

Basal T-cell media

RPMI-1640, 5%Human Serum, 1% Penicillin/Streptomycin, 1%L-Glutamine, 1%NEAA, 1%Sodium Pyruvate.

Media is filtered through 0.2um filters before use.

T-cell cloning media

Basal T-cell media, feeder cells ($0.5x10^6$cells/mL freshly purified allogeneic PBMCs irradiated at 50Gy), 1μg/mL PHA, 100U/mL hIL2.

T-cell expansion media

Basal T-cell media, feeder cells ($1x10^6$cells/mL fresh or thawed PBMCs irradiated at 33Gy), 1μg/mL PHA, 100U/mL hIL2.

2.2. Cell isolation

2.2.1. PBMC isolation

Peripheral blood mononuclear cells (PBMC) were isolated from blood leukocyte cones of adult healthy donors (NHS Blood and Transplant, UK). PBMCs were also isolated from 100-200mL blood from healthy internal donors from Immunocore Ltd or CRC donors.

Leucosep tubes were used to isolate PBMCs from blood samples. For this, 15mL Lymphoprep was spun in the tubes at 1000g for 1min using swinging bucket rotors. Blood or cone samples were diluted 1:2 in PBS before layering them in the Leucosep tubes. These were spun for 15min at 800g with breaks off during deceleration. After centrifugation, the enriched layer of PBMC was aspirated into R0 media and washed 2 times with R0 before resuspending in R10.

PBMCs were stored at -80ºC in 1mL aliquots of $20x10^6$cells/mL in freezing media. To thaw these aliquots, they were put into a water bath for 30sec and washed twice in 10mL R10 to remove the DMSO from the freezing media.

2.2.2. PanT-cell isolation

CD3+ cells were enriched from PBMCs using negative selection with the human PanT isolation kit (Miltenyi). Purities were consistently above 95%. For this, PBMCs were washed with MACS buffer and resuspended in 40μL MACS buffer and labelled with 10μL of antibody cocktail per 10^7cells. This cocktail binds to cell populations that are not T-cells. After 5min of incubation at room temperature, cells were magnetically labelled with 20μL Microbeads cocktail and 30μL MACS buffer for another 10min.

Cells were added to LS columns and washed with 3mL MACS buffer. Collected flowthrough contains the panT-cell fraction.

2.2.3. CD8+ isolation

CD8+ cells were enriched from PBMCs using positive selection with the human CD8 MicroBeads kit (Miltenyi). Purities were consistently above 85%. For this, PBMCs were washed with MACS buffer and magnetically labelled with 20μL CD8 MicroBeads and 80μL MACS per 10^7 cells. After 15min incubation at room temperature, cells were washed with 1mL MACS buffer for every 10^7cells and resuspended in a final volume of 500μL.

Cells were added to LS columns and washed 3 times with 3mL MACS buffer. The flowthrough contains the CD8 depleted PBMCs. To collect the CD8 cells, the LS columns were detached from the magnetic separator and flushed with 5mL MACS buffer.

2.2.4. PE-mediated positive selection (EasySep)

TRAV1-2+ T-cells were enriched from PBMCs or panT-cells using PE-based positive selection with the 3C10 anti-Vα.7.2 clone. For this, PBMCs or pre-isolated panT-cells were stained with 2μg/mL of PE-conjugated Vα.7.2 for 5min in 250μL MACS buffer and 100μL of FcR blocking reagent. After that, 100μL positive PE-selection cocktail (STEMCELL Technologies) were added to samples and incubated for 5min, followed by 100μL RapidSperes magnetic beads and incubated for another 5min.

Finally, samples (~500-600μL) were topped up to 2.5mL with MACS buffer and placed into FACS tubes for magnetic isolation. Sample pellets were washed 3 times with 2.5mL MACS buffer before eluting with 1x release buffer.

2.2.5. Reagents and Equipment

Culture Reagents	Provider	Catalogue number
Blood Leukocyte Cones	NHS Blood and Transplant, UK	NC24
Leucosep tubes	Greiner bio-one	Z642843-300EA
Lymphoprep	Stem Cell Technologies	07851
PanT isolation kit	Miltenyi Biotec	130-096-535
LS columns	Miltenyi Biotec	130-042-401
CD8 MicroBeads kit	Miltenyi Biotec	130-045-201
EasySep kit -PE selection cocktail -RapidSperes magnetic beads -Release Buffer	STEMCELL Technologies	17187741
3C10 Vα7.2-PE	Biolegend	351706
Human TrueStain FcX	Biolegend	422302

Table 2- 4. List of reagents used for T-cell isolation

2.3. Flow Cytometry and sorting

2.3.1. Surface cells staining

Cells were spun at 1600rpm for 4min in 96-well U-bottom plates, washed with 100μL PBS and pelleted again. The pellets were resuspended in 50μL of master-mix containing the different conjugated antibodies against the markers of interest and incubated in the dark at 4ºC for 30min. The master-mix was resuspended in PBS or Staining Buffer. After that, cells were washed with 100μL PBS and fixed with 100μL 2-4% of Formaldehyde (diluted in PBS) for 10min at room temperature. After fixation, cells were spun at 1800rpm for 2min. Samples were washed twice in PBS before analysis.

2.3.2. Intracellular cell staining (ICS)

Intracellular staining (ICS) can be used to stain both intracellular markers and some surface markers. For ICS, cellular secretion was blocked with BrefeldinA (eBioscience, 1:10000 final dilution) for 4h before starting the surface stain. Following fixation with 2-4% Formaldehyde and washing, cells were permeabilized with 100μL 1xPermeabilization Buffer (eBioscience, diluted in miliQ water) buffer for 10min at the dark and 4ºC. Next, cells were resuspended in 50μL master-mix of conjugated-antibodies (resuspended in 1xPermeabilization buffer) for 30min at 4ºC and dark. Cells were then washed once with 1xPermeabilization buffer and twice with PBS before analysis.

2.3.3. CTV staining

Cell Trace Violet (CTV) staining is performed before setting up T-cell activation or expansion assays. For this, rested PBMCs or PanT-cells were washed with 500μL MACS buffer twice and resuspended in CTV dye (at 1:2000 dilution in PBS) for 10min in the

dark. Next, cells were washed with cold FBS and incubated for 5min at 4ºC. Finally, cells were washed twice with the media that will be used for the assay. CTV signal was detected in the violet laser (405nm) and 450nm channel in FACS-based analysis.

2.3.4. Reagents and Equipment

Reagents	Provider	Catalogue number
Staining Buffer	Biolegend	420201
Formaldehyde 34%	Sigma Aldrich	47608-1L-F
Brefeldin A	eBioscience	00-4506-51
10 x Permeabilization buffer	eBioscience	00-8333-56
True-Phos Buffer	Biolegend	425401
Cell Trace Violet Proliferation kit	Invitrogen	C34557
LIVE/DEAD Fixable Near IR Dead Cell Stain Kit	Invitrogen	L10119
Zombie Green™ Fixable Viability Kit	Biolegend	423112

Table 2- 5. List of reagents used in the preparation of samples for Flow cytometry

Machine	Provider
LSRII	BD bioscience
LSR Fortessa	BD bioscience
Sony Sorter SH800S	Sony

Table 2- 6. List of hardware used for Flow Cytometry reading and sorting

Antibody Specificity (Clone #)	Conjugated Fluorochrome	Provider	Catalogue number
β2m (2M2)	FITC, PE, APC, PE-Cy7, APC Fire750	Biolegend	316304, 316306, 395712, 316318, 316314
MR1 (26.5)	PE, APC	Biolegend	361106, 361107
Anti-CD1c (L161)	PE, APC	Biolegend	331506, 331524
HLA-A2 (BB7.2)	FITC	Biolegend	343304
HLA-DR/DP/DQ (Tü39)	AF647	Biolegend	361704
HLA-DR (L243)	BV421	Biolegend	307636
CD3 (HIT3a) *OKT3 and UCHT1 clones were also used	FITC, PerCpCy5.5, PE, PE-Dazzle, PE-Cy7, APC	Biolegend	317306, 317338, 317308, 317346, 317334, 317318
CD3 (REA613)	VioBlue, VioGreen	Miltenyi	130-114-519, 130-113-142
CD4 (OKT4) *RPA-T4 and SK3 clones were also used	PerCpCy5.5, PE, PE-Cy7, APC, BV650	Biolegend	317428, 317409, 317414, 317416, 317436
CD4 (REA623)	VioBlue, VioGreen	Miltenyi	130-114-534, 130-113-230

CD8 (HIT8a) *RPA-T8 and SK1 clones were also used	PerCpCy5.5, PE, PE-Cy7, APC, BV605	Biolegend	300924, 300908, 300914, 300912, 300936
CD8 (REA734)	VioBlue, VioGreen	Miltenyi	130-110-683, 130-110-684
CD161 (HP-3G10)	PE, PECy7, APC, BV421	Biolegend	339904, 339918, 339912, 339914
CD161 (REA631)	PE, PEVio770, APC	Miltenyi	130-113-596, 130-113-597, 130-113-595
Vα7.2 (3C10)	FITC, PE, PECy7, APC, BV421, BV711	Biolegend	351704, 351706, 351712, 351708, 351716, 351732
CD14 (HCD14)	FITC	Biolegend	325604
CCR7 (G043H7)	FITC	Biolegend	353216
CD45RA (HI100)	PE, PEDazz	Biolegend	304108, 304146
CD69 (FN50)	FITC, PE, PECy7, APC	Biolegend	310904, 310906, 310912, 310910
CD137 (4B4-1)	PE, PECy7, APC	Biolegend	309804, 309818, 309810
OX40 (OX-86, ACT35)	PE	eBioscience, BD Bioscience	12-1341-82, 555838
CD25 (BC96)	PE, PECy7, APC	Biolegend	302606, 302612, 302610
PD-1 (EH12.2H7)	BV421	Biolegend	329920
IFNγ (REA600, 4S-B3)	FITC, APC, AF700, PE/Cy7	Miltenyi, Biolegend	130-113-497, 130-114-021, 502520, 502528
TNFα (MAb11)	FITC, PerCpCy5.5, APC	Biolegend,	502906, 502926, 502912
Granzyme-B (GB12, GB11)	APC, AF700	Invitrogen, BD Bioscience	MHGB05, 561016
IL17A (BL168)	BV421	Biolegend	512322
IL17F (9D3.1C8)	PE	Biolegend	517008
Furin (222722)	AF647	R&D Systems	IC1503R-100UG
IL10 (JES3-9D7)	PEDazz	Biolegend	501426
IL4 (11B11)	PE	Biolegend	504104
IL5 (TRFK5)	PE	Biolegend	504304
IL13 (JES10-5A2)	APC	Biolegend	501907
IL4R (G077F6)	PE	Biolegend	355004
CCL3 (93342)	APC	R&D Systems	AF270NA
GM-CSF (BVD2-21C11)	PerCpCy5.5	Biolegend	502312
pSTAT1–S727 (A15158B)	PE	Biolegend	686410
pSTAT3-Y705 (13A3-1)	PE	Biolegend	651006
pSTAT6-Y641 (A15137E)	PE	Biolegend	686008

Table 2- 7**. List of antibodies used for staining samples for Flow Cytometry reading**

2.4. Methods to measure T-cell activation

2.4.1. IFNγ ELISPOT

Human IFNγ ELISPOT Set contains capture or 1ry antibody, detection or 2ry antibody and streptavidin-HRP. Before setting the experiment, ELISPOT plates were coated with 100μL/well IFNγ capture antibody (1:400 in PBS) and incubated overnight at 4ºC. Next morning, the coating solution was removed, and each well was blocked with 100μL R10 for 2hour. After that, the assay was ready to set up.

To develop ELISPOTS, cells were washed off and plates were incubated at room temperature with 50μL/well detection antibody diluted 1:250 in assay diluent (PBS + 10% FBS) for 2h and 50μL/well Streptavidin-HRP (1:100 in assay diluent) for 1h. Between each step, plates were washed 3 times with 200uL/well washing-buffer (PBS + 0.05% Tween-20). Finally, the spots were developed up to 5min with 50μL/well AEC substrate. Spots were counted with the Immunospot software and analyser.

ELISPOTs measure the Spot forming units (SFU), which refers to the nº of cells or clusters of cells that are producing IFNγ.

2.4.2. IFNγ, TNFα and IL10 ELISA

ELISA assays work like ELISPOT assays; however, they quantify the total concentration of molecules in the supernatant instead of the nº of SFU. ELISA assays were conducted with T-cell supernatants that were utilised either after T-cell activation assays or kept at -80ºC. 100μL of diluted supernatants (1:2 and 1:4) in assay diluent (PBS + 10% FBS) were incubated in a plate shaker for 2h at 300rpm in a NUNC flat-bottom 96-well plate pre-coated with 1ry antibodies against the factor of interest.

To pre-coat the plate, these were incubated overnight at 4ºC with 100µL of 0.5-1µg/mL (1:200 in PBS) 1ry antibody (anti-IFNγ, -TNFα or -IL10), washed 3 time with 200µL/well washing-buffer (PBS + 0.05% Tween-20), and blocked with 200µL of assay diluent for 1h.

After 2h of incubating diluted supernatants, plates were washed 3 times with 200µL/well washing-buffer before adding 100µL of the corresponding biotinylated 2ry antibody (0.5-2µg/mL) and incubating for 1h at 300rpm. Samples were then washed and added 100µL of Avidin-HPR for 30min and developed for up to 15min with TMB substrate solution.

2.4.3. LegendPlex assays

Unlike ELISAs, which focus on a single factor with a high sensitivity, LegendPlex assays allow simultaneous quantification of several factors in supernatants. LegendPlex assays were conducted with T-cell supernatants that were either utilised after T-cell activation assays or kept at -80ºC. 25µL supernatants were mixed with 25µL of LegendPlex bead mix (Biolegend), each pre-coated with 1ry antibodies against different growth factors and inflammatory molecules, and 25µL biotinylated 2ry detection antibodies. Bead specificities could be segregated by their APC signal (pre-determined by provider).

The mixture was incubated for 2h at 300rpm in V-bottom 96-well plates. Afterwards, beads were spun down and incubated with 25µL Streptavidin-PE for 30min at 300rpm. Quantification of molecules of interest was measured by the PE-signal interpolated into a standard curve.

2.4.4. Proliferation assay

In proliferation assays, T-cells (either in PBMC or panT-cell isolated samples) are mildly activated through TCR signalling, either in the presence of 1μg/mL PHA, plate-coated 0.25-0.5μg/mL anti-CD3, 5μg/mL soluble MR1 molecules or, target cells presenting antigens through MR1 or CD1c.

T-cells and pre-stained with CTV (ThermoFisher), and their proliferation is monitored through the loss of signal intensity in the 450nm channel of the violet laser (405nm). For the proliferation, T-cells were incubated for 5-12 days in flat bottom wells (either in 0.32cm^2 or 1.9cm^2 of surface). With plate-coated 0.25-0.5μg/mL anti-CD3 stimulation (chapter 3), incubation periods were 5 days long with 1:2 media exchange on day 3. With other more specific T-cell triggers (chapter 4), proliferations were up to 12 days long with 1:2 media exchange every other day with 10U/mL IL2 supplementing (explained in more detail in chapter 4).

2.4.5. Reagents and Equipment

Reagents	Provider	Catalogue number
T Cell Activation Bioassay (NFAT)	Promega	J1621
MultiScreen$_{HTS}$ IP Filter Plate, 0.45 µm, white, sterile (ELISPOT plate)	Merck-Millipore	MSIPS4W10
Human IFNγ ELISPOT Set	BD	551849
Tween-20	Sigma Aldrich	P1379-100ML
Human IFNγ ELISA kit	Biolegend	430104
Human TNFα ELISA kit	Biolegend	430204
Human IL10 ELISA kit	Biolegend	430604
LegendPlex Growth Factor Panel	Biolegend	740180
LegendPlex Inflammation Panel	Biolegend	740809

Table 2- 8. List of reagents to prepare samples and measure T-cell activation (excluding Flow-Cytometry)

Machine	Provider
CLARIOstar plus (for NFAT luciferase and ELISA assays)	BMG Labtech
Immunospot Analyser (For ELISPOTs)	CTL

Table 2- 9. List of hardware used to measure T-cell activation

3. Tissue-repair and protective functions of MAIT cells

3.1. Introduction

Tissue-repair after an injury is a complex process with different cells and mechanisms coordinating to remove infiltrating pathogens and regenerate the damaged tissue without seriously impairing tissue functions. The immune system has a critical role throughout this process; its functions can be simplified into 2 phases. In the initial acute inflammatory phase, after detecting an injury, myeloid cells such as neutrophils and monocytes infiltrate the tissue and, along with resident macrophages and T-cells, sterilise the site of infection. Later, during the injury resolution phase, the immune system is dampened to allow the proliferation of local cells, angiogenesis, matrix remodelling and restoration of homeostasis. Fine control of these 2 stages of the immune response is crucial to avoid tissue scarring and fibrosis because of chronic wounds and dysregulated tissue-repair (Forbes and Rosenthal 2014; Eming, Wynn and Martin 2017).

How the immune system is modulated for tissue-repair is still poorly understood for many cell types. For example, in the case of macrophages, they often adopt intermediate phenotypes as they respond to mixed signals. However, the general trend is that macrophages transition towards the M2 anti-inflammatory or immuno-regulatory phenotypes after the acute inflammatory phase in response to IL4 and IL13 or IL10, respectively (Martinez and Gordon 2014; Wynn and Vannella 2016).

In the case of T-cells, Tregs are essential in tissue-repair as they modulate the immune activity against self- or nonself-antigens, therefore limiting chronic inflammation and autoimmunity. To exert those functions, they provide PDL1-mediated

regulation of antigen-reactive T-cell and secrete immunomodulatory cytokines such as IL10, TGFβ and IL35 (Vignali, Collison and Workman 2008; Forbes and Rosenthal 2014). Similar functions were also found in innate-like T-cells, such as iNKT cells in adipose tissue, which adopt mixed phenotypes and promote immune-suppressive environments with the secretion of IL4, IL13 and IL10 cytokines (Liu *et al.* 2008; Sag *et al.* 2014; Lynch *et al.* 2015).

MAIT cells are one of the major innate-like T-cell populations (Godfrey *et al.* 2015), representing most of the $CD161^{high}$ cells within circulating CD8 cells and being abundant in blood, liver, and barrier tissues (Dusseaux *et al.* 2011). Evidence suggests that MAIT cells can bind diverse bacterial ligands, but the most well-characterised one is 5OPRU. Despite 5OPRU being the most potent MAIT ligands known to date, TCR signalling tends to be insufficient to fully activate them (Turtle *et al.* 2011). However, in both mouse models and *in vitro* studies, co-signalling through TCR and non-TCR signals such as cytokines or TLR agonists generated more potent MAIT responses (Turtle *et al.* 2011; Ussher *et al.* 2014a, 2016). Studies at the Klenerman lab have also reported that MAIT cells can exert protective functions during viral infections through cytokines such as IL12, IL18, IL15 and type I Interferons (Ussher *et al.* 2014a; Sattler *et al.* 2015; van Wilgenburg *et al.* 2016; Wilgenburg *et al.* 2018). Most studies at the time showed expression of IFNγ, TNFα and GrzB (Kurioka *et al.* 2015); however, to obtain a more granular view of what pathways are triggered by cytokines and TCR signals in MAIT cells, in this chapter, we present bulk RNAseq results of MAIT cells under these different triggers.

In our studies, we focussed on the role of TNF-like protein 1A (TL1A) because it is a gut-associated cytokine secreted by different immune cell types (Migone *et al.* 2002; Meylan *et al.* 2008; Shih *et al.* 2009). Furthermore, it has been known to induce IFNγ and TNFα expression in CD161+CD4+ T-cells and in IL18Rα expressing T-cells when used in combination with TCR-ligation and other cytokines (Holmkvist *et al.* 2014). Given that CD161+ cells share a transcriptional signature (Fergusson *et al.* 2014; Provine and

Klenerman 2020) and MAIT cells also being CD161+IL18Rα+, we hypothesised that TL1A may play a role in MAIT activation.

The interplay between adaptive (TCR-ligation) and innate signals (such as IL12, IL18, IL15 and TL1A) is critical at barrier sites such as the gut lamina propria. In these mucosal sites, MAIT cells are constantly under challenge by the local microbiota and soluble but innocuous molecules from the diet. We hypothesised that the interplay of TCR-dependent and -independent signals might balance MAIT activation so they can elicit protective functions at mucosal sites without causing severe inflammation. At the time of the study, a report was published describing tissue-repair capabilities in murine skin-derived Th17 T-cells that were responsive to commensal ligands (in the context of H2M3) (Linehan *et al.* 2018). Considering the similarities between these H2M3 restricted cells and MAIT cells, which also can home to the skin, there were enough reasons to ask if MAIT cells also had a similar role at barrier sites.

To prove that MAIT cells have a protective function at barrier sites, we described 2 modules activated under TCR stimulation. One of these modules corresponded with the tissue-repair transcriptional signature described by Belkaid's group (Linehan *et al.* 2018). In addition, we provided evidence that MAIT cells can produce soluble factors to accelerate the recovery of damaged epithelia and have an overlapping immuno-regulatory module that may affect bystander T-cells and myeloid cells at the site of infection.

3.1.1. Aims

The aims of this chapter are:

- To investigate the single and combinatorial effects of TCR-dependent and TCR-independent signals in MAIT activation.
- To compare the impact of adaptive and innate signals at a transcriptional level in MAIT cells.
- To validate whether MAIT cells have a tissue-repair transcriptional signature like the murine Th17 skin-resident T-cells described in Belkaid's paper (Linehan *et al.* 2018)
- To explore immunoregulatory functions in MAIT cells which may or may not be linked to the tissue-repair module.

The wound-healing aspects of MAIT cells (Results until section 3.3.8) have already been published in Leng et al. 2019 with data generated by me, Dr Hackstein and preliminary work conducted by Dr Leng.

3.2. Materials and methods

3.2.1. Cells lines

THP1

THP1 (ECACC) cells were maintained with R10 media at 37ºC between 0.25-1x10^6cells/mL. For optimal growth, cells were split every 3 days.

CACO2

CACO2 (ATCC) are adherent cells and maintained with C10 media at 37ºC. For optimal growth, cells were split when they reached 70-80% confluency. During the split, cells were washed with PBS to remove traces of FBS, incubated at 37ºC with 1-3mL 0.25% Trypsin-EDTA solution for 10min to lift the cells and, split 1:5 into a new flask.

3.2.2. Isolation of LPMC from colonic tissues

Lamina propria mononuclear cells (LPMC) were isolated form colonic tissue (either unaffected or polyp mucosal samples) from colorectal-cancer patients. These samples were obtained and provided by the oxford biobank.

To isolate LPMC from colonic tissue samples were washed with warm R10 over cell strainer and homogenised with the gentleMACS (Miltenyi) in the presence of Collagenase D and DNAase for 1hour at 37ºC. Dissociated tissue was strained through 0.7μm filter and centrifuged at 500g for 10min. The resulting pellet was resuspended in 4mL R10 media with 40% Percoll (Sygma Aldrich), overlayed in PBMC with 80% Percoll and spun at 800g for 20min. The cells in the resulting interface were collected and washed with R10 for downstream applications.

CRC SAMPLE INFORMATION	
CRC patients	n = 21
AGE (AVERAGE, SD)	68, 12
SEX (MALE/FEMALE)	12/9
SAMPLES FROM SMALL INTESTINE	0
SAMPLES FROM LARGE INTESTINE	21
YEARS SINCE DIAGNOSTICS (AVERAGE, SD)	1, 1
***SD = STANDARD DEVIATION**	

Table 3- 1. CRC patient information table

3.2.3. *In-vitro* PBMC/LPMC activation

10^6 PBMCs were cultured in flat-bottom 96-well plates at 37ºC in R10 media. If anti-CD3/28 mediated activation was used, NUNC flat-bottom plates (Thermo Fisher) were pre-coated at 4ºC with 100μL of 1.25μg/mL anti-CD3 (UCHT or OKT3 from Biolegend). The day after, coated plates were washed 3 times with 200μL of R10 media before adding PBMCs with a final concentration of 1μg/mL anti-CD28 (Biolegend). These experiments were supplemented with cytokines (IL-12/18, IL-15, and TL1A) at the specified concentration in the results section. 4h before harvesting cells, Brefeldin A (eBioscience) was added at 1:10000 dilution to block the secretion of intracellular molecules. If PMA/ionomycin stimulation was added, these reagents were added 3h before harvesting cells. Cells were characterised by flow cytometry and, supernatants were analysed by LegendPlex kit.

3.2.4. *In-vitro* $CD8^+$ T-cell stimulation with THP1 cells

$2x10^5$ CD8+ T-cells were co-cultured in flat-bottom 96-well plates with 10^5 THP1 cells at 37ºC in R10 media. THP1 cells were pre-incubated for 2h with 5OPRU (10nM) or fixed *E.coli* (25bacteria/THP1 cell). These experiments were supplemented with 5μg/mL LEAF anti-MR1 blocking or co-signalling cytokines (IL-12/18, IL-15, and TL1A) at the specified concentration in the results section. 4h before harvesting cells, Brefeldin A was added at

1:10000 dilution. Cells were characterised by flow cytometry and, supernatants were analysed by LegendPlex kit.

3.2.5. Generation of fixed *E.coli*

E.coli (DH5α, Invitrogen) were thawed on ice for 10minute and diluted in 1mL LB and incubated overnight at 37ºC in LB agar plates at 1:100 dilution. The following day, a single colony was inoculated into 5mL LB and grown overnight at 37ºC and shaking at 225rpm. Grown *E.coli* were plated overnight in agar plates at 1:100, 1:1000 and 1:10000 dilutions. The rest were centrifuged at 4000rpm for 5min, washed once with PBS, fixed with 1% Formaldehyde for 20min at room temperature and washed 2 times more before resuspending in 1mL PBS. *E.coli* titre was estimated by counting the number of colonies formed on the agar plates. According to this, the concentration was re-adjusted at 10^7 colony-forming units (cfu)/μL. *E.coli* was used in experiments at 25 bacteria per cell (BpC) unless otherwise indicated.

3.2.6. *In-vitro* wound-healing assay

CACO2 cells were seeded at a density of 10^5 cells/well in flat-bottom 96-well plated and cultured with DMEM media for 5 days until 80-90% confluency was reached. In parallel, CD8 T-cells were co-cultured with THP1 cells and fixed *E.coli* for 72h in the presence or absence of anti-MR1. Supernatants were collected. CACO2 monolayers were scratched using WoundMaker (Essen Bio), washed twice with serum-free media and topped up with 200μL of $CD8^+$ T-cell supernatant diluted 1:2 with fresh media. To observe the closure of the scratch, time-course imaging was carried out with the IncuCyte S3 Live Cell Analysis System (Essen Bio) at 37ºC and intervals of 4h for a total of 36h. ImageJ (http://dev.mri.cnrs.fr/projects/imagej-macros/wiki/Wound_Healing_Tool) was used to detect wound edges and quantify the closure rate of the wound surface.

3.2.7. ICS of phosphorylated STAT molecules

This protocol for staining is like a regular ICS but used only to detect phosphorylation of STAT molecules. Staining other intracellular markers is not ideal with this method. After fixation and washing, cells were resuspended in 100μL True-Phos Buffer (pre-chilled at -20ºC, Biolegend) and incubated for 90min at -20ºC. Next, cells were washed with PBS and stained with 50μL master-mix of conjugated antibodies (resuspended in PBS) and incubated for 30min at 4ºC. Cells were then washed twice with PBS before analysis.

3.2.8. Other methods

Refer to chapter 2 for other methods not specified in this section. Lists of antibodies and providers are also specified in chapter 2.

3.3. Results

3.3.1. Co-stimulation with cytokines enhances TCR-mediated activation of CD8+ MAIT cells from resting blood

We focused on CD8+ MAIT cells in all our experiments because they represent over 70% of the total MAIT population in healthy PBMCs (**Figure 3- 1A, C, D**). Also, MAIT frequency in the DN (CD4- and CD8-) and CD8+ T-cell compartment is between 5-10%, being as high as 20% in some donors, while in the CD4 compartment, MAIT frequency is less than 1% (**Figure 3- 1B**).

MAIT cells, like other innate-like T-cells, are unique in their ability to be rapidly activated by cytokine signalling in the absence of TCR ligation. Within the circulating T-cell compartment, we gated on MAIT cells as CD161+ and TRAV1-2+ and, showed that they could produce IFNγ and TNFα in response to 50ng/mL IL12/IL18. Conversely, the TRAV1-2- sub-populations could not mount a similar response after 20h of cytokine stimulus (**Figure 3- 1E, F**).

To explore the effects of cytokines and TCR-crosslinking on PBMC-derived MAIT cells, we looked at the upregulation of inflammatory cytokines such as IFNγ, TNFα and GrzB in response to IL12/IL18 with or without anti-CD3/CD28. In the absence of TCR-ligation, MAIT cell activation is dose-dependent to the concentration of cytokines (**Figure 3- 2A, B**). To visualise any synergistic interplay between the 2 types of signalling, IL12/IL18 concentrations were reduced to sub-optimal concentrations (S.O., 2ng/mL), at which no significant upregulation of IFNγ, TFNα and GrzB could be observed **(Figure 3- 2D-F**). As expected TCR-dependent signalling is insufficient to fully activate MAIT cells; however co-signalling with S.O. cytokines induced a substantial amplification of the TCR-driven inflammatory response (**Figure 3- 2D-F**). This effect was also seen when 5OPRU was used as TCR-dependent trigger for MAIT cells instead of anti-CD3/CD28 (**Figure 3- 4A**).

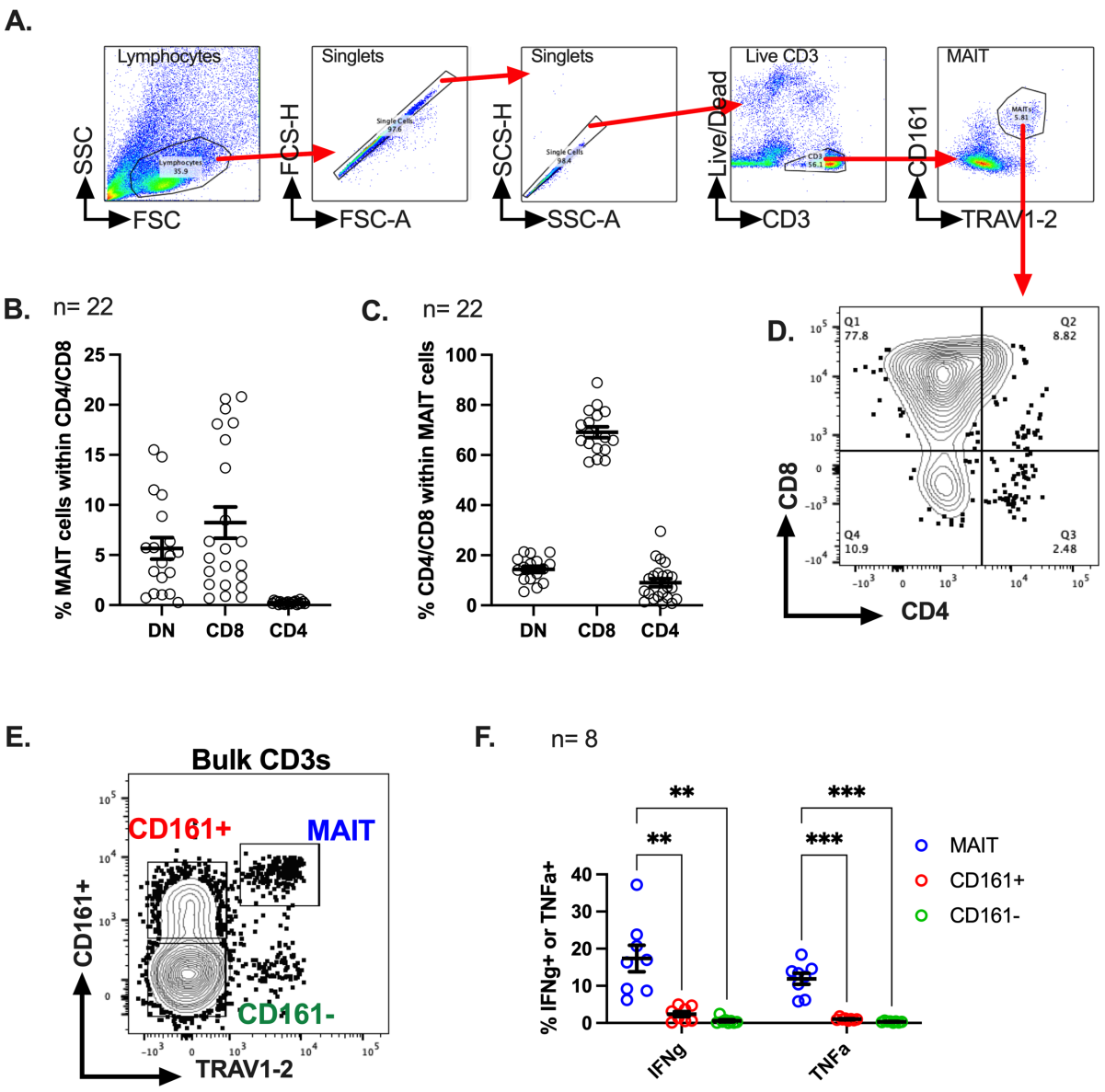

Figure 3- 1. MAIT cells are mostly CD8+ or DN and can be activated by IL12/IL18.

(**A-D**) Analysis of peripheral blood mononuclear cells (PBMCs) at steady-state. (**A**) Gating strategy of MAIT cells in PBMCs. (**B**) Frequency of MAIT cells inside the CD4, CD8 and DN compartments. (**C**) Frequencies and (**D**) representative FacsPlot elucidating the distribution of CD4, CD8 and DN T-cells inside the MAIT compartment. (**E-F**) PBMCs were stimulated overnight with 50ng/mL of IL12/IL18. € Gating strategy of MAIT cells (Blue) and, non-MAIT CD161+ (Red) and CD161- (Green) cells inside the CD3 compartment and, (**F**) frequency of IFNγ or TNFα producing T-cells following stimuli with IL12/IL18.

Data were acquired in 2-3 independent experiments. Every datapoint is a biological replicate. Error bars represent Mean ± SEM. Differences among conditions were analysed by RM One-way ANOVA with uncorrected Fisher's LSD test. *p < 0.05, **p < 0.01, ***p < 0.001, ****p < 0.0001.

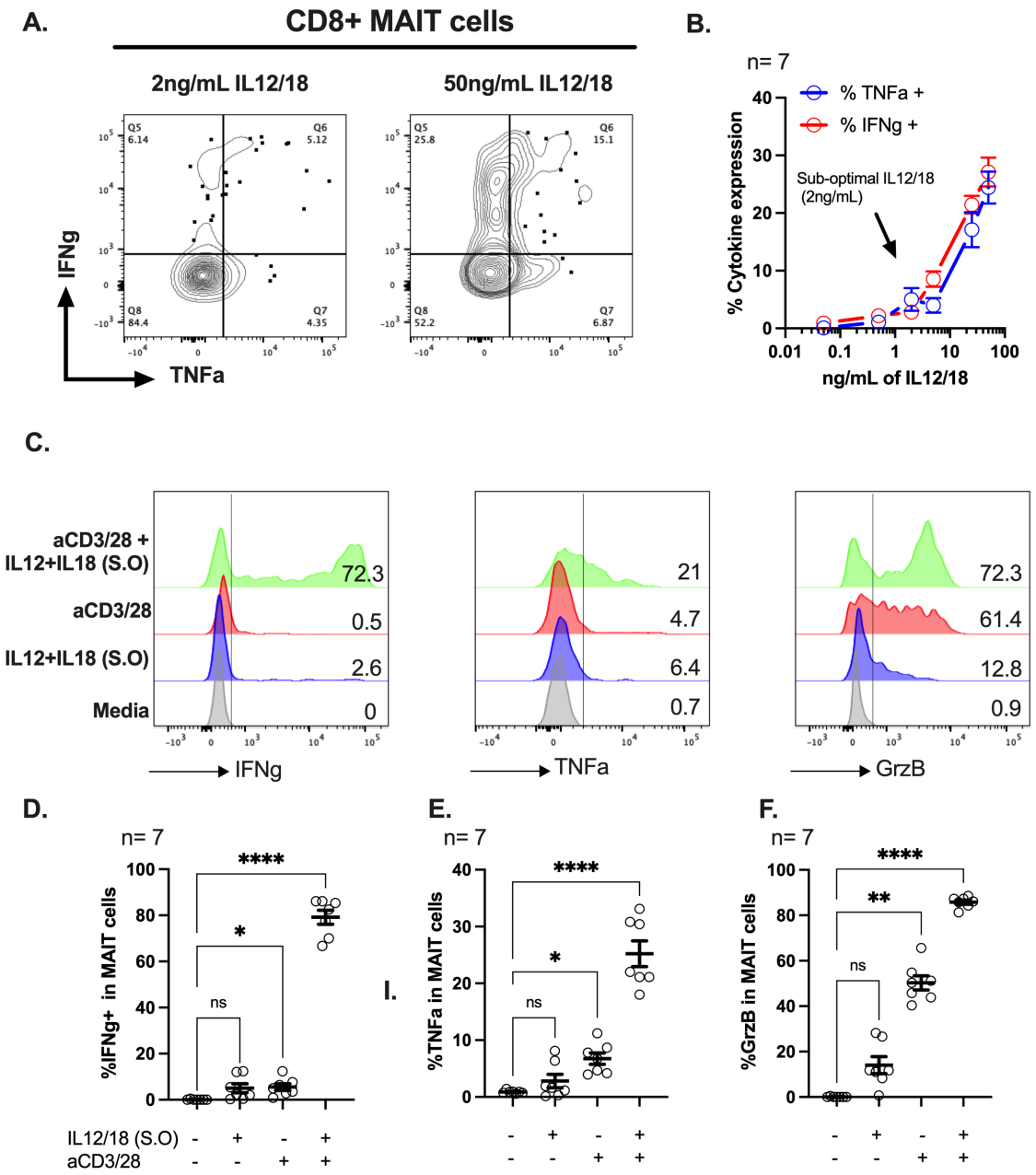

Figure 3- 2. Sub-optimal (S.O) co-stimulation of MAIT cells with IL12/IL18 significantly enhanced their activation in response to TCR ligation.

(A-B) PBMCs were stimulated overnight with different doses of IL12/IL18 from 50ng/mL of each down to 0.05ng/mL. (**A**) Representative FacsPlots and (**B**) frequencies of IFNγ (Red) and TNFα (Blue) expression in MAIT cells in response to different doses of IL12/IL18, represented in the titration curve.

(C-D) PBMCs were stimulated overnight with 2ng/mL of IL12/IL18 and/or 1.25µg/mL plate-bound anti-CD3/CD28. (**C-F**) Representative histogra€(**C**) and frequencies of IFNγ+ (**D**), €α+ (**E**) and GrzB+ (**F**) MAIT cells in response to either sub-optimal cytokine trigger, TCR trigger or a combination of the two.

Data were acquired in 2-3 independent experiments. Every datapoint is a biological replicate. Error bars represent Mean ± SEM. Differences among conditions were analysed by RM One-way ANOVA with uncorrected Fisher's LSD test. *p < 0.05, **p < 0.01, ***p < 0.001, ****p < 0.0001.

3.3.2. TL1A and IL15 can activate MAIT cells from resting blood in combination with IL12/IL18 and TCR-triggering

To understand the role of cytokines other than IL12/IL18, we explored the ability of TL1A and IL15 in MAIT cell activation. TL1A and IL15 could induce activation of CD161+ CD4+ T-cells when used in conjunction with IL12/IL18 (Cohavy *et al.* 2011). While TL1A and IL-15 cannot activate MAIT cells independently in titration experiments where PBMC were co-cultured with S.O L12/IL18 and different concentrations of TL1A and IL15, Dr Leng established that 100ng/mL and 50ng/mL were their optimal concentrations for *in-vitro* MAIT activation, respectively. Furthermore, within the CD8 compartment, MAIT cells were the only population that responded to these cytokines (Leng *et al.* 2019).

In our assays with PBMC, we found that TL1A (100ng/mL) and IL15 (25ng/mL) individually did not cause significant upregulation of IFNγ, TNFα and GrzB expression (**Figure 3- 3A-C**). However, in the presence of S.O IL12/IL18, they significantly increased the activation levels of MAIT cells in terms of IFNγ, TNFα, GrzB and CD69 expression (**Figure 3- 3D-G**). In our results, IL15 seemed more potent than TL1A as, when used singly with IL12/IL18, it drove most of the observed synergistic effect. Nevertheless, while the addition of TL1A to the IL12/IL18/IL15 mix did not affect GrzB expression (**Figure 3- 3G**), TL1A had a marginal contribution to IFNγ and TNFα production (**Figure 3- 3D,E**). Therefore, the cytokine combination of S.O IL12/IL18 and IL15/TL1A was used to generate bulk RNAseq datasets from pure MAIT cell populations.

To remove bystander effects from other cell populations in resting PBMC, CD8 cells were purified and co-cultured with THP1 monocytic cells in combination with cytokine and TCR triggers for 20h (**Figure 3- 4A**). To make the TCR signalling MAIT specific, 5OPRU was used as the cognate MAIT ligand.

The combination of 10nM 5OPRU and S.O IL12/IL18 could already elicit high levels of MAIT activation; however, the addition of TL1A and IL15 marginally increased the expression of IFNγ, TNFα and GrzB in MAIT cells for most donors (**Figure 3- 4B-E**).

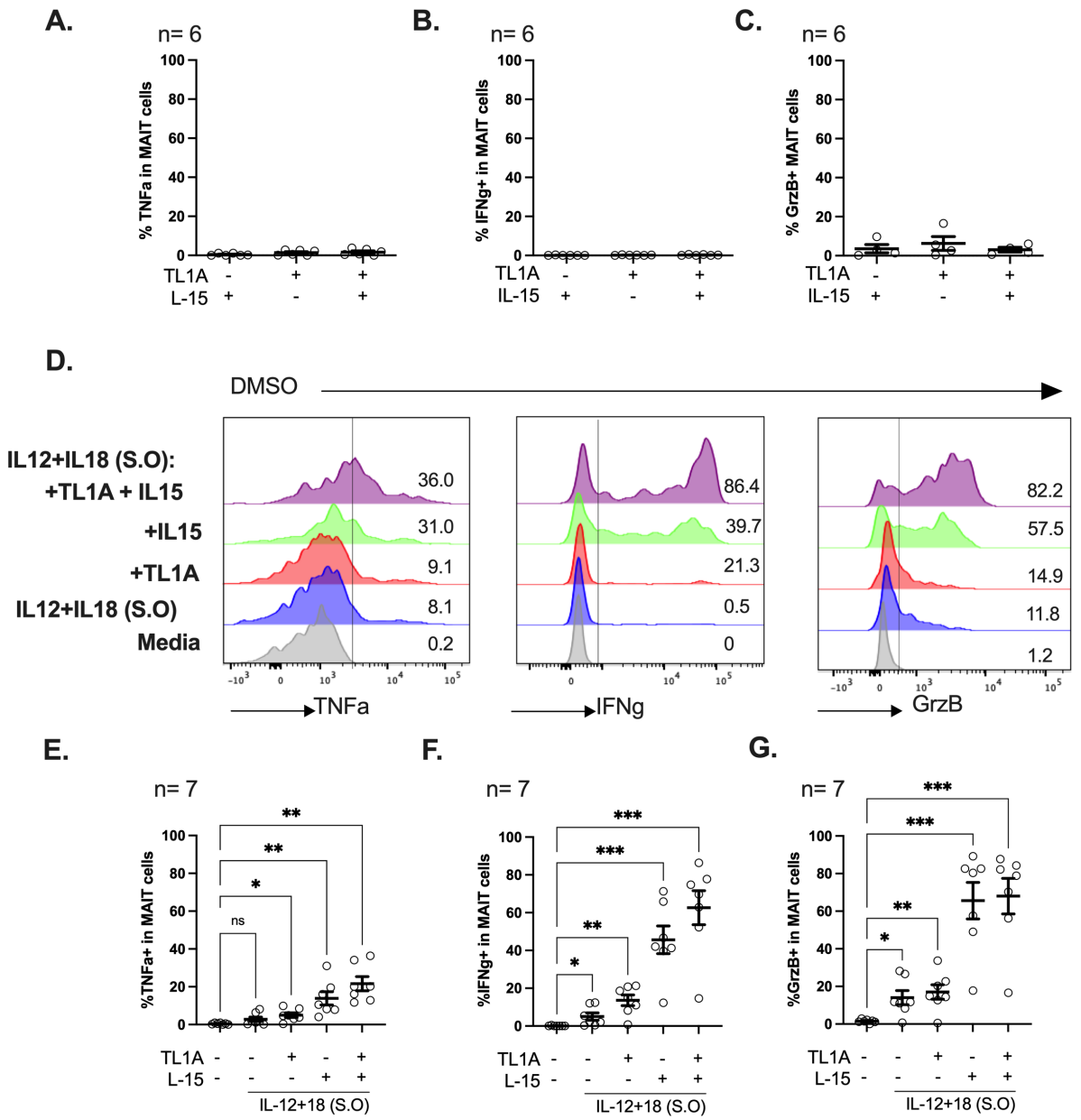

Figure 3- 3. TL1A and IL15 synergise with sub-optimal IL12/IL18 to enhance MAIT activation.
PBMCs were stimulated overnight with 100ng/ml TL1A and/or 25ng/ml IL15 on their own (**A-C**) or in combination with 2ng/mL IL12/IL18 (**D-G**). Plotted are the frequencies of TNFα (**A**), IFNγ (**B**) and GrzB (**C**) when stimulated by TL1A and/or IL15.
(**D**) Representative histograms and frequencies€ TNFα (**E**), IFNγ (**F**) and GrzB (**G**) in response to sub-optimal activation with 2ng/mL IL12/IL18 and addition of TL1A and/or IL15.
Data were acquired in 2-3 independent experiments. Every datapoint is a biological replicate. Error bars represent Mean ± SEM Differences among conditions were analysed by RM One-way ANOVA with uncorrected Fisher's LSD test. *p < 0.05, **p < 0.01, ***p < 0.001, ****p < 0.0001.

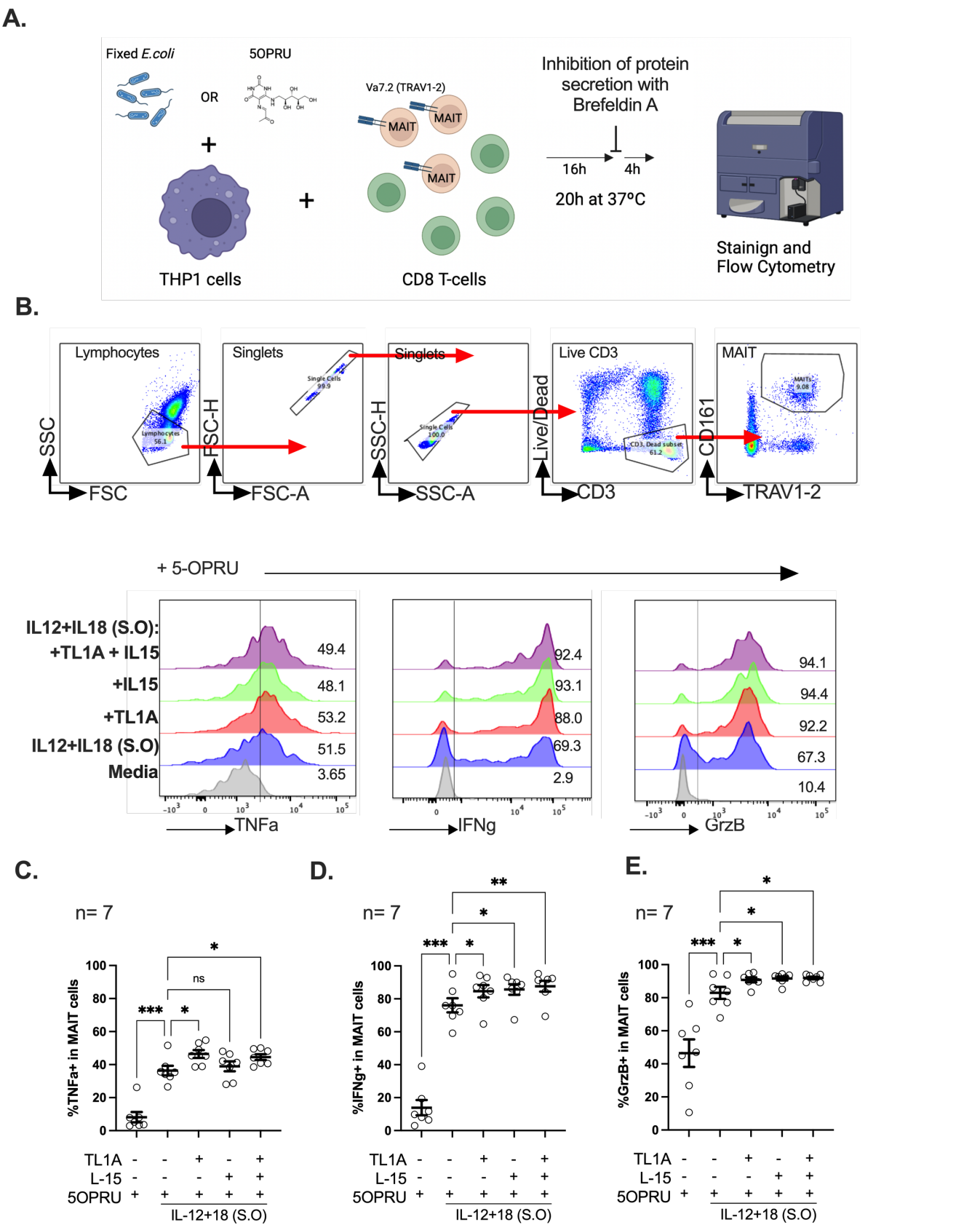

Figure 3- 4. Cytokine and TCR signals combine to stabilise peak levels of MAIT activation in *in vitro* activa model. (A) Diagram of overnight *in vitro* activation assay where CD8 T-cells were

purified from PBMCs and co-cultured overnight with THP1 monocytic cells in the presence of 5OPRU or fixed *E.coli* as MR1-specific signal.
(**B-E**) MAIT-rich CD8 T-cells were co-cultured with THP1 and 10nM 5OPRU in the presence or absence of 2ng/mL IL12/IL18 and/or 100ng/mL TL1A and 25ng/mL IL15. Gating strategy and representative histograms (**B**) and, plotted frequencies of TNFα (**C**), IFNγ (**D**) and GrzB (**E**) expression in MAIT cells activated by different cytokines and/or TCR stimuli.
Data were acquired in 2-3 independent experiments. Every datapoint is a biological replicate. Error bars represent Mean ± SEM. Differences among conditions were analysed by RM One-way ANOVA with uncorrected Fisher's LSD test. *p < 0.05, **p < 0.01, ***p < 0.001, ****p < 0.0001.

3.3.3. No significant changes are seen between circulating MAIT cells with their counterparts at barrier sites

To assess the behaviour of MAIT cells in barrier tissues, we isolated T-cells form the lamina propria and compared the activation of resident MAIT cells to their circulating counterparts. LPMC were obtained from uninvolved colonic tissues or polyp biopsies of patients with colorectal cancer (patient information found in section 3.2.2, **Table 3- 1**). In this study, T-cells were activated by combinations of anti-CD3/CD28, IL12/IL18 (50ng/mL) and TL1A/IL15; however, one caveat is that the datapoints corresponding to PBMC and gut biopsies are not matched. Gut-derived MAIT frequency was between 1-2% (**Supplementary Figure 3- 1**) and gated as CD161+ and Vα7.2+. Parallel work at the Klenerman lab showed that this gating strategy for CD8+ and DN cells encapsulated all the 5OPRU-tetramer+ MAIT cells (Phetsouphanh *et al.* 2021).

As we have established previously, MAIT cells from both blood and barrier tissues were able to upregulate IFNγ, TNFα and GrzB as part of their Th1 signature. They can also produce IL17A as part of their Th17 signature. At 50ng/mL, IL12/IL18 had a more substantial stimulatory effect than anti-CD3/CD28 for IFNγ production but not for TNFα, GrzB and IL17 production. In both PBMC or LPMC-derived MAIT cells, we observed a synergistic effect between IL12/IL18 and anti-CD3/CD28 stimulation and an additive effect of IL15/TL1A in terms for IFNγ, TNFα, GrzB and IL17A expression (**Figure 3- 5A-D**). However, when comparing the 2 compartments, a clear hyporesponsiveness was observed in MAIT cells from barrier tissues for Th1-related functions such as IFNγ, TNFα and GrzB expression. Nonetheless, lamina propria MAIT cells also had a more defined Th17 signature, as seen by the upregulation of IL17A compared to their blood counterparts (**Figure 3- 5A-D**).

Both PD1 and CD39 denote T-cells exhaustion and immunoregulation, and they have been associated with Th17 functions in CD161+ cells (Bai *et al.* 2014; Gupta *et al.* 2015;

Yong *et al.* 2018). Comparison of surface expression of CD39 and PD1 markers in circulating and tissue-resident MAIT cells at steady-state showed a significantly higher expression of these exhaustion markers in the LPMC-derived MAIT cells (**Figure 3- 5E, F**).

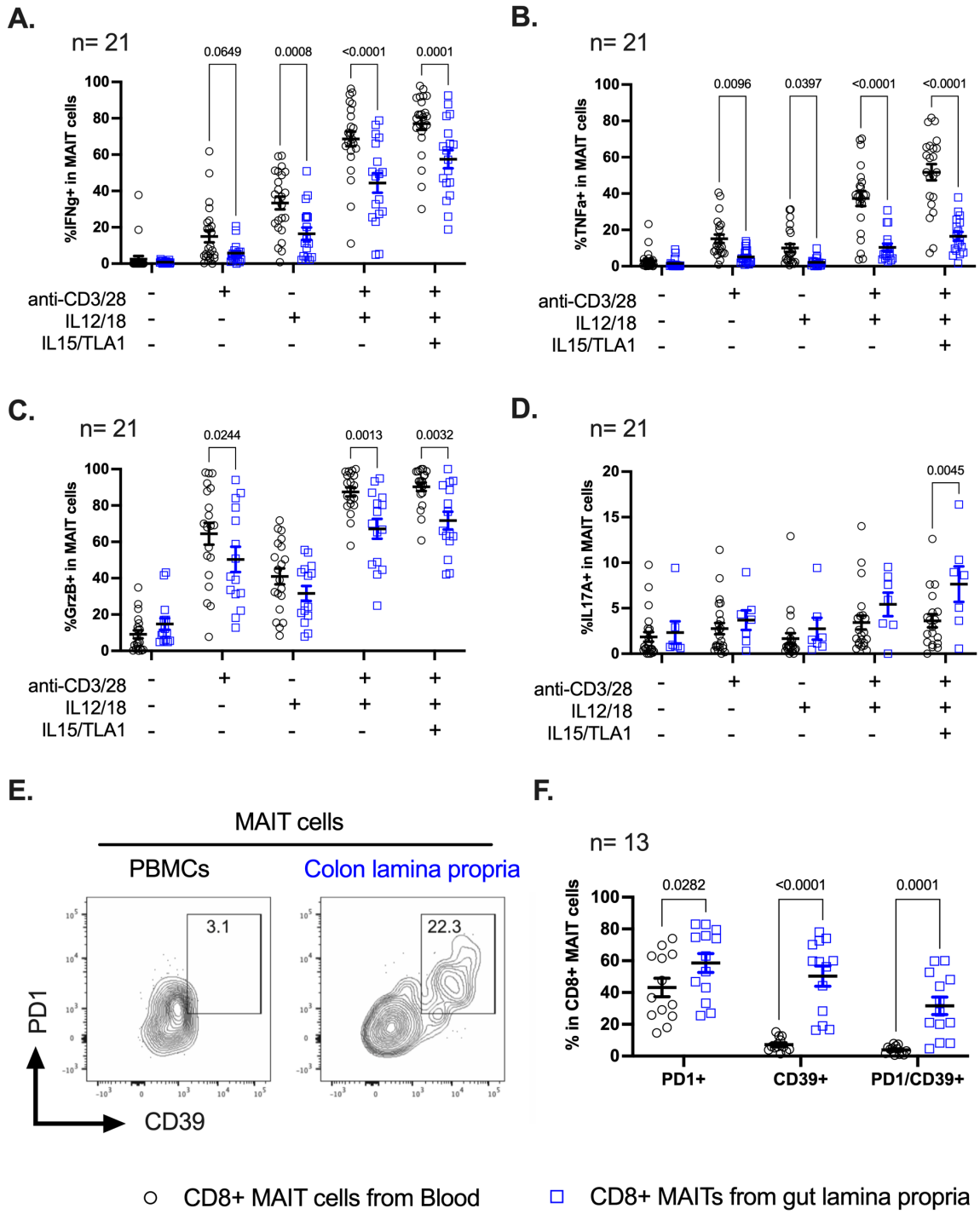

Figure 3- 5. Gut-derived MAIT cells have a dampened Th1 and increased Th17 response in comparison to their blood counterparts, when triggered by innate and adaptive stimuli.

(**A-D**) PBMC (Black) and lamina propria (Blue) derived MAIT cells were incubated overnight with 1.25μg/mL plate-bound anti-CD3/CD28 in the presence or absence of 50ng/mL IL12/IL18 and/or 100ng/mL and/or 25ng/mL IL15. Plotted are the frequencies of IFNγ (**A**), TNFα (**B**), GrzB (**C**) and IL17A (**D**) expression in MAIT cells. (**E**) Representative FacsPlot and (**F**) frequencies of PD1 and CD39 expressing MAIT cells at steady in blood (Black) and gut tissue (Blue).
Data were acquired in 2-3 independent experiments. Every datapoint is a biological replicate. Error bars represent Mean ± SEM. Differences among conditions were analysed by RM 2-way ANOVA with uncorrected Fisher's LSD test. *p < 0.05, **p < 0.01, ***p < 0.001, ****p < 0.0001.

3.3.4. MAIT cells have distinct transcriptional signatures with Cytokine and TCR activation

In our activation assays, the synergy between cytokine and TCR signalling, when used concomitantly, suggested that these 2 triggers activate MAIT cells through different pathways. To explore the underlying differences between cytokines and TCR activation, bulk RNA sequencing was used to characterise sorted CD8+ MAIT cells triggered *in vitro* with either or both. The accession number for the raw and pre-processed data from the RNAseq datasets reported in the publication of this data (Leng *et al*. 2019) is **GEO: GSE129906**. As TCR stimulus, plate-bound activation with 1μg/mL of anti-CD3/CD28 was used, whereas the cytokine stimulus contained 2ng/mL of IL12/IL18, 25ng/mL IL15 and 100ng/mL TL1A. Transcriptional data analysis was initially done by Dr Leng and further revised by Dr Hackstein and me. Recently I re-analysed the data using R packages DESeq2 and ClusterProfiler instead of Partek. Because R packages apply a different mathematical transformation to Partek when normalising the counts data, the differential expression data is slightly different to the data published in Leng *et al*., 2019 although the conclusions remain the same.

Transcriptional profiles of stimulated MAIT cells were compared to the untreated (Labelled as UT) condition to make lists of significantly modulated genes. To establish these lists, filtering was applied on variance-stabilising-transformed (VST) data to only keep genes with expression Log2 Fold-change > 1.5, false discovery rate < 0.05 and adjusted p-value across 3 donors < 0.05. At the transcriptional level, out of the total 3273 modulated genes, 154 were modulated with TCR stimulus (Labelled as T), 2343 with cytokines (Labelled as C) and 2893 genes were modulated by a combination of TCR and cytokine stimuli (Labelled as TC) (**Figure 3- 6A**). While the C and TC conditions had comparable numbers of upregulated and downregulated genes, in the case of TCR signalling, 150 out of the 154 genes were upregulated (**B,C**).

All 3 types of stimulations modulated 105 common genes, 100 of which were upregulated. From Gene Ontology (GO) enrichment analysis, these genes were associated with cytokine signalling pathways such as TNF signalling (TNF, NFKB1, NFKBIA) (**Figure 3- 6E**). 25, 349 and 887 genes were uniquely modulated in the T, C and TC conditions, respectively (**Figure 3- 6A**), indicating differences in the downstream signalling of TCR (T) and cytokine stimuli (C). It also highlighted new functions unique to the combination of anti-CD3/CD28 and cytokines (TC) stimuli, which may explain the strong synergy shown earlier in terms IFNγ and TNFα expression.

Among the 1830 (56%) upregulated genes (Appendix section 2), 996 genes were shared between the C and TC conditions (**Figure 3- 6B**); this represented 74% and 64% of genes upregulated in the C and TC conditions. In contrast, only 16 upregulated genes were shared between the TC and T conditions, representing only 1% and 11% of their total upregulated genes. These results suggest that most of the signal amplification seen at 20h timepoint in the TC condition is driven by the cytokines and not the TCR ligation.

Principal component analysis (PCA) using the first 2 components (PC1 and PC2) showed 4 clusters corresponding to the US, T, C and TC conditions. The T cluster segregated from the US cluster along the PC2 component while the C cluster segregated along the PC1 component, therefore suggesting different downstream effects (**Figure 3-6D**). Close placement of C and TC clusters confirmed again the dominant impact of cytokines over the TCR signal in MAIT activation. The changes caused by TCR stimulus are mostly represented by the PC2 component, which captures only 9% of the variance while, the effect of cytokines contributes to the PC1 component accounting for 64% of the variance. This indicated that while there are some changes happening due to TCR-ligation, these are not as ubiquitous or profound as those caused by TCR-independent signalling (**Figure 3- 6D**).

Given the limited number of upregulated genes distinctive to TCR stimulus, GO enrichment analysis did not show any interesting transcriptional profiles other than T-cell activation and Th17 function (RORC, BCL6, NFKBID). In contrast, more diverse functions were predicted from the list of genes exclusively upregulated by C and TC (**Figure 3- 6E**). Unique functions predicted in the presence of cytokines were T-cell polarisation by re-organisation of the cytoskeleton (ACTR2, ARPC1/2, TUBA/B, TPM4, PFN1), formation and traffic of vesicles from the ER and Golgi (COPI, FLOT1, TMED, SEC24, VAMP1), degranulation (STX11/12,) and, expression of adherent molecules involved in cell-to-cell contacts and migration (FERMT2, ICAM1, CD44). Unique functions predicted in the TC condition that were not predicted in T and C, included increased protein production and biogenesis of ribosomes (**Table 3- 2**)**.**

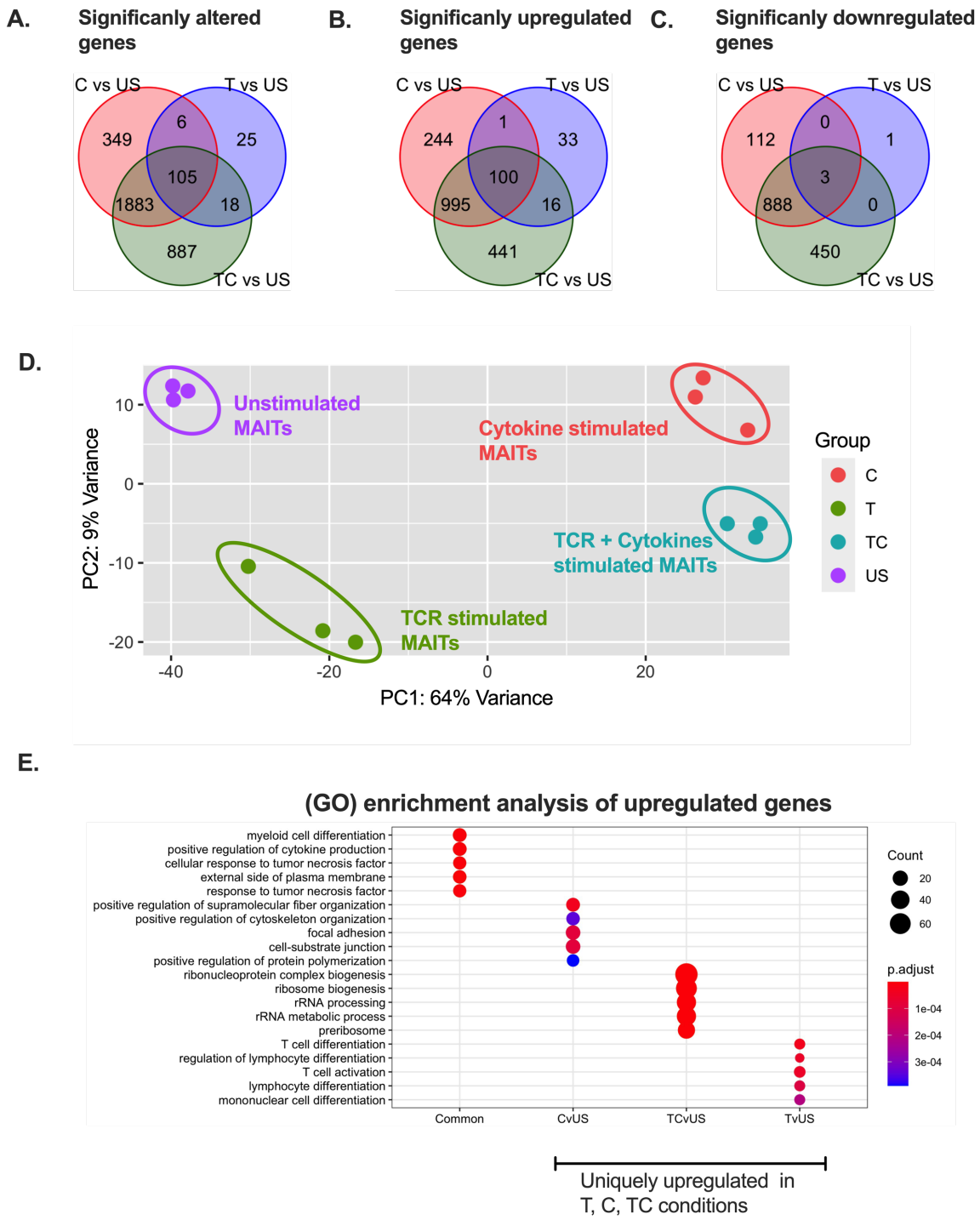

Figure 3- 6. TCR and cytokine signals prompt different transcriptional profiles in MAIT cells.
(**A-C**) Venn diagrams elucidating the total number (**A**) differentially expressed genes (Log2 Fold-change > 1.5, false discovery rate < 0.05 and adjusted p-value across 3 donors < 0.05) by cytokines (2ng/mL IL12/IL18, 100ng/mL TL1A and 25ng/mL IL15) (Red, C), anti-CD3/CD28 (Blue, T) and both (Green, TC) when compared to unstimulated (UT) MAIT cells. The cytokine stimulus consisted of a combination of 2ng/mL IL12/IL18, 25ng/mL IL15 and 100ng/mL of TL1A. Modulated genes are segregated based on positive regulation (**B**) and negative regulation (**C**).
(**D**) Principal component analysis (PCA) of CD8+ MAIT transcripts generated by the different stimulations in a 2-dimensional representation by the first 2 components. Samples are colour

coded: stimulated by cytokines (Red, C), anti-CD3/CD28 (Green, T), both (Cyan, TC) or, unstimulated (Purple, UT). (**E**) DotPlot of enriched Gene-Ontology pathways found in the lists of genes that are modulated by all 3 types of stimuli (C, T and TC), genes that are uniquely upregulated by cytokines (CvsUS), genes that are uniquely upregulated by TCR ligation (TvsUS) and genes that are uniquely upregulated when both signals are present (TCvsUS).
RNAseq data were analysed with R using DESeq2, ClusterProfiler, fgsea and VennDiagram packages.

Unique functions predicted in MAIT Cells under different stimuli

GENES	**Predicted GO functions**	**Genes**
Common Functions By C, T And Tc	Positive regulation of cytokine production	*LTA, FURIN, HIF1A, IRF4, SLC7A5, TNF, NFKB2, GAPDH, SEMA7A, CD83, NFKB1, IL23R, CCL3, PARK7*
	Myeloid Cell differentiation	*NFKBIA, HIF1A, IRF4, TFRC, TNF, JUNB, NME1, RELB, IL23R, CCL3, RBPJ*
	Cellular response to TNF	*NFKBIA, LTA, TNF, CCL20, ICAM1, TNFRSF18, BIRC3, TRAF4, TRAF1, TNFRSF9, NFKB1, CCL3, TNFRSF4*
Functions Unique To C	Positive regulation of cytoskeletal organization	*ACTR2, CORO1A, GPR65, ARPC1B, ARPC2, HSPA1B, CDC42, FCHSD2, WDR1, ARF6, RB1, ARFIP1, ARPC3, CLIP1*
	Focal Adhesion	*CAP1, ACTR2, ACTB, MAP2K1, RAC2, ARPC1B, CFL1, ARPC2, LPXN, CD44, CHP1, HSPA1B, CDC42, ARF6, YES1, YWHAZ, ARPC3*
	ER to Golgi vesicle-mediated transport	*TMED5, COPA, YIPF5, USO1, ARFGAP3, LMAN2, PPP6R1, TMED10*
Functions Unique To T	T-cell activation and differentiation	*CRTAM, RORC, ZFP36L1, TESPA1, BCL6, CD74, NFKBID, IL27RA*
Functions Unique To Tc	Ribosome Biogenesis	*DKC1, NOP56, RRS1, WDR36, NOL6, ZNHIT6, NOP2, URB1, RSL1D1, NOC2L, DDX18, NOB1, RRP15, UTP3, NPM3, PA2G4, SRFBP1, URB2, BMS1, MRPS7, WDR3, NAT10, FTSJ3, IMP4, DDX10, GAR1, LTV1, PAK1IP1, MYBBP1A, FASTKD2, AATF, DHX30, DDX47, RRP1, DCAF13, UTP15, PDCD11, PWP2, WDR75, DDX49, HEATR1, PWP1, MRPL36, UTP20, TFB2M, EMG1, PPAN, RRP9, UTP14A, NMD3, DDX56, EXOSC5, RPF1, RCL1, NLE1, KRR1, RRP1B, RRP7A, FCF1, MPHOSPH10*
	RNA splicing	*PRMT5, QKI, HNRNPF, NCBP2, PRPF19, PUF60, HNRNPU, PPP4R2, RBM14, HNRNPD, AAR2, SRSF10, WDR77, DHX9, DDX47, DHX15, HNRNPK, SRPK1, SRRT, DDX1, RNPS1, HNRNPM, PLRG1, GTF2F2, HNRNPLL, TGS1, PRPF4, NSRP1, SFPQ, RTCB, FUS, RRP1B, MPHOSPH10*
	RNA transport	*RRS1, NOL6, QKI, XPOT, NCBP2, HNRNPU, LTV1, NUP93, DHX9, NSUN2, NUTF2, LRPPRC, RNPS1, NUP35, PNPT1, NMD3, SSB, SFPQ*

Table 3- 2. Common and unique predicted functions in MAIT cells when activated. Functions predicted from unregulated genes in MAIT cells activated by cytokines (2ng/mL IL12/IL18, 100ng/mL TL1A and 25ng/mL IL15) (C), anti-CD3/CD28 (T) and both (TC)

3.3.5. Transcriptional signatures of TCR-activated MAIT cells predict tissue-repair functions

Given the range of functions driven by TCR and cytokines in other innate-like T-cells, we asked whether MAIT activity extended beyond the previously reported inflammatory and anti-microbial responses. Belkaid's group described a population of skin-homing unconventional T-cells in mice that displayed simultaneously anti-microbial and tissue-repair functions (Linehan *et al.* 2018). In functional assays, these T-cells were able to accelerate wound closure. This population have many similarities to MAIT cells, such as type-17 functions, innate-like phenotype, and reactivity to commensal formylated ligands presented by the non-classical MHCI receptor H2M3. Therefore, we asked whether MAIT cells also coupled inflammatory and anti-microbial function with tissue-repair and homeostasis.

Using Gene Set Enrichment Analysis (GSEA) on the total list of differentially expressed genes by activated MAIT cells, we found that upon stimulation with both anti-CD3/CD28 and cytokines (TC), there is a concomitant increase of inflammatory **(Figure 3- 7A)** and immunosuppressive functions **(Figure 3- 7C)**. These gene lists were obtained from the Gene-Ontology library of biological processes (GO:0006954 and GO:0002683, respectively). In addition, we run GSEA using the tissue-repair gene list compiled in Linehan et al. 2018 (**Table 3- 3**) and found upregulation of this gene signature in T and TC stimulated MAIT cells **(Figure 3- 7B)**. In 2-way scatter plots, we annotated the leading-edge genes from the GSEAs with the 3 different transcriptional programs. The leading edge for the immunosuppressive signature contained checkpoint markers such as CTLA4, PDL1 and Treg markers such as FOXP3 **(Figure 3- 7F)**. On the other hand, while the tissue-repair signature is not significant (p-adj of 0.07), the upregulation of genes such as Furin, TNF, CSF1, CCL3, among others including various growth factors such as VEGF and PDGF suggests that this gene signature could be genuine **(Figure 3- 7E, J)**.

The tissue-repair transcriptional signature was only close to significant in MAIT cells when triggered in the presence of TCR ligation (T and TC) but not by cytokines alone (C) **(Figure 3- 7G-I)**. Upon close analysis of volcano plots (**Supplementary Figure 3- 2**), we found that both TCR ligation and cytokines can upregulate some tissue-repair linked genes; however, cytokine signalling also had a negative regulation on other tissue-repair genes. Because of this, in the global statistical aggregate of the GSEAs, T and TC conditions had a p-adjust < 0.1 but not in the C condition.

Tissue-repair list

ANGPT1	*DEFB1*	*HGF*	*MMP25*	*VEGFB*
ANGPT2	*DEFB6*	*HIF1A*	*MMP28*	*VEGFC*
ANGPT4	*DHH*	*HMGB1*	*NGF*	*WNT1*
AREG	*DISP1*	*IGF1*	*NRG1*	*WNT2*
BMP2	*DLL1*	*IGF2*	*NRG2*	*WNT2B*
BMP4	*DLL3*	*IHH*	*NRG3*	*WNT3*
BMP7	*DLL4*	*IL1A*	*NRG4*	*WNT3A*
BTV	*EGF*	*IL1B*	*PDGFA*	*WNT4*
CCL2	*EPGN*	*IL6*	*PDGFB*	*WNT5A*
CCL3	*EREG*	*INHBA*	*PDGFC*	*WNT5B*
CHAT	*FGF1*	*INHBB*	*PGF*	*WNT6*
CSF1	*FGF2*	*JAG1*	*PTGES2*	*WNT7A*
CSF2	*FGF7*	*JAG2*	*SHH*	*WNT7B*
CTGF	*FGF10*	*LEP*	*TGFA*	*WNT8A*
CXCL1	*FGF22*	*MMP1A*	*TGFB1*	*WNT8B*
CXCL2	*FIGF*	*MMP2*	*TGFB2*	*WNT9A*
CXCL10	*FLG*	*MMP3*	*TGFB3*	*WNT10A*
CXCL12	*FLG2*	*MMP10*	*THBS1*	*WNT10B*
CXCL15	*FURIN*	*MMP13*	*TNF*	*WNT11*
CYR61	*HBEGF*	*MMP15*	*VEGFA*	*WNT16*

Significantly upregulated genes in TC vs US comparison

Significantly downregulated genes in TC vs US comparison

Table 3- 3. List of tissue-repair genes compiled by Linehan *et al.* Highlighted the genes that are upregulated (Blue) and downregulated (Orange) in the TC condition (1.25µg/mL anti-CD3/CD28, 2ng/mL IL12/IL18, 100ng/mL TL1A and 25ng/mL IL15) when compared to the unstimulated (UT) condition.

Upregulated genes in TC vs US

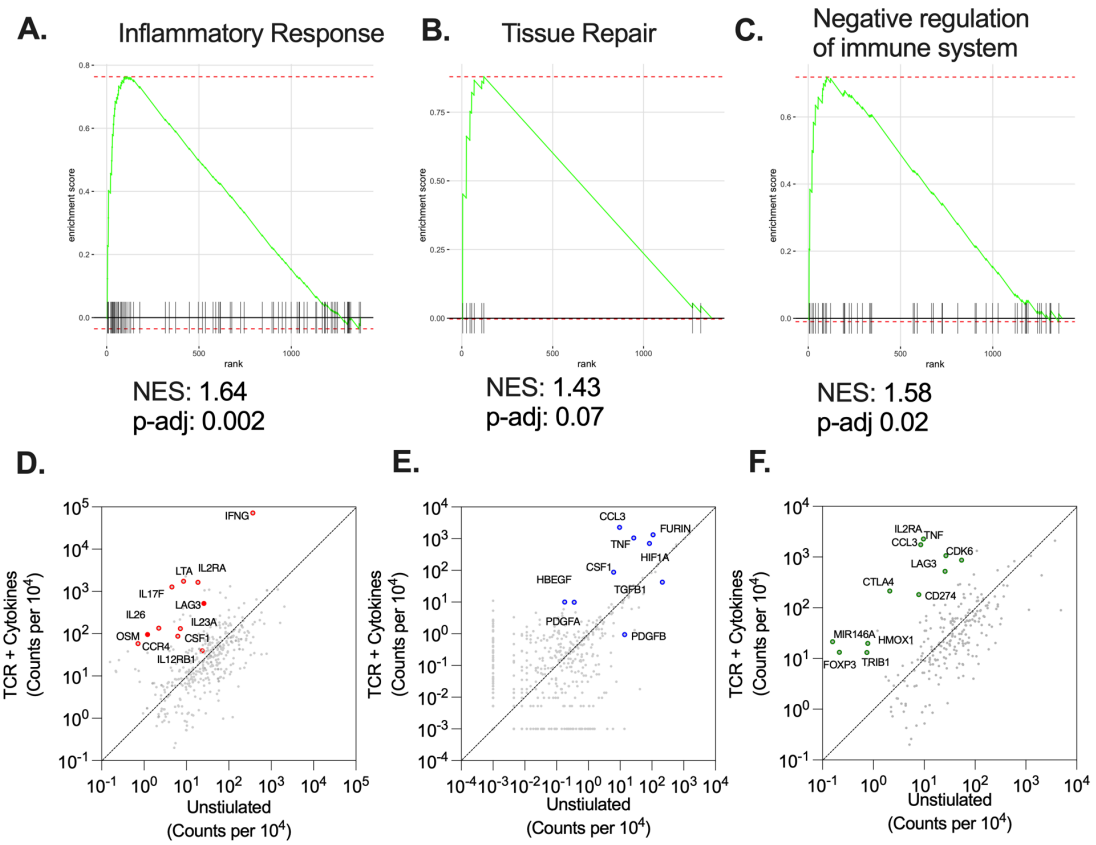

GSEA with Tissue Repair gene list

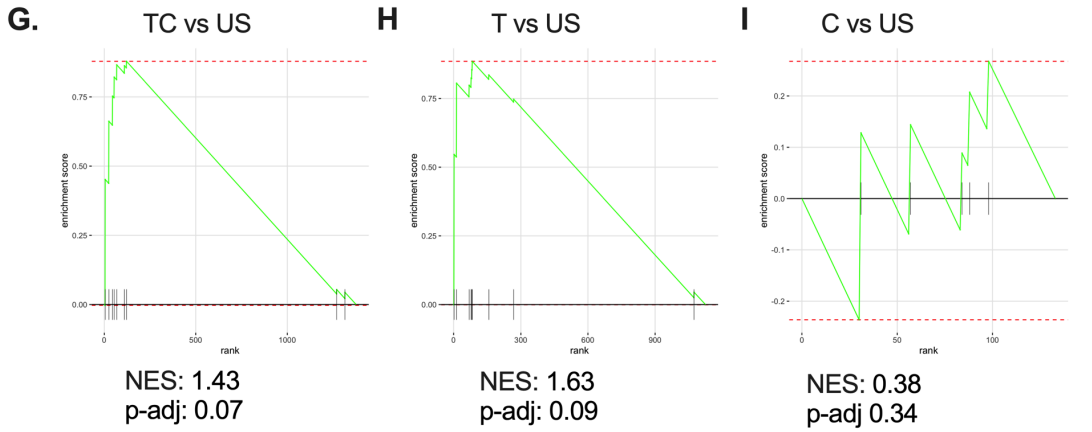

J.

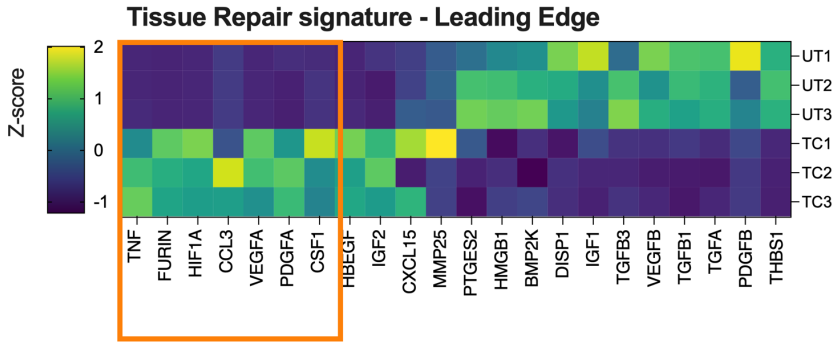

Figure 3- 7. MAIT cells can simultaneously elicit inflammatory, tissue-repair and immunoregulatory functions.

(A-C) Gene Set Enrichment Analysis (GSEA) of upregulated genes in MAIT cells by concomitant activation with anti-CD3/CD28, 2ng/mL IL12/IL18, 100ng/mL TL1A and 25ng/mL of IL15 (TC). Modulated genes were compared against Inflammatory (**A**), tissue-repair (**B**) and Negative regulation of the immune system (**C**) gene lists. The inflammatory and Negative regulation of the immune system gene lists originated from the GO-Term library of biological processes and, the tissue-repair gene list was compiled by Linehan *et al*. (see **Table 3- 3**).

(**D-F**) 2-way scatter plots of the differentially expressed genes in TC compared to the unstimulated condition (US) with underlined leading-edge genes from the Inflammatory (**D**), tissue-repair (**E**) and Negative regulation of the immune system (**F**) GSEAs.

(**G-I**) GSEAs of the tissue-repair gene list against the upregulated genes in the TC (**G**), anti-CD3/CD28 mediated (**H**) and cytokine (IL12/IL18 and TL1A/IL15) mediated stimulation (**I**) when compared to the US condition. (**J**) Heatmap of the tissue-repair leading-edge genes in the TC and US samples. Colour scheme represents z-score.

RNAseq data were analysed with R using DESeq2, ClusterProfiler, fgsea and VennDiagram packages.

3.3.6. MAIT cells can express Th17 and tissue-repair associated proteins during longer stimulation with *E.coli*

To validate the RNAseq analysis, we used flow cytometry to study if the transcriptional upregulation of tissue-repair genes also translated in terms of protein expression. To replicate the activation that MAIT cells would receive *in vivo*, we co-cultured CD8 cells with THP1 monocytic target cells in the presence of fixed *E.coli*. In these co-cultures, fixed bacteria are phagocyted and processed by THP1 cells to extract bacterial ligands, many of which are then presented by MR1 as intermediates of the riboflavin synthesis pathway (Harriff *et al.* 2016; Karamooz *et al.* 2019). In addition, the presence of microbes also is detected by TLRs from THP1 cells, which generates TCR-independent signals (**Figure 3- 4A**). Additionally, this experimental set up provides a natural trigger that mimics the TC condition from the bulk RNAseq data. In titration experiments, 25 BpC was the optimal ratio for IFNγ and TNFα expression in MAIT cells (**Figure 3- 8A, B**). Higher BpC led to cell death and reduced THP1 and MAIT cell populations. In our experiments, MAIT cells had a more robust activation with *E.coli* than with 5OPRU; however, bacteria-mediated activation could not be entirely blocked with anti-MR1 (**Figure 3- 8C**), indicating a partial TCR-independent effect. Blocking with anti-IL12 and anti-IL18 reduced the *E.coli*-mediated activation to the same level as with 5OPRU (**Figure 3- 8E**). On the other hand, THP1 cells exposed to 5OPRU or *E.coli* could also activate small populations of non-MAIT T-cells (**Figure 3- 8D**). These results could be caused by bystander activation of T-cells caused by MAIT activation or, because the non-MAIT compartment also contains fractions of MR1-restricted T-cells.

To optimise our activation assays, we did a time-course analysis to find the optimal timepoint post-stimulation to measure the production of tissue-repair proteins. TCR stimulation by either 5OPRU or fixed *E.coli*, but not with IL12/IL18 alone, induced a progressive increase of IL17A and IL17F expression in MAIT cells at longer stimulatory

timepoints up to 72h (**Figure 3- 8F, G, H**). The same pattern was observed, but to a lesser extent, with the expression of Furin (**Figure 3- 8F, I**).

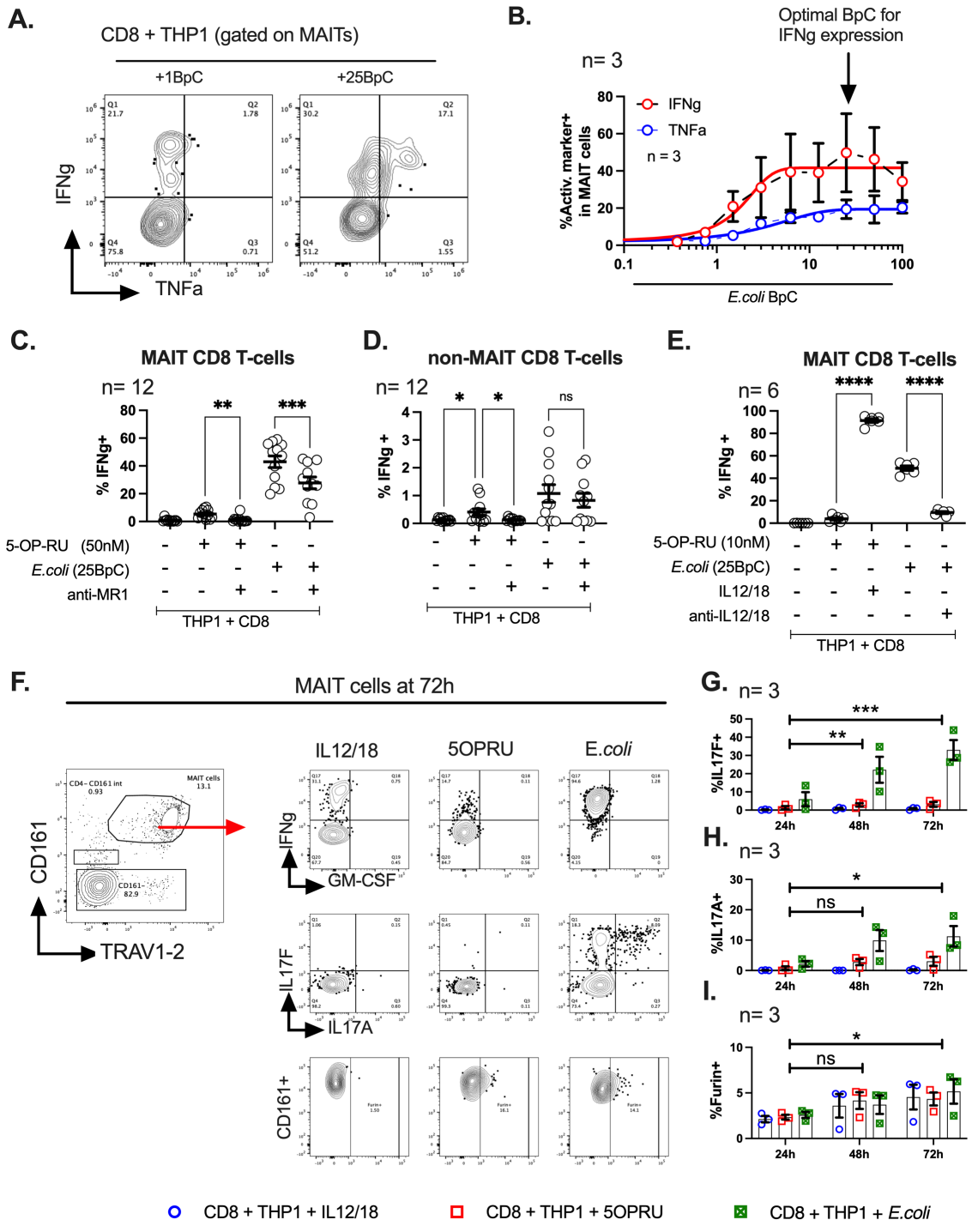

Figure 3- 8. Optimal MAIT activation for Th17 and tissue-repair functions require longer stimulations with *E.coli*.

(**A-E**) Purified CD8 T-cell were incubated overnight with THP1 cells with 0.5 to 100 fixed BpC or 10-50nM 5OPRU. Representative FacsPlots (**A**) and frequencies (**B**) of IFNγ (Red) and TNFα (Blue)

expression in MAIT cells activated by *E.coli* plotted in a titration curve. Frequencies of IFNγ expression in CD8+ MAIT cells (**C**) and non-MAIT cells (**D**) activated by 50nM 5OPRU or 25BpC *E.coli* in the presence or absence of 5μg/mL of anti-MR1. In (**E**) 10nM 5OPRU stimulation was supplemented by 50ng/mL of IL12/IL18 and, *E.coli* stimulation was blocked with 5μg/mL of anti-IL12/IL18.
(**F-I**) Purified CD8 T-cells were stimulated with THP1 in the presence of cytokine (Blue, 50ng/ml IL12/IL18), TCR (Red, 10nM 5OPRU) stimulus or both (Green, 25BpC) for 24h, 48h and 72h. Representative FacsPlots at 72h (**F**) and frequencies of IL17F (**G**), IL17A (**H**) and Furin (**I**) expression in MAIT cells during the time course from 24h to 72h.
Data were acquired in 2-3 independent experiments. Every datapoint is a biological replicate. Error bars represent Mean ± SEM. Differences among conditions in Figure **A-E** were analysed by Friedman's test with uncorrected Dunn's test. *p < 0.05, **p < 0.01, ***p < 0.001, ****p < 0.0001. Differences among conditions in **F-I** were analysed by RM 2-way ANOVA with uncorrected Fisher's LSD test. *p < 0.05, **p < 0.01, ***p < 0.001, ****p < 0.0001.

3.3.7. Flow cytometry experiments validated the upregulation of the tissue-repair program in MAIT cells

Activation assays with *E.coli* upregulated TNFα, Furin and CCL3 in MAIT cells. These responses were TCR-dependent as they could be fully and partially abrogated with anti-MR1 blocking at 20h and 72h, respectively (**Figure 3- 9A-E**). In addition, other proteins associated with tissue-repair, such as GM-CSF (CSF2), were also seen upregulated in extended cultures (72h) but not at 20h (**Figure 3- 9F**). GM-CSF was not present in the leading edge of our GSEAs and this could be explained because the transcriptomic dataset was generated after 20h MAIT stimulation, a timepoint at which many proteins from the tissue-repair program may be upregulated below detection levels.

Flow cytometry staining for other molecules from the leading edge (HIF1A, PDGFα, VEGF and CSF1) was challenging due to the lack of reliable reagents. Instead, some of these factors were measured from the supernatants of pure MAIT cells activated with anti-CD3/CD28 and IL12/IL18 (50ng/mL) for 72h using a LegendPlex kit from BioLegend. In the supernatants from activated MAIT cells, we found increased quantities of GM-CSF, VEGF, PDGFα and TGFα (**Figure 3- 9G**). Despite the low power in this experiment (3 donors), these results align with those previously attained in a setting where purified TRAV1-2+ cells were triggered by THP1, 5OPRU and cytokines (**Supplementary Figure 3-3**).

We did not detect any significant change in M-CSF (CSF1) concentration in response to anti-CD3/CD28 and IL12/IL18. The lack of statistical significance for this leading-edge protein could be attributed to the low experimental power (upregulation noted in 2 out of 3 donors). This result also underscores the fact that transcriptional changes do not always correspond to translational changes as there may be other factors involved, such as timing, activation co-factors and cross-regulation with other cellular pathways.

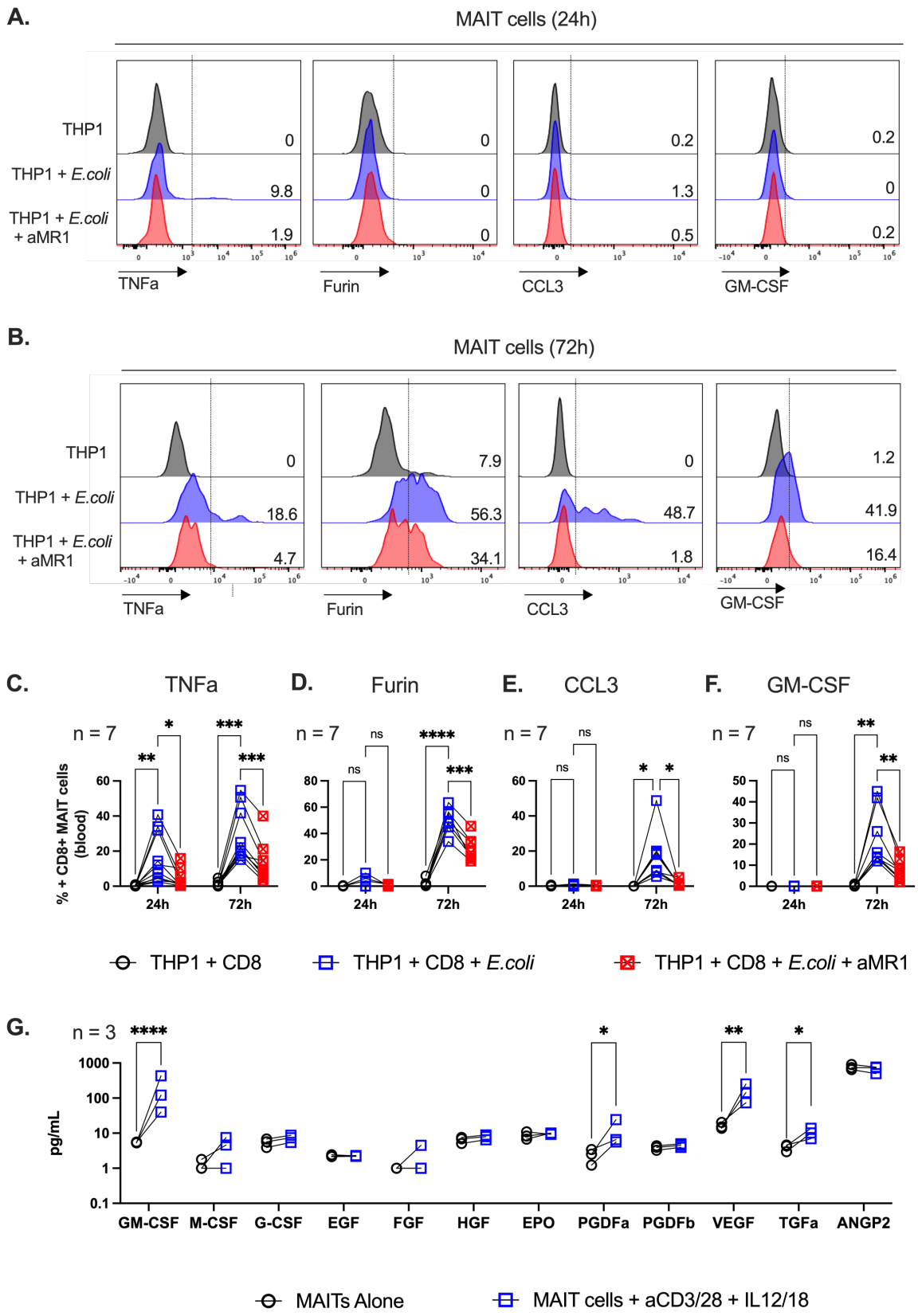

Figure 3- 9. MAIT cells elicit 5 out of 7 proteins from the tissue-repair leading-edge GSEA in prolonged cultures in the presence of bacteria.

(**A-F**) Purified CD8 T-cells were incubated with THP1 cells with 25BpC overnight (20h) or in prolonged cultures (72h). Representative histograms at 20h (**A**) and 72h (**B**) and, frequencies of TNFα (**C**), Furin (**D**), CCL3 (**E**) and GM-CSF (**F**) expression in CD8+ MAIT cells at 20h and 72h. Conditions are: CD8 T-cells incubated with THP1 cells without stimulus (Black), with *E.coli* stimulation in the absence (Blue) or presence (Red) of 5μg/mL anti-MR1.
(**G**) LegendPlex bead mediated quantification of tissue-repair growth-factors in 72h supernatants resulting from pure MAIT cells unstimulated (Black) and activated with 1.25μg/mL plate bound anti-CD3/CD28 and 50ng/mL IL12/IL18 (Blue).
Data in panels **A-F** were acquired in 2-3 independent experiments. Data in **G** were acquired for 3 donors in 1 single experiment. Every datapoint is a biological replicate. Error bars represent Mean ± SEM. Error bars represent Mean ± SEM. Differences among conditions were analysed by RM 2-way ANOVA with uncorrected Fisher's LSD test. *$p < 0.05$, **$p < 0.01$, ***$p < 0.001$, ****$p < 0.0001$.

3.3.8. Activated MAIT cells can accelerate wound-healing in a TCR-dependent manner

To assess whether the changes in protein expression had a functional effect, we conducted *in vitro* wound-healing assays where we generated scratches in monolayers of CACO2 cells, an intestinal epithelial cell line. In these assays, we measured the speed of recovery of these monolayers in the presence or absence of activated MAIT supernatants. These supernatants were harvested from 72h co-cultures of MAIT-rich CD8 cells with THP1 and fixed *E.coli* (**Figure 3- 10A, B**) and were added to the CACO2 monolayers at a 1:2 dilution with fresh media. CACO2 cells were used in this assay instead of other monolayer forming cells, such as HeLa, because they represent a better model for gut tissue, and their proliferation rate is slow, thus allowing us to measure the effects of supplemented supernatants. To measure the wound closure rate, images were taken every 4h, and the area of the wounds was measured and compared to the wound size and time 0 (before MAIT supernatants were added).

Supplemented supernatants significantly accelerated the recovery of the CACO2 monolayer compared to non-supplemented media. Furthermore, this effect was reduced in supernatants where MAIT activation was partially blocked with anti-MR1, emphasising the importance of the TCR-mediated signals in wound-healing (**Figure 3- 10B-D**. This result demonstrates that MAIT cells have the potential to orchestrate tissue homeostasis and repair, although the mechanisms behind these functions are still unknown.

In our *in vitro* model, supernatants from stimulated THP1s (without any MAIT cells) could also accelerate, but to a lesser extent, the recovery of CACO2 monolayers (**Figure 3- 10D**). This observation raises the question of whether the MAIT secretome directly affects the increased migration and proliferation of epithelial cells or if MAIT cells boost the homeostatic functions of bystander cells, such as THP1, in our *in vitro* system.

Images were analysed with ImageJ v1.8 (https://imagej.nih.gov/ij/index.html) to determine the area of wounds and normalise them as a percentage of the initial area.

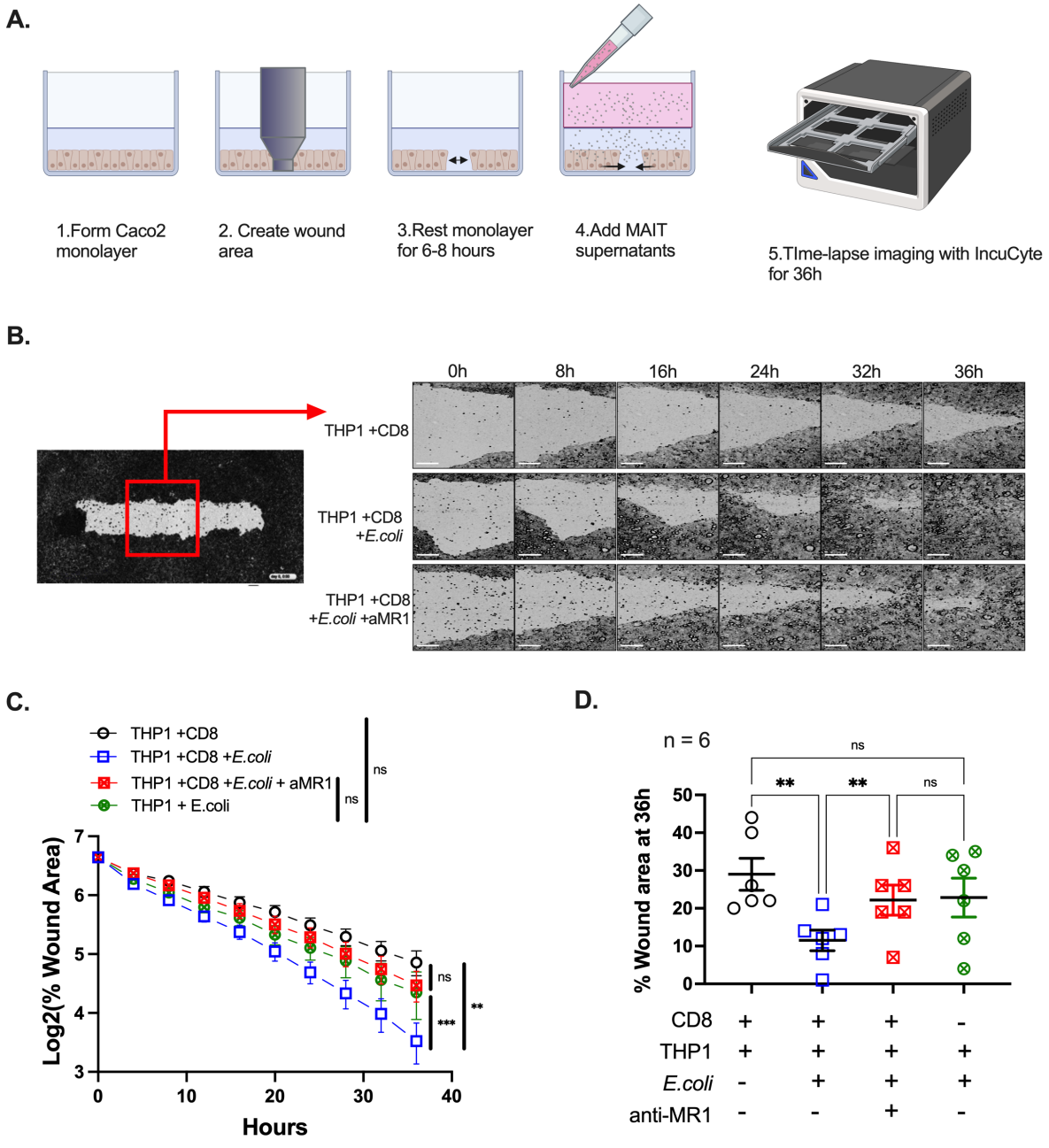

Figure 3- 10. Supernatants from MAIT cells activated with *E.coli* accelerate the recovery rate of epithelial monolayers. Supernatants from purified CD8 T-cell incubated for 72h with THP1 cells in the presence of *E.coli* (25BpC) were added on to scratched CACO2 epithelial monolayers. (**A**) Diagram of wound-healing assay where CACO2 monolayers are scratched, rested and, allowed to recover in the presence of MAIT supernatant during a 36h time-lapse imaging process conducted

in the IncuCyte at 37ºC. (**B**) Representative images of scratch in the epithelial monolayer (right) and time-lapse imaging of the recovering monolayer with different MAIT supernatants.
(**C**) Area of the wound (as a percentage of the are at Time = 0) during the time-lapse imaging with supernatants from unstimulated THP1 and CD8 T-cells (Black), stimulated with fixed *E.coli* in the absence (Blue) or presence (Red) of 5μg/mL anti-MR1 and, THP1 cells alone stimulated with fixed *E.coli* without T-cells (Green). (**D**) Area of the wound (as a percentage of the area at Time = 0) at 36h of incubation. Data from 6 biological replicated were acquired in 2-3 independent experiments. Every datapoint corresponds to a different donor and represents the mean of 3 technical replicates. Error bars represent Mean ± SEM. Differences among conditions were analysed by RM 2-way ANOVA with uncorrected Fisher's LSD test. *p < 0.05, **p < 0.01, ***p < 0.001, ****p < 0.0001. Scale bars are 250um.

3.3.9. Activated MAIT cells elicit paracrine effects on monocytic cells *in vitro*

The wound-healing assay showed an MR1-dependent accelerated recovery of the epithelial monolayer; however, it is yet unclear if this effect is directly driven by factors secreted by MAIT cells or whether MAIT cells coordinate a homeostatic signal amplification through paracrine effects on neighbouring immune cells, such as THP1 cells in our *in vitro* model. In *in vivo* settings, monocytes and macrophages are deeply involved in all stages of injury, from inflammatory response to wound-healing and injury resolution (Willenborg *et al.* 2012; Ramachandran, Iredale and Fallowfield 2015; Hos *et al.* 2016; Wynn and Vannella 2016).

We asked if THP1 cells underwent any phenotypical changes in response to MAIT activation. Following the proposed model by Wynn *et al.* (Wynn and Vannella 2016), we have characterised THP1 cells as inflammatory if they expressed IL1β, upregulated the phosphorylation of STAT1-Y701 and surface levels of HLA-DR; as wound-healing, if they express VEGF, PDGF and upregulate phosphorylation of STAT6-Y641 and surface levels of IL4R; and finally, as injury resolving if they express IL10, and upregulate the surface levels of IL10R and the phosphorylation of STAT3-Y705.

In our experiments, we have found a 5OPRU-MR1 dependent phosphorylation of STAT1, STAT6 and STAT3 in response to MAIT activation after 20h incubation, therefore indicating that all 3 phenotypes can be prompted by activated MAIT cells (**Figure 3- 11A, C, E, F**). In this result, it was unclear whether THP1 cells are adopting a mixed phenotype or if THP1 cells are being polarised into 3 different populations. This question could be answered by co-staining with anti-pSTAT1, anti-pSTAT3 and anti-pSTAT6 conjugated with different fluorochromes however, these reagents were not available to us at the time of the study. Moreover, in line with the pSTAT1 and pSTAT6 results, HLA-DR and IL4R surface markers, corresponding to the inflammatory and wound-healing phenotype, were also upregulated due to MAIT activation (**Figure 3- 11A, B, D**).

In further analysis of THP1 cells, we also observed an increased frequency of dead cells caused by MAIT cell activation (**Supplementary Figure 3- 4**). In the case of 5OPRU-driven MAIT activation, THP1 cell death is milder than in the case of *E.coli* and, it can be fully blocked with anit-MR1 (**Supplementary Figure 3- 4B-C**). The increased THP1 cell death with fixed *E.coli* could be attributed to cytokine driven inflammation, because it cannot be entirely prevented with anti-MR1 (**Supplementary Figure 3- 4B-C**); adding IL12/IL18 to 5OPRU increased the frequency of dead THP1 cells and reduces their counts (**Supplementary Figure 3- 4D-E**). These results align with the weaker inflammatory potential observed previously in MAIT cells under TCR trigger in comparison to simultaneous or single trigger by cytokines.

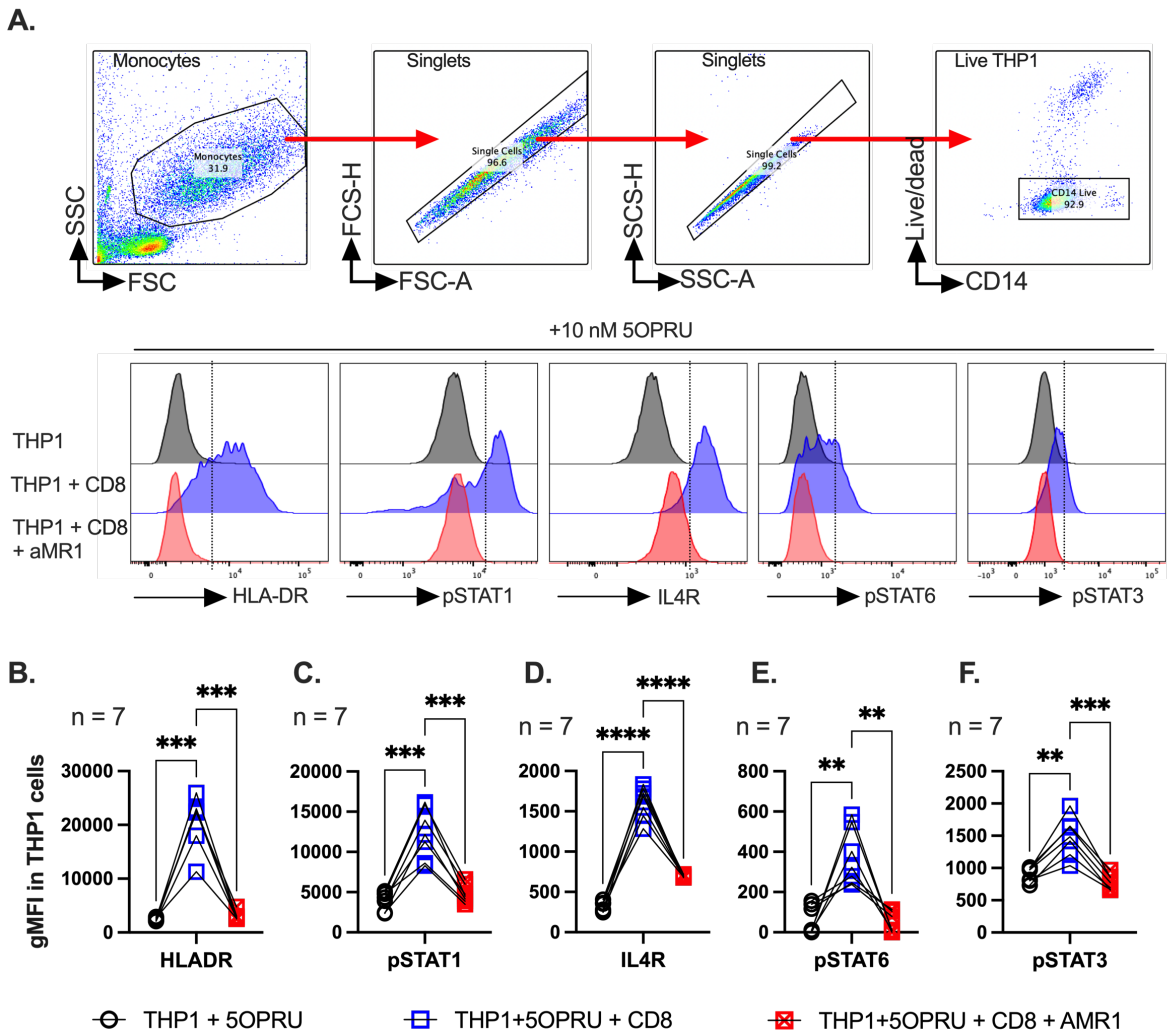

Figure 3- 11. MAIT cell activation can polarise THP1 monocytic cells to adopt inflammatory, tissue-repair or injury resolutive phenotypes. (A-F) Purified CD8 T-cells were incubated overnight

(20h) with THP1 cells with 10nM 5OPRU. Gating strategy of THP1 cells and representative histograms (**A**) and geometric means corresponding to the expression of HLA-DR (**B**), pSTAT1 (**C**), IL4R (**D**), pSTAT6 (**E**) and pSTAT3 (**F**) in THP1 cells when they are alone with 5OPRU (Black), in the presence of MAIT-rich CD8 T-cells in the absence (Blue) or presence (Red) of 5μg/mL of anti-MR1.
Data were acquired in 2-3 independent experiments. Every datapoint is a biological replicate. Error bars represent Mean ± SEM. Differences among conditions were analysed by RM One-way ANOVA with uncorrected Fisher's LSD test. *p < 0.05, **p < 0.01, ***p < 0.001, ****p < 0.0001.

3.3.10. MAIT cells can produce anti-inflammatory molecules upon TCR activation

We next questioned how MAIT cells could cause surface upregulation of IL4R and phosphorylation of different STAT molecules. Phosphorylation of STAT1, STAT3 and STAT6 are downstream of the IFNγ receptor (IFNGR), IL4R and IL10R, respectively (Stütz *et al.* 2003; Nakamura *et al.* 2015; Rahal *et al.* 2018; Yin *et al.* 2018; Chen *et al.* 2019), thus hinting potential expression of anti-inflammatory cytokine by activated MAIT cells. While Th1 functions have already been characterised in MAIT cells, expression of Th2 and Treg-associated anti-inflammatory cytokines such as IL4, IL13 and IL10 have not been previously described.

Expression of IL4 and IL13 cytokines was not seen in MAIT cells activated by TCR-ligation, cytokines, or a combination of the 2 (**Figure 3- 12B**). Addition of PMA/ionomycin 3 hours before harvesting T-cells also did not make any change, which suggests that circulating MAIT cells do not have the inherent capacity (not at transcriptional nor translational level) to produce these cytokines from steady-state or after 20h (**Figure 3-12B**) or 72h of stimulation (Data not shown). As a positive control, CD4 T-cells displayed the ability to produce IL4 (0.5%) and IL13 (1-2%) with only PMA/ionomycin after 3h stimulation or after 20h incubation with TCR and cytokine stimuli (**Figure 3- 12A, E, F**).

PMA/ionomycin on its own did not induce any IL10 expression after 3h incubation (**Figure 3- 12C**); however, TCR priming prompted the expression of IL10 in MAIT cells at 20h timepoint (**Figure 3- 12D, G**). After TCR activation, IL10 expression was further enhanced by PMA/ionomycin. On the other hand, virtually no IL10 expression was observed with IL12/IL18 stimulation. These results suggest that while circulating MAIT cells are not poised or do not have available tools to produce IL10, TCR signalling can unlock this function. The expression of IL10 in MAIT cells (5% frequency) was significantly higher than in CD4 T-cells (**Figure 3- 12G**).

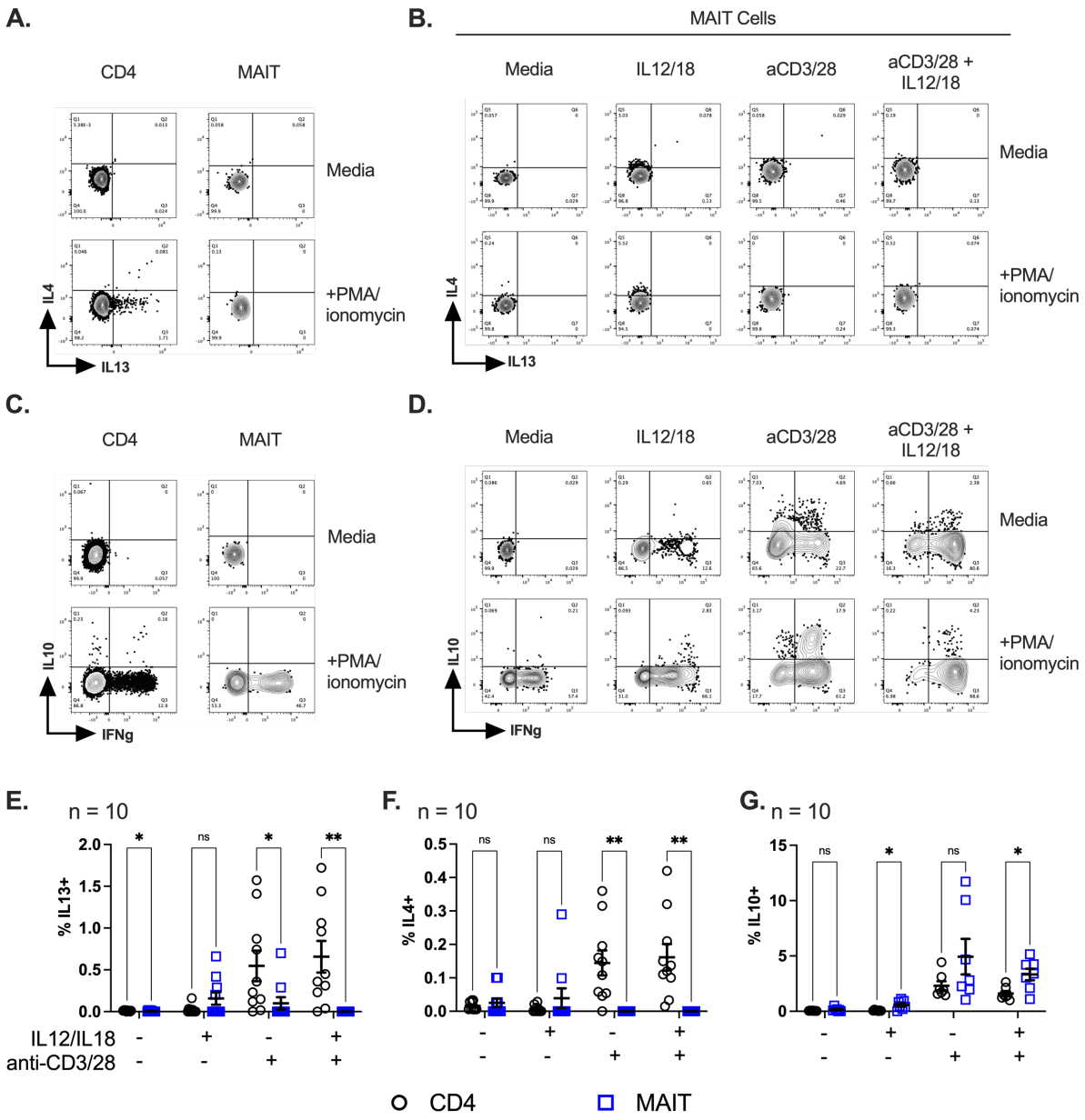

Figure 3- 12. MAIT cells can produce anti-inflammatory cytokines under TCR trigger. PBMCs were triggered overnight (20h) with cytokines (50ng/mL IL12/IL18), with 1.25μg/mL plate-bound anti-CD3/CD28 and a combination of the 2 in the presence or absence of PMA/ionomycin (20ng/mL and 1μM, respectively), which was added 3h before harvesting and analysing MAIT cells.
(**A, C**) Representative FacsPlots of baseline expression of IL4 and IL13 (**A**) and IFNγ and IL10 (**C**) in CD4 and MAIT cells at steady-state and with PMA/ionomycin. (**B, D, E-G**) Representative FacsPlots of MAIT cells (**B, D**) and frequencies of IL13 (**E**), IL4 (**F**) and IL10 (**G**) expression in MAIT cells (Blue) and CD4 T-cells (Black) when they are activated with cytokines, TCR-ligation, or both. Data were acquired in 2-3 independent experiments. Every datapoint is a biological replicate. Error bars represent Mean ± SEM. Differences among conditions were analysed by RM 2-way ANOVA with uncorrected Fisher's LSD test . *p < 0.05, **p < 0.01, ***p < 0.001, ****p < 0.0001.

3.3.11. Expression of IL10 in MAIT cells is tightly regulated in the presence of bacterial infections

To further validate the IL10 expression in MAIT cells, purified CD8 T-cells were stimulated with THP1 in the presence of MR1 ligands. 5OPRU triggered either IFNγ or IL10 expression in MAIT cells, pointing at two different routes of polarisation (**Figure 3-13A, B**). This expression of IL10 could be abrogated with anti-MR1 (**Figure 3- 13B**). When cytokine signalling was added on top of 5OPRU, there was a marginal increase in the frequency of IL10-producing MAIT cells, and half of them became double positives (IFNγ+ IL10+) (**Figure 3- 13A, C**).

While *E.coli* is a more potent stimulus than 5OPRU for the expression of IFNγ and many tissue-repair factors, it could not trigger IL10 production in MAIT cells (**Figure 3-13B**). Blocking the cytokine component of *E.coli*-mediated stimulations with anti-IL12, anti-IL18 and anti-IFNγ did not rescue the IL10 production in MAIT cells (**Figure 3- 13C**). The inability of circulating MAIT cells to produce IL10 in response to bacterial infection may suggest that this function is probably not part of the tissue-repair module and that IL10 expression might follow a different modulation mechanism than IFNγ or the tissue-repair factors.

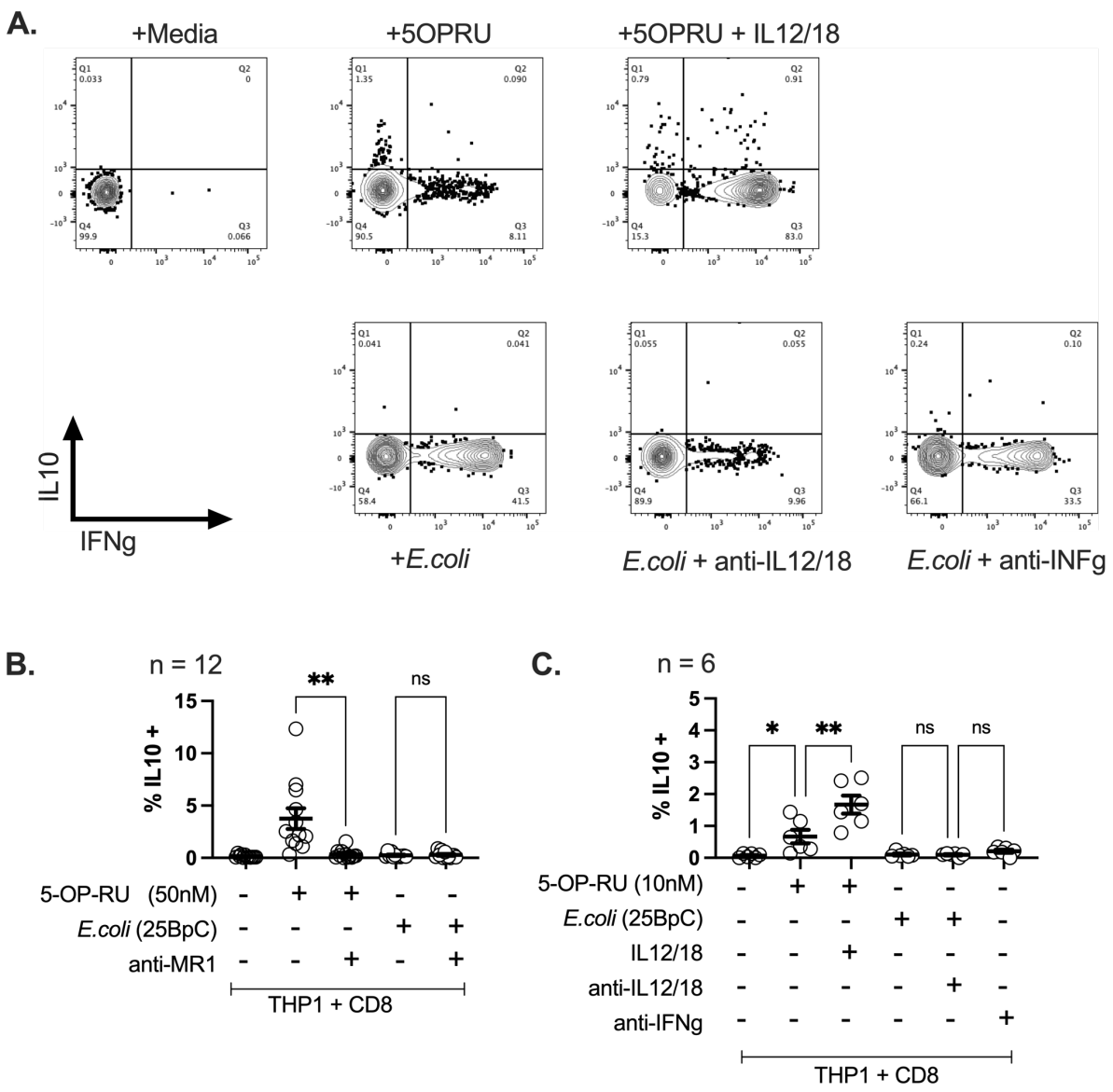

Figure 3- 13. Expression of IL10 in MAIT is tightly regulated in the presence of bacterial infections.

(**B**) Purified CD8 T-cells were stimulated overnight (20h) with THP1 in the presence of 50nM 5OPRU, 25BpC *E.coli* with or without 5μg/mL anti-MR1.

(**A, C**) CD8 T-cell stimulation with 10nM 5OPRU was supplemented with 50ng/mL IL12/IL18. On the other hand, *E.coli* mediated stimulation was blocked with anti-IL12/IL18 or anti-IFNγ. Representative FacsPlots (**A**) and frequencies (**C**) of IL10 expressing T-cells in MAIT cells after 20h stimulation.

Data were acquired in 2-3 independent experiments. Every datapoint is a biological replicate. Error bars represent Mean ± SEM. Differences among conditions were analysed by RM One-way ANOVA with uncorrected Fisher's LSD test. *p < 0.05, **p < 0.01, ***p < 0.001, ****p < 0.0001.

3.3.12. MAIT cells also have immunosuppressive functions as they inhibit the proliferation of bystander T-cells

The production of IL10 in MAIT cells is congruent with the positive regulation of immunomodulatory genes such as FOXP3, CTLA4, and PDL1 from RNAseq datasets generated in the Klenerman lab (**Figure 3- 7F**). Although transcriptional upregulation of the IL10 gene was not detected in our own RNAseq datasets, another study conducted with human MAIT cells by James Usher's lab showed significant transcriptional upregulation in both *E.coli* and 5OPRU stimulation (Lamichhane *et al.* 2019). The simultaneous upregulation of several regulatory genes at the RNA level may point to an unexplored immunoregulatory module in MAIT cells.

To investigate this, we set up preliminary proliferation assays with pan-triggered T-cells in the presence or absence of MAIT cells. To generate MAIT depleted samples, we removed the TRAV1-2+ fraction from panT-cells while MAIT enriched samples were spiked with autologous TRAV1-2+ T-cells (**Figure 3-14A**). These different samples were pre-stained with cell-trace-violet (CTV) and proliferation was assessed after 5 days under mild stimulation (plate-bound 0.25μg/mL anti-CD3). There was a significantly lower proliferation in the non-MAIT T-cell fraction (TRAV1-2-) of samples enriched with MAIT cells (**Figure 3-14B**). This could also be observed in CD4+, CD8+ and CD161+ sub-populations within the TRAV1-2- (or Vα7.2-) cells (**Figure 3-14A, C-E**).

While this result was consistent across 3 different experiments, the degree of inhibition in MAIT enriched samples did not strongly correlate with their MAIT frequency (**Figure 3-14F**). This result could be attributed to donor-to-donor variance however, experimental artifacts such as the total number of plated T-cells could have also influenced the level of proliferation. This experiment should be revised in a more accurate setting where the total number of cells in MAIT-enriched and -depleted samples

is consistent. This could be achieved by spiking an irrelevant T-cell population into MAIT depleted samples.

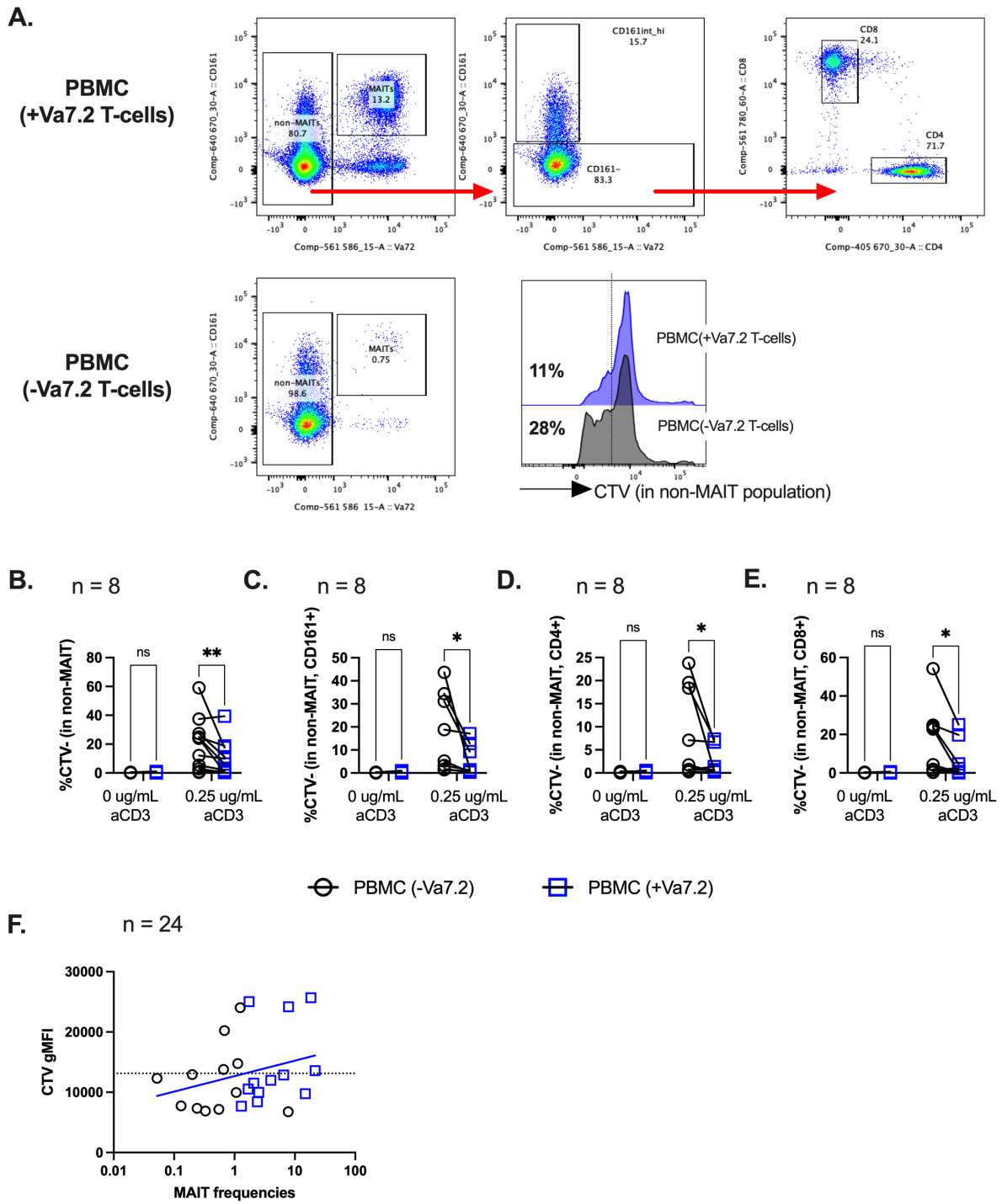

Figure 3- 14. TCR activated MAIT cells can dampen the proliferation of neighbouring activated T-cells. Purified TRAV1-2+ (or Vα7.2+) T-cell were isolated from PBMCs. Purified PanT-cells were depleted (PBMC -Vα7.2) or spiked with the previous isolated TRAV1-2+ fraction (PBMC +Vα7.2). Samples were pre-stained with CTV and activated with plate-bound 0.25μg/mL anti-CD3 for 5

days with media exchange on day 3. Gating strategy of different T-cell compartments and representative histograms (**A**) and frequency of CTV- T-cell in the total non-MAIT T-cells fraction (**B**), and the CD161+ (**C**) CD4+ (**D**) and CD8+ (**E**) fractions as shown in the gating strategy in (A). PBMC -Vα7.2 (Black) and PBMC +Vα7.2 (Blue). (**F**) Scatter plot of MAIT frequency and the proliferation level (gMFI of CTV) of the non-MAIT fraction.
Data were acquired in 2-3 independent experiments. Every datapoint is a biological replicate. Error bars represent Mean ± SEM. Differences among conditions were analysed by RM One-way ANOVA with uncorrected Fisher's LSD test. *p < 0.05, **p < 0.01, ***p < 0.001, ****p < 0.0001.

3.4. Discussion

From previous work in the Klenerman lab, CD161 expressing T-cells have been of interest as they share the common trait of being responsive to cytokine stimulus without TCR signalling (Fergusson *et al.* 2014). In circulating T-cells, MAIT cells represent most of the CD161^{high} population and are easily identifiable by the co-expression TRAV1-2 (or Vα7.2) (**Figure 3- 1E**). 60-80% of MAIT cells are CD8+ (**Figure 3- 1C**); hence our work primarily focused on those cells. It was known from previous reports that MAIT cells can respond to adaptive and innate signals. These findings prompted us to question, both in Dr Leng's thesis and mine, the underlying functional differences between innate and adaptive triggers in MAIT cells.

3.4.1. MAIT cells activation in barrier tissues and blood is boosted by synergies between TCR-dependent and independent triggers

In our *in-vitro* assays, we observed synergies between TCR signalling and sub-optimal levels of IL12/IL18 **(Figure 3- 2**). Sub-optimal levels of IL12/IL18, TL1A or IL15 could not trigger MAIT cells individually; however, they could synergise to induce MAIT activation (**Figure 3- 3**). These results show that synergies not only happen between TCR-dependent and TCR-independent triggers, but also between different types of TCR-independed signalling. Along with previous reports describing similar effects in CD161^{high} CD4+ T-cells with TL1A (Jin *et al.* 2012), these results underline the clinical relevance of TL1A and IL15 in inflammatory bowel disease (IBD) (Liu *et al.* 2000; Prehn *et al.* 2004) as enhancers of inflammation by exacerbating the production of inflammatory molecules such as IFNγ and TNFα.

We observed similar trends in the TCR-dependent and TCR-independent response when comparing MAIT cells from PBMCs and LPMCs (**Figure 3- 5A-C**). One important note

in gut-resident MAIT cells was the dampened inflammatory response with weak IFNγ and TNFα expression, although the IL17 expression was comparable or superior. In addition, LPMC-derived MAIT cells under steady-state had a higher surface expression of PD1 and CD39 exhaustion markers than their PBMC counterpart (Gupta *et al.* 2015; Yong *et al.* 2018),

3.4.2. Tissue-repair gene signature was validated in MAIT cells triggered by bacterial challenge in long cultures

Analysing the bulk transcriptomic data generated at the Klenerman lab, we observed that TCR and cytokine signalling stimulated TNF signalling pathways and enabled crosstalk with myeloid cells. On the other hand, while TCR-dependent stimuli activated pre-wired Th17 functions in MAIT cells, cytokine signalling promoted other biological processes related to cellular secretion and migration (**Figure 3- 6E**). The transcription profile of MAIT cells that have received both cytokine and TCR (TC) clustered closer to the C samples than the T samples in a plane set by the first 2 PCA components, underlining the dominant effect of cytokines over TCR activation (**Figure 3- 6D**).

GSEA analysis showed statistical significance for inflammatory, tissue-repair and immunoregulatory modules in circulating MAIT cells activated by TC (**Figure 3- 7A-F**). The tissue-repair signature was uniquely prompted with TCR ligation (T and TC) but not with cytokines alone (**Figure 3- 7G-J**). Although many of the leading-edge genes of the tissue-repair signature were also found upregulated by cytokines alone, cytokines also caused transcriptional downregulation of many relevant factors and induced many pro-inflammatory molecules (**Supplementary Figure 3- 2**).

Tissue-repair is a conglomeration of several co-occurring mechanisms such as matrix remodelling, revascularisation, regeneration of the damaged tissue and, modulation of the inflammatory microenvironment. Because transcriptional data do not always

correspond with translation and functional data, we validated the expression of the tissue-repair proteins by flow cytometry. Many tissue-repair linked proteins follow the same expression trend as IL17A and IL17F, increasing during prolonged stimulations (**Figure 3- 8F, G**)**.** Among the leading-edge proteins, we validated the expression of CCL3, TNFα, Furin, VEGF and PDGFα (**Figure 3- 9, Supplementary Figure 3- 3**). Furin is a protease that post-translationally cleaves and activates many growth factors such as TGFβ and matrix metalloproteases. In addition, Furin is an important factor in tissue protection and regulatory T-cell (Treg) development in a colitis model (Pesu *et al.* 2008). CCL3, GM-CSF and TNFα are involved with macrophage recruitment and differentiation and, epidermal homeostasis (DiPietro *et al.* 1998; Li *et al.* 2016). VEGF, PDGFα and TGFα are growth stimulating factors that are involved in the process of wound-healing (Schultz *et al.* 1987; Pierce *et al.* 1991, 1995; Schultz, Clark and Rotatori 1991; Eming and Krieg 2006; Fang *et al.* 2007; Wilgus *et al.* 2008).

In functional assays, we observed accelerated wound-healing with supernatant derived from MAIT cells under bacterial challenge (**Figure 3- 10**). In line with this, supporting results were obtained in mice models where improved epidermal recovery was mediated by MR1 and 5OPRU (Constantinides *et al.* 2019). Altogether, these experiments provide strong evidence of wound-healing functions in MAIT cells driven by TCR activation.

3.4.3. MAIT cells elicit immunoregulatory functions

Another aspect of tissue-repair is the suppression of inflammatory cells. In our *in vitro* system, co-cultured THP1 cells had significant phenotypical changes because of MAIT activation. Upon cross-talk with activated MAIT cells, THP1 cells simultaneously upregulated pro-inflammatory, tissue-repair and anti-inflammatory markers as seen by the increased phosphorylation of STAT1, STAT6 and STAT3, respectively (**Figure 3- 11C, E, F**). The dynamics of these phenotypical changes are still unclear; hence future work

should include a time-course study on the phosphorylation state of the different STAT intracellular markers driven by MAIT activation.

In our experiments, we did not detect MAIT cells expressing any Th2 cytokines; however, upon stimulation, they expressed higher IL10 than the CD4 compartment (**Figure 3- 12**). The phosphorylation of STAT3 in macrophages is downstream of the signalling pathways of IL10 (Nakamura *et al.* 2015; Yin *et al.* 2018), which could explain how MAIT cells induce M2 phenotypes in THP1 cells. Conversely, the M1 polarization of THP1 cells could be attributed to the expression of IFNγ and TNFα (Hu and Ivashkiv 2009; Wu *et al.* 2015). MAIT activation also affected negatively the anti-CD3 mediated proliferation of neighbouring T-cells (**Figure 3- 14**). As with macrophages, the T-cell regulation could also be mediated by IL10 (Akdis and Blaser 2001); additionally, other molecules such as VEGF can also be immunomodulatory (Gavalas et al. 2012; Bourhis et al. 2021).

Surprisingly, only 5OPRU but not fixed *E.coli* could trigger IL10 expression (**Figure 3-13**). The production of IL10 was not regulated by pro-inflammatory cues from IFNγ (Hu *et al.* 2006) or cross-regulation by IL12/IL18. Our current results do not answer how MAIT cells can discern the presence of soluble antigens from bacterial infections and, only produce IL10 in sterile conditions; however, these results underline MAIT cells' ability to balance tolerance and homeostasis with antimicrobial functions at barrier tissues. Parallel work by James Usher's group showed that IL10 is transcriptionally upregulated in MAIT cells stimulated with either 5OPRU or fixed *E.coli* (Lamichhane et al. 2019). This observation suggests that the lack of IL10 expression at a protein level following bacterial challenge could be due to post-transcriptional regulation.

3.4.4. Summary

Following Dr Leng's work on MAIT function, in this chapter, we provided evidence that MAIT cells can exert both inflammatory and homeostatic functions in response to TCR activation. Through GSEA predictions, Flow cytometry analysis and *in vitro* functional studies, we validated the tissue-repair transcriptional signature in MAIT cells, which resulted in accelerated wound-healing of epithelial monolayers and modulation of the activity of neighbouring immune cells.

We did not explore the immunoregulatory transcriptional signature in MAIT cells which contained upregulated genes such as CTLA4, PDL1 and FOXP3. This gene signature is likely to be tied to the immunoregulatory data elucidated in this chapter, such as the IL10 and VEGF expression, MAIT-driven regulation of T-cell proliferation and partial polarization of myeloid cells into M2 phenotype. In this chapter, we have not fully explored how this immunoregulatory signature is regulated in circulating and tissue-resident MAIT cells; however, the hyporesponsiveness and higher level of exhaustion markers such as CD39 and PD1 in gut-derived MAIT cells already hint that this module may become more prominent after tissue localisation. Similar results were found in studies conducted by Schmaler *et al*. where circulating MAIT cells clustered separately from gut-resident MAIT cells due to the increased expression of inhibitory receptors in gut-MAIT cells (Schmaler *et al*. 2018).

MAIT cells from barrier tissues, and potentially from the liver, are continuously exposed to MR1-ligands derived from commensal bacteria or the exterior. Taken together, our results and parallel work conducted in Hink's and Ussher's Lab (Hinks *et al*. 2019; Lamichhane *et al*. 2019; Leng *et al*. 2019) show that both human and mice MAIT cells have protective and homeostatic functions at barrier sites when triggered in the absence of TCR-independent signals associated with microbial infection. These results are aligned with later work in Belkaid's group (Constantinides *et al*. 2019), who also

demonstrated tissue-repair functions by MAIT cells in the skin of mice. This model explains why MR1-deficient NOD mice, which do not carry MAIT cells, have a dysfunctional mucosa and increased susceptibility to autoimmune diseases because of poor barrier integrity (Rouxel *et al.* 2017). Also, in IBD patients with compromised barrier integrity in the gut mucosa, MAIT activation was exacerbated compared to healthy patients; however, it is still unclear if this MAIT hyperresponsiveness was a consequence of the increased microbial infiltration or if MAIT cell dysregulation was contributing to the development of IBD (Serriari *et al.* 2014).

Given the shared type-17 functions between MAIT cells and murine H2M3 restricted skin-resident T-cells, it is plausible that the tissue-repair and immunoregulatory modules fall under the umbrella of the type-17 immunity. Although IL17 can be pro-inflammatory, it can also have a protective role in the gut (O'Connor *et al.* 2009; Lindemans *et al.* 2015). In several reports, Th17 cells have shown plasticity and the ability to elicit pleiotropic functions in response to microbial challenges, such as anti-inflammatory or regulatory functions. In fate reporter mouse models, a portion of Th17 cells fully trans-differentiated into FOXP3-, IL10-producing T-cells (Gagliani *et al.* 2015). Similarly, prolonged *in vitro* cultures of human Th17 cells have reported IL10 production after consecutive stimulations (Aschenbrenner *et al.* 2018). On the other hand, IL17A-producing CD161+ Tregs (FOXP3+) have also been described in humans and, they elicit a protective role in colitis by promoting wound-healing in the lamina propria (Povoleri *et al.* 2018). Taken together, the homeostatic role of MAIT cells in barrier tissues could be extrapolated to other Th17 or Tc17 cells such as NKT cells not only because of their anti-microbial role but also because they may also hold the potential plasticity to acquire Treg-like functions.

3.4.5. Limitations and future work

Some limitations of this study are that it only investigated the role of CD8+ MAIT cells. While CD8+ T-cells account for most of MAIT cells, there may be some functional differences between CD4+, DN and CD8+ MAIT subsets. Furthermore, while our experiment mostly used circulating MAIT cells, it is necessary to mention that there could be differences in MAIT activity depending on the disease and tissue localisation. In the comparative studies between circulating and tissue-resident MAIT cells (**Figure 3- 5**) the PBMC and LPMC samples were unmatched and underwent different sample processing protocols, which are factors that could have influenced the presented results.

The transcriptional study was only focused on the 20h timepoint, although we now know that many of the tissue-repair-linked proteins are expressed at later time points. This finding is congruent with the injury resolution phase during tissue-repair happening at time points beyond 3 days (Eming, Wynn and Martin 2017). Looking into different time points representing the inflammatory and resolution phases of tissue-repair may have provided a more holistic view of how MAIT behaviour changes in response to different types of triggers.

Finally, our *in vitro* activation and functional assays do not account for the interplay between different immune, epithelial, and stromal cells. Parallel *in vivo* work gave us confidence that our results had a biological relevance (Constantinides *et al.* 2019; Hinks *et al.* 2019); however, more understanding of the underlying molecular mechanisms that drive the tissue-repair process is needed. Other aspects of this work that require further attention are the biological and functional effect of the described immunoregulatory signature.

One open question of the immunoregulatory results is whether bacterial infections actively suppress the expression of IL10 in MAIT cells or whether fixed *E.coli* fail to

generate the necessary co-factors to prompt IL10 expression in MAIT cells. To understand if non-TCR components of microbial infections have an inhibitory effect on IL10 production, future experiments should include co-challenging MAIT cells with 5OPRU and *E.coli (*with impaired riboflavin synthesis pathway) or lipopolysaccharides (LPS). If non-TCR components of bacteria actively suppressed the immunoregulatory module, the presence of *E.coli* or LPS should abrogate the IL10 upregulation caused by 5OPRU.

Another pending question is how the presence of bacteria is detected. It is plausible that MAIT cells can use combinations of surface and soluble molecules to sense bacterial infections directly or indirectly through TLR sensors from APC. For example, in the case of CD161, its ligand Lectin-like transcript 1 (LLT1) and other soluble type 1 Interferons are upregulated in macrophages through TLR3 and TLR2/4 signalling in response to bacterial and viral infections (Germain *et al.* 2011; Satkunanathan *et al.* 2014). Both CD161 and IFNα/β can regulate Th1 functions in MAIT cells (Fergusson *et al.* 2014); however, their role in other MAIT functions has not been explored yet. Therefore, future experiments should also aim to dissect how bacterial challenge modulate the immunoregulatory signature of MAIT cells.

4. Discovery of MR1-specific T-cells reactive to cancer antigens

4.1. Introduction

Broadly speaking, most immunotherapies can be classified into 2 groups based on their antigen recognition method: antibody-mediated recognition and TCR-based recognition. While antibodies focus on surface epitopes (20% of proteome), TCRs recognise intracellular antigens (80% proteome) presented through antigen-presenting molecules such as MHC-I or MCH-II (Harper *et al.* 2018). One of the challenges for TCR-based therapies is the highly polymorphic nature of MHC molecules, causing significant variability across patients in therapeutic potency and off-target effects. This problem limits the patient population that can be treated by therapies that use TCR-based recognition.

Unconventional T-cells are unique for their ability to recognise non-peptide antigens outside the context of classical MHC molecules (Godfrey *et al.* 2015). The advantage for some of these non-classical antigen-presenting molecules is their homogeneity across the human population because of their lack of polymorphisms (Boudinot *et al.* 2016); this feature overcomes the MHC-restriction problem that current T-cell or TCR-based immunotherapies have (Godfrey *et al.* 2018). Non-polymorphic receptors include molecules such as CD1, MR1 and HLA-E, targeted by innate-like or adaptive T-cell populations (Godfrey *et al.* 2015). For example, in the case of the evolutionarily conserved MR1, it can be recognised by MAIT cells and MR1T cells (Kjer-Nielsen *et al.* 2012; Lepore *et al.* 2017). MAIT cells are defined by their specificity to 5OPRU-tetramers through the semi-invariant TRAV1-2+ TCR in humans (Corbett *et al.* 2014; Awad *et al.* 2020) and, for

their innate-like characteristics (described in more detail in chapter 3). On the other hand, the remainder of MR1-responsive cells is grouped into the MR1T category.

While MAIT cells sense bacterial and fungal infections by recognising microbe-derived pyrimidine intermediates from the riboflavin pathway (Eckle *et al.* 2015b; Corbett *et al.* 2020), antigens for MR1T cells are still poorly understood. Recent patents revealed MR1T cells recognising ligands that originate in metabolic environments with altered glycolysis and high oxidative stress (de Libero *et al.* 2021). The ability of MR1 to display infection and metabolic stress allows the immune system to use it as a surveillance platform for cellular fitness. This role as an immunological periscope (Chancellor, Vacchini and de Libero 2022) and its homogeneity across patients makes MR1 an attractive immunotherapy target for diseases associated with aberrant metabolic alterations such as cancer and infectious diseases. In work conducted in A. Sewell's group, the MC.7.G5 MR1T clone was described, which could recognise non-microbial ligands (hence potentially endogenous cancer-specific ligands) displayed by MR1 molecules on cancer cells, (Crowther *et al.* 2020). Another MR1T clone (D463-E4) was reactive to microbial infections through ligands outside the riboflavin synthesis pathway, although the ligand was not identified (Meermeier *et al.* 2016). Many of the identified MR1T clones so far can be stained with 5OPRU-tetramers; however, others had non-MAIT specificities (Gherardin *et al.* 2016; Harriff *et al.* 2018). Taken together, besides the nucleoside adducts described in (de Libero *et al.* 2021), the nature of naturally occurring MR1 ligands remains elusive; however, there are clear evidence for their existence and potential in therapy for diseases associated with cellular stress.

In silico screening of chemical compounds confirmed the existence of several structures around 300 MW that can fit the MR1 groove (Keller et al., 2017; Salio et al 2019). Even when the screening process was biased towards canonical MAIT-5OPRU-like interactions, many of these ligands failed to elicit MAIT activation. In fact, work conducted at Lewinson's lab showed that a significant portion of T-cell clones detected

with MR1-tetramers loaded with *E.coli*-derived antigens were TRAV1-2 negative (Harriff *et al.* 2018).

Considering the biases towards canonical interactions in *in silico* studies (Keller *et al.* 2017) and the MR1 pocket size, the repertoire of MR1-specific ligands is likely to be broader than initially thought. In line with this idea, ion elution from MR1 molecules expressed in insect cells in the presence and absence of live microbes showed the presence of several large and small non-uracil-based chemical clusters (Harriff *et al.* 2018), highlighting the existence of structural diversity of MR1 antigens. Within the riboflavin cluster, other ligands like FO, PLI, PLIII were identified as MR1T targets (Harriff *et al.* 2018). However, the reported frequency of non-MAIT MR1-restricted T cells remains low, and their relative contribution to MR1 biology remains to be explored.

To accelerate the discovery of MR1T TCRs and potential MR1 ligands, Immunocore Ltd. aimed to develop tools to identify MR1T TCR sequences without previous knowledge of relevant ligands (ligand blind method) and use these TCRs as tools for the posterior discovery of MR1 antigens. In this chapter, we describe a method to selectively expand MR1-specific cells using engineered target cells with removed expression of endogenous class-I and class-II molecules and overexpression of a stable MR1 construct that efficiently displays weak and strong MR1 antigens (**Figure 4- 1**). Using these reagents, we have identified 2 new MR1T clones with cancer specificity, although more work is required to discover their cognate antigens.

CD1c was included in this study as a non-polymorphic receptor to compare with MR1 in T-cell expansion studies. In addition, Immunocore had an interest in generating TCRs that recognise CD1c-associated cancer-specific antigens. Although the estimated frequency of CD1c-restricted T-cells in blood is considered low compared to the CD1a-specific populations (de Jong *et al.* 2010; de Lalla *et al.* 2011), studies have found CD1c to present self-lipids upregulated in leukaemia cells (Lepore *et al.* 2014b). In previous

reports, CD1c has only been described in immune cells such as DC, B-cells, monocytes and thymocytes (CD1c protein expression summary - The Human Protein Atlas, 2022), however in our studies we wanted to explore whether CRC target cell lines could induce activation of CD1c specific T-cells if over-expressing a CD1c molecule.

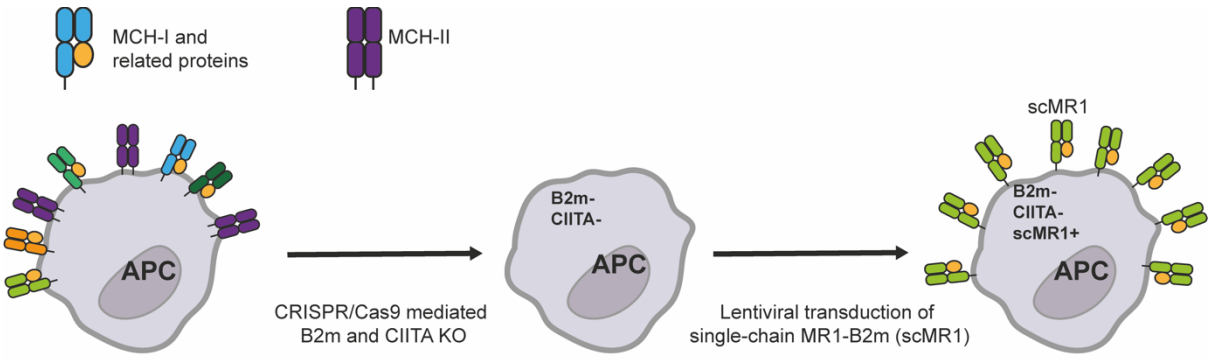

Figure 4- 1. Gene-editing strategy to generate modified target cells. Cancer cell lines had their class-I and class-II removed by CRISPR/Cas9-mediated β2m and CIITA knock-out, followed by lentiviral transduction to over-express MR1 in intracellular and extracellular membranes.

4.1.1. Aims

The aims of this chapter are:

- Gene-editing target cells to remove class-I and class-II expression and over-expression of MR1 and CD1c molecules presenting endogenous ligands.
- Validate the utility of modified target cells in discovering and identification of MR1 and CD1c reactive cells in TIL populations from colorectal tumours.
- Analyse the specificity of MR1T and CD1c cells and their reactivity to cancer cells.
- Explore the role of cellular stress in the generation of relevant MR1 and CD1c antigens.
- Identify the nature of the ligands recognised by the identified MR1T and CD1c cells.

Due to the Covid19 pandemic, commercial activity at Immunocore slowed down, impacting this project's progress. Due to time constraints, some of the objectives could not be met, such as the study of CD1c clones, the study of autophagy in generating MR1 ligands and establishing adequate in-house capabilities to conduct antigen discovery studies.

4.2. Materials and methods

4.2.1. Cells lines

THP1, U266, MOLT4

These cells grew in suspension and were maintained with R10 media at 37ºC between 0.25-1x10^6cells/mL. For optimal growth, cells were split every 3 days.

COLO205

These cells are semi-adherent; a significant portion are suspended while the rest remain lightly adhered. They were maintained with R10 media at 37ºC and split once weekly when cell media became acid and depleted. To split them, the depleted media and suspension cells were entirely removed and replaced with fresh media.

NCIH508, DLD1, PSN1, MEL526, MEL642, 7860

These cells are adherent and were maintained with R10 media at 37ºC. For optimal growth, cells were split when they reached 70-80% confluency. During the split, cells were washed with PBS to remove traces of FBS and incubated at 37ºC with 1-3mL 0.25%Trypsin-EDTA solution for 5-10min to lift the cells. Cells were split 1:5 into a new flask.

4.2.2. Gene editing

Reagents

Reagents	Provider	Catalogue number
CRISPRMAX kit: -Annealing buffer - Cas9 nuclease -Lypofectamine™ -Lipofectamine™ CRISPRMAX™ Transfection Reagent	Thermos Fisher Scientific	CMAX00001
β2m crRNA guides	Synthego	-
CIITA crRNA guides	Synthego	-
Opti-MEM™ I Reduced Serum Medium	Thermos Fisher Scientific	31985070
Cas9	IDT	1081061
Polyethylenimine (PEI)	Sigma Aldrich	764965
Lentiviral constructs (sequences in appendix)	GeneArt	-
pRSV.REV (plasmid)	Addgene	12253
pMDL.g (plasmid)	Addgene	12251
pMD2.g (plasmid)	Addgene	12259
Lenti-X-concentrator	TakaraBio	NC0448638
Polybrene	Sigma Aldrich	32160801

Table 4- 1. Reagents for gene editing

CRISPR/Cas9-mediated knock-out

Before lipofection, crRNA was annealed with the tracrRNA to form the guideRNA. For this, the following mixture was made in PCR tubes (**Table 4- 2**):

Pre-annealing of crRNA and tracrR	
CrRNA	12uL
TracRNA	6uL
5 x Annealing buffer	8uL
Nuclease free Water	14uL
*Incubate for 5min at room temperature	

Table 4- 2. Pre-annealing of crRNA and tracrRNA

This was incubated in the thermocycler at 72ºC for 10min and 37ºC for 30min. Next, the mix was rested at room temperature for at least 15min before freezing aliquots or using.

CRISPR/Cas9-mediated knock-out of target cells was conducted by lipofection of ribonucleoprotein complexed (RNP), following the protocol by Synthego. For that, THP1, COLO205, DLD1 target cells were seeded at $5x10^5$ cells/well and incubated for 24h in 9.5cm^2 flat wells. The next day (day 2), RNP (**Table 4- 3**) complexes were prepared and mixed with CRISPRMAX™ reagents (**Table 4- 4**) for 10min and added to the target cells.

Preparation of RNP complexes	
12 pMol Cas9 nuclease	0.6µL
12 pMol RNA guide (pre-annealed crRNA:tracrRNA)	0.6µL
Lypofectamine	5µL
Opti-MEM™ I Reduced Serum Medium	125µL
*Incubate for 5min at room temperature	

Table 4- 3. Mixture of components in the preparation of RNP complexes

Preparation of CRISPRMAX™ Transfection Reagents	
Lipofectamine™ CRISPRMAX™ Transfection Reagent	7.5µL
Opti-MEM™ I Reduced Serum Medium	125µL

Table 4- 4. Mixture of components in the CRISPRMAX™ Transfection Reagent

On day 5, cells were trypsinised if necessary and expanded in T25 flasks. A fraction was taken to analyse by flow cytometry. On day 7, the cells were lifted and sorted as β2m or HLA-II negative in the case of β2m and CIITA knock-outs, respectively. Guides for each knock-out are indicated in **Table 4- 5**.

RNA CRISPR guides	
β2m guide 1	CTCGCGCTACTCTCTCTTTCTG
β2m guide 2	GGCCGAGATGTCTCGCTCCGTGG
CIITA guide 1	TTCCTACACAATGCGTTGCC
CIITA guide 2	GATATTGGCATAAGCCTCCC

Table 4- 5. Sequence of RNA guides used for β2m and CIITA knock-out

Generation of lentiviral vectors and transductions

To generate lentiviral vectors, $5x10^6$ HEK293T cells were seeded in a T75 flask with 15mL D10 media and incubated overnight at 37ºC. The next day (day 2), the D10 supernatants were replaced with 12mL fresh DMEM media (not supplemented with FCS or antibiotics). HEK293Ts were transfected with 3mL polyplex nanoparticles coupled with DNA plasmids containing the constructs to be transduced and elements of the lentiviral capsid. The composition of the nanoparticles is detailed in **Table 4- 6**.

Preparation of Polyplex Nanoparticles	
PEI (1mg/ml)	156µL
Lenti construct	10µg
pRSV.REV (1mg/ml)	12µL
pMDL.g (1mg/ml)	12µL
pMD2.g (1mg/ml)	5µL
1.5M NaCl	300µL
Adjust total volume to 3000µl with OPTI-MEM	

*Vortex the transfection mix for 10 sec and incubate at room-temperature for 15min

Table 4- 6. Composition of Polyplex Nanoparticles coupled with DNA plasmids

After adding the nanoparticles, cells were incubated at 37ºC for 3 days. After that, the viral supernatant was collected, filtered through 0.45µm and mixed with Lenti-X at 3:1 ratio. Viral supernatants were left to precipitate overnight at 4ºC and spun at 1500g for 1h at 4ºC. Supernatants were discarded, and viral pellets were resuspended in 1mL R10 and frozen in 200µL aliquots.

Lentiviral vectors can be used fresh or kept frozen at -º80C. On the day of transduction, $2\text{-}5x10^5$ cells were incubated in a flat $0.32cm^2$ well with 100µL R10 containing 12µg/mL polybrene and 100µL lentivirus. This mix was spun at 700g and 32CºC for 90min before being transferred into the incubator at 37ºC. After 24h, cells were washed 2 times with fresh R10 to remove lentivirus and further incubated for 3

days in 9.5cm^2 wells. After that, cells were tested for transduction efficiency, expanded, and sorted.

4.2.3. T-cell expansion assays

In expansion assays, 10^6 pre-irradiated target cells (in Gammacell-1000 cell Irradiator, Best Theratronics) were incubated at 37ºC with 2x10^6 panT-cell in a 1.9cm^2 well with a total volume of 2mL T-cell media. panT-cells were isolated from fresh PBMCs and pre-stained with CTV to monitor their proliferation. We discarded 0.9mL media and resuspended with fresh 1mL T-cell media with 20U/mL IL2 (final IL2 concentration of 10U/mL) on days 4, 6, 8, 10 and 12. Every time, after the media split, 100μL of the culture was stained and analysed by flow cytometry to monitor the degree of T-cell proliferation. To control for scMR1, a control condition was used where T-cells were incubated with DKO target cells. In addition, scCD1c transduced targets were also used to get CD1c specific clones.

When significant scMR1 or scCD1c-specific proliferation was observed, CTV- cells were sorted and re-expanded in T-cell media with 10^6 cells/mL fresh feeders (irradiated PBMCs), 1μg/mL L-phytohemagglutinin (PHA) and 100 U/mL IL2.

4.2.4. T-cell cloning by limiting dilution

Polyclonal lines were resuspended in T-cell media with 5x10^5 cells/mL fresh feeders (irradiated PBMCs), 1μg/mL PHA and 100 U/mL IL2 using the following serial dilutions for plating in Terasaki plates:

T-cells /well	Cell/ml	N. of plates	Vol/plate (ml)*	Vol/group (ml)
10	500	2	1.2	2.4
3	166.66	3	1.2	3.6
1	55.55	5	1.2	6
0.3	18.51	10	1.2	12

* 0.02ml/well in Terasaki plates x 60 wells= 1.2ml

Table 4- 7. Summary of dilution in T-cell cloning by limiting dilution

20µL/well of each dilution were plated into Terasaki wells using a Terasaki dispenser. Terasaki plates were incubated at 37ºC for 10 days (to reduce evaporation, additional recipients of sterile water were added to the incubator).

After 10 days, Terasaki plates were screened and scored for plate efficiency (number of T-cells to be plated per well so that 63% of wells are positive, **Figure 4- 2**). Plate efficiency determines the maximum number of T-cells that can be plated per well so that statistically, only 1 of them grows into a clone. For example, if plate efficiency is 7, we can safely assume that the expanding T-cells from plates where 3 T-cells/well were plated are still monoclonal.

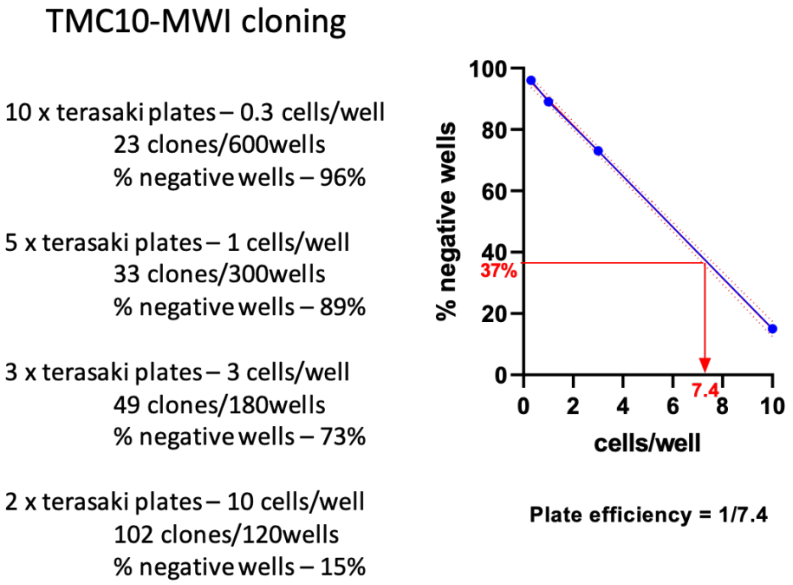

Figure 4- 2. Example of plate efficiency calculation.

Clones of interest were identified based on IFNγ production in response to target cells expressing scMR1 or scCD1c specifically blocked with anti-MR1 or anti-CD1c. Selected TCR clones were sequenced at Immunocore by rapid amplification of cDNA ends (RACE) followed by PCR and sequencing with TCR-specific primers.

4.2.5. Rapid amplification of cDNA ends (RACE)

4.2.5.1. Reagents

Reagents	Provider	Catalogue number
RNeasy Mini Kit	Qiagen	74004
Triton X-100	Sigma Aldrich	9036-19-5
RNase inhibitor	Promega	N2611
SuperScript II reverse transcriptase	Invitrogen	18064071
Betaine (5 M)	Sigma Aldrich	B0300
$MgCl_2$ (1 M)	Thermo Fisher Scientific	AM9530G
KAPA HiFi HotStart	Roche	KK5532
Platinum Hi Fi Taq	Thermo Fisher Scientific	11304011
96 well PCR plates	Thermo Fisher Scientific	403012

Table 4- 8. List of reagents for RACE

Primers	Provider	Sequence
5' Biosg TSO (Template switching oligo)	Exiqon	5BiosG/AAGCAGTGGTATCAACGCAGAGTACATrGrG+G
5' Biosg OligodT_{30}VN	IDT	/5BiosG/GGAATTCGACCGAGTACACATAAGGT_{30}VN
Biosg_ISPCRfwd primer	IDT	/5BiosG/AAGCAGTGGTATCAACGCAGAGT
Biosg_ISPCR$_{30}$rev primer	IDT	/5BiosG/GGAATTCGACCGAGTACACATAAGG
YOL237 primer	Eurofins	GAGTCTCTCAGCTGGTACACG
YOL240 primer	Eurofins	CAGTGTGGCCTTTTGGGTGTG

Table 4- 9. List of primers for RACE

Lysis buffer

480µl of the 2% Triton X-100, 240µl RNase inhibitor, 4.08mL Nuclease-free water.

Lysis plate

200µL Lysis buffer was mixed with 220µL 5' Biosg Oligo(dT)V_{30}N/dNTP. Plate 4µL per well in PCR plate and store at 4ºC.

4.2.5.2. Step 1: Reverse transcription

At around 10 days of T-cell expansion with PHA and feeder cells, once there were no feeders left, the expanded T-cells were spun and resuspended in 300µL of RNA protect. Cell RNA was extracted using the RNeasy Mini Kit (Qiagen).

5' Biosg TSO (Template Switching Oligo) contains 2 riboguanosines (rG) and a modified guanosine (G) in the 3' to facilitate template switching when the reverse transcriptase reaches the 5' of the mRNA. On the other hand, 5' Biosg OligodT_{30}VN Oligo contains a stretch of 30 thymines (T) that anneals to the poly-A tail of mRNA. For the reverse transcription, 1µL diluted RNA (1:10 in RNAase-free water) was mixed with 4µL lysis buffer (containing OligodT_{30}VN primers) and incubated in the thermocycler for 3min at 72ºC. This step allows the OligodT_{30}VN primers to anneal the mRNA. Next, the master mix for reverse transcription was added (**Table 4- 10**): (4 replicates per sample).

Component	Stock concentration	Final concentration	Volume per reaction (uL)
SuperScript II reverse transcriptase	200U/µL	100U	0.5
RNAse inhibitor	40U/µL	10U	0.25
Superscript II first-strand buffer	5×	1x	2
DTT (100 mM)	100mM	5mM	0.5
Betaine (5 M)	5M	1M	2
$MgCl_2$ (1 M)	1M	6mM	0.06
5' Biosg_TSO (100 uM)	100uM	1µM	0.1
Nuclease-free H_2O			0.29
Total Volume:			5.7

Table 4- 10. Reverse transcription mix

The mix was run on the thermocycler:

Cycle	Temperature (°C)	Time
1	42	90min
2–11 (10x)	50	2min
	42	2min
12	70	15min
13	4	Hold

Table 4- 11. Reverse transcription steps on thermocycler

During this amplification step, the 1st strand of cDNA generated though reverse transcription have the adaptors from 5' Biosg_TSO and the 5' Oligo(dT)V_{30}N primers as new adpators, which can be used in the subsequent cDNA amplification step.

4.2.5.3. Step 2: Universal cDNA amplification

The initial cDNA is then amplified to increase the total amount of cDNA available for downstream applications. The cDNA is amplified by PCR using the 5' Biosg ISPCRfwd and 5' Biosg ISPCR$_{30}$rev primers which bind to the PCR adaptor arms added to each cDNA molecule during reverse transcription via the 5' Biosg TSO and 5' Biosg Oligo(dT)V_{30}N primers, respectively. For the universal sDNA amplification, the PCR master mix (**Table 4- 12**) was added to the products from the reverse transcription:

Component	Stock concentration	Final concentration	Volume per reaction (uL)
First-strand		–	10
KAPA HiFi HotStart	2x	1×	12.50
Biosg_ISPCRfwd primer	10μM	0.1μM	0.25
Biosg_ISPCR$_{30}$rev	10μM	0.1μM	0.25
Nuclease-free water		–	2
Total volume		–	25

Table 4- 12. Universal cDNA amplification mix

The mix was run on the thermocycler:

Cycle	Temperature (°C)	Time
1	98	3min
2–19 (24x)	98	20sec
	67	15sec
	72	6min
20	72	5min
21	4	

Table 4- 13. Universal cDNA amplification steps on thermocycler

4.2.5.4. Step 3: Targeted amplification

After the PCR, high salt content and products under 200bp were cleaned up using Ampure XP SPRI beads. cDNA over 200bp was eluted in a final volume of 25μL.

In this step, multiplexed forward primers and TRAV and TRBV specific reverse primers are used to amplify the TRAV and TRBV sequences from each sample. The PCR master mix was as follows (**Table 4- 14**):

For TRAV amplification

Component	Stock concentration	Final concentration	Volume per reaction (μL)
Platinum Hi Fi Taq		1 U/rxn	0.10
PCR buffer	10x	1x	2.50
$MgSO_4$	50mM	2mM	1.00
10mM dNTPs	10mM	0.2mM	0.50
Fwd Primer mix*	2.5μM	0.1μM	1.00
YOL237 Rev primer	10μM	0.4μM	1.00
Nuclease-free water			16.4
Total volume			22.5

*Mix of primers binding to different TCR chain leader sequences.

Table 4- 14. Mix for targeted amplification of TCR sequences

For TRBV amplification, YOL240 is used as reverse primer.

The mix was run on the thermocycler:

Cycle	Temperature (°C)	Time
1	95	2 min
2–36 (35x)	95	30 sec
	62	30 sec
	72	1 min
37	72	7 min
38	4	

Table 4- 15. Steps on thermocycler for the amplification of TCR sequences

Amplification was verified by running a fraction of the product in agarose gel and sending 5μL for sequencing.

4.2.6. Luciferase assay

For this assay, Jurkat cells were modified to express the Nuclear Factor of Activated T-cells (NFAT) fused with Luciferase reporter (Promega). This cell line was transduced with the TCR of interest to study the reactivity against different target cells and antigens. Target cells and Jurkat cells were co-cultured in white flat-bottom 96-well plates in a total volume of 150μL per well. To read the bioluminescent signal, 100μL of BioGlo (Promega) reagent and incubate for 5min at room temperature. Signal was measured using the CLARIOstar plus plate-reader (BMG Labtech).

4.2.7. TCR Sequences

Lentiviral sequences are in the supplementary sections 8.2.8 and 8.2.9.

4.3. Results

4.3.1. The expression of MR1 and CD1 molecules can be upregulated in CRC lines with IFNγ-mediated stimulation

We chose 3 cancer-derived cell lines to gene-edit and generate the MHC-null target cell lines over-expressing MR1 and CD1 molecules. THP1 monocytic cell lines were selected because they could generate MR1-mediated MAIT responses *in vitro* in chapter 3. On the other hand, COLO205 and DLD1 are CRC derived cell lines, and they were chosen to screen tumour-infiltrated lymphocytes (TILs) from CRC patients. With that in mind, CRC cells are widely characterised by their genomic (MSI+) and epigenomic instability (CIMP+) phenotypes caused respectively by a deficient mismatch repair system or by hypermethylation of the chromatin (Ahmed *et al.* 2013; Berg *et al.* 2017). The rationale for choosing COLO205 and DLD1 cell lines was because they have different degrees of genomic and epigenomic stability (**Table 4- 16**), which, according to our hypothesis, could be an important factor when it comes to generating endogenous cancer-specific MR1 or CD1 ligands.

Cell lines	MSI status	CIMP status	Reference
COLO205	-	+	(Ahmed *et al.* 2013; Berg *et al.* 2017)
DLD1	+	+	(Ahmed *et al.* 2013; Berg *et al.* 2017)
THP1	-	Unknown	(Odero *et al.* 2000)

Table 4- 16. Genomic and epigenomic phenotypes of target cell lines. Genetic and epigenomics differences of target cells undergoing β2m and CIITA removal and lentiviral transduction of MR1 and CD1c.

Initial characterisation at steady-state showed that THP1 cells expressed HLA-A2, HLA-DP-DQ-DR, MR1 and all the CD1 molecules (a, b, c and d), while COLO205 cells only expressed MR1 and HLA-A2 **(Figure 4- 3A, B**). On the other hand, DLD1 cells did not

express any of the class-I, or related receptors nor any class-II molecules (**Figure 4- 3A, B**), which is explained because they lack expression of β2m at steady-state (Bicknell, Rowan and Bodmer 1994). Overnight stimulation of epithelial target cells using inflammatory cues such as IFNγ led to the upregulation of most class-I-like receptors (except for CD1c) and Class-II receptors in a dose-dependent manner (**Figure 4- 3C**). This indicated that despite their genetic or epigenetic status, they could upregulate MR1 and CD1 under inflammatory conditions.

In the case of DLD1, overnight stimulation with 10^4U/mL IFNγ, generated a small population (up to 12%) of β2m+ cells **(Supplementary Figure 4- 1**), which could explain the increased geometric mean for some class-I related molecules.

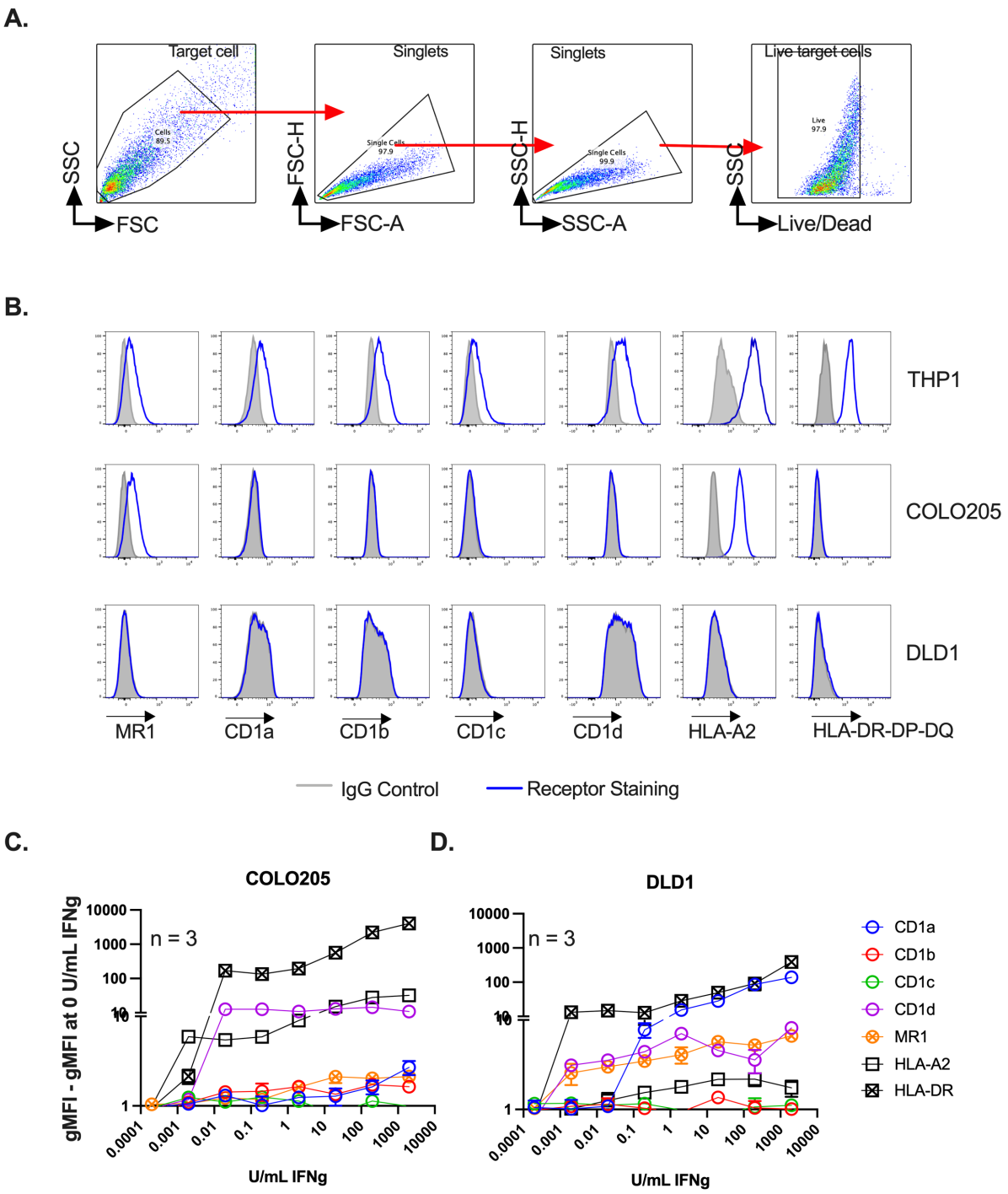

Figure 4- 3. IFNγ expression upregulated surface expression of antigen-presenting receptors. (**A**) Flow cytometry gating strategy of target cells ay steady state. (**B**) Representative histogram of isotype control (grey) and antigen-presenting receptors (Blue): MR1, CD1a, CD1b, CD1c, CD1d, HLA-I and HLA-II. (**C-D**) Fold-change (FC) compared to baseline expression in geometric mean of antigen-presenting receptors in overnight incubation at different concentrations of IFNγ (U/mL) in COLO205 (**C**) and DLD1 (**D**) cells compared to baseline.
Data were acquired in a single experiment. Error bars represent Mean ± SEM of 3 technical replicates.

4.3.2. β2m KO removes surface expression of MR1 and MCH-I

Using guide-RNAs designed by Dr Khanolkar, which target the β2m locus, we did CRISPR/Cas9-mediated knock-out (KO) for THP1 and CRC lines (**Figure 4- 4A**). To generate pure KO lines, we conducted 2 consecutive cell sortings using the gating strategy elucidated in **Figure 4- 4B**. After the sortings, the resulting populations did not have any β2m or HLA-A2 expression at steady-state nor after overnight stimulation with IFNγ (**Figure 4- 4C-E**).

In the case of the MR1 receptor, residual expression could be detected after β2m removal, although expression levels stopped increasing in response to IFNγ (**Figure 4- 4C, F**). In addition, in chapter 5, MAIT cells could be triggered by 5OPRU through β2m-KO target cell (explained in more detail in chapter 5) ; therefore, raising the question whether MR1 could have other mechanisms to be traffic to the plasmatic membrane without β2m. Although this topic has not been fully explored, it would align with the idea that murine MR1 affinity to β2m is weaker than conventional class-I molecules (Huang *et al.* 2005a), suggesting less β2m dependency. Surface staining with anti-MR1 reagents that detect the unfolded (β2m-free) and folded conformations of MR1 (8H3 and 8F2.F9 clones, respectively) (McWilliam *et al.* 2020) could indicate if there are any β2m-free conformations of MR1 that can be transiently trafficking to the plasmatic membrane.

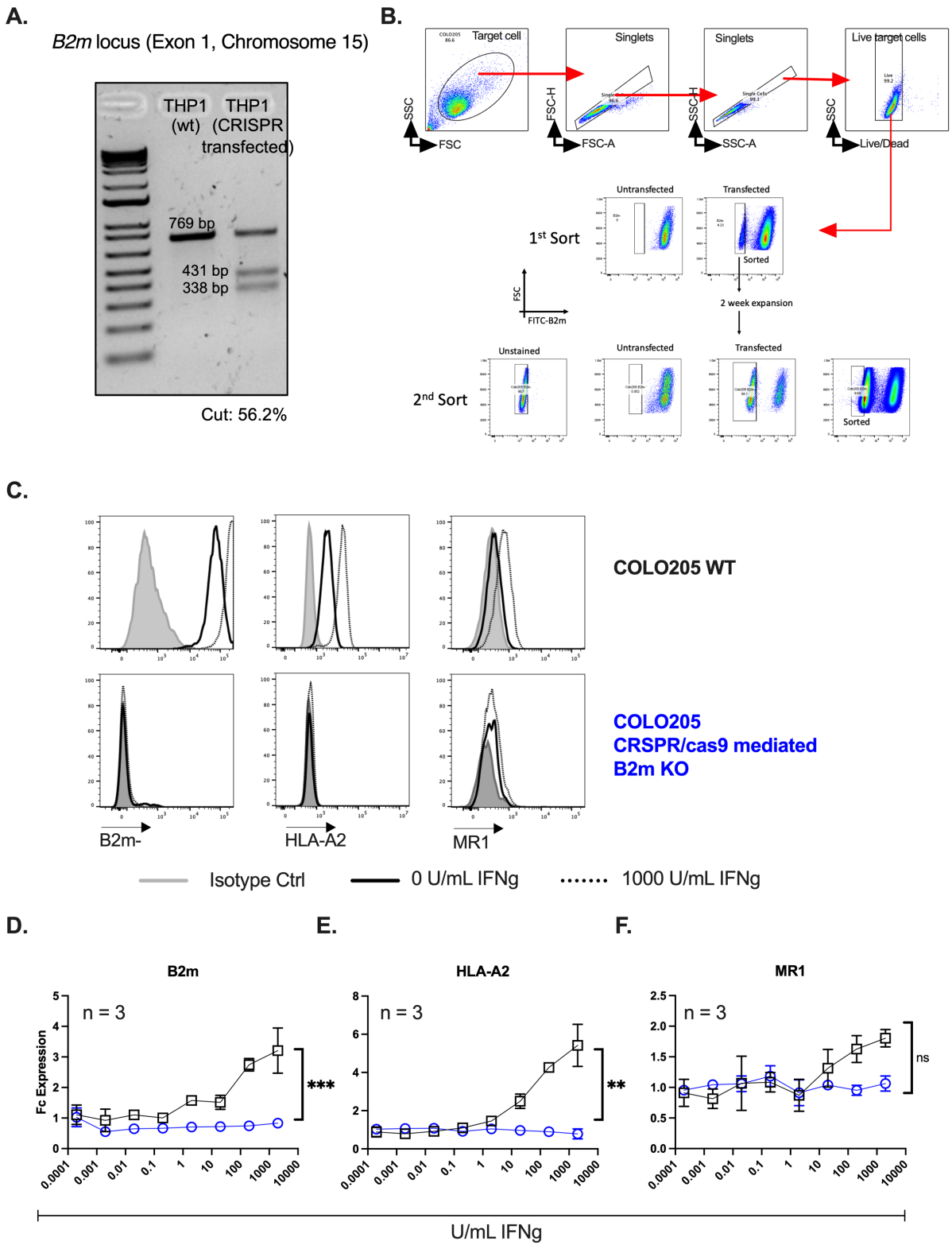

Figure 4- 4. β2m removal prevents surface upregulation of HLA-I and MR1 molecules in response to IFNγ. (**A**) PCR of β2m locus of wild-type THP1 and THP1 cells with CRISPR/Cas9-mediated β2m KO. (**B**) Representative gating strategy of target cells (top panel) and sorting gate of transfected cells with β2m crRNAs during 1st sort (middle panel) and consecutive 2nd sort (bottom panel). (**C**) Representative histograms of isotype control (grey), staining of β2m, HLA-A2 and MR1 at steady

state (black line) and overnight incubation with 1000U/mL IFNγ (discontinued line) in wild-type (top panels, black) and β2m-KO (bottom panels, blue) COLO205 cells. (**D-E**) FC in the geometric mean of β2m (**D**), HLA-A2 (**E**) and MR1 (**F**) in response to different concentrations of IFNγ (U/mL) in wild-type (black) and β2m KO (Blue) COLO205 cells.
Data were acquired in a single experiment. Error bars represent Mean ± SEM of 3 technical replicates.

4.3.3. CIITA KO reduces the baseline expression of HLA-II molecules but does not abrogate their surface expression and upregulation

Like section 2, the CIITA locus was truncated through CRISPR/Cas9-mediated KO (**Figure 4- 5A**). CIITA is the transactivator for the class-II major histocompatibility complex, and it is a nuclear protein that cannot be stained on the cell surface. We hypothesised that target cells that had the CIITA locus disrupted would not be able to express or upregulate MHC-II molecules on the plasmatic membrane. Therefore, following transfection, to select those cells that had successful KO of CIITA, we did 2 consecutive sortings of MHC-II negative target cells after overnight stimulation with 1000U/mL IFNγ. We denominated the resulting cells as double knockouts (DKO).

Incubating DKO cells with IFNγ showed that THP1 and COLO205 cells with truncated CIITA locus had a bimodal distribution of HLA-II^{low} and HLA-II^{high} cells (**Figure 4- 5B**). In contrast, DLD1 cells fully lost their ability to upregulate class-II molecules in the presence of I IFNγ (**Figure 4- 5B**). The resulting DKO target cells were transduced with single-chain MR1 (scMR1) and CD1 (scCD1) molecules (explained in detail in section 4.3.4). To generate stable homogeneous cell lines, we grew individual target clones for THP1, COLO205 and DLD1 cells; we selected the clones with the lowest surface expression of HLA-DP-DQ after stimulating overnight with 1000U/mL IFNγ (**Figure 4- 5C**). Nevertheless, as the heterogeneous parental lines, the selected clones elicited the ability to upregulate HLA-II in the presence of high concentrations of IFNγ (**Figure 4- 5D**).

Our results indicate that CRISPR/Cas9 mediated CIITA KO was insufficient to abrogate the expression or upregulation of class-II molecules in THP1 and COLO205 target cells. This is likely due to incomplete KO in the case of THP1 and COLO205 cells while, in the case of DLD1 cells, the CIITA KO completely removed the upregulation of HLA-DP-DQ-DR caused by IFNγ (**Figure 4- 5B**). For THP1 cells, CIITA KO reduced the baseline surface expression of HLA-DP-DQ-DR at a steady-state (**Figure 4- 5D**).

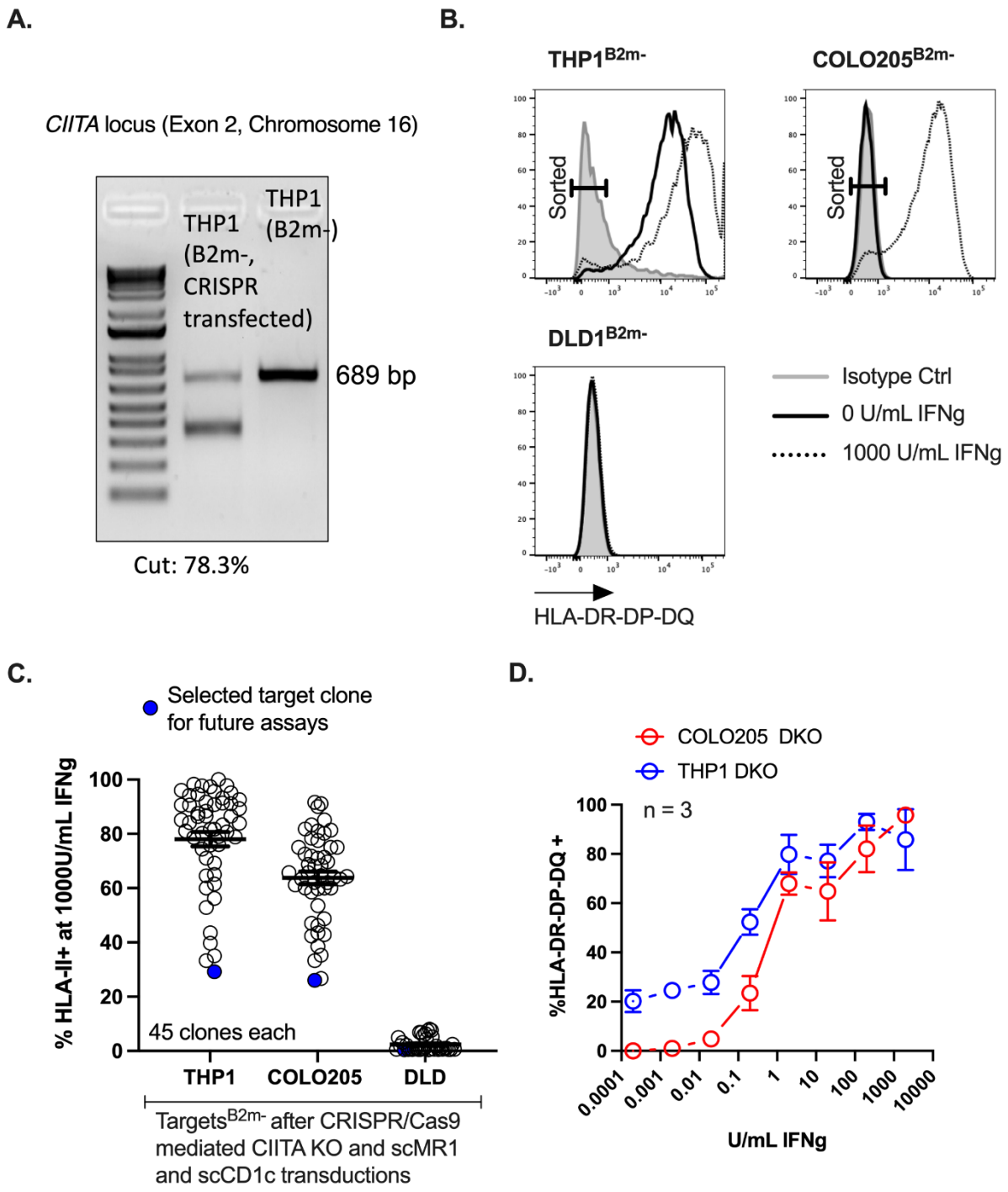

Figure 4- 5. CIITA KO was ineffective in removing HLA-II expression in target cells. (**A**) PCR of CIITA locus of wild-type THP1$^{\beta 2m-}$ and THP1 $^{\beta 2m-}$ cells after CRISPR/Cas9-mediated CIITA KO. (**B**) Representative histograms of isotype control (grey), staining of HLA- HLA-DR-DP-DQ at steady state (black line) and with 1000U/mL IFNγ (discontinued line) and, sorting gate in THP1$^{\beta 2m-}$, COLO2-5$^{\beta 2m-}$, DLD1$^{\beta 2m-}$ target cells. (**C**) Frequency of HLA-DR-DP-DQ positive cells in individual clones of target cells after overnight incubation with 1000U/mL IFNγ (selected clone was highlighted in blue). (**D**) Frequency of HLA-DR-DP-DQ positive cells in THP1 (blue) and COLO205 (Red) clones from (**C**) in response to IFNγ titration.
Data were acquired in a single experiment. Error bars represent Mean ± SEM of 3 technical replicates.

4.3.4. Single-chain MR1 and CD1c constructs allow stable surface expression of MR1 and CD1c, respectively, in DKO target cell lines

DKO cells were transduced with either scMR1 or scCD1c constructs using a lentiviral transduction system. These single-chain constructs consist of the monomorphic receptors fused with β2m in the N-terminal (**Figure 4- 6A**). This design was made because covalently linked β2m increases the surface expression of MR1 and other receptors (Miley *et al.* 2003). After lentiviral transduction, 2 consecutive sortings of the scMR1+ and scCD1c+ cell lines were conducted following the gating strategy depicted in **Figure 4- 6B**. The outcomes were MHC-null THP1, COLO205 and DLD1 cell lines over-expressing either scMR1 or scCD1 constructs (**Figure 4- 6C**). Unlike the endogenous MR1 or CD1c molecules, the surface expression of the single-chain constructs did not change because of IFNγ as they were under a lentiviral promoter (**Figure 4- 6C**). The CRC lines had a significantly higher expression of scMR1 construct than THP1 cells, while the expression of scCD1c was comparable for all 3 cell lines (**Figure 4- 6D, E**).

One caveat of these gene-editing procedures was the resulting heterogeneous cell populations. Lentiviral transductions randomly introduce several gene copies in different parts of the genome, while CRISPR/Cas9-mediated KO, although being a guided approach, has off-target effects on the genome. To generate homogenous populations for THP1, COLO205 and DLD1, new cell lines were generated from individually selected clones (clone selection is explained in more detail in section 4.3.3).

In our initial phenotyping of CRC cells, CD1c did not upregulate to the plasmatic membrane in response to high levels of IFNγ (**Figure 4- 3C, D**). Therefore, we asked whether CRC^{scCD1c} lines could activate or expand autoreactive CD1c-specific T-cells through the presentation of CD1c restricted antigens.

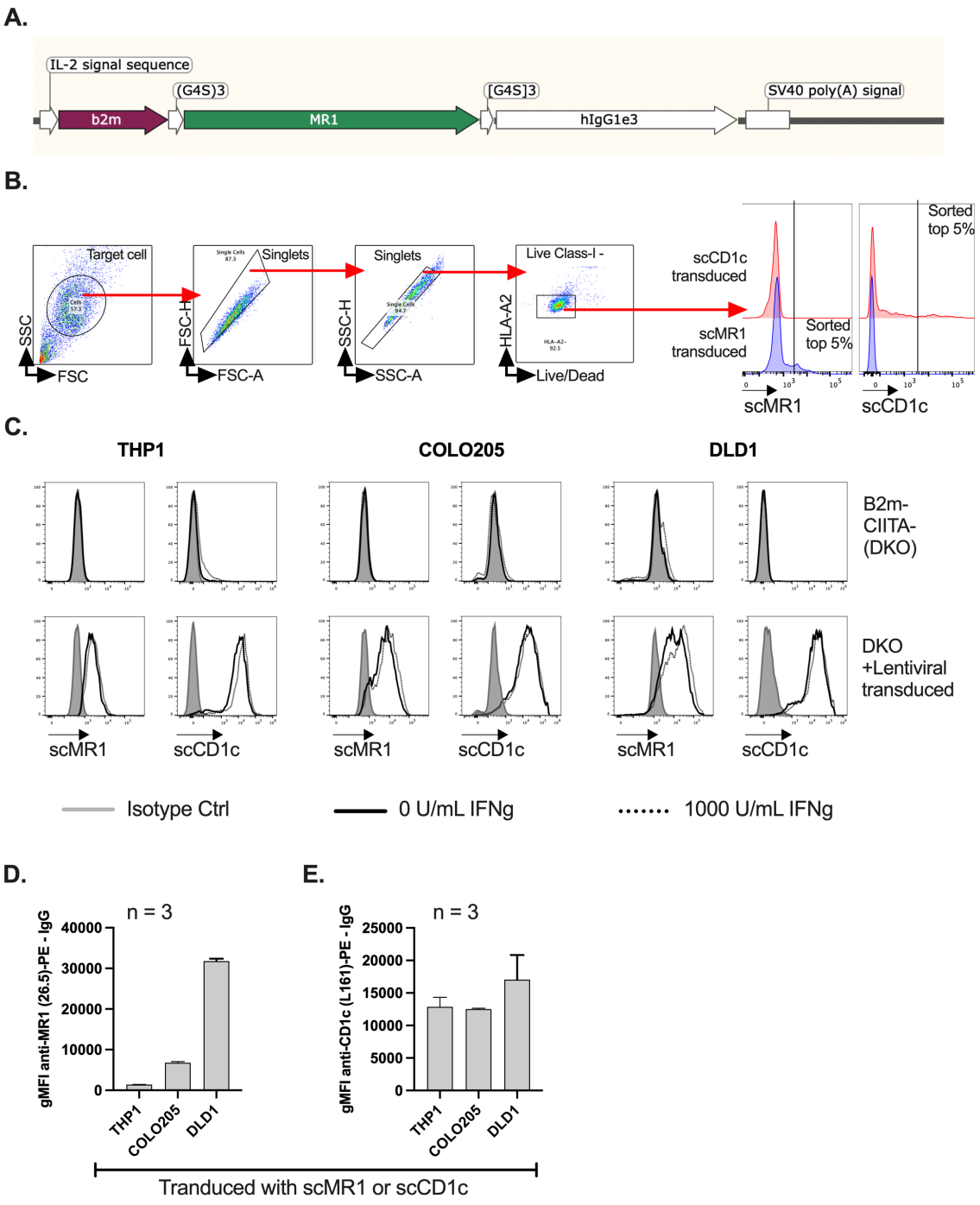

Figure 4- 6. Lentiviral transductions resulted into a stable surface expression of MR1 and CD1c. (**A**) Lentiviral backbone and diagram of scMR1 and scCD1c constructs. (**B**) Gating and sorting strategy of target cells transduced with scMR1 and scCD1c constructs. (**C**) Representative histograms of THP1, COLO205 and DLD1 cells with isotype control (grey), staining of scMR1 and scCD1c at steady state (black line) and after overnight incubation with 1000U/mL IFNγ (discontinued line) in DKO target cells (top panels) and transduced with lentiviral constructs (bottom panels). (**D-E**) Geometric mean (with substracted isotype staining) of scMR1 and scCD1c stained with 26.5 anti-MR1 (**D**) and L161 anti-CD1c (**E**) antibodies, respectively.
Data were acquired in a single experiment. Error bars represent Mean ± SEM of 3 technical replicates.

4.3.5. Target cells has functional scMR1 on their surface as they could activate MR1-specific Jurkats and primary T-cells

To validate the functionality of the scMR1 constructs, target cells were used to stimulate $2.5x10^4$ Jurkats transduced with 2 MR1-specific TCRs. The E8-TCR and VT001-TCR were developed at Immunocore using phage display technologies, screening artificial TCR libraries against 5OPRU-MR1 molecules. The E8-TCR can form extra bonds with the MR1 molecule and has been characterised at Immunocore as an antigen-agnostic TCR, meaning that it can bind MR1 independent from the associated ligands (Data not shown). Consequently, E8-Jurkat activation is generally used at Immunocore as a proxy to gauge surface levels of MR1 in different target cells. On the other hand, VT001 is a canonical MAIT-TCR, and it was generated using a filtered TCR library with a constant TRAV1-2 alpha chain. As with wild-type MAIT-TCRs, VT001 can bind MR1 only in the presence of 5OPRU.

In Jurkat activation assays, the E8-TCR could recognise the scMR1 in all target cells and did not react to the DKO target cells (**Figure 4- 7A**). This recognition was independent of any exogenous ligands, and the addition of 5OPRU did not inhibit or increase the activation of E8-Jurkat cells (**Figure 4- 7C**). On the other hand, VT001 MAIT-Jurkats could only react to target cells in the presence of 5OPRU (**Figure 4- 7B, D**). Similar to the 26.5 anti-MR1 staining results (**Figure 4- 6**), under non-saturating conditions (low number of target cells or low concentration of 5OPRU), both E8- and VT001-Jurkats showed significantly higher activation against CRC lines than THP1 target cells (**Figure 4- 7A, D**).

In ELISPOT assays using enriched MAIT cells and 10nM 5OPRU, only THP1 and COLO205 could elicit MR1-dependent MAIT activation (**Figure 4- 7F, G**). This was a surprising result considering that DLD1 cells had 10-fold and 3-fold higher surface levels of MR1 than THP1 and COLO205, respectively (**Figure 4- 6D**). These results indicated that MR1-mediated activation is not solely dependent on surface levels of MR1. Other factors

to weigh in are the presence of surface cofactors that allow effective T-cell response in both the target and effector cells.

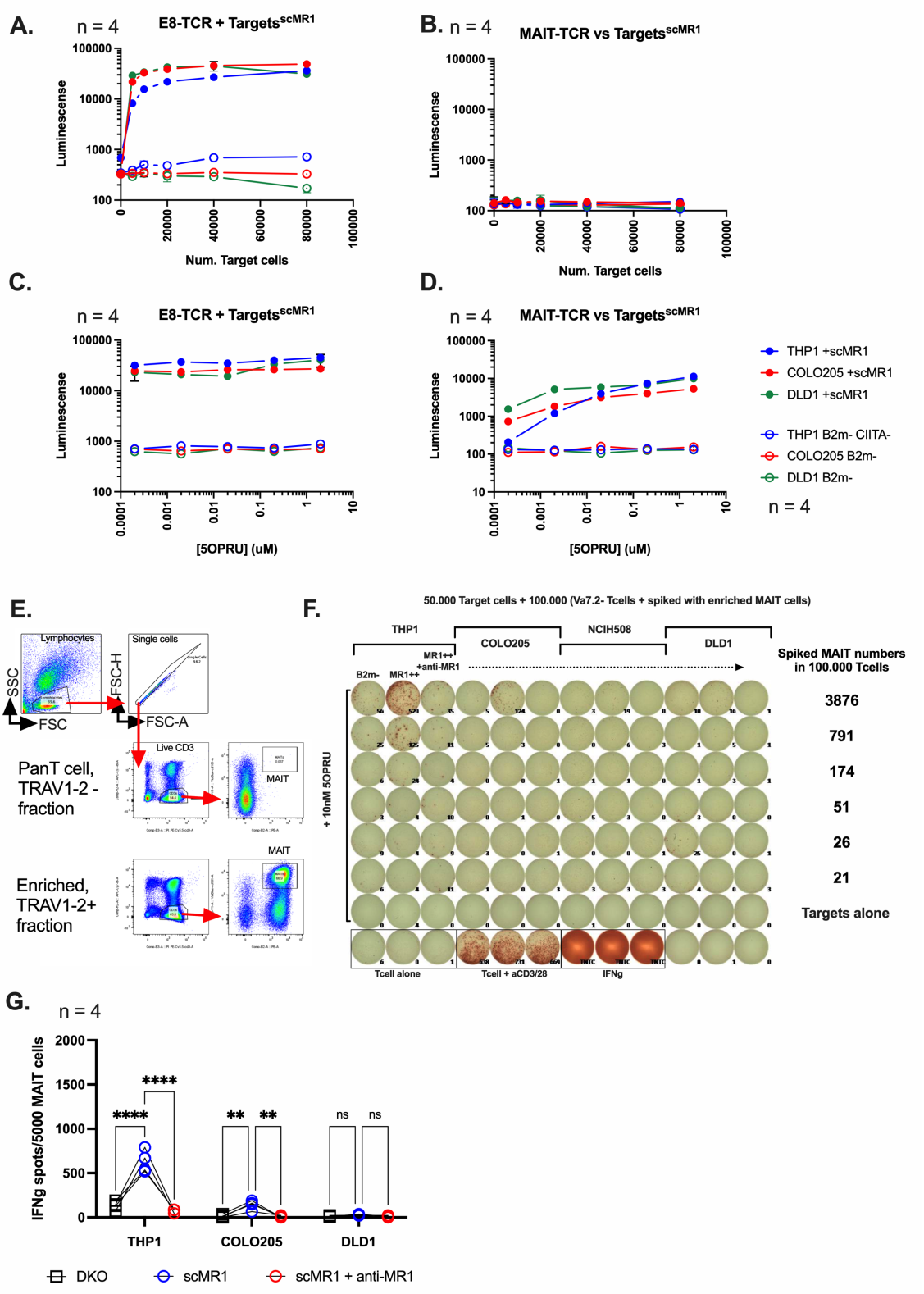

Figure 4- 7. scMR1 molecules are functional and can present 5OPRU on the cell surface. (**A-D**) NFAT-luciferase expression in Jurkats expressing with the E8 and VT001 (MAIT) TCRs after

overnight incubation with target cells^{DKO} and target cells^{scMR1}. (**A, B**) E8-Jurkats (**A**) and VT001-Jurkats (**B**) were incubated with different target cell numbers without exogenous ligands. (**C, D**) Jurkats expressing the E8 (**C**) and VT001 (**D**) TCRs were incubated with $2x10^4$ target cells at different concentrations of 5OPRU.
(**E-G**) ELISPOT assay of 10^5 panT-cells spiked with primary MAIT cells incubated with $5x10^4$ target cells. (**E**) Frequency check by flow cytometry of panT-cells depleted or spiked with TRAV1-2 positive primary T-cells. (**F**) Representative IFNγ ELISPOT of MAIT cells in response to target cells in the presence of 10nM 5OPRU and collated IFNγ SFU counts (**G**) for 5000 MAIT cells in response to the indicated targets: either DKO (black), scMR1 transduced in the absence (blue) or presence (red) of anti-MR1 (25.6) target cells.
Data were acquired in a single experiment. Error bars in (represent Mean ± SEM of 4 technical replicates in **A-D** and 4 biological replicates in **G**. Differences among conditions were analysed by 2-way ANOVA with uncorrected Fisher's LSD test. *p < 0.05, **p < 0.01, ***p < 0.001, ****p < 0.0001.

4.3.6. Target cells expressing scMR1 or scCD1c constructs could induce MR1- and CD1c-specific T-cell proliferations

T-cell expansion assays last over 5 days depending on the proliferation rate. During this time, optimal conditions must be used to prevent unspecific expansion of T-cells because of bystander activation or recognition of other target molecules. Target cells irradiation slowed their proliferation without killing them (**Figure 4- 8A**). 33Gy was the optimal irradiation dose for THP1 and COLO205 while, at 96 Gy, DLD1 cells still proliferated, although at a much slower rate (**Figure 4- 8B**). Beyond 96Gy, a significant portion of the target cells were dead (data not shown).

Although our initial intention was to use TIL populations, these samples became inaccessible to us during the COVID19 pandemic. Because of that, PBMCs from healthy internal donors were used instead. During proliferation assays, 10^5 target cells expressing either scMR1 or scCD1c were mixed 1:1 and incubated with T-cells in the presence of 10U/mL IL2 at an Effector:Target (E:T) ratio of 2:1 (**Figure 4- 8C-E, Figure 4- 9**).

In previous results, CRC lines had a limited capacity to activate MAIT cells in the presence of 5OPRU (**Figure 4- 7F, G**). Our initial hypothesis was that most MR1T cells had a naïve phenotype, and they required co-stimulations that epithelial cells could not provide. In the case of DLD1^{scMR1} cells, despite having 10-fold higher expression of MR1 than THP1^{scMR1}, they were unable to activate MAIT cells (**Figure 4- 7G**). To corroborate this result, we observed that only in 1/4 donors, DLD1^{scMR1} cells could induce MR1-specific T-cell proliferation; this was only reproducible in 1/3 technical replicates (**Figure 4- 8C, D**). To overcome the weak proliferation of panT-cells against CRC lines, 5ng/mL of IL7 and IL15 cytokines were added to the standard 10U/mL IL2. Throughout the literature, IL7 and IL15 cytokines have been reported to favour T-cell survival and proliferation (Rathmell *et al.* 2001; Wen *et al.* 2006; Cieri *et al.* 2013; Kohli *et al.* 2021). In our comparative assays, IL7 and IL15 increased T-cell proliferation against DLD^{scMR1} lines;

however, there was a large portion of unspecific expansion seen against DLD^{DKO} target cells (**Figure 4- 8C-E**). Because of the weak or unspecific expansion results, further proliferations against $DLD1^{scMR1}$ or $DLD1^{scCD1c}$ were not attempted.

As expected from previous results, $THP1^{scMR1}$ target cells could expand populations of MR1/CD1c-specific T-cells in 4/4 donors in all technical replicates (**Figure 4- 9B**). On the other hand, COLO205 elicited MR1/CD1c-specific T-cell expansion (below 1% expansion) in all technical replicates for 1/4 donors (**Figure 4- 9B, C**). Expanded T-cells (CTV- cells) were sorted following the gating strategy shown in **Figure 4- 9A** and further expanded twice with 1μg/mL PHA for 3 weeks to generate polyclonal T-cell lines. Nomenclature-wise, polyclonal lines generated with THP1 cells have the T10 extension, while those expanded against CRC have the N13 extension (**Figure 4- 9E**).

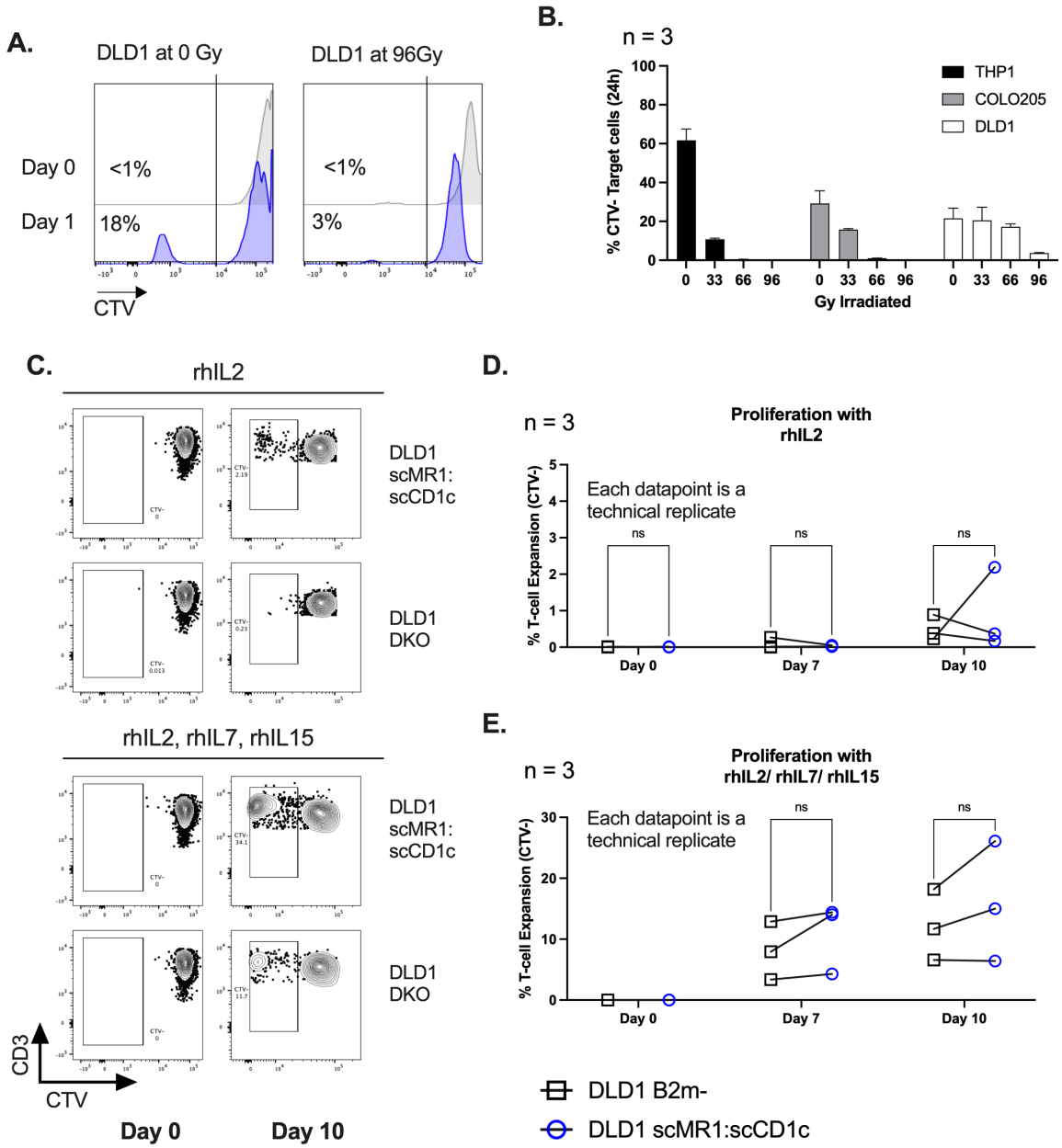

Figure 4- 8. DLD1 cells are not optimal target cells for MR1 or CD1c dependent T-cell proliferation. (**A-B**) Proliferation of target cells irradiated at different Gys with 0.5mm Cu filter and incubated overnight. (**A**) Representative histogram of CTV staining and quantification (**B**) of target cell proliferation (CTV-) at 24h after irradiation with 0, 33, 66, 96 Gys.
(**C-G**) Proliferation of $2x10^5$ panT-cells in a 10-day expansion assay against 10^5 target cells (1:1 mix of DLD1 cells expressing either scMR1 or scCD1c) in $0.32cm^2$ wells. © Representative frequencies of expanded panT-cells (CTV-) at days 0 and 10 in the presence of 10U/mL IL2 (top panels) or 10U/mL IL2 and 5ng/mL of IL7 and IL15 (bottom panel). (**D, E**) Frequencies of expanded panT-cells against DKO and scMR1:scCD1c DLD1 target cells in 3 technical replicates and the 2 conditions described ©(**C**).
Data were acquired in a single experiment. Error bars in B represent Mean ± SEM of 3 technical replicates. Differences among conditions in **D-E** were analysed by 2-way ANOVA uncorrected Fisher's LSD test. *p < 0.05, **p < 0.01, ***p < 0.001, ****p < 0.0001.

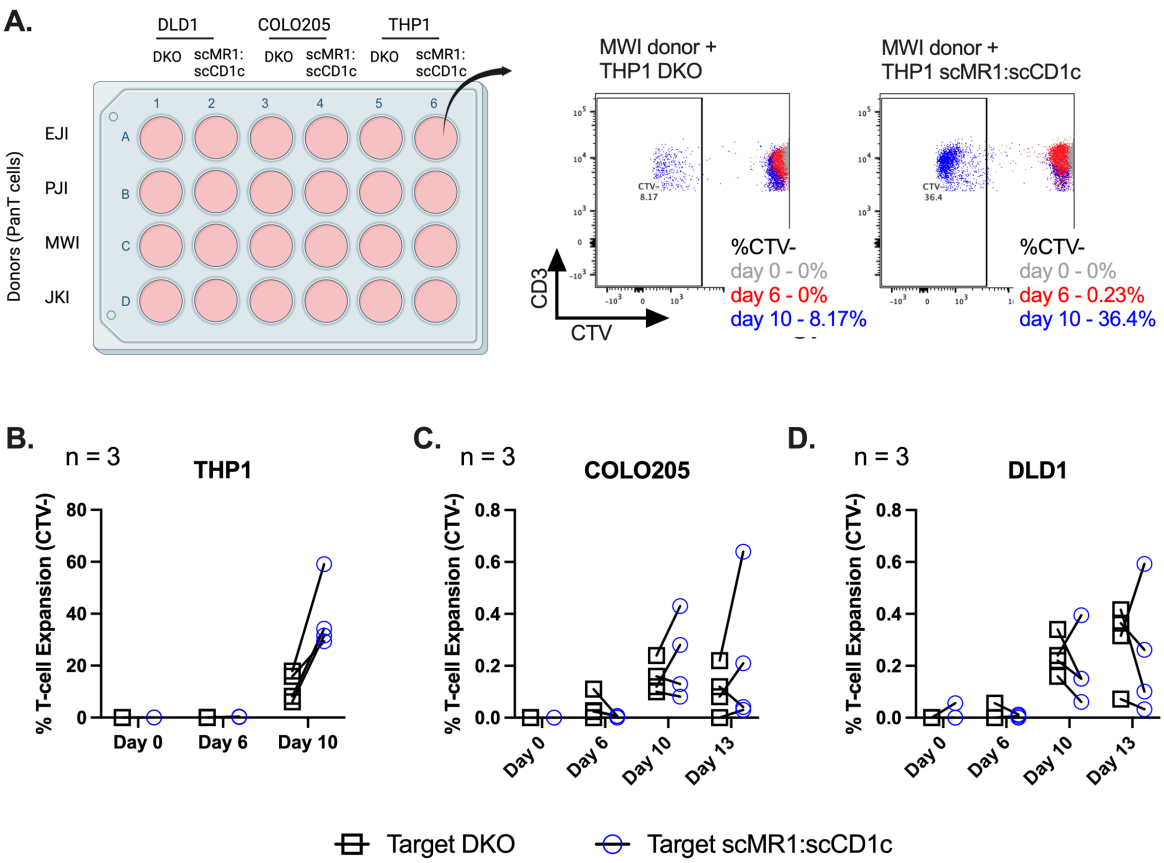

E.

Polyclonal T-cell line:	Expanded against
EJI_T10	THP1 scMR1:scCD1c
PJI_T10	THP1 scMR1:scCD1c
MWI_T10	THP1 scMR1:scCD1c
JKI_T10	THP1 scMR1:scCD1c
PJI_N13	COLO205 scMR1:scCD1c

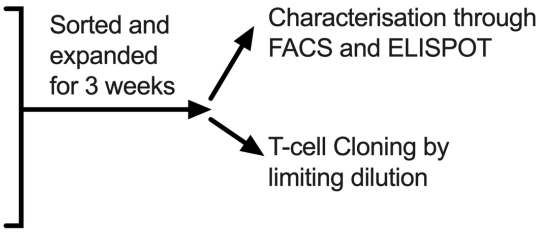

Figure 4- 9. T-cell expansion assays generated 5 polyclonal lines rich in MR1 or CD1c-restricted T-cells. (**A**) Representative experimental layout of 1 out of 3 technical replicates where $2x10^6$ T-cells from 4 donors were expanded against 10^6 target cells (1:1 mix of THP1 OR COLO205 cells expressing either scMR1 or scCD1c ,left panel). T-cell proliferation was monitored over a 10-day time-course (right panel). (**B-D**) Frequencies of T-cell expansion against DKO (black) and scMR1:scCD1c (Blue) THP1 (**B**), COLO205 (**C**), DLD1 (**D**) target cells. (**E**) Diagram of following expansion and experiments with sorted polyclonal T-cells.
Data were acquired in a single experiment. Each datapoints in **B-D** corresponds to a different donor and represents the average proliferation from 3 technical replicates.

4.3.7. Polyclonal lines contained both CD1c and MR1-specific T-cells

T10 and N13 polyclonal T-cells were re-challenged with wild-type (WT) THP1 and COLO205, respectively. Activation levels were measured by expression of CD137 or IFNγ. From the 5 polyclonal lines, only MWI_T10 and PJI_N13 showed MR1 and CD1c-reactivity against WT target cells in flow cytometry assays. The reactivity of MWI_T10 against $THP1^{WT}$ contained a mix of CD1c and MR1 specificities, whereas PJI_N13 activation against $COLO205^{WT}$ was primarily MR1-specific (**Figure 4- 10A-C**).

In IFNγ ELISPOT assays, T10 cell lines were challenged with CRC lines expressing scMR1 or scCD1c. T10 lines showed specific reactivity against both CD1c and MR1 (**Figure 4- 10D-G**), with 1 polyclonal line showing predominance of CD1c-mediated activation (**Figure 4- 10E**), 1 showing predominance of MR1-specificity (**Figure 4- 10G**) and 1 with similar frequencies of CD1c and MR1-reactive T-cells (**Figure 4- 10F**). Conversely, PJI_N13 was challenged with modified THP1 and DLD1 cells, showing over >90% MR1-specificity in the activated T-cells against both target cells (**Figure 4- 10H**).

While modified DLD1 cells did not induce MR1-specific activation nor proliferation in fresh PBMCs or panT-cells, they triggered higher MR1-specific responses than THP1 or COLO205 cells in pre-expanded polyclonal T-cells (**Figure 4- 10D-G**). This could indicate that most MR1T cells at steady-state in blood have a high activation threshold requiring co-signalling or a priming process to activate and expand, consistent with a potentially naïve phenotype (explained in more detail in chapter 5). On the other hand, in polyclonal lines, because they have been expanded several times or pre-primed with PHA, they may have a pronounced effector phenotype with a reduced activation threshold.

These results also suggest that different target cells have an overlapping expression of MR1 and CD1c antigens. Even the CRC^{scCD1c} epithelial cells, which did not express CD1c at steady-state, could activate pre-primed CD1c-specific T-cells that expanded against a

different target cell, in this case, THP1^{scCD1c} (**Figure 4- 10D-H**). On the other hand, panT-cells from the PJI donor had a considerable expansion of CD1c-reactive cells against THP1$^{scMR1:scCD1c}$ cells (**Figure 4- 10F**), but this was not the case against COLO205 $^{scMR1:scCD1c}$ cells (**Figure 4- 10H**), where a predominant response was of MR1-restricted. This initial result indicates that CRC lines cannot induce the proliferation of CD1c-specific T-cells because they are not natural expressors of CD1c; nevertheless they can produce CD1c specific antigens through which they can activate pre-primed CD1c-restricted T-cells. More biological replicates are needed to confirm whether CRC^{scCD1c} lines can induce CD1c-specific T-cell expansion or not.

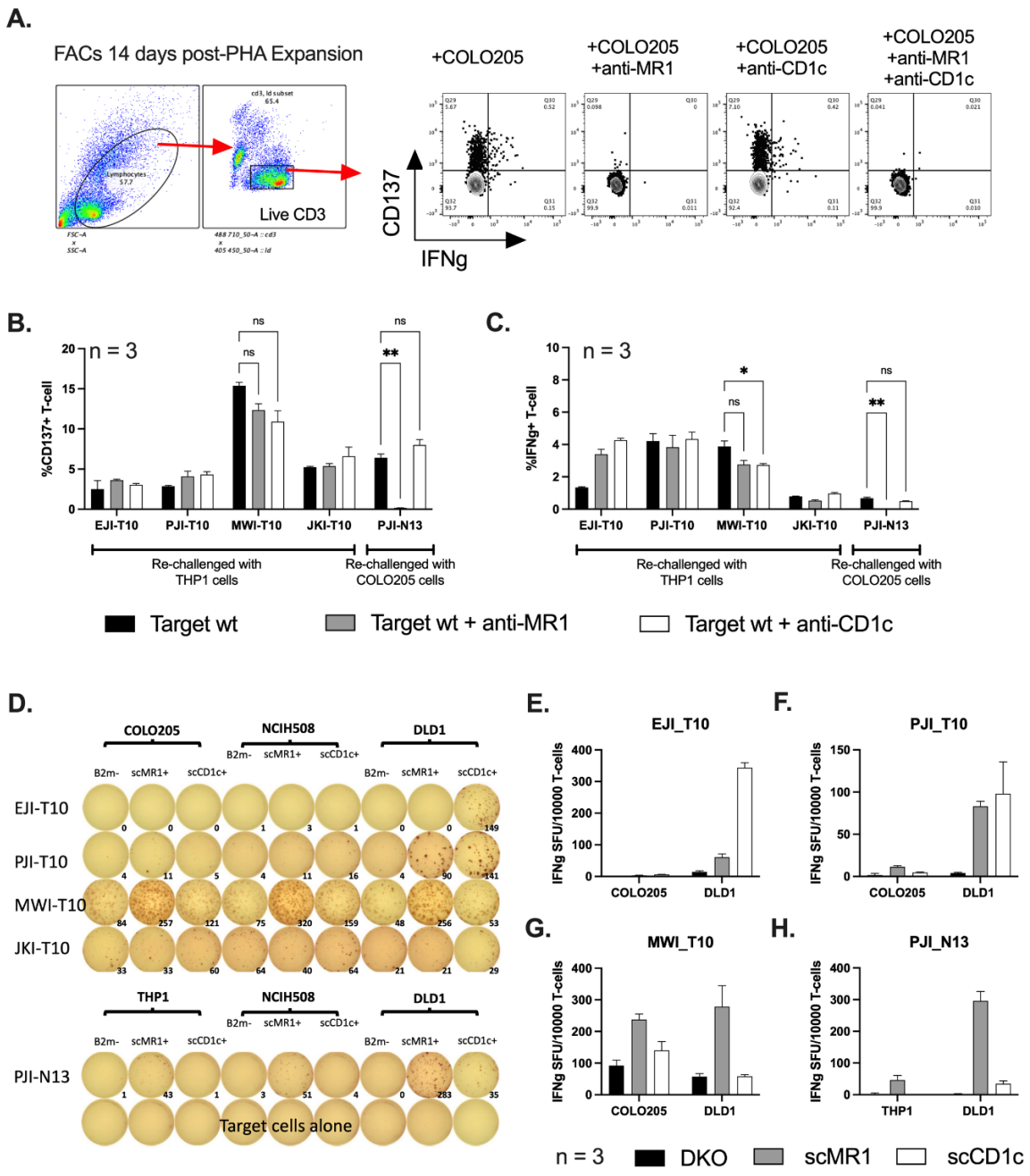

Figure 4- 10. MWI_T10 and PJI_N13 have high frequencies of MR1-specific T-cells. (**A-C**) $2x10^4$ T-cells from expanded polyclonal lines were incubated overnight with $5x10^4$ WT target cells. (**A**) Gating strategy (left panel) and representative FACSpots of CD137 and IFNγ expression in PJI_N13 polyclonal line against WT target cells (right panel). (**B-D**) Frequencies of CD137 (**B**) and IFNγ (**C**) in polyclonal T-cells against WT target cells alone (black) or in the presence of anti-MR1 (Grey) or anti-CD1c (White).
(**D-H**) ELISPOT assays of $2x10^4$ T-cells from polyclonal lines incubated overnight against $5x10^4$ DKO, scMR1 or scCD1 expressing target cells. (**D-H**) Representative technical replicate of ELISPOT assay (**D**) and normalised IFNγ SFU counts in 10^4 T-cells from EJI_T10 (**E**), PJI_T10 (**F**), MWI_T10 (**G**) and PJI_N13 (**H**) polyclonal lines across 3 separate ELISPOT assays.

Data were acquired in a single experiment. Error bars represent Mean ± SEM of 3 technical replicates. Differences among conditions in **D-C** were analysed by 2-way ANOVA with uncorrected Fisher's LSD test. *p < 0.05, **p < 0.01, ***p < 0.001, ****p < 0.0001.

4.3.8. Polyclonal lines are likely to contain polyfunctional T-cell populations

An in-depth analysis of the PJI_N13 polyclonal line showed that only ~20% of the T-cells were MR1-specific based on upregulation of CD69 and CD25 in response to different target cells expressing scMR1. In previous results, PJI_N13 contained virtually no CD1c-reactive T-cells; therefore, the remaining expanded T-cells were presumably MR1-unspecific (**Figure 4- 11A, B**) or specific to other activating molecules. One unclear aspect of these results is whether the reactive T-cells against the THP1 and CRC targets were the same T-cell clones. To answer that question, we would need to sort and sequence the reactive clones against different target cells.

When we analysed polyclonal lines based on CD69/CD25 upregulation, most MR1-reactive T-cells in PJI_N13 were CD4+ (**Figure 4- 11B**). Nevertheless, if we focus on IFNγ expressing cells, most of these are CD8+ (**Figure 4- 11C**). This is an important consideration, as IFNγ expression was used to select MR1-reactive T-cell clones in ELISA or ELISPOT assays (**Supplementary Figure 4- 3**). Although this analysis was not done for the other polyclonal lines, this finding could explain why most of the CD1c and MR1-reactive clones we found were CD8+ T-cells.

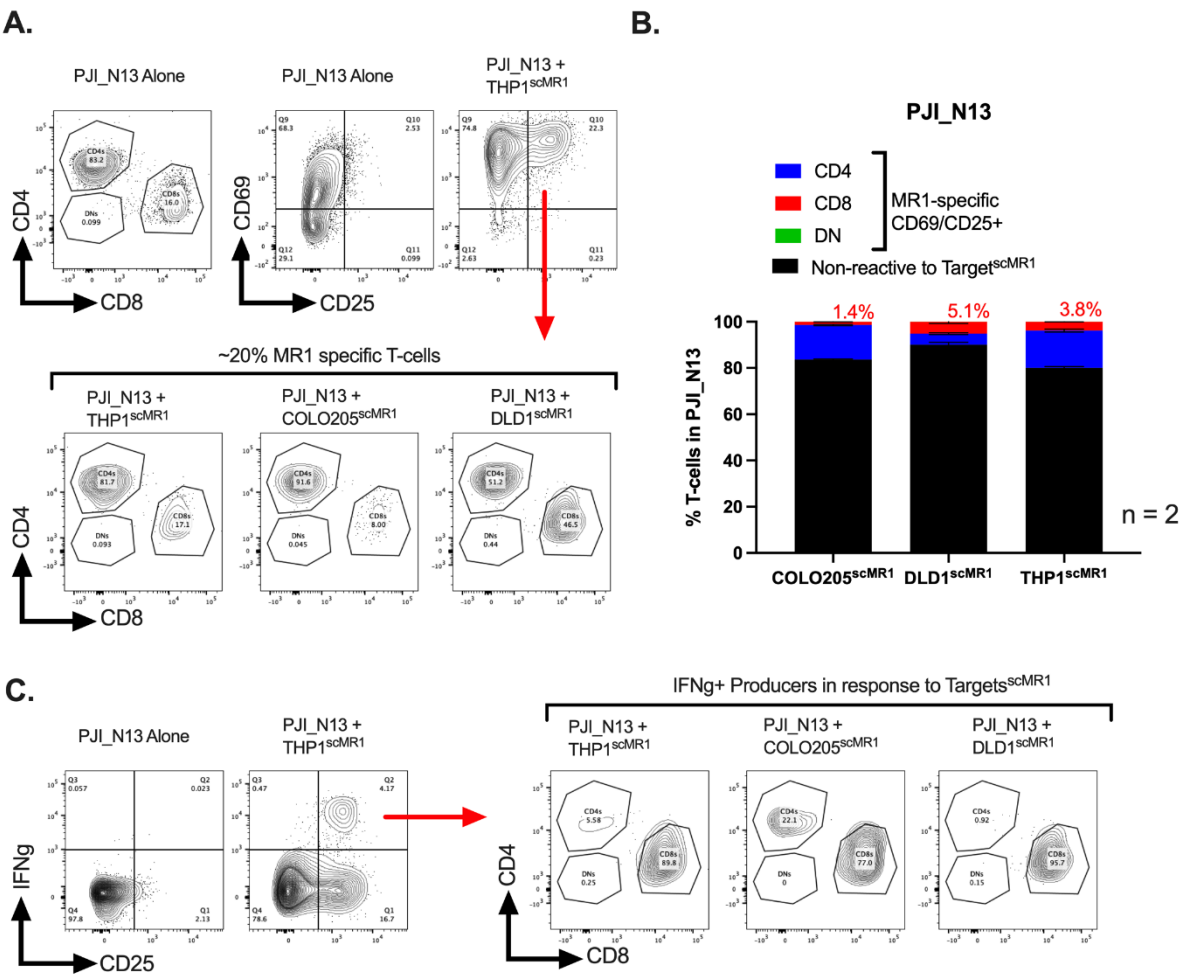

Figure 4- 11. MR1-reactivity in PJI_N13 is enriched in the CD4 T compartment, however I IFNγ-based detection is biased to CD8 T-cells. (**A-C**) $5x10^4$ T-cells from PJI_N13 polyclonal lines were incubated overnight with 10^5 $THP1^{scMR1}$. (**A**) Gating strategy of CD4, CD8 and DN T-cells (top-left panel). Representative FACSplots of bulk PJI_N13 activation against $THP1^{scMR1}$(top-right panel) and CD4, CD8 and DN T-cell composition within the activated cells (bottom panel). (**B**) Frequencies of unspecific (black) and MR1-reactive CD4 (blue), CD8(Red) and DN (Green) in PJI_N13. (**C**) Representative FACSplots of IFNγ expression in bulk PJI_N13 (left panel) and the frequencies of CD4, CD8 and DN T-cells within IFNγ producing cells against THP1, COLO205 and DLD1 cells expressing scMR1 (right panel).
Data were acquired in a single experiment. Error bars represent Mean ± SEM of 2 technical replicates.

4.3.9. Polyclonal lines contained CD1c and MR1-restricted T-cells

Next, we cloned the PJI_N13 and MWI_T10 lines by limiting dilution and plated them at 0.3, 1, 3, and 10 T-cells/well. T-cells were supplemented with irradiated feeders and expanded with 1μg/mL PHA and 100U/mL IL2 (**Figure 4- 12A**). The expanding T-cell clones were tested for IFNγ expression in response to THP1 or COLO205 cells expressing scMR1 or scCD1c. Out of the 2400 wells, ~400 had growing clones. From those, only ~166 clones were either CD1c or MR1 reactive. 27 came from the MWI_T10 polyclonal line and 139 clones from the PJI_N13 line (**Supplementary Figure 4- 3**), although strong TCR sequence convergence was seen in both cloning campaigns.

During TCR sequencing, a significant portion of clones were contaminated with more than 1 TCR pairing. After filtering, the resulting clean sequences converged into 11 TCR pairings (**Figure 4- 12B**); 6 of them were CD1c-specific (**Figure 4- 12C, D**), and 2 of them were MR1-specific (**Figure 4- 12C, E**). The remaining 3 sequences were initially deemed as MR1-specific based on IFNγ expression in screening ELISPOT assays; however, after transferring the TCR into primary CD8 cells, they did not retain the MR1-specificity (data not shown), indicating reactivity to other surface receptors.

The remaining of this chapter will focus on the 2 MR1-specific clones, referred to as MR1_C1 and MR1_C3. Both primary clones released IFNγ and TNFα in response to $THP1^{WT}$. This activation happened through the TCR complex because it could be blocked with monovalent anti-CD3 FLAG molecules (generated at Immunocore) (**Figure 4- 12F-I**). In addition, MR1_C1 and MR1_C3 activation could be blocked partially or fully with anti-CD8, respectively (**Figure 4- 12F-I**).

The CD8 dependency could be interpreted in several ways. Either CD8 provides stability to the TCR complex on the plasmatic membrane or CD8 favours productive TCR-MR1 interactions by increasing the avidity to MR1, as with HLA-I molecules. Furthermore,

the partial or full dependency on CD8 could be indicative of the weak affinity of MR1_C1 and MR1_C3 TCRs towards their cognate MR1-ligands.

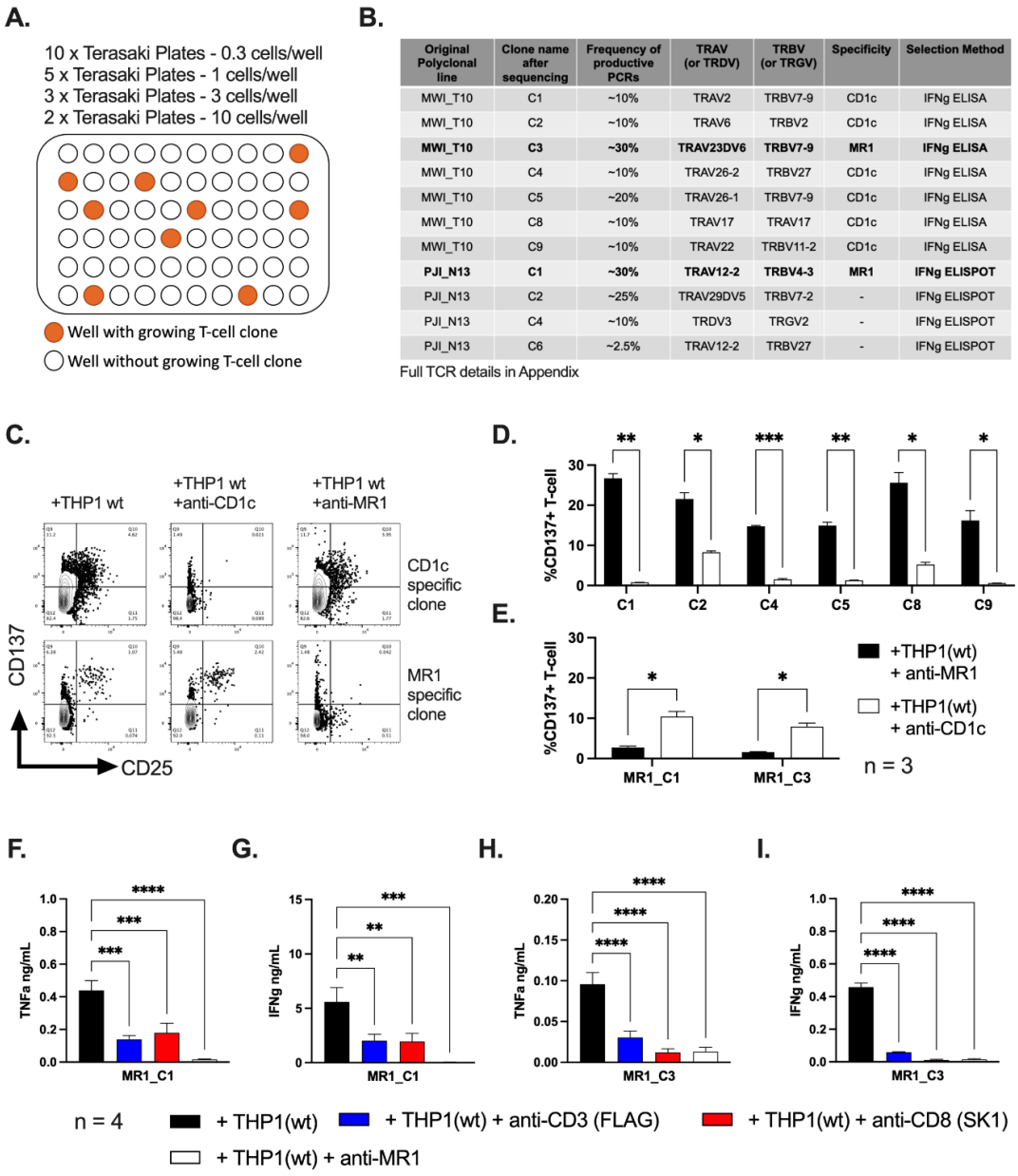

Original Polyclonal line	Clone name after sequencing	Frequency of productive PCRs	TRAV (or TRDV)	TRBV (or TRGV)	Specificity	Selection Method
MWI_T10	C1	~10%	TRAV2	TRBV7-9	CD1c	IFNg ELISA
MWI_T10	C2	~10%	TRAV6	TRBV2	CD1c	IFNg ELISA
MWI_T10	**C3**	**~30%**	**TRAV23DV6**	**TRBV7-9**	**MR1**	**IFNg ELISA**
MWI_T10	C4	~10%	TRAV26-2	TRBV27	CD1c	IFNg ELISA
MWI_T10	C5	~20%	TRAV26-1	TRBV7-9	CD1c	IFNg ELISA
MWI_T10	C8	~10%	TRAV17	TRAV17	CD1c	IFNg ELISA
MWI_T10	C9	~10%	TRAV22	TRBV11-2	CD1c	IFNg ELISA
PJI_N13	**C1**	**~30%**	**TRAV12-2**	**TRBV4-3**	**MR1**	**IFNg ELISPOT**
PJI_N13	C2	~25%	TRAV29DV5	TRBV7-2	-	IFNg ELISPOT
PJI_N13	C4	~10%	TRDV3	TRGV2	-	IFNg ELISPOT
PJI_N13	C6	~2.5%	TRAV12-2	TRBV27	-	IFNg ELISPOT

Figure 4- 12. MR1T clones isolated from polyclonal lines had a different dependency of CD8. (**A-B**) Representative diagram of seeded Terasaki plates in T-cell cloning campaigns (**A**) and list of validated CD1c and MR1-specific clones (**B**). (**C**) Representative FACSplots and frequency of CD137 and CD25 upregulation (**D-E**) in primary T-cell clones against THP1^{WT} cells alone or with anti-MR1 (black, **D**) and anti-CD1c blocking (white, **E**).
(**F-G**) Secretion of TNFα (**F, H**) and IFNγ (**G, I**) in MR1_C1 and MR1_C3, respectively, upon overnight incubation with THP1 alone (black) or in the presence of anti-CD3 (blue), anti-CD8 (red) and anti-MR1 (white).
Data were acquired in a single experiment. Error bars represent Mean ± SEM of technical replicates. Differences among conditions in **D-I** were analysed by 2-way ANOVA with uncorrected Fisher's LSD test. *p < 0.05, **p < 0.01, ***p < 0.001, ****p < 0.0001.

4.3.10. MR1 reactive clones have different specificity and sensitivity to the K43A mutation on MR1

MR1_C1 and MR1_C3 clones were challenged with THP1 cells transduced with scMR1^{wt} and scMR1^{K43A} mutant. The K43A mutation abrogates the ability of antigens to form a Schiff base in the A' pocket of MR1 (McWilliam *et al.* 2016; Mak *et al.* 2017). Therefore, it is reasonable to assume that the scMR1^{K43A} mutant might present a different repertoire of endogenous ligands than scMR1^{wt}. Of note, this mutation does not exclude ligands such as 5OPRU or 6FP from still sitting on scMR1^{K43A} without forming the covalent link; however, their binding-affinity to MR1 would be much lower, and other endogenous antigens can displace them (Awad *et al.* 2020; Seneviratna *et al.* 2022). In our assays, exogenous ligands such as 6FP or 5OPRU were not added, although it is possible that 6FP analogues can form spontaneously in folate-rich media.

In activation assays, MR1_C1 showed no sensitivity to the MR1^{K43A} mutation. On the other hand, the K43A mutation completely abrogated the activation of MR1_C3 TCR (**Figure 4- 13A, B**). This suggests that while MR1_C1 and MR1_C3 TCRs can recognise MR1^{wt}, their specificities differ. MR1_C3 specificity could be towards a group of ligands or a particular MR1 conformation that requires the formation of Schiff bases, while this might not be compulsory in the case for MR1_C1.

Next, we stained MR1_C1 and MR1_C3 clones with tetramers loaded with Schiff base-forming antigens: 5FSA, 6FP and 5OPRU (generated at Immunocore). As controls, E8 and MAIT-TCR were also stained. As positive and negative controls, the E8-TCR, which is ligand agnostic, can be stained by all 3 tetramers, the VT001-TCR could only be stained with the 5OPRU tetramers. In comparison, MR1_C1 and MR1_C3 TCR could not be stained for 5OPRU tetramers and showed binding only to 6FP tetramers (**Figure 4- 13C**). While MR1_C1 T-cells could also be weakly stained with 5FSA tetramers, MR1_C3 could not, underlining differences in their specificity (**Figure 4- 13C**).

To validate whether the tetramer staining data corresponds with ligand-mediated activation data, we incubated overnight MR1_C1 and MR1_C3 clones with THP1 cells in the presence of increasing amounts of 6FP, 5OPRU and 5FSA. Both T-cell clones secreted IFNγ and TNFα at higher concentrations when 6FP was present in the media. There was no change with 5OPRU and a significantly reduced T-cell activation with 5FSA (**Figure 4-13D, E**).

The inhibitory effects observed with 5FSA could be explained because it displaced relevant ligands. Nevertheless, we also observed this inhibitory effect on PHA-activated T-cells, suggesting that the observed inhibitory effects could be toxicity to the T-cells (**Supplementary Figure 4- 5**). The activating effects of 6FP happened at 100nM-10μM, which are concentrations that might not be biologically representative. On the other hand, 5OPRU could not displace the endogenous MR1 antigens in competitive assays.

Altogether, these results could suggest that both TCRs recognise Schiff base-forming antigens that cannot be displaced with concentrations as high as 10μM of exogenous 5OPRU. We also believe that while the cognate antigens for MR1_C1 might still be stable on MR1 without the covalent link, this might not be the case for MR1_C3 ligands. To further explore this hypothesis, this experiment should be repeated with THP1$^{MR1\text{-}K43A}$ mutant to remove the effects of the Schiff base and the intracellular trafficking of MR1 in competition assays.

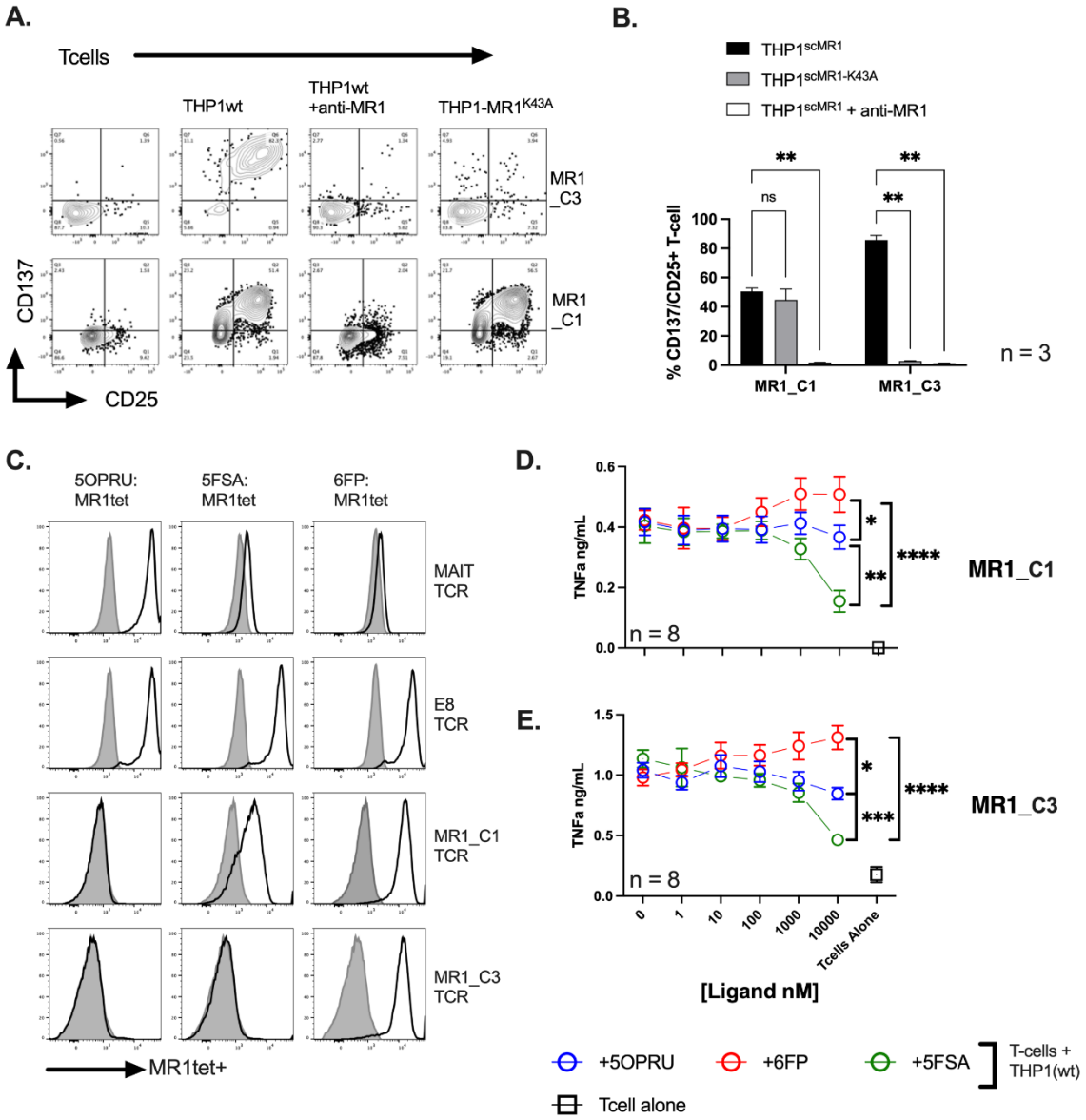

Figure 4- 13. MR1_C1 and MR1_C3 clones have different MR1 specificities and sensitibity to the K34A mutation. (**A-B**) Overnight incubation of MR1T clones with modified THP1 cells. (**A**) Representative FACSplots and frequencies (**B**) of CD137 and CD25 expression in MR1T cells in response to THP1^{scMR1} cells lines (black) or with anit-MR1 (white) and to THP1$^{scMR1\text{-}K43A}$ (grey). (**C**) Representative histograms of 5OPRU, 5FSA and 6FP tetramer staining of VT001, E8, MR1_C1 and MR1_C3 TCRs. (**D-E**) Secretion of TNFα in overnight incubation of MR1_C1 (**D**) and MR1_C3 (**E**) with THP1 cells spiked with different concentrations of 5OPRU (blue), 6FP (red) and 5FSA (green). Data were acquired in a single experiment in **C** and 2-3 independent experiments in **A**, **D, E**. Error bars represent Mean ± SEM of technical replicates. Differences among conditions in **B, D, E** were analysed by 2-way ANOVA with uncorrected Fisher's LSD test. *p < 0.05, **p < 0.01, ***p < 0.001, ****p < 0.0001.

4.3.11. Transduced primary CD8 T-cells provided higher antigen-specific responses than their Jurkat counterparts

MR1_C1 and MR1_C3 TCRs were transferred into TCR null Jurkats without endogenous TCRs and into primary CD8 T-cells. The TCR transfer was conducted using a lentiviral vector with a polycistronic format where the TCRα and the TCRβ chains were separated by a P2A sequence (**Figure 4- 14A**). Lentiviral constructs also had a puromycin resistance gene used to enrich transduced cells.

We chose TCR null Jurkat cells as an ideal effector line because they proliferate indefinitely and do not carry endogenous TCRs, which would make their maintenance easy and ensures that the Jurkat response is specific to the transduced TCRs. The main challenge with Jurkat effectors is their inability to express cytotoxic molecules; therefore, they cannot be used in killing assays or IFNγ-based assays. After the TCR transduction to Jurkats, we observed that a significant portion of MR1_C1 and MR1_C3 TCRs (70% and 90%, respectively) were located intracellularly (**Figure 4- 14B**). Although it is unknown how stable the TCR is on E8-Jurkats, PHA stimulations showed significantly higher activation in E8-Jurkats compared to C1 and C3-Jurkats, suggesting that the E8-TCR is more accessible and stable (**Figure 4- 14C**). Accordingly, C1 and C3-Jurkats only weakly recognized $THP1^{WT}$ cells (**Figure 4- 14C**).

On the other hand, primary CD8 cells require PHA and feeder-mediated expansion and cannot proliferate indefinitely. Moreover, they also carry an endogenous TCR, which can misspair with the transduced TCR chains, generating 4 potential TCR populations in each CD8 T-cell. To favour the correct pairing of the transduced TCRs, these were introduced with an extra disulphide bond (ds) in the TCR constant domains (**Figure 4-14A**). With these modifications, C3ds-CD8 cells showed increased MR1-specific activation whereas no changes were seen in C1ds-CD8 (**Supplementary Figure 4- 4**). We could not quantify the surface expression of the transduced TCR in CD8 cells because they carry

endogenous TCRs and we did not have Vbeta specific antibodies. However, unlike Jurkats, C1ds and C3ds-CD8 cells responded to $THP1^{WT}$ cells by significantly upregulating CD69, CD25 (**Figure 4- 14D-F**), CD137 and IFNγ (data not shown).

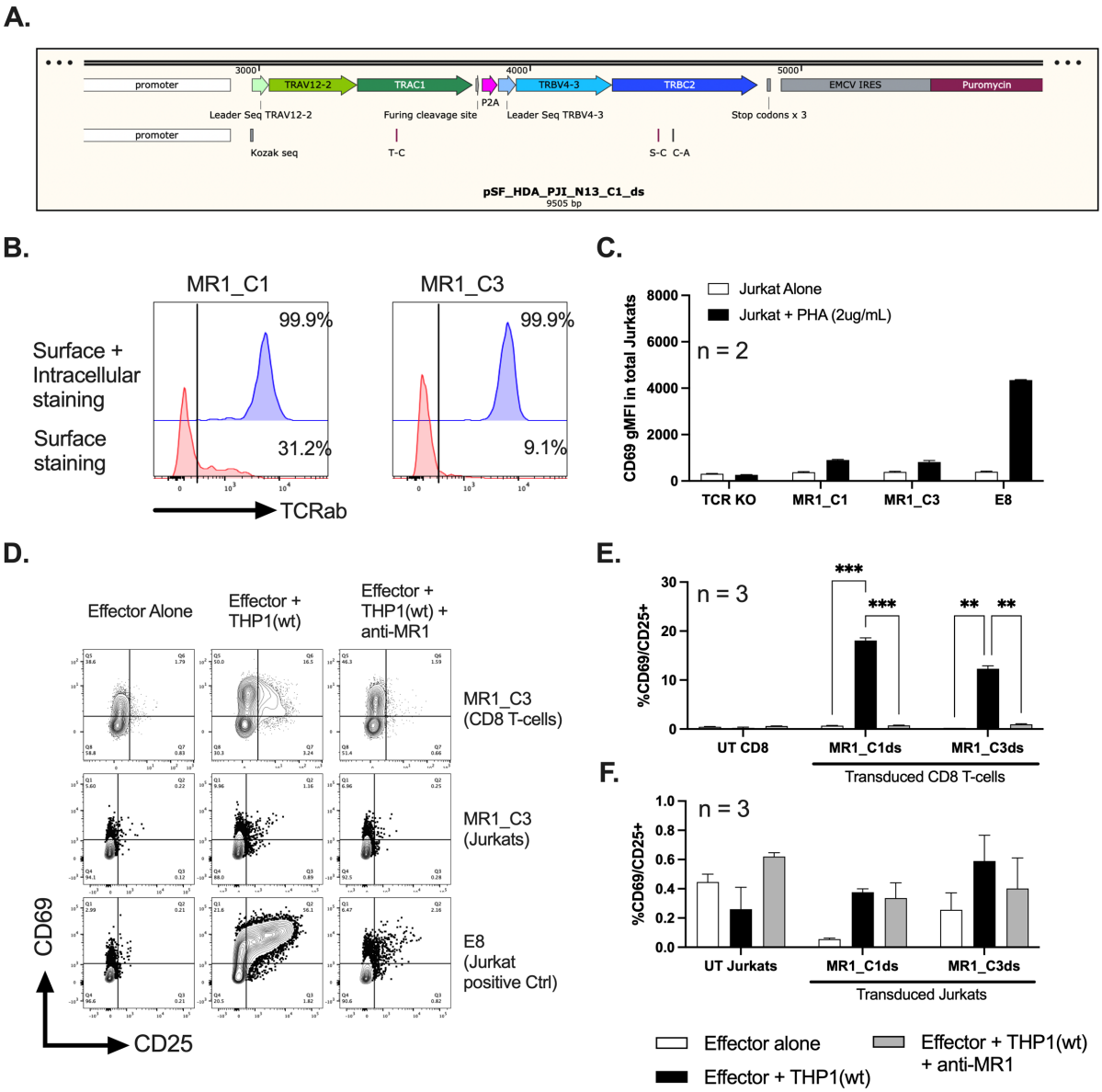

Figure 4- 14. MR1_C1 and MR1_C3 TCRs have better expression and antigen sensitivity on primary CD8 cells than on Jurkat cells. (**A**) Structure of polycistronic expression of TCRα and TCRβ chains separated by P2A ribosome shifting sequence. (**B**) Representative histograms of surface (red) and total (blue) staining of transduced TCRαβ in Jurkats. (**C**) CD69 geometric mean in PHA activated Jurkats that have been transduced with vector, MR1_C1, MR1_C3 and E8 TCRs. (**D**) Representative FACSplots and activation levels of CD8 T-cells (**E**) and Jurkats (**F**) transduced with MR1_C1ds and MR1_C2ds.

Data were acquired in a single experiment in **B** and 2-3 independent experiments in **C_E**. Error bars represent Mean ± SEM of technical replicates. Differences among conditions in **C, E, F** were analysed by 2-way ANOVA with uncorrected Fisher's LSD test. *p < 0.05, **p < 0.01, ***p < 0.001, ****p < 0.0001.

4.3.12. MR1-mediated activation is not purely dependent on expression levels of MR1

To remove the cellular component in the MR1-specific activation, Immunocore generated soluble MR1 molecules expressed in Expi293 mammalian cells. We assumed that these MR1 monomers are loaded with endogenous metabolites from Expi293. These purified MR1 monomers were used in plate-bound activation assays with 5μg/mL monomer to activate C1ds and C3ds-CD8 cells. In our flow cytometry assays, transduced CD8 cells can respond in an MR1-specific manner to plate-bound monomers without additional components from target cells (**Figure 4- 15A-C**). Like the results seen in section **Figure 4- 13**, C3ds-CD8 ligation could be abrogated with the K43A mutation on MR1 (**Figure 4- 15C**). Also, C1ds-CD8 showed a partially weaker response of the $MR1^{K43A}$ mutant compared to $MR1^{WT}$ molecules (**Figure 4- 15B**), agreeing with previous hypothesis that both MR1_C1 and MR1_C3 TCRs may be recognising Schiff base-forming antigens.

Recently a patient lacking MAIT cells was reported to have an MR1 mutation called R9H, which prevents the binding of 5OPRU and selection of MAIT cells in the thymus. We therefore expressed and tested this mutant in our plate-bound assay to gain further insights into the differential antigen specificity of MR1_C1 and MR1_C3 (Howson et al., 2020). The R9H mutation affects MR1's stability and capacity to go to the cell surface (Howson *et al.* 2020). Because of this, we could not use target cells to assess if MR1_C1 and MR1_C3 TCRs are sensitive to this mutation; however, in plate-bound assays, neither of the 2 TCRs could recognise the $MR1^{R9H}$ mutant (**Figure 4- 15B**). It is unclear if the R9H can present any antigens; however, its inability to egress the ER suggests that the structural changes to the ligand-binding region are impairing antigen presentation. Therefore, the absence of recognition by C1_MR1 and C3_MR1 TCRs confirms again that both TCRs are specific to self-antigens.

Next, we wanted to assess the reactivity of the MR1T TCRs to different WT cancer cell lines. We used E8-Jurkat activation to determine and rank the target cells' capacity to activate effector cells through MR1 (**Figure 4- 15E**). In our activation assays, MR1_C1ds and MR1_C3ds TCRs followed a very similar pattern of recognition to the E8-TCR; however, they differed in their activation against THP1 cells, which the E8-TCR recognised weakly (**Figure 4- 15E-G**). Although more analysis needs to be done, MR1_C1 and MR1_C3 TCRs had different recognition patterns to the E8-TCR, therefore this strongly indicating that the activation of transduced CD8 cells may not be purely dependent on MR1 levels, but also on the specific recognition of endogenous metabolites.

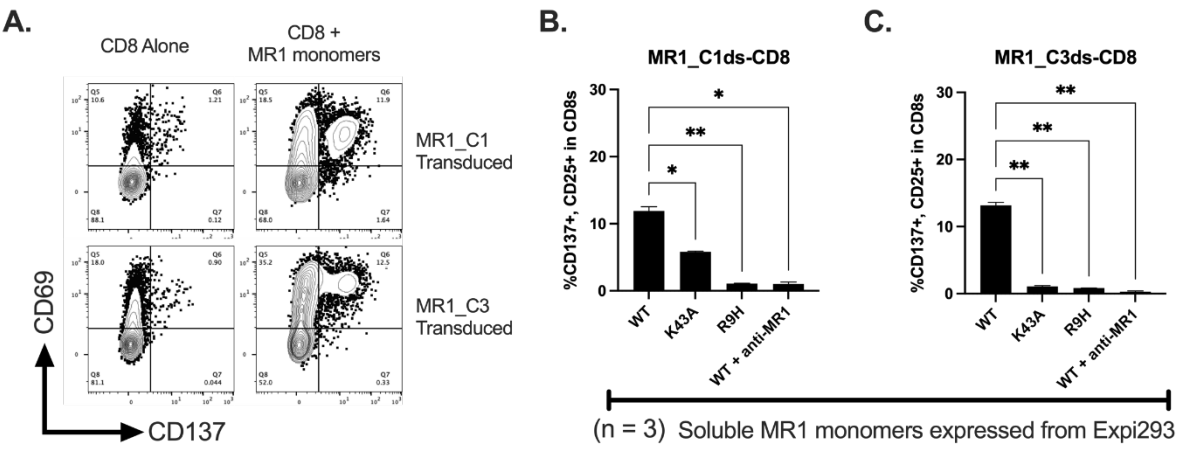

D.

Tissue	Cell name	Cell type	Disease
Lymphoid/Blood	U266	B-cell	Myeloma
Lymphoid/Blood	MOLT4	T-lymphoblast	Lymphoblastic Leukaemia
Myeloid/Blood	THP1	Monocyte	Monocytic leukaemia
Gut	COLO205	(Colon) Epithelial	Dukes' type D, colorectal
Skin	MEL624	Skin	Melanoma
Skin	MEL526	Skin	Melanoma
Kidney	786O	Epithelial	Renal carcinoma
Pancreas	PSN1	Epithelial-like	Adenocarcinoma

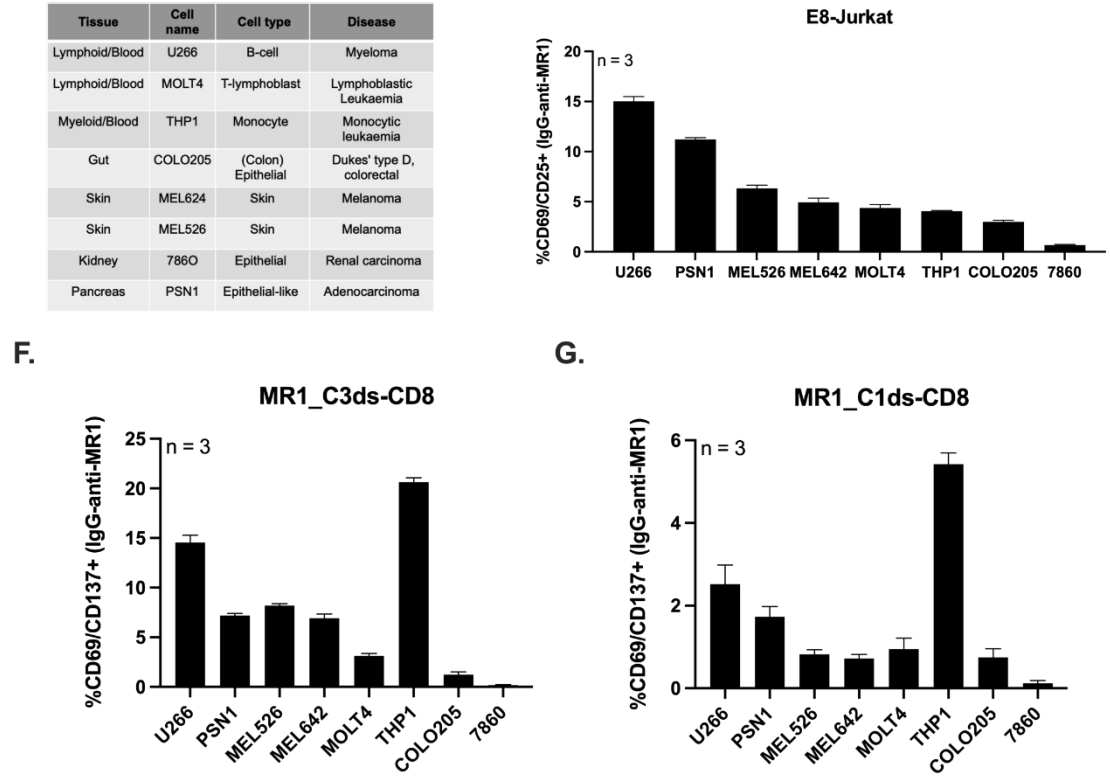

Figure 4- 15. MR1T TCRs are reactive to different cancer lines by recognising endogenous targets. (**A-B**) CD8 T-cells transduced with MR1T TCRs were activated overnight in plate-coated MR1 purified from mammalian cells. (**A**) Representative FACSplots and frequencies (**B**) of CD137+ and CD25+ CD8 T-cells in response to $MR1^{WT}$, $MR1^{K43A}$ and $MR1^{R9H}$ with and without anti-MR1 blocking. (**D**) Table of cancer target cells and their surface levels of MR1 determined by E8-TCR activation (**E**). (**F-G**) activation of MR1_C3ds (**F**) and MR1_C1ds (**G**) transduced CD8 T-cells in overnight activation assays with a panel of WT target cells.

Data were acquired in a single experiment. Error bars represent Mean ± SEM of technical replicates. Differences among conditions in **B,C** were analysed by 2-way ANOVA with uncorrected Fisher's LSD test. *p < 0.05, **p < 0.01, ***p < 0.001, ****p < 0.0001.

4.3.13. MR1T TCRs showed the preferential killing of blood-derived cancer cell lines than their healthy counterparts

Next, we established killing assays by quantifying the number of target cells after overnight incubation with MR1T transduced CD8 cells. To standardise this quantification, sterile counting beads were used (**Figure 4- 16A**) as a reference to count the loss of live target cells due to CD8 activity in killing assays. To calculate the number of target cells per bead, the following formula was applied:

$$\text{Standardised target count (STC)} = {}^{\#\text{ Target cells}}/_{\#\text{ Beads}}$$

In overnight killing assays, C1ds and C3ds-CD8 cells elicited MR1-dependent THP1 killing. This effect could be blocked with anti-MR1 (**Figure 4- 16B**). To determine the amount of killing of different target cells, the following formula was used:

$$\text{MR1 mediated killing} = 100 \text{ x } \frac{(\text{STC without CD8} - \text{STC with CD8})}{\text{STC without CD8}}$$

MR1-mediated killing was seen against all target cells, with a preferential killing of THP1 cells (**Figure 4- 16C, D**). This agrees with the activation data where MR1T TCR transduced CD8 cells had higher activation against $THP1^{WT}$ target cells than other cell lines.

In preliminary assays, we also quantified the amount of killing of healthy and cancer cells. Because fresh PBMCs were easily accessible, we purified CD19, CD3 and CD14 cells and compared the overnight killing of healthy cells with cancer cell counterparts (U266, MOLT4 and THP1, respectively). In 3 biological replicates, these healthy cells elicited comparable E8-Jurkat activation to their cancer counterparts (**Figure 4- 16E**). Killing assays showed a significantly higher MR1-mediated killing activity against THP1 and

MOLT4 cancer lines than CD14 and CD3 cells, respectively (**Figure 4- 16F, G**). No significant differences were seen between the killing of U266 and CD19 cells (**Figure 4-16F, G**). These results could suggest that MR1_C1 and MR1_C3 TCRs have some specificity towards some cancer cells over their healthy counterparts.

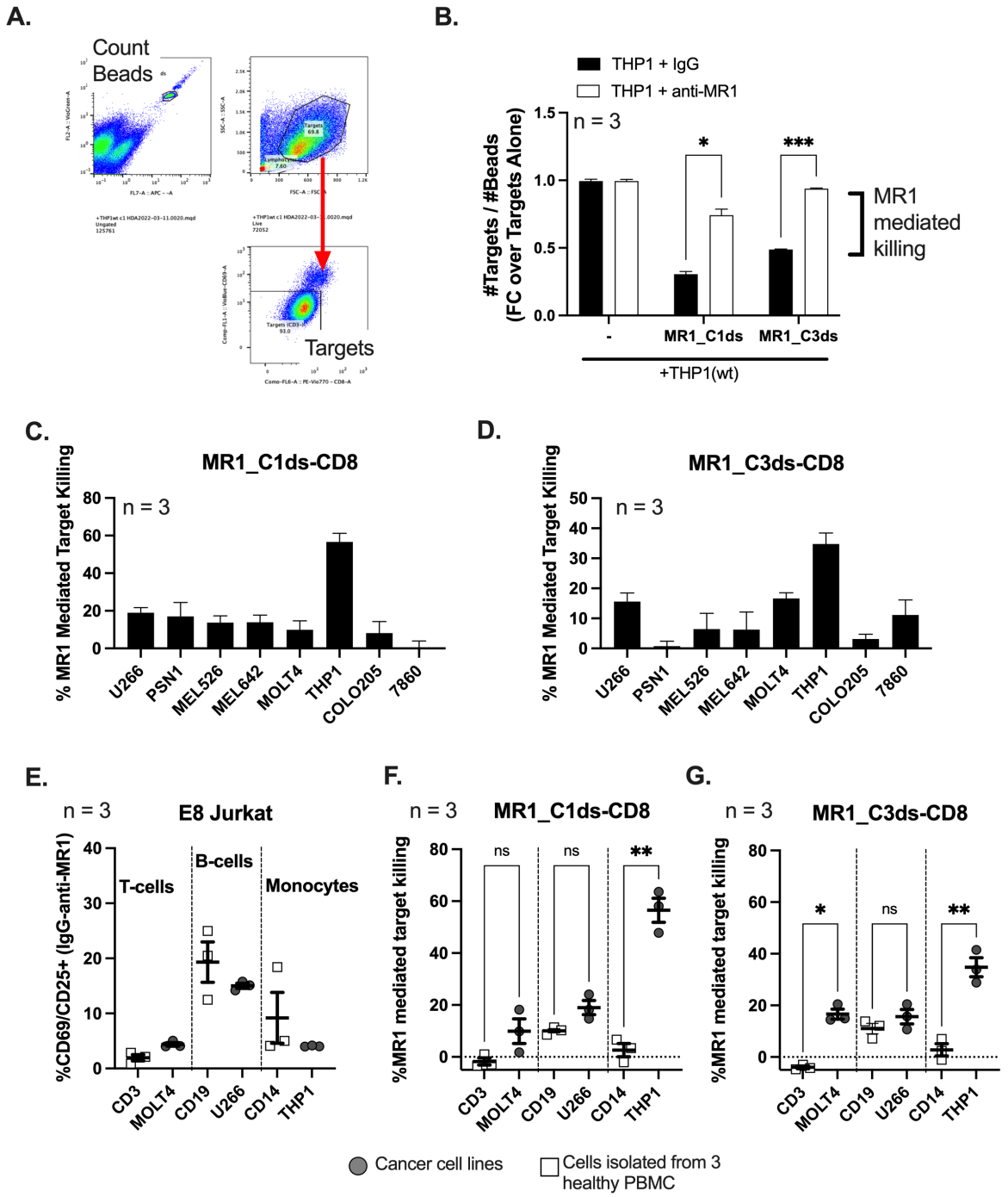

Figure 4- 16. CD8 cells transduced with MR1T TCRs can elicit specific killing of cancer target cells. (**A**) Gating strategy of beads and target cells and frequencies of live THP1 cells per bead (**B**)

after overnight incubation with CD8 cells with transduced MR1T cells alone (black) or with anti-MR1 (white). The difference between the 2 is the MR1-mediated killing. (**C-D**) Killing of cancer-derived panel of WT target cells by CD8 cells transduced with MR1_C1ds (**C**) and MR1_C3ds (**D**). (**E-G**) MR1 levels in cancer (grey) and healthy (white) blood-derived cell lines determined by E8-Jurkat activation (**E**) and, killing of healthy and cancer cells by CD8 cells transduced with MR1_C1ds (**F**) and MR1_C3ds (**G**).

Data were acquired in a single experiment. Error bars represent Mean ± SEM of 3 technical replicates in **B-D** and 3 biological replicated in **E-G**. Differences among conditions were analysed by 2-way ANOVA with uncorrected Fisher's LSD test. *p < 0.05, **p < 0.01, ***p < 0.001, ****p < 0.0001.

4.3.14. The blocking of autophagy in THP1 cells did not impact the activity of the MR1T transduced CD8 cells

One topic of interest in the Klenerman group was the role of autophagy in MR1 trafficking and the generation of MR1 antigens. A recent patent showed that abnormal redox conditions and accumulation of reactive adducts such as glyoxal inside cells could favour the generation of MR1 ligands (de Libero *et al.* 2021). Considering these results, we asked whether autophagy had any role in the generation of MR1 ligands.

To analyse the role of autophagy, Dr Phalora treated THP1 cells with Bafilomycin A1, 3MA, and Wortmannin drugs. While Bafilomycin-A1 inhibits autophagy by blocking the acidification and fusion of lysosomes with autophagosomes (Klionsky *et al.* 2008; Wang *et al.* 2021), 3MA and Wortmannin are inhibitors of class-III PI3K, which prevent the formation of autophagosomes (Blommaart *et al.* 1997; Wu *et al.* 2010; Jaber *et al.* 2012; Iershov *et al.* 2019). In our results, autophagy-blocking drugs caused an increase in surface levels of MR1 in THP1 cells (**Figure 4- 17A**). In addition, knock-down (KD) of Atg7, a protein involved in the formation of autophagic vesicles, led to an increase in MAIT response to fixed *E.coli* or 5OPRU (**Figure 4- 17C, D**). On the other hand, enhancing autophagy by starving THP1 cells with EBSS caused a slight reduction in the surface staining of MR1 (**Figure 4- 17A**).

To understand more about the antigens for MR1_C1 and MR1_C3, we asked if blocking autophagy would increase the activation of MR1T transduced CD8 cells. In pilot activation and killing assays, we did not convincingly see any correlation in the CD8 activity against $THP1^{WT}$, $THP1^{Atg7\text{-}KD}$ (**Figure 4- 17E-H**) and, their respective expression of Atg7 (**Figure 4- 17B)**. One problem in these assays is that Atg7 KD causes changes in morphology and proliferation rate, which are factors that require additional controls. Future assays should focus initially on how the treatments of THP1 cells with autophagy-blocking drugs affect the activation of the MR1T TCRs.

Overall, these results did not fully answer whether autophagy is directly or indirectly related to MR1-mediated antigen presentation. One possibility is that autophagy is directly involved in the degradation of MR1 antigens or MR1 receptors. Alternatively, the blocking of autophagy could be causing other metabolic changes that increase the generation of MR1 ligands. More experiments are needed to show a correlation between MR1-related signals (either surface expression, MAIT or MR1T activation) and the autophagy flux, witch could be monitored by measuring the processing of LC3 into LC3-I and -II.

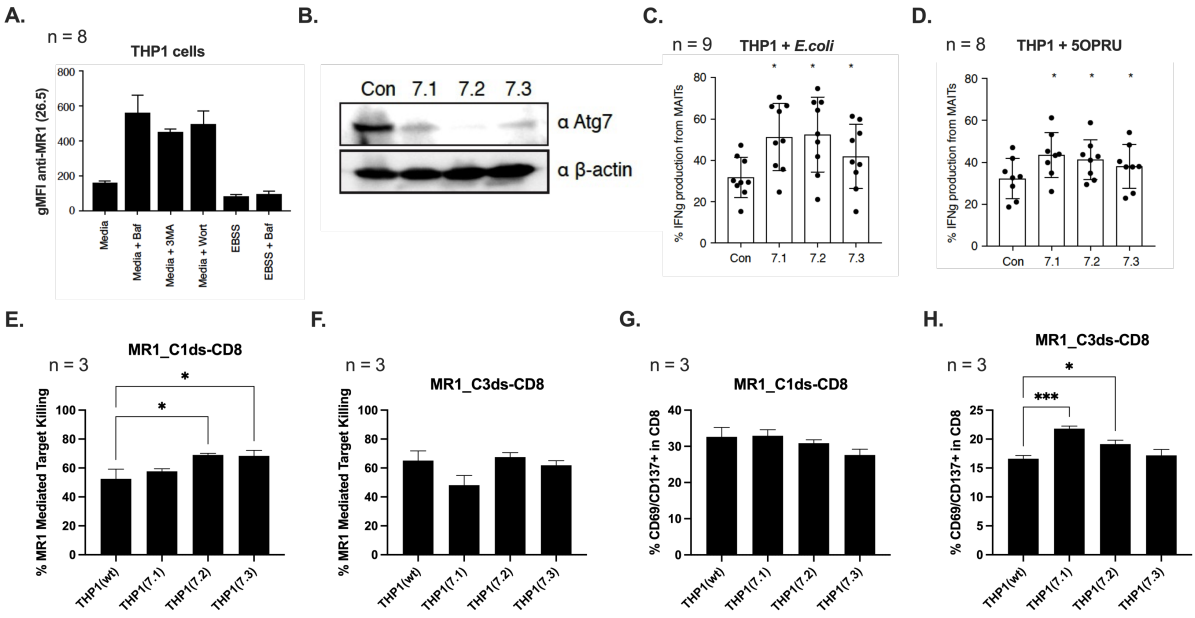

Figure 4- 17. Autophagy blocking induces increased MR1-mediated antigen presentation and response. (**A**) Surface expression of MR1 was determined by the 26.5 anti-MR1 in THP1 treated with autophagy inhibitors (Bafilomycin, 3MA and Wortmannin) and enhancer (EBBS). (**B**) Western blot of ATG7 expression compared to the β-actin housekeeping protein after shRNA-mediated KD. (**C-D** IFNγ production in MAIT cells after overnight incubation with $THP1^{ATG7\text{-}KD}$ expression and stimulation with fixed *E.coli* and 5OPRU. (**E-H**) Killing (**E, F**) and activation (**G, H**) of CD8 cells transduced with MR1_C1ds and MR1_C3ds, respectively.
Data were acquired in a single experiment in all figures except in **C-D**, where 3 independent experiments were conducted. Error bars represent Mean ± SEM of 3 technical replicates in all figures except in **C-D,** where datapoints are biological replicates. Differences among conditions were analysed by 2-way ANOVA with uncorrected Fisher's LSD test. *p < 0.05, **p < 0.01, ***p < 0.001, ****p < 0.0001.

4.4. Discussion

Some of the focuses of the immune-oncology field have been either the use of adoptive T-cell therapy, T-cells transduced with chimeric antigen receptors (CAR-T cells) or engineered T-cells and soluble TCRs (Saez-Ibañez *et al.* 2022). In all these approaches, the targets have always been protein-based, either in the form of membrane epitopes or peptides presented in the context of classical HLA molecules (Marshall and Djamgoz 2018; Murciano-Goroff, Warner and Wolchok 2020). The study of unconventional T-cells potentially unlocks new strategies to target diseases through immunotherapy. Some of these strategies imply using non-protein targets such as lipids and metabolites presented in CD1 and MR1, respectively (Godfrey *et al.* 2018). In this chapter, we have developed a method to identify unconventional TCR sequences without previous knowledge of antigens.

4.4.1. Modified target cells can expand T-cell populations specific to MR1 and CD1c

In our experiments, we have been using IFNγ titrations to determine whether target cells still held the capacity to upregulate antigen-presenting-receptors under inflammatory conditions (**Figure 4- 3**). DKO of β2m and CIITA successfully removed surface expression of HLA-I, HLA-II molecules and the majority of endogenous MR1. Although it is plausible that residual MR1 can temporality traffic through the surface without β2m (Lion *et al.* 2013), DKO-target cells failed to prompt significant activation of primary MAIT cells and MR1-reactive Jurkats (**Figure 4- 7**), indicating that the residual MR1 detected in the plasmatic membrane is either an experimental artifact, non-functional, or absent of ligands.

Single-chain constructs of CD1c or MR1 molecules are expressed in the plasma membrane at significantly higher levels than the endogenous receptors. This is because WT MR1 and CD1c molecules associate non-covalently to β2m, and this interaction requires the binding of antigens (McWilliam *et al.* 2016). However, in the case of scMR1 and scCD1c molecules, these are readily available to leave the ER because they are covalently linked and stabilised by β2m. We believe that this inherent stability of the single-chain constructs allows them to present high and low-affinity antigens and saturate intracellular and extracellular membranes. Under natural conditions, only high-affinity antigens could stabilise CD1 and MR1 molecules to reach the cell surface. In T-cell proliferation assays, these target cells induced higher T-cell proliferation than their DKO counterparts (**Figure 4- 9**), indicating that the expansion is specific to CD1c and MR1.

4.4.2. T-cell cloning campaigns may have yielded more MR1 and CD1c-specific TCR sequences had they been conducted before polyclonal expansions

Expanded polyclonal populations against engineered target cells are enriched in MR1 and CD1c specific T-cells. Our results also showed that different target cells drive the expansion of diverse T-cell populations. In the case of PJI_donor, the polyclonal T-cells that expanded against transduced THP1 cells had comparable frequencies of CD1c and MR1 reactive T-cells (**Figure 4- 10F**) whereas, in the case of modified COLO205 cells, over 90% of expanded T-cells were MR1-specific (**Figure 4- 10H**). Considering that CD1c was not found in wild-type CRC epithelial lines (CD1c protein expression summary - The Human Protein Atlas, 2022), one possibility would be that they cannot prompt CD1c-specific expansions despite over-expressing scCD1c molecules because they lack significant expression of appropriate antigens. Nevertheless, primed and expanded CD1c-specific T-cells could be activated by CRC lines expressing scCD1c (**Figure 4- 10D**),

confirming that CRC lines can generate CD1c-specific antigens. To explain the disparity between proliferation and activation data, it is possible that in proliferation assays, most CD1c reactive T-cells in fresh blood might be close in their naïve state. In contrast, after priming and PHA expansions, CD1c reactive T-cells have an effector-phenotype with higher antigen sensitivity and lower activation threshold.

From T-cell cloning assays, we identified several CD1c and MR1 reactive TCR sequences (**Figure 4- 12**). We were surprised to find only 2 MR1-specific clones from 2 T-cell cloning campaigns. Obtaining this low number of MR1T sequences could be either because the circulating MR1T diversity is low or because of flaws in the experimental design. Polyclonal lines were sorted on days 10-13, at which time-point there was at least 20% unspecific T-cell proliferation (**Figure 4- 9**). After PHA expansions, unspecific T-cells could have taken over and further reduced the proportions of MR1 and CD1c-reactive T-cells. Characterisation of PJI_N13 showed that almost 80% of T-cells were MR1 or CD1c-unspecific (**Figure 4- 11**). On the other hand, we have seen that primarily CD8 T-cells are IFNγ producers (**Figure 4- 11**); therefore, IFNγ-based ELISAs or ELISPOTs could have favoured the selection process toward a few CD8 clones.

In retrospect, expanded T-cells should have been sorted straight as single cells (at 1cells/well) instead of conducting polyclonal expansions, thus, avoiding TCR convergence and loss of diversity. In addition, unbiased screening and selection methods should be developed to prevent the selection of only CD8 clones. Potential options to consider pleiotropic markers such as IL2, TNFα or GM-CSF ELISA assays or flow-cytometry analysis of broader surface activation markers such as CD69, OX40, PD1, ICOS, CD25 or CD137.

4.4.3. MR1-specific activity had a significant dependency on CD8

MR1T cells were the focus of this chapter. Anti-CD3 blocking data (**Figure 4- 12**) indicated that the 2 primary clones (MR1_C1 and MR1_C3) are activated through the TCR complex. Moreover, MR1_C1 and MR1_C3 showed partial or complete CD8 dependency in their MR1 recognition, respectively (**Figure 4- 12**). Given that most MR1-specific T-cells (MAIT or non-MAIT cells) described in the literature are CD8+ (Gherardin *et al.* 2018a), CD8 may play a role in the MR1-mediated immunology by increasing the avidity of the TCR-complex to MR1 (Gold *et al.* 2012); a similar effect has been described with CD1b (James *et al.* 2020) and conventional HLA-I molecules. In addition, the degree of inhibition by anti-CD8 could reflect the weak affinity of the 2 MR1T TCRs. For example, given that any MR1_C3 activity requires the presence of CD8, it may have a weaker affinity to MR1 than MR1_C1, which does not require it. In future work, surface plasmon resonance with soluble MR1 and TCR reagents could give us more accurate affinity data of MR1_C1 and MR1_C3 TCRs.

One hypothesis not fully explored in this chapter is whether the presence of functional CD8 influences the structural stability of the TCR complex on the surface. In Jurkat cells, which do not have endogenous CD8 expression, we saw that only 30% and 10% of total MR1_C1 and MR1_C3 TCRs were present on the cell surface, respectively (**Figure 4- 14B**). Moreover, co-transduction of the CD8α chain in Jurkats showed a meaningful improvement in the surface levels of the 2 MR1T TCRs (**Supplementary Figure 4- 2**). In addition, transduced CD8 were significantly more sensitive effector reagents than transduced Jurkats (**Figure 4- 14E**). These findings were consistent with the CD8 dependency data and suggested that CD8, besides increasing the affinity to MR1, may also provide stability to the TCR complex on the cell surface. These results need further validation by comparing transduced CD8 cells with transduced CD4s and DN T-cells.

4.4.4. MR1-specific TCRs are antigen-specific

MR1_C1 and MR1_C3 recognised $MR1^{WT}$ monomers expressed in mammalian cells but could not recognise the $MR1^{R9H}$ mutant (**Figure 4- 16**). The R9H mutation impairs ligand association to MR1, preventing MR1 release outside the ER and abrogating the development of MAIT cells in humans and mice (Howson *et al.* 2020). As a result, the $MR1^{R9H}$ mutant may be the closest conformation to an empty MR1 molecule, and the lack of recognition by MR1_C1 and MR1_C3 indicates that these TCRs are not ligand agnostic.

On the other hand, MR1_C1ds-CD8 and MR1_C3ds-CD8 cells showed different sensitivity to the $MR1^{K43A}$ mutant in experiments conducted with plate-bound monomers and transduced target cells (**Figure 4- 13, Figure 4- 15**). The absence of the K43 residue on MR1 prevents the formation of the Schiff base covalent bond with some metabolites (Kjer-Nielsen *et al.* 2012) and, consequently, skews the repertoire of the presented antigens. In the case of MR1_C1, the K43A mutation partially inhibited the activation of primary T-cell clones and transduced-CD8 cells, suggesting specificity to ligands that may form Schiff bases but can be presented by MR1 without the covalent link. On the other hand, MR1_C3 activation was entirely hindered by the absence of K43, indicating specificity to less stable ligands that require covalent binding with MR1.

Staining with MR1-tetramers showed that MR1T TCRs could recognise 6FP but not 5OPRU (**Figure 4- 13C**). Furthermore, MR1_C1, but not MR1_C3, could bind 5FSA-tetramers (**Figure 4- 13C**), confirming differences in their specificity. Because 6FP can be presented by both $MR1^{WT}$ and $MR1^{K43A}$ (Awad *et al.* 2020; Seneviratna *et al.* 2022), it is unlikely that 6FP was present in cell cultures as otherwise, we should see MR1_C3 activity against the $MR1^{K43A}$ monomers and $targets^{K43A}$. Nevertheless, given that T-cell expansions were not conducted in folate-free media we cannot discard the possibility that the 2 MR1T clones expanded through folate derivates from the growth media, such as 6FP analogues generated by photodegradation,

From classical immunology, it is widely accepted that TCRs are promiscuous and recognise several antigens, and different TCRs can recognise the same antigen (Pittet *et al.* 2002; Sewell 2012). Similarly, MR1_C1 can recognise 6FP and 5FSA (**Figure 4- 13C**), and MAIT cells can interact with diverse ligands other than 5OPRU (Meermeier *et al.* 2016; Keller *et al.* 2017). The fact that both MR1_C1 and MR1_C3 share 6FP specificity only indicates that they have an overlapping ligandome; however, it does not exclude recognition of other endogenous antigens that might resemble 6FP in the interactions they make with MR1. To shed more light on this, future experiments at Immunocore aim to use lysate sub-fractionation and mass-spectrometry methods to identify MR1-binding metabolites that can be recognised by MR1_C1 or MR1_C3 TCRs.

4.4.5. MR1-specific TCRs can recognise a wide range of cancer cells

In screening assays, MR1_C1ds and MR1_C3ds-CD8 cells recognise different skin and gut-derived carcinoma, myeloma, and leukaemia-derived cell lines. No recognition was observed for 7860 kidney carcinoma cells as these had weak MR1 expression (**Figure 4-15**). Overall, activation levels of transduced CD8 cells corresponded with surface levels of MR1 (determined by activation of the ligand agnostic E8-Jurkats) except in the case of THP1 cells. THP1 monocytic lines weakly activated the E8-Jukats, which suggests they have low levels of MR1; however, they also prompted the highest MR1_C1 and MR1_C3 mediated recognition in both activation and killing assays (**Figure 4- 15E-H**).

In our results, MR1_C1 and MR1_C3 showed different recognition patterns to the E8-TCR, indicating that their preferential recognition for THP1 is not solely due to MR1 levels but also due to other factors, potentially higher availability of cognate ligands. Blood-derived healthy cells (CD3, CD14 and CD19) and their leukaemia and myeloma counterparts (MOLT4, THP1 and U266, respectively) had comparable MR1 levels (**Figure 4- 16E**), but there was a preferential killing of the cancer lines by MR1_C1ds and

MR1_C3ds-CD8 cells (**Figure 4- 16F, G**). These results aligned with the study of other MR1T clones (Crowther *et al.* 2020) and the relationship between MR1 ligands, cancer, and altered metabolism. To explore in more detail the role of cellular stress in generating MR1 ligands, in the Klenerman lab, Dr Phalora investigated the involvement of autophagy in modulating MAIT activation and surface levels of MR1 (**Figure 4- 17**). Nevertheless, our preliminary data did not show any convincing change in the killing or activation of MR1_C1ds and MR1_C3ds-CD8 cells against target cells with altered autophagy (**Figure 4- 17E-H**). Further work needs to be done in optimising these assays and exploring the role of autophagy in generating MR1-antigens.

4.4.6. Summary

To summarise the results of this chapter, removing HLA-I and HLA-II molecules and transducing stable MR1 receptors (scMR1) allowed us to find TCR sequences specific to these receptors. Our results showed that different target cells induce the expansion of diverse T-cell populations, which may be subject to the antigens present in each target cell. The 2 MR1T cells we found showed differences in their dependency on CD8. However, it is still unclear if CD8 is aiding in the T-cell activation by stabilising the TCR complex or by increasing the avidity to MR1.

The inability of 2 MR1T cells to recognise the $MR1^{R9H}$ mutant indicates that they are not autoreactive to the MR1 molecule, but to self-antigens. The 2 MR1T TCRs showed differences in specificity as they behave differently in response to the K43A mutation on MR1; however, they still share recognition of 6FP tetramers and, unlike MAIT cells, cannot recognise 5OPRU. Because 6FP is not a naturally occurring ligand and we did not use it during our expansion assays, we believe that both MR1T cells can have other specificities, such as cancer-specific endogenous ligands.

Both MR1T cells can recognise different cancer cell lines, and this recognition partially correlates with their surface levels of MR1; however, they also show very high reactivity to THP1 cells relative to their expression of MR1 (determined by E8-Jurkats), thus suggesting that THP1 cells may have a higher concentration of cognate antigens for the 2 MR1T TCRs. Comparing THP1 cells to healthy CD14 cells, which have similar MR1 levels to their cancer counterparts, the 2 MR1T TCRs showed preferential recognition of the cancer cell line, indicating that their cognate antigens maybe associated with cancer-like behaviour and cellular stress.

4.4.7. Limitations and future work

There are several limitations to the design of the modified target cells. One is that T-cells can still expand against target cells through innate-like recognition such as NKG2D ligands (MICA, MICB, ULBP1–3, and RAE-1b) (Sivori *et al.* 2019). Moreover, populations like γδT-cells can also recognise phospho-antigens in addition to forming Ig-like interactions with surface epitopes (Deseke and Prinz 2020). Therefore, despite β2m and CIITA removal, there is still a wide range of stimulatory molecules on the targets cells that can activate irrelevant T-cells.

Moreover, CIITA KO did not result into full HLA-II expression loss; hence, target cells may still be able to elicit class-II mediated T-cell expansions. On the other hand, bystander T-cells can also expand due to cytokine-mediated stimulus from antigen-specific T-cells. These technical challenges and sub-optimal cloning strategies could have contributed to the proliferation and selection of T-cells that are unspecific to MR1 and CD1c.

Another unknown in these modified target cells is the proportion of surface scMR1 molecules loading antigens from the serum-rich media. This could happen as scMR1 molecules reach the plasmatic membrane in an empty state or bound to weak ligands,

which could be exchanged on the surface. This could be one important aspect to consider as we assume that the scMR1 and scCD1c molecules present endogenous ligands; however, we do not know how rich the intracellular environment is on MR1-specific metabolites or CD1c-specific lipids. Therefore, we cannot exclude the possibility that a proportion of surface scMR1 or CD1c molecules on the surface are empty or presenting serum-derived components instead of cancer-specific endogenous antigens.

Despite the details to be polished, we have proven the utility of these modified target cells as tools for the discovery of unconventional T-cells. The next steps would be to develop a metabolomics platform to deconvolute the cognate antigens for the MR1T TCRs found using this ligand-blind approach. In future work, Immunocore is developing a ligand discovery pipeline that integrates methods in metabolite extraction, chemical and physical sub-fractionation of cellular extracts, screening of fractions to identify MR1T responses and mass-spectrometry methods to identify enriched metabolic species in the fractions of interest.

One of the challenges to overcome in the short term is the development of optimal effector reagents that allow the use of discovered TCRs for the subsequent ligand identification process. Transduction of TCRs into Jurkat cells showed weak sensitivity to antigens and, stability problems in both MR1T TCRs. It is unclear if this stability issue persists in transduced CD8 cells; however, they show better sensitivity than Jurkats. The downside of CD8 cells is that these have endogenous TCR chains that form heterogeneous pairing and could influence the readout from activations assays. To overcome this, one possibility is the re-engineering of the TCRs with murine constant domains (Cohen *et al.* 2006; Sommermeyer and Uckert 2010), which may circumvent the stability problems in Jurkat cells and potentially increase their sensitivity. In transduced CD8 cells, the chimeric constructs would impede mixed TCR pairings and allow us to discriminate the transduced TCR from the endogenous TCR. Another option is to generate a TCR-deficient hybridoma to transduce TCRs onto or, convert T-cell clones of interest

into hybridomas by fusing them with immortalised cell lines (Canaday 2013; Kisielow, Obermair and Kopf 2019).

Immunocore specialises in producing soluble TCRs and TCR-bispecific (Harper *et al.* 2018; Lowe *et al.* 2019). Generation of soluble reagents with the MR1T TCRs would also be helpful for the study of affinity, thermostability and ligand screening assays, potentially being a more versatile solution than the cell-based effector reagents.

5. *Ex-vivo* detection of MR1T cells

5.1. Introduction

From the results in chapter 3, we understand the importance of MR1 in protecting against bacteria at barrier sites. MAIT cells are an innate-like T-cell populations that generates rapid anti-microbial responses to pathogens with the riboflavin synthesis pathway (Ussher *et al.* 2016; Kurioka *et al.* 2017; Legoux *et al.* 2019a). Some MR1T cells (defined as being outside the TRAV1-2+/CD161+ gate in circulating human T-cells) can also recognise 5OPRU-MR1 complexes, in addition to other microbial antigens that cannot be recognised by MAIT cells (Gherardin *et al.* 2016; Meermeier *et al.* 2016; Koay *et al.* 2019a). Similarly, non-microbial specificities have also been described in MR1T cells (Keller *et al.* 2017), some of which correspond to autoreactivity through the recognition of endogenous melabolites in the context of MR1 (Lepore *et al.* 2017; Crowther *et al.* 2020). The existence of these specificities opens the possibility of using MR1 as a target molecule for cancer therapy (explained in detail in chapter 4) and infectious diseases. For that, it is paramount to develop methods that increase our understanding of MR1-associated antigens and MR1-reactive TCRs.

In most studies, the discovery of MR1T sequences used tetramer fishing methods with MR1 molecules refolded with either 5OPRU, 6FP or synthetic analogues replicating specific MR1-antigens (Gherardin et al., 2016; De Libero et al., 2021). The limitation of this method is that it requires previous knowledge of the antigens of interest. In chapter 4, we presented a method to discover autoreactive MR1T cells using target cells overexpressing a β2m-fused MR1 construct that remains stable on the cell surface, potentially presenting high and low-affinity antigens. In cloning campaigns using this ligand-blind method, we discovered and validated only 2 MR1T clones. We hypothesised that our experimental design using proliferation assays loses information about the TCR

sequence diversity, *ex-vivo* frequency, and phenotypical and functional characteristics of autoreactive MR1T cells. In this chapter, we aim to optimise the methods used in chapter 4 to detect and isolate MR1T cells under *ex-vivo* conditions.

5.1.1. Aims

The aims of this chapter are:

- Optimise method to detect MR1T cells *ex-vivo*
- Assess the *ex-vivo* frequency of MR1T cells
- Comparing MR1T frequencies from healthy donors and cancer patients
- Isolation and sequencing of TCRs from *ex-vivo* detected MR1T cells
- Study of MR1T repertoire activated against different target cells
- Phenotype characterisation of isolated MR1T cells

Due to the Covid19 pandemic, commercial activity at Immunocore slowed down, impacting this project's progress. Due to time constraints, some of the objectives could not be met, such as the isolation, sequencing, and functional characterisation of MR1T cells detected *ex-vivo*.

5.2. Materials and methods

5.2.1. *Ex-vivo* AIM assays (using target cells or plate-bound Endo-MR1 monomers)

For *ex-vivo* AIM (activation induced markers) assays using target cells, $2x10^5$ target cells were incubated with $4x10^5$ PBMC or CD3 T-cells (purified by negative selection) overnight at 37ºC in the presence of 5μg/mL anti-CD28.

In the case of plate-bound Endo-MR1 mediated AIM assays, 100μL of 5μg/mL Endo-MR1 molecules were plated in MAXISORP flat-bottom 96-well plates and incubated at 4ºC overnight. The day after, the plates were flicked to remove unbound MR1 molecules and washed with 200L R10. After that, $4x10^5$ PBMC were added and incubated overnight at 37ºC in the presence of 5μg/mL anti-CD28.

5.2.2. Approved ethics

Blood from CRC patients was obtained using a subproject of the GI Biobank (ethics code REC 16/YH/0247), see appendix for subproject (stick this part below in the appendix as the approved subproject)

Date	08.10.2018
Study Title	Analysis of human colon polyps and colorectal cancer and healthy tissue
Lead Applicant (e.g. HoD, PI…)	Paul Klenerman, PI
Research Group[1]	Klenerman Group (collaborating with Simon Leedham)
Contact Person (person coordinating requests)	**Joachim Hagel,** Hossain Delowar Akther, **Philipp Hackstein,**

Consenters and Data entry personnel[2]	Cohort/BRC theme biobankers
Funding	Wellcome, DFG, MRC iCase,
Ethical Approval Details[3]	GI Illness Biobank
Follow-up Duration	2 years
Planned Study Period	2 years
Interventions[4]	Surgery and endoscopy: analysis of cancer resection and polypectomy samples taken for standard clinical care
Summary of Project	The project investigates the phenotypes and functions of human gut cells including immune and non-immune cells in healthy tissue compared to colon polyps and colorectal cancer. We would like to understand the difference in immune infiltration between healthy gut and colon polyps/colorectal cancer and characterise the immune cells by phenotyping and functional studies. On the other hand, we want to investigate the phenotype of non-immune gut cells, including cancer cells, and investigate their effect on immune cells. Understanding the interaction network of specific immune cells and cancer we will be able to develop therapeutically interventions for a positive clinical outcome in patients. Further we wish to clone out T cells which show anti-tumour recognition properties. If these show sustained anti-tumour responses we will sequence the TCRs in collaboration with Immunocore and use these TCRs to screen for the relevant ligands in cancer cell lines.
Aims and Objectives (Scientific background, plan of investigation, methods, pilot data)	The aim of the project is to deep-phenotype immune and non-immune cells and investigate their function. This will include analysis by multiple approaches including: - Expression of intra- and extracellular markers e.g. by flow cytometry, chip cytometry, western blot, ELISA (e.g. lineage markers, activation markers, cytokines) - Immunohistological analysis - Functional responses to antigen and nonspecific stimuli (e.g. cytokines, proliferation) - Gene expression studies at the resting state and following stimulation (e.g. RNAseq, single cell gene expression, 10x) - FACS sorting of purified cell populations - Genetic testing for specific genes - Epigenetic analyses (e.g. ATACseq)

	- Analyses of metabolic responses to stimulation - Short-term and long-term cultures - Testing supernatants of cultured cells for the presence of certain molecules - testing functional properties of supernatants of cultured cells on target cells - produce clones of selected cell types - extract and clone genetic information of selected cell clones - transfer material to Immunocore (established MRC iCase studentship programme) for cloning of cells, cloning of TCR and development of TCR-based tools for detection and killing of cancer.
NHS Personnel (if you have discussed with endoscopist, pathologists and/or surgeon)[5]	Discussed with Simon Leedham who is co-ordinating cancer sampling and Michael Yewdell from the CRUK centre
Sample requirements (numbers and description)	- 30 colorectal cancer donors with paired healthy tissue - 30 colon polyps - 15 blood samples from CRC patients (treatment naïve or ideally in remission).
How will the material be used	The material will be either used and processed as frozen tissue sections for histology or processed to cell suspension for all other applications. Blood samples will be processed to isolate PBMCs or T-cells, which will be frozen in vials. T-cells will be expanded and used for study of clones and TCR sequences.
Summary of the project in layman's terms	We would like to understand the role of immune cells in cancer and the effect of cancer cells on immune cells. We hope to define immune cell subsets in the human gut including healthy tissue, polyps and cancer and investigate their status and function. We aim to draw conclusions by comparing healthy tissue, polyps and cancer about the impact of specific subsets. *Vice versa* we aim to investigate the effect of the cancer microenvironment on the immune infiltrate. Furthermore, we would like to use the genetic information of single immune cells that show a promising anti-cancer effects to develop clinical anti-tumour strategies.

5.2.3. Donor information

Healthy PBMCs were isolated from leukocyte cones (NHS Blood Services). These samples are fully anonymized, so data on age and gender are not available for comparison. On the other hand, 10-20mL bloods collected for a cohort of patients with colorectal cancer. These samples were processed as detailed in section 2.2.1.

CRC sample information	
CRC patients	n = 26
Age (Average, SD)	70, 16
Sex (Male/Female)	20/6
Samples from blood	26
Frequent comorbidities (n)	Type 2 diabetes (2) Type I diabetes (3) Hypertension (5) Ischaemic heart disease (4)
Years since diagnostics (Average, SD)	1, 1
*SD = Standard deviation	

Table-5 1. CRC patient information

5.3. Results

5.3.1. Non-MAIT cells have specificities to 5OPRU and other antigens presented in the context of MR1

Blood-derived T-cells from internal donors were stained with tetramers made from MR1-5OPRU, MR1-6FP or MR1-Endogenous ligands (MR1-Endo), generated at Immunocore Ltd. MR1-5OPRU and MR1-6FP were generated from refolding bacterially expressed soluble MR1 in the presence of the ligands of interest and, as a result, the resulting tetramers are homogenous in the antigens they present. On the other hand, MR1-Endo were recombinantly expressed in mammalian cells (Expi293), and these are presumably presenting a heterogeneous pool of antigens found inside the expressing cell line. As a result, unlike 5OPRU- or 6FP-tetramers, Endo-tetramers contain heterogenous MR1-antigen populations.

5OPRU-tetramers stained principally TRAV1-2+ T-cells (**Figure 5- 1B**), most of them being MAIT cells (gated as CD161+ and TRAV1-2+); however, we also observed many non-MAIT CD161- T-cells that could be stained by 5OPRU-tetramers (**Figure 5- 1E**). In contrast, a significantly lower frequency of T-cells could be stained with 6FP- and Endo-tetramers (**Figure 5- 1C, D**). In 3/12 and 7/12 donors, MAIT cells could also be stained with 6FP- and Endo-tetramers, with frequencies between 1/1000 and 1/10000, respectively (**Figure 5- 1F, G**).

In the case of non-MAIT T-cells, there were differences between the TRAV1-2+ and TRAV1-2- compartments. The TRAV1-2+ compartment had a higher frequency of 5OPRU-tetramer staining (1:100) than TRAV1-2- cells (**Figure 5- 1E**); however, the opposite was seen for 6FP and Endo-tetramer binding (**Figure 5- 1F, G**). TRAV1-2- T-cell could recognise 6FP and Endo-tetramers with frequencies of 1:10000, while this frequency was several orders of magnitude lower for TRAV1-2+ cells.

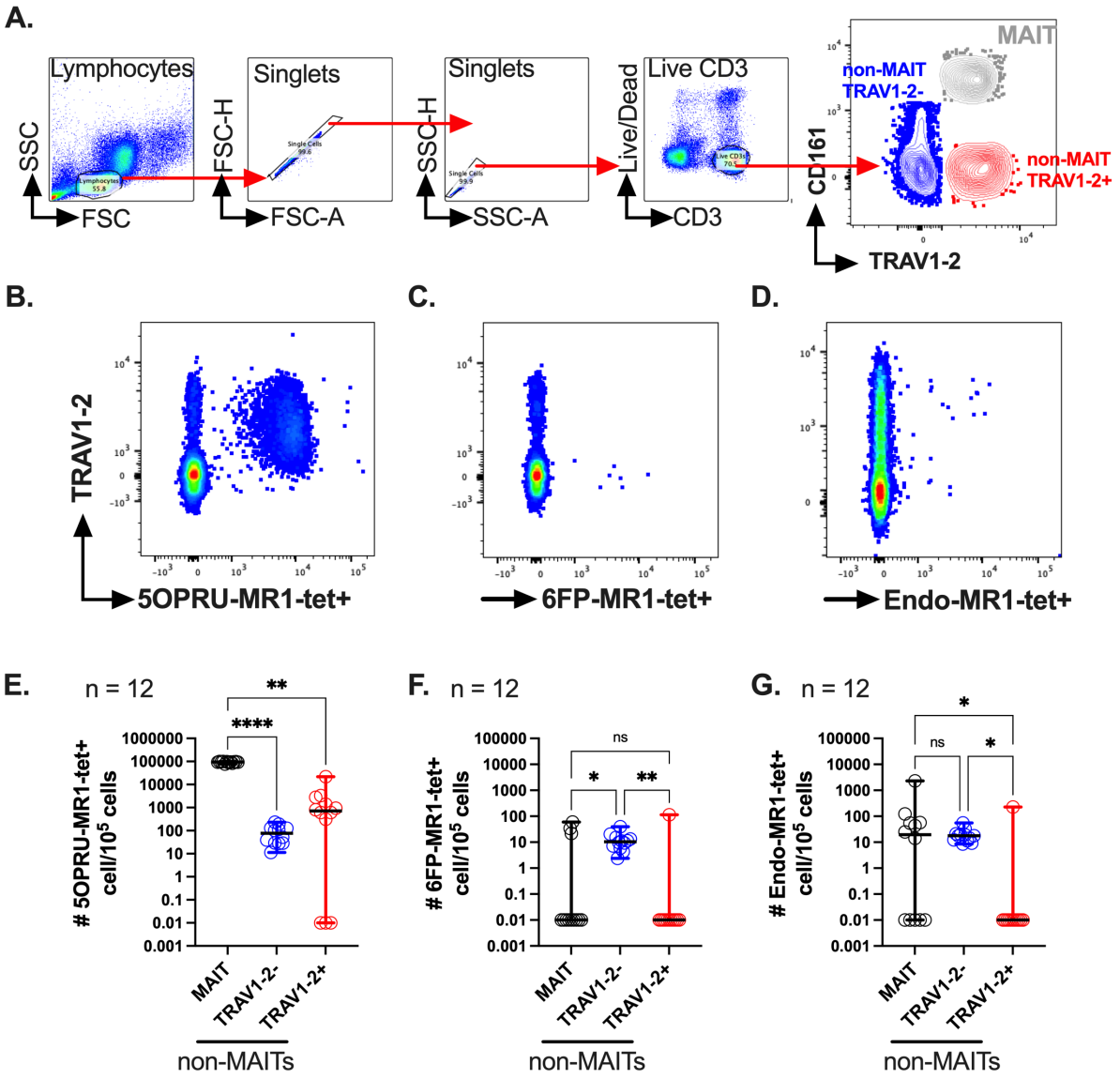

Figure 5- 1. MR1T cells can bind 5OPRU, 6FP and endogenous ligands expressed in mammalian cells. (**A**) Representative gating strategy of MAIT cells (grey), non-MAIT TRAV1-2- (blue) and non-MAIT TRAV1-2+ (red). (**B-G**) Representative FACSplots (**B-D**) and frequencies (**E-F**) of T-cells stained with 5OPRU-tetramer (**B, E**), 6FP-tetramer (**C, F**) and, Endo-tetramers (**D, G**).
Data were acquired in 2-3 independent experiments. Error bars represent Mean ± SEM of biological replicates. Differences among conditions were analysed by Friedman's test with uncorrected Dunn's test. *p < 0.05, **p < 0.01, ***p < 0.001, ****p < 0.0001.

5.3.2. AIM assays overcome avidity problems caused by the heterogeneity of Endo-tetramers

The low frequency of Endo-tetramer staining observed in **Figure 5- 1** could be explained by the low avidity of these heterogenous tetramers compared with the homogenous 5OPRU- and 6FP-tetramers. This problem could also be observed in CD8 T-cells transduced with MR1_C1 and MR1_C3 TCRs (Explained in more detail in chapter 4). Transduced T-cells are likely to have 4 TCR populations on their surface as the 2 endogenous TCR chains pair with the 2 transduced chains, although this has not been experimentally shown yet.

While the primary T-cell clones, with a pure MR1-reactive TCR population, could be stained by the 6FP-tetramer, this staining was lost in transduced CD8 cells (**Figure 5- 2A, B**). One explanation for this is that, like with the Endo-tetramers, the TCR heterogeneity on the surface may have reduced the binding avidity to the 6FP-tetramer. Similarly, primary transduced CD8 cells could not be stained by the Endo-tetramers (**Figure 5- 2C**).

To overcome the avidity problem of Endo-MR1 molecules, instead of tetramer staining we performed activation assays where T-cells were incubated overnight with 5μg/mL plate-bound MR1 molecules. During activation assays, the MR1-reactivity was measured by the upregulation of activation-induced markers (AIM) (**Figure 5- 2D, E**). In AIM assays, transduced CD8 cells upregulated CD137 and CD25 activation markers, confirming their ability to recognise specific Endo-MR1 molecules. In chapter 4, these experiments are explained in more detail.

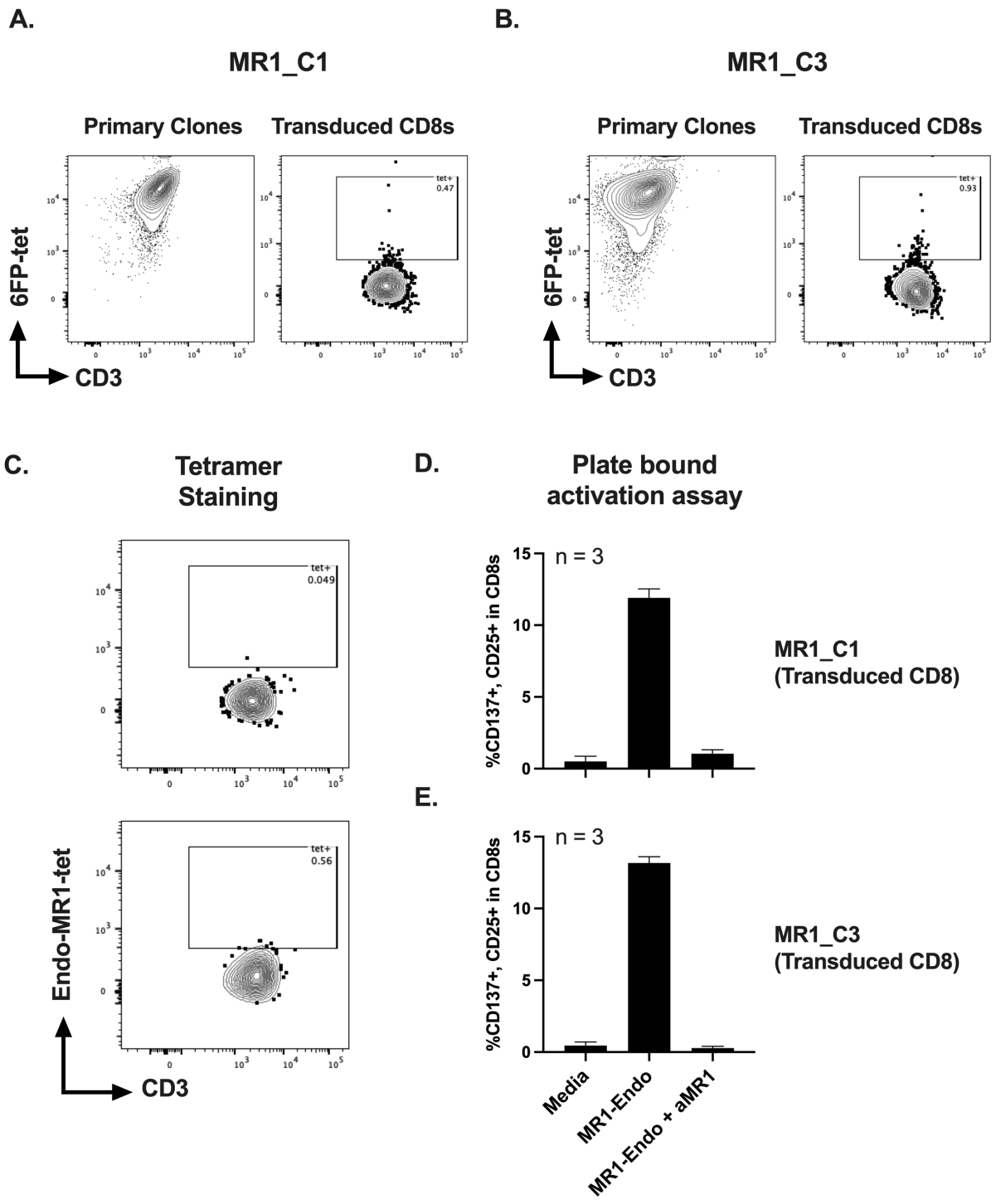

Figure 5- 2. Heterogeneity in Endo-MR1 tetramers reduces their affinity to bind to MR1T cells. (**A-B**) Representative staining of a bona fide primary MR1T clone (left panel) and transduced CD8 cells with the corresponding TCR (right panel) with 6FP-tetramers. (**C-D**) Representative FACSplot of transduced CD8 cells stained with Endo-tetramers (**C**) and activated with plate-bound Enod-MR1 molecules (**D-E**).

Data were acquired in a single experiment. Error bars represent Mean ± SEM of 3 technical replicates.

5.3.3. *Ex-vivo* AIM assays do not elicit MR1T activation against endogenous ligands in PBMCs

AIM assays were repeated with THP1^{scMR1} and THP1^{DKO} target cells using healthy PBMCs. THP1^{DKO} cells did not elicit any T-cell activation; however, in the presence of 50nM 5OPRU, they could activate <0.5% of non-MAIT cells and around 10% of MAIT cells (**Figure 5- 3B-E**). This could mean that THP1^{DKO} target cells, which had β2m and CIITA removed through CRISPR/Cas9 mediated KO, can still have MR1 on the surface in a β2m independent way. This result needs to be re-tested to exclude the possibility of self-presentation of 5OPRU by PBMCs.

Around 4% of MAIT cells activated against THP1^{scMR1} cells by producing IFNγ in the absence of 5OPRU (**Figure 5- 3C, E**). This aligns with their ability to recognise Endo-tetramers (**Figure 5- 1G**) and highlights that MAIT cells may have other specificities in addition to 5OPRU, as also shown in previous studies (Keller *et al.* 2017).

On the other hand, non-MAIT cells (gated as CD161-) showed virtually no reactivity against THP1^{scMR1} in the absence of 5OPRU and <0.5% of them elicited IFNγ expression in the presence of 5OPRU (**Figure 5- 3B, D**). Given that the expression of IFNγ in non-MAIT cells was very similar against THP1^{scMR1} and THP1^{DKO} presented with 5OPRU, the observed activation could be MR1 unspecific or PBMC-mediated 5OPRU presentation. Similar results were seen when using plate-bound Endo-MR1 monomers for the AIM assays (data not shown).

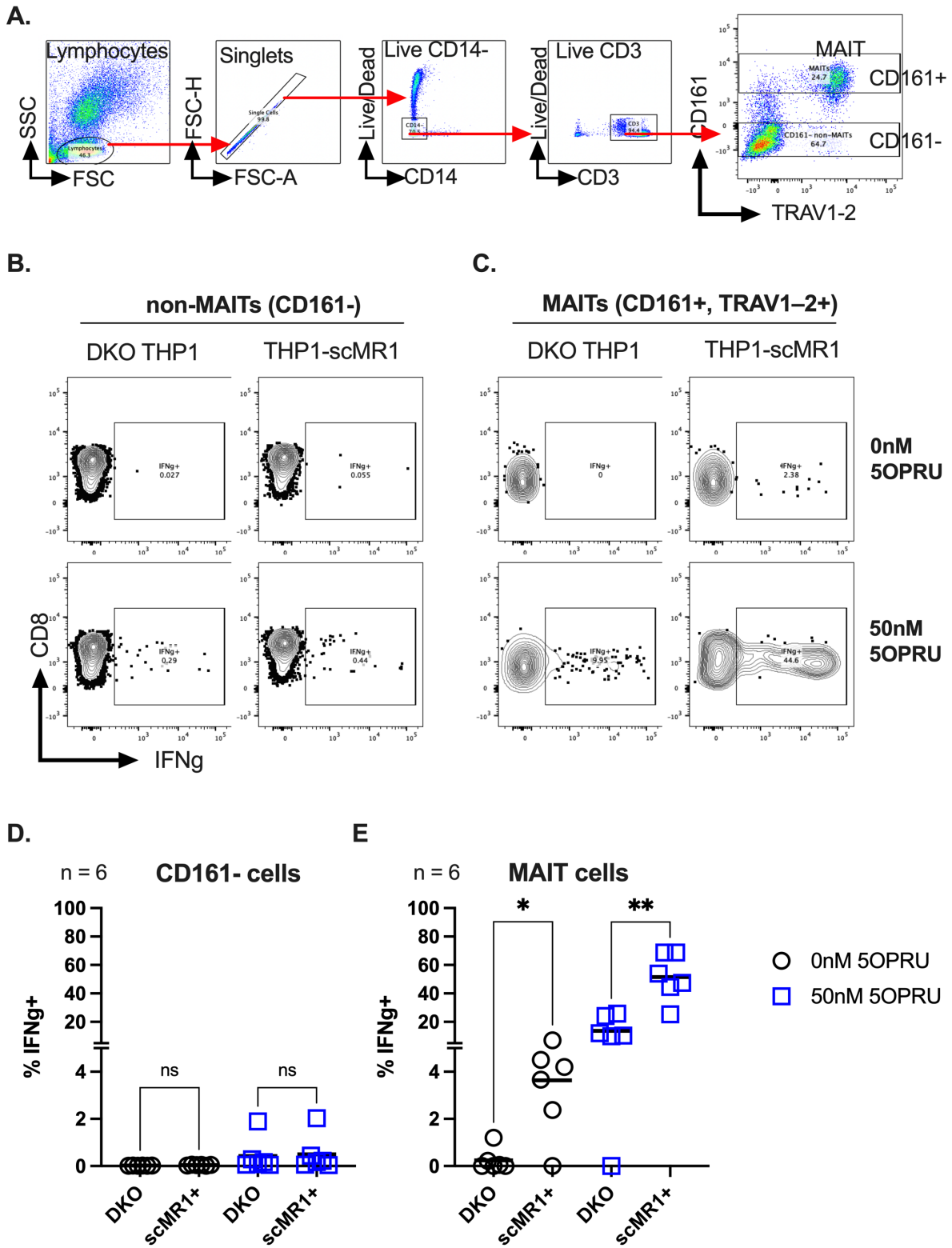

Figure 5- 3. MAIT and MR1T cells were not triggered by endogenous ligands presented by THP1^{scMR1} in ex-vivo AIM assays (**A**) Gating strategy of MAIT cells and CD161- T-cells. (**B-E**) Representative FACSplots (**B, C**) and frequencies (**D, E**) of IFNγ expression in CD161- (**B, D**) and MAIT cells (**C, E**) against THP1^{DKO} and THP1^{scMR1} target cells in the absence (black) or presence (blue) of 50nM 5OPRU.

Data were acquired in 2-3 independent experiments. Error bars represent Mean ± SEM of biological replicates. Differences among conditions were analysed by RM One-way ANOVA with uncorrected Fisher's LSD test. *p < 0.05, **p < 0.01, ***p < 0.001, ****p < 0.0001.

5.3.4. Co-stimulation with anti-CD28 can reduce the threshold to activate MR1T cells and facilitate their detection in *ex-vivo* AIM assays

Healthy PBMCs were incubated overnight at different concentrations of plate-bound Endo-MR1 molecules in the presence or absence of 5OPRU. In line with the previous results with THP1^{scMR1}, MAIT cells showed a concentration-dependent response to Endo-MR1 only in the presence of 50nM 5OPRU (**Figure 5- 4B**). The highest upregulation of CD137 and OX40 was achieved when plates were coated with at least 5μg/mL Endo-MR1 (**Figure 5- 4B**).

Using plates coated with 5μg/mL Endo-MR1, non-MAIT T-cells could elicit MR1-mediated responses in the presence of co-stimulatory reagents such as anti-CD28 antibodies (**Figure 5- 4C**). In a titration assay, non-MAIT cells showed increased activation in the presence of a high concentration of anti-CD28 (at least 5μg/mL). This activation was MR1-specific because it could be partially blocked with anti-MR1 (**Figure 5- 4C**). non-MAIT activation against MR1 did not require 5OPRU, indicating that the elicited response was against endogenous antigens. These results showed that co-stimulatory signals provided by anti-CD28 decreased the activation threshold of autoreactive MR1T cells and allowed their detection through activation markers in *ex-vivo* assays.

The MR1-specific response was calculated as the difference in the frequency of activated T-cells with and without anti-MR1 blocking:

$$\text{Freq.}(\text{E}+\text{T}) = \text{ Frequency of Tcells activated without antiMR1 blocking}$$
$$\text{Freq.}(\text{E}+\text{T}+\text{aMR1}) = \text{ Frequency of Tcells activated with antiMR1 blocking}$$
$$\text{MR1 specific response} = \text{Freq.}(\text{E}+\text{T}) - \text{ Freq.}(\text{E}+\text{T}+\text{aMR1})$$

If we assess the MR1-specific response by the upregulation of OX40 and CD137 activation markers, MR1T cells require a high concentration of anti-CD28 to respond

against Endo-MR1 molecules in overnight activation assays. In contrast, MAIT cells showed little response against Endo-MR1 molecules and were unaffected by the presence of anti-CD28 (**Figure 5- 4D**). On the other hand, if we analyse IFNγ expression in the presence of 10nM 5OPRU, MR1T cells had little activation in overnight activation assays (<0.5%), while MAIT cells showed a significantly higher expression of IFNγ (5-10%). In both cases, activation was dose-dependent to anti-CD28 (**Figure 5- 4E).**

In chapter 3, we have shown that MAIT cells can respond to innate cues by expressing IFNγ and other effector molecules. To explain the dose dependent effect of anti-CD28 on MAIT activation, it is possible that anti-CD28 can trigger innate signals in other cell populations within PBMCs, which increase the activation of MAIT cells through paracrine effects.

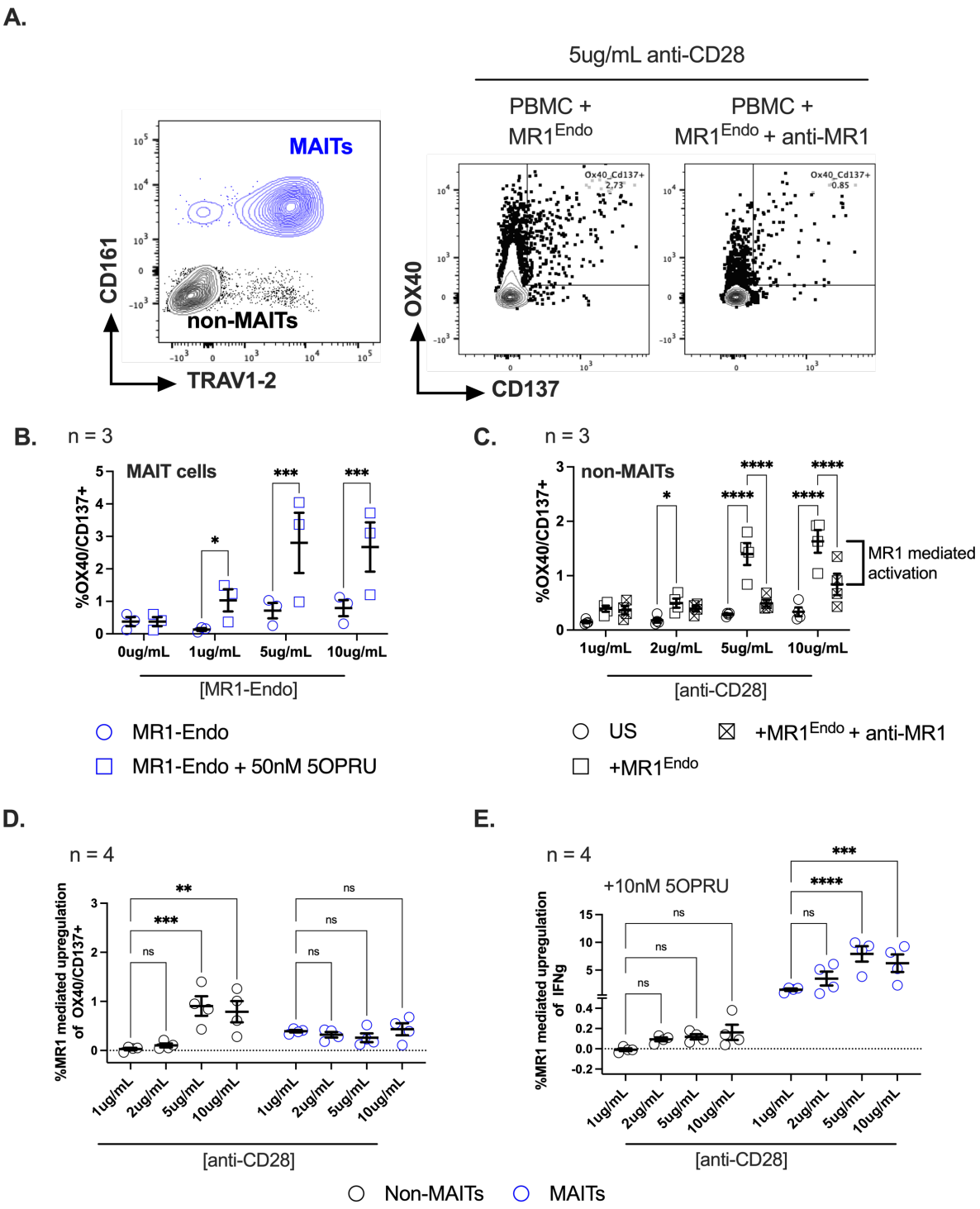

Figure 5- 4. Co-stimulation with anti-CD28 reduced the activation threshold of MR1T cells in *ex-vivo* AIM assays. (**A**) Representative gating of MAIT (blue) and CD161- (black) T-cells (left panel) and representative FACSplot of CD137 and OX40 surface expression of CD161- T-cells activated overnight against plate-coated Endo-MR1 with and without anti-MR1 in the presence of 5μg/mL anti-CD28 (right panel). (**B**) Frequency of CD137 and OX40 upregulation in MAIT cells activated overnight with increasing amounts of plate-bound Endo-MR1 alone (round symbol) or with 50nM 5OPRU (square symbol). (**C**) Frequency of CD137 and OX40 upregulation in CD161- T-cells activated overnight with 5μg/mL plate-bound Endo-MR1 without (square symbol) and with anti-

MR1 blocking (crossed square symbol) in the presence of increasing concentrations of anti-CD28. (**D**) MR1-driven upregulation of OX40/CD137 in MAIT (blue) and non-MAIT CD161- (black) cells at 5μg/mL Endo-MR1 and increasing concentrations of anti-CD28. (**E**) MR1-driven upregulation of IFNγ in MAIT (blue) and non-MAIT CD161- (black) cells at 5μg/mL Endo-MR1, 10nM 5OPRU and increasing concentrations of anti-CD28.
Data were acquired in 2-3 independent experiments. Error bars represent Mean ± SEM of biological replicates. Differences among conditions were analysed by RM 2-way ANOVA with uncorrected Fisher's LSD test. *$p < 0.05$, **$p < 0.01$, ***$p < 0.001$, ****$p < 0.0001$.

5.3.5. MR1-specific responses remain the same after consecutive challenges, confirming that activated T-cells have bona fide MR1T TCRs

In our results so far, we have seen that MR1T cells can be triggered by both target cells overexpressing scMR1 and plate-bound MR1, both in the presence of anti-CD28. This activation can be blocked with anti-MR1; hence it is MR1 specific. In chapter 4, we have seen that different target cells had different capacity to elicit T-cell activation. For example, in the case of epithelial cells, despite 5OPRU and over-expression of scMR1 on their surface, they failed to trigger MAIT cells. Similarly, here we saw that in the case of MR1T cells, epithelial cells such as DLD1^{scMR1} also weakly triggered autoreactive MR1T cells from PBMCs (**Figure 5- 5A, B**). Unlike in chapter 4, where MAIT cells were incubated with target cells in the presence of 5OPRU, from this experimental setting, we cannot tell whether the low MR1T activation with DLD1 cells happened because of the co-factor composition on DLD1 cells or because they lack the appropriate intracellular ligands.

The system with plate-coated MR1 molecules also lacks any additional co-factor signalling other than anti-CD28; however, it activated MR1T cells at comparable levels to THP1^{scMR1} (**Figure 5- 5A**). To validate whether the observed responses in these AIM assays were genuinely MR1-specific, purified CD161- T-cells were activated *ex-vivo* with THP1^{scMR1} target cells (**Figure 5- 5B**). Activated T-cells were sorted and re-challenged with the same target cells in an IFNγ ELISPOT assay (**Figure 5- 5C-F**). Our results showed MR1-specific responses after re-challenge confirming that they were genuine MR1T cells. This confirmed that we could detect MR1T cells through *ex-vivo* AIM assays.

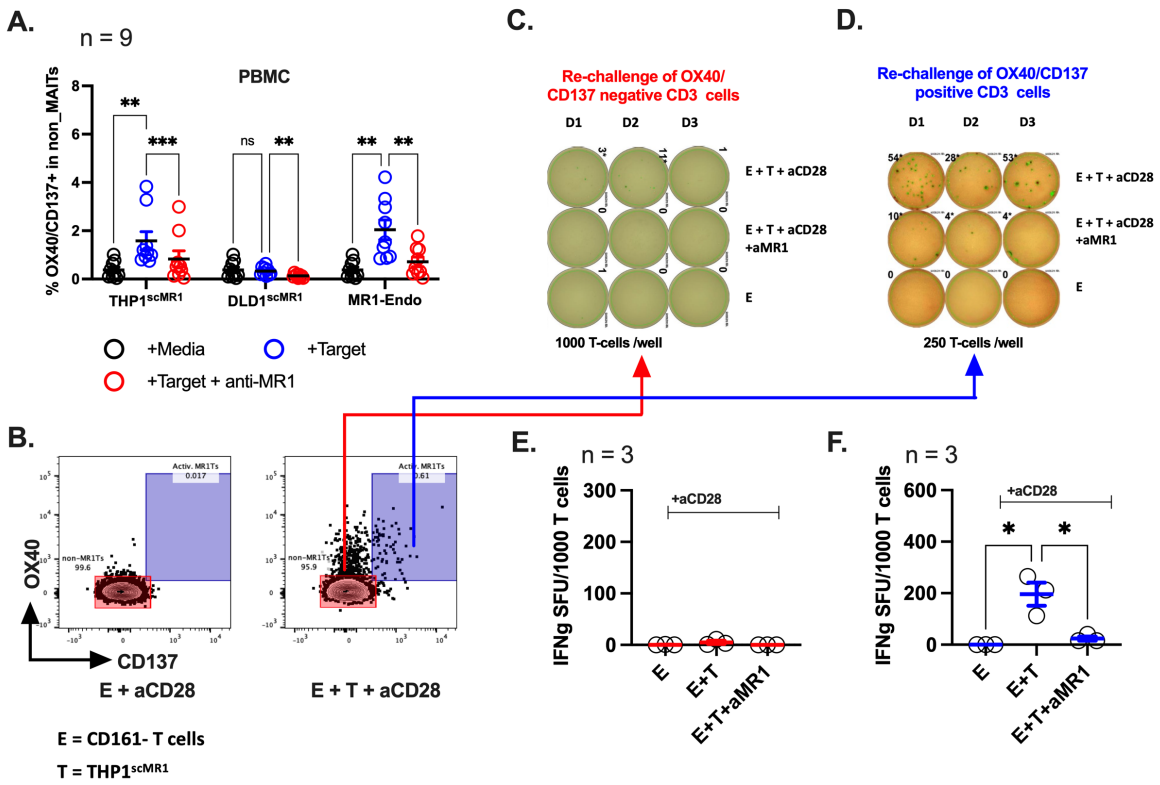

Figure 5- 5. Detected T-cells through ex-vivo AIM assays and genuinely MR1-restricted. (A) Frequency of CD137 and OX40 upregulation in CD3s from PBMCs alone (Black), against THP1^{scMR1}, DLD1^{scMR1} or 5μg/mL plate-bound Endo-MR1 alone (blue) or in the presence of anti-MR1 (red). AIM assays were conducted in the presence of 5μg/mL anti-CD28. (**B**) Representative FACSplot of OX40 and CD137 upregulation in CD161- T-cells from purified panT-cells activated overnight against THP1^{scMR1}and 5μg/mL anti-CD28. Highlighted are the T-cells responsive (blue) and unresponsive (red) to MR1. (**C-F**) Representative ELISPOTs (**C, D**) and IFNγ SFU (**E, F**) of sorted MR1-responsive (**D, F**) and unresponsive (**C, E**) after overnight re-challenge with THP1^{scMR1} and 5μg/mL anti-CD28.

Data in **A** were acquired in 2-3 independent experiments, while data in **C-F** were acquired from a single experiment. Error bars represent Mean ± SEM of biological replicates. Differences among conditions were analysed by RM 2-way ANOVA with uncorrected Fisher's LSD test. *p < 0.05, **p < 0.01, ***p < 0.001, ****p < 0.0001.

5.3.6. MR1T cells represent between 0.4-1.3% of total circulating T-cells

Next, we estimated the frequency of MR1-specific responses against Endo-MR1 using PBMCs from cohorts of healthy donors and CRC patients. In the AIM assays, we used OX40/CD137 double-positive gating to measure the frequency of MR1T cells. From 51 donors, we found that the median frequency of MR1T cells was ~0.7% in the total CD3 compartment, with an interquartile range between 0.4% to 1.3% (**Figure 5- 6A, B**). In parallel studies using IFNγ ELISPOTs, we saw similar frequencies of MR1-specific activation (**Supplementary Figure 5- 1**).

We also measured the frequency of MR1T cells in different T-cell sub-compartments, gated as shown in **Figure 5- 6C**. To reduce the noise caused by donor-to-donor variability (**Figure 5- 6D**), the frequencies in each compartment were transformed into FC over the frequency of MR1T cells in the total CD3 compartment (**Figure 5- 6E**):

$$\text{Normalised MR1 response in compartment X in donor Y} = \frac{\text{MR1 specific response in compartment X in donor Y}}{\text{MR1 specific response in total CD3s in donor Y}}$$

Analysing the transformed data in **Figure 5- 6E,** we saw a weak MR1-autoreactive response in the MAIT compartment. Within non-MAIT cells, the CD161+ compartment had a wide distribution in the frequency of responding autoreactive MR1T cells, indicating a significant donor-to-donor variability. Inside the CD161- compartment, autoreactive MR1T cells were enriched in CD4 T-cells compared to CD8 or DN T-cells.

Comparing the MR1-mediated response in PBMCs triggered with THP1^{scMR1} and plate-bound Endo-MR1, we did not find a clear correlation in the frequencies of T-cells activated by these 2 methods **(Supplementary Figure 5- 2**). This difference could be attributed to the apparent differences between these 2 systems as we are comparing

target cells overexpressing MR1 with pure monomeric MR1 molecules. In addition, Endo-MR1 molecules were expressed in Expi293 cells, which could have a different composition of antigens to those presented by THP1 target cells, thus triggering different populations of MR1T cells. From these results and the differences in activation seen with THP1^{scMR1} and DLD1^{scMR1} cells, we could assume that different target cells would activate different T-cell populations; therefore, the presented results could be biased to Endo-MR1 molecules produced in Expi293 cells.

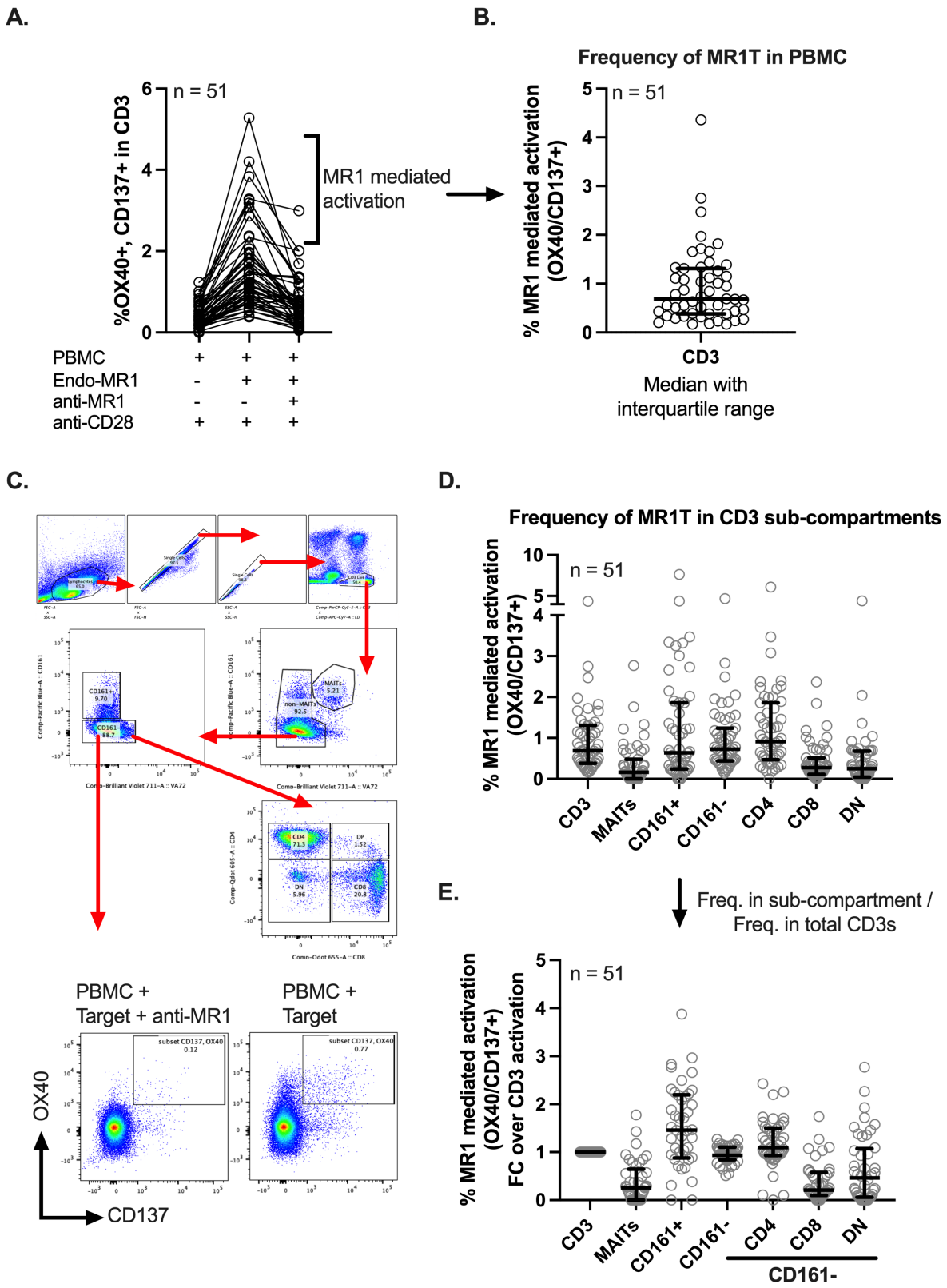

Figure 5- 6. MR1-responsive T-cells represent between 0.4% to 1.3% of circulating T-cells. (**A**) Surface expression of OX40 and CD137 in circulating T-cells after overnight activation with 5µg/mL Endo-MR1 with and without anti-MR1 blocking and, in the presence of 5µg/mL of anti-CD28. (**B**) Frequency of MR1-mediated activation in blood from healthy donors and CRC patients.

(**C-E**) Gating strategy (**C**) and, absolute (**D**) and normalised (**E**) frequency of MR1-response in different T-cell compartments in blood. To normalise the frequency in each compartment, data were transformed as fold-change (FC) over the activation in the bulk CD3 compartment.
Data were acquired in 4-6 independent experiments. Error bars represent Median and interquartile range of biological replicates. Differences among conditions were analysed by RM 2-way ANOVA with uncorrected Fisher's LSD test. *p < 0.05, **p < 0.01, ***p < 0.001, ****p < 0.0001.

5.3.7. Circulating MR1T cells in CRC donors have a higher frequency of memory cells than in healthy donors

Next, we compared the frequencies of MR1T cells in circulating T-cell from healthy donors and CRC patients (patient information found in section 5.2.3, **Table-5 1**). Our results showed no significant differences between the 2 groups. In the healthy and CRC patient cohorts, the median frequency of MR1T cells was ~0.55% and ~0.62%, respectively (**Figure 5- 7A**).

Analysing the different T-cell compartments, we observed an enrichment of MR1T cells in the CD161+ compartment of CRC patients compared to healthy donors, while no differences were seen in the CD161- gate (**Figure 5- 7B**). We also measured the frequency of MR1T cells in the different naïve and memory compartments gated through the surface expression of CCR7 and CD45RA, as indicated in **Figure 5- 7C**. We observed that in cancer patients, MR1-mediated responses were slightly (=ns) reduced in naïve T-cells while significantly enriched in T-cells with central-memory phenotype (**Figure 5- 7D**). These findings suggest that some MR1T cells might undergo differentiation in colorectal cancer by recognising MR1-associated ligands.

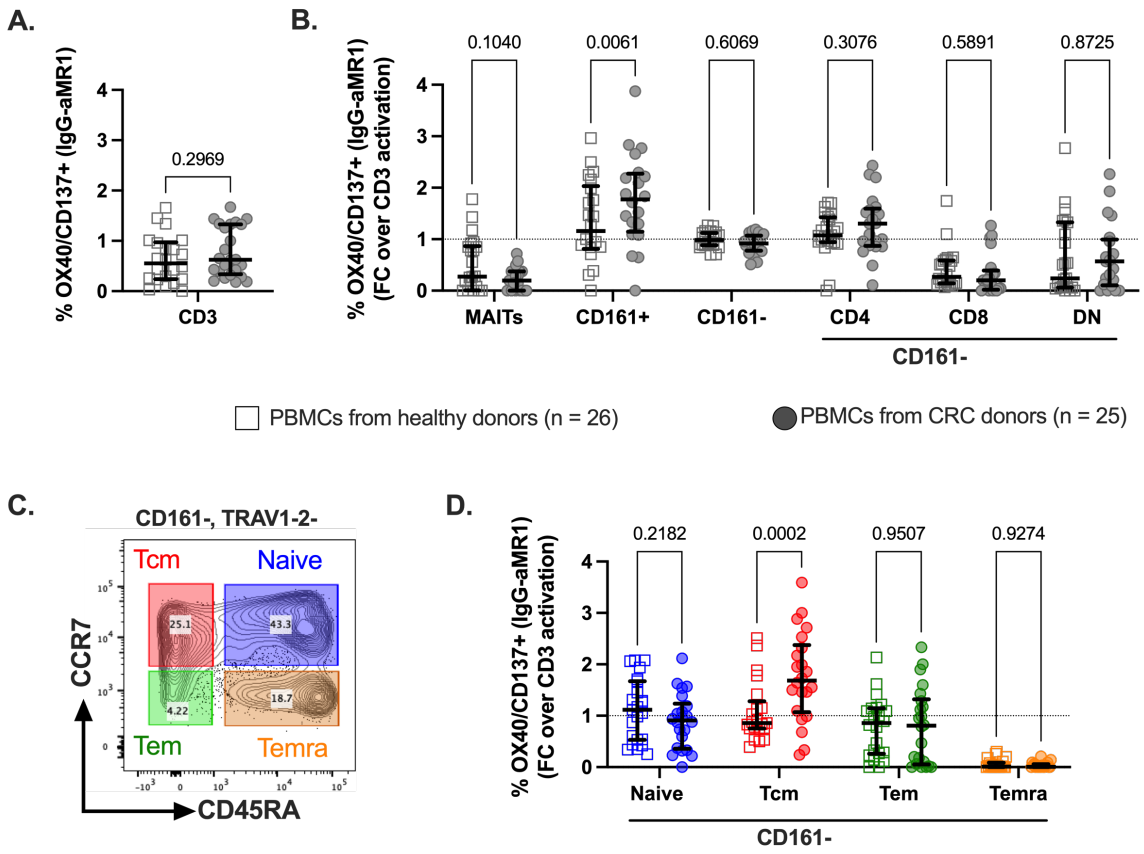

Figure 5- 7. MR1T cells undergo differentiation from naïve to memory phenotype in CRC patients. (**A**) Frequency of MR1-mediated activation in circulating CD3s of healthy donors (clear square symbol) and CRC patients (grey round symbol). (**B**) Frequency of MR1-mediated activation in T-cells subcompartments of healthy donors (clear square symbol) and CRC patients (grey round symbol). Data were transformed as FC over total CD3 activation. (**C**) Gating strategy of naïve (blue), Tcm (red), Tem (green) and Temra (orange) T-cells through the surface expression of CCR7 and CD45RA. (**D**) Frequency of MR1-response in circulation naïve (blue), Tcm (red), Tem (green) and Temra (orange) T-cell compartments of healthy donors (clear square symbol) and CRC patients (filled round symbol).

Data were acquired in 4-6 independent experiments. Error bars represent Median and interquartile range of biological replicates. Differences among conditions were analysed by RM 2-way ANOVA with uncorrected Fisher's LSD test. *p < 0.05, **p < 0.01, ***p < 0.001, ****p < 0.0001.

5.4. Discussion

5.4.1. Co-stimulation with anti-CD28 allows ex-vivo detection of MR1T cells through overnight AIM assays

Within non-MAIT cells (gated as CD161- T-cells), the bulk of T-cells that could be stained with 5OPRU-tetramers were TRAV1-2+ cells (0.5-10%) (**Figure 5- 1E**). Despite having low expression of CD161, these TRAV1-2+/5OPRU-tetramer+ T-cells could still be MAIT cells if they expressed PLZF (Gherardin *et al.* 2018b). The link between 5OPRU and TRAV1-2+ cells (in both MR1T and MAIT cells) highlights the relevance of the riboflavin pathways as a source of MR1 antigens (Boudinot *et al.* 2016; Legoux *et al.* 2019a) However, although not fully characterised, other clusters of non-bacterial MR1-ligands have also been suggested (Harriff et al., 2018). At Immunocore, through the expression of a soluble MR1 constructs in mammalian cells, we generated tetramers loaded with heterogenous endogenous ligands. Excluding MAIT cells, Endo-tetramers stained predominantly TRAV1-2- cells with a frequency of 1:1000 or 0.1% (**Figure 5- 1**). This frequency was lower than expected, considering that the frequency of 6FP-tetramer+ T-cells, a synthetic ligand that does not occur naturally, was also 1:1000 or 0.1%. This prompted us to hypothesise whether Endo-tetramers, due to their heterogeneity, have low avidity to detect MR1T cells. In line with that, Endo-tetramers could not stain previously validated MR1T cells (C1 and C3 TCRs generated in chapter 4), while in plate-bound activation assays with the same Endo-MR1 molecules, they elicited 10% activation from both C1 and C3 TCRs (**Figure 5- 2**).

While CD8 cells transduced with C1 and C3 TCRs could be activated by endogenous ligands in overnight assays, no activation was seen in freshly purified PBMCs (**Figure 5-3**). This could be explained because, like MAIT cells, transduced CD8 cells have a low activation threshold as they may have acquired an effector/memory phenotype during consecutive PHA-mediated expansion. To elicit MR1-mediated responses in fresh PBMC,

co-stimulation with anti-CD28 was necessary (**Figure 5- 4, Figure 5- 5**). In *ex-vivo* AIM assays, the MR1-dependent reactivity could be measured by the surface expression of OX40 and CD137 or the upregulation of IFNγ (**Figure 5- 4**). Both activation signals could be triggered by either plate-bound Endo-MR1 or target cells overexpressing scMR1 and, blocked with anti-MR1.

5.4.2. There is an unexpectedly high frequency of autoreactive MR1T cells in the blood

Using *ex-vivo* AIM assay, we observed around 1/133 or 0.75% of circulating MR1-responsive T-cells across healthy and CRC donors (**Figure 5- 6B**). This frequency only represents the reactivity to endogenous antigens and, did not include specificities to microbial-derived antigens (Meermeier *et al.* 2016), potentially amounting to even higher frequencies of MR1T cells.

Studies have shown that some TRAV1-2- MR1T cells with specificity to 5OPRU have MAIT-like phenotypes (CD161+, IL18Ra+, CD26+, PLZF+) (Koay *et al.* 2019a). Similarly, in our results with non-MAIT cells, we observed that some donors had significant enrichment of autoreactive MR1T cells within the CD161+ compartment (reaching up to 4%) compared to the frequency in the CD161- compartment (~1%) (**Figure 5- 6E**). Although we have not analysed the expression of PLZF or IL18Ra in MR1T cells, these markers, along with RORγt have been transcriptionally linked to the expression of CD161 (Fergusson *et al.* 2014). On the other hand, because these CD161+ MR1T cells cannot be detected without using co-stimulatory reagents such as anti-CD28, it is unlikely that they have the same level of innateness as MAIT cells.

In the CD161- compartment, which represented the largest segment of the peripheral T-cells, MR1T cells were enriched in CD4 T-cells rather than in CD8 and DN T-cells (**Figure 5- 6E**). These results are opposed to those expected from 5OPRU-reactive cells,

where there is a predominance of CD8 T-cells (Koay et al., 2019). Finally, our analysis also showed a low autoreactivity in the MAIT compartment, emphasising their restriction to riboflavin derivates.

Comparing the donors by their healthy or CRC status, we saw no significant difference in the frequency of circulating autoreactive MR1T cells (**Figure 5- 7A**). However, further analysis of T-cell compartments elucidated changes in the distribution of MR1T cells in CRC patients. Fundamental changes were the increase of CD161+ autoreactive MR1T cells and the increase of MR1T cells with memory phenotype in the CD161- compartment (**Figure 5- 7B, D**). These changes suggest a potential role for MR1 as a platform to display cancer-associated antigens and, underline the potential of autoreactive MR1-specific TCRs in targeting cancer diseases.

5.4.3. Summary

In chapter 4, from proliferation assays using different target cells overexpressing scMR1, we identified 2 MR1T sequences. Sequencing assays showed a significant number of clones carrying the same TCR. This could be explained because either the MR1T population is not as diverse as we initially hypothesised, or there was sequence convergence during the proliferation assays or after PHA-mediated expansion. To improve future MR1T identification campaigns, in chapter 4, we argued that T-cell cloning should be conducted close to *ex-vivo* conditions. In this chapter, we proposed using overnight AIM stimulation assays to detect MR1T cells. In addition, with this detection method we estimated an unexpectedly high frequency of circulating autoreactive MR1T cells in healthy donors and CRC patients. Phenotype analysis also showed increased circulating MR1-specific memory T-cells in CRC patients compared to healthy patients.

5.4.4. Limitations and future work

Although AIM assays can be used to estimate *ex-vivo* frequencies of MR1T cells, the T-cell populations that upregulate generic surface activation markers such as OX40 or CD137 cannot be labelled as genuine MR1T cells without further validation. This is because a portion of this activation cannot be blocked with anti-MR1 (**Figure 5- 6A**). These MR1-unspecific T-cells were probably activated by the presence of coreceptors in target cells or other cell populations in PBMCs, by high concentrations of anti-CD28 or by signal amplification through bystander T-cell activation. In the Klenerman lab, Dr Hackstein showed that a significant portion of bystander signal amplification could be prevented with anti-IFNGR1 blocking (**Supplementary Figure 5- 3**).

The upregulation of intracellular markers such as IFNγ is more tightly regulated than surface markers; however, this activation marker is also restricted to specific T-cell populations. Moreover, the intracellular staining of IFNγ requires permeabilisation of T-cells, which is incompatible with posterior sorting and T-cell cloning. One solution is the use of detection kits to tag T-cells secreting multifunctional cytokines (ex: TNFα or GM-CSF); however, we have not tested that approach in our experiments. Further study of other surface activation markers, such as PD-1, HLA-DR and ICOS, and time-course analysis for their optimal expression could also improve the accuracy of MR1T detection.

In future experiments, the aim will be to conduct T-cell cloning of MR1T cells detected through *ex-vivo* AIM assays in the presence or absence of microbial infections. In addition, this pipeline could also be applied to compare the repertoire of reactive MR1T cells to different target cells or, Endo-MR1 molecules produced in different target cells. Sequencing the resulting T-cell clones would provide a better understanding of the TCR diversity in autoreactive and microbe sensing MR1T cells, their promiscuousness to different antigens, and the overlap of antigens across different target cells. These experiments applied to TIL samples would also point out whether there are converging

MR1T sequences within tumours, which could become potential candidates for MR1-mediated immunotherapy.

Other potential experiments involve more detailed characterisation of the innateness and functional aspects of MR1T cells. This could be addressed by analysing the frequency of transcription factors such as PLZF, RORγt, T-bet, GATA3 and FOXP3.

6. General discussion

This thesis explored several facets of MR1-mediated immunology, consisting of 2 distinct categories of T-cells. On one side, we have MAIT cells, which are defined by the TRAV1-2+ semi-invariant TCR and 5OPRU specificity. These acquire innate-like properties during their development in the thymus, defined by the expression of PLZF and, can colonise mucosal and barrier tissues early in the life of individuals. On the other hand, not much is known about MR1T cells, which are vaguely defined as MR1-reactive T-cells that do not fit into the MAIT category. MR1T cells have variable TCR sequences, antigens, and levels of innateness, and their selection process in the thymus is still unclear.

6.1. MAIT cells protect barrier integrity at mucosal sites

MAIT cells are known as highly inflammatory with Tc1 and Tc17 signatures that conferred protection against viral and microbial infections, respectively; the former, through cytokine triggers from APC such as IL12/IL18 and IFNα (Ussher *et al.* 2014b; van Wilgenburg *et al.* 2016). At the time of the study, it was unclear how MAIT activation was regulated at barrier and mucosal sites. Given the inflammatory and cytotoxic potential of MAIT cells, if unregulated, the constant exposure to commensal-derived agonistic antigens should lead to severe tissue damage and scarring because of chronic inflammation.

In chapter 3, we hypothesised that the MAIT regulation at barrier sites is conditioned by the interplay between TCR-dependent and -independent signals; however, the downstream effects of these triggers in MAIT cells remained unexplored. In this chapter,

we elucidate that cytokine signalling was the main driver of inflammatory and cytotoxic, functions in MAIT cells (IFNγ, TNFα, GrzB). On the other hand, we identified a TCR-dependent tissue-repair and immunoregulatory signature in MAIT cells which can be potentiated by interleukins (IL12/IL18/IL15). Unlike the tissue-repair signature, the immunoregulatory module was tightly regulated and only seen under TCR-trigger by soluble antigens but not by bacterial infections. In both TCR-associated or cytokine-associated signatures, these were amplified with co-stimulation by both TCR-dependent and TCR-independent stimulation. In our transcriptional analysis, we saw that concomitant stimulation with TCR and cytokines enhanced the biogenesis of ribosomes and increased the translational capacity of MAIT cells; these changes could explain the observed synergies between TCR-dependent and TCR-independent triggers.

Considering these results, we propose a new model where MAIT cells primarily focus on maintaining barrier integrity and homeostasis at steady-state. Commensal-derived metabolites such as 5OPRU and related molecules can cross barrier tissues (Legoux *et al.* 2019a) and potentially stimulate the tissue-repair and immunoregulatory modules of MAIT cells under sterile conditions, dampening the immune response and promoting homeostasis at barrier and mucosal sites. The hyporesponsiveness of MAIT cells in terms of inflammatory and anti-microbial responses by TCR-signalling means that they can be constantly activated against microbiota-derived soluble antigens without damaging their local microenvironment. In our analysis of blood and gut-derived MAIT cells, we observed a reduced inflammatory potential (IFNγ, TNFα, GrzB) in the tissue-resident MAIT cells accompanied by immunosuppressive surface markers such as PD-1 and CD39; nonetheless, these cells conserved their anti-microbial functions with higher production of IL17A.

Surprisingly, in vitro stimulation of MAIT cells with fixed bacteria did not elicit IL10 expression, which is otherwise upregulated by 5OPRU-mediated triggers. This could mean that MAIT cells can switch off their immunosuppressive module under bacterial

infections. The presence of microbial infections generates additional TCR-independent signals from APC, which shift the profile of MAIT cells into highly inflammatory and cytotoxic to clear the milieu from invading pathogens. Additionally, several tissue-repair factors were expressed by concomitant TCR and cytokine signalling or *E.coli*-mediated triggers, indicating that MAIT cells may promote wound-healing under microbial infections. The synergies observed between TCR and cytokine signalling also suggest that both the inflammatory and tissue-repair functions may wane after the clearance of pathogens and TCR agonists from the local microenvironment.

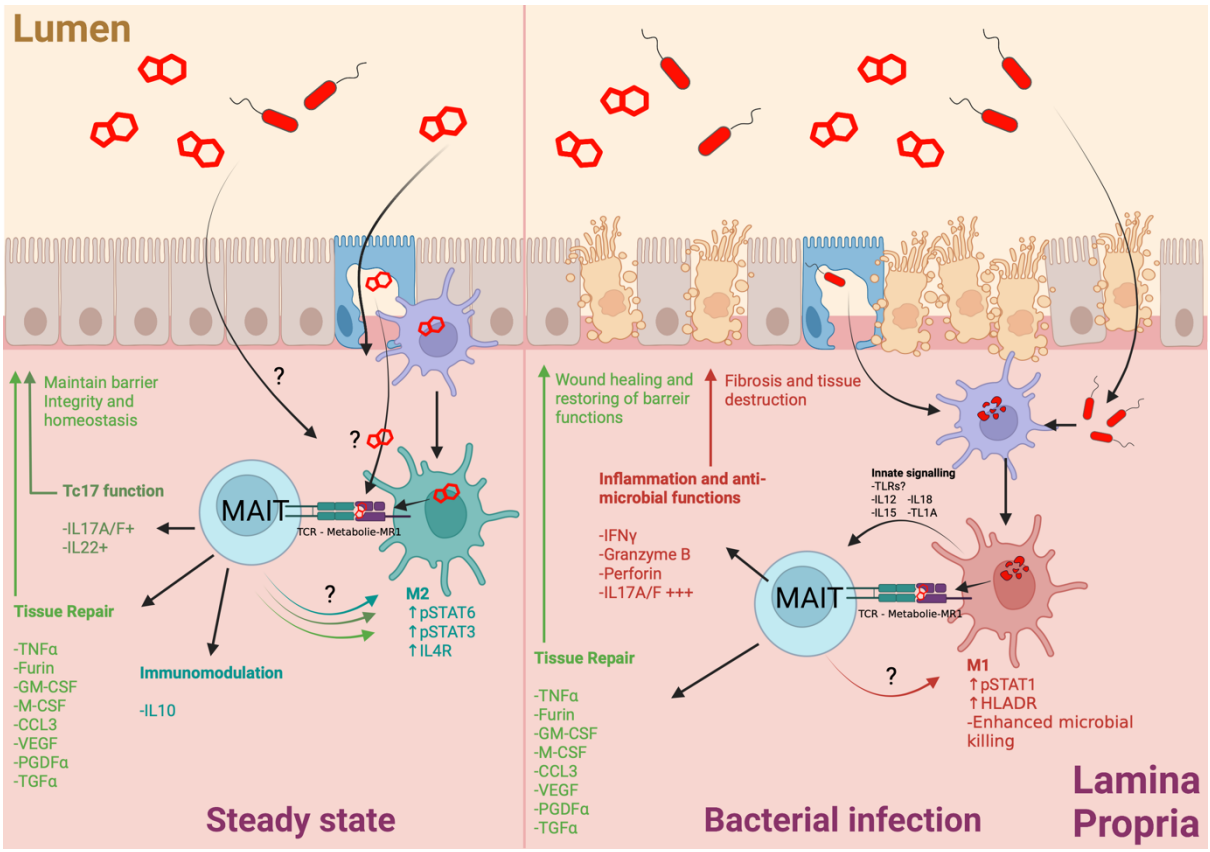

Figure 6- 1. MAIT cells elicit protective and homeostatic functions at steady-state. TCR triggers from soluble commensal-derived antigens induce homeostatic functions in MAIT cells. However, under bacterial infections, the presence of cytokine co-stimulation induces inflammatory and anti-microbial functions in addition to accelerated wound-healing properties. Created with BioRender.com

This model explains why MAIT cells, despite their constant exposure to microbial antigens, do not cause tissue damage. In the case of IBD syndrome, the combination of

factors such as increased gut permeability, dysbiosis and changing concentrations of carbohydrate sources and oxygen (Kiesslich *et al.* 2012; Schmaler *et al.* 2018) may have profound effects on MAIT responses, potentially leading to chronic inflammation and fibrosis and further contributing to the progression of the disease. Increased mucosal permeability may also exacerbate MAIT activation in distal tissues due to the increase of translocating microbiota compounds; thus, contributing to the development of autoimmune diseases such as liver fibrosis and T1D disease, where microbial compounds migrate to the liver and pancreas, respectively (Rouxel *et al.* 2017; Böttcher *et al.* 2018; Hegde *et al.* 2018; Rouland *et al.* 2021; Lett *et al.* 2022). On the other hand, the immunoregulatory module at a steady state may also explain why MAIT infiltration into CRC and HCC tumours correlated with poor prognostics, as they may dampen the immune response against cancer cells. In addition, the expression of growth factors such as VEGF, PDGF and TGFα and recruitments of myeloid cells may also contribute to the pro-tumour role of MAIT cells.

One remaining question is whether the observed homeostatic functions of MAIT cells also apply to other CD161+ or innate-like T-cell populations such as NKT and $\gamma\delta$T-cells, which also play a role at barrier sites and often compete with MAIT cells for the early colonisation of different tissues (Constantinides and Belkaid 2021). Given the transcriptional overlap between CD161+ T-cells (Fergusson *et al.* 2014), this topic should be explored in more detail.

6.1.1. Future work

Future experiments should entail:

- Dissection of the immunoregulatory module in MAIT cells and how it is regulated.
- Effect of MAIT cell activation in the functionality and phenotype of other immune cells.

6.2. Circulating auto-reactive MR1T cells can be used to kill cancer cells

Besides MAIT cells, MR1 is also interesting as an antigen-presenting molecule due to its low number of polymorphisms across the human population and species (Godfrey *et al.* 2015) and, because it presents a new group of antigens that have not been explored before in classical immunology. In TCR-recognition-based immunotherapies, targeting polymorphic HLA molecules limits the size of patient populations, making them less cost-effective to develop. Monomorphic receptors such as MR1 circumvent the HLA-restriction problem; however, the antigen domain of MR1 is poorly understood other than the cluster of metabolic intermediates generated in the synthesis pathway of Vitamin B_2; this poses a challenge in the discovery of MR1-specific TCR sequences that could be used for TCR-based immunotherapies.

In chapter 4, we elucidated that it is possible to isolate and study auto-reactive MR1T cells using HLA-null target cells that overexpress a stable construct of MR1 without adding bacterial-derived antigens. Our results showed data from 2 MR1T clones with distinct specificities capable of recognising and killing cancer cells. Surprisingly in the killing assay, blood-derived healthy cells were not as affected as their cancer counterparts. While our studies did not attempt to identify the cognate antigens for the 2 MR1T clones, our data suggest that these clones may be specific to antigens that are structurally similar or forming similar bonds as 6FP. In addition, we also found that MR1-antigens do not require the formation of Schiff bases to trigger autoreactive MR1T cells. These results add to the growing body of data that describes autoreactive MR1T cells that recognise differentially expressed antigens in cells undergoing metabolic and oxidative stress, such as cancer cells (Lepore *et al.* 2017; Crowther *et al.* 2020; de Libero *et al.* 2021). In this chapter, we also introduced a ligand-blind method using enhanced target cells to identify MR1-specific T-cells without previous knowledge of their antigens.

In chapter 5, we explored the possibility of using modified target cells or soluble MR1 molecules (expressed recombinantly in mammalian cells) to detect and isolate MR1T cells under *ex-vivo* conditions using AIM assays. Our preliminary results showed that while most circulating MR1T cells *in vivo* are naïve, there is an increased frequency of memory MR1T cells in CRC donors. These results further validate the role of MR1T cells in cancer disease.

6.2.1. Future work

Future experiments should entail:

- Developing capabilities in chemical sub-fractionation and mass-spectrometry to unveil the nature of MR1-specific ligands for generated MR1T clones.
- Improving the *ex-vivo* AIM assays by blocking unspecific activation of innate-like T-cells using anti-IFNGR or excluding innate-like T-cells from the AIM assay.

Generating libraries of MR1T TCR sequences and further characterising the nature, functions, and innateness of MR1T cells using single-cell analysis methods such as RNAseq or BD-Rapsody.

7. Bibliography

Abós B, Gómez del Moral M, Gozalbo-López B *et al.* Human MR1 expression on the cell surface is acid sensitive, proteasome independent and increases after culturing at 26°C. *Biochem Biophys Res Commun* 2011;**411**:632–6.

Ahmed D, Eide PW, Eilertsen IA *et al.* Epigenetic and genetic features of 24 colon cancer cell lines. *Oncogenesis* 2013;**2**, DOI: 10.1038/oncsis.2013.35.

Ahmed R, Gray D. Immunological Memory and Protective Immunity: Understanding Their Relation. *Science (1979)* 1996;**272**:54–60.

Akdis CA, Blaser K. Mechanisms of interleukin-10-mediated immune suppression. *Immunology* 2001;**103**:131.

Alevy YG, Patel AC, Romero AG *et al.* IL-13–induced airway mucus production is attenuated by MAPK13 inhibition. *J Clin Invest* 2012;**122**:4555–68.

Aschenbrenner D, Foglierini M, Jarrossay D *et al.* An immunoregulatory and tissue-residency program modulated by c-MAF in human TH17 cells. *Nat Immunol* 2018;**19**:1126–36.

Awad W, Ler GJMM, Xu W *et al.* The molecular basis underpinning the potency and specificity of MAIT cell antigens. *Nat Immunol* 2020;**21**:400–11.

Bachmann MF, Odermatt B, Hengartner H *et al.* Induction of long-lived germinal centers associated with persisting antigen after viral infection. *J Exp Med* 1996;**183**:2259–69.

Bai A, Moss A, Kokkotou E *et al.* CD39 and CD161 modulate Th17 responses in Crohn's disease. *J Immunol* 2014;**193**:3366–77.

Bai H, Gao X, Zhao L *et al.* Respective IL-17A production by γδ T and Th17 cells and its implication in host defense against chlamydial lung infection. *Cellular & Molecular Immunology 2017 14:10* 2016;**14**:850–61.

Bakos E, Thaiss CA, Kramer MP *et al*. CCR2 Regulates the Immune Response by Modulating the Interconversion and Function of Effector and Regulatory T Cells. *The Journal of Immunology* 2017;**198**:4659–71.

Banchereau J, Steinman RM. Dendritic cells and the control of immunity. *Nature* 1998;**392**:245–52.

Bendelac A. Positive selection of mouse NK1+ T cells by CD1-expressing cortical thymocytes. *J Exp Med* 1995;**182**:2091–6.

Bendelac A, Rivera MN, Park SH *et al*. Mouse CD1-specific NK1 T cells: Development, specificity, and function. *Annu Rev Immunol* 1997;**15**:535–62.

Berg KCG, Eide PW, Eilertsen IA *et al*. Multi-omics of 34 colorectal cancer cell lines - a resource for biomedical studies. *Mol Cancer* 2017;**16**, DOI: 10.1186/s12943-017-0691-y.

Bicknell DC, Rowan A, Bodmer WF. Beta 2-microglobulin gene mutations: a study of established colorectal cell lines and fresh tumors. *Proceedings of the National Academy of Sciences* 1994;**91**:4751–5.

Billerbeck E, Kang YH, Walker L *et al*. Analysis of CD161 expression on human CD8+ T cells defines a distinct functional subset with tissue-homing properties. *Proc Natl Acad Sci U S A* 2010;**107**:3006–11.

Blommaart EFC, Krause U, Schellens JPM *et al*. The phosphatidylinositol 3-kinase inhibitors wortmannin and LY294002 inhibit autophagy in isolated rat hepatocytes. *Eur J Biochem* 1997;**243**:240–6.

Bolte FJ, Rehermann B. Mucosal-Associated Invariant T Cells in Chronic Inflammatory Liver Disease. *Semin Liver Dis* 2018;**38**:60–5.

Bonneville M, O'Brien RL, Born WK. γδ T cell effector functions: a blend of innate programming and acquired plasticity. *Nat Rev Immunol* 2010;**10**, DOI: 10.1038/nri2781.

Booth JS, Salerno-Goncalves R, Blanchard TG *et al*. Mucosal-Associated Invariant T Cells in the Human Gastric Mucosa and Blood: Role in Helicobacter pylori Infection. *Front Immunol* 2015;**6**, DOI: 10.3389/FIMMU.2015.00466.

Böttcher K, Rombouts K, Saffioti F *et al.* MAIT cells are chronically activated in patients with autoimmune liver disease and promote profibrogenic hepatic stellate cell activation. *Hepatology* 2018;**68**:172–86.

Boudinot P, Mondot S, Jouneau L *et al.* Restricting nonclassical MHC genes coevolve with TRAV genes used by innate-like T cells in mammals. *Proc Natl Acad Sci U S A* 2016;**113**:E2983–92.

le Bourhis L, Martin E, Péguillet I *et al.* Antimicrobial activity of mucosal-associated invariant T cells. *Nat Immunol* 2010;**11**:701–8.

Bourhis M, Palle J, Galy-Fauroux I *et al.* Direct and Indirect Modulation of T Cells by VEGF-A Counteracted by Anti-Angiogenic Treatment. *Front Immunol* 2021;**12**:853.

Camelo A, Rosignoli G, Ohne Y *et al.* IL-33, IL-25, and TSLP induce a distinct phenotypic and activation profile in human type 2 innate lymphoid cells. *Blood Adv* 2017;**1**:577.

Campbell JJ, Ebsworth K, Ertl LS *et al.* IL-17-Secreting γδ T Cells Are Completely Dependent upon CCR6 for Homing to Inflamed Skin. *J Immunol* 2017;**199**:3129–36.

Canaday DH. Production of $CD4^+$ and $CD8^+$ T cell hybridomas. *Methods Mol Biol* 2013;**960**:297–307.

Carding SR, Egan PJ. The importance of gdT cells in the resolution of pathogen-induced inflammatory immune responses. *Immunol Rev* 2000;**173**:98–108.

Carolan E, Tobin LM, Mangan BA *et al.* Altered Distribution and Increased IL-17 Production by Mucosal-Associated Invariant T Cells in Adult and Childhood Obesity. *The Journal of Immunology* 2015;**194**:5775–80.

Casetti R, Agrati C, Wallace M *et al.* Cutting edge: TGF-beta1 and IL-15 Induce FOXP3+ gammadelta regulatory T cells in the presence of antigen stimulation. *J Immunol* 2009;**183**:3574–7.

CD1C protein expression summary - The Human Protein Atlas.

Cesare A di, Meglio P di, Nestle FO. The IL-23/Th17 Axis in the Immunopathogenesis of Psoriasis. *Journal of Investigative Dermatology* 2009;**129**:1339–50.

Chancellor A, Vacchini A, de Libero G. MR1, an immunological periscope of cellular metabolism. *Int Immunol* 2022;**34**:141–7.

Chang SH, Dong C. A novel heterodimeric cytokine consisting of IL-17 and IL-17F regulates inflammatory responses. *Cell Research 2007 17:5* 2007;**17**:435–40.

Chen S, Crabill GA, Pritchard TS *et al*. Mechanisms regulating PD-L1 expression on tumor and immune cells. *J Immunother Cancer* 2019;**7**, DOI: 10.1186/S40425-019-0770-2.

Chen Z, Wang H, D'Souza C *et al*. Mucosal-associated invariant T-cell activation and accumulation after in vivo infection depends on microbial riboflavin synthesis and co-stimulatory signals. *Mucosal Immunol* 2017;**10**:58–68.

Cheroutre H, Lambolez F. Doubting the TCR Coreceptor Function of CD8αα. *Immunity* 2008;**28**:149–59.

Chiba A, Tajima R, Tomi C *et al*. Mucosal-associated invariant T cells promote inflammation and exacerbate disease in murine models of arthritis. *Arthritis Rheum* 2012;**64**:153–61.

Cieri N, Camisa B, Cocchiarella F *et al*. IL-7 and IL-15 instruct the generation of human memory stem T cells from naive precursors. *Blood* 2013;**121**:573–84.

Cohavy O, Shih DQ, Doherty TM *et al*. CD161 defines effector T cells that express light and respond to TL1A-DR3 signaling. *Eur J Microbiol Immunol (Bp)* 2011;**1**:70.

Cohen CJ, Zhao Y, Zheng Z *et al*. Enhanced Antitumor Activity of Murine-Human Hybrid T-Cell Receptor (TCR) in Human Lymphocytes Is Associated with Improved Pairing and TCR/CD3 Stability. *Cancer Res* 2006;**66**:8878.

Constant P, Davodeau F, Peyrat M-A *et al*. Stimulation of Human γδ T Cells by Nonpeptidic Mycobacterial Ligands. *Science (1979)* 1994;**264**:267–70.

Constantinides MG, Belkaid Y. Early-life imprinting of unconventional T cells and tissue homeostasis. *Science (1979)* 2021;**374**, DOI: 10.1126/science.abf0095.

Constantinides MG, Link VM, Tamoutounour S *et al.* MAIT cells are imprinted by the microbiota in early life and promote tissue repair. *Science (1979)* 2019;**366**:eaax6624.

Corbett AJ, Awad W, Wang H *et al.* Antigen Recognition by MR1-Reactive T Cells; MAIT Cells, Metabolites, and Remaining Mysteries. *Front Immunol* 2020;**11**:1–18.

Corbett AJ, Eckle SBG, Birkinshaw RW *et al.* T-cell activation by transitory neo-antigens derived from distinct microbial pathways. *Nature 2014 509:7500* 2014;**509**:361–5.

Cosgrove C, Ussher JE, Rauch A *et al.* Early and nonreversible decrease of CD161++ /MAIT cells in HIV infection. *Blood* 2013;**121**:951–61.

Crosby CM, Kronenberg M. Tissue-specific functions of invariant natural killer T cells. *Nat Rev Immunol* 2018;**18**:559–74.

Crotzer VL, Blum JS. Autophagy and adaptive immunity. *Immunology* 2010;**131**:9–17.

Crowther MD, Dolton G, Legut M *et al.* Genome-wide CRISPR–Cas9 screening reveals ubiquitous T cell cancer targeting via the monomorphic MHC class I-related protein MR1. *Nat Immunol* 2020;**21**:178–85.

Davey MS, Willcox CR, Joyce SP *et al.* Clonal selection in the human Vδ1 T cell repertoire indicates γδ TCR-dependent adaptive immune surveillance. *Nat Commun* 2017;**8**, DOI: 10.1038/ncomms14760.

Deseke M, Prinz I. Ligand recognition by the γδ TCR and discrimination between homeostasis and stress conditions. *Cellular & Molecular Immunology 2020 17:9* 2020;**17**:914–24.

Dias J, Boulouis C, Gorin JB *et al.* The CD4 - CD8 - MAIT cell subpopulation is a functionally distinct subset developmentally related to the main CD8 + MAIT cell pool. *Proc Natl Acad Sci U S A* 2018;**115**:E11513–22.

DiPietro LA, Burdick M, Low QE *et al.* MIP-1alpha as a critical macrophage chemoattractant in murine wound repair. *J Clin Invest* 1998;**101**:1693–8.

Do J, Fink PJ, Li L *et al*. Cutting Edge: Spontaneous Development of IL-17–Producing γδ T Cells in the Thymus Occurs via a TGF-β1–Dependent Mechanism. *The Journal of Immunology* 2010;**184**:1675–9.

Domae E, Hirai Y, Ikeo T *et al*. Cytokine-mediated activation of human ex vivo-expanded Vγ9Vδ2 T cells. *Oncotarget* 2017;**8**:45928.

Dong C. Diversification of T-helper-cell lineages: finding the family root of IL-17-producing cells. *Nature Reviews Immunology 2006 6:4* 2006;**6**:329–34.

Doyle C, Strominger JL. Interaction between CD4 and class II MHC molecules mediates cell adhesion. *Nature 1987 330:6145* 1987;**330**:256–9.

D'Souza C, Pediongco T, Wang H *et al*. Mucosal-Associated Invariant T Cells Augment Immunopathology and Gastritis in Chronic Helicobacter pylori Infection. *J Immunol* 2018;**200**:ji1701512.

Duan M, Goswami S, Shi JY *et al*. Activated and exhausted MAIT cells foster disease progression and indicate poor outcome in hepatocellular carcinoma. *Clinical Cancer Research* 2019;**25**:3304–16.

Dubin PJ, Kolls JK. Interleukin-17A and interleukin-17F: a tale of two cytokines. *Immunity* 2009;**30**:9–11.

Dunkelberger JR, Song WC. Complement and its role in innate and adaptive immune responses. *Cell Research 2010 20:1* 2009;**20**:34–50.

Dusseaux M, Martin E, Serriari N *et al*. Human MAIT cells are xenobiotic-resistant, tissue-targeted, CD161 hi IL-17-secreting T cells. *Blood* 2011;**117**:1250–9.

van Dyken SJ, Locksley RM. Interleukin-4- and interleukin-13-mediated alternatively activated macrophages: roles in homeostasis and disease. *Annu Rev Immunol* 2013;**31**:317–43.

Eberl G, Brawand P, MacDonald HR. Selective Bystander Proliferation of Memory CD4 + and CD8 + T Cells Upon NK T or T Cell Activation . *The Journal of Immunology* 2000;**165**:4305–11.

Eberl G, Colonna M, Santo JPD *et al*. Innate lymphoid cells: A new paradigm in immunology. *Science (1979)* 2015;**348**, DOI:

10.1126/SCIENCE.AAA6566/ASSET/86BE18C9-7159-455B-89A8-BD6B8E8FA5CD/ASSETS/GRAPHIC/348_AAA6566_FA.JPEG.

Eckle SBG, Corbett AJ, Keller AN *et al*. Recognition of Vitamin B precursors and byproducts by mucosal associated invariant T cells. *Journal of Biological Chemistry* 2015a;**290**:30204–11.

Eckle SBGG, Birkinshaw RW, Kostenko L *et al*. A molecular basis underpinning the T cell receptor heterogeneity of mucosal-associated invariant T cells. *Journal of Experimental Medicine* 2014;**211**:1585–600.

Eckle SBGG, Corbett AJ, Keller AN *et al*. Recognition of Vitamin B precursors and byproducts by mucosal associated invariant T cells. *Journal of Biological Chemistry* 2015b;**290**:30204–11.

Eisenstein EM, Williams CB. The T reg /Th17 Cell Balance: A New Paradigm for Autoimmunity. 2009.

Eming SA, Krieg T. Molecular mechanisms of VEGF-A action during tissue repair. *J Investig Dermatol Symp Proc* 2006;**11**:79–86.

Eming SA, Wynn TA, Martin P. Inflammation and metabolism in tissue repair and regeneration. *Science (1979)* 2017;**356**:1026–30.

Ennamorati M, Vasudevan C, Clerkin K *et al*. Intestinal microbes influence development of thymic lymphocytes in early life. *Proc Natl Acad Sci U S A* 2020;**117**:2570–8.

Fang D, Zhu J. Dynamic balance between master transcription factors determines the fates and functions of CD4 T cell and innate lymphoid cell subsets. *Journal of Experimental Medicine* 2017;**214**:1861–76.

Fang Y, Gong SJ, Xu YH *et al*. Impaired cutaneous wound healing in granulocyte/ macrophage colony-stimulating factor knockout mice. *British Journal of Dermatology* 2007;**157**:458–65.

Fergusson JR, Smith KE, Fleming VM *et al*. CD161 defines a transcriptional and functional phenotype across distinct human T cell lineages. *Cell Rep* 2014;**9**:1075–88.

Forbes SJ, Rosenthal N. Preparing the ground for tissue regeneration: from mechanism to therapy. *Nature Publishing Group* 2014;**20**, DOI: 10.1038/nm.3653.

Fort MM, Cheung J, Yen D *et al*. IL-25 Induces IL-4, IL-5, and IL-13 and Th2-Associated Pathologies In Vivo. *Immunity* 2001;**15**:985–95.

Fowlkes BJ, Edison E, Mathieson BJ *et al*. Cell-cell adhesion mediated by CDS and MHC class I molecules. *J A Proc natn Acad Sci USA* 1985;**19**:2275–785.

Gagliani N, Vesely MCA, Iseppon A *et al*. TH17 cells transdifferentiate into regulatory T cells uring resolution of inflammation. *Nature* 2015;**523**:221–5.

Gagnon E, Duclos S, Rondeau C *et al*. Endoplasmic reticulum-mediated phagocytosis is a mechanism of entry into macrophages. *Cell* 2002;**110**:119–31.

Gavalas NG, Tsiatas M, Tsitsilonis O *et al*. VEGF directly suppresses activation of T cells from ascites secondary to ovarian cancer via VEGF receptor type 2. *Br J Cancer* 2012;**107**:1869.

Georgel P, Radosavljevic M, Macquin C *et al*. The non-conventional MHC class I MR1 molecule controls infection by Klebsiella pneumoniae in mice. *Mol Immunol* 2011;**48**:769–75.

Germain C, Meier A, Jensen T *et al*. Induction of Lectin-like Transcript 1 (LLT1) Protein Cell Surface Expression by Pathogens and Interferon-γ Contributes to Modulate Immune Responses *. *Journal of Biological Chemistry* 2011;**286**:37964–75.

Gherardin NA, Keller AN, Woolley RE *et al*. Diversity of T Cells Restricted by the MHC Class I-Related Molecule MR1 Facilitates Differential Antigen Recognition. *Immunity* 2016;**44**:32–45.

Gherardin NA, McCluskey J, Rossjohn J *et al*. The Diverse Family of MR1-Restricted T Cells. *The Journal of Immunology* 2018a;**201**:2862–71.

Gherardin NA, Souter MNT, Koay HF *et al*. Human blood MAIT cell subsets defined using MR1 tetramers. *Immunol Cell Biol* 2018b;**96**:507–25.

Gibbs A, Leeansyah E, Introini A *et al*. MAIT cells reside in the female genital mucosa and are biased towards IL-17 and IL-22 production in response to bacterial stimulation. *Mucosal Immunol* 2017;**10**:35–45.

Girardi E, Maricic I, Wang J *et al*. Type II natural killer T cells use features of both innate-like and conventional T cells to recognize sulfatide self antigens. *Nature Immunology 2012 13:9* 2012;**13**:851–6.

Girardi M, Lewis J, Glusac E *et al*. Resident Skin-specific γδ T Cells Provide Local, Nonredundant Regulation of Cutaneous Inflammation. *Journal of Experimental Medicine* 2002;**195**:855–67.

Gleimer M, von Boehmer H, Kreslavsky T. PLZF controls the expression of a limited number of genes essential for NKT cell function. 2012, DOI: 10.3389/fimmu.2012.00374.

Godfrey DI, MacDonald HR, Kronenberg M *et al*. NKT cells: what's in a name? *Nat Rev Immunol* 2004;**4**, DOI: 10.1038/nri1309.

Godfrey DI, le Nours J, Andrews DM *et al*. Unconventional T Cell Targets for Cancer Immunotherapy. *Immunity* 2018;**48**:453–73.

Godfrey DI, Uldrich AP, McCluskey J *et al*. The burgeoning family of unconventional T cells. *Nat Immunol* 2015;**16**:1114–23.

Gold MC, Cerri S, Smyk-Pearson S *et al*. Human mucosal associated invariant T cells detect bacterially infected cells. *PLoS Biol* 2010;**8**, DOI: 10.1371/JOURNAL.PBIO.1000407.

Gold MC, Eid T, Smyk-Pearson S *et al*. Human thymic MR1-restricted MAIT cells are innate pathogen-reactive effectors that adapt following thymic egress. *Mucosal Immunology 2013 6:1* 2012;**6**:35–44.

Goldfinch N, Reinink P, Connelley T *et al*. Conservation of mucosal associated invariant T (MAIT) cells and the MR1 restriction element in ruminants, and abundance of MAIT cells in spleen. *Vet Res* 2010;**41**:62.

Golebski K, Ros XR, Nagasawa M *et al.* IL-1β, IL-23, and TGF-β drive plasticity of human ILC2s towards IL-17-producing ILCs in nasal inflammation. *Nat Commun* 2019;**10**, DOI: 10.1038/S41467-019-09883-7.

Grusby MJ, Johnson RS, Papaioannou VE *et al.* Depletion of CD4+ T cells in major histocompatibility complex class II-deficient mice. *Science* 1991;**253**:1417–20.

Gu S, Nawrocka W, Adams EJ. Sensing of Pyrophosphate Metabolites by Vδ9Vγ2 T Cells. *Front Immunol* 2015;**5**, DOI: 10.3389/fimmu.2014.00688.

Gupta PK, Godec J, Wolski D *et al.* CD39 Expression Identifies Terminally Exhausted CD8+ T Cells. *PLoS Pathog* 2015;**11**, DOI: 10.1371/JOURNAL.PPAT.1005177.

Gutierrez-Arcelus M, Teslovich N, Mola AR *et al.* Lymphocyte innateness defined by transcriptional states reflects a balance between proliferation and effector functions. *Nat Commun* 2019;**10**, DOI: 10.1038/s41467-019-08604-4.

Haga K, Chiba A, Shibuya T *et al.* MAIT cells are activated and accumulated in the inflamed mucosa of ulcerative colitis. *J Gastroenterol Hepatol* 2016;**31**:965–72.

Hama I, Tominaga K, Yamagiwa S *et al.* Different distribution of mucosal-associated invariant T cells within the human cecum and colon. *Cent Eur J Immunol* 2019;**44**:75–83.

Harper J, Adams KJ, Bossi G *et al.* An approved in vitro approach to preclinical safety and efficacy evaluation of engineered T cell receptor anti-CD3 bispecific (ImmTAC) molecules. Unutmaz D (ed.). *PLoS One* 2018;**13**:e0205491.

Harriff MJ, Cansler ME, Toren KG *et al.* Human lung epithelial cells contain Mycobacterium tuberculosis in a late endosomal vacuole and are efficiently recognized by CD8+ T Cells. *PLoS One* 2014;**9**:e97515.

Harriff MJ, Karamooz E, Burr A *et al.* Endosomal MR1 Trafficking Plays a Key Role in Presentation of Mycobacterium tuberculosis Ligands to MAIT Cells. *PLoS Pathog* 2016;**12**:e1005524.

Harriff MJ, McMurtrey C, Froyd CA *et al.* MR1 displays the microbial metabolome driving selective MR1-restricted T cell receptor usage. *Sci Immunol* 2018;**3**:2556.

Hayashi E, Chiba A, Tada K *et al.* Involvement of Mucosal-associated Invariant T cells in Ankylosing Spondylitis. *J Rheumatol* 2016;**43**:1695–703.

Hayday AC. γδ T Cells and the Lymphoid Stress-Surveillance Response. *Immunity* 2009;**31**, DOI: 10.1016/j.immuni.2009.08.006.

He X, He X, Dave VP *et al.* The zinc finger transcription factor Th-POK regulates CD4 versus CD8 T-cell lineage commitment. *Nature* 2005;**433**:826–33.

Hegde P, Weiss E, Paradis V *et al.* Mucosal-associated invariant T cells are a profibrogenic immune cell population in the liver. *Nature Communications 2018 9:1* 2018;**9**:1–12.

Hinks TSC, Marchi E, Jabeen M *et al.* Activation and In Vivo Evolution of the MAIT Cell Transcriptome in Mice and Humans Reveals Tissue Repair Functionality. *Cell Rep* 2019;**28**:3249-3262.e5.

Holmkvist P, Roepstorff K, Uronen-Hansson H *et al.* A major population of mucosal memory CD4+ T cells, coexpressing IL-18Rα and DR3, display innate lymphocyte functionality. *Mucosal Immunology 2015 8:3* 2014;**8**:545–58.

Hoorweg K, Peters CP, Cornelissen F *et al.* Functional differences between human NKp44- and NKp44+ RORC+ innate lymphoid cells. *Front Immunol* 2012;**3**:72.

Hoq MM, Suzutani T, Toyoda T *et al.* Role of gamma delta TCR+ lymphocytes in the augmented resistance of trehalose 6,6'-dimycolate-treated mice to influenza virus infection. *J Gen Virol* 1997;**78 (Pt 7)**:1597–603.

Hos D, Bucher F, Regenfuss B *et al.* IL-10 Indirectly Regulates Corneal Lymphangiogenesis and Resolution of Inflammation via Macrophages. *Am J Pathol* 2016;**186**:159–71.

Howson LJ, Awad W, Borstel A von *et al.* Absence of mucosal-associated invariant T cells in a person with a homozygous point mutation in MR1. *Sci Immunol* 2020;**5**:1–14.

Hsieh CS, Macatonia SE, Tripp CS *et al.* Development of TH1 CD4+ T cells through IL-12 produced by Listeria-induced macrophages. *Science* 1993;**260**:547–9.

Hu G, Wu P, Cheng P *et al*. Tumor-infiltrating CD39+ γδTregs are novel immunosuppressive T cells in human colorectal cancer. *Oncoimmunology* 2017;**6**, DOI: 10.1080/2162402X.2016.1277305.

Hu X, Ivashkiv LB. Cross-regulation of Signaling Pathways by Interferon-γ: Implications for Immune Responses and Autoimmune Diseases. *Immunity* 2009;**31**:539–50.

Hu X, Paik PK, Chen J *et al*. IFN-γ Suppresses IL-10 Production and Synergizes with TLR2 by Regulating GSK3 and CREB/AP-1 Proteins. *Immunity* 2006;**24**:563–74.

Huang S, Gilfillan S, Cella M *et al*. Evidence for MR1 antigen presentation to mucosal-associated invariant T cells. *Journal of Biological Chemistry* 2005a;**280**:21183–93.

Huang S, Gilfillan S, Cella M *et al*. Evidence for MR1 Antigen Presentation to Mucosal-associated Invariant T Cells. *Journal of Biological Chemistry* 2005b;**280**:21183–93.

Huang S, Gilfillan S, Kim S *et al*. MR1 uses an endocytic pathway to activate mucosal-associated invariant T cells. *Journal of Experimental Medicine* 2008;**205**:1201–11.

Huang S, Martin E, Kim S *et al*. MR1 antigen presentation to mucosal-associated invariant T cells was highly conserved in evolution. *Proc Natl Acad Sci U S A* 2009;**106**:8290–5.

Iershov A, Nemazanyy I, Alkhoury C *et al*. The class 3 PI3K coordinates autophagy and mitochondrial lipid catabolism by controlling nuclear receptor PPARα. *Nature Communications 2019 10:1* 2019;**10**:1–18.

Jaber N, Dou Z, Chen JS *et al*. Class III PI3K Vps34 plays an essential role in autophagy and in heart and liver function. *Proc Natl Acad Sci U S A* 2012;**109**:2003–8.

James CA, Xu Y, Aguilar MS *et al*. CD4 and CD8 co-receptors modulate functional avidity of CD1b-restricted T cells. *bioRxiv* 2020:2020.10.17.332072.

Jameson JM, Cauvi G, Witherden DA *et al*. A Keratinocyte-Responsive γδ TCR Is Necessary for Dendritic Epidermal T Cell Activation by Damaged Keratinocytes

and Maintenance in the Epidermis. *The Journal of Immunology* 2004;**172**:3573–9.

Jin S, Chin J, Seeber S *et al.* TL1A/TNFSF15 directly induces proinflammatory cytokines, including TNFα, from CD3+CD161+ T cells to exacerbate gut inflammation. *Mucosal Immunology 2013 6:5* 2012;**6**:886–99.

Jo J, Tan AT, Ussher JE *et al.* Toll-Like Receptor 8 Agonist and Bacteria Trigger Potent Activation of Innate Immune Cells in Human Liver. *PLoS Pathog* 2014;**10**:e1004210.

Joffre OP, Segura E, Savina A *et al.* Cross-presentation by dendritic cells. *Nature Reviews Immunology 2012 12:8* 2012;**12**:557–69.

de Jong A, Peña-Cruz V, Cheng TY *et al.* CD1a-autoreactive T cells are a normal component of the human αβ T cell repertoire. *Nature Immunology 2010 11:12* 2010;**11**:1102–9.

Kain L, Webb B, Anderson BL *et al.* The Identification of the Endogenous Ligands of Natural Killer T Cells Reveals the Presence of Mammalian α-Linked Glycosylceramides. *Immunity* 2014;**41**, DOI: 10.1016/j.immuni.2014.08.017.

Kallies A, Xin A, Belz GT *et al.* Blimp-1 transcription factor is required for the differentiation of effector CD8(+) T cells and memory responses. *Immunity* 2009;**31**:283–95.

Kara EE, McKenzie DR, Bastow CR *et al.* CCR2 defines in vivo development and homing of IL-23-driven GM-CSF-producing Th17 cells. *Nat Commun* 2015;**6**, DOI: 10.1038/NCOMMS9644.

Karamooz E, Harriff MJ, Narayanan GA *et al.* MR1 recycling and blockade of endosomal trafficking reveal distinguishable antigen presentation pathways between Mycobacterium tuberculosis infection and exogenously delivered antigens. *Sci Rep* 2019;**9**:1–11.

Keller AN, Eckle SBGG, Xu W *et al.* Drugs and drug-like molecules can modulate the function of mucosal-associated invariant T cells. *Nat Immunol* 2017;**18**:402–11.

Kiesslich R, Duckworth CA, Moussata D *et al*. Local barrier dysfunction identified by confocal laser endomicroscopy predicts relapse in inflammatory bowel disease. *Gut* 2012;**61**:1146–53.

Kimura A, Naka T, Kishimoto T. IL-6-dependent and -independent pathways in the development of interleukin 17-producing T helper cells. *Proc Natl Acad Sci U S A* 2007;**104**:12099–104.

Kisielow J, Obermair FJ, Kopf M. Deciphering CD4+ T cell specificity using novel MHC–TCR chimeric receptors. *Nature Immunology 2019 20:5* 2019;**20**:652–62.

Kjer-Nielsen L, Patel O, Corbett AJ *et al*. MR1 presents microbial vitamin B metabolites to MAIT cells. *Nature* 2012;**491**:717–23.

Klein L, Kyewski B, Allen PM *et al*. Positive and negative selection of the T cell repertoire: what thymocytes see (and don't see). *Nature Reviews Immunology 2014 14:6* 2014;**14**:377–91.

Klionsky DJ, Elazar Z, Seglen PO *et al*. Does bafilomycin A1 block the fusion of autophagosomes with lysosomes? *Autophagy* 2008;**4**:849–50.

Koay HF, Gherardin NA, Enders A *et al*. A three-stage intrathymic development pathway for the mucosal-associated invariant T cell lineage. *Nat Immunol* 2016;**17**:1300–11.

Koay HF, Gherardin NA, Xu C *et al*. Diverse MR1-restricted T cells in mice and humans. *Nat Commun* 2019a;**10**:1–15.

Koay HF, Su S, Amann-Zalcenstein D *et al*. A divergent transcriptional landscape underpins the development and functional branching of MAIT cells. *Sci Immunol* 2019b;**4**, DOI: 10.1126/SCIIMMUNOL.AAY6039/SUPPL_FILE/AAY6039_SM.PDF.

Kohli K, Yao L, Nowicki TS *et al*. IL-15 mediated expansion of rare durable memory T cells following adoptive cellular therapy. *J Immunother Cancer* 2021;**9**:e002232.

Kolaczkowska E, Kubes P. Neutrophil recruitment and function in health and inflammation. *Nature Reviews Immunology 2013 13:3* 2013;**13**:159–75.

Kulicke C, Karamooz E, Lewinsohn D *et al.* Covering All the Bases: Complementary MR1 Antigen Presentation Pathways Sample Diverse Antigens and Intracellular Compartments. *Front Immunol* 2020;**11**:2034.

Kurioka A, Jahun AS, Hannaway RF *et al.* Shared and Distinct Phenotypes and Functions of Human CD161++ Vα7.2+ T Cell Subsets. *Front Immunol* 2017;**8**, DOI: 10.3389/FIMMU.2017.01031.

Kurioka A, Ussher JE, Cosgrove C *et al.* MAIT cells are licensed through granzyme exchange to kill bacterially sensitized targets. *Mucosal Immunol* 2015, DOI: 10.1038/mi.2014.81.

Kurioka A, Walker LJ, Klenerman P *et al.* MAIT cells: new guardians of the liver. *Clin Transl Immunology* 2016;**5**:e98.

de Lalla C, Lepore M, Piccolo FM *et al.* High-frequency and adaptive-like dynamics of human CD1 self-reactive T cells. *Eur J Immunol* 2011;**41**:602–10.

Lamichhane R, Schneider M, de la Harpe SM *et al.* TCR- or Cytokine-Activated CD8+ Mucosal-Associated Invariant T Cells Are Rapid Polyfunctional Effectors That Can Coordinate Immune Responses. *Cell Rep* 2019;**28**:3061-3076.e5.

Lange J, Anderson RJ, Marshall AJ *et al.* The Chemical Synthesis, Stability, and Activity of MAIT Cell Prodrug Agonists That Access MR1 in Recycling Endosomes. *ACS Chem Biol* 2020;**15**:437–45.

Lee CH, Zhang HH, Singh SP *et al.* C/EBPd drives interactions between human MAIT cells and endothelial cells that are important for extravasation. *Elife* 2018;**7**, DOI: 10.7554/ELIFE.32532.

Lee SK, Rigby RJ, Zotos D *et al.* B cell priming for extrafollicular antibody responses requires Bcl-6 expression by T cells. *J Exp Med* 2011;**208**:1377.

Lee YJ, Holzapfel KL, Zhu J *et al.* Steady-state production of IL-4 modulates immunity in mouse strains and is determined by lineage diversity of iNKT cells. *Nat Immunol* 2013;**14**, DOI: 10.1038/ni.2731.

Lee YJ, Wang H, Starrett GJ *et al.* Tissue-Specific Distribution of iNKT Cells Impacts Their Cytokine Response. *Immunity* 2015;**43**:566–78.

Leeansyah E, Ganesh A, Quigley MF *et al*. Activation, exhaustion, and persistent decline of the antimicrobial MR1-restricted MAIT-cell population in chronic HIV-1 infection. *Blood* 2013;**121**:1124–35.

Leeansyah E, Svärd J, Dias J *et al*. Arming of MAIT Cell Cytolytic Antimicrobial Activity Is Induced by IL-7 and Defective in HIV-1 Infection. *PLoS Pathog* 2015;**11**, DOI: 10.1371/JOURNAL.PPAT.1005072.

Legoux F, Bellet D, Daviaud C *et al*. Microbial metabolites control the thymic development of mucosal-associated invariant T cells. *Science (1979)* 2019a;**366**:494–9.

Legoux F, Gilet J, Procopio E *et al*. Molecular mechanisms of lineage decisions in metabolite-specific T cells. *Nature Immunology 2019 20:9* 2019b;**20**:1244–55.

Leng T, Akther HD, Hackstein CP *et al*. TCR and Inflammatory Signals Tune Human MAIT Cells to Exert Specific Tissue Repair and Effector Functions. *Cell Rep* 2019;**28**:3077-3091.e5.

Lepore M, Kalinicenko A, Colone A *et al*. Parallel T-cell cloning and deep sequencing of human MAIT cells reveal stable oligoclonal TCRβ repertoire. *Nature Communications 2014 5:1* 2014a;**5**:1–15.

Lepore M, Kalinichenko A, Calogero S *et al*. Functionally diverse human T cells recognize non-microbial antigens presented by MR1. *Elife* 2017;**6**:e24476.

Lepore M, de Lalla C, Gundimeda SR *et al*. A novel self-lipid antigen targets human T cells against CD1c+ leukemias. *J Exp Med* 2014b;**211**:1363–77.

Lett MJ, Mehta H, Keogh A *et al*. Stimulatory MAIT cell antigens reach the circulation and are efficiently metabolised and presented by human liver cells. *Gut* 2022;**0**:gutjnl-2021-324478.

Levin-Konigsberg R, Grinstein S. Phagosome-endoplasmic reticulum contacts: Kissing and not running. *Traffic* 2020;**21**:172–80.

Levy JMM, Towers CG, Thorburn A. Targeting autophagy in cancer. *Nat Rev Cancer* 2017;**17**:528–42.

Li Z, Hodgkinson T, Gothard EJ *et al*. Epidermal Notch1 recruits RORγ+ group 3 innate lymphoid cells to orchestrate normal skin repair. *Nature Communications 2016 7:1* 2016;**7**:1–14.

Liang HE, Reinhardt RL, Bando JK *et al*. Divergent expression patterns of IL-4 and IL-13 define unique functions in allergic immunity. *Nature Immunology 2011 13:1* 2011;**13**:58–66.

de Libero G, Mori L, Vacchini A *et al*. MR1 LIGANDS AND PHARMACEUTICAL COMPOSITIONS FOR IMMUNOMODULATION. 2021.

Lin Q, Kuypers M, Philpott DJ *et al*. The dialogue between unconventional T cells and the microbiota. *Mucosal Immunology 2020 13:6* 2020;**13**:867–76.

Lindemans CA, Calafiore M, Mertelsmann AM *et al*. Interleukin-22 Promotes Intestinal Stem Cell-Mediated Epithelial Regeneration. *Nature* 2015;**528**:560.

Linehan JL, Harrison OJ, Han SJ *et al*. Non-classical Immunity Controls Microbiota Impact on Skin Immunity and Tissue Repair. *Cell* 2018;**172**:784-796.e18.

Ling L, Lin Y, Zheng W *et al*. Circulating and tumor-infiltrating mucosal associated invariant T (MAIT) cells in colorectal cancer patients. *Sci Rep* 2016;**6**, DOI: 10.1038/SREP20358.

Lion J, Debuysscher V, Wlodarczyk A *et al*. MR1B, a natural spliced isoform of the MHC-related 1 protein, is expressed as homodimers at the cell surface and activates MAIT cells. *Eur J Immunol* 2013;**43**:1363–73.

Liu TY, Uemura Y, Suzuki M *et al*. Distinct subsets of human invariant NKT cells differentially regulate T helper responses via dendritic cells. *Eur J Immunol* 2008;**38**:1012–23.

Liu Z, Geboes K, Colpaert S *et al*. IL-15 is highly expressed in inflammatory bowel disease and regulates local T cell-dependent cytokine production. *J Immunol* 2000;**164**:3608–15.

Loh L, Wang Z, Sant S *et al*. Human mucosal-associated invariant T cells contribute to antiviral influenza immunity via IL-18-dependent activation. *Proc Natl Acad Sci U S A* 2016;**113**:10133–8.

López-Sagaseta J, Dulberger CL, Crooks JE *et al.* The molecular basis for Mucosal-Associated Invariant T cell recognition of MR1 proteins. *Proc Natl Acad Sci U S A* 2013;**110**:E1771–8.

Lowe KL, Cole D, Kenefeck R *et al.* Anti-Tumour Treatment Novel TCR-based biologics: mobilising T cells to warm "cold" tumours. 2019, DOI: 10.1016/j.ctrv.2019.06.001.

Lynch L, Michelet X, Zhang S *et al.* Regulatory iNKT cells lack expression of the transcription factor PLZF and control the homeostasis of T reg cells and macrophages in adipose tissue. *Nat Immunol* 2015;**16**:85–95.

Maher CO, Dunne K, Comerford R *et al.* Candida albicans Stimulates IL-23 Release by Human Dendritic Cells and Downstream IL-17 Secretion by Vδ1 T Cells. *The Journal of Immunology* 2015;**194**:5953–60.

Mak JYW, Xu W, Reid RC *et al.* Stabilizing short-lived Schiff base derivatives of 5-aminouracils that activate mucosal-associated invariant T cells. *Nature Communications 2017 8:1* 2017;**8**:1–13.

Mao Y, Yin S, Zhang J *et al.* A new effect of IL-4 on human γδ T cells: promoting regulatory Vδ1 T cells via IL-10 production and inhibiting function of Vδ2 T cells. *Cell Mol Immunol* 2016;**13**:217–28.

Marshall HT, Djamgoz MBA. Immuno-oncology: Emerging targets and combination therapies. *Front Oncol* 2018;**8**:315.

Martin E, Treiner E, Duban L *et al.* Stepwise Development of MAIT Cells in Mouse and Human. Cerundolo V (ed.). *PLoS Biol* 2009;**7**:e1000054.

Martinez FO, Gordon S. The M1 and M2 paradigm of macrophage activation: time for reassessment. *F1000Prime Rep* 2014;**6**, DOI: 10.12703/P6-13.

McKenzie DR, Comerford I, Silva-Santos B *et al.* The emerging complexity of γδT17 Cells. *Front Immunol* 2018;**9**:796.

McLeod JJA, Baker B, Ryan JJ. Mast Cell Production and Response to IL-4 and IL-13. *Cytokine* 2015;**75**:57.

McShan AC, Devlin CA, Papadaki GF *et al.* TAPBPR employs a ligand-independent docking mechanism to chaperone MR1 molecules. *Nature Chemical Biology 2022* 2022:1–10.

McWilliam HEG, Eckle SBG, Theodossis A *et al.* The intracellular pathway for the presentation of Vitamin B-related antigens by the antigen-presenting molecule MR1. *Nat Immunol* 2016;**17**:531–7.

McWilliam HEG, Mak JYW, Awad W *et al.* Endoplasmic reticulum chaperones stabilize ligand-receptive MR1 molecules for efficient presentation of metabolite antigens. *Proc Natl Acad Sci U S A* 2020;**117**:24974–85.

McWilliam HEGG, Villadangos JA. How MR1 Presents a Pathogen Metabolic Signature to Mucosal-Associated Invariant T (MAIT) Cells. *Trends Immunol* 2017;**38**:679–89.

Medzhitov R, Janeway CA. Innate immune recognition and control of adaptive immune responses. *Semin Immunol* 1998;**10**:351–3.

Meermeier EW, Laugel BF, Sewell AK *et al.* Human TRAV1-2-negative MR1-restricted T cells detect S. pyogenes and alternatives to MAIT riboflavin-based antigens. *Nat Commun* 2016;**7**:1–12.

Meierovics A, Yankelevich WJC, Cowley SC. MAIT cells are critical for optimal mucosal immune responses during in vivo pulmonary bacterial infection. *Proc Natl Acad Sci U S A* 2013;**110**, DOI: 10.1073/PNAS.1302799110.

Mempel TR, Henrickson SE, von Andrian UH. T-cell priming by dendritic cells in lymph nodes occurs in three distinct phases. *Nature 2004 427:6970* 2004;**427**:154–9.

Meylan F, Davidson TS, Kahle E *et al.* The TNF-Family Receptor DR3 is Essential for Diverse T Cell-Mediated Inflammatory Diseases. *Immunity* 2008;**29**:79–89.

Michel ML, Keller AC, Paget C *et al.* Identification of an IL-17-producing NK1.1neg iNKT cell population involved in airway neutrophilia. *Journal of Experimental Medicine* 2007;**204**:995–1001.

Migone TS, Zhang J, Luo X *et al.* TL1A Is a TNF-like Ligand for DR3 and TR6/DcR3 and Functions as a T Cell Costimulator. *Immunity* 2002;**16**:479–92.

Miley MJ, Truscott SM, Yu YYL *et al.* Biochemical Features of the MHC-Related Protein 1 Consistent with an Immunological Function. *The Journal of Immunology* 2003;**170**:6090–8.

Mittrücker HW, Visekruna A, Huber M. Heterogeneity in the Differentiation and Function of CD8+ T Cells. *Arch Immunol Ther Exp (Warsz)* 2014;**62**:449–58.

Mosser DM, Edwards JP. Exploring the full spectrum of macrophage activation. *Nature Reviews Immunology 2008 8:12* 2008;**8**:958–69.

Muñoz-Fernández MA, Fernández MA, Fresno M. Synergism between tumor necrosis factor-alpha and interferon-gamma on macrophage activation for the killing of intracellular Trypanosoma cruzi through a nitric oxide-dependent mechanism. *Eur J Immunol* 1992;**22**:301–7.

Murciano-Goroff YR, Warner AB, Wolchok JD. The future of cancer immunotherapy: microenvironment-targeting combinations. *Cell Research 2020 30:6* 2020;**30**:507–19.

Murphy K, Weaver C. Janeway 's Immunology. *America (NY)* 2017:1–277.

Nakai K, He YY, Nishiyama F *et al.* IL-17A induces heterogeneous macrophages, and it does not alter the effects of lipopolysaccharides on macrophage activation in the skin of mice. *Scientific Reports 2017 7:1* 2017;**7**:1–14.

Nakamura R, Sene A, Santeford A *et al.* IL10-driven STAT3 signalling in senescent macrophages promotes pathological eye angiogenesis. *Nat Commun* 2015;**6**, DOI: 10.1038/NCOMMS8847.

Neefjes J, Jongsma MLMM, Paul P *et al.* Towards a systems understanding of MHC class i and MHC class II antigen presentation. *Nat Rev Immunol* 2011;**11**:823–36.

Ness-Schwickerath KJ, Jin C, Morita CT. Cytokine Requirements for the Differentiation and Expansion of IL-17A– and IL-22–Producing Human Vγ2Vδ2 T Cells. *The Journal of Immunology* 2010;**184**, DOI: 10.4049/jimmunol.1000600.

Nishikawa K, Seo N, Torii M *et al*. Interleukin-17 Induces an Atypical M2-Like Macrophage Subpopulation That Regulates Intestinal Inflammation. *PLoS One* 2014;**9**:e108494.

le Nours J, Gherardin NA, Ramarathinam SH *et al*. A class of gd T cell receptors recognize the underside of the antigen-presenting molecule MR1. *Science (1979)* 2019;**366**:1522–7.

Novak J, Dobrovolny J, Novakova L *et al*. The decrease in number and change in phenotype of mucosal-associated invariant T cells in the elderly and differences in men and women of reproductive age. *Scand J Immunol* 2014;**80**:271–5.

O'Connor W, Kamanaka M, Booth CJ *et al*. A protective function for interleukin 17A in T cell-mediated intestinal inflammation. *Nat Immunol* 2009;**10**:603–9.

Odero MD, Zeleznik-Le NJ, Chinwalla V *et al*. Cytogenetic and molecular analysis of the acute monocytic leukemia cell line THP-1 with an MLL-AF9 translocation. *Genes Chromosomes Cancer* 2000;**29**:333–8.

Ohnmacht C, Schwartz C, Panzer M *et al*. Basophils orchestrate chronic allergic dermatitis and protective immunity against helminths. *Immunity* 2010;**33**:364–74.

Park JH, Lee HK. Function of γδ T cells in tumor immunology and their application to cancer therapy. *Experimental & Molecular Medicine 2021 53:3* 2021;**53**:318–27.

Patel O, Kjer-Nielsen L, le Nours J *et al*. Recognition of vitamin B metabolites by mucosal-associated invariant T cells. *Nat Commun* 2013;**4**:1–9.

Payne KK, Mine JA, Biswas S *et al*. BTN3A1 governs antitumor responses by coordinating αβ and γδ T cells. *Science* 2020;**369**:942–9.

Pearce EL, Mullen AC, Martins GA *et al*. Control of effector CD8+ T cell function by the transcription factor Eomesodermin. *Science* 2003;**302**:1041–3.

Pei B, Vela JL, Zajonc D *et al*. Interplay between carbohydrate and lipid in recognition of glycolipid antigens by natural killer T cells. *Ann N Y Acad Sci* 2012;**1253**, DOI: 10.1111/j.1749-6632.2011.06435.x.

Pellicci DG, Koay HF, Berzins SP. Thymic development of unconventional T cells: how NKT cells, MAIT cells and γδ T cells emerge. *Nature Reviews Immunology 2020 20:12* 2020;**20**:756–70.

Peng G, Wang HY, Peng W *et al*. Tumor-Infiltrating γδ T Cells Suppress T and Dendritic Cell Function via Mechanisms Controlled by a Unique Toll-like Receptor Signaling Pathway. *Immunity* 2007;**27**:334–48.

Pesu M, Watford WT, Wei L *et al*. T-cell-expressed proprotein convertase furin is essential for maintenance of peripheral immune tolerance. *Nature 2008 455:7210* 2008;**455**:246–50.

Petermann F, Rothhammer V, Claussen MC *et al*. γδ T Cells Enhance Autoimmunity by Restraining Regulatory T Cell Responses via an Interleukin-23-Dependent Mechanism. *Immunity* 2010;**33**:351–63.

Phetsouphanh C, Phalora P, Hackstein CP *et al*. Human MAIT cells respond to and suppress HIV-1. *Elife* 2021;**10**, DOI: 10.7554/ELIFE.50324.

Pichavant M, Goya S, Meyer EH *et al*. Ozone exposure in a mouse model induces airway hyperreactivity that requires the presence of natural killer T cells and IL-17. *Journal of Experimental Medicine* 2008;**205**:385–93.

Pierce GF, Mustoe TA, Altrock BW *et al*. Role of platelet-derived growth factor in wound healing. *J Cell Biochem* 1991;**45**:319–26.

Pierce GF, Tarpley JE, Tseng J *et al*. Detection of platelet-derived growth factor (PDGF)-AA in actively healing human wounds treated with recombinant PDGF-BB and absence of PDGF in chronic nonhealing wounds. *J Clin Invest* 1995;**96**:1336–50.

Pittet MJ, Zippelius A, Valmori D *et al*. Degeneracy instead of specificity: is this a solution to cancer immunotherapy? *Trends Immunol* 2002;**23**:344.

Porcelli S, Brenner MB, Greenstein JL *et al*. Recognition of cluster of differentiation 1 antigens by human CD4–CD8>– cytolytic T lymphocyte. *Nature* 1989;**341**, DOI: 10.1038/341447a0.

Porcelli S, Yockey CE, Brenner MB *et al*. Analysis of T cell antigen receptor (TCR) expression by human peripheral blood CD4-8- alpha/beta T cells demonstrates preferential use of several V beta genes and an invariant TCR alpha chain. *J Exp Med* 1993;**178**:1–16.

Povoleri GAMM, Nova-Lamperti E, Scottà C *et al*. Human retinoic acid–regulated CD161 + regulatory T cells support wound repair in intestinal mucosa. *Nat Immunol* 2018;**19**:1403–14.

Prehn JL, Mehdizadeh S, Landers CJ *et al*. Potential role for TL1A, the new TNF-family member and potent costimulator of IFN-γ, in mucosal inflammation. *Clinical Immunology* 2004;**112**:66–77.

Provine NM, Binder B, FitzPatrick MEB *et al*. Unique and common features of innate-like human Vδ2+ γδT cells and mucosal-associated invariant T cells. *Front Immunol* 2018;**9**:756.

Provine NM, Klenerman P. MAIT Cells in Health and Disease. *Annu Rev Immunol* 2020;**38**:203–28.

Qin H, Wang L, Feng T *et al*. TGF-β promotes Th17 cell development through inhibition of SOCS3. *J Immunol* 2009;**183**:97.

Rahal OM, Wolfe AR, Mandal PK *et al*. Blocking Interleukin (IL)4- and IL13-Mediated Phosphorylation of STAT6 (Tyr641) Decreases M2 Polarization of Macrophages and Protects Against Macrophage-Mediated Radioresistance of Inflammatory Breast Cancer. *Int J Radiat Oncol Biol Phys* 2018;**100**:1034–43.

Rahimpour A, Koay HF, Enders A *et al*. Identification of phenotypically and functionally heterogeneous mouse mucosal-associated invariant T cells using MR1 tetramers. *J Exp Med* 2015;**212**:1095–108.

Ramachandran P, Iredale JP, Fallowfield JA. Resolution of Liver Fibrosis: Basic Mechanisms and Clinical Relevance. *Liver Dis* 2015;**35**:119–31.

Rathmell JC, Farkash EA, Gao W *et al*. IL-7 Enhances the Survival and Maintains the Size of Naive T Cells. *The Journal of Immunology* 2001;**167**:6869–76.

Reantragoon R, Corbett AJ, Sakala IG *et al*. Antigen-loaded MR1 tetramers define T cell receptor heterogeneity in mucosal-associated invariant T cells. *Journal of Experimental Medicine* 2013;**210**:2305–20.

Reinink P, van Rhijn I. Mammalian CD1 and MR1 genes. *Immunogenetics* 2016;**68**:515–23.

van Rhijn I, le Nours J. CD1 and MR1 recognition by human γδ T cells. *Mol Immunol* 2021;**133**:95–100.

Rhost S, Sedimbi S, Kadri N *et al*. Immunomodulatory Type II Natural Killer T Lymphocytes in Health and Disease. *Scand J Immunol* 2012;**76**, DOI: 10.1111/j.1365-3083.2012.02750.x.

Ribot JC, Ribeiro ST, Correia D v. *et al*. Human γδ Thymocytes Are Functionally Immature and Differentiate into Cytotoxic Type 1 Effector T Cells upon IL-2/IL-15 Signaling. *The Journal of Immunology* 2014;**192**, DOI: 10.4049/jimmunol.1303119.

Roche PA, Furuta K. The ins and outs of MHC class II-mediated antigen processing and presentation. *Nat Rev Immunol* 2015;**15**:203–16.

Rock EP, Sibbald PR, Davis MM *et al*. CDR3 length in antigen-specific immune receptors. *Journal of Experimental Medicine* 1994;**179**, DOI: 10.1084/jem.179.1.323.

Rouland M, Beaudoin L, Rouxel O *et al*. Gut mucosa alterations and loss of segmented filamentous bacteria in type 1 diabetes are associated with inflammation rather than hyperglycaemia. *Gut* 2021;**71**:296–308.

Rouxel O, da Silva J, Beaudoin L *et al*. Cytotoxic and regulatory roles of mucosal-associated invariant T cells in type 1 diabetes. *Nature Immunology 2017 18:12* 2017;**18**:1321–31.

Roy KC, Maricic I, Khurana A *et al*. Involvement of Secretory and Endosomal Compartments in Presentation of an Exogenous Self-Glycolipid to Type II NKT Cells. *The Journal of Immunology* 2008;**180**:2942–50.

Rutishauser RL, Martins GA, Kalachikov S *et al*. Transcriptional repressor Blimp-1 promotes CD8(+) T cell terminal differentiation and represses the acquisition of central memory T cell properties. *Immunity* 2009;**31**:296–308.

Rutkowski MR, Stephen TL, Svoronos N *et al*. Microbially driven TLR5-dependent signaling governs distal malignant progression through tumor-promoting inflammation. *Cancer Cell* 2015;**27**:27–40.

Saez-Ibañez AR, Upadhaya S, Partridge T *et al*. Landscape of cancer cell therapies: trends and real-world data. *Nat Rev Drug Discov* 2022, DOI: 10.1038/D41573-022-00095-1.

Sag D, Krause P, Hedrick CC *et al*. IL-10-producing NKT10 cells are a distinct regulatory invariant NKT cell subset. *Journal of Clinical Investigation* 2014;**124**:3725–40.

Salio M, Awad W, Veerapen N *et al*. Ligand-dependent downregulation of MR1 cell surface expression. *Proc Natl Acad Sci U S A* 2020;**117**:10465–75.

Salou M, Legoux F, Gilet J *et al*. A common transcriptomic program acquired in the thymus defines tissue residency of MAIT and NKT subsets. *J Exp Med* 2019;**216**:133–51.

Salou M, Legoux F, Lantz O. MAIT cell development in mice and humans. *Mol Immunol* 2021;**130**:31–6.

Satkunanathan S, Kumar N, Bajorek M *et al*. Respiratory Syncytial Virus Infection, TLR3 Ligands, and Proinflammatory Cytokines Induce CD161 Ligand LLT1 Expression on the Respiratory Epithelium. *J Virol* 2014;**88**:2366–73.

Sattler A, Dang-Heine C, Reinke P *et al*. IL-15 dependent induction of IL-18 secretion as a feedback mechanism controlling human MAIT-cell effector functions. *Eur J Immunol* 2015;**45**:2286–98.

Savage AK, Constantinides MG, Han J *et al*. The Transcription Factor PLZF Directs the Effector Program of the NKT Cell Lineage. *Immunity* 2008;**29**:391–403.

Schatz DG, Oettinger MA, Baltimore D. The V(D)J recombination activating gene, RAG-1. *Cell* 1989;**59**:1035–48.

Schilbach K, Welker C, Krickeberg N *et al*. In the Absence of a TCR Signal IL-2/IL-12/18-Stimulated γδ T Cells Demonstrate Potent Anti-Tumoral Function Through Direct Killing and Senescence Induction in Cancer Cells. *Cancers 2020, Vol 12, Page 130* 2020;**12**:130.

Schmaler M, Colone A, Spagnuolo J *et al*. Modulation of bacterial metabolism by the microenvironment controls MAIT cell stimulation. *Mucosal Immunology 2018 11:4* 2018;**11**:1060–70.

Schultz G, Clark W, Rotatori DS. EGF and TGF-alpha in wound healing and repair. *J Cell Biochem* 1991;**45**:346–52.

Schultz GS, White M, Mitchell R *et al*. Epithelial wound healing enhanced by transforming growth factor-alpha and vaccinia growth factor. *Science* 1987;**235**:350–2.

Schumacher TNM, Heemels MT, Neefjes JJ *et al*. Direct binding of peptide to empty MHC class I molecules on intact cells and in vitro. *Cell* 1990;**62**:563–7.

Seach N, Guerri L, Bourhis L le *et al*. Double Positive Thymocytes Select Mucosal-Associated Invariant T Cells. *The Journal of Immunology* 2013a;**191**:6002–9.

Seach N, Guerri L, Bourhis L le *et al*. Double Positive Thymocytes Select Mucosal-Associated Invariant T Cells. *The Journal of Immunology* 2013b;**191**:6002–9.

Seneviratna R, Redmond SJ, McWilliam HEG *et al*. Differential antigenic requirements by diverse MR1-restricted T cells. *Immunol Cell Biol* 2022;**100**:112–26.

Serriari NE, Eoche M, Lamotte L *et al*. Innate mucosal-associated invariant T (MAIT) cells are activated in inflammatory bowel diseases. *Clin Exp Immunol* 2014;**176**:266–74.

Sewell AK. Why must T cells be cross-reactive? *Nature Reviews Immunology 2012 12:9* 2012;**12**:669–77.

Shaler CR, Tun-Abraham ME, Skaro AI *et al*. Mucosa-associated invariant T cells infiltrate hepatic metastases in patients with colorectal carcinoma but are rendered dysfunctional within and adjacent to tumor microenvironment. *Cancer Immunol Immunother* 2017;**66**:1563–75.

Shen J, Sun X, Pan B *et al*. IL-17 induces macrophages to M2-like phenotype via NF-κB. *Cancer Manag Res* 2018;**10**:4217.

Shi S, Zhang Q, Atsuta I *et al*. IL-17-mediated M1/M2 macrophage alteration contributes to pathogenesis of bisphosphonate-related osteonecrosis of the jaws. *Clinical Cancer Research* 2013;**19**:3176–88.

Shih DQ, Kwan LY, Chavez V *et al*. Microbial induction of inflammatory bowel disease associated gene TL1A (TNFSF15) in antigen presenting cells. *Eur J Immunol* 2009;**39**:3239–50.

Shimamura M, Huang YY, Goji H *et al*. Regulation of immunological disorders by invariant Vα19-Jα33 TCR-bearing cells. *Immunobiology* 2011;**216**:374–8.

Shulman Z, Gitlin AD, Weinstein JS *et al*. Germinal centers: Dynamic signaling by T follicular helper cells during germinal center B cell selection. *Science (1979)* 2014;**345**:1058–62.

Singer A, Adoro S, Park JH. Lineage fate and intense debate: myths, models and mechanisms of CD4/CD8 lineage choice. *Nat Rev Immunol* 2008;**8**:788.

Singh SP, Zhang HH, Tsang H *et al*. PLZF Regulates CCR6 and is Critical for the Acquisition and Maintenance of the Th17 Phenotype in Human Cells. *J Immunol* 2015;**194**:4350.

Sivori S, Vacca P, del Zotto G *et al*. Human NK cells: surface receptors, inhibitory checkpoints, and translational applications. *Cellular & Molecular Immunology 2019 16:5* 2019;**16**:430–41.

Slichter CK, McDavid A, Miller HW *et al*. Distinct activation thresholds of human conventional and innate-like memory T cells. *JCI Insight* 2016;**1**:86292.

Sobkowiak MJ, Davanian H, Heymann R *et al*. Tissue-resident MAIT cell populations in human oral mucosa exhibit an activated profile and produce IL-17. *Eur J Immunol* 2019;**49**:133–43.

Sommermeyer D, Uckert W. Minimal amino acid exchange in human TCR constant regions fosters improved function of TCR gene-modified T cells. *J Immunol* 2010;**184**:6223–31.

Spaan M, Hullegie SJ, Beudeker BJB *et al.* Frequencies of Circulating MAIT Cells Are Diminished in Chronic HCV, HIV and HCV/HIV Co-Infection and Do Not Recover during Therapy. *PLoS One* 2016;**11**:e0159243.

Stout RD, Suttles J, Xu J *et al.* Impaired T cell-mediated macrophage activation in CD40 ligand-deficient mice. *The Journal of Immunology* 1996;**156**:8 LP – 11.

Stütz AM, Pickart LA, Trifilieff A *et al.* The Th2 Cell Cytokines IL-4 and IL-13 Regulate Found in Inflammatory Zone 1/Resistin-Like Molecule α Gene Expression by a STAT6 and CCAAT/Enhancer-Binding Protein-Dependent Mechanism. *The Journal of Immunology* 2003;**170**:1789–96.

Sun JC, Lanier LL. NK cell development, homeostasis and function: parallels with CD8+ T cells. *Nature Reviews Immunology 2011 11:10* 2011;**11**:645–57.

Sundström P, Ahlmanner F, Akéus P *et al.* Human Mucosa-Associated Invariant T Cells Accumulate in Colon Adenocarcinomas but Produce Reduced Amounts of IFN-γ. *J Immunol* 2015;**195**:3472–81.

Szabo SJ, Kim ST, Costa GL *et al.* A novel transcription factor, T-bet, directs Th1 lineage commitment. *Cell* 2000;**100**:655–69.

Tang X-Z, Jo J, Tan AT *et al.* IL-7 licenses activation of human liver intrasinusoidal mucosal-associated invariant T cells. *J Immunol* 2013;**190**:3142–52.

Tatituri RVV, Watts GFM, Bhowruth V *et al.* Recognition of microbial and mammalian phospholipid antigens by NKT cells with diverse TCRs. *Proc Natl Acad Sci U S A* 2013;**110**:1827–32.

Taylor A, Verhagen J, Blaser K *et al.* Mechanisms of immune suppression by interleukin-10 and transforming growth factor-β: the role of T regulatory cells. *Immunology* 2006;**117**:433.

Thomas SY, Scanlon ST, Griewank KG *et al.* PLZF induces an intravascular surveillance program mediated by long-lived LFA-1-ICAM-1 interactions. *Journal of Experimental Medicine* 2011;**208**:1179–88.

Tilloy F, Treiner E, Park SH *et al.* An invariant T cell receptor alpha chain defines a novel TAP-independent major histocompatibility complex class Ib-restricted alpha/beta T cell subpopulation in mammals. *J Exp Med* 1999;**189**:1907–21.

Toussirot É, Laheurte C, Gaugler B *et al.* Increased IL-22- and IL-17A-Producing Mucosal-Associated Invariant T Cells in the Peripheral Blood of Patients With Ankylosing Spondylitis. *Front Immunol* 2018;**9**:1.

Treiner E, Duban L, Bahram S *et al.* Selection of evolutionarily conserved mucosal-associated invariant T cells by MR1. *Nature* 2003;**422**:164–9.

Turtle CJ, Delrow J, Joslyn RC *et al.* Innate signals overcome acquired TCR signaling pathway regulation and govern the fate of human CD161hi CD8α+ semi-invariant T cells. *Blood* 2011;**118**:2752–62.

Ussher JE, Bilton M, Attwod E *et al.* CD161++CD8+ T cells, including the MAIT cell subset, are specifically activated by IL-12+IL-18 in a TCR-independent manner. *Eur J Immunol* 2014a;**44**:195–203.

Ussher JE, Bilton M, Attwod E *et al.* CD161++ CD8+ T cells, including the MAIT cell subset, are specifically activated by IL-12+IL-18 in a TCR-independent manner. *Eur J Immunol* 2014b;**44**:195–203.

Ussher JE, van Wilgenburg B, Hannaway RF *et al.* TLR signaling in human antigen-presenting cells regulates MR1-dependent activation of MAIT cells. *Eur J Immunol* 2016;**46**:1600–14.

Vantourout P, Hayday A. Six-of-the-best: unique contributions of γδ T cells to immunology. *Nat Rev Immunol* 2013;**13**, DOI: 10.1038/nri3384.

Vignali DAA, Collison LW, Workman CJ. How regulatory T cells work. *Nature Reviews Immunology 2008 8:7* 2008;**8**:523–32.

Vincent MS, Leslie DS, Gumperz JE *et al.* CD1-dependent dendritic cell instruction. *Nat Immunol* 2002;**3**, DOI: 10.1038/ni851.

Voillet V, Buggert M, Slichter CK *et al.* Human MAIT cells exit peripheral tissues and recirculate via lymph in steady state conditions. *JCI Insight* 2018;**3**, DOI: 10.1172/JCI.INSIGHT.98487.

Walch M, Dotiwala F, Mulik S *et al.* Cytotoxic cells kill intracellular bacteria through Granulysin-mediated delivery of Granzymes. *Cell* 2014;**157**:1309.

Walker LJ, Kang YH, Smith MO *et al.* Human MAIT and CD8αα cells develop from a pool of type-17 precommitted CD8+ T cells. *Blood* 2012;**119**:422–33.

Wang C, Kang SG, Lee J *et al.* The roles of CCR6 in migration of Th17 cells and regulation of effector T cell balance in the gut. *Mucosal Immunol* 2009;**2**:173.

Wang H, D'Souza C, Lim XY *et al.* MAIT cells protect against pulmonary Legionella longbeachae infection. *Nature Communications 2018 9:1* 2018;**9**:1–15.

Wang R, Wang J, Hassan A *et al.* Molecular basis of V-ATPase inhibition by bafilomycin A1. *Nature Communications 2021 12:1* 2021;**12**:1–8.

Wax Ma N SG, Ritchie JM, Sandie . C *et al.* Development of CD4–CD8+ cytotoxic T cells requires interactions with class I MHC determinants. *Nature 1988 333:6169* 1988;**333**:180–3.

Wei B, Wingender G, Fujiwara D *et al.* Commensal Microbiota and CD8+ T Cells Shape the Formation of Invariant NKT Cells. *The Journal of Immunology* 2010;**184**:1218–26.

Wen QL, Jiang Q, Aleem E *et al.* IL-7 promotes T cell proliferation through destabilization of p27Kip1. *Journal of Experimental Medicine* 2006;**203**:573–82.

Wilgenburg B van, Loh L, Chen Z *et al.* MAIT cells contribute to protection against lethal influenza infection in vivo. *Nature Communications 2018 9:1* 2018;**9**:1–9.

van Wilgenburg B, Scherwitzl I, Hutchinson EC *et al.* MAIT cells are activated during human viral infections. *Nat Commun* 2016;**7**, DOI: 10.1038/ncomms11653.

Wilgus TA, Ferreira AM, Oberyszyn TM *et al.* Regulation of scar formation by vascular endothelial growth factor. *Laboratory Investigation 2008 88:6* 2008;**88**:579–90.

Willcox BE, Willcox CR. γδ TCR ligands: the quest to solve a 500-million-year-old mystery. *Nature Immunology 2019 20:2* 2019;**20**:121–8.

Willcox CR, Pitard V, Netzer S *et al.* Cytomegalovirus and tumor stress surveillance by binding of a human γδ T cell antigen receptor to endothelial protein C receptor. *Nature Immunology 2012 13:9* 2012;**13**:872–9.

Willenborg S, Lucas T, van Loo G *et al*. CCR2 recruits an inflammatory macrophage subpopulation critical for angiogenesis in tissue repair. *Blood* 2012;**120**:613–25.

Willing A, Leach OA, Ufer F *et al*. CD8$^+$ MAIT cells infiltrate into the CNS and alterations in their blood frequencies correlate with IL-18 serum levels in multiple sclerosis. *Eur J Immunol* 2014;**44**:3119–28.

Wingender G, Krebs P, Beutler B *et al*. Antigen-Specific Cytotoxicity by Invariant NKT Cells In Vivo Is CD95/CD178-Dependent and Is Correlated with Antigenic Potency. *The Journal of Immunology* 2010;**185**, DOI: 10.4049/jimmunol.1001018.

Winter SJ, Kunze-Schumacher H, Imelmann E *et al*. MicroRNA miR-181a/b-1 controls MAIT cell development. *Immunol Cell Biol* 2019;**97**:190–202.

Won EJ, Ju JK, Cho YN *et al*. Clinical relevance of circulating mucosal-associated invariant T cell levels and their anti-cancer activity in patients with mucosal-associated cancer. *Oncotarget* 2016;**7**:76274–90.

Wu L, van Kaer L. *Natural Killer T Cells in Health and Disease*.

Wu X, Xu W, Feng X *et al*. TNF-a mediated inflammatory macrophage polarization contributes to the pathogenesis of steroid-induced osteonecrosis in mice. *Int J Immunopathol Pharmacol* 2015;**28**:351–61.

Wu YT, Tan HL, Shui G *et al*. Dual role of 3-methyladenine in modulation of autophagy via different temporal patterns of inhibition on class I and III phosphoinositide 3-kinase. *J Biol Chem* 2010;**285**:10850–61.

Wynn TA, Vannella KM. Macrophages in Tissue Repair, Regeneration, and Fibrosis. *Immunity* 2016;**44**:450–62.

Xiao X, Li K, Ma X *et al*. Mucosal-Associated Invariant T Cells Expressing the TRAV1-TRAJ33 Chain Are Present in Pigs. *Front Immunol* 2019;**10**:2070.

Yamaguchi H, Hashimoto K. Association of MR1 protein, an MHC class I-related molecule, with β2-microglobulin. *Biochem Biophys Res Commun* 2002;**290**:722–9.

Ye G, Wang P, Xie Z *et al*. Autophagy-Mediated Activation of Mucosal-Associated Invariant T Cells Driven by Mesenchymal Stem Cell-Derived IL-15. *Stem Cell Reports* 2021;**16**:926–39.

Yin Z, Ma T, Lin Y *et al*. IL-6/STAT3 pathway intermediates M1/M2 macrophage polarization during the development of hepatocellular carcinoma. *J Cell Biochem* 2018;**119**:9419–32.

Yong YK, Saeidi A, Tan HY *et al*. Hyper-expression of PD-1 is associated with the levels of exhausted and dysfunctional phenotypes of circulating CD161++TCR iVα7.2+ Mucosal-associated invariant T cells in chronic hepatitis B virus infection. *Front Immunol* 2018;**9**:472.

Youssef G ben, Tourret M, Salou M *et al*. Ontogeny of human mucosal-associated invariant T cells and related T cell subsets. *J Exp Med* 2018;**215**:459–79.

Yuseff MI, Pierobon P, Reversat A *et al*. How B cells capture, process and present antigens: a crucial role for cell polarity. *Nature Reviews Immunology 2013 13:7* 2013;**13**:475–86.

Zabijak L, Attencourt C, Guignant C *et al*. Increased tumor infiltration by mucosal-associated invariant T cells correlates with poor survival in colorectal cancer patients. *Cancer Immunol Immunother* 2015;**64**:1601–8.

Zeissig S, Blumberg RS. Life at the beginning: Perturbation of the microbiota by antibiotics in early life and its role in health and disease. *Nat Immunol* 2014;**15**:307–10.

Zhao J, Chen X, Herjan T *et al*. The role of interleukin-17 in tumor development and progression. *Journal of Experimental Medicine* 2020;**217**, DOI: 10.1084/JEM.20190297.

Zheng C, Zheng L, Yoo JK *et al*. Landscape of Infiltrating T Cells in Liver Cancer Revealed by Single-Cell Sequencing. *Cell* 2017;**169**:1342-1356.e16.

Zheng Y, Valdez PA, Danilenko DM *et al*. Interleukin-22 mediates early host defense against attaching and effacing bacterial pathogens. *Nature Medicine 2008 14:3* 2008;**14**:282–9.

8. Appendices

8.1. Chapter 3 Supplementary Figures

8.1.1. Tetramer staining of LPMC-derived MAIT cells

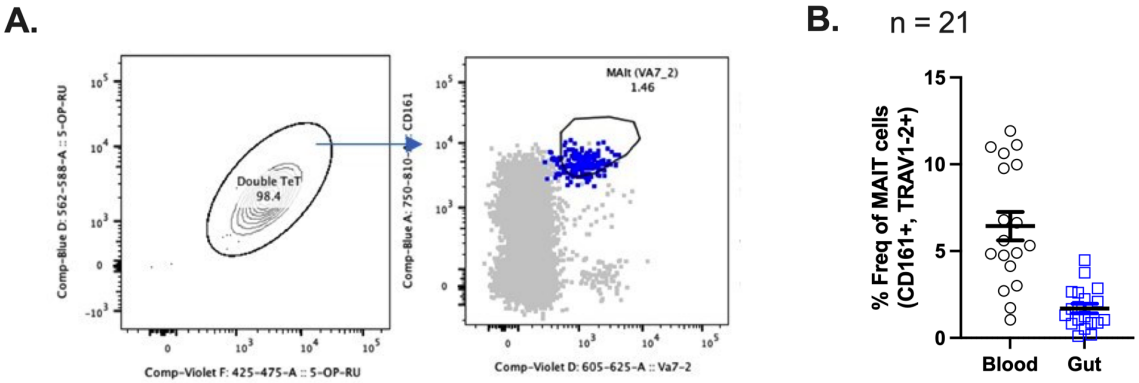

Supplementary Figure 3- 1. 5OPRU-tetramer+ MAIT cells in the gut as also CD161+TRAV1-2+. (**A**) FACSplot of 5OPRU-tetramer staining (left) and CD161+/TRAV1-2+ gating of MAIT cells (right). Tetramer+ cells are highlighter in blue in the right panel. (**B**) Frequency of MAIT cells, gated as CD161+/TRAV1-2+, in PBMCs and LPMCs.
Data were acquired in 2-3 independent experiments. Error bars represent Mean ± SEM.

8.1.2. Differential expression of genes in bulk RNASeq data

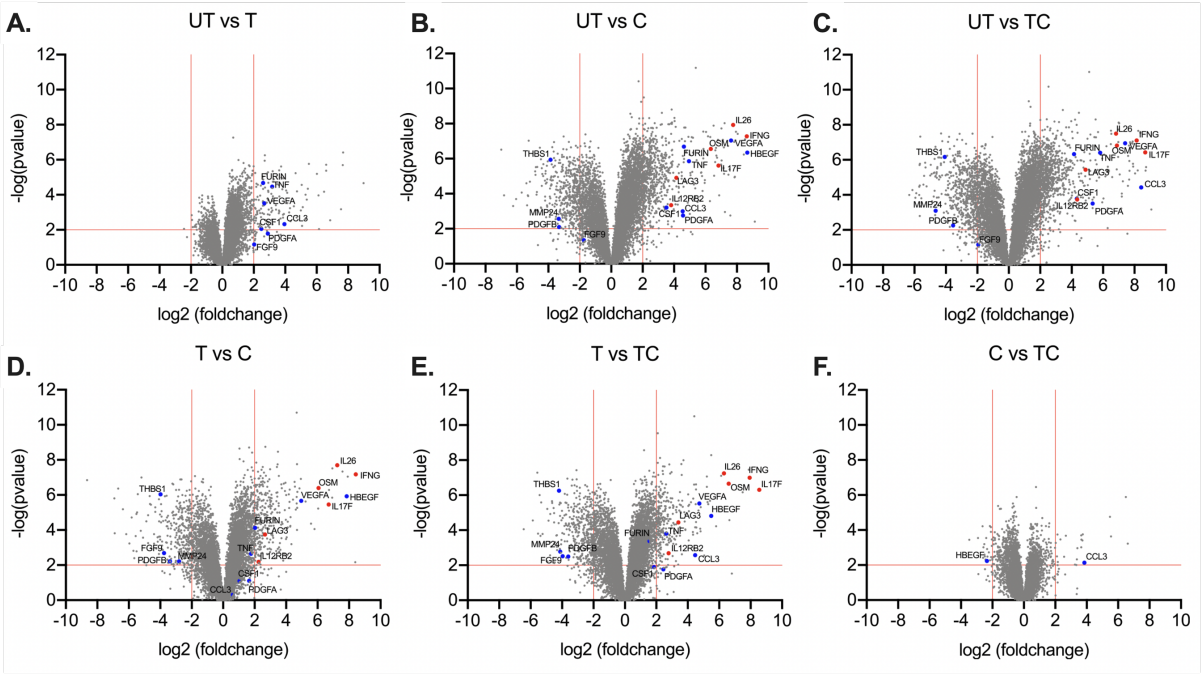

Supplementary Figure 3- 2. Volcano plots of differentially expressed MAIT transcripts under different stimuli. Purified MAIT cells were stimulated for 20h with cytokines (C), with 1µg/mL of anti-CD3/CD28 (T) or both (TC). Cytokine signal is comprised by 2ng/ml IL12/IL18, 100ng/mL TL1A and 25ng/mL IL15. Plotted are the log2FoldChange and -log(-value) of different MAIT transcripts when comparing unstimulated MAIT cells (UT) with T (**A**), UT with C (**B**), UT with TC (**C**), T with C (**D**), T with TC (**E**) and C with TC (**F**).
Differential gene expression data was obtained using R DESeq2 package.

8.1.3. Quantification of growth-factors in MAIT supernatants

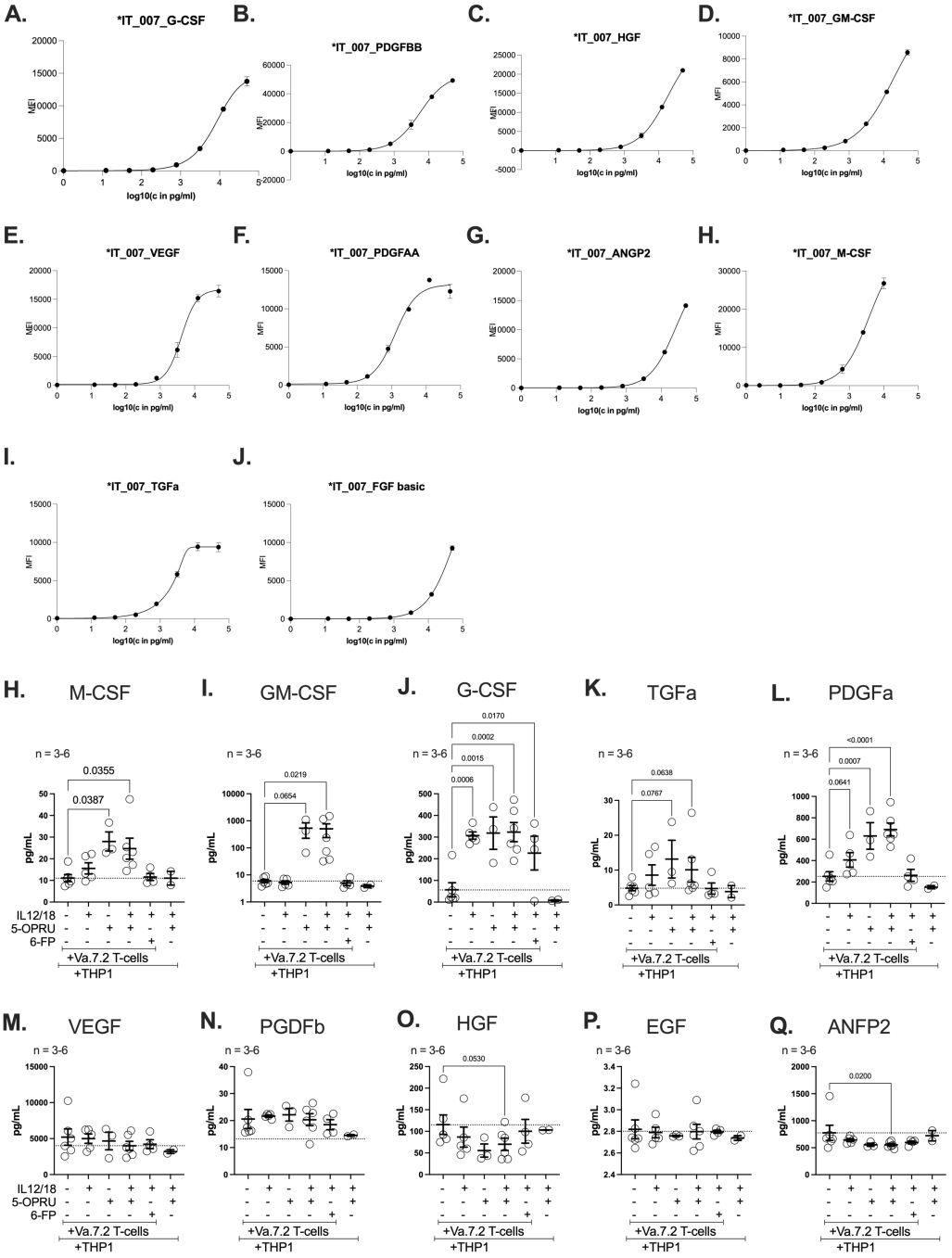

Supplementary Figure 3- 3. LegendPlex bead mediated quantification of tissue-repair growth-factors in MAIT supernatants in *in vitro* system. LegendPlex bead were used to quantify tissue-repair growth-factors in 72h supernatants resulting from purified TRAV1-2+ (or Vα7.2+) cells incubated with THP1 cells with combinations of 50ng/mL IL12/IL18, 10nM 5OPRU and 10nM of 6FP. (**A-J**) Standard curves of different growth factors named in the tittle of each curve. (**H-Q**) Quantification of different growth factors (title of the graph) in 72h MAIT supernatants.
Data were acquired in 2-3 independent experiments. Every datapoint is a biological replicate. Error bars represent Mean ± SEM. Differences among conditions were analysed by RM One-way ANOVA with uncorrected Fisher's LSD test. *p < 0.05, **p < 0.01, ***p < 0.001, ****p < 0.0001.

8.1.4. THP1 viability in response to MAIT activation

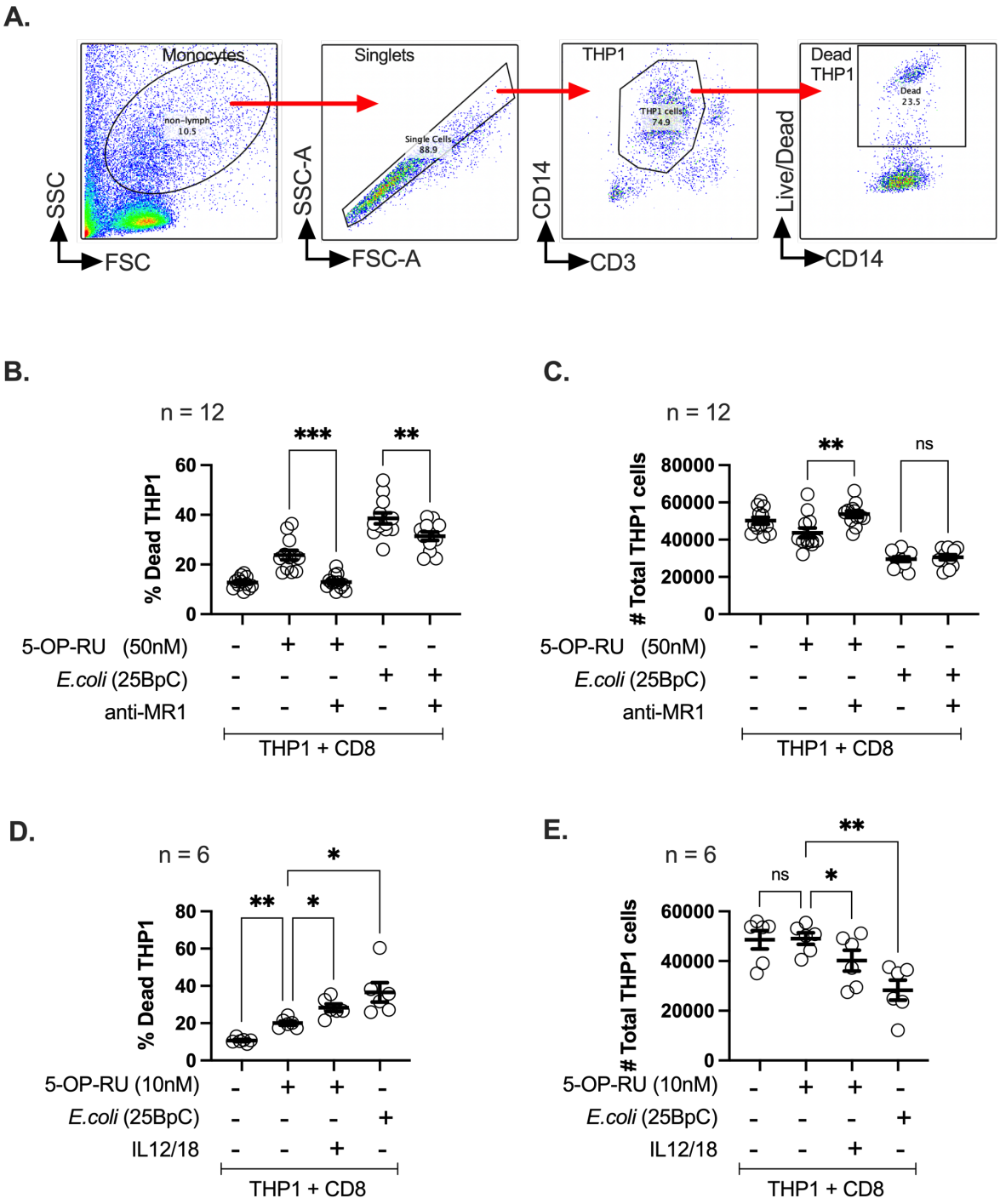

Supplementary Figure 3- 4. Bacteria mediated triggers cause significant amount of cell-death in THP1 cells compared to 5OPRU. (**A**) Gating strategy of dead THP1 cells. (**B-E**) Frequency of dead THP1 (**B, D**) and count of total THP1 cells after *in-vitro* stimulation assays (**C-E**). Data were acquired in 2-3 independent experiments. Every datapoint is a biological replicate. Error bars represent Mean ± SEM. Differences among conditions were analysed by RM One-way ANOVA with uncorrected Fisher's LSD test. *p < 0.05, **p < 0.01, ***p < 0.001, ****p < 0.0001.

8.2. Chapter 4 Supplementary Figures

8.2.1. β2m upregulation in DLD1 cells

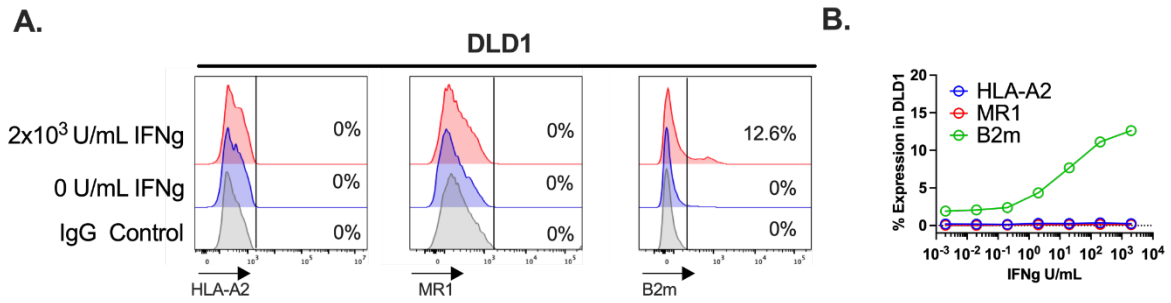

Supplementary Figure 4- 1. DLD1 cells can weakly express β2m with IFNγ stimulation. (**A**) Representative histograms and frequencies (**B**) of HLA-A2 (blue), MR1 (red) and β2m (green) producing cells.

8.2.2. TCR stability in Jurkat cells pre-transduced with CD8α

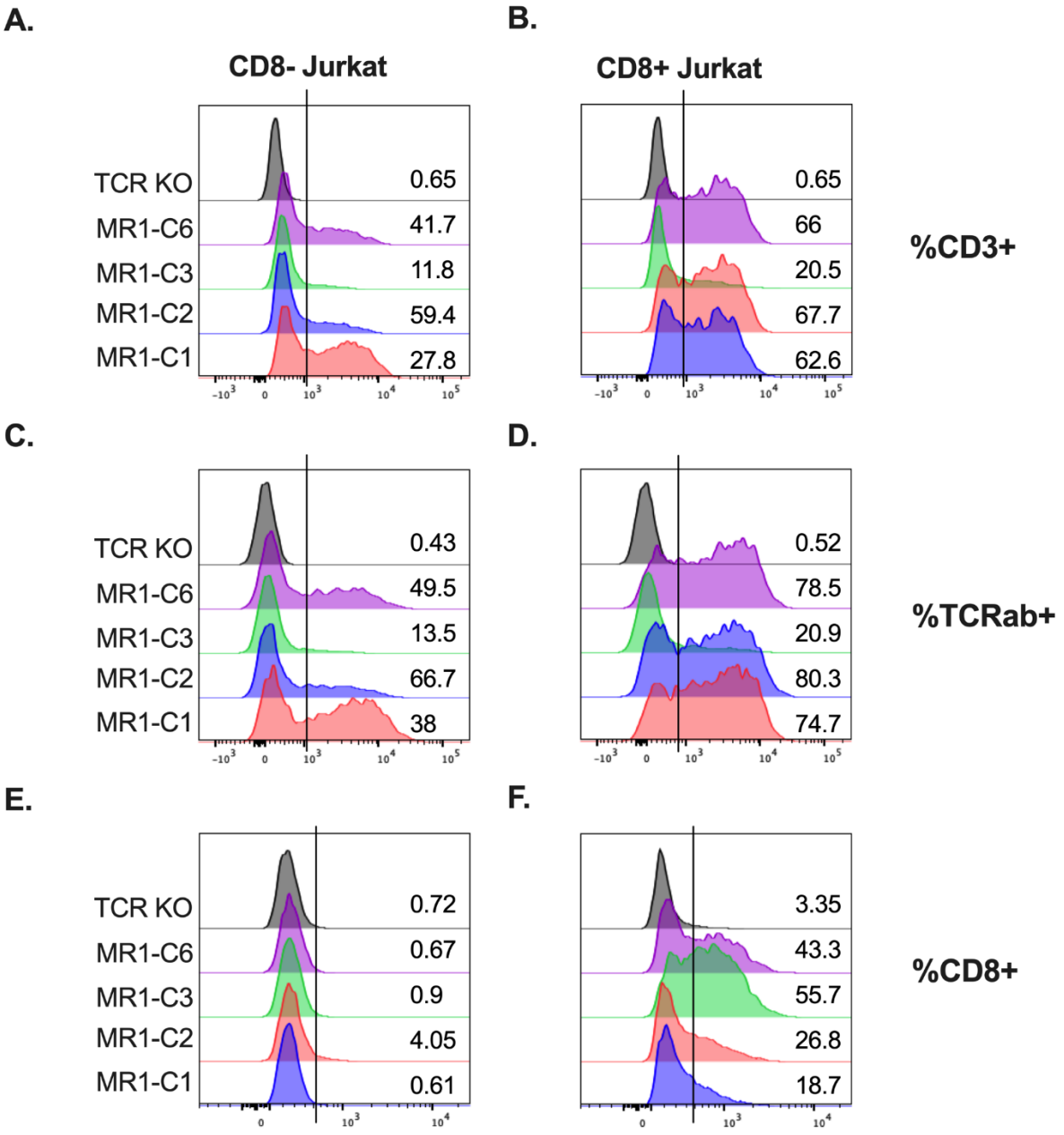

Supplementary Figure 4- 2. Stability of the TCR complex increases in Jurkats when TCRs are co-transduced with CD8α. (**A-E**) Representative histograms of CD3 (**A, B**), TCRαβ (**C, D**) and CD8 (**E, F**) of Jurkat cells with MR1T TCRs co-transduced with (**B, D, F**) and without CD8α (**A, C, E**).

8.2.3. T-cell cloning campaigns

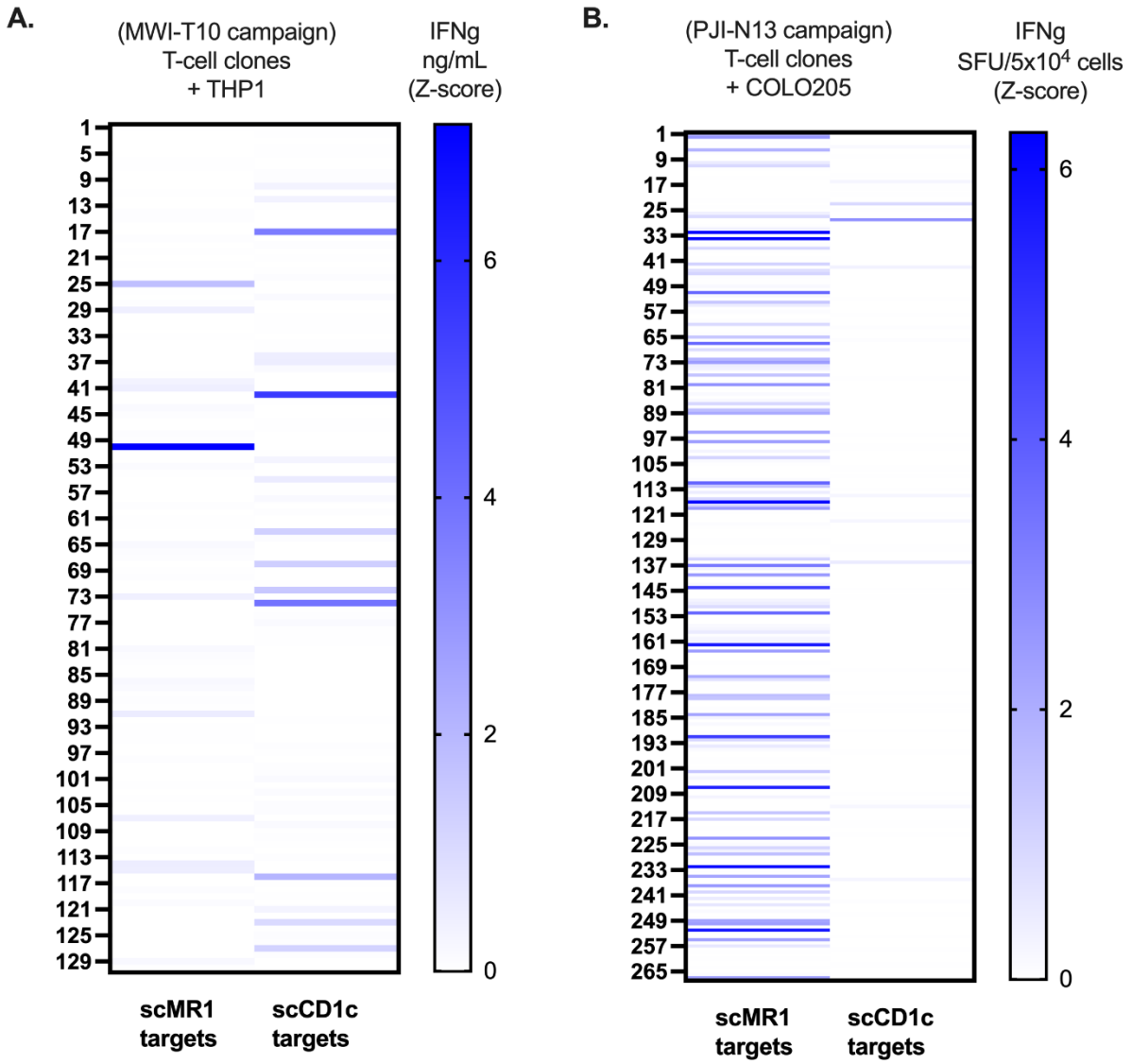

Supplementary Figure 4- 3. Reactivity of T-cell clones isolated from MWI-T10 and PJI-N13. (**A-B**) Individual clones were grown by limiting dilution from MWI-T10 (**A**) and PJI-N13 (**B**) polyclonal lines and activated overnight with modified THP1 and COLO205 cells, respectively.

8.2.4. **Disulphide-bridge increases activity of MR1_C3 TCR**

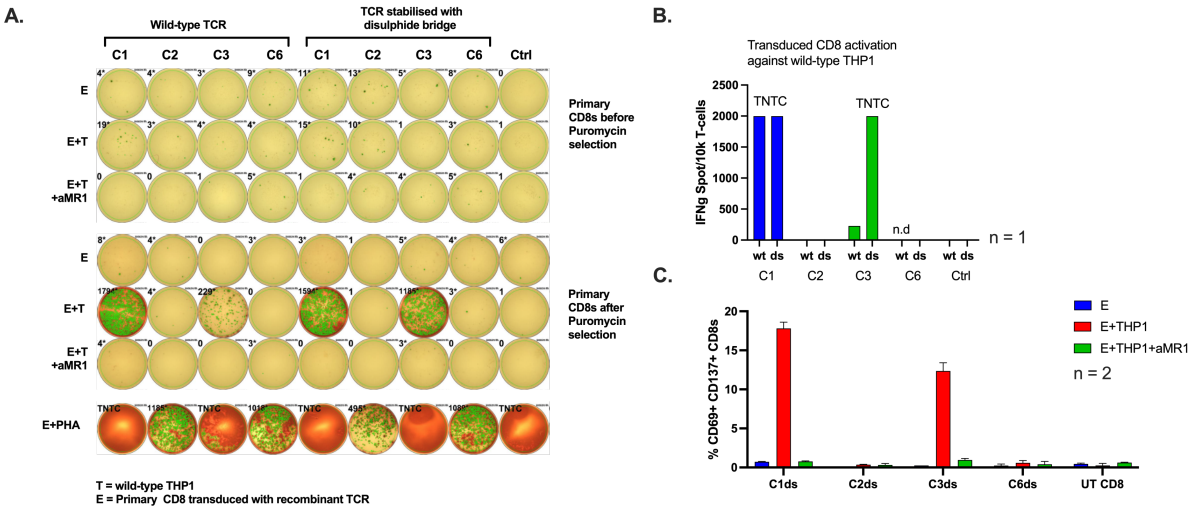

Supplementary Figure 4- 4. The addition of disulphide bridges increased the activity of MR1_C3 TCRs on CD8 cells. (**A-C**) Overnight incubation of 10^4 CD8 cells transduced with MR1T cells with $5x10^4$ THP1 cells. (**A**) Representative ELISPOT and IFNγ SFU (**B**) per 10^4 transduced effector cells of wild-type and stabilised TCRs with disulphide bonds. (**C**) Frequency of CD137+ and CD69+ cells in MR1T transduced CD8 cells after overnight incubation with target cells.

8.2.5. Toxic effects of 6FP, 5OPRU and 5FSA

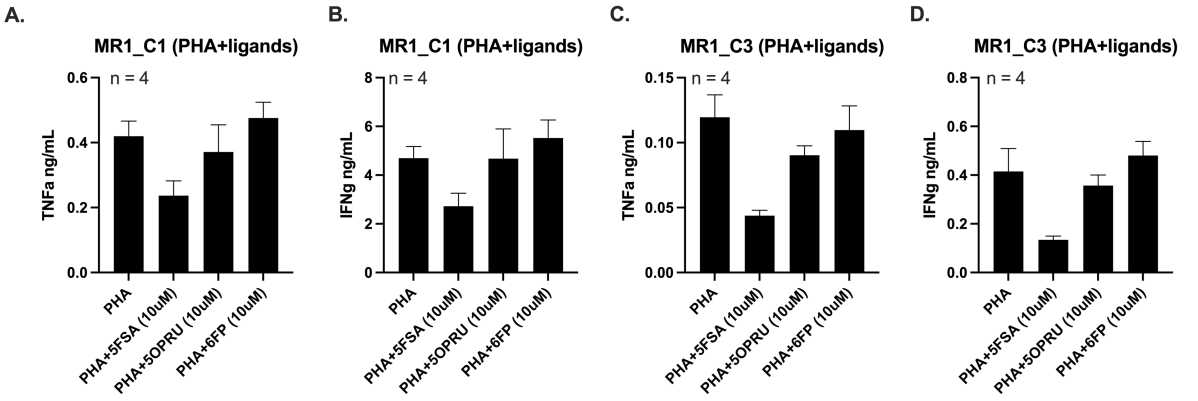

Supplementary Figure 4- 5. Toxic effects of MR1 ligands on T-cell clones. (**A-D**) $5x10^4$ MR1_C1 (**A, B**) and MR1_C3 (**C, D**) primary clones were activated with PHA in the presence of MR1 ligands (10nM of 5FSA, 5OPRU, 6FP). Represented are the secreted TNFα (**A, B**) and IFNγ (**C, D**).
Data were acquired in 2-3 independent experiments. Error bars represent Mean ± SEM of biological replicates. Differences among conditions were analysed by RM One-way ANOVA with uncorrected Fisher's LSD test. *p < 0.05, **p < 0.01, ***p < 0.001, ****p < 0.0001.

8.2.6. Lentiviral backbone

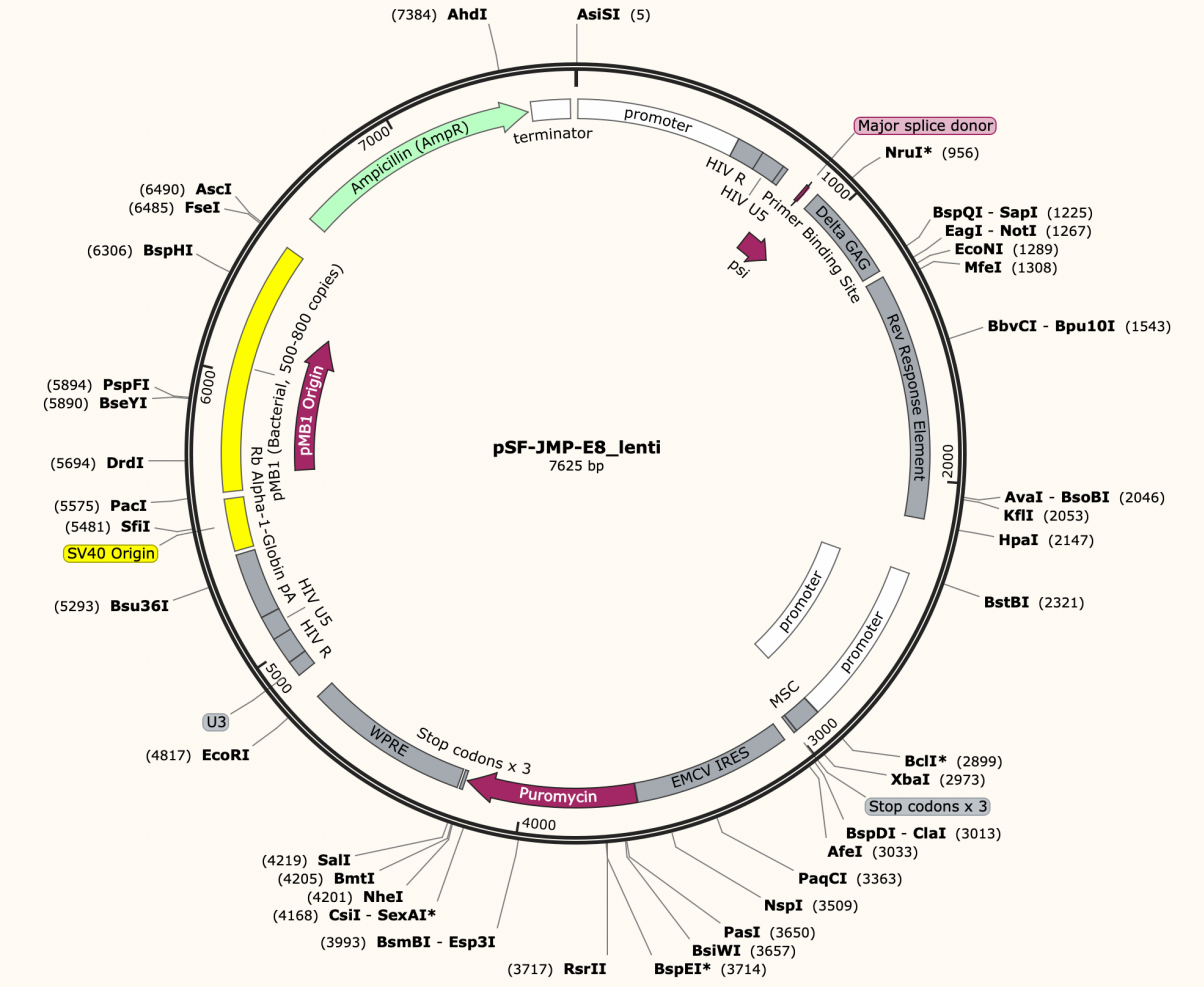

Supplementary Figure 4- 6. Lentiviral backbone used for scMR1, scCD1c and TCR transductions

8.2.7. scMR1 sequence

Structure:

IL2 leader sequence – β2m – Linker – MR1 Sequence

IL2 leader sequence

MYRMQLLSCIALSLALVT

β2m sequence

NSIQRTPKIQVYSRHPAENGKSNFLNCYVSGFHPSDIEVDLLKNGERIEKVEHSDLSFSKDWSFYL
LYYTEFTPTEKDEYACRVNHVTLSQPKIVKWDRD

Linker sequence

GGGGSGGGGSGGGGS

MR1 sequence

RTHSLRYFRLGVSDPIHGVPEFISVGYVDSHPITTYDSVTRQKEPRAPWMAENLAPDHWERYTQL
LRGWQQMFKVELKRLQRHYNHSGSHTYQRMIGCELLEDGSTTGFLQYAYDGQDFLIFNKDTLS
WLAVDNVAHTIKQAWEANQHELLYQKNWLEEECIAWLKRFLEYGKDTLQRTEPPLVRVNRKET
FPGVTALFCKAHGFYPPEIYMTWMKNGEEIVQEIDYGDILPSGDGTYQAWASIELDPQSSNLYSC
HVEHSGVHMVLQVPQESE

8.3. Chapter 5 Supplementary Figures

8.3.1. IFNγ ELISPOT

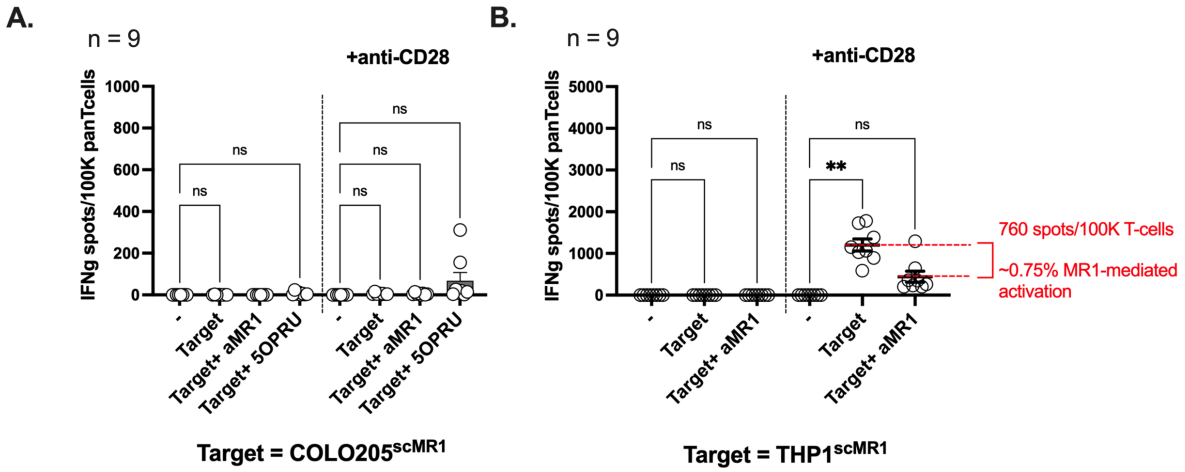

Supplementary Figure 5- 1. MR1T can be detected by using anti-CD28 co-stimulation IFNγ ELISPOT assays. (**A-B**) IFNγ SFU from 10^5 T-cells activated with COLO205^{scMR1} (**A**) and THP1^{scMR1} (**B**).

Data were acquired in 2-3 independent experiments. Error bars represent Mean ± SEM of biological replicates. Differences among conditions were analysed by RM One-way ANOVA with uncorrected Fisher's LSD test. *p < 0.05, **p < 0.01, ***p < 0.001, ****p < 0.0001.

8.3.2. Comparison of MR1T detection results between plate-coated Endo-MR1 and THP1^{scMR1}

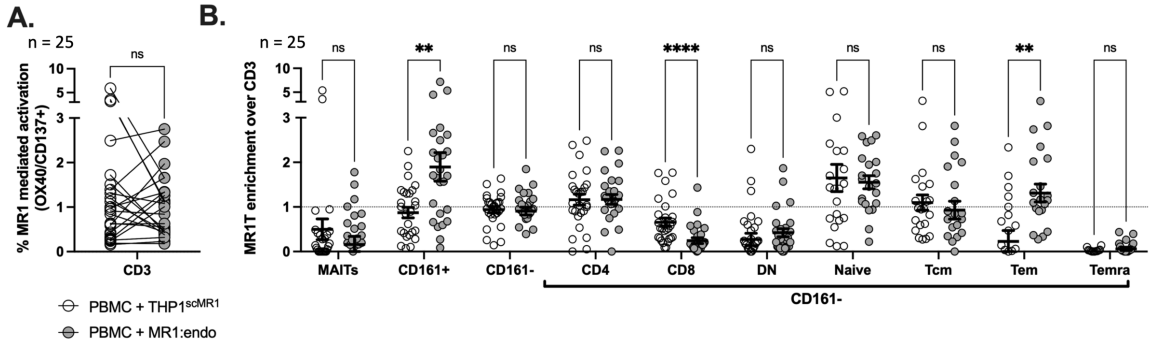

Supplementary Figure 5- 2. Different profiles of MR1T activation are seen when using THP1^{scMR1} and Endo-MR1. (**A-B**) MR1-mediated activation (IgG-aMR1) of total circulating (**A**) and T-cell sub-compartment (**B**). Data were transformed as FC over total CD3 activation.
Data were acquired in 2-3 independent experiments. Error bars represent Mean ± SEM of biological replicates. Differences among conditions were analysed by RM One-way ANOVA with uncorrected Fisher's LSD test. *p < 0.05, **p < 0.01, ***p < 0.001, ****p < 0.0001.

8.3.3. Blocking of IFNGR1 can reduce unspecific T-cell activation due to signal amplification

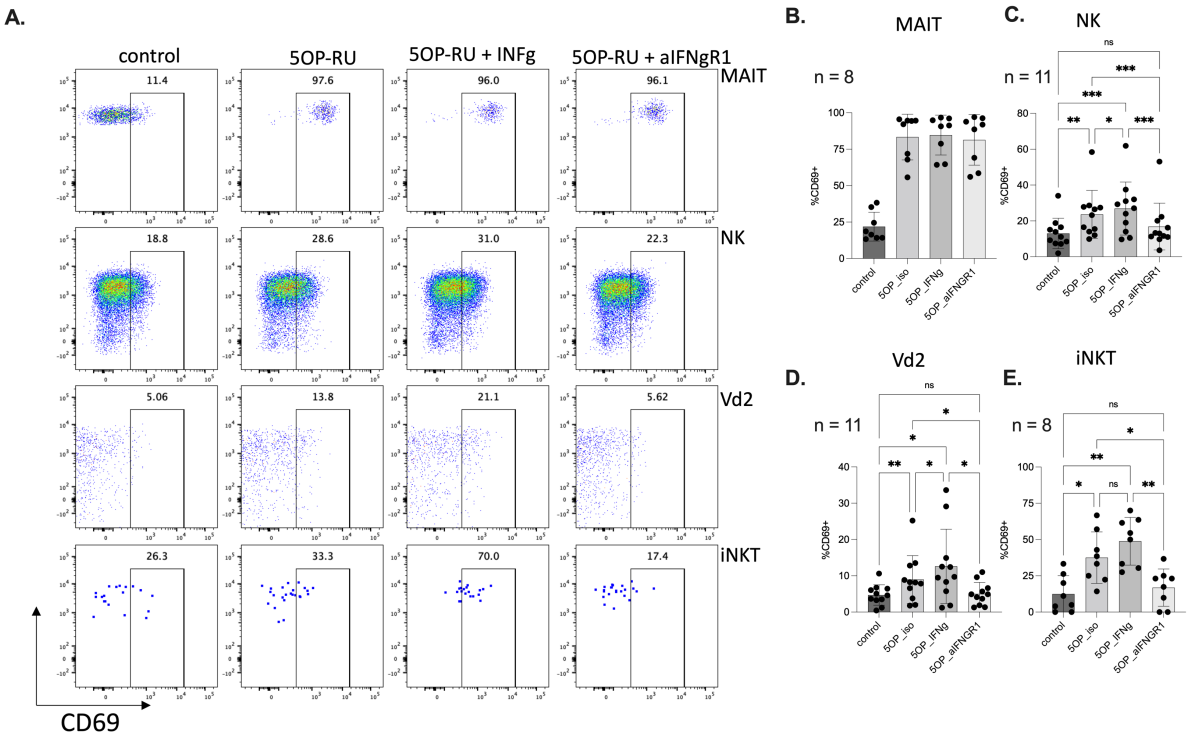

Supplementary Figure 5- 3. IFNGR1 blocking reduced bystander T-cell activation. (**A-E**) Representative FACSplots (**A**) and frequencies of CD69 expression (**B-E**). NK (**C**), Vd2 (**D**) and iNKT (**E**) cells by 5OPRU mediated MAIT activation (**B**) in the presence of **IFNγ** (100U/mL) or 10μg/mL IFNGR1.

Data were acquired in 2-3 independent experiments. Error bars represent Mean ± SEM of biological replicates. Differences among conditions were analysed by RM One-way ANOVA with uncorrected Fisher's LSD test. *p < 0.05, **p < 0.01, ***p < 0.001, ****p < 0.0001.

8.4. Chapter 3 RNAseq data tables

Upregulated MAIT transcripts (Log2 Fold-change > 1.5, false discovery rate < 0.05 and adjusted p-value across 3 donors < 0.05) when activated with 2ng/mL IL12/Il18, 100ng/mL of TL1A and 25ng/mL IL15 (C) or plate bound 1.25ug/mL anti-CD3/CD28 (T) or both (TC). Tables are comparison of each stimulus against transcripts at unstimulated (US) condition.

C vs US

GeneID	log2FC	padj
IFNG	8.25	#######
CYTIP	3.46	2.9E-87
GZMB	7.53	7.2E-81
ENO1	3.47	4.3E-68
MTHFD2	5.82	5.9E-64
PIM2	3.84	1.1E-62
NAMPTL	6.39	4.5E-60
NFKBIA	4.79	2.0E-58
ENO1P1	3.50	9.0E-57
LTA	5.65	1.5E-55
SLC1A5	4.69	7.3E-54
TPI1P1	3.25	1.1E-49
NAMPT	6.32	1.1E-49
FURIN	4.25	5.4E-47
HIF1A	4.09	2.7E-45
GARS	3.73	1.4E-44
PSAT1	6.16	2.4E-42
SHMT2	4.29	4.4E-41
CD274	4.94	4.2E-39
VCP	2.18	1.5E-38
SOCS3	5.88	3.0E-38
PKM	3.52	5.0E-37
SLC7A1	3.29	8.3E-37
NFKBIZ	4.78	1.1E-33
IRF4	6.32	8.0E-32
IL2RA	7.09	1.2E-31
TFRC	4.28	2.7E-31
MTHFD2P7	5.76	3.6E-31
PIM1	3.11	1.3E-30
SLC7A5	4.25	2.6E-30
TPM4	3.32	3.5E-30
TNF	4.62	6.7E-30
TUBA1C	2.77	9.9E-30
EDARADD	3.03	1.0E-28
SESN2	3.33	1.0E-28
BATF	4.32	1.2E-28
VASP	2.53	2.4E-27
H3F3B	1.63	2.9E-27
HK2	4.46	4.1E-27
DDX21	2.82	5.3E-27
PMAIP1	4.54	1.0E-26
XBP1	2.43	3.9E-26
FTH1	2.87	5.2E-26
PSMA6P1	3.30	5.5E-26
FASLG	3.64	6.5E-26
FAM46C	2.44	1.0E-25
NFE2L1	2.24	1.3E-25
CCR1	3.51	2.5E-25
EIF1	1.82	3.5E-25
MAP3K8	4.27	4.1E-25
ADAM19	4.95	4.2E-25
EIF2S2P4	2.56	4.2E-25
RP11-121L10.3	2.79	4.9E-25
CD40LG	3.89	8.7E-25
TIFA	3.54	9.4E-25
ACTR3	2.03	1.0E-24
EIF5AL1	2.59	1.1E-24
SLC16A1	3.45	1.3E-24
IL17F	6.54	2.2E-24
TARS	3.11	7.8E-24
SGK1	6.54	1.6E-23
SCD	3.48	2.6E-23
GADD45B	3.43	4.4E-23
FRMD4B	3.10	4.7E-23
WARS	4.67	5.4E-23
EIF4A1P10	2.06	6.0E-23
EIF5A	2.47	7.2E-23
CCL20	5.31	1.5E-22
CDKN1A	4.79	2.2E-22
TUBA1B	2.83	3.7E-22
NDUFV2P1	2.90	9.2E-22
FTH1P10	2.99	1.4E-21
NFKB2	3.62	1.4E-21
PKMP1	3.49	1.5E-21
P2RX5	5.10	3.9E-21
MARS	2.56	6.5E-21
RSL24D1	2.27	1.4E-20

T vs US

GeneID	log2FC	padj
EGR2	7.37	7.2E-23
RBPJ	2.49	9.6E-23
EGR1	5.67	1.1E-21
IRF4	5.34	3.6E-21
EGR3	7.37	5.9E-20
NR4A1	6.36	1.7E-15
PKM	2.31	3.4E-13
SHMT2	2.64	1.6E-12
FURIN	2.38	1.1E-11
TRAF4	3.92	2.3E-11
NFKBIA	2.34	1.0E-10
SDC4	3.34	2.2E-10
TNF	2.98	2.2E-10
TAGAP	2.35	6.1E-10
VDR	4.84	7.1E-10
TNFRSF18	4.66	1.5E-09
DUSP5	4.54	1.6E-09
TNFRSF9	6.63	5.7E-09
BTG2	1.94	9.1E-09
PIM2	1.74	9.1E-09
RELB	2.72	1.4E-08
ARHGAP31	3.04	1.5E-08
SLC1A5	2.19	1.7E-08
NFKB2	2.48	3.3E-08
TRAF1	2.69	5.8E-08
IL4I1	3.66	1.2E-07
PKMP1	2.33	1.2E-07
CRTAM	3.95	1.9E-07
IL2RG	1.15	4.2E-07
BIRC3	2.38	6.0E-07
CCL4	3.17	8.2E-07
ADO	1.78	1.0E-06
IL2RA	3.60	1.3E-06
GNG4	8.70	1.4E-06
CD69	2.37	2.9E-06
NAB2	2.40	3.2E-06
CCL20	3.09	5.8E-06
IER5	1.66	6.3E-06
CD83	3.46	6.7E-06
DUSP4	2.77	1.1E-05
HNRNPA1P48	1.15	1.6E-05
JUNB	1.55	2.7E-05
HSP90AB1	1.44	2.8E-05
HSP90AB3P	1.43	2.9E-05
HIVEP3	3.62	3.1E-05
HNRNPA1P10	1.21	4.2E-05
RGS16	5.23	4.9E-05
SLC7A1	1.50	7.8E-05
CCL4L2	4.46	8.4E-05
C17orf96	2.95	1.0E-04
WARS	2.43	1.0E-04
HNRNPA1P7	1.12	1.0E-04
IER3	6.34	1.3E-04
REL	2.28	2.1E-04
NR4A3	3.70	2.4E-04
STX11	2.22	2.4E-04
RAB8B	1.64	3.5E-04
PSAT1	2.40	3.8E-04
BHLHE40	1.91	4.2E-04
C2CD4A	7.64	6.0E-04
RORC	1.66	6.4E-04
EIF5AL1	1.31	7.1E-04
BZW1	1.26	7.8E-04
BZW1P2	1.12	8.1E-04
EIF5A	1.28	8.1E-04
GAPDHP1	1.25	8.1E-04
IL27RA	1.48	8.6E-04
NFKB1	1.81	9.1E-04
MTHFD2	1.82	1.0E-03
SRGN	1.55	1.1E-03
TNFRSF4	6.29	1.1E-03
SHF	3.72	1.3E-03
PARK7	1.45	1.4E-03
MIR146A	5.99	1.5E-03
PTPN7	1.83	1.6E-03
HNRNPA1L2	1.17	1.7E-03
SNX9	2.03	1.7E-03

TC vs US

GeneID	log2FC	padj
IFNG	7.78	1.6E-89
GZMB	7.84	7.8E-88
LTA	6.65	8.3E-79
MTHFD2	6.20	2.4E-73
PIM2	4.06	2.7E-71
SLC1A5	5.15	4.3E-66
GARS	4.15	3.5E-57
CYTIP	2.81	4.0E-54
PSAT1	6.66	5.4E-50
NAMPTL	5.81	4.6E-49
ENO1	2.99	1.1E-48
SHMT2	4.61	3.2E-48
SLC7A1	3.67	2.2E-47
IRF4	7.41	9.7E-45
TNF	5.51	8.4E-44
NFKBIA	4.09	2.7E-41
IL17F	8.39	5.3E-41
DDX21	3.38	6.3E-41
ENO1P1	3.03	7.1E-41
TFRC	4.79	3.1E-40
NAMPT	5.72	3.8E-40
IL2RA	7.84	3.8E-39
FURIN	3.79	1.7E-36
PIM3	3.48	4.9E-36
MTHFD2P7	6.15	5.8E-36
CD274	4.69	7.9E-35
EIF5AL1	2.98	1.4E-34
SESN2	3.59	1.7E-34
SLC43A3	4.15	1.2E-33
SLC7A5	4.41	5.6E-33
EIF5A	2.85	4.3E-32
RSL24D1	2.70	1.6E-31
EIF4A1P10	2.34	2.3E-31
NFKBIZ	4.60	4.3E-31
PMAIP1	4.82	1.0E-30
WARS	5.28	6.6E-30
CDK6	4.20	3.1E-29
HSP90AB3P	2.77	5.5E-29
HSP90AB1	2.77	1.7E-28
EIF2S2P4	2.68	5.0E-28
MARS	2.88	9.0E-28
HK2	4.50	9.4E-28
SOCS3	5.07	9.4E-28
H3F3B	1.62	2.7E-27
VCP	1.88	3.4E-27
HIF1A	3.25	3.5E-27
IARS	2.87	3.9E-27
LAG3	4.54	6.4E-27
NFE2L1	2.27	1.5E-26
MIR155HG	7.39	1.7E-26
ASNS	4.34	1.7E-26
TUBA1C	2.61	6.3E-26
TARS	3.20	1.4E-25
GADD45B	3.57	2.8E-25
FRMD4B	3.21	5.1E-25
BATF	4.04	7.8E-25
TAP1	2.30	2.8E-24
ICOS	4.36	7.4E-24
FASLG	3.50	8.5E-24
CCL20	5.36	4.9E-23
PKM	2.83	9.7E-23
TPI1P1	2.32	1.5E-22
SLC3A2	2.64	2.1E-22
CYCS	3.08	2.9E-22
CCL4	5.18	4.4E-22
PAICS	3.84	1.1E-21
SLC16A1	3.23	4.1E-21
ODC1	3.50	4.6E-21
EIF4A1	2.22	6.1E-21
PRMT1	3.15	1.4E-20
STIP1	2.51	4.5E-20
EIF1	1.66	5.6E-20
EIF4A1P2	2.37	6.9E-20
NFKB2	3.49	7.2E-20
BCL2L1	2.92	3.1E-19
EDARADD	2.55	3.1E-19
PSMA6P1	2.89	3.2E-19

PRDM1	2.37	1.6E-20
SLC43A3	3.33	1.9E-20
PTGER4	2.32	3.9E-20
ASNS	3.86	3.9E-20
PGAM1	2.16	8.0E-20
GAPDHP1	2.27	1.2E-19
CYCS	2.90	2.4E-19
MIR155HG	6.35	3.1E-19
PSMA6	3.07	5.1E-19
ICOS	3.89	1.6E-18
STIP1	2.43	1.9E-18
TMSB10	1.85	2.2E-18
ICAM1	4.08	2.9E-18
RP11-516A11.1	2.68	2.9E-18
HSPA13	2.61	3.1E-18
LAG3	3.78	4.4E-18
SLC2A3	2.08	4.4E-18
SOD2	3.14	5.1E-18
IARS	2.43	5.3E-18
GAPDH	2.29	8.5E-18
PTMS	3.53	9.6E-18
SLC3A2	2.39	1.0E-17
IER5	2.47	1.5E-17
IL2RB	2.02	1.6E-17
CCDC71L	2.89	1.8E-17
TUBB4B	2.19	1.8E-17
SLC4A10	2.02	2.1E-17
FTH1P20	2.93	2.4E-17
GAPDHP65	2.27	2.9E-17
PGK1P2	2.69	3.5E-17
ZC3H12A	3.14	4.3E-17
TNFRSF18	5.82	4.7E-17
FTH1P2	2.87	5.1E-17
HSP90AB3P	2.20	5.3E-17
LDHA	2.50	6.7E-17
ALDOA	1.61	7.0E-17
HSP90AB1	2.20	7.0E-17
CDK6	3.26	7.3E-17
ATP2A2	1.78	9.1E-17
TXNP6	3.90	9.1E-17
FTH1P11	2.91	1.1E-16
VDAC1	2.36	1.2E-16
RP6-145B8.3	2.58	1.6E-16
RAB7L1	1.90	1.8E-16
BHLHE40	3.27	2.3E-16
LDLR	2.39	2.8E-16
CD53	1.50	3.3E-16
JUNB	2.31	5.4E-16
NRAS	2.14	6.5E-16
AC098614.2	3.21	1.3E-15
GCH1	2.33	1.5E-15
PRMT1	2.79	1.7E-15
DUSP5	5.42	2.0E-15
B4GALT5	2.34	2.0E-15
FEZ1	5.55	2.1E-15
KIF3B	2.31	2.2E-15
MIF	2.10	3.0E-15
RP11-466P24.2	1.58	5.0E-15
FTH1P7	2.84	5.5E-15
TNFRSF1B	3.13	5.7E-15
EIF4A1P2	2.10	5.9E-15
SATB1	2.07	6.7E-15
TAP1	1.87	7.3E-15
TANK	2.39	8.0E-15
STX11	3.50	9.4E-15
MAFG	2.28	9.5E-15
PIM3	2.38	9.8E-15
ARCN1	1.62	1.2E-14
ODC1	2.98	1.2E-14
IL26	7.64	1.5E-14
IER3	10.12	2.2E-14
GS1-44D20.1	3.22	2.4E-14
INSIG1	2.85	2.4E-14
CREM	3.15	2.6E-14
PSMC1P1	2.12	3.1E-14
EIF2S2	2.35	3.1E-14
NUPL1	2.17	3.9E-14
FTH1P8	2.78	4.8E-14
GNG2	2.04	5.2E-14
PLEK	3.04	6.9E-14
HAX1	2.08	1.0E-13
BCL2L1	1.53	1.8E-03
IL21R	2.63	1.8E-03
IGFLR1	1.42	2.0E-03
GAPDH	1.25	2.1E-03
IL23R	2.73	2.2E-03
PMAIP1	2.02	2.2E-03
SEMA7A	2.39	2.2E-03
PKMP4	2.58	2.3E-03
PIM3	1.40	2.4E-03
HIF1A	1.43	2.4E-03
FCGBP	2.79	3.1E-03
ZFP36L1	2.04	3.5E-03
CCL4L1	4.68	3.5E-03
PKMP5	2.59	3.9E-03
NAMPTL	1.84	4.2E-03
ZBED2	5.19	4.6E-03
YARS	1.36	5.1E-03
TESPA1	1.64	5.6E-03
PYCR1	5.28	6.2E-03
FEZ1	2.82	6.3E-03
BACH2	1.90	7.0E-03
GAPDHP65	1.19	7.0E-03
TARS	1.40	9.0E-03
BCL6	1.42	9.1E-03
JUND	1.48	9.1E-03
ICAM1	1.95	9.4E-03
NCS1	2.07	9.6E-03
ASNS	1.82	9.7E-03
C17orf49	1.63	1.0E-02
CCL3	3.72	1.2E-02
IPO4	2.20	1.2E-02
RHOG	1.18	1.4E-02
ENO1	1.00	1.5E-02
RPSAP58	0.94	1.5E-02
GARS	1.27	1.6E-02
CD97	1.60	1.7E-02
ASB2	5.43	1.7E-02
CTLA4	3.43	1.7E-02
DNAJA1	1.09	1.8E-02
ID2	1.61	1.8E-02
NME1	2.41	1.9E-02
SEC14L1	1.45	1.9E-02
MSN	0.90	2.0E-02
NAMPT	1.79	2.2E-02
LTA	1.57	2.2E-02
AC021224.1	1.03	2.2E-02
LYST	1.68	2.3E-02
CTC-308K20.3	1.44	2.5E-02
ENO1P1	1.05	2.7E-02
HNRNPA1	1.00	2.8E-02
RP11-373L24.1	2.26	3.0E-02
BZRAP1-AS1	1.37	3.2E-02
AARS	1.23	3.2E-02
SLC7A5	1.48	3.3E-02
SPRY4	4.87	3.6E-02
NINJ1	1.94	3.7E-02
NDFIP2	3.44	3.7E-02
CXXC5	1.49	3.8E-02
SGK1	2.43	3.8E-02
CD74	1.44	3.9E-02
RCC2	1.01	3.9E-02
NR4A2	2.91	4.0E-02
TFRC	1.48	4.2E-02
TPI1P1	1.00	4.2E-02
C9orf16	1.16	4.4E-02
NACC1	1.17	4.4E-02
MFSD2A	4.26	4.4E-02
MARS	1.11	4.4E-02
SCD	1.38	4.9E-02
MSNP1	0.92	4.9E-02
NFKBID	1.87	4.9E-02
NFKBIE	1.68	4.9E-02
NUP62	0.98	4.9E-02
C4orf32	4.36	5.1E-19
DUSP4	4.48	5.8E-19
TNFAIP8	2.30	8.6E-19
HSPA13	2.63	1.3E-18
RP11-121L10.3	2.45	1.5E-18
CCT5	2.41	2.0E-18
TIFA	3.10	2.1E-18
HSPD1	2.97	2.3E-18
TXNP6	4.03	4.2E-18
RAN	2.25	4.6E-18
ICAM1	4.05	5.8E-18
PLAGL2	2.74	6.0E-18
MAP3K8	3.68	6.0E-18
RANP1	2.29	9.1E-18
ATP2A2	1.81	1.1E-17
ADAM19	4.20	1.2E-17
IL23A	4.36	1.3E-17
PCK2	4.08	1.3E-17
TNFRSF18	5.90	1.4E-17
RP6-145B8.3	2.64	1.6E-17
DNAJA1	2.13	2.4E-17
HSP90AA1	1.91	2.8E-17
PTMS	3.47	4.9E-17
CREM	3.40	5.3E-17
TUBA1B	2.50	1.1E-16
TRAF4	4.47	1.2E-16
CCL3	8.10	2.0E-16
LIF	7.89	2.1E-16
EIF2S2	2.48	3.3E-16
P2RX5	4.51	3.3E-16
SRPRB	2.59	3.9E-16
CD40LG	3.21	3.9E-16
NPM1	2.14	5.0E-16
ATP5B	1.68	5.0E-16
TNFRSF9	8.30	6.4E-16
PIM1	2.32	7.0E-16
ILF2	2.25	1.0E-15
TBX21	2.79	1.1E-15
XPO5	2.56	1.3E-15
HSPD1P1	2.99	1.4E-15
JUNB	2.27	2.1E-15
DUSP5	5.39	3.2E-15
ETF1	2.08	3.5E-15
IL6ST	2.14	3.5E-15
PSAT1P3	6.63	4.2E-15
CISH	3.27	4.6E-15
RBPJ	2.04	5.2E-15
NME1	4.89	6.5E-15
BHLHE40	3.12	8.5E-15
RP11-1033A18.1	1.92	9.6E-15
VDAC1	2.23	1.3E-14
IQCG	4.03	1.8E-14
YARS	2.39	2.1E-14
MAFG	2.25	2.2E-14
PSMC1P1	2.12	2.2E-14
EGR2	5.71	2.4E-14
NARS	1.98	2.4E-14
PGAM1	1.88	2.4E-14
XBP1	1.88	2.8E-14
KIF3B	2.23	2.9E-14
VASP	1.92	2.9E-14
EPRS	1.87	3.1E-14
PRDM1	2.03	3.1E-14
CCDC6	2.61	3.6E-14
STX11	3.43	3.9E-14
IER3	9.97	5.9E-14
TXNDC5	2.24	6.2E-14
PSMA6	2.68	6.6E-14
CTLA4	6.93	6.9E-14
HSPA9	2.06	7.4E-14
SARS	1.90	8.2E-14
YRDC	3.34	1.1E-13
HAX1	2.06	1.3E-13
RGS16	7.82	1.3E-13
UBE2D3	1.42	1.4E-13
IRF8	7.43	1.6E-13
EIF4H	1.33	1.6E-13
EIF3J	2.12	2.2E-13
PKMP1	2.82	2.5E-13
AK2	2.47	2.5E-13
DESI1	2.75	2.6E-13

PAICS	3.14	1.0E-13
CPD	2.57	1.0E-13
EIF4A1	1.86	1.2E-13
HMGCS1	2.27	1.7E-13
IRF8	7.41	1.8E-13
ATP5B	1.57	2.1E-13
DDIT4	3.76	2.3E-13
FLOT1	2.67	2.6E-13
SPTY2D1	1.65	3.7E-13
ATF4	2.13	4.1E-13
SLC1A4	3.02	4.3E-13
SARS	1.87	4.4E-13
PCK2	3.56	6.6E-13
DNAJA1	1.89	6.7E-13
SLAMF7	2.49	7.5E-13
PSAT1P3	6.12	9.1E-13
VEGFA	7.16	9.1E-13
EML5	3.02	1.0E-12
BZW1P2	1.65	1.1E-12
LMAN1	2.38	1.5E-12
CTLA4	6.60	1.5E-12
HSP90AA1	1.67	1.6E-12
IDI1	1.95	2.1E-12
PSMA1	2.27	2.2E-12
HYOU1	1.96	2.5E-12
BZW1	1.86	2.6E-12
UBE2N	1.80	2.7E-12
DESI1	2.66	3.1E-12
UBALD2	2.18	3.4E-12
FTH1P23	2.97	3.5E-12
ILF2	2.03	3.7E-12
RP11-386G11.10	2.67	3.9E-12
TNFAIP8	1.90	4.0E-12
RP11-887P2.3	2.25	4.7E-12
BIRC3	2.87	5.9E-12
TBX21	2.47	7.2E-12
SRPRB	2.27	7.4E-12
BEST1	3.03	7.9E-12
BCL2L1	2.36	8.7E-12
ARHGDIA	1.33	8.8E-12
CD69	2.94	1.3E-11
MANF	2.47	1.7E-11
PSME2P2	2.28	1.7E-11
SELK	3.00	2.0E-11
CCT5	1.98	2.3E-11
YARS	2.15	3.0E-11
CHAC1	7.79	3.4E-11
GOT1	2.86	3.4E-11
NDFIP2	6.57	3.6E-11
PPIF	2.36	3.8E-11
TYMP	4.11	4.1E-11
TRAF4	3.70	4.5E-11
ZBTB32	6.99	4.7E-11
TXNDC5	2.04	5.2E-11
RP11-312J18.5	3.28	5.2E-11
UBE2D3	1.31	8.2E-11
CISH	2.83	8.3E-11
NME1	4.22	8.3E-11
ANXA2P2	1.87	8.9E-11
HSPA5	2.24	9.2E-11
YWHAE	1.95	1.1E-10
CTD-2301A4.5	3.13	1.2E-10
IQCG	3.50	1.2E-10
CALR	1.70	1.6E-10
RP11-1033A18.1	1.66	1.8E-10
RNF145	1.70	2.4E-10
RAP1B	1.68	2.6E-10
PSMB4	1.49	3.1E-10
CAP1	1.27	3.8E-10
AARS	2.05	4.0E-10
PHLDA1	3.20	4.5E-10
NCS1	3.29	4.8E-10
HAPLN3	3.61	5.0E-10
GHITM	1.55	5.4E-10
HSPD1	2.27	5.5E-10
YRDC	2.91	5.5E-10
TMED9	1.68	5.5E-10
CHPF	2.77	5.7E-10
AK2	2.18	6.5E-10
RP11-1136G11.6	2.18	6.5E-10
TRAF1	2.81	6.8E-10
EIF4H	1.18	7.0E-10
NOLC1	2.24	2.7E-13
GOT1	3.06	2.8E-13
LARP4	2.51	3.3E-13
BZW1P2	1.67	3.4E-13
CCR4	6.03	3.5E-13
PSMA1	2.31	4.6E-13
CTD-2301A4.5	3.42	4.7E-13
YWHAE	2.11	4.8E-13
NPM1P27	2.08	5.1E-13
TSEN15	2.14	5.5E-13
HSPA9P1	2.12	5.8E-13
TXNRD1	2.34	5.9E-13
SLC39A14	2.42	7.1E-13
GCH1	2.14	7.9E-13
RP11-312J18.5	3.50	8.1E-13
SRSF1	2.02	8.6E-13
TPM4	2.26	1.1E-12
HNRNPAB	2.36	1.1E-12
EIF4G1	1.61	1.2E-12
CCT2	2.61	1.3E-12
NCL	1.90	1.3E-12
SERBP1	1.98	1.4E-12
SERBP1P5	2.14	1.4E-12
AARS	2.23	1.4E-12
CCDC71L	2.50	1.5E-12
PSME2P2	2.35	1.8E-12
RP11-1136G11.6	2.38	1.9E-12
BZW1	1.86	2.2E-12
TRAF1	3.10	2.5E-12
HYOU1	1.95	2.7E-12
NDUFV2P1	2.26	2.7E-12
PAICSP4	3.99	3.0E-12
HSPA5	2.37	3.1E-12
CHAC1	8.12	3.2E-12
HNRNPC	1.30	3.2E-12
SCD	2.62	3.4E-12
MRTO4	3.45	3.9E-12
CCT6A	2.08	4.7E-12
NUPL1	2.02	4.8E-12
VEGFA	6.94	4.8E-12
GHITM	1.65	5.4E-12
ATP1B3	2.71	5.5E-12
PGK1	1.65	5.8E-12
RP11-466P24.2	1.44	7.2E-12
C17orf96	4.13	8.2E-12
EIF4EBP1	3.17	9.1E-12
SLAMF7	2.38	9.4E-12
ATF4	2.00	1.8E-11
PRDX1	2.30	2.0E-11
ACTR3	1.48	2.1E-11
ARHGAP31	3.28	2.1E-11
IL26	6.77	2.3E-11
MYC	2.44	2.4E-11
CDK4	2.42	2.4E-11
RAB7L1	1.63	2.6E-11
SLMO2	2.14	3.0E-11
NDFIP2	6.57	3.1E-11
POFUT1	1.99	3.1E-11
PSMB2	2.20	3.3E-11
ZBTB32	7.01	3.6E-11
RBM8B	2.35	3.7E-11
CD83	4.33	3.8E-11
YBX1P1	1.72	3.9E-11
FTH1	1.97	4.2E-11
HSP90AB2P	2.88	4.3E-11
SLC38A2	1.48	4.3E-11
PTGER4	1.80	4.5E-11
EML5	2.82	4.8E-11
RP11-153M3.1	3.00	4.8E-11
SGK1	4.56	4.9E-11
PSME3	1.56	5.1E-11
TXN	3.75	5.5E-11
PPIAP22	1.38	6.0E-11
CCT7	1.92	6.0E-11
MAK16	2.51	6.2E-11
DDIT4	3.40	6.8E-11
EGR1	4.00	8.1E-11
SOD2	2.49	8.2E-11
SLC1A4	2.76	9.5E-11
LARP1	1.55	9.7E-11
EPT1	2.26	1.1E-10
FAM60A	1.85	1.1E-10

NARS	1.71	7.2E-10
SAMSN1	2.94	8.0E-10
MAFF	3.60	8.9E-10
CHCHD2	2.03	9.5E-10
CANX	1.36	1.0E-09
ARF4	2.15	1.1E-09
ARPC5L	2.05	1.2E-09
DNAJB9	2.03	1.3E-09
TXN	3.54	1.4E-09
VLDLR	3.12	1.5E-09
IRAK2	3.04	1.6E-09
TNFRSF9	6.45	1.6E-09
DCUN1D3	2.96	1.9E-09
HK2P1	4.68	1.9E-09
LDHAP4	2.32	1.9E-09
TXNRD1	2.04	2.0E-09
VIMP	2.70	2.3E-09
PSMB2	2.05	2.3E-09
H3F3C	1.67	2.5E-09
RP11-490H24.5	2.15	2.8E-09
PSMC4	2.13	3.0E-09
PKMP4	3.69	3.6E-09
EPRS	1.58	3.7E-09
SEC61B	2.48	3.8E-09
TMED2	1.43	4.0E-09
RAB9A	2.25	4.1E-09
SLC16A3	2.81	4.2E-09
PPIAP22	1.29	4.3E-09
RANP1	1.73	4.5E-09
SEMA7A	3.36	4.9E-09
EIF4G1	1.41	5.0E-09
MXD1	2.35	5.5E-09
AK4	8.63	5.6E-09
GAPDHP60	2.17	5.9E-09
ETV3	1.70	5.9E-09
SOCS1	4.35	5.9E-09
RGS1	4.55	6.0E-09
PRDX1	2.09	6.0E-09
ATP1B3	2.39	6.7E-09
XPO5	2.02	8.4E-09
EIF4EBP1	2.80	8.5E-09
ETF1	1.67	8.9E-09
BLM	3.30	9.0E-09
RAN	1.66	1.1E-08
DUSP6	4.96	1.1E-08
PKMP5	3.69	1.3E-08
SRSF1	1.71	1.4E-08
HSPD1P1	2.29	1.6E-08
ARHGAP31	2.89	1.7E-08
PSMD14	3.11	1.7E-08
HBEGF	8.30	1.8E-08
STK40	1.39	1.8E-08
SEC24D	2.54	1.9E-08
KDELR2	1.84	2.0E-08
MYL6	1.43	2.1E-08
IL6ST	1.68	2.4E-08
TPM3	1.30	2.4E-08
RBM8B	2.08	2.4E-08
ADM2	3.32	2.6E-08
EIF3J	1.74	2.7E-08
BCL2A1	3.87	2.8E-08
CALU	2.15	2.9E-08
CCT2	2.18	3.1E-08
PSMD1	1.96	3.7E-08
RP4-592A1.2	2.54	4.0E-08
LRRC59	1.96	4.1E-08
BAK1	2.08	4.4E-08
SLC38A2	1.31	4.4E-08
HERPUD1	1.61	4.9E-08
GZMH	6.32	4.9E-08
C4orf32	2.94	5.1E-08
TSEN15	1.76	5.1E-08
HAVCR2	6.12	5.3E-08
IL23A	3.05	5.4E-08
KBTBD8	3.06	5.4E-08
P4HB	1.17	5.8E-08
ARF1	1.11	5.9E-08
PAICSP4	3.29	6.4E-08
MAPK6	2.15	9.2E-08
UBB	1.15	9.6E-08
SNX22	1.67	9.8E-08
FICD	2.51	1.1E-07
UBE2N	1.69	1.3E-10
RP4-592A1.2	2.83	1.4E-10
SEMA7A	3.58	1.5E-10
IER5	1.97	2.0E-10
FTH1P10	2.16	2.2E-10
LMAN1	2.18	2.2E-10
SAMSN1	3.00	2.2E-10
MCM6	2.06	2.4E-10
ARPC5L	2.09	2.6E-10
ID2	2.70	2.8E-10
NUS1	2.41	3.8E-10
DPH2	2.62	4.3E-10
GART	2.13	4.4E-10
DNAJA1P3	2.35	4.7E-10
MANF	2.32	4.7E-10
C1QBP	2.50	5.6E-10
PYCR1	8.57	5.6E-10
EIF3CL	2.05	5.7E-10
BYSL	3.35	5.8E-10
ZC3H12A	2.46	5.9E-10
HERPUD1	1.75	6.0E-10
YBX1	1.64	6.3E-10
HK2P1	4.75	6.9E-10
SLC25A5	1.74	7.2E-10
FKBP4	2.42	7.6E-10
GZMH	6.94	8.8E-10
CCT6P2	2.05	1.0E-09
YWHAG	1.58	1.0E-09
EGR3	5.08	1.1E-09
CTC-308K20.3	2.34	1.1E-09
EIF2S1	1.80	1.2E-09
SERBP1P1	2.12	1.3E-09
USP12	2.34	1.3E-09
RP11-887P2.3	2.03	1.3E-09
SEH1L	2.56	1.4E-09
FOXP4	2.44	1.4E-09
NCS1	3.20	1.4E-09
TOMM40	2.52	1.4E-09
IPO4	3.46	1.7E-09
CCT3	1.96	1.7E-09
IL12RB2	3.90	1.8E-09
CDKN1A	3.24	1.8E-09
PA2G4P4	1.76	1.8E-09
UBALD2	1.94	1.9E-09
TANK	1.96	2.0E-09
NRAS	1.72	2.1E-09
CARS	2.28	2.1E-09
EIF5AP4	2.82	2.3E-09
UBB	1.23	2.3E-09
GPT2	6.07	2.7E-09
VDR	4.44	3.1E-09
RP11-137N23.1	2.27	3.5E-09
EIF3C	2.00	3.7E-09
B4GALT5	1.86	3.9E-09
GRPEL1	2.01	4.9E-09
EED	2.96	5.4E-09
INSIG1	2.30	5.5E-09
DCTPP1	2.52	5.5E-09
PTPN11	1.37	5.7E-09
RCN1	3.41	6.1E-09
FEZ1	4.26	6.1E-09
CCDC86	3.08	6.1E-09
H3F3C	1.63	6.1E-09
RRP12	3.51	6.1E-09
LRRC59	2.02	7.0E-09
TUBE1	2.80	7.0E-09
EBNA1BP2	3.05	7.3E-09
NOP16	3.02	7.5E-09
PSMD14	3.14	7.8E-09
PTBP1	1.24	8.1E-09
PTP4A1	1.60	8.6E-09
HSPH1	2.16	9.2E-09
CAMTA2	1.96	1.0E-08
SYTL3	2.78	1.0E-08
CANX	1.30	1.0E-08
IL15RA	2.54	1.0E-08
ABCF2	1.75	1.1E-08
SETP14	1.41	1.1E-08
GNPNAT1	2.31	1.1E-08
CMTM6	1.50	1.1E-08
RPL7L1	1.61	1.1E-08
CERS6	2.59	1.2E-08

VDAC1P1	2.23	1.1E-07
SLC25A5	1.57	1.2E-07
TWSG1	2.47	1.2E-07
PTPN11	1.29	1.2E-07
CARS	2.10	1.2E-07
MMD	2.81	1.3E-07
TICAM1	2.07	1.3E-07
DNAJA1P3	2.10	1.3E-07
EPT1	1.96	1.3E-07
PTP4A1	1.51	1.4E-07
ULBP1	7.49	1.5E-07
C21orf91	1.52	1.6E-07
SEC24A	2.03	1.7E-07
NUS1	2.11	1.7E-07
BLOC1S6	1.57	1.7E-07
RPN1	1.33	1.8E-07
TCP1	1.55	1.8E-07
RP11-274E7.2	2.23	1.8E-07
SYTL3	2.60	1.9E-07
C20orf24	1.78	1.9E-07
PSMD11	1.68	2.0E-07
YBX1P1	1.46	2.1E-07
PFN1	1.52	2.1E-07
SH3BP5	3.77	2.2E-07
GPT2	5.44	2.3E-07
CCT7	1.64	2.4E-07
CAPZA1	1.20	2.4E-07
TCP1P1	1.92	2.7E-07
NFE2L2	1.27	2.8E-07
BAK1P1	2.05	2.9E-07
ACTR2	1.12	3.0E-07
GFPT1	1.94	3.1E-07
GNA15	5.06	3.2E-07
SLMO2	1.79	3.2E-07
NFE2L3	2.36	3.3E-07
SF3B5	1.58	3.4E-07
ETV5	7.71	3.6E-07
HIGD1A	1.93	4.5E-07
SREBF1	2.65	4.8E-07
EHD4	2.08	4.8E-07
HSP90AB2P	2.37	4.9E-07
LDHAP7	2.42	5.0E-07
HNRNPC	1.06	5.1E-07
RAB33A	2.99	5.3E-07
HSPA9	1.55	5.5E-07
ATF4P4	2.16	5.6E-07
MAPRE1	1.27	5.6E-07
PPIB	1.57	5.7E-07
ITK	1.89	6.5E-07
GLUD1	1.25	6.5E-07
EIF5AP4	2.48	6.9E-07
HNRNPA3P6	1.44	6.9E-07
GBP5	1.84	6.9E-07
IL12RB2	3.35	7.0E-07
RGS16	5.59	7.2E-07
SEC61A1	1.38	7.3E-07
BATF3	6.76	7.5E-07
RP11-137N23.1	2.02	7.6E-07
NOP10	1.82	7.6E-07
NUDCD1	2.74	7.6E-07
YBX1	1.41	7.6E-07
CLIC4	6.29	7.7E-07
LYRM1	2.11	7.8E-07
LARP4	1.90	7.8E-07
RP11-567G24.1	1.64	8.1E-07
MYO1B	6.24	8.7E-07
NDUFV2	2.97	8.7E-07
DNAJC3	1.68	8.8E-07
PEA15	1.49	1.0E-06
CCR4	4.36	1.0E-06
BYSL	2.82	1.1E-06
MTHFD1L	4.65	1.1E-06
PSME3	1.29	1.1E-06
MGAT2	1.39	1.2E-06
CCT6A	1.63	1.2E-06
GRPEL1	1.77	1.2E-06
PFN1P1	1.56	1.3E-06
SRPR	1.39	1.4E-06
TMEM64	1.86	1.5E-06
PYCR1	6.94	1.5E-06
MIR146A	7.24	1.6E-06
TNFRSF8	7.20	1.7E-06
TWSG1	2.58	1.3E-08
HAPLN3	3.35	1.3E-08
SRM	2.51	1.4E-08
CD69	2.55	1.5E-08
YBX1P10	1.68	1.5E-08
GTPBP4	2.24	1.6E-08
TCP1	1.63	1.6E-08
MTHFD1L	5.20	1.7E-08
PSMC4	2.03	1.7E-08
CCT4	1.79	1.7E-08
WDR43	2.31	1.8E-08
PSMD11	1.76	1.9E-08
ABCE1	2.26	2.0E-08
KPNB1	1.40	2.2E-08
MRPL3P1	2.43	2.3E-08
TCP1P1	2.01	2.4E-08
NOP14	2.53	2.4E-08
MAPK6	2.20	2.5E-08
CALR	1.54	2.6E-08
RP4-775C13.1	1.82	2.6E-08
NME2P1	1.98	2.8E-08
PSMB4	1.37	2.8E-08
PPIF	2.06	2.9E-08
PNO1	2.75	3.0E-08
TUBB4B	1.59	3.0E-08
NFKB1	2.32	3.3E-08
HMGCS1	1.83	3.3E-08
FTH1P2	2.07	3.4E-08
TNFRSF8	8.07	3.5E-08
RAP1B	1.52	3.5E-08
SATB1	1.59	4.1E-08
FTH1P11	2.11	4.2E-08
SET	1.24	4.2E-08
NFE2L3	2.47	4.3E-08
RP11-298C3.2	2.65	4.3E-08
WDR12	2.93	4.4E-08
PSMB5	2.24	4.4E-08
ULBP1	7.70	4.7E-08
FTH1P20	2.08	4.8E-08
ADM2	3.25	4.8E-08
HNRNPA1P48	1.25	5.1E-08
IL2RB	1.45	5.2E-08
SDC4	2.82	5.2E-08
TSR1	2.01	5.3E-08
DKC1	1.91	5.4E-08
SEC61B	2.32	5.7E-08
CSF1	4.04	5.8E-08
VLDLR	2.86	5.9E-08
NPM1P39	2.06	6.0E-08
SUB1	2.05	6.1E-08
BATF3	7.24	6.3E-08
KBTBD8	3.02	6.8E-08
ARCN1	1.26	7.8E-08
CTPS1	2.95	8.2E-08
PHB	1.98	8.2E-08
ATP1B3P1	2.70	8.2E-08
RP11-274E7.2	2.26	8.3E-08
SELK	2.52	8.3E-08
CTH	5.14	8.5E-08
CEBPG	1.64	9.0E-08
TICAM1	2.07	9.5E-08
PSMD1	1.89	9.8E-08
MIF	1.57	1.0E-07
PSMD12	2.24	1.1E-07
FOSL1	7.83	1.1E-07
VDAC1P1	2.21	1.2E-07
C10orf2	2.31	1.2E-07
TMED9	1.49	1.3E-07
CHCHD2	1.81	1.3E-07
ATF3	3.38	1.6E-07
RP11-386G11.10	2.15	1.6E-07
FASN	1.90	1.6E-07
PSMD12P	2.67	1.6E-07
GPATCH4	2.45	1.8E-07
PIPSL	1.46	1.8E-07
NPM1P6	1.98	1.9E-07
RP11-490H24.5	1.94	1.9E-07
NIP7	1.84	1.9E-07
CLIC4	6.51	2.1E-07
UBE2D3P1	1.60	2.2E-07
CCL4L2	5.01	2.2E-07
HNRNPCP2	1.31	2.4E-07

SND1	1.48	1.8E-06
UFM1	1.68	1.8E-06
SERBP1	1.49	1.8E-06
HSPA9P1	1.59	1.8E-06
MT2A	3.51	1.9E-06
GNAI3	1.41	2.1E-06
MIR22HG	2.70	2.2E-06
CCT8P1	1.65	2.3E-06
SLC41A2	4.60	2.4E-06
SERBP1P5	1.61	2.5E-06
SEC23B	2.06	2.5E-06
EIF2S1	1.52	2.7E-06
PPP1CB	1.55	2.7E-06
RP11-446E9.1	1.63	2.7E-06
COX6A1P2	1.50	2.7E-06
HSP90B1	1.36	2.8E-06
PFKP	2.22	2.9E-06
ZEB2	2.90	2.9E-06
CBFB	1.39	3.0E-06
CORO1A	1.22	3.0E-06
SUB1	1.86	3.1E-06
GNPNAT1	2.01	3.1E-06
RELB	2.26	3.2E-06
ATF3	3.11	3.3E-06
CCDC6	1.82	3.4E-06
FAS	2.34	3.5E-06
GORASP2	1.39	3.7E-06
PSMD8	1.66	3.9E-06
ACTB	1.53	4.0E-06
FOSL1	7.02	4.0E-06
NPM1	1.43	4.0E-06
OSM	6.09	4.0E-06
SLAMF1	2.13	4.1E-06
ID2	2.13	4.3E-06
IPO4	2.84	4.4E-06
MRTO4	2.53	4.5E-06
BCL3	2.46	4.6E-06
PSMD12	2.03	4.7E-06
SRP72	1.50	4.7E-06
SPRY4	6.91	4.8E-06
HSP90B2P	1.41	4.8E-06
PDIA6	1.82	5.0E-06
SBNO2	1.77	5.0E-06
RP11-153M3.1	2.29	5.1E-06
C17orf96	3.03	5.1E-06
PIPSL	1.34	5.1E-06
NABP1	2.14	5.3E-06
PLEKHB2	1.15	5.4E-06
UBE2D3P1	1.48	5.7E-06
PSMD12P	2.42	5.7E-06
RP11-9L18.2	1.35	5.7E-06
SEC13	1.83	5.8E-06
TMED5	1.35	5.9E-06
RCN1	2.85	5.9E-06
SLC39A14	1.75	6.2E-06
YWHAG	1.30	6.3E-06
ACTR3P2	1.92	6.7E-06
FKBP4	1.94	6.8E-06
ANXA2	1.95	7.0E-06
APOL6	1.59	7.4E-06
ALG2	1.54	7.8E-06
HOXB9	6.65	7.9E-06
PTPN1	1.19	8.0E-06
PSMD2	1.52	8.6E-06
RP11-550F7.1	1.24	8.9E-06
PSMD13	1.53	9.1E-06
YBX1P10	1.44	9.2E-06
TCEB3	1.67	9.8E-06
MTFP1	2.01	1.0E-05
EIF3CL	1.63	1.1E-05
RP1-232L22__B.1	3.92	1.1E-05
GLUD2	1.22	1.2E-05
AP000350.4	1.98	1.2E-05
EBNA1BP2	2.50	1.2E-05
PSMB5	1.93	1.2E-05
PRDX6	1.47	1.2E-05
DCTPP1	2.07	1.3E-05
HNRNPAB	1.66	1.3E-05
SMS	3.36	1.4E-05
CYP51A1	1.72	1.4E-05
MCM6	1.60	1.4E-05
NSMF	2.87	1.4E-05
ELL2	2.60	2.5E-07
OSM	6.63	2.6E-07
HNRNPA1P10	1.30	2.6E-07
HOXB9	7.40	2.8E-07
ARHGEF2	1.75	3.1E-07
BIRC3	2.27	3.1E-07
IL23R	3.47	3.1E-07
PTPN1	1.29	3.2E-07
RAB9A	2.02	3.2E-07
BZW2	2.81	3.4E-07
PSMD8	1.76	3.4E-07
SYNCRIP	1.57	3.5E-07
NETO2	3.05	3.6E-07
NOP58	2.27	4.4E-07
NUS1P1	2.32	4.4E-07
SSRP1	1.39	4.4E-07
MFSD2A	6.72	4.5E-07
AC098614.2	2.26	4.5E-07
ZBED2	6.95	4.7E-07
RPF2P1	2.91	4.7E-07
RP11-446E9.1	1.69	4.7E-07
TIMM17A	2.36	5.1E-07
POLR1B	1.75	5.1E-07
MRPL3	2.11	5.2E-07
LMNB2	1.71	5.4E-07
NAA15	1.87	5.5E-07
NUDCD1	2.74	5.5E-07
UFM1	1.73	5.6E-07
RPF2	2.76	5.7E-07
BCL2A1	3.54	5.7E-07
FTH1P7	2.01	6.2E-07
HNRNPA1P7	1.21	6.3E-07
SLC25A32	2.01	6.6E-07
SMAP2	1.35	6.7E-07
SFXN1	1.84	7.3E-07
CCT8P1	1.70	7.3E-07
BCAT1	7.35	7.4E-07
SLC6A9	7.11	7.6E-07
MPDU1	2.33	7.7E-07
KIAA0020	3.10	8.0E-07
NIFK	2.10	8.3E-07
CALU	1.96	8.3E-07
AC104297.1	2.54	8.7E-07
ZEB2	3.00	9.0E-07
TUFM	1.60	1.0E-06
RP11-9L18.2	1.41	1.0E-06
LMNA	2.53	1.2E-06
RCN1P2	3.27	1.3E-06
CHPF	2.29	1.4E-06
ARF4	1.80	1.4E-06
ZFR	1.34	1.4E-06
GLUD1	1.22	1.4E-06
RP11-567G24.1	1.60	1.4E-06
PPIL1	2.17	1.5E-06
METRNL	2.53	1.5E-06
SMS	3.58	1.7E-06
EIF6	1.77	1.7E-06
PPP1R15B	1.41	1.7E-06
PSMD7	1.55	2.0E-06
SND1	1.46	2.1E-06
BEST1	2.29	2.1E-06
FTH1P8	1.96	2.1E-06
PRMT5	2.32	2.2E-06
SNRPB	1.60	2.3E-06
TYMP	3.15	2.3E-06
RP11-861A13.4	2.48	2.3E-06
BAK1	1.86	2.3E-06
PPA1	2.93	2.3E-06
C9orf91	2.08	2.5E-06
NUP188	1.68	2.6E-06
C8orf33	1.69	2.6E-06
BLM	2.82	2.6E-06
MIR146A	7.06	2.8E-06
ATF4P4	2.04	2.9E-06
PMF1	2.14	2.9E-06
TIMM23	2.48	2.9E-06
PKMP4	3.08	2.9E-06
GAPDHP1	1.39	3.0E-06
TOMM70A	1.52	3.3E-06
NOP56	1.52	3.3E-06
NFE2L2	1.18	3.3E-06
CFLAR	1.69	3.3E-06

NME2P1	1.68	1.4E-05
CCT4	1.50	1.5E-05
C19orf10	2.56	1.5E-05
MORF4L2	1.55	1.5E-05
FEN1	1.99	1.6E-05
CTH	4.37	1.6E-05
DUSP4	2.52	1.8E-05
RBBP7	1.42	1.9E-05
ATF4P3	2.10	2.0E-05
CCT6P2	1.62	2.0E-05
USP12	1.82	2.0E-05
TALDO1	1.62	2.0E-05
RP11-39C10.1	2.51	2.0E-05
BCL2	2.27	2.0E-05
PSMD3	1.73	2.1E-05
RP5-940J5.9	2.20	2.1E-05
NUS1P1	2.07	2.1E-05
IL4I1	2.92	2.1E-05
FNDC3B	2.59	2.1E-05
FTH1P5	2.82	2.1E-05
PSMD7	1.45	2.2E-05
USP14	1.36	2.3E-05
STK17B	1.45	2.3E-05
SLC6A9	6.30	2.3E-05
MB21D1	2.37	2.3E-05
COX17P1	2.36	2.4E-05
CCT3	1.54	2.4E-05
ADRM1	1.64	2.5E-05
MTMR6	1.48	2.6E-05
SNRPB	1.49	2.8E-05
TMEM208	2.21	2.8E-05
CD83	3.06	2.8E-05
MAP2K1	1.42	2.9E-05
PXK	1.65	2.9E-05
LDHAP2	2.33	3.0E-05
ST8SIA4	1.70	3.0E-05
LIF	4.50	3.1E-05
ATP1B3P1	2.26	3.1E-05
PPP1R15B	1.30	3.2E-05
KIF21B	1.52	3.3E-05
TRAM1	1.31	3.4E-05
VMP1	1.56	3.4E-05
CHCHD2P6	2.26	3.4E-05
NFKB1	1.89	3.4E-05
DPY19L1	1.77	3.4E-05
SERBP1P1	1.63	3.4E-05
TDPX2	2.31	3.5E-05
COPA	1.21	3.6E-05
EIF3C	1.57	3.7E-05
RHBDD1	1.59	3.7E-05
SNRPB2	1.95	3.8E-05
P4HA1	2.13	3.9E-05
ABTB2	4.69	3.9E-05
HNRNPA2B1	1.12	3.9E-05
STAT4	1.70	4.0E-05
RP11-334L9.1	2.22	4.1E-05
PRNP	1.25	4.1E-05
MSC	2.79	4.4E-05
COPG1	1.53	4.4E-05
TUBE1	2.20	4.5E-05
LONP1	1.92	4.8E-05
NFIL3	2.40	4.8E-05
SRP54	1.89	4.8E-05
RHOH	1.30	4.8E-05
RP11-64K7.1	1.99	4.9E-05
FOXP4	1.84	5.0E-05
SRA1	1.96	5.1E-05
CDK2AP2	1.34	5.3E-05
JAKMIP1	3.34	5.4E-05
CSF1	3.23	5.4E-05
GPI	1.36	5.7E-05
LRP8	2.19	5.7E-05
PSMA2P3	1.85	5.9E-05
PSMA4	1.57	6.0E-05
NEDD4	2.18	6.0E-05
POLR2K	1.69	6.1E-05
MAK16	1.79	6.1E-05
TRIB3	1.92	6.1E-05
ATP6V0B	1.74	6.2E-05
PSMB6	1.76	6.4E-05
IL15RA	1.99	6.6E-05
UBE2MP1	1.79	6.6E-05
TXLNA	1.49	3.4E-06
LDHA	1.60	3.6E-06
WDR46	2.02	3.6E-06
CCL3L1	5.77	3.7E-06
LRP8	2.39	3.7E-06
SF3B5	1.47	3.7E-06
CDV3	0.96	3.7E-06
AK4	7.09	3.7E-06
ATP13A3	1.45	3.9E-06
HAVCR2	5.31	4.1E-06
SLC25A22	2.15	4.3E-06
RIOK1	2.39	4.4E-06
POLD2	1.97	4.5E-06
PSMD2	1.54	4.8E-06
MDFIC	1.83	4.9E-06
PPIA	1.08	5.0E-06
RSL24D1P11	2.74	5.2E-06
DDX39A	1.69	5.4E-06
PSMD3	1.80	5.5E-06
HNRNPA2B1	1.19	5.5E-06
PFAS	2.41	5.5E-06
AC093724.2	2.71	5.9E-06
NR4A3	3.89	5.9E-06
TRIB3	2.07	6.0E-06
H2AFZ	1.64	6.3E-06
RP11-334L9.1	2.36	6.7E-06
PES1	1.90	7.1E-06
CBFB	1.35	7.3E-06
HOMER1	3.55	7.3E-06
PSMB3	1.93	7.4E-06
SRP72	1.47	7.4E-06
SREBF1	2.42	7.6E-06
TIMM13	2.23	7.8E-06
IPO5	1.50	7.8E-06
NME1-NME2	1.92	7.8E-06
POLR2K	1.80	8.0E-06
TRIM25	1.41	8.0E-06
RP11-39C10.1	2.57	8.0E-06
FTH1P23	2.12	8.3E-06
GNL2	2.13	8.5E-06
RP11-142L4.3	2.09	8.6E-06
TDPX2	2.41	8.8E-06
SPTY2D1	1.19	9.1E-06
TFAM	1.63	9.1E-06
RAB33A	2.70	9.5E-06
TOMM22	1.65	9.8E-06
DUSP6	4.03	9.9E-06
CSNK2A3	1.45	1.0E-05
FABP5P7	5.19	1.0E-05
IMPDH2	1.62	1.0E-05
GS1-44D20.1	2.13	1.0E-05
SRXN1	1.91	1.0E-05
LONP1	2.01	1.1E-05
GLUD2	1.21	1.1E-05
MAFF	2.77	1.2E-05
SNRPD1	2.65	1.2E-05
AHCY	2.04	1.2E-05
DCUN1D5	2.73	1.2E-05
FAS	2.22	1.3E-05
SIAH2	1.63	1.3E-05
SZRD1	1.12	1.3E-05
HNRNPA3P6	1.31	1.3E-05
GAPDH	1.38	1.4E-05
PDIA6	1.75	1.4E-05
NOP10	1.65	1.4E-05
PSAT1P4	5.64	1.5E-05
SLC2A3	1.26	1.5E-05
PXK	1.68	1.5E-05
PKMP5	2.99	1.5E-05
DNAJB9	1.59	1.5E-05
PIGW	2.80	1.5E-05
HNRNPA1L2	1.28	1.5E-05
BAK1P1	1.81	1.6E-05
COX6A1P2	1.41	1.6E-05
METTL1	3.62	1.6E-05
ARL8B	1.25	1.6E-05
HSPA8	1.39	1.7E-05
BAZ1A	1.57	1.7E-05
COA4	2.02	1.7E-05
RHBDD1	1.62	1.7E-05
AC007318.5	1.42	1.8E-05
SLC41A2	4.25	1.8E-05

GART	1.58	6.7E-05
PDCD1	2.32	6.8E-05
COPB2	1.45	6.9E-05
SZRD1	1.07	6.9E-05
RP11-349K21.1	2.08	7.1E-05
CEBPG	1.36	7.1E-05
TIMM17A	2.02	7.1E-05
G6PD	1.45	7.2E-05
KPNB1	1.13	7.3E-05
EAF1	1.34	7.3E-05
RAB21	1.27	7.6E-05
CMAHP	2.49	7.9E-05
PMF1	1.92	8.1E-05
RP11-365H23.1	1.92	8.1E-05
RFTN1	1.58	8.2E-05
OSTC	1.62	8.6E-05
GAPDHP38	2.23	8.9E-05
TOMM40	1.86	9.6E-05
FASN	1.57	9.8E-05
GALNT4	1.65	9.8E-05
PA2G4P4	1.33	9.8E-05
CDK4	1.67	1.0E-04
CCDC86	2.30	1.0E-04
RP11-395L14.17	2.32	1.0E-04
MAPK1IP1L	1.13	1.0E-04
RP11-134K13.2	3.50	1.1E-04
LDHAP5	2.55	1.1E-04
NPM1P27	1.34	1.1E-04
MPDU1	1.98	1.1E-04
CCND3	1.79	1.1E-04
CLIC1P1	1.93	1.1E-04
CDC37	1.39	1.2E-04
ACVR1B	1.69	1.2E-04
CAP1P2	1.29	1.2E-04
IL23R	2.84	1.2E-04
U40455.1	2.25	1.2E-04
SFXN1	1.57	1.2E-04
Sep-15	1.31	1.2E-04
ACO2	1.76	1.2E-04
DNAJB11	1.66	1.2E-04
EIF6	1.54	1.3E-04
MLF2	1.18	1.3E-04
PSMB3	1.75	1.4E-04
STT3A	1.28	1.4E-04
CCL3	4.24	1.4E-04
PRDX3	1.56	1.4E-04
NDUFB8	1.71	1.4E-04
PSAT1P4	5.13	1.4E-04
RHOA	0.95	1.4E-04
RPF2	2.30	1.4E-04
RRP12	2.58	1.4E-04
CTC-308K20.3	1.69	1.5E-04
MRPL3P1	1.86	1.5E-04
RP11-416K24.2	1.84	1.5E-04
C2CD4A	7.28	1.5E-04
METRNL	2.14	1.5E-04
GPR65	1.26	1.6E-04
RPF2P1	2.39	1.6E-04
SPCS2P4	1.35	1.6E-04
SLC25A32	1.68	1.6E-04
GMPPB	1.82	1.6E-04
PFDN2	2.30	1.6E-04
TMED7	1.41	1.6E-04
RP11-298C3.2	2.05	1.6E-04
PNO1	2.10	1.7E-04
BCAT1	5.92	1.7E-04
GAPDHP72	2.30	1.7E-04
ARSB	2.08	1.8E-04
MYB	6.33	1.9E-04
ADSL	1.91	1.9E-04
TXLNA	1.30	1.9E-04
ADAM8	1.37	1.9E-04
LRRFIP1	1.08	1.9E-04
HSPH1	1.61	2.0E-04
TUBBP1	1.52	2.0E-04
OXSR1	1.30	2.0E-04
DPP3	2.05	2.1E-04
HK1	1.29	2.1E-04
EIF4A3	1.53	2.1E-04
GPR132	1.35	2.2E-04
LYN	2.32	2.2E-04
GOLT1B	1.61	2.2E-04
KDELR2	1.52	1.8E-05
SNRPA	1.69	1.8E-05
NSMF	2.82	1.9E-05
PSMA2P3	1.92	1.9E-05
PMM2	2.23	1.9E-05
STRAP	1.58	1.9E-05
PGK1P2	1.63	2.0E-05
CD53	0.98	2.1E-05
MYO1B	5.52	2.1E-05
TWISTNB	1.74	2.2E-05
FLOT1	1.79	2.3E-05
CMAHP	2.60	2.3E-05
MB21D1	2.35	2.4E-05
UCK2	2.12	2.4E-05
ITK	1.67	2.5E-05
BLOC1S6	1.35	2.5E-05
EIF4HP1	1.29	2.5E-05
ALDOA	1.02	2.5E-05
PTGES3	1.07	2.5E-05
ARSB	2.23	2.5E-05
SPRY4	6.44	2.6E-05
SOCS2	3.96	2.7E-05
BCL2	2.23	2.7E-05
GNL3	2.00	2.7E-05
NHP2	1.95	2.7E-05
STAT5A	1.65	2.7E-05
HNRNPR	1.25	2.8E-05
CCT5P2	2.41	2.9E-05
SEC61A1	1.23	2.9E-05
CCL4L1	5.30	3.0E-05
FEN1	1.93	3.0E-05
RP11-516A11.1	1.57	3.0E-05
EBI3	6.53	3.1E-05
USP14	1.34	3.2E-05
RRS1	2.02	3.3E-05
MRPL15	2.45	3.3E-05
TOMM34	2.18	3.3E-05
FARSA	1.92	3.4E-05
IDH3A	1.82	3.4E-05
NHP2P1	2.24	3.5E-05
TMSB10	1.11	3.5E-05
CAPRIN1	1.15	3.5E-05
DHX33	1.96	3.6E-05
IL4I1	2.84	3.6E-05
MORF4L2	1.49	3.6E-05
EIF4A3	1.63	3.7E-05
SRSF3	1.50	3.7E-05
BRIX1	2.19	3.8E-05
HSPE1	2.51	3.8E-05
PSMA4	1.58	3.9E-05
TCEB3	1.57	4.0E-05
RP11-395L14.17	2.39	4.1E-05
NACC1	1.48	4.1E-05
NAA20	2.11	4.2E-05
PRDX3	1.62	4.2E-05
TIMM10	2.75	4.2E-05
HNRNPABP1	2.55	4.3E-05
SUB1P1	2.18	4.4E-05
WDR36	1.85	4.5E-05
ANP32A	1.23	4.6E-05
PHF5A	1.78	4.7E-05
RP11-134K13.2	3.60	4.8E-05
RELB	2.04	4.8E-05
CD3EAP	2.75	4.9E-05
NFIL3	2.37	4.9E-05
TMEM208	2.14	5.0E-05
C17orf49	1.87	5.9E-05
RP11-570P14.1	2.53	5.9E-05
XRCC6P2	1.09	5.9E-05
NOL6	1.73	6.1E-05
PARK7	1.50	6.1E-05
AC018804.7	1.87	6.1E-05
RPN1	1.12	6.2E-05
TMED2	1.11	6.2E-05
ETF1P2	2.45	6.4E-05
NR4A1	3.52	6.6E-05
NPM1P24	2.03	6.6E-05
DPP3	2.13	6.8E-05
RP11-405A12.1	1.98	6.8E-05
POLR2D	1.79	6.9E-05
RABGGTB	1.82	7.1E-05
GAPDHP65	1.32	7.1E-05

ANP32A	1.17	2.2E-04
MYO1G	1.81	2.2E-04
CYB5B	1.24	2.3E-04
RTN4	1.25	2.3E-04
SRM	1.86	2.4E-04
RP11-861A13.4	2.10	2.4E-04
SUB1P1	2.05	2.4E-04
TMEM39A	1.60	2.5E-04
TAF13	2.52	2.6E-04
TMEM165	1.74	2.6E-04
CALCOCO2	1.38	2.6E-04
CEBPB	1.85	2.6E-04
PELO	1.51	2.6E-04
RSL24D1P11	2.36	2.7E-04
RP11-819M15.1	2.02	2.7E-04
RAB1A	1.38	2.7E-04
HSP90B3P	1.38	2.7E-04
IPO5	1.32	2.8E-04
NAA15	1.51	2.9E-04
C17orf49	1.76	2.9E-04
NOP16	2.17	3.1E-04
EIF3I	1.34	3.1E-04
SSR3	1.37	3.3E-04
STRAP	1.42	3.3E-04
SQLE	1.60	3.4E-04
NCL	1.19	3.5E-04
RP11-405A12.1	1.85	3.6E-04
ARRB2	1.81	3.6E-04
ARL8B	1.13	3.6E-04
DAP	1.26	3.7E-04
AC007318.5	1.27	3.8E-04
RP4-775C13.1	1.36	3.8E-04
TIMM23	2.07	3.8E-04
DOCK10	1.72	3.8E-04
CDV3	0.83	3.8E-04
SRF	1.09	3.9E-04
YME1L1	1.10	4.0E-04
CPEB4	1.71	4.0E-04
C12orf23	1.45	4.1E-04
GMFB	1.51	4.2E-04
RP11-296P7.4	1.83	4.2E-04
RP1-273G13.2	2.78	4.2E-04
H2AFZ	1.41	4.3E-04
FAM96B	1.84	4.3E-04
TPD52	1.53	4.4E-04
TRIP10	2.34	4.4E-04
AC131180.1	1.55	4.5E-04
RDX	1.63	4.5E-04
EGR2	3.13	4.6E-04
SOCS2	3.49	4.6E-04
RCN1P2	2.62	4.6E-04
NETO2	2.34	4.6E-04
C1QBP	1.68	4.7E-04
PPP2CA	1.03	4.7E-04
PMVK	1.82	4.7E-04
CMTM6	1.10	4.9E-04
SEH1L	1.75	5.0E-04
Z82188.1	1.25	5.0E-04
NOLC1	1.33	5.1E-04
ELL2	1.99	5.1E-04
PPIA	0.93	5.1E-04
SPRED2	3.94	5.1E-04
GTPBP4	1.61	5.2E-04
CAMTA2	1.40	5.3E-04
CERS6	1.84	5.4E-04
LGALS1	3.70	5.6E-04
IRGQ	1.74	5.6E-04
PSMC3	1.85	5.6E-04
SLCO4A1	3.58	5.8E-04
HNRNPCP2	1.03	5.8E-04
IMPAD1	1.27	5.9E-04
IGF2R	1.27	6.1E-04
NAA20	1.89	6.1E-04
SNRPA	1.47	6.3E-04
PTBP1	0.91	6.3E-04
VAV1	1.77	6.3E-04
SDF2L1	2.25	6.3E-04
TIMM10	2.45	6.3E-04
PTPN2P1	1.91	6.5E-04
ATP5G3	1.39	6.6E-04
UBE2V1	0.97	6.6E-04
PSMC2	1.70	6.7E-04
BANF1	1.61	7.2E-05
RCC2	1.23	7.2E-05
ADRM1	1.56	7.2E-05
CCT5P1	2.55	7.3E-05
NEDD4	2.14	7.5E-05
ACVR1B	1.70	7.8E-05
PSMD13	1.40	7.9E-05
ZNHIT6	1.82	8.1E-05
CCND2	1.94	8.2E-05
VIMP	1.98	8.2E-05
ATP5G3	1.50	8.3E-05
PFDN2	2.34	8.3E-05
NOP2	1.53	8.4E-05
PSMB6	1.73	8.4E-05
FERMT2	3.00	8.4E-05
PNPT1P1	2.47	9.2E-05
IPO7	1.22	9.6E-05
QKI	1.27	1.0E-04
MRPL17	1.90	1.0E-04
SOCS1	3.17	1.0E-04
TNFRSF4	6.28	1.1E-04
RP1-273G13.2	2.95	1.1E-04
YBX3P1	6.25	1.2E-04
XRCC6	1.10	1.2E-04
MAT2A	1.24	1.2E-04
AC006026.9	2.02	1.2E-04
SNRPB2	1.84	1.3E-04
RP11-64K7.1	1.90	1.3E-04
LRRC8B	2.19	1.3E-04
FKBP1A	1.72	1.4E-04
CAMK2D	1.79	1.5E-04
ATP6V0B	1.67	1.5E-04
RANGAP1	1.32	1.6E-04
ATF4P3	1.92	1.6E-04
CD55	1.71	1.7E-04
MTFP1	1.79	1.7E-04
C2CD4A	7.18	1.7E-04
RP11-737O24.3	2.28	1.8E-04
SNX22	1.31	1.8E-04
NIPA2	1.28	1.8E-04
AC004797.1	1.50	1.8E-04
EIF3I	1.36	1.8E-04
MED8	1.73	1.8E-04
NFAT5	1.67	1.9E-04
FAM98A	1.96	1.9E-04
RP3-406P24.1	1.93	1.9E-04
STK40	1.07	1.9E-04
HBEGF	5.94	1.9E-04
RFTN1	1.52	1.9E-04
MMD	2.18	1.9E-04
XPOT	1.29	1.9E-04
RPIA	1.83	1.9E-04
HNRNPF	0.91	1.9E-04
TMEM64	1.55	1.9E-04
RANBP1	2.10	2.0E-04
SEC13	1.59	2.0E-04
TXNL1	1.60	2.0E-04
CPD	1.54	2.0E-04
SLC41A1	1.29	2.1E-04
G6PD	1.38	2.1E-04
ABTB2	4.29	2.2E-04
EHD4	1.66	2.2E-04
GLS	1.00	2.3E-04
PSMC3	1.92	2.3E-04
PSMB1	1.45	2.3E-04
URB1	1.63	2.3E-04
U40455.1	2.16	2.3E-04
NCBP2	1.24	2.4E-04
SEC24D	1.86	2.4E-04
C1orf43	1.16	2.4E-04
CHCHD2P6	2.06	2.5E-04
RP11-296P7.4	1.86	2.5E-04
EIF3B	1.31	2.5E-04
PRNP	1.16	2.5E-04
MKX	6.16	2.6E-04
COPB1	1.28	2.6E-04
CAPZA1	0.97	2.6E-04
IDI1	1.25	2.6E-04
SLC4A10	1.13	2.6E-04
SNHG16	1.17	2.6E-04
MTMR1	1.29	2.6E-04
SEC23B	1.72	2.7E-04

CDKN2B	5.96	6.8E-04
CTSH	1.81	6.9E-04
VBP1	1.51	7.1E-04
VDAC1P2	2.37	7.1E-04
MTDH	1.31	7.1E-04
PFKFB3	2.11	7.2E-04
PHB	1.46	7.2E-04
UPP1	1.81	7.5E-04
P2RX5-TAX1BP3	2.60	7.7E-04
CCND2	1.75	7.7E-04
RAC2	1.27	7.8E-04
RPN2	1.22	7.8E-04
MZT1	2.38	7.9E-04
AP1B1	1.22	8.0E-04
GBE1	2.49	8.1E-04
LYSMD3	1.24	8.1E-04
TMEM214	1.24	8.1E-04
TOMM22	1.39	8.2E-04
NME1-NME2	1.60	8.2E-04
SERPINB8	1.47	8.3E-04
WSB2	1.33	8.3E-04
CLTC	0.96	8.6E-04
EIF4HP1	1.13	8.6E-04
P2RY14	1.99	8.6E-04
COPB1	1.22	8.8E-04
SNX10	2.07	8.9E-04
TXNL1	1.50	8.9E-04
TCEB1	2.12	9.0E-04
XXbac-BPG252P9.9	2.08	9.1E-04
PDIA3	1.27	9.2E-04
GPR171	1.09	9.2E-04
MRPL3	1.60	9.2E-04
TMEM65	2.20	9.3E-04
CSTF2	2.52	9.4E-04
NFAT5	1.54	9.4E-04
SLC27A2	5.76	9.5E-04
SDC4	1.99	9.6E-04
RP3-406P24.1	1.80	9.7E-04
FTH1P12	2.91	9.8E-04
MFSD2A	4.83	9.9E-04
KSR1	2.08	1.0E-03
KIAA0020	2.35	1.0E-03
RBPJ	1.14	1.0E-03
PTGES3	0.94	1.0E-03
WDR12	2.06	1.0E-03
HNRNPA1P48	0.92	1.1E-03
TUBB	1.36	1.1E-03
PTPN2	1.43	1.1E-03
ABCF2	1.23	1.1E-03
HM13	1.34	1.1E-03
TREML2	5.44	1.1E-03
IKBIP	1.84	1.2E-03
ENSA	1.04	1.2E-03
RP11-215G15.5	3.20	1.2E-03
FKBP1A	1.56	1.2E-03
SLC35B1	1.80	1.2E-03
CCT8	1.53	1.2E-03
SLC41A1	1.19	1.2E-03
DPH2	1.66	1.3E-03
PPA1	2.26	1.3E-03
PTGER2	1.44	1.3E-03
BANF1	1.42	1.3E-03
LIG4	1.39	1.3E-03
STARD4	2.03	1.3E-03
SCDP1	3.43	1.3E-03
SLC2A1	1.24	1.3E-03
PPIL1	1.67	1.4E-03
ABAT	1.51	1.4E-03
LGALS3	2.06	1.4E-03
SQRDL	1.38	1.4E-03
BZW2	2.04	1.4E-03
COA4	1.67	1.5E-03
IMPA1	1.78	1.5E-03
FOXP3	5.79	1.5E-03
MTPN	0.90	1.5E-03
EIF2S2P3	2.68	1.5E-03
DDX39A	1.35	1.5E-03
ACTBP2	1.42	1.6E-03
GSG2	4.07	1.6E-03
NOTCH1	1.35	1.6E-03
HOMER1	2.79	1.6E-03
RRBP1	1.82	1.6E-03
AGPAT5	1.70	2.8E-04
RP11-365H23.1	1.80	2.8E-04
RAD23B	1.23	2.9E-04
RHOH	1.21	2.9E-04
FOXP3	6.34	3.0E-04
COPS2	1.53	3.1E-04
ZNF593	3.03	3.1E-04
POLR3D	1.76	3.1E-04
TMEM33	1.29	3.1E-04
EEF1E1	2.33	3.2E-04
GORASP2	1.18	3.2E-04
LYPLA1	1.86	3.2E-04
CD226	2.15	3.4E-04
ELL2P1	3.09	3.4E-04
RSL1D1	1.17	3.5E-04
PLEK	1.73	3.5E-04
RP11-215G15.5	3.40	3.5E-04
PLEKHB2	0.99	3.6E-04
MRPL12	2.24	3.6E-04
CLUH	1.77	3.7E-04
KARS	1.17	3.7E-04
TOP1	1.44	3.7E-04
RBBP8	3.88	3.8E-04
ARF1	0.86	3.9E-04
RDH10	2.83	3.9E-04
PPP2CA	1.03	3.9E-04
EPAS1	4.63	4.0E-04
MAPK13	2.13	4.0E-04
MSC	2.50	4.0E-04
AIMP2	2.99	4.0E-04
CCT8	1.61	4.0E-04
YWHAEP5	2.23	4.0E-04
TIMM44	1.91	4.0E-04
DNAJC3	1.34	4.0E-04
ZMPSTE24	1.50	4.0E-04
FNDC3B	2.26	4.1E-04
AC073869.20	2.03	4.1E-04
UTP11L	2.09	4.2E-04
NOC2L	1.62	4.4E-04
SLC35F2	1.91	4.5E-04
DDX18	1.17	4.6E-04
GOLT1B	1.55	4.7E-04
ABCF2P1	1.69	4.7E-04
GFPT1	1.49	4.8E-04
GADD45A	2.12	4.8E-04
AHSA1	1.45	4.8E-04
ADO	1.34	4.8E-04
TLCD1	5.73	4.9E-04
JAKMIP1	2.98	4.9E-04
TRIB1	4.48	4.9E-04
ADSL	1.81	5.0E-04
NOB1	1.60	5.1E-04
RSL24D1P1	2.61	5.1E-04
EIF5B	1.48	5.1E-04
RP13-383K5.4	2.01	5.1E-04
NDUFV2	2.30	5.1E-04
YWHAEP1	2.26	5.1E-04
RPL22L1	2.19	5.4E-04
MYB	5.92	5.5E-04
TRMT6	1.92	5.6E-04
PEA15	1.19	5.8E-04
RP11-173E2.1	1.62	5.9E-04
GFM1	1.62	5.9E-04
OSTC	1.48	6.0E-04
PSMA7	1.42	6.2E-04
MLF2	1.09	6.3E-04
ALG2	1.28	6.3E-04
SRPR	1.11	6.3E-04
TAF13	2.38	6.4E-04
RAD23A	1.11	6.4E-04
RUVBL1	1.61	6.5E-04
EIF2S2P3	2.79	6.5E-04
PRDX6	1.25	6.5E-04
SUMO1	1.24	6.5E-04
CTD-2256P15.4	2.13	6.6E-04
HIGD1A	1.48	6.6E-04
MAP3K14	1.37	6.7E-04
POP1	2.65	6.7E-04
ANP32B	1.13	6.8E-04
PDAP1	1.33	6.8E-04
APEX1	1.38	6.8E-04
RRP15	1.85	7.2E-04

SLC25A22	1.68	1.6E-03
SRXN1	1.54	1.6E-03
SERP1	1.11	1.6E-03
FAM107B	1.24	1.7E-03
AKR1A1	1.75	1.7E-03
YBX3P1	5.41	1.7E-03
AC104297.1	1.88	1.7E-03
TNIP2	1.34	1.8E-03
FES	5.61	1.8E-03
HBS1L	1.85	1.8E-03
GK	4.04	1.8E-03
ARL1	1.49	1.9E-03
UBE2SP1	2.00	1.9E-03
IPMK	1.72	1.9E-03
PSMB1	1.32	1.9E-03
ARID5B	2.54	2.0E-03
FERMT2	2.57	2.0E-03
YWHAEP5	2.06	2.0E-03
NIP7	1.32	2.0E-03
MTMR2	1.58	2.0E-03
TOMM70A	1.18	2.0E-03
UBE2NL	2.35	2.1E-03
IER3IP1	1.58	2.1E-03
LYPLA1	1.70	2.1E-03
MSMO1	1.36	2.2E-03
AC005795.1	1.19	2.3E-03
VDR	2.71	2.4E-03
SNRPD1	2.09	2.4E-03
PMM2	1.78	2.5E-03
YWHAEP1	2.08	2.5E-03
PSMA7	1.33	2.6E-03
PSMC5	1.15	2.6E-03
CHSY1	1.21	2.6E-03
NIPA2	1.14	2.6E-03
BNIP3P1	2.44	2.6E-03
CCT5P1	2.14	2.6E-03
TXNP4	3.84	2.6E-03
CSNK2A3	1.16	2.7E-03
FAM60A	1.14	2.7E-03
ABCE1	1.48	2.7E-03
AC093724.2	2.06	2.7E-03
G3BP2	0.78	2.7E-03
RIOK3	1.19	2.8E-03
SELT	1.09	2.8E-03
PLAA	1.46	2.9E-03
POTEJ	1.63	2.9E-03
GDI2	0.99	2.9E-03
AK4P1	5.48	2.9E-03
HNRNPA1P10	0.94	3.0E-03
YIPF5	1.19	3.0E-03
AL139819.1	3.33	3.1E-03
MTHFD2P1	5.24	3.1E-03
MKX	5.33	3.1E-03
HSD17B12	1.66	3.1E-03
ARPC1B	1.29	3.1E-03
SYNCRIP	1.12	3.2E-03
COX8A	1.23	3.2E-03
HSPE1	2.02	3.3E-03
LACC1	2.47	3.3E-03
COQ10B	1.40	3.3E-03
MAP3K14	1.27	3.3E-03
SRSF3	1.22	3.4E-03
CKAP4	1.56	3.4E-03
RP13-383K5.4	1.82	3.4E-03
UBE2A	1.24	3.5E-03
ETF1P2	2.01	3.5E-03
RP11-815J4.5	5.24	3.5E-03
CCDC47	1.22	3.5E-03
HNRNPR	1.02	3.5E-03
PGD	1.54	3.6E-03
EBI3	5.06	3.7E-03
CTPS1	1.95	3.7E-03
STAT3	1.25	3.7E-03
ZNRF1	1.74	3.7E-03
RP11-297L17.6	1.26	3.7E-03
IL32	1.46	3.7E-03
CCT5P2	1.90	3.7E-03
HNRNPA1P7	0.89	3.8E-03
KIAA0247	1.06	3.8E-03
CASP4	1.15	3.8E-03
GNE	1.35	3.8E-03
HILPDA	4.02	3.8E-03
CEBPB	1.74	7.2E-04
SRA1	1.72	7.5E-04
SLC38A5	2.78	7.5E-04
AC021224.1	1.10	7.5E-04
CCDC59	1.70	7.5E-04
PITPNB	1.44	7.6E-04
PRPF19	1.36	7.7E-04
RAB21	1.14	7.8E-04
PFN1	1.14	7.8E-04
MTHFD2P1	5.68	7.8E-04
TUFMP1	1.65	7.9E-04
FKBP1C	1.81	7.9E-04
YBX3	4.85	7.9E-04
UTP3	1.45	8.0E-04
HSPA8P1	1.45	8.1E-04
PUF60	1.11	8.2E-04
LMNB1	1.77	8.2E-04
MRPS23	1.91	8.3E-04
G3BP1	1.01	8.3E-04
COX17P1	2.00	8.3E-04
BCCIP	1.75	8.4E-04
ZNF259P1	1.91	8.5E-04
CALM2	1.09	8.6E-04
CCDC124	1.59	8.6E-04
CDC37	1.26	8.8E-04
NPM3	3.27	8.9E-04
ZC3H15	1.41	9.0E-04
CSNK2A1	1.06	9.1E-04
PA2G4	1.17	9.2E-04
GBP5	1.38	9.2E-04
FARSB	2.28	9.4E-04
ARID5B	2.63	9.8E-04
DLD	1.66	9.8E-04
RP11-61N20.3	2.48	1.0E-03
PSMC5	1.19	1.0E-03
TTC4	1.64	1.0E-03
EVI5	6.48	1.0E-03
PSMC2	1.65	1.1E-03
PPIAP31	1.44	1.1E-03
HNRNPKP4	0.84	1.1E-03
IGF2R	1.23	1.1E-03
POLR2H	1.77	1.1E-03
RNF19A	1.49	1.1E-03
SCFD2	2.55	1.1E-03
AC005822.1	1.68	1.1E-03
SERPINB8	1.44	1.1E-03
AC010878.3	1.71	1.1E-03
PPIB	1.19	1.1E-03
API5	0.98	1.1E-03
SRFBP1	2.29	1.1E-03
AC000110.1	2.29	1.1E-03
HNRNPA1	1.05	1.1E-03
MTDH	1.27	1.1E-03
YIF1A	1.77	1.1E-03
PFN1P1	1.20	1.1E-03
GABPB1	1.65	1.1E-03
NUDT15	2.31	1.1E-03
TNIP2	1.35	1.2E-03
NDUFAF4	2.00	1.2E-03
HSP90B2P	1.13	1.2E-03
HNRNPU	0.82	1.2E-03
URB2	1.61	1.2E-03
LYRM1	1.57	1.2E-03
TCEB1	2.06	1.2E-03
XPO1	1.12	1.2E-03
HSP90B1	1.07	1.3E-03
RCC1	1.68	1.3E-03
PTPN7	1.64	1.3E-03
MGAT2	1.07	1.3E-03
PHGDH	5.79	1.3E-03
ECE2	3.35	1.3E-03
POLR1A	1.31	1.3E-03
TRA2B	1.31	1.3E-03
CS	0.99	1.3E-03
SPHK1	4.64	1.3E-03
MZT1	2.28	1.4E-03
C19orf10	2.06	1.4E-03
CCL3L3	5.28	1.4E-03
XPOTP1	1.27	1.4E-03
AMD1	1.22	1.4E-03
AKR1A1	1.75	1.4E-03
DNAJB11	1.46	1.4E-03

EIF2S2P2	2.47	3.8E-03
XRCC6P2	0.92	3.8E-03
EMP1	4.58	3.9E-03
USO1	1.24	4.0E-03
BZW1P1	1.47	4.0E-03
SERPINB1	1.11	4.0E-03
C9orf91	1.53	4.0E-03
CFLAR	1.24	4.1E-03
UBE2V2	1.29	4.1E-03
JUN	1.87	4.1E-03
MED8	1.49	4.1E-03
LMNB1	1.62	4.2E-03
AC002056.3	1.93	4.2E-03
DDOST	1.10	4.2E-03
FTLP3	1.40	4.2E-03
INSIG2	1.45	4.2E-03
DCUN1D5	2.06	4.3E-03
UNC119	1.68	4.4E-03
RPS6KA1	1.07	4.4E-03
SMIM15	1.39	4.4E-03
XRCC5	0.87	4.5E-03
RP11-570P14.1	2.03	4.5E-03
COX6A1	1.34	4.5E-03
FAM129A	0.98	4.6E-03
FBXO6	2.42	4.6E-03
ADORA2A	1.38	4.6E-03
LMNB2	1.21	4.7E-03
ARFGAP3	1.30	4.8E-03
YIF1A	1.63	5.0E-03
GNL2	1.58	5.1E-03
AC026271.5	1.32	5.2E-03
ACTN1	3.51	5.2E-03
MCTP2	1.63	5.2E-03
FABP5P7	3.72	5.3E-03
MAP2K1P1	1.45	5.4E-03
CFL1	0.86	5.4E-03
GABPB1	1.51	5.5E-03
UBE2S	1.98	5.6E-03
AC015987.2	2.38	5.7E-03
EI24	1.43	5.7E-03
DARS	1.40	5.8E-03
GNL3	1.54	5.8E-03
PHGDH	5.24	5.8E-03
TNFRSF4	4.96	5.8E-03
TMEM33	1.11	5.9E-03
DSE	1.84	5.9E-03
SUMO1	1.11	5.9E-03
RP11-737O24.3	1.88	6.0E-03
ALDOAP2	1.57	6.1E-03
DLD	1.50	6.2E-03
CS	0.92	6.3E-03
BTG3	1.81	6.4E-03
SEC11C	1.56	6.4E-03
GPATCH4	1.59	6.4E-03
CTC-444N24.11	1.51	6.4E-03
RP11-295H24.3	1.68	6.6E-03
WDR46	1.44	6.6E-03
RIOK1	1.70	6.8E-03
TIPIN	3.57	6.8E-03
UTP11L	1.78	6.8E-03
GLS	0.86	6.9E-03
ARPC3P1	1.40	6.9E-03
TXNP5	5.06	7.1E-03
IDH3A	1.40	7.1E-03
CAPRIN1	0.91	7.1E-03
SRGN	1.23	7.1E-03
UBE2Z	0.87	7.1E-03
PIGW	2.05	7.2E-03
PIP5K1A	1.17	7.3E-03
NIFK	1.43	7.3E-03
DERL1	0.86	7.3E-03
FKBP1C	1.59	7.4E-03
ARPC2	0.94	7.6E-03
TWISTNB	1.32	7.6E-03
YBX3	4.16	7.6E-03
HSPA8	1.04	7.6E-03
ATP5F1	1.07	7.6E-03
LPXN	0.82	7.6E-03
TIPRL	1.51	7.7E-03
FTL	1.39	7.7E-03
SPCS3	0.87	7.7E-03
SLC31A1	1.75	7.7E-03
HSP90AA4P	1.88	1.4E-03
EIF1AXP1	2.11	1.4E-03
TRAP1	2.15	1.4E-03
VDAC1P2	2.25	1.4E-03
AC015849.14	2.48	1.4E-03
TAF9	1.31	1.5E-03
AC002056.3	2.04	1.5E-03
ECHDC1	1.38	1.5E-03
C19orf48	1.54	1.6E-03
BMS1	1.45	1.6E-03
UQCRFS1	1.26	1.6E-03
DDB1	0.98	1.6E-03
ABCF1	1.19	1.6E-03
TPM3	0.92	1.6E-03
EIF4G2	0.75	1.6E-03
RP11-349K21.1	1.77	1.6E-03
COPG1	1.28	1.7E-03
RP5-850E9.3	2.19	1.7E-03
TIPIN	3.92	1.7E-03
PIP5K1A	1.26	1.7E-03
EAF1	1.15	1.7E-03
PDCD1	1.95	1.7E-03
PPAT	1.89	1.7E-03
B4GALT2	2.45	1.8E-03
NOTCH1	1.33	1.8E-03
MRPS7	1.51	1.8E-03
CCR1	1.44	1.8E-03
SERBP1P6	2.23	1.8E-03
PELO	1.36	1.8E-03
RP11-700P18.1	1.31	1.8E-03
WDR3	1.67	1.9E-03
SLC35B1	1.73	1.9E-03
TRMT10C	1.63	1.9E-03
OTUD4	1.05	1.9E-03
KDM6B	1.34	1.9E-03
RP11-1079K10.4	2.43	1.9E-03
KLHL8	1.65	1.9E-03
MYO1G	1.60	1.9E-03
IRAK2	1.87	1.9E-03
TXNP4	3.88	2.0E-03
MAPK1IP1L	0.99	2.0E-03
SNHG15	1.87	2.0E-03
RP11-75L1.2	1.12	2.0E-03
CSTF2	2.38	2.1E-03
TMEM165	1.55	2.1E-03
PSPH	3.35	2.1E-03
DPM2	1.57	2.1E-03
TALDO1	1.31	2.1E-03
DCAF13P3	2.20	2.2E-03
SLC31A1	1.89	2.2E-03
SF3B14	1.58	2.2E-03
SMIM15	1.43	2.2E-03
EIF2S2P2	2.53	2.2E-03
NAT10	1.43	2.2E-03
SYNGR2	1.03	2.2E-03
EFTUD2	1.27	2.2E-03
NOL10	1.94	2.2E-03
ESF1	2.19	2.3E-03
MRRF	2.01	2.3E-03
SLCO4A1	3.25	2.3E-03
VBP1	1.40	2.3E-03
CACYBPP2	1.56	2.3E-03
CCDC47	1.23	2.3E-03
RP11-819M15.1	1.78	2.4E-03
HSPA8P5	1.49	2.4E-03
SRSF6	1.13	2.4E-03
BZW1P1	1.50	2.4E-03
UBE2MP1	1.49	2.4E-03
ANP32BP1	1.31	2.4E-03
CASP3	1.45	2.4E-03
ATAD3A	2.33	2.4E-03
PGAM5	1.36	2.5E-03
RP11-63E16.1	2.05	2.5E-03
UQCRQ	1.53	2.5E-03
PLAGL1	2.48	2.6E-03
FICD	1.69	2.6E-03
RP1-159M24.1	1.83	2.6E-03
KCTD15	3.02	2.6E-03
SRP54	1.55	2.6E-03
UBE2SP1	1.94	2.6E-03
FTSJ3	1.36	2.6E-03
HMOX1	4.46	2.6E-03

API5	0.89	7.7E-03
WIPI1	2.69	7.8E-03
CHCHD2P9	2.16	7.8E-03
NPM1P39	1.31	7.8E-03
SLC2A3P4	2.52	7.8E-03
RP11-680H20.1	1.13	7.9E-03
CDYL2	2.04	7.9E-03
UQCRFS1	1.15	8.0E-03
CD44	1.22	8.1E-03
TSR1	1.27	8.3E-03
SMAP2	0.94	8.3E-03
AHSA1	1.24	8.3E-03
TMEM167A	1.09	8.4E-03
COPS2	1.28	8.5E-03
HMOX1	4.10	8.5E-03
HAT1	1.49	8.6E-03
STX12	1.49	8.6E-03
MDH1	1.27	8.6E-03
MAGOHB	2.84	8.7E-03
SNRNP27	1.68	8.7E-03
LARP1	0.90	8.8E-03
TRMT6	1.63	8.8E-03
NHP2P1	1.68	8.9E-03
METTL1	2.58	9.1E-03
ABCF1	1.08	9.1E-03
MRPS10	1.24	9.1E-03
ATP6V1C2	1.69	9.2E-03
PPIAP31	1.27	9.2E-03
AC010878.3	1.50	9.3E-03
BUD31	1.50	9.3E-03
TPM3P8	1.40	9.3E-03
MSN	0.83	9.4E-03
HNRNPABP1	1.91	9.5E-03
AC005822.1	1.48	9.5E-03
MFHAS1	1.14	9.6E-03
EPAS1	3.72	9.8E-03
SLC39A1	1.11	9.8E-03
ECHDC1	1.24	9.8E-03
HINT1	0.98	9.9E-03
C15orf38-AP3S2	2.98	1.0E-02
PES1	1.35	1.0E-02
MAGOH2	1.80	1.0E-02
ACTBP11	1.42	1.0E-02
UBE2J1	1.08	1.0E-02
IVNS1ABP	1.14	1.0E-02
TUFM	1.08	1.0E-02
RAD23B	1.02	1.0E-02
SSR1	1.05	1.0E-02
TOP1	1.20	1.0E-02
NOP14	1.49	1.0E-02
CHP1	1.00	1.1E-02
IL18RAP	1.20	1.1E-02
PTPN7	1.42	1.1E-02
SMN2	2.37	1.1E-02
CYP51A1P2	1.67	1.1E-02
MYBL1	1.68	1.1E-02
B4GALT2	2.17	1.1E-02
ANP32AP1	1.50	1.1E-02
RBBP8	3.11	1.1E-02
RP11-512F24.1	1.60	1.1E-02
RP11-311C24.1	1.86	1.1E-02
XRCC6	0.88	1.1E-02
BCAS2	1.56	1.1E-02
POLD2	1.36	1.1E-02
CTB-52I2.4	1.11	1.1E-02
NOL7	1.78	1.1E-02
ZDHHC18	1.23	1.1E-02
SLC25A3	0.83	1.1E-02
PDK1	1.43	1.2E-02
PPP2CB	1.47	1.2E-02
UQCRQ	1.39	1.2E-02
AZIN1	0.96	1.2E-02
NOP58	1.44	1.2E-02
POLR2H	1.52	1.2E-02
PHF5A	1.34	1.2E-02
HSPA1B	1.08	1.2E-02
RSL24D1P1	2.14	1.2E-02
CLN6	1.68	1.2E-02
NPM1P6	1.25	1.2E-02
ARHGEF2	1.12	1.2E-02
FAM98A	1.53	1.2E-02
SF3B14	1.42	1.2E-02
CALCOCO2	1.21	2.6E-03
CMSS1	2.65	2.6E-03
GTF3C6	2.12	2.6E-03
DCUN1D3	1.81	2.6E-03
REL	1.77	2.6E-03
XRCC5	0.88	2.7E-03
ACSL4	1.37	2.8E-03
SBNO2	1.34	2.8E-03
CLN6	1.84	2.8E-03
SRSF2	1.23	2.8E-03
MXD1	1.47	2.9E-03
PUS1	1.83	2.9E-03
PFDN6	1.91	2.9E-03
RP11-417L14.1	3.22	3.0E-03
LDHAP4	1.41	3.0E-03
PPP4R2	1.10	3.0E-03
IFRD1	1.78	3.1E-03
MCM4	1.85	3.1E-03
TMEM39A	1.38	3.1E-03
CTSH	1.64	3.1E-03
RP11-64B16.2	1.59	3.1E-03
CACYBP	1.35	3.2E-03
SLC29A1	3.92	3.2E-03
ALDH18A1	1.35	3.2E-03
CHORDC1	1.52	3.2E-03
TOMM5	1.33	3.3E-03
RP11-416K24.2	1.54	3.3E-03
ARMC6	1.77	3.3E-03
IMP4	1.30	3.3E-03
RP1-232L22__B.1	2.92	3.3E-03
ERH	1.56	3.4E-03
DDX10	1.89	3.4E-03
NDUFB8	1.43	3.5E-03
GSG2	3.81	3.5E-03
RP11-304F15.5	3.29	3.5E-03
TRMT61A	1.78	3.6E-03
USP12PX	2.23	3.7E-03
SLC19A2	2.19	3.7E-03
RBM14	1.08	3.8E-03
SPRED2	3.43	3.8E-03
SLC39A10	1.61	3.9E-03
SERP1	1.05	3.9E-03
FABP5	5.36	3.9E-03
SLC16A6	2.99	3.9E-03
SPCS2P4	1.14	3.9E-03
C20orf24	1.21	3.9E-03
HNRNPD	0.99	4.0E-03
SLC5A6	1.51	4.0E-03
RP11-142L4.2	2.11	4.0E-03
BUD31	1.57	4.0E-03
SMN2	2.54	4.1E-03
IMPAD1	1.13	4.1E-03
MCM2	1.54	4.1E-03
RDX	1.42	4.2E-03
ZHX1	1.39	4.2E-03
GAR1	2.32	4.3E-03
HSPD1P6	2.83	4.3E-03
FAM96B	1.60	4.3E-03
CHSY1	1.16	4.3E-03
LTV1	1.69	4.3E-03
UBE2S	1.99	4.3E-03
LYRM4	2.02	4.4E-03
HPRT1	1.94	4.4E-03
RP11-154D3.1	2.92	4.4E-03
RAB11FIP1	1.05	4.4E-03
RP11-658F2.3	2.74	4.4E-03
SRD5A3	2.07	4.4E-03
APOL6	1.18	4.4E-03
RP11-144L1.8	2.12	4.4E-03
Sep-15	1.09	4.4E-03
SH3BP5	2.40	4.4E-03
AAR2	1.15	4.5E-03
NXT1	1.54	4.5E-03
ACTN1	3.50	4.5E-03
PPRC1	1.27	4.6E-03
GRWD1	1.22	4.7E-03
SRGN	1.26	4.7E-03
HSPBP1	1.64	4.7E-03
TMA16	2.60	4.8E-03
HNRNPDL	1.12	4.8E-03
SLC25A3	0.87	4.9E-03
PFKP	1.57	4.9E-03

MAGT1	1.08	1.2E-02
CHMP2B	1.23	1.2E-02
ATP6V1B2	0.98	1.2E-02
LDHAP3	2.36	1.2E-02
GSTP1	1.20	1.3E-02
ATP6V1E1	1.15	1.3E-02
SRP19	1.44	1.3E-02
SNRPGP15	2.01	1.3E-02
PSMD6	1.21	1.3E-02
HNRNPA1L2	0.94	1.3E-02
TIMM13	1.53	1.3E-02
GNG5	1.61	1.3E-02
AHR	1.56	1.4E-02
IQSEC1	1.01	1.4E-02
RPL7L1	0.97	1.4E-02
CD226	1.69	1.4E-02
HIPK2	1.09	1.4E-02
PDAP1	1.12	1.4E-02
CTD-2528L19.3	2.76	1.4E-02
RP11-566K19.8	1.67	1.4E-02
GTF3C6	1.88	1.4E-02
TMCO1	1.12	1.4E-02
IMMT	1.01	1.4E-02
KARS	0.96	1.5E-02
BAZ1A	1.13	1.5E-02
CRELD2	1.84	1.5E-02
MRPL17	1.43	1.5E-02
LOC124685	1.88	1.5E-02
BRIX1	1.57	1.5E-02
RP11-1079K10.4	2.11	1.5E-02
FKBP11	1.21	1.5E-02
CDC42	0.81	1.5E-02
CAB39	0.82	1.5E-02
POTEI	1.62	1.5E-02
TRIM25	1.00	1.5E-02
PARK7	1.13	1.5E-02
VDAC3	1.19	1.5E-02
ANKRD12	1.34	1.5E-02
COX7A2P2	2.06	1.5E-02
FCHSD2	1.23	1.5E-02
POU2F2	1.67	1.5E-02
AC000110.1	1.91	1.5E-02
RAP2C	1.10	1.6E-02
TMEM70	1.49	1.6E-02
SETP14	0.86	1.6E-02
ZNF593	2.34	1.6E-02
ALAS1	1.30	1.6E-02
MYL6P3	1.81	1.6E-02
RPIA	1.41	1.6E-02
AC018804.7	1.37	1.6E-02
WDR1	0.88	1.6E-02
SLC2A3P2	2.62	1.6E-02
MT2P1	3.23	1.6E-02
IL4R	1.58	1.7E-02
PLAGL2	1.14	1.7E-02
TRAF3IP2	1.64	1.7E-02
ELL2P1	2.38	1.7E-02
C1orf43	0.92	1.7E-02
LARS	1.07	1.7E-02
ATP6V1E1P1	1.36	1.7E-02
FARSA	1.37	1.7E-02
WDR43	1.32	1.7E-02
PCYT1A	0.96	1.7E-02
AC140481.1	1.56	1.7E-02
CDC6	4.59	1.8E-02
SERTAD1	1.39	1.8E-02
GALE	2.49	1.8E-02
GLRX3	1.98	1.8E-02
PDCD10	1.57	1.8E-02
RNF181	1.65	1.8E-02
RP11-309G3.3	3.88	1.8E-02
LMAN2	0.98	1.8E-02
KCNN4	3.30	1.8E-02
RP11-793I11.1	2.47	1.8E-02
AIMP2	2.30	1.9E-02
HSP90AA4P	1.58	1.9E-02
AC004797.1	1.15	1.9E-02
C1GALT1C1	1.43	1.9E-02
NELFE	2.74	2.0E-02
PSMC1	1.68	2.0E-02
SPCS2	1.39	2.0E-02
RP11-325E14.5	2.26	2.0E-02
FTH1P5	2.11	4.9E-03
UMPS	1.57	5.0E-03
IRGQ	1.51	5.1E-03
PITRM1	1.33	5.1E-03
EIF1AX	1.63	5.1E-03
HSPA8P9	1.39	5.2E-03
HDAC2	1.34	5.3E-03
SRR	1.91	5.3E-03
SRSF10	1.12	5.4E-03
KM-PA-2	3.11	5.4E-03
MRPL37	1.49	5.5E-03
HIPK2	1.15	5.5E-03
RARS	1.61	5.5E-03
WDR77	1.64	5.5E-03
ETV5	4.85	5.5E-03
MAPRE1	0.89	5.6E-03
AC005229.7	2.64	5.6E-03
FAM91A1	1.41	5.7E-03
RAB1A	1.16	5.7E-03
UBE2V2	1.25	5.7E-03
LA16c-60H5.7	2.77	5.7E-03
GLRX3	2.16	5.8E-03
CHAC2	3.39	5.8E-03
TREML2	4.77	5.8E-03
PDGFA	4.99	5.8E-03
PAK1IP1	2.34	5.9E-03
C4orf46	1.80	5.9E-03
TMED3	1.50	5.9E-03
MARS2	1.51	5.9E-03
TMEM70	1.59	5.9E-03
ARRB2	1.51	5.9E-03
RNF145	1.00	6.0E-03
AP1AR	1.50	6.1E-03
NUP93	1.49	6.1E-03
MTMR2	1.46	6.1E-03
HBS1L	1.68	6.1E-03
IMMT	1.06	6.1E-03
DHX9	0.91	6.1E-03
TMEM217	5.13	6.1E-03
TRIP10	1.96	6.1E-03
AP000350.4	1.45	6.2E-03
COX6A1	1.29	6.2E-03
TAF4B	2.03	6.3E-03
MYBBP1A	1.51	6.3E-03
QTRTD1	1.39	6.4E-03
TXNP5	5.04	6.4E-03
ARID3B	1.32	6.5E-03
FES	5.03	6.5E-03
SLC27A2	4.94	6.5E-03
LARS	1.14	6.6E-03
FASTKD2	1.47	6.6E-03
SERTAD1	1.49	6.7E-03
METAP2	1.24	6.8E-03
LYN	1.86	6.9E-03
MAGOH2	1.83	7.0E-03
RP11-807E13.3	5.04	7.0E-03
AATF	1.23	7.0E-03
TP53	1.16	7.0E-03
DHX30	1.10	7.1E-03
VDAC3	1.24	7.1E-03
TNFRSF1B	1.42	7.2E-03
PSMD6	1.25	7.2E-03
TPD52	1.29	7.3E-03
RNPS1P1	1.03	7.3E-03
DDX47	1.34	7.4E-03
RRP1	1.82	7.4E-03
UBE2NL	2.13	7.4E-03
DCAF13	1.61	7.5E-03
AGPS	1.30	7.5E-03
DLAT	1.46	7.5E-03
TNPO1	0.91	7.5E-03
HSPA4	1.09	7.5E-03
FAM84B	1.21	7.6E-03
NOL7	1.81	7.8E-03
KCNN4	3.54	7.8E-03
PPP1CC	0.92	7.8E-03
GSTP1	1.23	7.8E-03
UBA2	1.14	7.9E-03
PSMD7P1	1.83	8.0E-03
RP11-815J4.5	4.84	8.2E-03
DHX15	0.96	8.2E-03
MRPS10	1.23	8.2E-03

TXNDC17	2.05	2.1E-02
GTF2A2	1.62	2.1E-02
DDB1	0.84	2.1E-02
CISD1	2.03	2.1E-02
CTD-2256P15.4	1.69	2.1E-02
FAM57A	1.90	2.1E-02
MCM4	1.61	2.1E-02
PIK3AP1	1.92	2.1E-02
PRDX4	1.98	2.1E-02
AC015849.14	2.04	2.2E-02
CALM2	0.90	2.2E-02
CXCL16	2.24	2.2E-02
POLR3D	1.35	2.2E-02
ARF6	0.83	2.2E-02
YES1	1.53	2.2E-02
PPP2R1A	0.86	2.2E-02
MRPL15	1.69	2.2E-02
EMC7	1.39	2.2E-02
KLC2	1.36	2.2E-02
PSMD7P1	1.70	2.2E-02
FAM91A1	1.28	2.2E-02
PGDP1	1.68	2.2E-02
ALDH18A1	1.18	2.2E-02
HIAT1	1.01	2.3E-02
TVP23B	1.36	2.3E-02
MRPL28	1.19	2.3E-02
EEF1E1	1.76	2.3E-02
CHRM3-AS2	2.12	2.3E-02
GNG5P2	1.36	2.3E-02
PSMB7	1.51	2.3E-02
RP11-552O4.2	1.55	2.3E-02
PDIA4	1.02	2.3E-02
PSENEN	1.38	2.3E-02
ESRRA	1.28	2.3E-02
RNF144A-AS1	3.25	2.4E-02
POLR2L	1.25	2.4E-02
NDUFAF4	1.61	2.4E-02
LAMTOR5	1.51	2.4E-02
RP11-64B16.2	1.37	2.4E-02
ZNF267	1.12	2.4E-02
EIF1AXP1	1.70	2.5E-02
RASA2	1.06	2.5E-02
AIFM2	1.91	2.5E-02
NACC1	1.04	2.5E-02
CTB-47B8.5	1.53	2.6E-02
HPRT1	1.69	2.6E-02
MMADHC	1.20	2.6E-02
EIF5B	1.14	2.6E-02
NXT1	1.35	2.6E-02
FDPSP1	1.57	2.6E-02
ASCC3	1.03	2.7E-02
UCHL5	1.36	2.7E-02
YWHAZ	0.75	2.7E-02
TRIB1	3.30	2.7E-02
CHST11	1.02	2.7E-02
ACSL4	1.17	2.7E-02
GPAA1	1.05	2.7E-02
SRSF2	1.05	2.7E-02
SRP72P2	1.41	2.8E-02
RP11-144L1.8	1.82	2.8E-02
WARS2	1.74	2.8E-02
ZNF259P1	1.49	2.8E-02
SCFD2	1.99	2.8E-02
BTG2	1.00	2.9E-02
FAM210A	1.38	2.9E-02
AC125238.2	1.30	2.9E-02
RB1	1.27	2.9E-02
YIPF6	1.27	2.9E-02
SRP9	0.86	2.9E-02
CAMK2D	1.27	2.9E-02
PPP6R1	0.79	2.9E-02
FAM3C2	1.39	2.9E-02
SLC16A6	2.52	2.9E-02
NUCB1	0.88	2.9E-02
AC073869.20	1.52	3.0E-02
GBP2	1.01	3.0E-02
GZMA	1.73	3.0E-02
PDGFA	4.28	3.0E-02
NHP2	1.31	3.0E-02
CDC42P6	0.88	3.0E-02
POP1	2.01	3.0E-02
KIF5B	1.05	3.0E-02
UTP15	1.77	8.2E-03
SLC35D1	1.03	8.2E-03
SNRPEP4	1.83	8.3E-03
RGS1	2.48	8.3E-03
AP1B1	1.06	8.3E-03
NUDC	1.31	8.3E-03
PSMD4	1.31	8.3E-03
COPB2	1.12	8.3E-03
HNRNPLP2	0.87	8.4E-03
OTUD6B	2.17	8.4E-03
WARS2	1.92	8.4E-03
ACTR3P2	1.35	8.6E-03
TSTA3	1.41	8.6E-03
BCL3	1.68	8.6E-03
SLAMF1	1.44	8.7E-03
SPNS3	2.95	8.7E-03
GGCT	1.88	8.7E-03
GTF2H3	1.33	8.8E-03
LDHAP7	1.55	8.8E-03
C12orf44	1.44	8.9E-03
HIVEP1	1.43	9.0E-03
GNA15	3.04	9.0E-03
SEC24A	1.29	9.0E-03
HNRNPK	0.80	9.1E-03
SIGMAR1	1.26	9.1E-03
CISD1	2.16	9.2E-03
DOCK10	1.40	9.2E-03
LARP4P	2.54	9.3E-03
ANP32AP1	1.50	9.3E-03
DNTTIP2	1.03	9.3E-03
TMEM185B	1.28	9.3E-03
TGIF2	1.24	9.3E-03
POLDIP2	1.23	9.4E-03
GMFB	1.24	9.4E-03
FUBP1	1.18	9.5E-03
PUS7	2.61	9.6E-03
ARL1	1.32	9.6E-03
ATP5G1	1.95	9.6E-03
SNRPGP15	2.03	9.7E-03
YME1L1	0.92	9.7E-03
CTB-52I2.4	1.11	9.7E-03
PDCD11	1.15	9.7E-03
SRPK1	1.08	9.7E-03
HSPE1P3	2.54	9.8E-03
NFKBIB	1.46	9.8E-03
IVNS1ABP	1.13	9.9E-03
TIMM8A	2.66	1.0E-02
FAM89A	1.99	1.0E-02
NSUN2	1.14	1.0E-02
PPM1G	1.03	1.0E-02
AEBP2	1.47	1.0E-02
PWP2	1.42	1.0E-02
RAB39B	1.24	1.0E-02
ALAS1	1.32	1.0E-02
DDX10P2	1.98	1.0E-02
TDG	1.37	1.0E-02
CSE1L	1.22	1.1E-02
ENSA	0.90	1.1E-02
HSP90B3P	1.11	1.1E-02
GNG4	4.94	1.1E-02
HS6ST1	1.63	1.1E-02
NBN	1.19	1.1E-02
OAT	1.49	1.1E-02
RPL23	0.98	1.1E-02
PLAA	1.31	1.1E-02
WDR75	1.52	1.1E-02
HPDL	4.73	1.1E-02
LMO4	1.32	1.1E-02
MRPL24	2.05	1.1E-02
AC125238.2	1.39	1.1E-02
EDEM1	0.81	1.1E-02
HSPE1P2	2.44	1.1E-02
DIEXF	1.21	1.1E-02
ALYREF	1.74	1.1E-02
TFDP1	1.59	1.1E-02
SEC11C	1.47	1.2E-02
C6orf211	1.39	1.2E-02
RHOB	2.15	1.2E-02
TCEA1	1.05	1.2E-02
PSMB7	1.58	1.2E-02
STARD7	0.88	1.2E-02
ATP6V1C2	1.63	1.2E-02

KLHL8	1.35	3.1E-02
PYROXD1	1.70	3.1E-02
TXNDC9	1.47	3.1E-02
AC009506.2	1.11	3.1E-02
TUBA1A	1.23	3.1E-02
KCTD10	0.94	3.1E-02
CD48	0.98	3.1E-02
ERAP2	1.08	3.1E-02
ZMPSTE24	1.14	3.2E-02
ZDHHC16	1.66	3.2E-02
SPHK1	3.54	3.2E-02
DLEU2	4.20	3.3E-02
TMED3	1.31	3.3E-02
PNPT1P1	1.70	3.3E-02
ARFIP1	1.47	3.3E-02
RP11-417L14.1	2.62	3.3E-02
RNASEK-C17orf49	2.13	3.4E-02
PDE4B	1.02	3.4E-02
CHAC2	2.88	3.4E-02
TLCD1	4.15	3.4E-02
TBXAS1	2.35	3.4E-02
RABGGTB	1.25	3.4E-02
CD55	1.22	3.4E-02
AC005229.7	2.26	3.4E-02
CLPP	1.30	3.4E-02
PJA1	1.07	3.4E-02
LYPLA2	1.01	3.4E-02
NTRK2	3.81	3.5E-02
OAT	1.35	3.5E-02
POMP	2.18	3.5E-02
ECE2	2.56	3.5E-02
SBDS	1.03	3.6E-02
SET	0.74	3.6E-02
DAD1	0.93	3.6E-02
FAM3C	1.32	3.6E-02
RP11-334A14.2	1.85	3.6E-02
MMP25	2.29	3.6E-02
SH2D1A	1.10	3.6E-02
IL1RL1	3.83	3.6E-02
GAPDHP71	2.49	3.6E-02
EFTUD2	1.04	3.6E-02
RAD23A	0.87	3.7E-02
CSGALNACT2	0.96	3.7E-02
MRPL12	1.61	3.7E-02
ATP5G1	1.73	3.7E-02
HSPA8P1	1.11	3.8E-02
TMED10	0.68	3.8E-02
RP11-63E16.1	1.65	3.8E-02
RP11-154D3.1	2.42	3.8E-02
MYCBP	1.18	3.8E-02
B4GALT3	0.99	3.8E-02
NOL10	1.56	3.8E-02
VAPA	0.90	3.8E-02
SPPL2A	1.69	3.9E-02
COX7A2	1.52	3.9E-02
SLC25A5P2	1.71	3.9E-02
NUP188	1.04	3.9E-02
VDAC2	1.32	3.9E-02
TTC4	1.27	3.9E-02
NSFL1C	1.16	3.9E-02
C4orf46	1.54	3.9E-02
POLR2D	1.22	3.9E-02
PITPNB	1.10	3.9E-02
C5orf28	1.50	3.9E-02
DNTTIP2	0.92	4.0E-02
UBA6	1.08	4.0E-02
CHORDC1	1.25	4.0E-02
PANK3	0.82	4.1E-02
RP11-350G8.7	1.65	4.1E-02
NDRG1	1.06	4.1E-02
SUMO2	0.99	4.2E-02
RP11-142L4.3	1.30	4.2E-02
TP53INP2	2.35	4.2E-02
XPO1	0.89	4.2E-02
PDE4D	0.89	4.3E-02
KIF2A	0.88	4.3E-02
UBE2E1	1.16	4.3E-02
UBA2	1.00	4.3E-02
TMED8	1.02	4.4E-02
ALYREF	1.54	4.5E-02
RAB5A	1.02	4.5E-02
ADPRH	1.84	4.5E-02
POLR1C	1.56	1.2E-02
PA2G4P2	1.58	1.2E-02
HSD17B12	1.48	1.2E-02
GAPDHP60	1.24	1.2E-02
EIF3A	0.80	1.2E-02
SDF2L1	1.81	1.2E-02
VAPA	0.98	1.2E-02
AC026271.5	1.22	1.3E-02
C17orf51	1.73	1.3E-02
KIF5B	1.12	1.3E-02
INO80B	1.52	1.3E-02
PICALM	0.90	1.3E-02
IL21R	1.98	1.3E-02
HSPD1P5	4.84	1.3E-02
SLC25A19	2.21	1.3E-02
STAT4	1.23	1.3E-02
BCAS2	1.52	1.3E-02
LACC1	2.18	1.3E-02
MDH1	1.21	1.3E-02
YBX1P2	1.64	1.3E-02
PSMA5	1.39	1.3E-02
TIPRL	1.43	1.3E-02
PPP1CB	1.03	1.3E-02
CYB5B	0.98	1.3E-02
GNAI3	0.96	1.3E-02
MTPN	0.78	1.4E-02
VDAC2	1.43	1.4E-02
RP11-507E23.1	1.59	1.4E-02
PABPC4	1.00	1.4E-02
NUDT4	1.10	1.4E-02
EMP1	4.04	1.4E-02
POU2F2	1.67	1.4E-02
PIGV	1.39	1.4E-02
PHBP8	2.58	1.4E-02
FAM60CP	1.60	1.4E-02
C1orf109	1.30	1.4E-02
C16orf87	1.97	1.4E-02
GTF2A2	1.65	1.4E-02
SRP72P2	1.47	1.4E-02
P4HB	0.75	1.4E-02
RPN2	1.01	1.4E-02
RP11-325E14.5	2.30	1.4E-02
NLN	3.93	1.4E-02
AC013460.1	4.67	1.5E-02
EIF2S3L	0.91	1.5E-02
AC064850.4	1.25	1.5E-02
RP11-512F24.1	1.54	1.5E-02
TTC1	1.17	1.5E-02
RP11-119N19.1	2.47	1.5E-02
CHCHD2P9	2.02	1.5E-02
UPP1	1.46	1.5E-02
DUSP2	1.61	1.5E-02
P2RX5-TAX1BP3	2.08	1.5E-02
MBD2	1.07	1.5E-02
RP11-295H24.3	1.55	1.5E-02
SRRT	1.08	1.5E-02
PDF	3.93	1.5E-02
DDX1	1.84	1.5E-02
NSFL1C	1.25	1.5E-02
RPS6KA2	1.72	1.5E-02
AC097711.1	3.89	1.5E-02
HM13	1.12	1.5E-02
AC005523.2	1.33	1.5E-02
POMP	2.34	1.5E-02
C17orf58	3.41	1.5E-02
DDOST	0.99	1.6E-02
GSPT1	0.89	1.6E-02
DDX49	1.62	1.6E-02
MTHFD1P1	1.77	1.6E-02
FAM46C	0.92	1.6E-02
TIMM9	1.84	1.6E-02
TNFRSF25	0.99	1.6E-02
NDUFAB1	2.00	1.6E-02
EIF2B3	2.86	1.6E-02
AGMAT	3.40	1.6E-02
HEATR1	1.11	1.6E-02
HNRNPRP1	1.31	1.6E-02
MAGOHB	2.64	1.6E-02
NTRK2	4.10	1.7E-02
NUTF2	1.23	1.7E-02
SRF	0.87	1.7E-02
BTG3	1.64	1.7E-02

MORF4L1P1	0.76	4.5E-02
PSMA5	1.25	4.5E-02
FUBP1	1.04	4.5E-02
ARPC3	1.09	4.5E-02
COX7A2L	0.94	4.5E-02
NDUFAB1	1.82	4.5E-02
UBE2V1P2	1.34	4.5E-02
FARSB	1.69	4.6E-02
RP11-473I1.9	1.36	4.6E-02
SSRP1	0.84	4.6E-02
ZC3H15	1.07	4.6E-02
TRA2B	1.01	4.6E-02
RP11-465B22.3	3.55	4.6E-02
BOLA2B	1.62	4.7E-02
RANBP1	1.44	4.7E-02
DBNL	0.91	4.7E-02
NIPA1	1.03	4.7E-02
ERH	1.26	4.7E-02
UBE2M	1.28	4.8E-02
CSNK1A1	0.84	4.8E-02
RNF41	1.00	4.8E-02
SRD5A3	1.68	4.8E-02
DHDDS	1.21	4.8E-02
SF3B4	0.90	4.8E-02
CLIP1	0.94	4.8E-02
KCTD20	0.77	4.9E-02
ABCF2P1	1.22	4.9E-02
PSMD4	1.13	4.9E-02
CHUK	1.23	4.9E-02
AC013269.1	1.41	4.9E-02
LLPH	1.27	4.9E-02
SRSF6	0.90	4.9E-02
ESF1	1.68	4.9E-02
BCAS2P2	1.49	5.0E-02
DCP1A	0.90	1.7E-02
LRPPRC	1.11	1.7E-02
PRELID1	1.20	1.7E-02
RNPS1	0.89	1.7E-02
KCNK5	4.28	1.7E-02
ITPA	1.70	1.7E-02
HNRNPM	0.91	1.7E-02
MIR22HG	1.68	1.7E-02
TMED7	1.07	1.7E-02
POLR2L	1.27	1.7E-02
PPIAP29	1.33	1.7E-02
CYP51A1	1.17	1.8E-02
VTA1	1.10	1.8E-02
BOLA2B	1.76	1.8E-02
MRPS35	1.39	1.8E-02
PWP1	1.37	1.8E-02
OXSR1	0.99	1.8E-02
MRPL36	1.53	1.8E-02
NUP35	1.95	1.8E-02
SELT	0.95	1.9E-02
IMPA1	1.46	1.9E-02
RP11-443N24.1	1.67	1.9E-02
SLC39A6	0.97	1.9E-02
GNG2	0.95	1.9E-02
DESI2	1.00	1.9E-02
RP11-345J4.5	2.30	1.9E-02
MRPS28	1.82	1.9E-02
ALG3	1.54	1.9E-02
CD320	1.53	2.0E-02
PLRG1	1.26	2.0E-02
POLR3G	3.46	2.0E-02
GTF2F2	1.79	2.0E-02
C5orf28	1.59	2.0E-02
MYCBP	1.23	2.0E-02
UTP20	1.44	2.0E-02
GALE	2.42	2.1E-02
GMPPB	1.33	2.1E-02
VAV1	1.38	2.1E-02
SLC9B2	1.60	2.1E-02
ESRRA	1.28	2.1E-02
STOML2	1.59	2.1E-02
LDHAP2	1.57	2.1E-02
TFB2M	1.82	2.1E-02
NELFE	2.68	2.1E-02
RHOA	0.73	2.2E-02
LCLAT1	1.48	2.2E-02
OTUD5	0.95	2.2E-02
PDE12	1.01	2.2E-02
PTPN2P1	1.47	2.2E-02
MRPS16	1.04	2.2E-02
PNPT1	1.82	2.3E-02
SBDS	1.06	2.3E-02
RUVBL2	1.60	2.3E-02
RP4-647J21.1	2.12	2.3E-02
RP11-629O4.1	4.62	2.3E-02
GPR114	1.41	2.3E-02
SNX10	1.60	2.3E-02
ZNF259	1.46	2.3E-02
B4GALT3	1.03	2.3E-02
CBX6	0.82	2.3E-02
RNASEK-C17orf49	2.18	2.3E-02
UBE2D3P2	1.82	2.3E-02
EMG1	1.29	2.3E-02
PPAN	1.34	2.3E-02
SRP9	0.87	2.4E-02
RRP9	2.64	2.4E-02
NAA25	1.19	2.4E-02
ATP5F1	0.97	2.4E-02
PRDX4	1.93	2.4E-02
UTP14A	1.51	2.4E-02
AZIN1	0.90	2.4E-02
GRPEL2	1.12	2.4E-02
NMD3	1.34	2.4E-02
DDX56	1.32	2.4E-02
EXOSC5	2.21	2.5E-02
RPF1	1.46	2.5E-02
DRG1	1.56	2.5E-02
SRP19	1.33	2.5E-02
PTRH2	1.46	2.5E-02
PARVB	1.99	2.5E-02
C12orf23	1.10	2.5E-02
CLTC	0.78	2.5E-02

IPO7P2	1.25	2.5E-02
MEMO1P1	1.41	2.5E-02
GNG5	1.49	2.5E-02
SLC25A5P2	1.76	2.5E-02
DARS	1.22	2.5E-02
ACOT7	2.55	2.6E-02
DOT1L	1.30	2.6E-02
RPS6KA1	0.93	2.6E-02
RP11-311C24.1	1.69	2.6E-02
RP11-10L12.2	3.30	2.6E-02
LLPH	1.33	2.6E-02
CIRH1A	2.19	2.6E-02
COPS3	1.35	2.6E-02
DDHD1	1.20	2.6E-02
CLPB	2.08	2.7E-02
TXNDC17	1.97	2.7E-02
STAT3	1.05	2.7E-02
RP11-467J12.1	2.31	2.7E-02
CPEB4	1.26	2.8E-02
GPI	0.95	2.8E-02
COQ10B	1.17	2.8E-02
PPP2CB	1.33	2.8E-02
ACO2	1.24	2.8E-02
MCTP2	1.39	2.8E-02
RCC2P6	1.63	2.8E-02
MMADHC	1.17	2.8E-02
ILF2P1	2.18	2.8E-02
RP1-305B16.3	2.42	2.9E-02
RCL1	1.61	2.9E-02
ESPL1	4.50	2.9E-02
RP11-49C9.2	1.18	2.9E-02
MAPKAPK3	1.13	2.9E-02
PHLDA1	1.49	2.9E-02
HSPA8P8	1.37	2.9E-02
RP11-373L24.1	1.85	2.9E-02
NLE1	1.44	2.9E-02
SHFM1	1.67	2.9E-02
HNRNPLL	1.25	2.9E-02
PSMC1	1.59	2.9E-02
TGS1	1.06	3.0E-02
SSR3	1.01	3.0E-02
KPNA3	0.97	3.0E-02
TP53BP2	1.02	3.0E-02
NEDD9	1.32	3.0E-02
PPP5C	1.32	3.1E-02
KIF2A	0.90	3.1E-02
SSB	1.27	3.1E-02
RIOK3	0.98	3.1E-02
POLR3H	0.96	3.1E-02
PRR5L	1.23	3.1E-02
PRPF4	1.13	3.1E-02
SYP	4.62	3.2E-02
RP11-350G8.7	1.67	3.2E-02
PCYT1A	0.90	3.2E-02
IER3IP1	1.26	3.2E-02
SLC19A1	1.93	3.2E-02
SEMA4A	2.20	3.2E-02
AC015987.2	1.99	3.2E-02
KSR1	1.55	3.2E-02
ARL5A	1.14	3.2E-02
GLA	1.76	3.3E-02
KCNQ5	3.82	3.3E-02
RP11-680A11.5	4.33	3.3E-02
ZNF281	1.00	3.3E-02
FOSB	2.55	3.3E-02
TMCO1	1.02	3.3E-02
GDI2	0.82	3.4E-02
RP11-496I2.5	2.50	3.4E-02
MRPL4	1.43	3.4E-02
DHX9P1	0.91	3.4E-02
MRPS18A	1.55	3.4E-02
TMEM167A	0.95	3.4E-02
RP11-793I11.1	2.27	3.4E-02
RP11-334A14.2	1.83	3.4E-02
RP11-473I1.9	1.38	3.4E-02
SCDP1	2.56	3.5E-02
CTB-47B8.5	1.45	3.5E-02
URM1	1.03	3.5E-02
FTH1P12	2.14	3.6E-02
GPAA1	1.00	3.6E-02
MRPL13	1.83	3.6E-02
SNHG3	1.53	3.6E-02

GDAP1	2.33	3.6E-02
BTG2	0.97	3.6E-02
TOMM6	1.09	3.7E-02
ADAM8	0.98	3.7E-02
SLC25A33	2.11	3.7E-02
NSRP1	1.30	3.7E-02
SFPQ	0.95	3.7E-02
CTD-2314B22.3	4.36	3.7E-02
LONRF1	1.58	3.8E-02
MCUR1	1.41	3.8E-02
MRPL51	1.22	3.8E-02
MT2A	1.92	3.8E-02
KRR1	1.07	3.8E-02
PDIA3	0.97	3.9E-02
UCHL5	1.29	3.9E-02
IRAK1	0.96	4.0E-02
FASTKD1	1.87	4.0E-02
PTGES3P1	0.92	4.0E-02
AUP1	0.91	4.0E-02
BTF3	0.80	4.0E-02
SACS	0.99	4.0E-02
ATP5C1	1.26	4.0E-02
NAB1	1.12	4.0E-02
CHCHD3P3	1.61	4.1E-02
EIF4A1P7	2.40	4.1E-02
STT3A	0.90	4.1E-02
CDC6	4.08	4.1E-02
MIR29A	3.06	4.2E-02
DPY19L1	1.13	4.2E-02
SUB1P3	2.40	4.2E-02
USP12PY	2.56	4.2E-02
AC016732.2	1.77	4.3E-02
USP10	0.96	4.3E-02
ME2	1.23	4.3E-02
NCLP1	1.71	4.3E-02
ZNF267	1.04	4.3E-02
FBXO6	1.93	4.3E-02
CLPP	1.24	4.3E-02
KIF21B	0.98	4.3E-02
LSM12	1.19	4.4E-02
PSMA2	1.15	4.4E-02
RTCB	1.08	4.4E-02
AIFM2	1.76	4.4E-02
IPO8P1	1.24	4.4E-02
FUS	0.92	4.4E-02
FLAD1	1.11	4.5E-02
TUBBP1	1.04	4.5E-02
RRP1B	0.90	4.6E-02
SCAMP3	1.03	4.6E-02
SMIM13	1.26	4.6E-02
IL1RL1	3.65	4.6E-02
NDUFAF2	2.18	4.6E-02
RP5-837I24.1	1.59	4.7E-02
SNRNP27	1.41	4.7E-02
ASCC3	0.96	4.7E-02
RRP7A	0.96	4.7E-02
ECE1	1.38	4.8E-02
TMEM126A	1.99	4.8E-02
NIFKP6	2.10	4.8E-02
GPN3	1.80	4.8E-02
RPL5P29	2.77	4.8E-02
C1orf216	1.23	4.8E-02
HAT1	1.25	4.9E-02
CCDC58P3	3.98	4.9E-02
B4GALT4	1.63	4.9E-02
EMC7	1.26	4.9E-02
RP5-940J5.9	1.32	4.9E-02
FCF1	1.05	4.9E-02
NUTF2P2	1.70	4.9E-02
COX5A	1.52	4.9E-02
PYROXD1	1.58	4.9E-02
TMX1	1.10	4.9E-02
TTC27	1.77	4.9E-02
SSBP1	1.68	4.9E-02
ATIC	1.19	4.9E-02
PDCD10	1.39	4.9E-02
SLC39A1	0.95	4.9E-02
CCT7P1	2.06	4.9E-02
PLK3	1.39	4.9E-02
CKS2	2.56	4.9E-02
AC016734.2	1.07	5.0E-02
MPHOSPH10	1.20	5.0E-02

9. List of publications

-Leng T, Akther HD, Hackstein CP, Powell K, King T, Friedrich M, Christoforidou Z, McCuaig S, Neyazi M, Arancibia-Cárcamo CV, Hagel J, Powrie F; Oxford IBD Investigators, Peres RS, Millar V, Ebner D, Lamichhane R, Ussher J, Hinks TSC, Marchi E, Willberg C, Klenerman P. TCR and Inflammatory Signals Tune Human MAIT Cells to Exert Specific Tissue Repair and Effector Functions. Cell Rep. 2019 Sep 17;28(12):3077-3091.e5. doi: 10.1016/j.celrep.2019.08.050. PMID: 31533032; PMCID: PMC6899450.

-Buckland MS, Galloway JB, Fhogartaigh CN, Meredith L, Provine NM, Bloor S, Ogbe A, Zelek WM, Smielewska A, Yakovleva A, Mann T, Bergamaschi L, Turner L, Mescia F, Toonen EJM, Hackstein CP, Akther HD, Vieira VA, Ceron-Gutierrez L, Periselneris J, Kiani-Alikhan S, Grigoriadou S, Vaghela D, Lear SE, Török ME, Hamilton WL, Stockton J, Quick J, Nelson P, Hunter M, Coulter TI, Devlin L; CITIID-NIHR COVID-19 BioResource Collaboration; MRC-Toxicology Unit COVID-19 Consortium, Bradley JR, Smith KGC, Ouwehand WH, Estcourt L, Harvala H, Roberts DJ, Wilkinson IB, Screaton N, Loman N, Doffinger R, Lyons PA, Morgan BP, Goodfellow IG, Klenerman P, Lehner PJ, Matheson NJ, Thaventhiran JED. Treatment of COVID-19 with remdesivir in the absence of humoral immunity: a case report. Nat Commun. 2020 Dec 14;11(1):6385. doi: 10.1038/s41467-020-19761-2. PMID: 33318491; PMCID: PMC7736571.

-Poster at EMBO workshop: CD1/MR1-restricted T lymphocytes

Article

Cell Reports

TCR and Inflammatory Signals Tune Human MAIT Cells to Exert Specific Tissue Repair and Effector Functions

Graphical Abstract

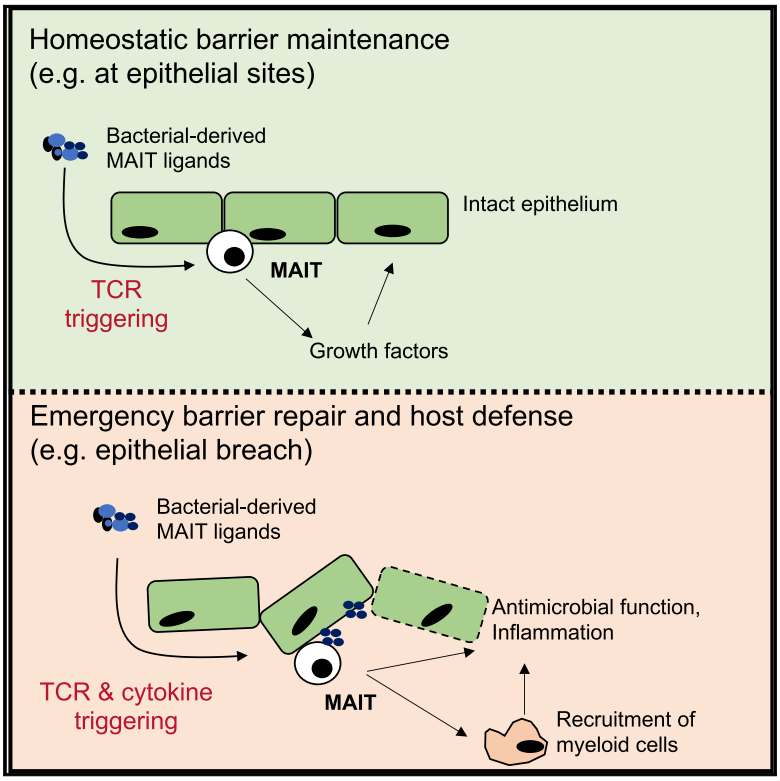

Highlights

- Activation of human MAIT cells is TCR-dependent or TCR-independent and enhanced by TL1A
- TCR-dependent and TCR-independent triggering induces distinct transcriptional responses
- TCR-dependent triggering of MAIT cells induces a tissue-repair program
- Data integration with *in vivo* studies in mice indicates a shared transcriptome

Authors

Tianqi Leng, Hossain Delowar Akther, Carl-Philipp Hackstein, ..., Emanuele Marchi, Chris Willberg, Paul Klenerman

Correspondence

paul.klenerman@medawar.ox.ac.uk

In Brief

Leng et al. explore the consequences of activation of human MAIT cells via their TCR and/or cytokines, including the gut-associated TNF-superfamily member TL1A. TCR triggering reveals a transcriptional program linked to tissue-repair functions seen *in vivo*, consistent with a homeostatic role for these cells in epithelia.

Leng et al., 2019, Cell Reports *28*, 3077–3091
September 17, 2019
https://doi.org/10.1016/j.celrep.2019.08.050

CellPress

Cell Reports
Article

TCR and Inflammatory Signals Tune Human MAIT Cells to Exert Specific Tissue Repair and Effector Functions

Tianqi Leng,[1,9] Hossain Delowar Akther,[1,3,9] Carl-Philipp Hackstein,[1,3,9] Kate Powell,[1,5] Thomas King,[1] Matthias Friedrich,[2] Zoe Christoforidou,[3] Sarah McCuaig,[2] Mastura Neyazi,[2] Carolina V. Arancibia-Cárcamo,[3] Joachim Hagel,[1] Fiona Powrie,[2] Oxford IBD Investigators,[3] Raphael Sanches Peres,[2] Val Millar,[4] Daniel Ebner,[4] Rajesh Lamichhane,[5] James Ussher,[5] Timothy S.C. Hinks,[6,7,8] Emanuele Marchi,[1] Chris Willberg,[1] and Paul Klenerman[1,3,6,10,*]

[1]Peter Medawar Building for Pathogen Research, South Parks Road, Oxford OX1 3SY, UK
[2]The Kennedy Institute of Rheumatology, Roosevelt Dr., Oxford OX3 7FY, UK
[3]Translational Gastroenterology Unit, Nuffield Department of Medicine, University of Oxford, Oxford OX3 9DU, UK
[4]Target Discovery Institute, Roosevelt Dr., Oxford OX3 7FZ, UK
[5]Department of Microbiology and Immunology, University of Otago, Otago, New Zealand
[6]NIHR Biomedical Research Centre, John Radcliffe Hospital, Oxford OX3 9DU, UK
[7]Respiratory Medicine Unit, Nuffield Department of Medicine Experimental Medicine, University of Oxford, Oxford OX3 9DU, UK
[8]Department of Microbiology and Immunology, Peter Doherty Institute for Infection and Immunity, University of Melbourne, Melbourne, VIC 3000, Australia
[9]These authors contributed equally
[10]Lead Contact
*Correspondence: paul.klenerman@medawar.ox.ac.uk
https://doi.org/10.1016/j.celrep.2019.08.050

SUMMARY

MAIT cells are an unconventional T cell population that can be activated through both TCR-dependent and TCR-independent mechanisms. Here, we examined the impact of combinations of TCR-dependent and TCR-independent signals in human CD8$^+$ MAIT cells. TCR-independent activation of these MAIT cells from blood and gut was maximized by extending the panel of cytokines to include TNF-superfamily member TL1A. RNA-seq experiments revealed that TCR-dependent and TCR-independent signals drive MAIT cells to exert overlapping and specific effector functions, affecting both host defense and tissue homeostasis. Although TCR triggering alone is insufficient to drive sustained activation, TCR-triggered MAIT cells showed specific enrichment of tissue-repair functions at the gene and protein levels and in *in vitro* assays. Altogether, these data indicate the blend of TCR-dependent and TCR-independent signaling to CD8$^+$ MAIT cells may play a role in controlling the balance between healthy and pathological processes of tissue inflammation and repair.

INTRODUCTION

Human innate and adaptive immune systems form a critical partnership in immune defense against microorganisms. Studies have revealed several types of unconventional T lymphocytes that sit at the bridge between innate and adaptive immunity, including mucosal-associated invariant T (MAIT) cells (Godfrey et al., 2015). MAIT cells are abundant in human blood and enriched most substantially in the liver (Dusseaux et al., 2011). They are marked by high surface expression of the C-type lectin molecule CD161, and they bear the semi-invariant T cell receptor (TCR) Vα7.2-Jα33/12/20, which restricts them to the evolutionary conserved, non-polymorphic major histocompatibility complex (MHC) class I-related protein 1 (MR1) (Kjer-Nielsen et al., 2012; Reantragoon et al., 2013). MAIT cells recognize microbially derived riboflavin synthesis intermediates presented by MR1 (López-Sagaseta et al., 2013; Ussher et al., 2014a). MR1 tetramers loaded with riboflavin and folate intermediates have been developed, enabling the specific detection and characterization of human and mouse MAIT cells (López-Sagaseta et al., 2013; Rahimpour et al., 2015; Reantragoon et al., 2013).

Despite this specific antigen recognition as an effector T cell, MR1-TCR signaling alone is insufficient to fully activate MAIT cells (Turtle et al., 2011). To achieve sufficient activation, TCR signaling is supported by other costimulatory signals, such as CD28, and by cytokines, such as interleukin (IL)-18 and IL-12 (Ussher et al., 2014b). This is true in mouse cells examined *in vivo*. Normal expansion is only seen if ligand is delivered with a toll-like receptor (TLR) stimulus (Chen et al., 2017).

This behavior has prompted investigation into the responsiveness of MAIT cells to innate signals, including IL-12, IL-18, IL-15, and type I interferons (IFNs) (Sattler et al., 2015; Ussher et al., 2014b; van Wilgenburg et al., 2016). *In vitro* studies in human cells have shown that cytokines such as IL-12 and IL-18 can, in combination, activate MAIT cells in a fully TCR-independent manner (Ussher et al., 2014b). Cytokine-stimulated

$CD161^{2+}CD8^+$ T cells, including MAIT cells, may exert effector functions by secretion of cytokines and upregulation of granzyme (Gr) B (Billerbeck et al., 2010; Kurioka et al., 2015). We and others have highlighted a role for MAIT cells in viral infections, in which MAIT cell activation was TCR independent but depended on IL-18 in synergy with IL-12, IL-15, and/or the type I interferons IFN-α/β (Loh et al., 2016; van Wilgenburg et al., 2016), with a critical protective role *in vivo* (Wilgenburg et al., 2018). Thus, it is clear that MAIT cells can be activated via TCR-dependent and TCR-independent pathways. However, the diversity of functions triggered by different cytokines compared with those triggered by TCR signaling has yet to be defined.

The specific functions of MAIT cells elicited by cytokines are particularly relevant in mucosal tissues, such as the gut, where local signaling may be critical in defining the balance between host defense responses and tolerance. Data on IL-17-expressing skin-homing mouse $CD8^+$ T cells, an innate-like T cell population that mirrors some critical features of MAIT cells, indicate that they display a tissue-repair phenotype rather than a pure inflammatory phenotype in response to TCR triggering via commensal-associated ligands (formyl peptides restricted by H2M3) (Linehan et al., 2018). The authors propose that responses to commensals driven by TCR could support a role for such T cells in tissue homeostasis. This behavior may extend to more broadly include innate-like T cells restricted by MHC1b molecules, which are evolutionarily ancient (Klenerman and Ogg, 2018).

Tumor necrosis factor (TNF)-like protein 1A (TL1A)/TNF superfamily member 15 (TNFSF15) is a gut-associated proinflammatory cytokine originally characterized in a screen for TNF-α homologous molecules. It is expressed by activated T cells, dendritic cells, and monocytes and signals through death receptor-3 (DR3) (Meylan et al., 2008; Migone et al., 2002; Shih et al., 2009). TL1A is particularly relevant because it has previously been described as activating a subset of $CD4^+$ memory T cells expressing IL-18Rα and DR3 (Holmkvist et al., 2015). More specifically, it has been shown to increase production of IFN-γ and TNF-α by $CD161^+CD4^+$ T cells in the presence of anti-CD3 or IL-12+IL-18 (Jin et al., 2013). This may be relevant to MAIT cell functions, because we have previously identified a phenotypic, functional, and transcriptional program shared by CD161-expressing cells (Fergusson et al., 2014).

Here, we addressed how TCR-dependent and TCR-independent signals synergize and drive the activation of *in vitro* blood- and gut-derived MAIT cells. We find that IL-12 and IL-18, in synergy with TCR triggering, promote the activation of MAIT cells and that additional TL1A signaling can optimize this response in a dose-dependent manner. Triggering with TCR alone or supported by cytokines drives a set of functions linked to a tissue-repair gene expression signature, accompanied by relevant protein expression and function. Overall, our data provide insight into the precise nature of TCR- and cytokine-mediated human MAIT cell activation, characterized by a range of effector functions including not only emergency host defense but also ongoing homeostasis maintenance. This feature may be relevant to other innate-like T cell subsets found at barrier sites in humans.

RESULTS

TL1A and IL-15 Enhance Effector Functions of Human MAIT Cells

To explore the full impact of cytokine triggering of MAIT cells, we first examined extended combinatorial signaling. The ability of TL1A and IL-15 to promote T cell activation in the presence of a suboptimal IL-12 and IL-18 trigger has been shown in the CD161-expressing $CD4^+$ T cells (Sattler et al., 2009; Cohavy et al., 2011; Jin et al., 2013; Holmkvist et al., 2015; Sattler et al., 2015). We therefore addressed whether MAIT cells possess similar responsiveness.

TL1A triggered MAIT cell activation (as judged by expression of IFN-γ, TNF-α, and granzyme B) in combination with suboptimal doses of IL-12 and IL-18 in a dose-dependent manner (Figures 1A–1C). Expression of IFN-γ, TNF-α, and granzyme B by stimulated MAIT cells from a representative donor is shown in Figure 1D. IL-15 (50 ng/mL), TL1A (100 ng/mL), or the combination of both markedly promoted IL-12 (2 ng/mL)/IL-18 (50 ng/mL)-induced MAIT cell activation, measured by MAIT cell expression of IFN-γ, TNF-α, GrB, and CD69 (Figures 1E–1H).

Overall, we found that TL1A and IL-15 individually increased MAIT cell expression of IFN-γ and TNF-α and upregulated GrB and CD69 expression. IL-15 was more potent than TL1A when added singly to the IL-12+IL-18 culture, but the peak level of MAIT cell activation was achieved by a combination of both cytokines in the presence of IL-12 and IL-18. This combination was therefore used in downstream experiments. TL1A and IL-15 alone do not promote MAIT cell effector functions and have only a limited effect on $CD161^+$ and $CD161^-$ $CD8^+$ T cells (Figure S1).

MAIT Cells Respond to Combinations of Cytokines and TCR Triggering and Enhance Effector Functions in a Dose-Dependent Manner

Studies have addressed the hypo-responsiveness of $CD8^+$ MAIT cells to anti-CD3 by comparing their ability to proliferate and produce cytokines *in vitro* to their $CD161^-$ $CD8^+$ counterparts (Turtle et al., 2011). We hypothesized that this could result from a lack of complementary inflammatory signals. Thus, we first asked how TCR and cytokine signaling combined (Figure 2). For these experiments, we used the optimized MR1 ligand 5-OP-RU and compared this to anti-CD3/CD28 bead stimulations.

Enriched $CD8^+$ T cells were stimulated by suboptimal concentrations of IL-12 (2 ng/mL) and IL-18 (50 ng/mL) with or without TL1A and/or IL-15 in combination with 5-OP-RU (Figures 2A–2E). TCR signaling via 5-OP-RU had a profound synergy with added cytokines—with the major impact from IL-12 and IL-18—as measured by release of IFN-γ and TNF-α and upregulation of GrB, and CD69 (representative histograms in Figure 2A and combined data in Figures 2B–2E).

We repeated these protocols using anti-CD3/CD28 beads as the TCR trigger (Figures 2F–2J). The frequency of MAIT cells that responded to anti-CD3/CD28 by producing IFN-γ or TNF-α positively correlated with the bead-to-cell ratio (Figures S2A and S2B). Similar data were obtained to those using the 5-OP-RU trigger (histograms in Figure 2F and combined data in Figures 2G–2J). Again, in these combined TCR-cytokine stimulation

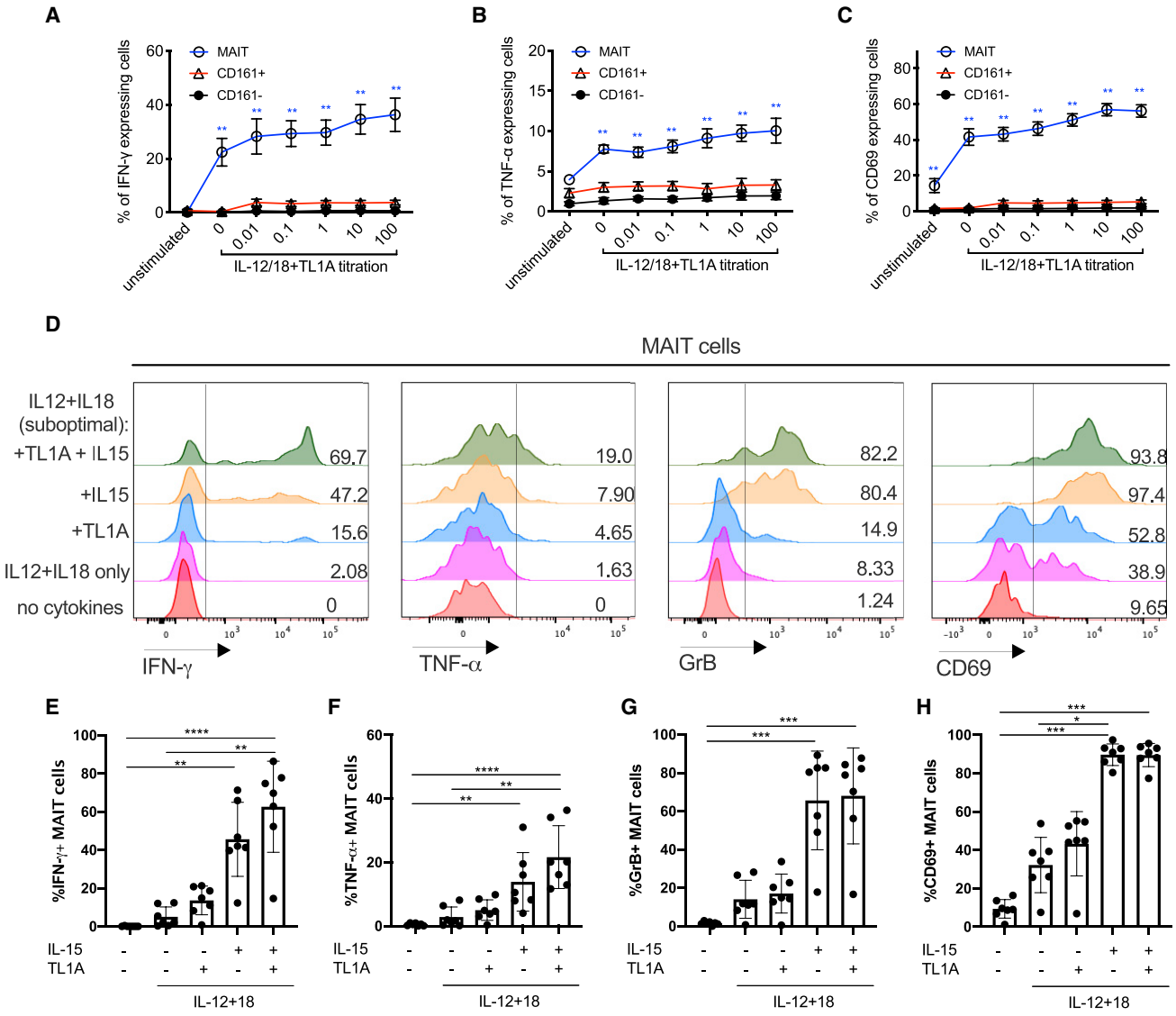

Figure 1. TL1A Enhances the Activation of MAIT Cells Suboptimally Stimulated with IL-12 and IL-18

CD8$^+$ T cells were enriched from healthy peripheral blood mononuclear cells (PBMCs) and stimulated overnight with different combinations of cytokines: IL-12 at 2 ng/mL, IL-18 at 50 ng/mL, IL-15 at 25 ng/mL, and TL1A from 0.01 to 100 ng/mL as indicated.

(A–C) Proportions of CD8$^+$ MAIT/CD161$^+$ or CD161$^-$ cells producing IFN-γ (A), TNF-α (B), or CD69 (C) following overnight stimulation with suboptimal concentrations of IL-12 and IL-18, plus varying concentrations of TL1A.

(D) Representative histograms showing the expression of IFN-γ, TNF-α, GrB, and CD69 by MAIT cells after stimulation with different combinations of cytokines.

(E–H) Frequency of MAIT cells expressing IFN-γ (E), TNF-α (F), GrB (G), and CD69 (H) upon stimulation with the indicated cytokines.

Data were acquired from seven donors in 2–3 experiments. Error bars represent means ± SEM. Differences among conditions were analyzed by Friedman tests with Dunn's multiple comparison tests. *p < 0.05, **p < 0.01, ***p < 0.001, ****p < 0.0001.

See also Figure S1.

studies, IFN-γ expression correlated with that of CD161, consistent with previous findings (Fergusson et al., 2015, 2014), and TL1A and IL-18 had no impact individually (Figure S2C).

In the periphery, MAIT cells can be exposed to various stimuli that could alter the way they respond to TCR and cytokine stimulation. To test to what extent the response patterns described earlier are preserved in barrier tissues, we analyzed MAIT cells isolated from the adjacent normal tissue taken at surgery for colonic cancer. The data may be affected by the presence of malignancy in the patients studied, and we have only examined broad patterns of responsiveness, rather than differences between tissues. In these tissue-derived cells, TCR and suboptimal IL-12/IL-18 triggers synergized strongly, and maximal activation was seen using combined stimulations, including IL-15 and TL1A, as was seen previously in blood-derived cells (Figure 3; Figure S3). We repeated these experiments with *E. coli* as a

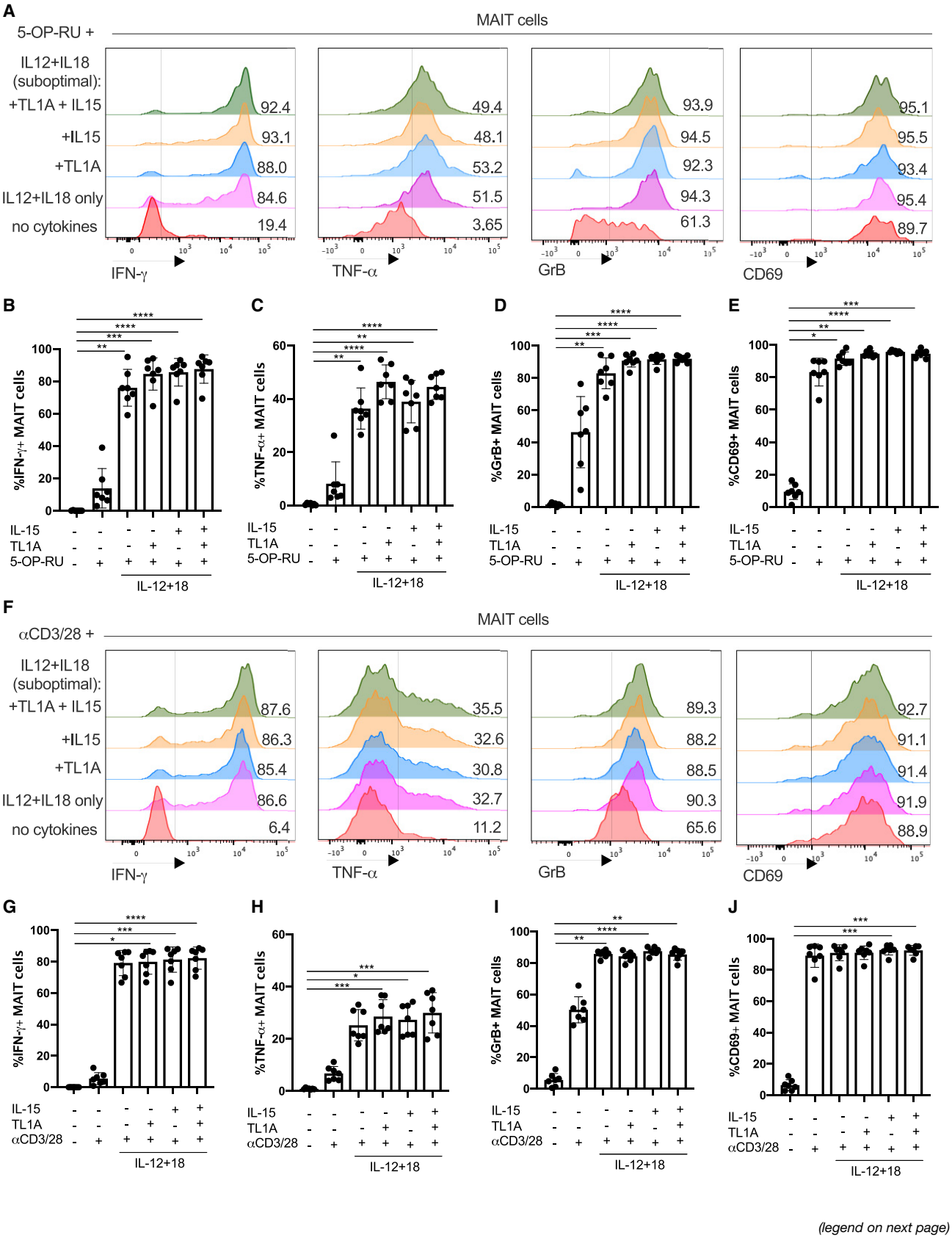

(legend on next page)

natural trigger of combined TCR- and cytokine-mediated stimulation (Figures 3G and 3H; Figure S3D), again observing a similar overall pattern of responsiveness.

MAIT Cells Possess Distinct Transcriptional Signatures upon Activation by TCR or Cytokines

To explore the full breadth of effector functions of MAIT cells elicited by TCR or cytokine signals, we used RNA sequencing (RNA-seq) to characterize transcriptional profiles of MAIT cells under different treatments: TCR (anti-CD3/CD28, labeled here as T), cytokines (IL-12/IL-15/IL-18/TL1A, labeled here as C), and a combination thereof (labeled here as TC). Transcriptional profiles of differentially stimulated MAIT cells were compared with those of untreated (UT) cells. TCR beads were used at a 1:1 bead-to-cell ratio, and cytokines were used at the concentrations optimized earlier. To confirm activation, MAIT cells from the same donors were examined for their release of IFN-γ, TNF-α, and expression of GrB in response to the same stimulations (Figures S4A–S4C).

The mRNA levels of 132, 1,124, or 1,375 genes were significantly modulated ($p < 0.01$, $|\text{fold change}| > 4$, false discovery rate [FDR] < 0.05, including upregulation and downregulation) by TCR, cytokines, or combined TCR and cytokine stimulation, respectively. Venn diagrams highlight the overlapping and unique transcriptional signatures elicited by these 3 stimulations (Figures 4A–4C; Table S1). We found that stimulating MAIT cells with TCR beads and/or cytokines resulted in significant alteration of 89 common mRNA transcripts in MAIT cells, consisting of 88 upregulated genes (Figure 4B; Table S1) and 1 downregulated gene (Figure 4C). Gene Ontology (GO) enrichment analysis on these common 88 upregulated genes by MAIT cells predicted that they are involved in C production and signaling, including, of relevance, IL-12-mediated signaling (IL23R, EBI3, IL2RA, RELB, NFKB1, NFKB2, and CCL3), and TNF signaling (TNF, NFKB1, and NFKBIA).

Analysis of the other genes unique to TCR and cytokines (TC) indicates these two signals induce diverse physiological functions in MAIT cells (Figure 4A). Among 1,594 modulated genes (Table S2), 960 (60.2%) were upregulated and the rest were downregulated (Figures 4A and 4B). MAIT cells stimulated via TC shared 572 upregulated genes with their counterparts that were only stimulated with cytokines. They constitute 82.1% of upregulated gene transcripts elicited by cytokines and 70.8% elicited by TCR beads and cytokines (Figure 4B).

The 1,594 genes with significantly altered expression levels among conditions were then plotted in a heatmap according to their normalized expressions using average linkage hierarchical clustering (Figure 4D). We also performed a principal-component analysis (PCA) using the first two principal components of the 1,594 mRNA transcripts and visualized the correlation of the transcriptional profiles of differentially stimulated MAIT cells (Figure 4E). Clustering of C− and TC− conditions confirmed that cytokine stimulation at this time point had a dominant impact on MAIT cell activation. However, the finding of 221 upregulated genes (Figure 4B) and 208 downregulated genes (Figure 4C) unique to TC stimulation also suggests a strong synergy between TCR signaling and cytokines to drive MAIT cell activation and promote their effector functions. Furthermore, the PCA analysis indicates that a TCR stimulus alone can trigger a pronounced level of activation, because TCR clustering was clearly separate from UT.

We next analyzed volcano plots that show differentially expressed transcriptional profiles of stimulated MAIT cells compared with their unstimulated counterparts (Figures 4F–4H) and compared among stimulations (Figures 4I–4K). Overall, a more limited number of genes were significantly altered by a single dose of TCR stimulation, after filtering for transcripts with $p < 0.01$ and fold change > 4 (Figure 4F), compared with more dynamic transcriptional profiles seen following stimulation with cytokines (Figures 4G and 4H). The transcriptional impact of cytokines on top of TCR stimulation (TCR versus TC) is shown in Figure 4J.

To confirm these findings from RNA-seq, we first used qPCR to validate 3 of the most highly upregulated genes—*IL-26*, oncostatin M (*OSM*), and heparin binding early growth factor (*HBEGF*) (Figures 4G and 4H)—on RNA samples extracted from activated MAIT cells (Figures S4E–S4G). In all 3 cases, we demonstrate a similar pattern of responsiveness by an independent method. Overall, these data indicated that a range of responses can be generated by MAIT cells in response to TCR and cytokine triggers and that the pattern of these differ between the triggers used. We therefore went on to explore the significance of this in more depth.

Transcriptional Signatures of Activated MAIT Cells Predict Not Only Antimicrobial but also Tissue-Repair Functions

Given the range of responses seen after TCR- and cytokine-mediated activation, we speculated that functions of MAIT cells extended beyond conventional antimicrobial responses. The discovery of a skin-homing Tc17 subset in mouse responsive to commensal ligands has shed light on a unique form of

Figure 2. TCR and Cytokine Signaling Combine to Promote MAIT Cell Effector Functions

(A–J) Magnetic-activated cell sorting (MACS)-enriched CD8 T cells from the blood were cultured overnight in the presence of the indicated cytokines, together with the THP1 cell pulsed with DMSO or the MAIT-antigen 5-OP-RU (A–E) or with αCD3/CD28 beads (F–J).

(A) Representative histograms showing the expression of IFN-γ, TNF-α, GrB, and CD69 by MAIT cells after stimulation with different cytokines in the presence of 5-OP-RU.

(B–E) Frequency of MAIT cells expressing IFN-γ (B), TNF-α (C), GrB (D), or CD69 (E) upon stimulation with the indicated cytokines.

(F) Representative histograms showing the expression of IFN-γ, TNF-α, GrB, and CD69 by MAIT cells after stimulation with different cytokines in the presence of 5-OP-RU.

(G–J) Frequency of MAIT cells expressing IFN-γ (G), TNF-α (H), GrB (I), or CD69 (J) upon stimulation with the indicated cytokines.

Data were acquired from seven donors in two experiments. Error bars represent means ± SEM. Differences among conditions were analyzed by Friedman tests with Dunn's multiple comparison tests. *$p < 0.05$, **$p < 0.01$, ***$p < 0.001$, ****$p < 0.001$.

See also Figure S2.

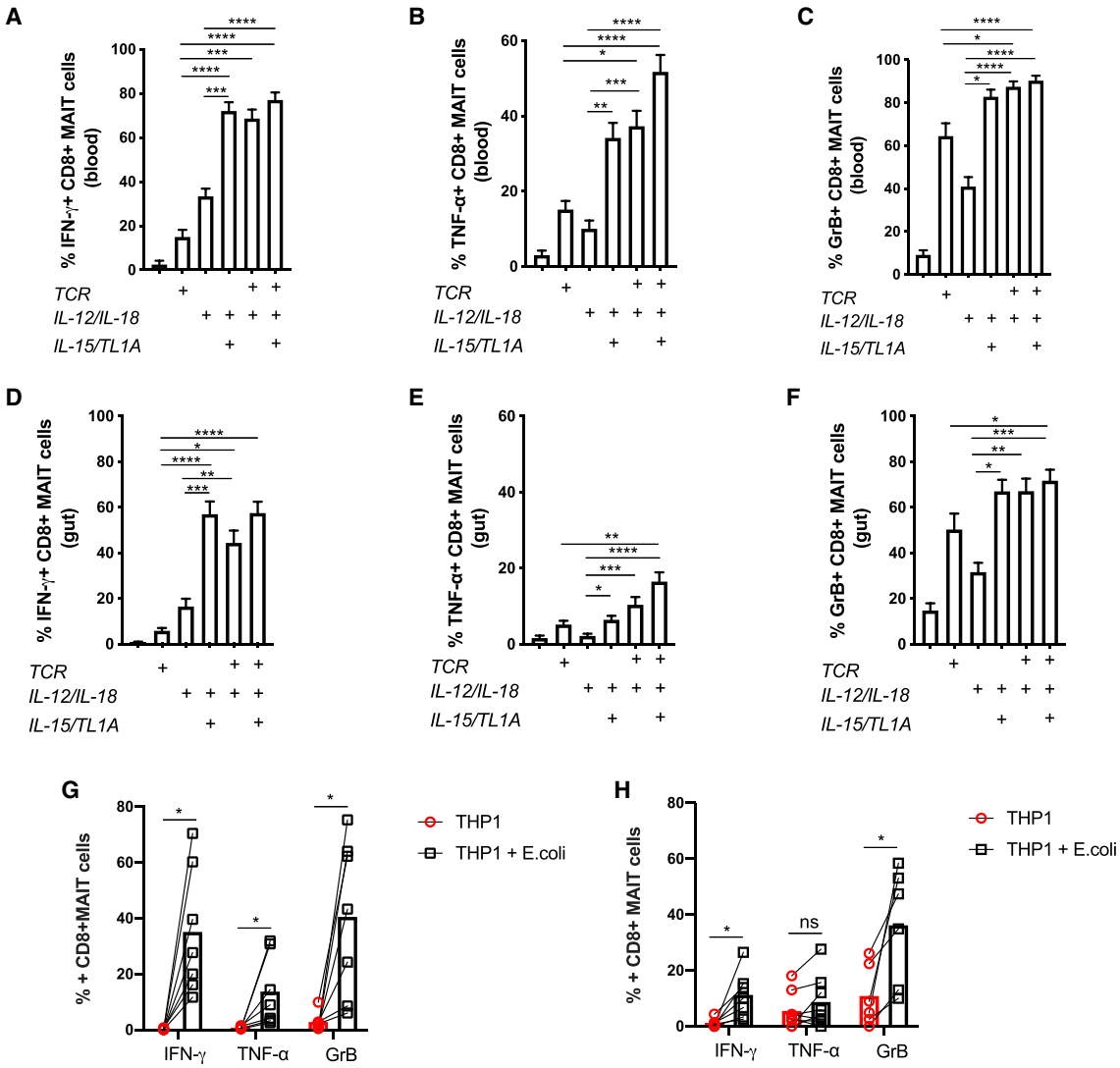

Figure 3. Gut-Derived MAIT Cells Show a Broadly Similar Response Pattern toward Innate and Adaptive Stimuli Compared with Their Blood-Derived Counterparts

Representative plots showing the percentage of cells positive for the indicated effector molecules as a proportion of $CD8^+$ MAIT cells.

(A–C) Proportions of blood-derived (n = 32) $CD8^+$ MAIT cells producing IFN-γ (A), TNF-α (B), or GrB (C) following overnight stimulation with combinations of suboptimal concentrations of IL-12 and IL-18, TL1A, and αCD3/CD28 beads as indicated.

(D–F) Proportions of gut-derived (n = 13) $CD8^+$ MAIT cells producing IFN-γ (D), TNF-α (E), or GrB (F) stimulated in the same way as in (A)–(C).

(G and H) Expression of IFN-γ, TNF-α, and GrB by blood-derived (G, n = 7) or gut-derived (H, n = 6) $CD8^+$ MAIT cells 20 h after coculture with THP1 cells alone or THP1 cells incubated with 25 fixed *E. coli* bacteria per cell.

Data were acquired from multiple donors as indicated in 3–5 experiments. Error bars represent means ± SEM. Differences among conditions were analyzed by Friedman tests with Dunn's multiple comparison tests (A–F), two-way ANOVA (G), or Wilcoxon tests (H). *p < 0.05, **p < 0.01, ***p < 0.001, ****p < 0.001.

See also Figure S3.

adaptive immunity in which antimicrobial functions and tissue repair are coupled within the same subset of unconventional T cells (Harrison et al., 2019; Linehan et al., 2018). These commensal-specific T cells elicited a tissue-repair signature and accelerated wound closure, in addition to promoting protection against pathogens. MAIT cells are commensal responsive and similarly have been associated with a type-17 phenotype (Billerbeck et al., 2010; Dusseaux et al., 2011; Sobkowiak et al., 2019). Therefore, we investigated functional overlap using a genomic comparison between activated human MAIT cells and mouse skin-homing Tc17 cells.

First, we examined the volcano plots in Figures 4F–4K and annotated the genes from the tissue-repair gene list used in the study of Linehan et al. (2018) (Table S3). The genes on these plots (Figures 4F–4K) are color coded according to whether they associated with a proinflammatory and an antimicrobial response, as has been classically associated with MAIT cells (red) or tissue-repair signature (blue). Substantial numbers of

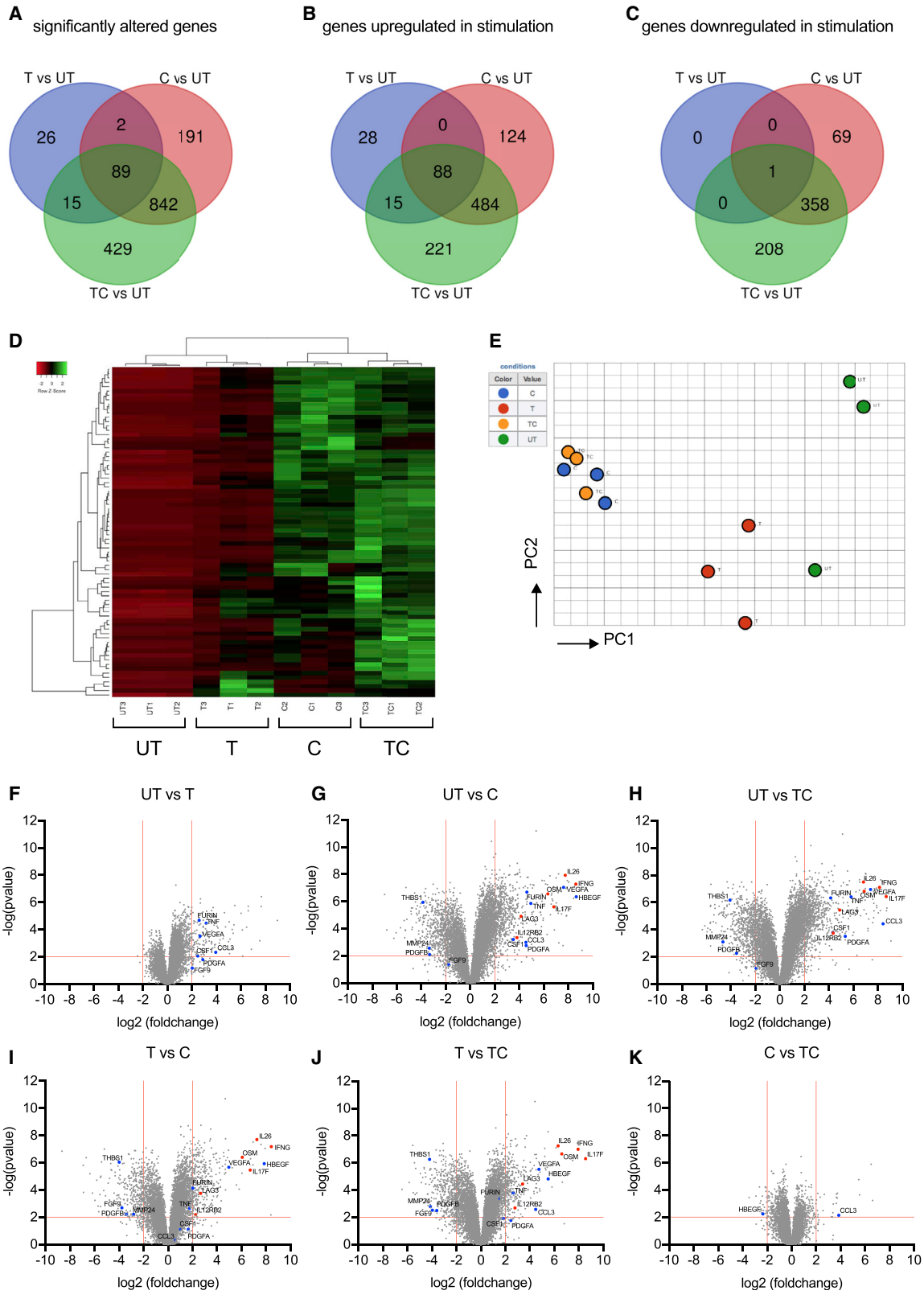

(legend on next page)

genes linked with the tissue-repair signature were observed, including genes such as Furin, TNF, CSF1, and CCL3 and various growth factors.

Next, genes that were significantly differentially expressed compared with unstimulated MAIT cells were identified from TCR-, C-, and TC-stimulated MAIT cells and statistically compared in aggregate to the tissue-repair gene dataset (Linehan et al., 2018). Gene set enrichment analysis demonstrated significant enrichment ($p < 0.0002$) of these tissue repair-related genes in MAIT cells stimulated by TCR with or without cytokines (Figures 5A and 5B), but not by cytokines alone (Figure 5C). The significant leading edge genes from these analyses are indicated in Figures S5A and S5B. These data suggest that TCR triggering by MAIT cells may be important in driving a tissue-repair program.

Examination of MAIT Cell Functions Confirms a Tissue-Repair Activity

To test these findings, we analyzed the expression of 3 of these genes from the tissue-repair signature on the protein level by flow cytometry. Triggering of MAIT cells by *E. coli* led to the production of TNF, Furin, and CCL3 in a TCR-dependent manner, because it could be blocked fully or partially by anti-MR1 at 20 or 72 h, respectively (Figures 5D and 5E; Figures S5C and S5D). We also validated upregulation of granulocyte-monocyte colony-stimulating factor (GM-CSF; CSF2), a tissue-repair-associated gene not upregulated at earlier time points, which again was most evident in extended cultures (72 h) and triggered in an MR1-dependent fashion (Figures S5E and S5F).

To assess this, we used *in vitro* wound-healing assays, combining the intestinal epithelial cell line Caco2 (see STAR Methods) (Povoleri et al., 2018) with supernatants derived from MAIT-containing $CD8^+$ T cell cultures stimulated with *E. coli* in the presence or absence of anti-MR1 blocking antibodies for 72 h. Supernatants obtained from *E. coli*-stimulated $CD8^+$ T cell cultures significantly accelerated wound closure in this system, which was most evident at later time points (e.g., 24–36 h) (Figure 5G). This effect was significantly reduced when MR1 was blocked, underscoring the importance of MR1-dependent TCR signaling in the process (Figures 5F and 5G). Altogether, these data provide further evidence that TCR-dependent activation is essential for the expression of tissue-repair-associated molecules by MAIT cells and that it, in principle, allows MAIT cells to affect key aspects of tissue repair like the migration and/or proliferation of epithelial-type cells.

Comparative Analyses of Human and Mouse MAIT and Tissue-Repair Datasets

We performed a data integration analysis by fusing RNA-seq datasets containing mouse data from activation studies *in vivo* and *in vitro* (Hinks et al., 2019) with our human data and applying a protocol for such integration (Marchi et al., 2019). First, we examined how our data aligned with those obtained by Hinks et al. (2019), who examined mouse MAIT cell activation *in vitro* (5-OP-RU stimulation) and *in vivo* (bacterial challenge), because these were shown to align with activated H2M3-restricted cells from publicly available data from Linehan et al. (2018) (Figure 6). The accompanying dendrogram shows the close transcriptional relationship between our *in vitro*-activated human T cells and those in the mouse. In this analysis, the closest neighbors of the maximally activated cells (TC and C) were the Tc17 cells activated in the mouse skin and the *in vivo* chronically or *in vitro*-activated MAIT cells from Hinks et al. (2019). In the less activated condition (TCR), the human MAIT cells from our study cluster with H2M3-restricted CD8 T cells from the murine secondary lymphoid organs, which were shown to be less capable of cytokine production compared with their skin-derived counterparts and with murine MAIT cells acutely activated *in vivo*. Hence, despite the cross-species comparison, stronger stimulation creates an important and relevant shift in the position on the dendrogram. These data indicate, in an unsupervised analysis, that closely shared transcriptional patterns exist between our *in vitro*-stimulated cells and different subsets that are performing tissue-repair functions (as well as host defense functions) *in vivo* in mice.

Finally, we performed, using an extension of this bioinformatic approach, alignment among all 3 generated datasets on human and mouse MAIT cell activation to assess their comparability. All 3 have shown that under conditions in which the TCR is stimulated, there is a tissue-repair signature, but when tested in both our dataset and that of Lamichhane et al. (2019), the statistical association in gene set enrichment analysis (GSEA) studies was lost under conditions of cytokine stimulation alone. In Figure S6, all unstimulated human MAIT cells clustered (indicating both good data fusion and consistency between studies), with

Figure 4. TCR- and Cytokine-Activated MAIT Cells Possess Distinct Transcriptional Profiles

(A–C) Venn diagrams showing genes that are significantly differentially modulated ($p < 0.05$, fold change > 4) in TCR (T)-, cytokine (C)-, or TCR and cytokine (TC)-treated $CD8^+$ MAIT cells compared with untreated (UT) MAIT cells of three healthy individuals. The cytokine (C) stimulation consisted of a cocktail of 4 cytokines: IL-12 (2 ng/mL), IL-18 (50 ng/mL), IL-15 (25 ng/mL), and TL1A (100 ng/mL). Genes with significantly altered expression levels (A) are divided into two sets: those are that are upregulated upon stimulation (B) and those that are downregulated upon stimulation (C).

(D) Heatmap showing 1,594 significantly differentially expressed transcripts ($p < 0.05$, fold change > 4) between TCR/C/TC-stimulated and UT $CD8^+$ MAIT cells among the same three healthy individuals.

(E) Visualization of the $CD8^+$ MAIT cell transcripts elicited by differential stimulations in the subspace of the first principle components (PCs). Each colored circle represents a sample and is color coded in accordance with the conditions with which cells were stimulated, as illustrated on the right-hand side of the graph.

(F–K) Volcano plots to visualize differentially expressed transcriptional profiles of activated $CD8^+$ MAIT cells stimulated in different ways. Each point represents a single gene, and genes expressed at significantly higher or lower levels between the compared conditions are depicted, respectively, in the upper-right or upper-left corner of each plot. Genes discussed in the text are highlighted in blue (tissue repair associated) or in red (inflammation associated). The gene expression of untreated MAIT cells was compared to (F) T-, (G) C-, or (H) TC-stimulated MAIT cells. Further, gene expression in those cells was also compared directly between the different stimulation conditions: (I) T- to C- stimulation, (J) T- to TC-stimulation, and finally (K) C- to TC-stimulation.

Data were acquired from three donors in one experiment.

See also Figure S4 and Tables S1, S2, and S3.

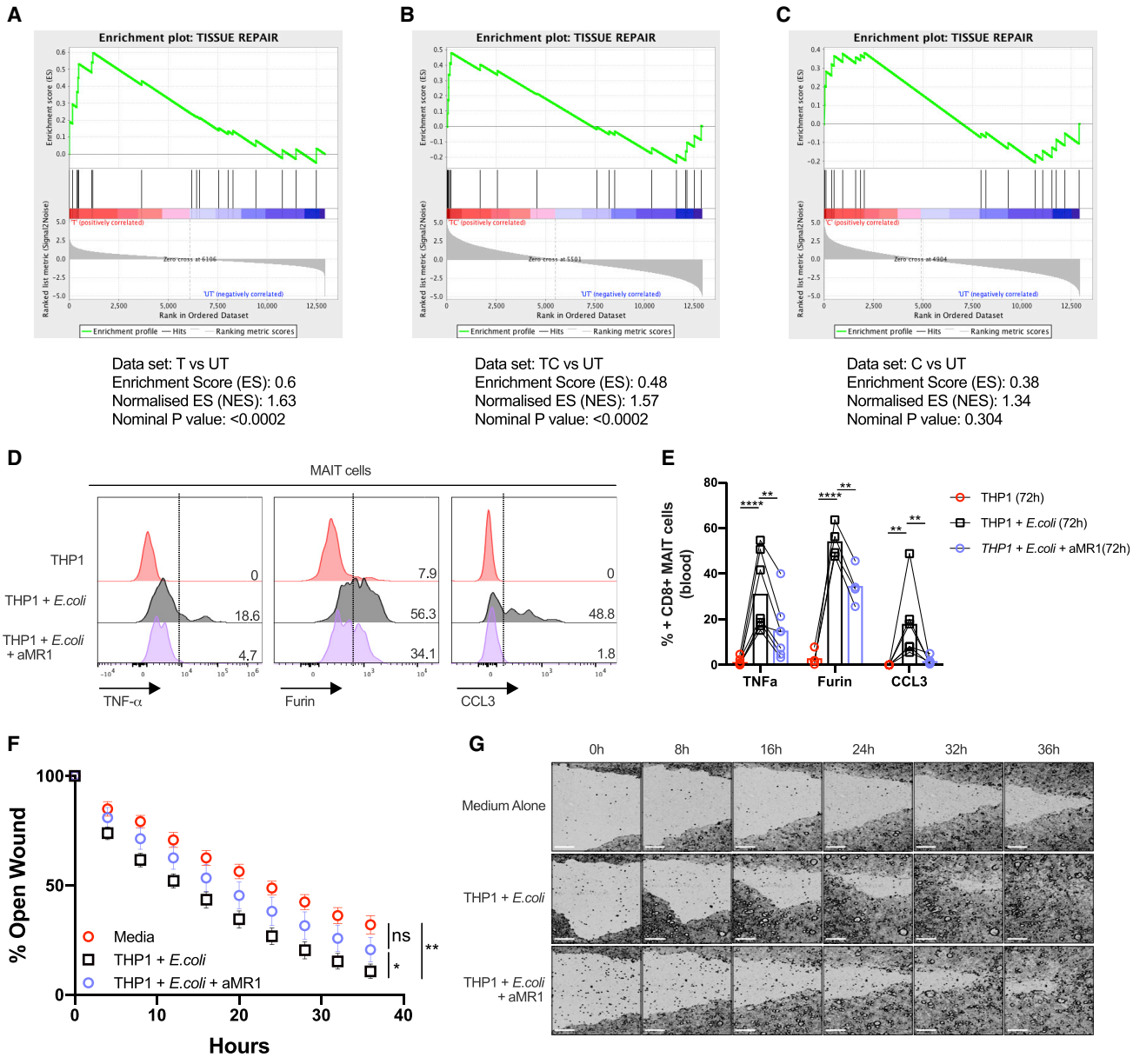

Figure 5. TCR-Mediated Activation of MAIT Cells Leads to the Expression of Tissue-Repair-Associated Molecules and Accelerates Wound Healing

(A–C) Gene set enrichment summary plots for stimulated sorted MAIT cell-versus-unstimulated cell-ranked genes. Depicted are the individual plots for TCR-stimulated versus UT in (A), TC-stimulated versus UT in (B), and C versus unstimulated in (C). Non-significant for C versus UT, normalized enrichment score (NES) = 1.63; $p < 0.0002$ for TCR versus UT, NES = 1.57; and $p < 0.0002$ for TC versus UT. Data were acquired from three donors in one experiment.

(D) Flow cytometry analysis of the expression of TNF-α, furin, and CCL3 by CD161^{++}/MAIT CD8^{+} T cells in response to fixed *E. coli* presented by THP1 cells in the presence or absence of an anti-MR1 (αMR1) blocking antibody at the 72-h time point.

(E) Statistical analysis of the expression of the effector molecules shown in (D).

(F) Caco2 cells were grown to confluency and scratched with a WoundMaker device to perform *in vitro* wound-healing assays. Cells were supplemented with different supernatants collected from 72-h cocultures of enriched CD8 T cells with *E. coli*-loaded THP1 cells in the presence or absence of αMR1, as indicated. The open wound areas were quantified as percentages of the initial wound size in the Caco2 cultures. Data points are mean ± SEM and were acquired from five biological replicates in two experiments.

(G) Representative pictures of the closure of the wounds in Caco2 cultures treated as in (F) were assessed with time-lapse imaging over a time course of 36 h. Data were acquired from seven donors in three experiments.

Differences among conditions were analyzed by two-way ANOVA. ns, not significant; *$p < 0.05$, **$p < 0.01$, ****$p < 0.001$. Scale bars, 250 μm.

See also Figure S5 and Table S3.

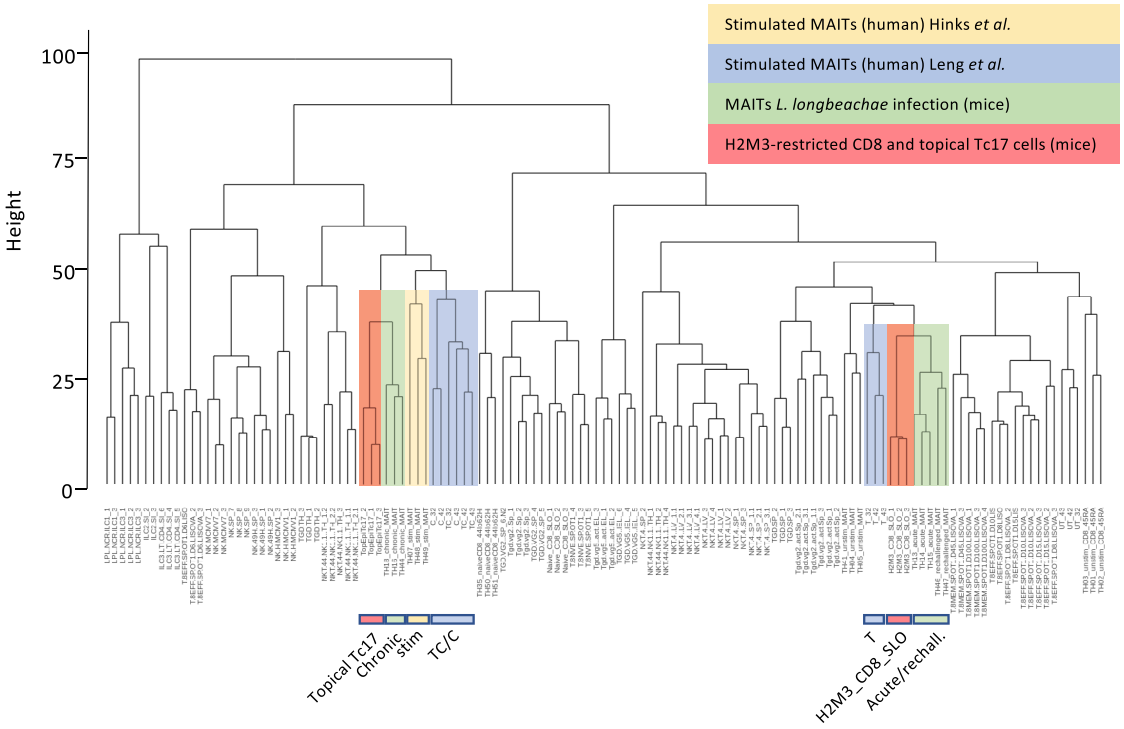

Figure 6. Integrated Transcriptional Analyses Reveal the Relationship between *In Vitro*-Activated Human MAIT Cells and *In Vivo*-Activated Murine MAIT and Tc17 Cells

Hierarchical clustering analysis of the transcriptomic profiles of the indicated cell populations is shown. Similarity between the expression profiles is measured using a Euclidean distance (height). Datasets were derived from ImmGen (Heng et al., 2008), Linehan et al. (2018), and Hinks et al. (2019) and were integrated as described in the STAR Methods section. The relevant datasets are colored. UT, TCR, C, and TC refer to the conditions used in this paper on *in vitro*-activated human $CD8^+$ MAIT cells (blue). Topical Tc17 and H2M3_CD8_SLO refer to the H2M3-restricted populations identified in Linehan et al. (2018) in the skin and secondary lymphoid organs of mice, respectively (red). The cells described in Hinks et al. (2019) are marked in yellow (stimulated human MAIT cells) or green (chronic or acute, derived during a late or an early time point after *L. longbeachae* infection in mice, respectively). See also Figure S6.

a large block of long-term activated mouse and strongly activated human MAIT cells sitting in a distinct clade. In this analysis, we could split TCR and UT conditions, and the TCR conditions clustered closely with the acutely activated murine MAIT cells, indicating even this relatively modest response in our assay conditions parallels a transcriptional state observed *in vivo*. Overlap was seen between the different human datasets (e.g., between bacterial- and ligand-stimulated cells from different sources), indicating the comparability of the studies despite the different protocols and sites.

A Local Model for MAIT Cells in Epithelial Defense and Tissue Repair

Given the relationship between MAIT cells and epithelial maintenance, we wished to assess how closely associated such cells are with the epithelial layer. Because only limited data are available on this (partly because of the availability of suitable antibodies and the need for antibody combinations to reliably identify MAIT cells), we developed a high content imaging protocol based on chip cytometry. By costaining for multiple relevant markers (CD3, CD8, CD161, Vα7.2, and PLZF) in colonic tissue, we could observe apposition between MAIT cells and intact epithelium, suggesting two-way cross talk is possible under homeostatic conditions (Figure 7).

DISCUSSION

CD161-expressing human TCR lymphocytes possess shared transcriptional and functional phenotypes, and their enhanced innate ability to respond to inflammatory cues has been investigated with transcriptomic approaches (Fergusson et al., 2014). MAIT cells comprise a large proportion of these CD161-expressing T cells and have previously been described as showing limited responses to conventional TCR signals, although combinatorial signaling can markedly augment this *in vitro* and *in vivo* (Slichter et al., 2016; Turtle et al., 2011) (see also accompanying papers by Hinks et al., 2019, and Lamichhane et al., 2019). However, MAIT cells can respond in a fully TCR-independent manner, via cytokine signaling, and such behavior can trigger protection *in vivo* (Wilgenburg et al., 2018). The functional consequences of TCR-dependent versus TCR-independent activation of MAIT cells have not been fully defined; thus, dissecting the differential signals that promote and sustain MAIT cell effector function is of central importance in defining the role of MAIT cells in both health and disease. Here we probed the contribution of innate and adaptive signals to MAIT cell activation in the blood and gut, describing segregating functions of MAIT cells in response to different activation stimuli.

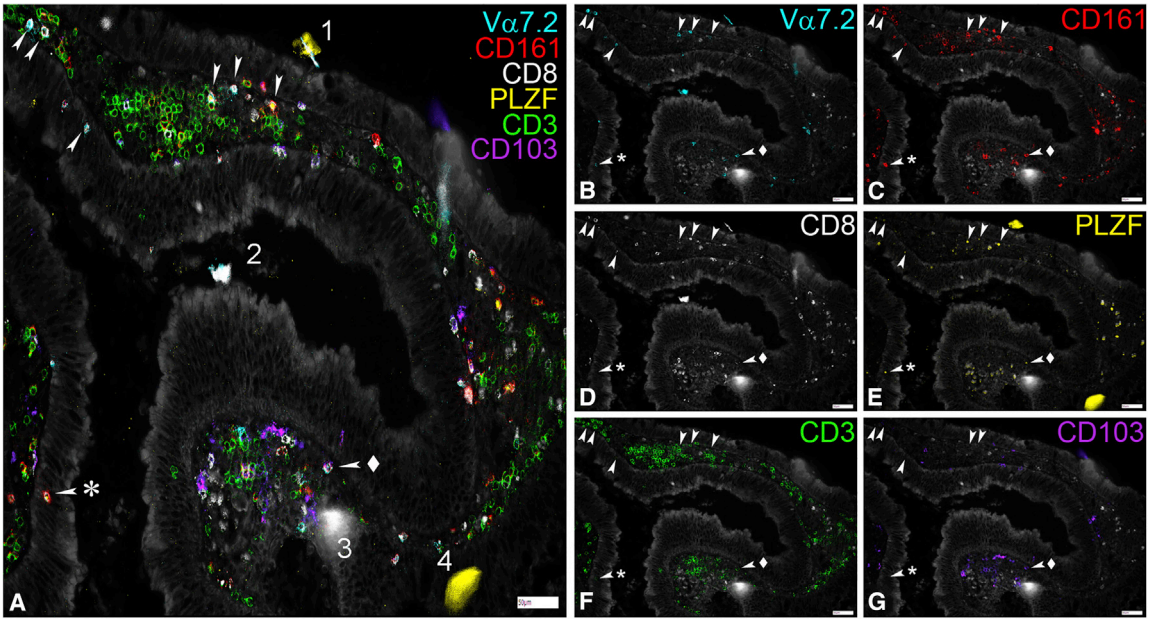

Figure 7. MAIT Cells Can Be Found Close to and within the Colonic Epithelium

(A–G) Representative images showing the expression of Va7.2, CD161, CD8, PLZF, CD3, and CD103 in the lamina propria and the epithelium of fixed samples of colonic polyp tissue. Samples were mounted on cytometer chips and iteratively stained with sets of three directly fluorochrome-conjugated antibodies as described in the methods section. Depicted are a merged picture (A) and all the individual stains for Va7.2 (B), CD161(C), CD8 (D), PLZF (E), CD3 (F), and CD103 (G). White arrows mark cells showing co-expression of Va7.2, CD161, PLZF, and CD3 that were defined as MAIT cells here. Note that while CD8 was co-expressed in most of them, CD8− MAITs (arrow + asterisk) could also be found. In contrast, CD103 was rarely co-expressed on MAITs (arrow + diamond). During the iterative staining process dust particles and other detritus can be picked up by the solution flowing over the tissue creating autofluorescent artifacts (1–4). While some of these get washed away after completion of the staining cycle (1, 4), others present during multiple imaging rounds (2, 3). Scale bars, 50μm.

We defined MAIT cells in both human blood and human gut as $CD161^{2+}V\alpha7.2^{+}CD8^{+}CD4^{-}CD3^{+}$ T cells, a common approach used by several studies to dissect MAIT cell effector function elicited by cytokines or the TCR (Kurioka et al., 2015, 2017; Sattler et al., 2015; Ussher et al., 2014b; van Wilgenburg et al., 2016). MR1 tetramers, combined with CD161 staining, identify MR1-restricted MAIT cells unequivocally, but these reagents only became available at the end of this study. We also stained freshly isolated colonic lymphocytes using the MR1 tetramer, with Vα7.2 and CD161 antibodies on the same panel. These provided similar estimates of frequency (as they commonly do in blood). An example is shown in Figure S3C.

Responses following a TCR stimulation of MAIT cells and conventional CD8 T cells differ in magnitude and in quality. We and others (Slichter et al., 2016) initially explored this using bead-based protocols. This allowed a direct comparison with non-MAIT populations and simplified some downstream sorting procedures. Although CD3/CD28 beads do not represent a true physiological TCR stimulus, here we confirmed the bead-based data using 5-OP-RU, an optimized MR1 ligand, and *E. coli* stimulation, which represents a more physiological trigger. In each case, there is clearly activation in response to TCR triggering, but this is markedly amplified and sustained through combinatorial signals via cytokines. These broad features were recapitulated in MAIT cells derived from the human gut.

Resting MAIT cells express a higher level of IL-18Rα on the cell surface compared with their $CD161^{2+}V\alpha7.2^{-}$ or $CD161^{-}$ counterparts (Fergusson et al., 2014; Ussher et al., 2014b). However, we and others found that IL-18 alone has a limited role in activating lymphocytes, including MAIT, natural killer (NK), and T cells (Tominaga et al., 2000; Sareneva et al., 2000). A signal combining IL-12 and IL-18 has been described as activating a range of lymphocytes, including T helper 1 (Th1) cells, B cells, NK cells, and more recently, MAIT cells, independently from the TCR. Expanding on this, our data also show TL1A can synergize with these cytokines to enhance MAIT cell activation. In addition to its proinflammatory and costimulatory role in the human blood, TL1A is a gut-associated cytokine and has been linked to inflammatory bowel disease (IBD) (Jin et al., 2013; Shih et al., 2009). Patients with IBD have higher levels of DR3 and TL1A expression in their mucosal T cells and macrophages (Bamias et al., 2003; Prehn et al., 2004). We highlight that TL1A enhances the effector function of gut MAIT cells in the presence of a suboptimal dose of IL-12+IL-18, suggesting that TL1A may contribute to the amplification of inflammatory responses. Thus, TL1A blockade *in vivo* could potentially achieve an anti-inflammatory response while maintaining barrier function. These data confirm and extend the importance of TNF superfamily members in MAIT cell activation—as revealed for TNF-α in responses to opsonized bacteria at limiting doses (Banki et al., 2019)—and suggest a context-specific and antigen-presenting cell (APC)-dependent role for these signals.

Genes controlling the TCR signaling pathway have been shown to be differentially regulated in MAIT cells compared

with conventional $CD8^+$ T cells ($CD161^-$ cells) (Turtle et al., 2011), yet full implications of a partial response by TCR-triggered MAIT cells have been unclear so far. We therefore explored this using RNA-seq of MAIT cells stimulated *in vitro* via TCR-dependent and TCR-independent pathways. Our RNA-seq data reveal both shared and independent response patterns between TCR-dependent and TCR-independent stimulation. Although the magnitude of change seen in our experiments was greater in the cytokine-stimulated cells, the transcripts associated with TCR triggering alone provided a clear insight into potential function. We linked, using GSEA, the MAIT TCR-driven transcriptional profile with a tissue-repair signature from a report on IL-17+ innate-like $CD8^+$ T cells in a murine skin model (Linehan et al., 2018) (later confirmed in the gut by Harrison et al., 2019). The tissue-repair profile in the unconventional (H2M3-restricted) mouse skin $CD8^+$ T cells was shown to be linked to an encounter with commensal microbes and to affect cutaneous wound healing. In our model, we have shown a functional impact of TCR-dependent microbe-triggered MAIT cells *in vitro* using a monolayer scratch assay.

We validated expression of some of the most critical genes underpinning this signature by MAIT cells on the protein level. These genes included furin, which plays an important role in tissue repair through its broad proprotein convertase activity, leading to activation of proteins like transforming growth factor β (TGF-β) and matrix metalloproteinases. T cell-derived furin has been shown to be critical in tissue protection in a transfer colitis model and affects regulatory T cell (Treg) development (Pesu et al., 2008). CCL3 (MIP1α), which is more broadly expressed and has been better studied in T cells, has a critical role in macrophage recruitment (DiPietro et al., 1998). Both of these mediators and TNF-α, which has a described role in tissue repair in concert with CCL3 (Li et al., 2016), were produced by activated MAIT cells in a sustained and TCR-dependent manner. The repair signature was most evident in MAIT cells triggered via their TCR, either with or without cytokines, but there was no statistical enrichment in the cytokine-only stimulation. This is most evident in Figures 4F–4K, in which some key genes are marked. For example, the cytokine-alone stimulus induces many relevant genes, but there is a slight abundance of inflammatory and host defense genes upregulated in the cytokine versus TCR comparison (Figures 4I versus 4F), together with some downregulation of tissue-repair genes from the GSEA list (Table S3). These findings were corroborated by the results of an *in vitro* wound-healing assay, because blocking MR1-dependent TCR signaling in CD8 T cell cultures abolished the accelerating effect that these supernatants otherwise had on wound closure (Figures 5F and 5G).

Beyond the list of tissue-repair factors identified in the work of Linehan et al. (2018) and used in the GSEA comparison, other MAIT cell-derived factors were found through the RNA-seq study (and validated in independent assays), with potential roles in inflammation and in tissue homeostasis. For example, IL-26 is part of the IL-20 family of cytokines (including IL-22, also made by MAIT cells; Gibbs et al., 2017), which all strongly affect epithelial cell function, including wound repair (Rutz et al., 2014). Similarly, OSM, which is upregulated in the gut during inflammation *in vivo* (West et al., 2017), has been shown to induce migration of keratinocytes *in vitro* and skin repair *in vivo* (Boniface et al., 2007; Hoffmann et al., 2011), while HBEGF, which was highly expressed by activated MAIT cells, has a long track record in tissue regeneration (reviewed in Dao et al., 2018). Altogether, these data substantially broaden the known functions of MAIT cells and include a range of functions on a spectrum of host defense, inflammation, and barrier repair.

A similar set of RNA-seq data, functional data, and conclusions has been obtained using parallel experiments in human MAIT cells *ex vivo* with a 5-OP-RU and bacterial trigger and most importantly in an *in vivo* challenge incorporating a TCR trigger with and without cytokines (Hinks et al., 2019; Lamichhane et al., 2019). Several observations can be made from a comparison of the transcriptional data. First, in all 3 cases, a GSEA analysis using TCR-triggered MAIT cells revealed a statistically robust congruence with the tissue-repair signature. In both studies in which this was addressed, this was not seen with cytokine stimulation alone (IL-12/IL-18 in the parallel study) (Lamichhane et al., 2019). Looking more broadly at transcriptional regulation of MAIT cells in mouse and man, the data fusion analyses also showed a strong link between the activation of human MAIT cells shown here (and in parallel studies) and the Tc17 tissue-repair subset of Linehan et al. (2018). This is an interesting, and we feel important, extension of the work, allowing a direct comparison between *in vivo* mouse data and multiple parallel sets of *in vitro*-stimulated human data across species, platforms, experimental protocols, and sites. Because this is an unsupervised and hypothesis-free approach, it lends weight to the associations seen here and the triggering model we have produced. We propose that it provides a useful template for future studies of such populations for which the aggregation of data enhances its biological impact (as well as providing independent validation). Thus, a reasonable body of data has emerged in parallel among the three studies that suggests MAIT cells possess tissue-repair activity of relevance in barrier defense.

Taking together the data here and those of Hinks et al. (2019) and Lamichhane et al. (2019), we propose a model whereby in the human gut and potentially in the liver, MAIT cells are continuously exposed to MR1-bound ligand derived from the commensal bacteria present in the microbiome. In the absence of inflammatory signals, this only drives the circumscribed transcriptional signature associated with local homeostatic function. This model would fit well with emerging data that in tissues such as the gut, MAIT cells can play a protective role. This is most clearly seen in the study of non-obese diabetic (NOD) mice, in which the genetic absence of MR1 leads to loss of mucosal integrity and bacterial translocation in the steady state (Rouxel et al., 2017). A similar epithelial protective role is seen in a model of graft versus host disease (Varelias et al., 2018). This adds to existing data indicating a classical immune protective role against infection, for example, in the lung, following bacterial challenge (Wang et al., 2018). During loss of bowel integrity associated, for example, with IBD, MAIT cells have been shown to be further activated in some studies (Serriari et al., 2014), but whether this is a response to tissue injury or they play a causative role has yet to be defined. Our data suggest that during tissue injury, the innate cytokines induced would drive the full activation signal seen, which includes a broad inflammatory response. For example, IL-17F, which has been shown to be pathogenic in IBD

models (Tang et al., 2018), is not induced by TCR signals alone but is strongly induced in the presence of inflammatory cytokines (fold change > 400, $p < 10^{-6}$).

There are some limitations to the study presented. This includes the analysis of gut tissue, in which the material was obtained from patients with a colonic tumor, potentially affecting uninvolved mucosa. The study also focused on the majority $CD8^+$ MAIT cells. Their triggering behavior reflects that of other MAIT subsets in which this has been studied, although some functional differences may exist (Kurioka et al., 2017). Analysis of transcriptional changes was limited to a single time point, and analysis of shorter and longer stimulations could prove impactful. In such studies, it would also be of interest to specifically address the influence of both age and gender, which were not studied in this analysis because of the anonymized nature of the blood cones. Finally, the analysis of MAIT cell location using high content cytometry (Figure 7) was limited to intact epithelium and should be extended in future studies to identify the transcription factors and cytokines expressed both in the steady state and in an inflammatory state to test these ideas *in situ*.

Overall, we have defined combinatorial pathways to activate MAIT cells, extending the role of TNF superfamily members such as TL1A, and we have dissected the consequences of activation via TCR-dependent and TCR-independent pathways in human blood and gut. Given the overlap between tissue repair and host defense and inflammatory programs found in MAIT cells (and related populations in the mouse), our model suggests that ongoing maintenance of the barrier is an integral part of the function of such unconventional cells concentrated in epithelia, which goes hand-in-hand with control of microbial invasion.

STAR★METHODS

Detailed methods are provided in the online version of this paper and include the following:

- KEY RESOURCES TABLE
- LEAD CONTACT AND MATERIALS AVAILABILITY
- EXPERIMENTAL MODEL AND SUBJECT DETAILS
  - Human samples
  - Cell lines
- METHOD DETAILS
  - Isolation and short-term culture of human lymphocytes
  - *In vitro* stimulations
  - Flow cytometry
  - RNA sequencing (RNaseq)
  - qPCR
  - *In vitro* wound-healing assay
  - Chip Cytometry
- QUANTIFICATION AND STATISTICAL ANALYSIS
- DATA AND CODE AVAILABILITY

SUPPLEMENTAL INFORMATION

Supplemental Information can be found online at https://doi.org/10.1016/j.celrep.2019.08.050.

CONSORTIA

The members of Oxford IBD Investigators are Carolina Arancibia-Carcamo, Adam Bailey, Eillie Barnes, Beth Bird-Lieberman, Oliver Brain, Barbara Braden, Jane Collier, James East, Alessandra Geremia, Lucy Howarth, Satish Keshav, Paul Klenerman, Simon Leedham, Rebecca Palmer, Fiona Powrie, Astor Rodrigues, Alison Simmons, Peter B. Sullivan, Simon P.L. Travis, and Holm H. Uhlig.

ACKNOWLEDGMENTS

This research was supported by the Wellcome Trust (WT109965MA, 104553/z/14/z, and 211050/Z/18/z), an NIHR Senior Fellowship (to P.K.), the NIH (U19 I082360), the Chinese Scholarship Council (to T.L.), and the Deutsche Forschungsgemeinshaft (DFG; project number: 403193363 to C.-P.H.). The authors acknowledge the BRC Oxford GI Biobank and BRC Oxford IBD Cohort for collecting and making available the samples and data used in the generation of this publication. The research was supported by the National Institute for Health Research (NIHR) Oxford Biomedical Research Centre (BRC). The views expressed are those of the authors and not necessarily those of the NHS, the NIHR, or the Department of Health. We thank Ahmed Hegazy, Nathaniel West, James Chivenga, Cloe Vassart, and David Maldonado-Perez for their effort and help. We additionally thank Chan Phetsouphanh for sorting the cells in the Peter Medawar Building. We thank Simon J. Leedham (Translational Gastroenterology Unit, University of Oxford, John Radcliffe Hospital, Oxford, UK) for collecting polyp tissue samples used for chip cytometry. This work benefited from data assembled by the ImmGen consortium (Heng et al., 2008). 5-OP-RU was a gift from David Fairlie, University of Queensland.

AUTHOR CONTRIBUTIONS

Conceived and designed the experiments: T.L., H.D.A., C.-P.H., V.M., P.K., C.W., and D.E. Performed the experiments: T.L., H.D.A., C.-P.H., K.P., J.H., V.M., and T.K. Analyzed the data: T.L., H.D.A., C.-P.H., T.K., and P.K. Contributed to the collection of clinical samples: T.L., T.K., M.F., Z.C., S.M., M.N., and R.S.P. Contributed to the writing of this manuscript: T.L., H.D.A., C.-P.H., P.K., and C.W.

DECLARATION OF INTERESTS

The authors declare no competing interests.

Received: December 8, 2018
Revised: April 17, 2019
Accepted: August 15, 2019
Published: September 17, 2019

REFERENCES

Bamias, G., Martin, C., 3rd, Marini, M., Hoang, S., Mishina, M., Ross, W.G., Sachedina, M.A., Friel, C.M., Mize, J., Bickston, S.J., et al. (2003). Expression, localization, and functional activity of TL1A, a novel Th1-polarizing cytokine in inflammatory bowel disease. J. Immunol. *171*, 4868–4874.

Banki, Z., Krabbendam, L., Klaver, D., Leng, T., Kruis, S., Mehta, H., Müllauer, B., Orth-Höller, D., Stroiber, H., Willberg, C.B., and Klenerman, P. (2019). Antibody opsonization enhances MAIT cell responsiveness to bacteria via a TNF-dependent mechanism. Immunol. Cell Biol. *97*, 538–551.

Billerbeck, E., Kang, Y.H., Walker, L., Lockstone, H., Grafmueller, S., Fleming, V., Flint, J., Willberg, C.B., Bengsch, B., Seigel, B., et al. (2010). Analysis of CD161 expression on human CD8+ T cells defines a distinct functional subset with tissue-homing properties. Proc. Natl. Acad. Sci. USA *107*, 3006–3011.

Boniface, K., Diveu, C., Morel, F., Pedretti, N., Froger, J., Ravon, E., Garcia, M., Venereau, E., Preisser, L., Guignouard, E., et al. (2007). Oncostatin M secreted by skin infiltrating T lymphocytes is a potent keratinocyte activator involved in skin inflammation. J. Immunol. *178*, 4615–4622.

Chen, Z., Wang, H., D'Souza, C., Sun, S., Kostenko, L., Eckle, S.B.G., Meehan, B.S., Jackson, D.C., Strugnell, R.A., Cao, H., et al. (2017). Mucosal-associated invariant T-cell activation and accumulation after *in vivo* infection depends on microbial riboflavin synthesis and co-stimulatory signals. Mucosal Immunol. *10*, 58–68.

Cohavy, O., Shih, D.Q., Doherty, T.M., Ware, C.F., and Targan, S.R. (2011). CD161 defines effector T cells that express light and respond to TL1A-DR3 signaling. Eur. J. Microbiol. Immunol. (Bp) *1*, 70–79.

Dao, D.T., Anez-Bustillos, L., Adam, R.M., Puder, M., and Bielenberg, D.R. (2018). Heparin-Binding Epidermal Growth Factor-Like Growth Factor as a Critical Mediator of Tissue Repair and Regeneration. Am. J. Pathol. *188*, 2446–2456.

DiPietro, L.A., Burdick, M., Low, Q.E., Kunkel, S.L., and Strieter, R.M. (1998). MIP-1alpha as a critical macrophage chemoattractant in murine wound repair. J. Clin. Invest. *101*, 1693–1698.

Dusseaux, M., Martin, E., Serriari, N., Péguillet, I., Premel, V., Louis, D., Milder, M., Le Bourhis, L., Soudais, C., Treiner, E., and Lantz, O. (2011). Human MAIT cells are xenobiotic-resistant, tissue-targeted, CD161hi IL-17-secreting T cells. Blood *117*, 1250–1259.

Fergusson, J.R., Smith, K.E., Fleming, V.M., Rajoriya, N., Newell, E.W., Simmons, R., Marchi, E., Björkander, S., Kang, Y.H., Swadling, L., et al. (2014). CD161 defines a transcriptional and functional phenotype across distinct human T cell lineages. Cell Rep. *9*, 1075–1088.

Fergusson, J.R., Hühn, M.H., Swadling, L., Walker, L.J., Kurioka, A., Llibre, A., Bertoletti, A., Holländer, G., Newell, E.W., Davis, M.M., et al. (2015). CD161(int) CD8+ T cells: a novel population of highly functional, memory CD8+ T cells enriched within the gut. Mucosal Immunol. *9*, 401–413.

Geremia, A., Arancibia-Cárcamo, C.V., Fleming, M.P.P., Rust, N., Singh, B., Mortensen, N.J., Travis, S.P.L., and Powrie, F. (2011). IL-23-responsive innate lymphoid cells are increased in inflammatory bowel disease. J. Exp. Med. *208*, 1127–1133.

Gibbs, A., Leeansyah, E., Introini, A., Paquin-Proulx, D., Hasselrot, K., Andersson, E., Broliden, K., Sandberg, J.K., and Tjernlund, A. (2017). MAIT cells reside in the female genital mucosa and are biased towards IL-17 and IL-22 production in response to bacterial stimulation. Mucosal Immunol. *10*, 35–45.

Godfrey, D.I., Uldrich, A.P., McCluskey, J., Rossjohn, J., and Moody, D.B. (2015). The burgeoning family of unconventional T cells. Nat. Immunol. *16*, 1114–1123.

Harrison, O.J., Linehan, J.L., Shih, H.-Y., Bouladoux, N., Han, S.-J., Smelkinson, M., Sen, S.K., Byrd, A.L., Enamorado, M., Yao, C., et al. (2019). Commensal-specific T cell plasticity promotes rapid tissue adaptation to injury. Science *363*, eaat6280.

Heng, T.S., and Painter, M.W.; Immunological Genome Project Consortium (2008). The Immunological Genome Project: networks of gene expression in immune cells. Nat. Immunol. *9*, 1091–1094.

Hennig, C., Adams, N., and Hansen, G. (2009). A versatile platform for comprehensive chip-based explorative cytometry. Cytometry A *75*, 362–370.

Hinks, T.S.C., Marchi, E., Jabeen, M., Olshansky, M., Kurioka, A., Pediongco, T.J., Meehan, B.S., Kostenko, L., Turner, S.J., Corbett, A.J., et al. (2019). Activation and In Vivo Evolution of the MAIT Cell Transcriptome in Mice and Humans Reveals Tissue Repair Functionality. Cell Rep. *28*, 3249–3262.

Hoffmann, D.C., Textoris, C., Oehme, F., Klaassen, T., Goppelt, A., Römer, A., Fugmann, B., Davidson, J.M., Werner, S., Krieg, T., and Eming, S.A. (2011). Pivotal role for alpha1-antichymotrypsin in skin repair. J. Biol. Chem. *286*, 28889–28901.

Holmkvist, P., Roepstorff, K., Uronen-Hansson, H., Sandén, C., Gudjonsson, S., Patschan, O., Grip, O., Marsal, J., Schmidtchen, A., Hornum, L., et al. (2015). A major population of mucosal memory CD4+ T cells, coexpressing IL-18Rα and DR3, display innate lymphocyte functionality. Mucosal Immunol. *8*, 545–558.

Jin, S., Chin, J., Seeber, S., Niewoehner, J., Weiser, B., Beaucamp, N., Woods, J., Murphy, C., Fanning, A., Shanahan, F., et al. (2013). TL1A/TNFSF15 directly induces proinflammatory cytokines, including TNFα, from CD3+CD161+ T cells to exacerbate gut inflammation. Mucosal Immunol. *6*, 886–899.

Johnson, W.E., Li, C., and Rabinovic, A. (2007). Adjusting batch effects in microarray expression data using empirical Bayes methods. Biostatistics *8*, 118–127.

Kjer-Nielsen, L., Patel, O., Corbett, A.J., Le Nours, J., Meehan, B., Liu, L., Bhati, M., Chen, Z., Kostenko, L., Reantragoon, R., et al. (2012). MR1 presents microbial vitamin B metabolites to MAIT cells. Nature *491*, 717–723.

Klenerman, P., and Ogg, G. (2018). Killer T cells show their kinder side. Nature *555*, 594–595.

Kurioka, A., Ussher, J.E., Cosgrove, C., Clough, C., Fergusson, J.R., Smith, K., Kang, Y.-H., Walker, L.J., Hansen, T.H., Willberg, C.B., and Klenerman, P. (2015). MAIT cells are licensed through granzyme exchange to kill bacterially sensitized targets. Mucosal Immunol. *8*, 429–440.

Kurioka, A., Jahun, A.S., Hannaway, R.F., Walker, L.J., Fergusson, J.R., Sverremark-Ekström, E., Corbett, A.J., Ussher, J.E., Willberg, C.B., and Klenerman, P. (2017). Shared and Distinct Phenotypes and Functions of Human CD161++ Vα7.2+ T Cell Subsets. Front. Immunol. *8*, 1031.

Lamichhane, R., Schneider, M., de la Harpe, S.M., Harrop, T.W.R., Hannawat, R.F., Dearden, P.K., Kirman, J.R., Tyndall, J.D., Vernall, A.J., and Ussher, J.E. (2019). TCR- or Cytokine-Activated CD8+ Mucosal-Associated Invariant T Cells Are Rapid Polyfunctional Effectors That Can Coordinate Immune Responses. Cell Rep. *28*, 3061–3076.

Leek, J.T., Johnson, W.E., Parker, H.S., Fertig, E.J., Jaffe, A.E., Storey, J.D., Zhang, Y., and Torres, L.C. (2019). sva: Surrogate Variable Analysis. R package version 3.32.1 (Bioconductor).

Li, Z., Hodgkinson, T., Gothard, E.J., Boroumand, S., Lamb, R., Cummins, I., Narang, P., Sawtell, A., Coles, J., Leonov, G., et al. (2016). Epidermal Notch1 recruits RORγ(+) group 3 innate lymphoid cells to orchestrate normal skin repair. Nat. Commun. *7*, 11394.

Linehan, J.L., Harrison, O.J., Han, S.-J., Byrd, A.L., Vujkovic-Cvijin, I., Villarino, A.V., Sen, S.K., Shaik, J., Smelkinson, M., Tamoutounour, S., et al. (2018). Non-classical Immunity Controls Microbiota Impact on Skin Immunity and Tissue Repair. Cell *172*, 784–796.e18.

Loh, L., Wang, Z., Sant, S., Koutsakos, M., Jegaskanda, S., Corbett, A.J., Liu, L., Fairlie, D.P., Crowe, J., Rossjohn, J., et al. (2016). Human mucosal-associated invariant T cells contribute to antiviral influenza immunity via IL-18-dependent activation. Proc. Natl. Acad. Sci. USA *113*, 10133–10138.

López-Sagaseta, J., Dulberger, C.L., McFedries, A., Cushman, M., Saghatelian, A., and Adams, E.J. (2013). MAIT recognition of a stimulatory bacterial antigen bound to MR1. J. Immunol. *191*, 5268–5277.

Mak, J.Y., Xu, W., Reid, R.C., Corbett, A.J., Meehan, B.S., Wang, H., Chen, Z., Rossjohn, J., McCluskey, J., Liu, L., and Fairlie, D.P. (2017). Stabilizing short-lived Schiff base derivatives of 5-aminouracils that activate mucosal-associated invariant T cells. Nat. Commun. *8*, 14599.

Marchi, E., Lee, L.N., and Klenerman, P. (2019). Inflation vs. Exhaustion of Antiviral CD8+ T-Cell Populations in Persistent Infections: Two Sides of the Same Coin? Front. Immunol. *10*, 197.

Meylan, F., Davidson, T.S., Kahle, E., Kinder, M., Acharya, K., Jankovic, D., Bundoc, V., Hodges, M., Shevach, E.M., Keane-Myers, A., et al. (2008). The TNF-family receptor DR3 is essential for diverse T cell-mediated inflammatory diseases. Immunity *29*, 79–89.

Migone, T.S., Zhang, J., Luo, X., Zhuang, L., Chen, C., Hu, B., Hong, J.S., Perry, J.W., Chen, S.F., Zhou, J.X.H., et al. (2002). TL1A is a TNF-like ligand for DR3 and TR6/DcR3 and functions as a T cell costimulator. Immunity *16*, 479–492.

Pesu, M., Watford, W.T., Wei, L., Xu, L., Fuss, I., Strober, W., Andersson, J., Shevach, E.M., Quezado, M., Bouladoux, N., et al. (2008). T-cell-expressed proprotein convertase furin is essential for maintenance of peripheral immune tolerance. Nature *455*, 246–250.

Povoleri, G.A.M., Nova-Lamperti, E., Scottà, C., Fanelli, G., Chen, Y.-C., Becker, P.D., Boardman, D., Costantini, B., Romano, M., Pavlidis, P., et al.

(2018). Human retinoic acid-regulated CD161^{+} regulatory T cells support wound repair in intestinal mucosa. Nat. Immunol. *19*, 1403–1414.

Prehn, J.L., Mehdizadeh, S., Landers, C.J., Luo, X., Cha, S.C., Wei, P., and Targan, S.R. (2004). Potential role for TL1A, the new TNF-family member and potent costimulator of IFN-γ, in mucosal inflammation. Clin. Immunol. *112*, 66–77.

Rahimpour, A., Koay, H.F., Enders, A., Clanchy, R., Eckle, S.B.G., Meehan, B., Chen, Z., Whittle, B., Liu, L., Fairlie, D.P., et al. (2015). Identification of phenotypically and functionally heterogeneous mouse mucosal-associated invariant T cells using MR1 tetramers. J. Exp. Med. *212*, 1095–1108.

Reantragoon, R., Corbett, A.J., Sakala, I.G., Gherardin, N.A., Furness, J.B., Chen, Z., Eckle, S.B.G., Uldrich, A.P., Birkinshaw, R.W., Patel, O., et al. (2013). Antigen-loaded MR1 tetramers define T cell receptor heterogeneity in mucosal-associated invariant T cells. J. Exp. Med. *210*, 2305–2320.

Ritchie, M.E., Phipson, B., Wu, D., Hu, Y., Law, C.W., Shi, W., and Smyth, G.K. (2015). limma powers differential expression analyses for RNA-sequencing and microarray studies. Nucleic Acids Res. *43*, e47.

Rouxel, O., Da Silva, J., Beaudoin, L., Nel, I., Tard, C., Cagninacci, L., Kiaf, B., Oshima, M., Diedisheim, M., Salou, M., et al. (2017). Cytotoxic and regulatory roles of mucosal-associated invariant T cells in type 1 diabetes. Nat. Immunol. *18*, 1321–1331.

Rutz, S., Wang, X., and Ouyang, W. (2014). The IL-20 subfamily of cytokines—from host defence to tissue homeostasis. Nat. Rev. Immunol. *14*, 783–795.

Sareneva, T., Julkunen, I., and Matikainen, S. (2000). IFN-alpha and IL-12 induce IL-18 receptor gene expression in human NK and T cells. J. Immunol. *165*, 1933–1938.

Sattler, A., Wagner, U., Rossol, M., Sieper, J., Wu, P., Krause, A., Schmidt, W.A., Radmer, S., Kohler, S., Romagnani, C., and Thiel, A. (2009). Cytokine-induced human IFN-gamma-secreting effector-memory Th cells in chronic autoimmune inflammation. Blood *113*, 1948–1956.

Sattler, A., Dang-Heine, C., Reinke, P., and Babel, N. (2015). IL-15 dependent induction of IL-18 secretion as a feedback mechanism controlling human MAIT-cell effector functions. Eur. J. Immunol. *45*, 2286–2298.

Serriari, N.E., Eoche, M., Lamotte, L., Lion, J., Fumery, M., Marcelo, P., Chatelain, D., Barre, A., Nguyen-Khac, E., Lantz, O., et al. (2014). Innate mucosal-associated invariant T (MAIT) cells are activated in inflammatory bowel diseases. Clin. Exp. Immunol. *176*, 266–274.

Shih, D.Q., Kwan, L.Y., Chavez, V., Cohavy, O., Gonsky, R., Chang, E.Y., Chang, C., Elson, C.O., and Targan, S.R. (2009). Microbial induction of inflammatory bowel disease associated gene TL1A (TNFSF15) in antigen presenting cells. Eur. J. Immunol. *39*, 3239–3250.

Slichter, C.K., McDavid, A., Miller, H.W., Finak, G., Seymour, B.J., McNevin, J.P., Diaz, G., Czartoski, J.L., McElrath, M.J., Gottardo, R., and Prlic, M. (2016). Distinct activation thresholds of human conventional and innate-like memory T cells. JCI Insight *1*, 1–16.

Sobkowiak, M.J., Davanian, H., Heymann, R., Gibbs, A., Emgård, J., Dias, J., Aleman, S., Krüger-Weiner, C., Moll, M., Tjernlund, A., et al. (2019). Tissue-resident MAIT cell populations in human oral mucosa exhibit an activated profile and produce IL-17. Eur. J. Immunol. *49*, 133–143.

Subramanian, A., Tamayo, P., Mootha, V.K., Mukherjee, S., Ebert, B.L., Gillette, M.A., Paulovich, A., Pomeroy, S.L., Golub, T.R., Lander, E.S., and Mesirov, J.P. (2005). Gene set enrichment analysis: a knowledge-based approach for interpreting genome-wide expression profiles. Proc. Natl. Acad. Sci. USA *102*, 15545–15550.

Tang, C., Kakuta, S., Shimizu, K., Kadoki, M., Kamiya, T., Shimazu, T., Kubo, S., Saijo, S., Ishigame, H., Nakae, S., and Iwakura, Y. (2018). Suppression of IL-17F, but not of IL-17A, provides protection against colitis by inducing T_{reg} cells through modification of the intestinal microbiota. Nat. Immunol. *19*, 755–765.

Tominaga, K., Yoshimoto, T., Torigoe, K., Kurimoto, M., Matsui, K., Hada, T., Okamura, H., and Nakanishi, K. (2000). IL-12 synergizes with IL-18 or IL-1beta for IFN-gamma production from human T cells. Int. Immunol. *12*, 151–160.

Turtle, C.J., Delrow, J., Joslyn, R.C., Swanson, H.M., Basom, R., Tabellini, L., Delaney, C., Heimfeld, S., Hansen, J.A., and Riddell, S.R. (2011). Innate signals overcome acquired TCR signaling pathway regulation and govern the fate of human CD161(hi) CD8α^{+} semi-invariant T cells. Blood *118*, 2752–2762.

Ussher, J.E., Bilton, M., Attwod, E., Shadwell, J., Richardson, R., de Lara, C., Mettke, E., Kurioka, A., Hansen, T.H., Klenerman, P., and Willberg, C.B. (2014a). CD161++ CD8+ T cells, including the MAIT cell subset, are specifically activated by IL-12+IL-18 in a TCR-independent manner. Eur. J. Immunol. *44*, 195–203.

Ussher, J.E., Klenerman, P., and Willberg, C.B. (2014b). Mucosal-associated invariant T-cells: new players in anti-bacterial immunity. Front. Immunol. *5*, 450.

van Wilgenburg, B., Scherwitzl, I., Hutchinson, E.C., Leng, T., Kurioka, A., Kulicke, C., de Lara, C., Cole, S., Vasanawathana, S., Limpitikul, W., et al.; STOP-HCV Consortium (2016). MAIT cells are activated during human viral infections. Nat. Commun. *7*, 11653.

Varelias, A., Bunting, M.D., Ormerod, K.L., Koyama, M., Olver, S.D., Straube, J., Kuns, R.D., Robb, R.J., Henden, A.S., Cooper, L., et al. (2018). Recipient mucosal-associated invariant T cells control GVHD within the colon. J. Clin. Invest. *128*, 1919–1936.

Wang, H., D'Souza, C., Lim, X.Y., Kostenko, L., Pediongco, T.J., Eckle, S.B.G., Meehan, B.S., Shi, M., Wang, N., Li, S., et al. (2018). MAIT cells protect against pulmonary *Legionella longbeachae* infection. Nat. Commun. *9*, 3350.

West, N.R., Hegazy, A.N., Owens, B.M.J., Bullers, S.J., Linggi, B., Buonocore, S., Coccia, M., Görtz, D., This, S., Stockenhuber, K., et al.; Oxford IBD Cohort Investigators (2017). Oncostatin M drives intestinal inflammation and predicts response to tumor necrosis factor-neutralizing therapy in patients with inflammatory bowel disease. Nat. Med. *23*, 579–589.

Wilgenburg, B.V., Loh, L., Chen, Z., Pediongco, T.J., Wang, H., Shi, M., Zhao, Z., Koutsakos, M., Nüssing, S., Sant, S., et al. (2018). MAIT cells contribute to protection against lethal influenza infection *in vivo*. Nat. Commun. *9*, 4706.

STAR★METHODS

KEY RESOURCES TABLE

REAGENT or RESOURCE	SOURCE	IDENTIFIER
Antibodies		
LEAF-purified mouse anti-human CD3 (clone UCHT1)	Biolegend	Discontinued Alternative: Cat# 300438; RRID: AB_11146991
LEAF-purified mouse anti-human CD28 (clone CD28.2)	Biolegend	Cat# 302914; RRID: AB_314316
LEAF-purified mouse anti mouse/rat/human MR1 (clone 26.5)	Biolegend	Cat# 361103; RRID: AB_2563041
Anti-human CD3 (clone UCHT1) PerCp/Cy.5	Biolegend	Cat# 300428; RRID: AB_893298
Anti-human CD3 (clone OKT3) eFluor450	eBioScience	Cat# 48-0037-42; RRID: AB_1272055
Anti-human CD3 (clone OKT3) BV605	Biolegend	Cat# 317321; RRID: AB_11126166
Anti-human CD4 (clone M-T466) VioGreen	Miltenyi	Cat# 130-113-259; RRID: AB_2726060
Anti-human CD4 (clone OKT4) PerCP/Cy5.5	eBioScience	Cat# 45-0048-42; RRID: AB_10804390
Anti-human CD8 (clone SK1) FITC	Biolegend	Cat# 344704; RRID: AB_1877178
Anti-human CD8 (clone REA734) VioGreen	Miltenyi	Cat# 130-110-684; RRID: AB_2659245
Anti-human CD8 (clone REA734) PE-Vio770	Miltenyi	Cat# 130-110-680; RRID: AB_2659245
Anti-human CD39 (clone A1) PE	Biolegend	Cat# 328207; RRID: AB_940427
Anti-human CD69 (clone H1.2F3) eFluor450	eBioScience	Cat# 48-0691-82; RRID: AB_10719430
Anti-human CD103 (Ber-ACT8) PE	Biolegend	Cat# 350206; RRID: AB_10641843
Anti-human CD161 (clone 191B8) APC	Miltenyi	Cat# 130-113-590; RRID: AB_2733346
Anti-human CD161 (clone 191B8) PE	Miltenyi	Cat# 130-113-593; RRID: AB_2733772
Anti-human CD161 (clone 191B8) PE-Vio770	Miltenyi	Cat# 130-113-594; RRID: AB_2751134
Anti-human CCL3/(4) (clone 93342) APC	R&D Systems	Cat# AF270NA; RRID: AB_354436
Anti-human Furin (clone 222722) AF647	R&D Systems	Cat# IC1503R-100UG; https://www.rndsystems.com/products/human-furin-alexa-fluor-647-conjugated-antibody-222722_ic1503r
Anti-human GM-CSF (clone BVD2-21C11) PerCP/Cy5.5	Biolegend	Cat# 502312; RRID: AB_11147946
Anti-human GrB (clone GB12) APC	Initrogen	Cat# MHGB05; RRID: AB_1500190
Anti-human GrB (clone GB11) AF700	BD BioSciences	Cat# 561016; RRID: AB_2033973
Anti-human IFNγ (clone 4S.B3) AF700	Biolegend	Cat# 502520; RRID: AB_528921
Anti-human IFNγ (clone 45-15) FITC	Miltenyi	Cat# 130-091-641; RRID: AB_244194
Anti-human IFNγ (clone 4S.B3) PE/Cy7	Biolegend	Cat# 502528; RRID: AB_2123323
Anti-human IgG2bκ (clone 133303) AF647	R&D Systems	Cat# IC0041R; RRID: AB_2737095
Anti-human PD-1 (clone EH12.2H7) BV421	Biolegend	Cat# 329920; RRID: AB_10960742
Anti-human/mouse PLZF (clone R17-809) PE	BD Pharmigen	Cat# 564850; RRID: AB_2738984
Anti-human TNFα (clone Mab11) FITC	Biolegend	Cat# 502906; RRID: AB_315258
Anti-human TNFα (clone Mab11) PerCP/Cy5.5	Biolegend	Cat# 502926; RRID: AB_2204081
Anti-human Vα7.2 (clone 3C10) APC	Biolegend	Cat# 351708; RRID: AB_10933246
Anti-human Vα7.2 (clone 3C10) FITC	Biolegend	Cat# 351704; RRID: AB_10900975
Anti-human Vα7.2 (clone 3C10) PE	Biolegend	Cat# 351710; RRID: AB_2561954
Anti-human Vα7.2 (clone 3C10) PE/Cy7	Biolegend	Cat# 31712; RRID: AB_2561994
Anti-human TCRγ/δ (clone IMMU510) FITC	Beckman Coulter	Cat# IM1571U; https://www.mybeckman.uk/reagents/coulter-flow-cytometry/antibodies-and-kits/single-color-antibodies/tcr-pan-g-d/im1571u
Anti-human TCRγ/δ (clone 11F2) APC-Vio770	Miltenyi	Cat# 130-113-501; RRID: AB_2751120

(*Continued on next page*)

Continued

REAGENT or RESOURCE	SOURCE	IDENTIFIER
Bacterial and Virus Strains		
E.coli DH5α	Invitrogen	Cat# 18265017
Biological Samples		
Leukocyte cones	NHS Blood and Transplant	https://www.nhsbt.nhs.uk/
Patient-derived resections (CRC)	TGU Biobank	https://www.expmedndm.ox.ac.uk/tgu/tgu-biobank-ibd-cohort
Patient-derived resection (IBD)	TGU Biobank	https://www.expmedndm.ox.ac.uk/tgu/tgu-biobank-ibd-cohort
Chemicals, Peptides, and Recombinant Proteins		
Brefeldin A solution (1000X)	eBioScience	Cat# 00-4506-51
5-OP-RU	Fairlie group, Mak et al., 2017	N/A
Collagenase A	Roche (mft)/ Merck	Cat# 10103578001
DNase I	Roche (mft)/ Merck	Cat# 11284932001
SuperScript III Reverse Transcriptase	Invitrogen	Cat# 18080093
Human IL-12, premium grade	Miltenyi	Cat# 130-096-705
Human IL-15, premium grade	Miltenyi	Cat# 130-095-764
Recombinant Human IL-18	MBL	Cat# B001-5
Recombinant Human TL1A/TNFSF15	R&D Systems	Cat# 1319-TL-010
Critical Commercial Assays		
T cell Activation/Expansion Kit, human	Miltenyi	Cat# 130-091-441
RNeasy Micro Kit	Quiagen	Cat# 74004
LIVE/DEAD Fixable Near IR Dead Cell Stain Kit	Invitrogen	Cat# L10119
Permeabilization buffer (10x)	eBioScience	Cat# 00-8333-56
CD8 MicroBeads, human	Miltenyi	Cat# 130-045-201
Deposited Data		
RNA-seq files (UT, T, C, CT)	This Paper	GEO GSE129906
Experimental Models: Cell Lines		
THP-1	ATCC	TIB-202; RRID: CVCL 0006
Caco2	ATCC	HTB-37; RRID: CVCL 0025
Oligonucleotides		
Primer specific for *OSM*: Forward > cttccccagtgaggagacc	Roche	N/A
Primer specific for *OSM*: Reverse > ctgctctaagtcggccagtc	Roche	N/A
Primer specific for *HBEGF*: Forward > tggggcttctcatgtttagg	Roche	N/A
Primer specific for *HBEGF*: Reverse > catgcccaacttcactttctc	Roche	N/A
Primer specific for *GAPDH*: Forward > ccccggtttctataaattgagc	Roche	N/A
Primer specific for *GAPDH*: Reverse > cttccccatggtgtctgag	Roche	N/A
Software and Algorithms		
Bioinformatics & Evolutionary Genomics	Ghent University	http://bioinformatics.psb.ugent.be/webtools/Venn/
FlowJo 10	Tree Star	https://www.flowjo.com
GSEA version 3.0	Subramanian et al., 2005	https://software.broadinstitute.org/gsea/index.jsp
Heatmapper	Wishart group, University of Alberta	http://www.heatmapper.ca

(*Continued on next page*)

Continued

REAGENT or RESOURCE	SOURCE	IDENTIFIER
ImageJ Version 1.8	NIH	https://imagej.nih.gov/ij/index.html
Partek Flow	Partek	http://www.partek.com/partek-flow/
Prism Version 6.0b	Graphpad	https://www.graphpad.com
ZellExplorer	Zellkraftwerk GmbH	http://www.zellkraftwerk.com/products/
Other		
5-OP-RU-MR1-Tetramer PE	NIH tetramer core facility	N/A
PerColl	GE Healthcare (mft)/ Merck	Cat# GE17-0891-01
Human *IL26* TaqMan Probe	Thermo Fisher Scientific	Hs00218189_m1
TaqMan Fast Advanced Master Mix	Thermo Fisher Scientific	Cat# 4444557
Zellsafe Tissue chips	Zellkraftwerk GmbH	no. 28050606/02-010

LEAD CONTACT AND MATERIALS AVAILABILITY

Further information and requests for resources and reagents should be directed to and will be fulfilled by the Lead Contact, Paul Klenerman (paul.klenerman@medawar.ox.ac.uk). Please note that this study did not generate new unique reagents.

EXPERIMENTAL MODEL AND SUBJECT DETAILS

Human samples

All tissue samples were collected with appropriate patient consent and NHS REC provided ethical approval (reference numbers 09/H0606/5 for IBD patients and 16/YH/0247 for CRC patients and polyp biopsies).

Healthy PBMCs were isolated from leukocyte cones (NHS Blood Services). For long-term storage, PBMCs were kept in liquid nitrogen with freezing media (10% DMSO, 90% fetal calf serum, both Sigma-Aldrich). These samples are fully anonymized, so data on age and gender are not available for comparison. Colonic tissues were collected in the form of polyp biopsies or from the uninvolved mucosa of patients with colorectal cancer. Patient information is shown in the table below. All patients involved gave written consent. Colonic tissues were digested at 37°C for overnight with Collagenase A (Roche) and DNase I (Sigma-Aldrich). Colonic lymphocytes were then isolated from the cell suspension by a Percoll- (GE Healthcare) gradient: cells were resuspended in 4ml of a 40% Percoll solution that was carefully overlayed over 4ml of 80% Percoll. After centrifugation (2000rpm, 20min, brake turned off), lymphocytes were obtained from the interphase between the two Percoll layers. A detailed protocol has been described by Geremia et al. (2011).

Characteristics of the CRC patients.

CRC patients	n = 21
Age (Average, SD*)	68, 12
Sex (Male/Female)	12/9
Uninflamed, tumor-free tissue origin	
Small intestine	0
Large intestine	21
Time since diagnosis (years)	1, 1
Average, SD	

*SD: standard deviation

Cell lines

Cell lines were cultured at 37°C in 5% CO_2. Caco2 cells (Colorectal adenocarcinoma cell line, ATCC) were cultured at a starting density of $4x10^5$ cell/cm^2 in T-175 cell-culture flasks, using GlutaMAX medium supplemented with 10% fetal bovine serum (FBS), 1% MEM Non-essential-amino acid solution (NEAA), 100ug/mL Penicillin-Streptomycin, 2mM L-glutamine (Sigma Aldrich). Cultures were maintained with media exchange every second day and routinely split every week when cells had reached approximately 70% confluency.

THP1 cells (Human monocyte cell line, ATCC) were cultured at a density between $2x10^5$ to 10^6 cells/mL in T-175 cell-culture using RPMI-1640 medium (Sigma Aldrich) supplemented with FBS, Penicillin-Streptomycin and L-glutamine.

METHOD DETAILS

Isolation and short-term culture of human lymphocytes

PBMCs were thawed, washed and maintained in RPMI 1640 with 10% fetal calf serum, 1% L-glutamine, and 1% penicillin/streptomycin (R10) (all Sigma-Aldrich). $CD8^+$ T cells were positively labeled with CD8 Microbeads (Miltenyi Biotech, purities were $\geq$ 90%), and enriched from PBMCs using MS or LS columns following the manufacturer's instructions (Miltenyi Biotech). Colonic lymphocytes were used without prior enrichment by CD8 microbeads and were maintained in R10 supplemented with 25ng/mL amphotericin B (GIBCO), 40 μg/mL gentamicin (GIBCO), and 10 μg/mL ciprofloxacin (Sigma-Aldrich).

In vitro stimulations

For non-specific TCR triggering, PBMCs, enriched CD8 T cells, sorted cells or colonic lymphocytes were stimulated with plate bound anti-CD3/28 antibodies (Miltenyi), or anti-CD3/28 beads (Miltenyi) at 1:1 ratio. ELISA plates (Greiner) were coated with 5 μg/mL anti-CD3/28 with the final volume of 100 μL at 4°C for overnight. Antibody mix was washed off the next morning, and plates were used after 1-hour 37°C incubation with R10. Anti-CD3/28 beads were prepared following the manufacturer's instructions.

MAIT-specific TCR triggering was achieved by co-culturing of $2x10^5$ MACS-enriched CD8s with $1x10^5$ THP1 cells which had been previously pulsed with 10nM 5-OP-RU (kindly provided by David Fairlie) for 2 hours. Unpulsed THP1s were used as controls.

For cytokine triggering, cells were stimulated for 20 hours with IL-12 (Miltenyi) at 2ng/mL, IL-18 (MBL) at 50ng/ml, IL-15 (Miltenyi) at 25ng/ml, TL1A (R&D) at 100ng/ml, unless otherwise stated.

For activation of MAIT cells by bacteria-derived ligands, THP1 cells were loaded with PFA-fixed (2%, 20min) *E. coli* (DH5α, Invitrogen) at a 25 bacteria per cell (BpC) ratio overnight. Bacterially loaded THP1s were washed and co-cultured with MACS-enriched CD8s at a 1:2 ratio. In order to block the TCR-dependent component of this activation, in some experiments an anti-MR1 blocking antibody (26.5, Biolegend) was added to the co-cultures.

Flow cytometry

Brefeldin A (eBioscience, 1000x) was added into the cell cultures for the last 4 hours before intracellular staining.

Cells were stained with the antibodies and dyes listed in the Key Resources Table and were fixed with 2% Paraformaldehyde for 10 min before acquisition on a MACSQuant cytometer (Miltenyi) or LSRII (BD Biosciences). Data were analyzed with FlowJo (Tree Star Inc.), a representative gating strategy is shown in Figure S3A.

RNA sequencing (RNaseq)

$CD8^+$ T cells were enriched from PBMCs of three healthy individuals and were rested overnight prior to sorting. On the next day, MAIT ($CD161^{2+}$ $V\alpha7.2^+$) cells were sorted using a Beckman Coulter MoFlo XDP and stimulated with a range of conditions including anti-CD3/28, cytokines (IL-12/IL-18/IL-15/TL1A), or the combination of both, or left untreated in R10 media for 24 hours. RNA was then extracted from these 12 samples using an RNeasy Micro kit (QIAGEN). The quantity and quality of extracted RNA was first evaluated using both a nanodrop spectrophotometer and the Agilent 2100 bioanalyzer. All samples had RNA integrity (RIN) values greater than 9 and were free from contaminating protein and organic compounds. RNaseq was performed by Wellcome Trust Centre for Human Genetics (University of Oxford) on a HiSeq4000v platform. Gene lists that were differentially expressed (> 4 fold, $p < 0.01$, FDR < 0.05) between various conditions and their normalized expression values, as well as the principle component analysis (PCA) plots, were generated with Partek® Flow®, an online analysis platform for Next Generation Sequencing data (http://www.partek.com/partek-flow/), following the user's guide. Volcano plots were generated with Prism software. Heatmaps were generated using normalized counts with Heatmapper (http://www.heatmapper.ca/expression/) with the averaged linkage clustering method and Pearson distance measurement method. Venn diagrams were drawn with an online diagram drawing platform developed by Ghent University, Belgium (http://bioinformatics.psb.ugent.be/webtools/Venn/). Gene set enrichment analysis (GSEA) was performed using GSEA version 3.0 (Subramanian et al., 2005), comparing gene expression data as a whole with the reference gene list obtained from the publication by Linehan et al. (2018).

qPCR

$CD161^{2+}$ $V\alpha7.2^+$ (MAIT) and $CD161^-$ $V\alpha7.2^-$ cells were sorted from pre-enriched blood $CD8^+$ T cells. These cells were then stimulated with anti-CD3/28, cytokines (IL-12/IL-18/IL-15/TL1A), the combination of both or left untreated in R10 media for 20 hours. The total RNA of sorted T cells was extracted with an RNeasy Micro kit (QIAGEN) and reverse transcribed using reverse transcribed using SuperScript III Reverse Transcriptase (Invitrogen). For detection of IL-26 mRNA, a 20X IL-26 human TaqMan® probe was used (Hs00218189_m1) with 2X TaqMan® Fast Advanced Master Mix (both from ThermoFisher Scientific). OSM and HEBGF cDNA quantification was performed with Roche ® hydrolysis probes (*OSM*: forward primer sequence, 5′-cttccccagtgaggagacc-3′, reverse sequence, 5′-ctgctctaagtcggccagtc-3′; HBEGF: forward primer sequence, 5′-tggggcttctcatgtttagg-3′, reverse sequence, 5′-catgcc caacttcactttctc-3′), with GAPDH as the internal control (forward primer sequence, 5′-ccccggtttctataaattgagc-3′, reverse sequence, 5′-cttccccatggtgtctgag-3′).

In vitro wound-healing assay

Enriched $CD8^+$ were co-cultured with THP1 cells loaded with fixed *E. coli* at 25 BpC in the presence or absence of 20 μg/mL LEAF anti-MR1 Antibody (Biolegend). Supernatants were collected at 72 hours. A total of $1.5x10^4$ Caco2 cells were seeded per well in a 96-well clear flat bottom plate (Corning) and grown to confluency at 37°C for 5 days with media exchange every 2 days. Monolayers were scratched using a WoundMaker (Essen Bioscience), washed with serum-free medium and incubated with $CD8^+$ 72h hour supernatants diluted 1:4 with fresh media. As a negative control, fresh media was used. Time lapse imaging was recorded every 4 hours using IncuCyte S3 Live Cell Analysis System (Essen Bioscience) for 36 hours at 37°C. GlutaMAX medium supplemented with 10% FBS, 1% NEAA, Penicillin-Streptomycin and L-glutamine was used throughout this experiment.

Chip Cytometry

Samples were snap frozen and cryosectioned onto cytometer chips (Zellsafe Tissue chips, Zellkraftwerk, GmbH, Deutscher Platz 5c, 04103 Leipzig, Germany). Sections were fixed *in situ* at room temperature for 10 minutes using 4% paraformaldehyde solution, then washed with 10-20 mL of PBS. Non-specific binding was blocked by incubating in 5% normal goat serum (Thermo Fisher cat016201) in PBS for at least one hour at room temperature. All antibodies were directly conjugated to their fluorophore and were diluted for the staining step in PBS. Immunostaining was performed using an iterative approach where up to three colors could be applied simultaneously. Fluorophores were subsequently bleached and a new round of antibodies applied to build up the panel (Hennig et al., 2009). Images were acquired using a Zellscanner One Chip cytometer (Zellkraftwerk) using the dedicated ZellExplorer software.

Data Integration

A selection of ImmGen (https://www.immgen.org/) samples (Heng et al., 2008) (microarrays) were merged first with a selection of RNA-Seq data from Hinks et al. (2019) and Linehan et al. (2018) (see also Fergusson et al., 2014). Raw read counts data were transformed to log2-counts per million (logCPM) using *voom* function in *limma* R package (Ritchie et al., 2015). RNA-Seq from Human MAIT cells were merged to mouse dataset using a common set of genes, using homologous ids from MGI database (http://www.informatics.jax.org/orthology.shtml). Batch effects were removed using *ComBat* function in 'sva' R package (Leek et al., 2019), using a procedure described in Johnson et al. (2007). Hierarchical clustering analysis of integrated expression profiles was performed using Euclidian distance as similarity measure and filtering genes by variance (IQR > 0.95).

QUANTIFICATION AND STATISTICAL ANALYSIS

All graphs and statistical analyses, except RNaseq data analysis, were performed using GraphPad Prism Software Version 6.0b (La Jolla, CA). Statistical significance was assessed using paired Student's t test, or repeated-measures two-way analysis of variances, with Bonferroni's correction for multiple comparison assays. For the analysis of the RNaseq dataset, Partek Flow was used. For the *in vitro* wound-healing assay, ImageJ v1.8 was used to determine the area of wounds. Area at different time points were normalized as a percentage of the initial area. All data were presented as means ± SEM.

DATA AND CODE AVAILABILITY

The accession number for the raw and pre-processed data from the RNaseq datasets reported in this paper is GEO: GSE129906.

Cell Reports, Volume *28*

Supplemental Information

TCR and Inflammatory Signals Tune Human MAIT Cells to Exert Specific Tissue Repair and Effector Functions

Tianqi Leng, Hossain Delowar Akther, Carl-Philipp Hackstein, Kate Powell, Thomas King, Matthias Friedrich, Zoe Christoforidou, Sarah McCuaig, Mastura Neyazi, Carolina V. Arancibia-Cárcamo, Joachim Hagel, Fiona Powrie, Oxford IBD Investigators, Raphael Sanches Peres, Val Millar, Daniel Ebner, Rajesh Lamichhane, James Ussher, Timothy S.C. Hinks, Emanuele Marchi, Chris Willberg, and Paul Klenerman

Supplementary Figure 1

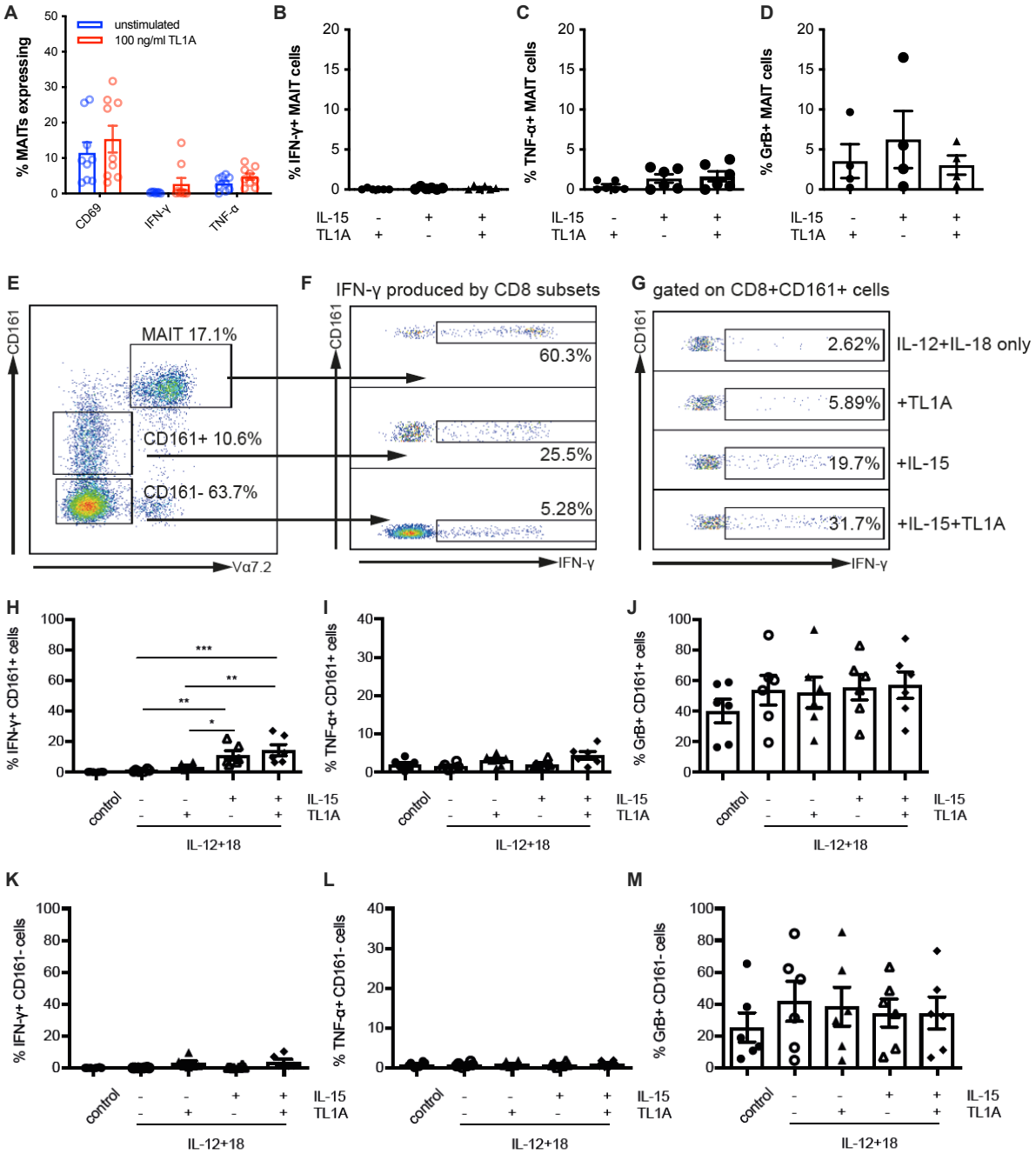

SFigure 1 (related to Fig 1). **TL1A and IL-15 alone do not promote MAIT cell effector functions and have only a limited effect on CD161+ and CD161- CD8+ T-cells.** CD8+ T cells were enriched from healthy PBMCs and stimulated overnight with combinations of the indicated cytokines. **(A)** Proportion of CD8+ MAIT cells producing CD69, IFN-γ, and TNF-αwhen left untreated, or stimulated singly with 100ng/ml TL1A. **(B-D)** Frequency of MAIT cells expressing IFN-γ (B), TNF-α (C) or GrB (D) upon stimulation with TL1A (100ng/ml), IL- 15 (25ng/ml) or both cytokines. **(E)** Gating strategy for CD8+ MAIT (CD161++Vα7.2+)/CD161+Vα7.2-/CD161-Vα7.2-cells **(F)** Proportion of CD8+MAIT (CD161++Vα7.2+), CD161+Vα7.2-, or CD161-Vα7.2-cells producing IFN-γ when stimulated with IL-12, IL-15, IL-18 and TL1A. **(G)** Proportion of CD8+CD161+Vα7.2-cells producing IFN-γ when stimulated with a range of conditions. **(H-M)** Proportion of CD8+CD161+Vα7.2- cells (H-J) or CD8+CD161-Vα7.2- cells (K-M) producing IFN-γ (H and K), TNF-α (I and L), or GrB (J and M) when treated with combinations of TL1A (100ng/ml) and IL-15 (25ng/ml) with suboptimal IL-12/18 (2ng/ml). Data were acquired from 6-8 donors in 2-3 experiments. Error bars represents mean ± SEM. Differences between the conditions were analysed by Friedman tests with Dunn's multiple comparison tests.

Supplementary Figure 2

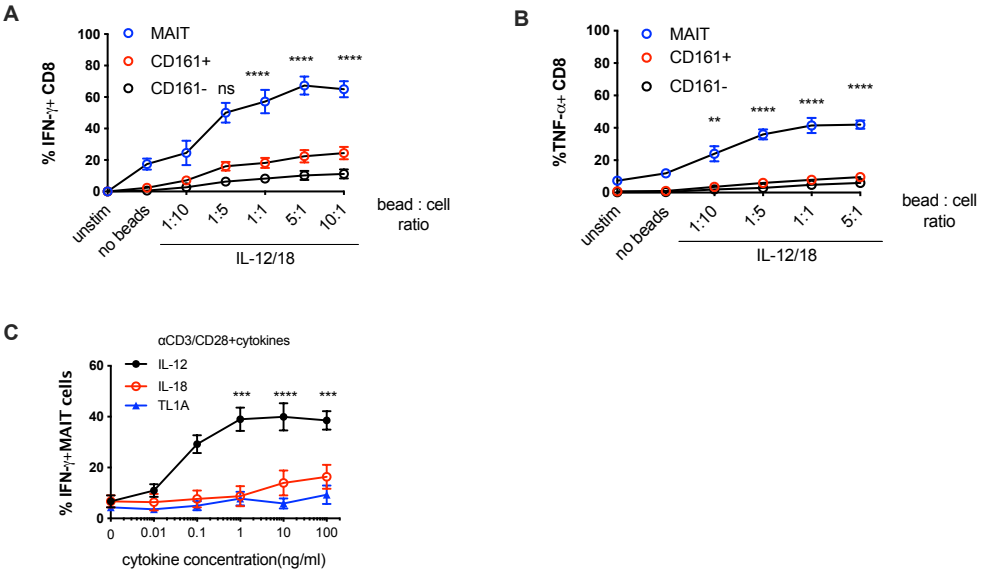

SFigure 2 (related to Fig. 2). **Functional studies on the impact of combined TCR and cytokine signalling.** CD8+ T cells were enriched from healthy PBMCs and stimulated in different ways. **(A, B)** Proportion of CD8+ MAIT (CD161++Vα7.2+)/CD161+/CD161- cells producing IFN-γ (A) or TNF-α (B) following overnight incubation with suboptimal concentrations of IL-12 and IL-18, plus αCD3/CD28 beads at increasing bead-to-cell ratios. **(C)** Proportion of CD8+MAIT cells producing IFN-γ (following stimulation with increasing concentrations of cytokines: IL-12, IL-18, or TL1A, respectively in the presence of plate-bound αCD3/CD28 antibodies. Data were acquired from 7-8 donors in three experiments. Differences between the conditions were analysed by 2way ANOVA with Tuckeys multiple comparison tests (A-C). Error bars represents mean ± SEM. ns = not significant, **p<0.01, ***p<0.001, ****p<0.0001.

Supplementary Figure 3

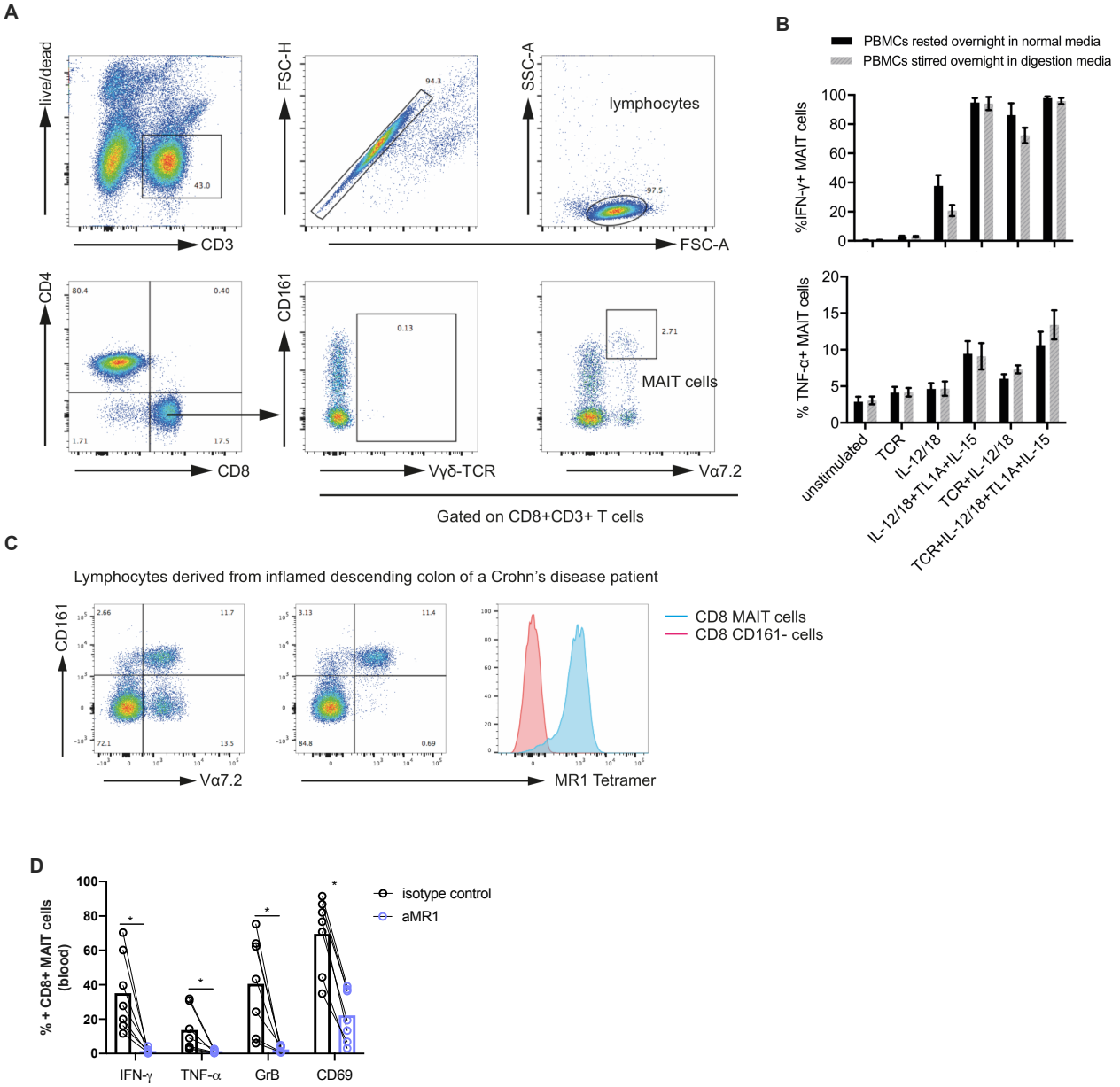

SFigure 3 (related to Fig. 3). **Identification of MAIT cells in the colonic lamina propria and additional functional studies on blood-derived MAITs. (A)** Gating strategy to identify CD8+MAIT cells from gut LPLs. **(B)** Proportion of CD8+MAIT cells producing IFN-γ or TNF-α after overnight stimulations. CD8+MAIT cells were derived from PBMCs, which, prior to stimulation, were either rested in the normal media or stirred in the digestion media containing DNase and Collagenase A for 12 hours. (**C)** Representative plot showing how to identify MAIT cells from the gut by using either a conventional Vα7.2 TCR staining antibody or the MR1-tetramer staining antibody, in combination with CD161 staining. **(D)** Proportion of CD8+ MAIT cell expressing the indicated molecules after overnight co-culture with THP1 cells incubated with 25 fixed *E. coli* bacteria per cell in the presence of a blocking antibody directed against MR1 or an isotype control. Data were acquired from 1-7 donors in 1-3 experiments. Differences between the conditions were analysed by Wilcoxon tests (D). *p<0.05

Supplementary Figure 4

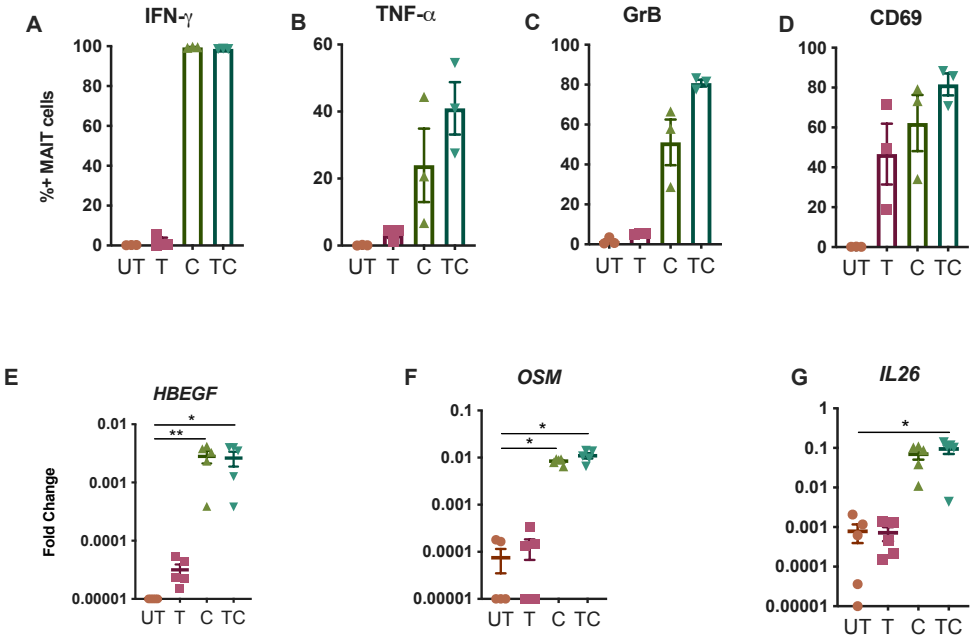

SFigure 4 (related to Fig. 4). **Expression of effector molecules by MAITs treated with the conditions used in the RNAseq study.** CD8+ T-cells were MACS enriched and left untreated (UT) or were stimulated with αCD3/28 beads (T), suboptimal IL-12/18 in combination with TL1A and IL-15 (C) or with a combination of the aforementioned cytokines and αCD3/28 beads (TC) overnight. **(A-D)** Proportion of CD8+MAIT cells isolated from parts of the samples used for the RNAseq experiment producing IFN-γ (A), TNF-α (B), GrB (C) or CD69 (D). Each dot corresponds to a donor of the RNAseq study, data were acquired from 3 donors in one experiment. **(E-G)** Expression levels of *HBEGF* (E), *OSM* (F) and *IL26* (G) in CD8+MAIT cells (n=5) examined by qPCR. GAPDH was used as house-keeping gene. Data were acquired from five donors in two experiments. Error bars represents mean ± SEM. Differences between conditions were analysed by Friedman tests with Dunn's multiple comparisons tests. *p<0.05, **p<0.01.

Supplementary Figure 5

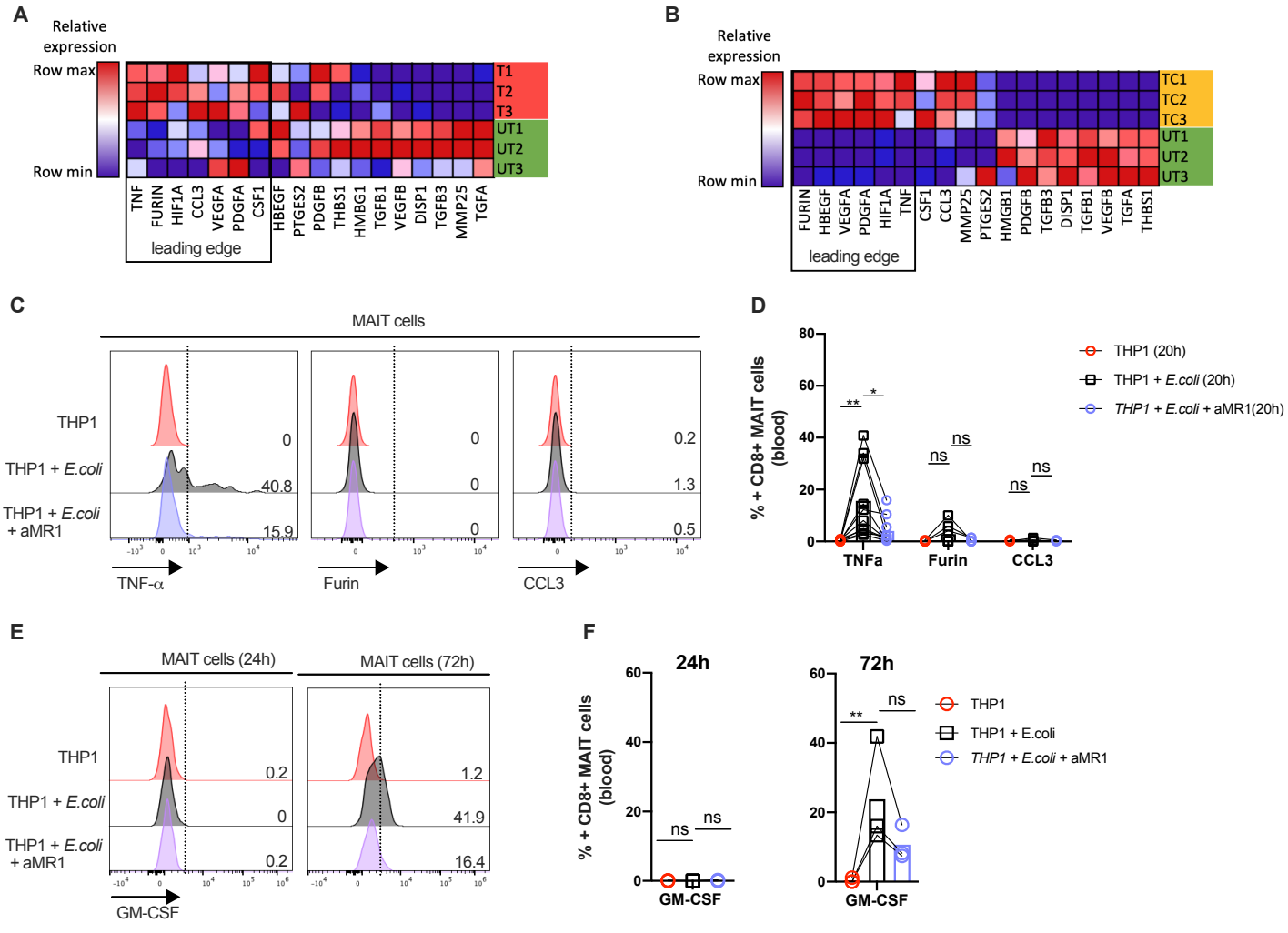

SFigure 5 (related to Fig. 5). **Further investigation of tissue repair related functions of MAIT cells. (A, B)** Relative expression of the genes of the tissue repair gene set by MAIT cells stimulated by TCR (A) or TCR+cytokines (B) compared to unstimulated controls. The leading edge genes of the corresponding GSEA plots (F6) are marked. The original tissue repair gene set of 101 genes was restricted to the genes present in our dataset. Data were acquired from 3 healthy donors in one experiment. **(C)** Flow cytometry analysis of the expression of TNF-α, Furin and CCL3 by CD161++/MAIT CD8+ T cells in response to fixed *E. coli* presented by THP1 cells in the presence or absence of an anti-MR1 (αMR1) blocking antibody at 20h timepoint. (**D**) Statistical analysis of the expression of the effector molecules shown in (A). Data were acquired from seven donors in three experiments. **(E)** Flow cytometry and **(F)** statistical analysis of the expression of GM-CSF by CD161++/MAIT CD8+ T cells at 20h and 72h timepoints using the conditions described in (A). Data were acquired from three donors in one experiment.

Supplementary Figure 6

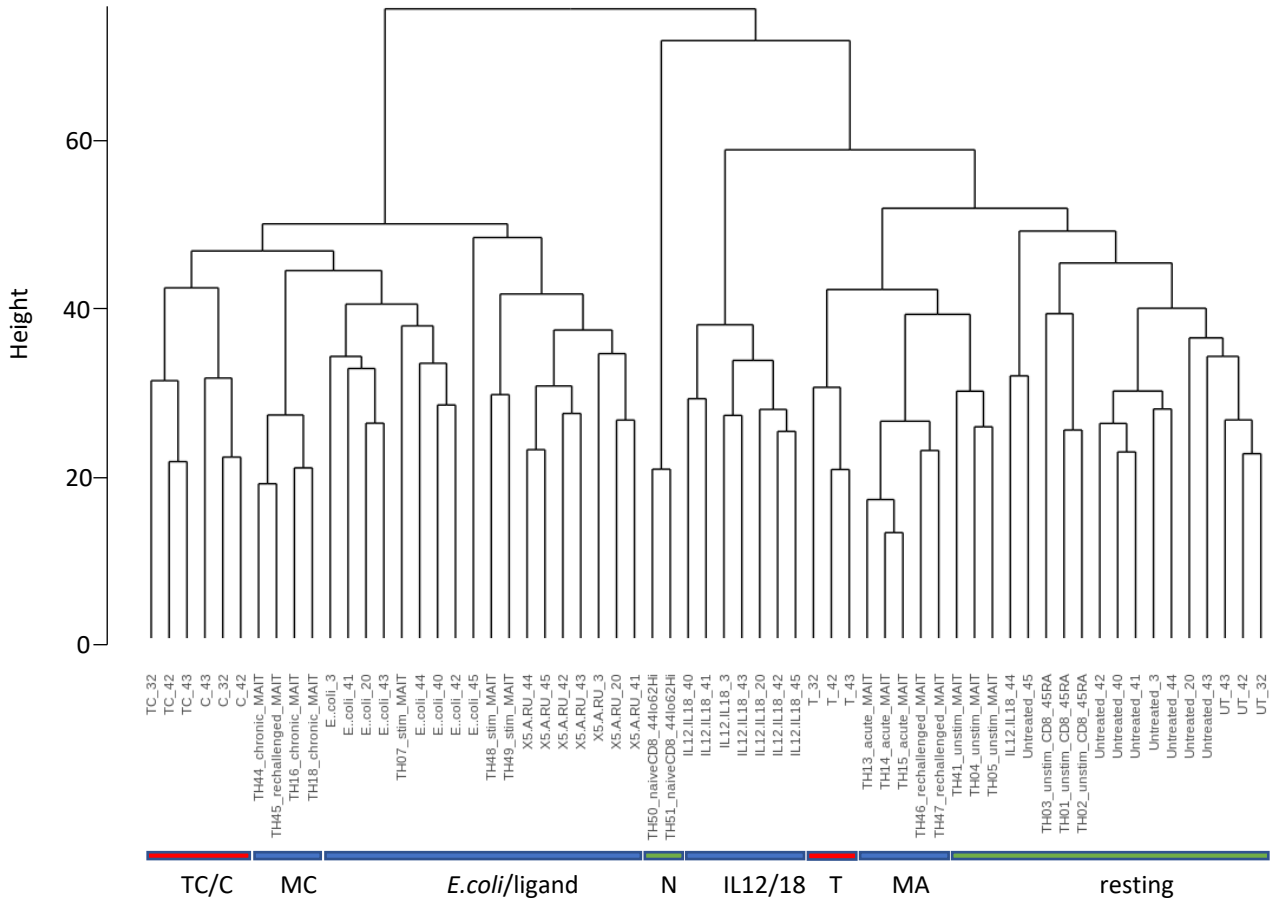

SFigure 6 (related to Fig. 6). **Data fusion of three recently generated human and mouse MAIT datasets.** In this plot we have extended the data fusion shown in Figure 6, by including the human datasets from Lamichhane et al (Lamichhane et al., 2019). The other background data have been removed. Cells are indicated as either naïve or unstimulated (N), acutely activated in vivo (MA) or chronically activated in vivo (MC). Similarity between the expression profiles is measured using a Euclidean distance (Height).

Ex-vivo identification and characterisation of MR1-restricted T cells in healthy donors and colorectal cancer patients

Hossain Delowar Akther[1, 2, 3], Rahul Khanolkar[3], Richard Suckling[3], Robert Simmons[3], Lauren Chessum[3], Shaliny Ramachandran[3], Nicola Smith[3], Carl-Philipp Hackstein[1, 2], Mariolina Salio[3], Carolina V. Arancibia-Cárcamo[2], David Cole[3], Marco Lepore[3], Paul Klenerman[1, 2]
1 Peter Medawar Building for Pathogen Research, University of Oxford, United Kingdom
2 Nuffield Department of Medicine, University of Oxford, United Kingdom
3 Immunocore Ltd, Abingdon, Oxford, United Kingdom

Introduction: MR1 as a target for cancer therapy

-MR1 is a non-polymorphic antigen-presenting molecule that can accommodate small metabolites. Riboflavin and folate derivates such as 5-OP-RU and 6FP are two of the most well-studied MR1 ligands, with the former one being able to stimulate mucosal-associated invariant T (MAIT) cells (1).

-Although the nature of other natural MR1 ligands remains elusive, recent reports suggest a link between cell metabolism, generation of endogenous MR1 ligands and MR1-specific T-cell (MR1-T) recognition. This highlights the potential of harnessing MR1-T cells for treating diseases associated with aberrant metabolic alterations, such as cancer (2,3).

-The heterogeneity of MR1-Ts and the lack of specific markers represent challenges for *ex-vivo* identification and characterisation of these T cells. To overcome this challenge, we developed an assay to isolate MR1-Ts using MHCI and MHCII negative antigen-presenting cells (APC) over-expressing MR1. These will be referred to as Targets^{scMR1}.

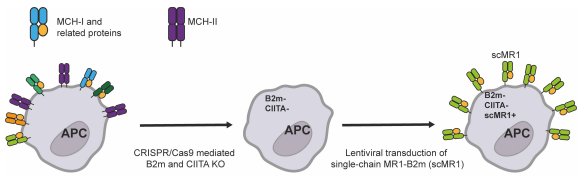

-Our objective was to validate these modified target cells as a tool to identify and detect MR1-T cells reactive to cancer cells through endogenous ligands presented via MR1. In addition, we also developed a higher-throughput phenotypic assay based on activation-induced markers (AIM) in the presence of APC and co-stimulation with anti-CD28.

1. Target cells over-expressing MR1 can be used to identify and isolate MR1 specific T-cells

- Targets^{scMR1} induce proliferation of T-cells pre-stained with Cell-Trace Violet (CTV) in a 10-day co-culture **(Figure 1A).**

-Expanded T-cells (CTV-) were sorted and grown individually through limiting dilution and sequenced (**Figure 1B).**

-MR1 specific TCRs (C1 and C3) were transduced into primary CD8 to assess their reactivity to MR1 molecules (wild-type, K43A) expressed in mammalian cells **(Figure 1C, D, E).** Shown is the activation of transduced CD8 as detected by FACS.

A. Proliferation assay

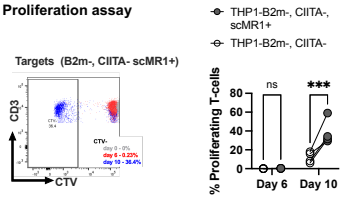

B. MR1T sequences identified though limiting dilution

TRAV	TRBV	Clone ID
TRAV12-2	TRBV4-3	C1
TRAV23DV6	TRBV7-9	C3

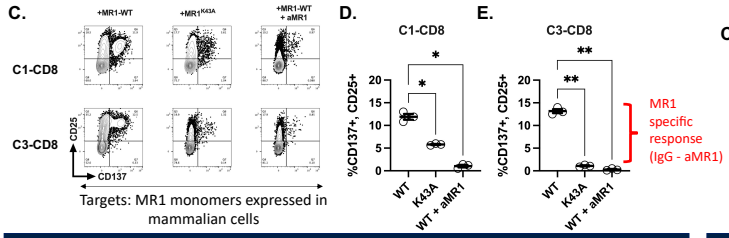

2. MR1 specific TCRs can react to different cancer cells lines

-We measured the reactivity of MR1 specific TCRs (transduced CD8) to different wild-type cancer cell lines **(Figure 2C, E)** and target cells of myeloid and lymphoid origin **(Figure 2D, F).** The plots depict MR1 specific responses (IgG-anti MR1 activation) as detected by FACS

-E8 is a ligand agnostic TCR generated at Immunocore Ltd. Target recognition by CD8 transduced with the E8 TCR is used as a proxy for MR1 expression **(Figure 2A, B).**

-C1- and C3-TCR expressing CD8 cells show a preferential reactivity against THP1 cells **(Figure 2C, E).**

-In 20h killing assays, higher killing activity was observed by C1 and C3-expressing CD8 T cells against cancer cell lines compared to their healthy blood-derived counterparts **(Figure 2D, F).**

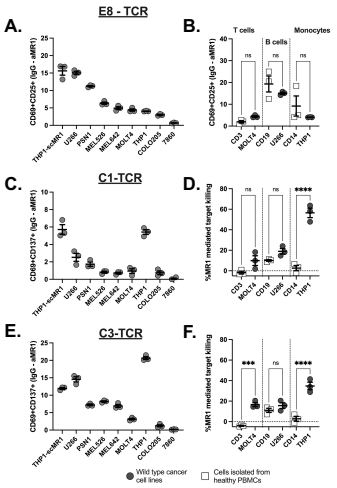

3. MR1-T cell can be detected *ex-vivo* through activation-induced marker (AIM) assays

-We detected MR1 specific responses (IgG-aMR1) *ex-vivo* through AIM assays where T-cells are co-cultured for 20-24h with targets^{scMR1} and anti-CD28.

-We observed an anti-CD28 dose-dependent upregulation of activation markers (CD137 and OX40) for CD161^{low} and CD161^{int} cells, but not in MAIT and CD161^{High} **(Figure 3A-D).**

-To validate whether CD137/OX40+ T-cells included MR1-T cells, both activated and non-activated T-cells were sorted and re-challenged. We confirmed MR1 dependent response only in the CD137/OX40+ fraction **(Figure 3E-I)**.

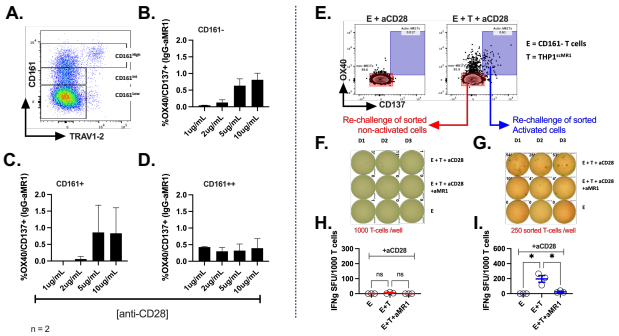

4. AIM assays can be used to estimate frequencies of MR1-T cells in blood from healthy and cancer donors

-By AIM assay, we did not observe differences in the frequency of MR1-T cells in total blood CD3 cells from healthy and colorectal cancer (CRC) donors **(Figure 4A).**

-However, compared to healthy donors, a higher frequency of MR1-T cells was observed in the CD161+ compartment of CRC patients **(Figure 4B).**

-Within the CD161- compartment, CRC patients have an increased frequency of circulating MR1-T cells with central memory phenotype and a reduction of naïve MR1T cells **(Figure 4C, D).**

-The activation data from different T-cell compartments was normalised as FC over bulk CD3 activation to reduce donor-to-donor variance and bystander effects **(Figure 4C, D)**.

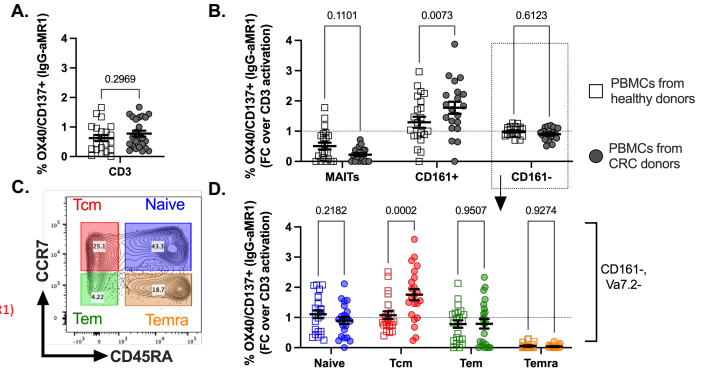

Conclusions

-Our results indicate that Targets^{scMR1} can be used to specifically expand MR1-T cells in a 10-day proliferation assay. MR1-T cells can also be identified in a shorter 20h AIM assay in the presence of anti-CD28 co-stimulation.

-We characterised two MR1-restricted TCR (C1 and C3) which show different sensitivity to the K43A mutation, suggesting different specificities.

-Both C1 and C3 TCRs show reactivity against different cancer cell lines, with a preferential reactivity against THP1 cells. C1 and C3 TCRs are only weakly reactive to cell populations isolated from healthy PBMCs.

-Results from AIM assays showed an unexpectedly high frequency (~1/133 or ~0.75%) of MR1-T cells in peripheral blood. Furthermore, comparing PBMCs from healthy and CRC donors, we found an increased circulation of MR1-T cells with central memory phenotype in the latter.

-The observed high frequency of MR1-T cells may include bystander T-cell activation driven by the presence of APCs, anti-CD28 and signal amplification. More validation needs to be done.

References

1.Eckle, S. B. G. G. et al. A molecular basis underpinning the T cell receptor heterogeneity of mucosal-associated invariant T cells. Journal of Experimental Medicine 211, 1585–1600 (2014).
2.Keller, A. N. et al. Drugs and drug-like molecules can modulate the function of mucosal-associated invariant T cells. Nature Immunology 18, 402–411 (2017).
3.Crowther, M. D. et al. Genome-wide CRISPR–Cas9 screening reveals ubiquitous T cell cancer targeting via the monomorphic MHC class I-related protein MR1. Nature Immunology 21, 178–185 (2020).